THE UNIVERSITY
of EDINBURGH

THE UNIVERSITY *of* EDINBURGH

Spatial and temporal variations in potentially toxic elemental (Sb, Pb, Cu and Zn) and PAH concentrations and associations in run-off from urban and rural areas of Scotland

Kenneth G.N. Macgregor

PhD THESIS

The University of Edinburgh

2016

Declaration

This thesis has not been submitted as part of any other degree or professional qualification. The work presented in this thesis is original, and has been composed by the author.

Kenneth Macgregor February 2016

Acknowledgement

Firstly, I would like to thank National Environment Research Council (NERC) for providing funds and support to complete this project, which otherwise, would not have been possible. I would also like to express my appreciation to the University of Edinburgh (UoE) and Scottish Universities Environmental Research Centre (SUERC) for their personal support and administration.

I owe a great debt of gratitude to my PhD supervisors Dr Gillian MacKinnon, Professor John Farmer and in particular, Dr Margaret Graham, which have provided excellent technical expertise and mentoring over the PhD duration. I am privileged to have met and worked alongside such esteemed individuals, and their presence and input has been extremely inspirational. The assistance from facility staff is also recognised and greatly appreciated, particularly Dr Lorna Eades and Caroline Donnelly, and in addition, Dr Justin Hargreaves, Michael Beglan and Harry Jackson from the University of Glasgow (UoG). My fellow PhD students, David, Peerapat, Ellen, Michael and Gavin have been a real asset to have around, and their daily encouragement was greatly valued. Finally, I would like thank the unconditional love and support from my devoted family, specifically my wife Jennifer, who has kept me smiling throughout the challenging times and given me the belief to successfully complete this project.

Abstract

Since the UK industrial revolution, coal combustion, ore smelting and other industrial activities have resulted in a marked increase in emissions of potentially toxic elements (PTEs) such as antimony (Sb), lead (Pb), arsenic (As), copper (Cu) and zinc (Zn), along with polycyclic aromatic hydrocarbons (PAHs), to the atmosphere. Although stricter environmental regulation and improved technology has led to a notable decline for some contaminant emissions in recent decades, this has not been observed for all elements, e.g. Sb, where only a modest reduction in emissions have been recorded. Once emitted, Sb along with Pb, As, Cu, Zn and PAHs may persist in the environment for considerable periods of time after their release; although their chemical associations may change, elements are not broken down over time and organic contaminants may break down slowly. Above all, PTEs and PAHs are detrimental to human and environmental health, with chemical forms of Sb, Pb, As and PAHs categorised as carcinogenic. Understanding their behaviour and fate in the environment is therefore an important step towards evaluating their likely impact on both ecosystem and human health. Consequently, this study focuses on the release, behaviour and fate of contaminants from current and past anthropogenic sources in the urban and rural environment, with a specific interest in Sb and PAHs, where emissions originate from similar anthropogenic sources, with Pb, As, Cu and Zn also included for comparison purposes.

Current and past industrial activity was identified as the dominant source of PTEs and PAHs to the urban environment, with emissions from vehicle, coal combustion and metal smelting identified as main contributors to total contaminant concentrations. Using road dust collected from Edinburgh at five high- and low-traffic roads at a distance of 10 and 50 m from the closest road junction, concentrations of Sb, Pb, Cu, Zn, PAHs and Pb isotope ratios were determined, with road dust undergoing further characterisation using chemical (sequential

extraction) and spectroscopic (X-ray diffraction, SEM-EDX) techniques. No consistent trend for the element concentrations released from vehicles braking at 10 and 50 m from the closest road junction was observed. Mean concentrations for Sb, Cu and Zn were 5.3 ± 2.8 mg kg^{-1}, 91.4 ± 48 mg kg^{-1} and 237 ± 144 mg kg^{-1}, respectively, and were similar to road dust sampled from five high- and five low-traffic locations in Glasgow (Sb 4.5 ± 2.1 mg kg^{-1}; Cu 117 ± 71.9 mg kg^{-1}; Zn: 283 ± 146 mg kg^{-1}). This was in contrast to mean concentrations for Pb and Σ16PAHs obtained from Glasgow (Pb 250 ± 283 mg kg^{-1}, Σ16PAH 7.7 ± 4.3 mg kg^{-1}) where values were approximately double and two-thirds greater than those found in Edinburgh (Pb 135 ± 129 mg kg^{-1}, Σ16PAH 4.7 ± 2.9 mg kg^{-1}), respectively. Lead isotopic analysis of Glasgow road dust ($^{206}Pb/^{207}Pb$ range of 1.140-1.174) showed a strong influence of past emissions from coal combustion and metal smelting, and was in agreement with Glasgow's industrial history. For Edinburgh, the isotopic signature was considerably lower ($^{206}Pb/^{207}Pb$ range of 1.116-1.151), and was influenced moreso by emissions of Australian sourced Pb in leaded fuel. Isotopic signatures in Edinburgh were lowest at easterly locations within 5 km of Edinburgh airport ($^{206}Pb/^{207}Pb$ ~ 1.12), and corresponded with past vehicle emissions from leaded petrol use, and to a lesser degree, emissions from avgas, which was consistent with the mean annual wind direction for Edinburgh. The mobility of elements from the road dust to the aqueous phase were assessed by sequential extraction, and by using road surface water samples which showed mobility decreased in the order of Zn>Cu>Pb>Sb. Road dust characterised by XRD and SEM-EDX had a high proportion of quartz present (~55%), whilst the presence of less abundant minerals such as calcite were found to increase Pb mobility through ease of dissolution into the aqueous phase.

For the rural environment, the behaviour and fate of elemental pollution originating from two former mining sites, an Sb mine at Glendinning, SW Scotland, and a Pb mine at Tyndrum in central Scotland was examined. Under specific environmental conditions, Sb was found to be both mobile and immobile in the environment. The chemical weathering of

stibnite found in spoil heaps at Glendinning Sb mine demonstrated that ~3% of total Sb can be mobilised during the chemical weathering process, while hydrous Fe oxides and organic matter in the surrounding soil favoured its retention. The retention of Sb, along with Pb, was similarly observed in Loch Tay sediment downstream of Tyndrum Pb mine, where upon deposition, Sb and Pb remained immobile in sediment and allowed the construction of deposition chronologies for two sediment cores to be established. Excellent agreement between the sediment core deposition chronologies was observed, with both chronologies identifying atmospheric deposition as the primary source of Sb to Loch Tay sediment, whilst the dominant source of Pb was from Tyndrum Pb mine ~25 km upstream of Loch Tay. Relative to Sb and Pb, As had the greatest mobility, with its geochemical behaviour and partial retention by the solid phase influenced by the presence of Fe. This was evident in the surrounding soil at Glendinning Sb mine, where As was associated with hydrous Fe oxides present in the solid phase, while at Loch Tay, the redox cycling of Fe resulted in the post-depositional mobility of As in sediment.

The use of ombrotrophic peat bogs for this study provided an effective means to assess atmospheric deposition of contaminants over past centuries; they continually accumulate and receive all their nutrients and contaminants exclusively by deposition from the atmosphere. The deposition archives of Sb and Pb from two Scottish peat cores sampled from Great Moss, Cairngorms Mountains, and, Auchencorth Moss, Midlothian, were used to construct chronologies for historic and contemporary emissions, particularly in relation to current and historic anthropogenic activities observed in urban and rural environments. At Great Moss, the deposition of Sb and Pb during the 19th century increased by a factor of 10 and 4, respectively, as a result of the industrial revolution and emissions from the combustion of coal and metal smelting. The trend continued into the 20th century where Sb and Pb deposition peaked ~1950, followed by a decline towards the early 21st century by a factor of 5 and 11, respectively. Over this period of time, the contribution from coal combustion and

metal smelting towards total anthropogenic emissions was on the decline, while emissions from the combustion of leaded fuel increased until the ~1980s. Although deposition chronologies before 1970 for Sb and Pb at Auchencorth Moss were generally in agreement with those from Great Moss, several differences were observed after 1970, or more specifically, in the top ~10 cm of the peat core. This was a result of sub-surface perturbations for Ti, Sb, Pb and ^{210}Pb concentrations, and indicated once deposited, elements were susceptible to post-depositional mobility brought about from a change in environmental conditions. The thicker acrotelm layer present at Auchencorth Moss, and the vertical movement of the peat water-table within this layer, resulted in a change in redox conditions and led to the redox cycling of Mn and Fe, which in turn, influenced vertical concentrations of Ti, Sb, Pb and ^{210}Pb. While Sb and Pb are usually found immobile in peat systems, the post-deposition mobility of Sb and Pb at Auchencorth Moss was comparable to a peat core sampled from Flanders Moss, and indicated that under specific environmental conditions, both elements can become mobile in ombrotrophic peat bogs. It is worth bearing in mind however, that these results are the exception, and in all other cases ombrotrophic peat bogs remain a reliable archival material to use.

Lay Abstract

Human activity from past and current practices including mining, coal combustion and vehicular transportation, have led to large quantities of potentially toxic contaminants such as antimony, lead, arsenic and polycyclic aromatic hydrocarbons released to the environment. Although environmental regulation has reduced the amounts of contaminants currently released to the atmosphere, a reduction in the extent of environmental contamination may not be observed for all. One such contaminant is antimony, where global production has tripled since the mid-1980's, partly due to its use in brake-linings, where upon vehicle braking, small quantities of antimony, as well as lead, copper and zinc are deposited on the road surface. Using road dust sampled from Edinburgh and Glasgow, this research showed that vehicle emissions had a variable impact on the quantity of contaminants present in road dust at each location; past industrial activities also had an impact on contaminant concentrations in some dust samples. The impact of past mining activities was also still evident in rural areas; antimony, along with lead and arsenic, continue to be released from spoil heaps, in the vicinity of two abandoned mines in Scotland, Glendinning antimony mine and Tyndrum lead mine. The release of contaminants downslope into rivers, soils and sediments were observed at both locations. At Glendinning, elevated concentrations of dissolved antimony were found in nearby stream waters whilst at Loch Tay, contaminant transport in association with particulate matter meant that the impact of mining was evident up to 25 km downstream. The emission of antimony and lead from past and current human activity, and the rate of deposition was assessed using two Scottish peat cores sampled from Great Moss, Cairngorm Mountains, and Auchencorth Moss, Midlothian. Although the atmospheric deposition of antimony and lead had considerably declined since the last century, unlike lead, no decline in atmospheric deposition for antimony was observed in the 21st century.

Contents

List of Figures

List of tables

List of acronyms and definitions

AADF	Atomic Absorption Spectroscopy
AAS	Annual Average Daily Flow
ACE	Acenaphthene
ACY	Acenaphthylene
ANT	Anthracene
AOD	Above Ordnance Datum
ATP	Adenosine Triphosphate
ASTM	American Society for Testing and Materials
BaA	Benzo(a)anthracene
BaP	Benzo(a)pyrene
BbF	Benzo(b)fluoranthene
BCR	Community Bureau of Reference
BghiP	Benzo(g,h,i)perylene
Bidentate	A lewis base that donates two pairs of electrons to a metal atom.
BkF	Benzo(k)fluoranthene
CCME	Canadian Council of Ministers of the Environment
CE	Capillary Electrophoresis
CEH	Centre for Ecology & Hydrology
Chalcophilic	An element that has a low affinity for oxgen and prefers to bond to sulfur.
CHR	Chrysene
CIC	Constant Initial Concentration
CLEA	Contaminant Land Exposure Assessment
CL:aire	Contaminated Land Applications in Real Environment
CONCAWE	Conservation of Clean Air and Water in Europe
CRJ	Closest Roadside Junction
CRS	Constant Rate of Supply
CRM	Certified Reference Material
DaHA	Dibenzo(a,h)anthracene
DEFRA	Department for Environment, Food and Rural Affairs
DOC	Dissolved Organic Carbon
DMA	Dimethylarsinic Acid
EDTA	Ethylenediaminetetraacetic Acid
EDX	Energy-dispersive X-ray spectroscopy
EEA	European Environment Agency
ELV	End of Life Vehicles
EQS	Environmental Quality Standard
EC	European Commission
EU	European Union
FL	Fluorene
FLA	Fluoranthene
FOREGS	Forum of European Geological Surveys
GC	Gas Chromatography
HPLC	High Performance Liquid Chromatography
HS	Humic Substances
IcdP	Indeno(1,2,3-c,d)pyrene
ICP	Inductively Coupled Plasma
IARC	International Agency for Research on Cancer

IQ	Intelligence Quotient
LOD	Limit of Detection
LQM	Land Quality Management
MARS	Microwave Accelerated Reaction System
MMA	Monomethylarsonic Acid
Monodentate	A Lewis base that donates a single pair of electrons to a metal atom.
MS	Mass Spectrometry
Multidentate	A Lewis base that donates more than two pair of electrons to a metal atom.
MWCO	Molecular Weight Cut Off
NERC	Natural Environment Research Council
NIST	National Institute of Standards and Technology
NP	Naphthalene
OES	Optical emission spectroscopy
OM	Organic matter
PAH	Polycyclic Aromatic Hydrocarbon
PE	Polyethylene
pe	Reduction potential
PET	Polyethylene terephthalate
PHE	Phenanthrene
PHS	Priority Hazardous Substance
POP	Persistent Organic Pollutant
PM	Particular Matter
PS	Priority Substance
PTFE	Polytetrafluoroethylene
PYR	Pyrene
RSC	Royal Society of Chemistry
SEM	Scanning Electron Microscopy
SEPA	Scottish Environment Protection Agency
SGV	Soil Guideline Value
SIM	Selective Ion Monitoring
SPRI	Scottish Pollutant Release Inventory
SNH	Scottish Natural Heritage
SRM	Standard Reference Material
SUDS	Sustainable Drainage Systems
SUERC	Scottish Universities Environmental Research Centre
TDI	Tolerable daily intake
TTC	Total Traffic Count
UKTAG	United Kingdom Technical Advisory Group
UNEP	United Nations Environment Programme
USEPA	United States Environmental Protection Agency
USDA	United States Department of Agriculture
USGS	United States Geological Survey
UV/Vis	Ultraviolet and/or Visible
VROM	Ministry of Housing, Spatial Planning and the Environment
WFD	Water Framework Directive
WHO	World Health Organisation
XANES	X-ray Absorption Near Edge Structure
XRD	X-Ray Diffraction
XRS	Xikuangshan

Chapter 1 Introduction

1.1. Introduction

From the start of the UK Industrial Revolution in the mid-19th century, coal combustion, ore smelting and other industrial activities resulted in a marked increase in emissions of potentially toxic elements (PTEs) such as antimony (Sb), lead (Pb), arsenic (As), copper (Cu) and zinc (Zn), as well as polycyclic aromatic hydrocarbons (PAHs), to the atmosphere. Contaminant emissions continued to increase from the early to mid-20th century, where emissions from coal combustion and ore smelting were dominant. Although no significant increase for contaminant emissions were observed after ~1950s, the dominant source of emissions had changed from coal combustion and ore smelting, to the combustion of leaded petrol (Farmer *et al.*, 1999). Since the late 20th century, however, stricter environmental regulation and improved technology resulted in a considerable decline in emissions of many contaminants. For some contaminants such as Sb, however, new uses have emerged and emissions in recent years have shown no similar decline, with future emissions expected to increase twofold between 2010 and 2050 (Tian *et al*, 2014; Zhou *et al.*, 2015). It is important to remember that elements and certain pollutants may persist in the environment for considerable periods of time after their release; although their chemical associations may change, elements are not broken down over time and organic contaminants may break down slowly over time to more recalcitrant forms.

In addition to their classification as PTEs, Sb, Pb, As, Cu and Zn are defined as chalcophilic, meaning that they have a low affinity for oxygen and prefer to bond to sulfur. As a result, they are often found together in sulfidic ores and coals, and consequently were released to the atmosphere from similar anthropogenic activities for much of the 19th and early 20th centuries. PAHs are often formed and subsequently released during high temperature

processes such as coal combustion, metallurgical processes and vehicle emissions. Thus, similar anthropogenic activities have released both PTEs and PAHs to the atmosphere. Based on their likely impact upon human health, a group of 16 PAHs have been defined by the USEPA as priority pollutants, and include 8 PAHs that have been categorised as either Priority Hazardous Substances (PHS) or Priority Substances (PS) under the Water Framework Directive (WFD) (2000/60/EC). Whilst the chemical properties of each PAH may vary depending on their individual structure, they are all considered environmentally persistent and are classed as carcinogens.

Understanding their behaviour and fate in the environment is therefore an important step towards evaluating their likely impact on both ecosystem and human health. Although this has been well documented in past studies for some contaminants such as Pb (McLean and Bledsoe, 1992; Drever, 1997; Farmer *et al*., 1997; MacKenzie *et al*., 1998; Shotyk *et al*., 2002;) and, to some extent, PAHs (Kogel-Knaber and Totsche, 1998; Yang *et al.*, 2001; Wang *et al.,* 2007; Dong and Lee, 2009), even less is known about the environmental behaviour of Sb, specifically its associations and mobility in both urban and rural settings. Therefore, the main focus of this study will be on Sb and PAHs; because they originate from similar anthropogenic sources, whilst the co-occurrence of Pb, As, Cu and Zn with Sb in minerals and coal have also been included for comparison purposes.

Although the mechanism of release is different, vehicle use is currently the major source of Sb and PAHs to the urban environment in Scotland; Sb in brake-linings is released during their operation whilst PAHs are emitted during combustion of petrol or diesel (Dore *et al.,* 2005; SEPA SPRI, 2015). Globally, vehicle emissions have shown a considerable decline in recent years for other contaminants such as Pb however, emissions of Sb and PAHs have remained largely the same (Tian *et al*., 2014; Shen *et al.,* 2011). A further concern is that the decline in atmospheric concentrations of Pb (and Cu and Zn) has not been reflected in a similar decline for riverine concentrations, with run-off containing chalcophilic contaminants

identified as a major source of inner city water pollution (Zhao *et al.*, 2011; Zhang *et al*., 2014). This places a greater importance on understanding the source of chalcophilic contaminants and PAHs to road dust, as well as their retention or release in the urban environment.

In the rural environment, the source of chalcophilic elements can be very different from that in the urban environment. For example, the traffic numbers in rural roads are much lower than urban roads, and as a consequence, the release of contaminants from vehicle use is considerably lower. Past anthropogenic activities may therefore remain the main source of contaminants to the rural environment, particularly in areas where previous land use included metal ore mining. At former mining sites, mineral-rich soil has often been excavated, deposited and left on the surface soil potentially acting as a continuing source of chalcophilic elements to nearby receiving waters. A number of studies have shown that metals released from mine spoils can bind to solid phase organic matter and mineral phases rendering them largely immobile (McLean and Bledsoe 1992; Filella, 2002a). For example, Pb may bind to humic substances via ionic or electrostatic interactions with carboxylic and phenolic groups, or may become adsorbed onto mineral surfaces such as hydrous metal oxides in slightly acidic soils (McLean and Bledsoe 1992; McKenzie 1998b; Tipping, 2002; Scheetz and Rimstidt, 2008). A change in environmental conditions, however, has the potential to mobilise these soil-bound elements, with soil drainage (and E_h) and pH being particularly important influential factors. Whilst the behaviour and fate of Pb in soil-water systems has been the focus of numerous past studies, there are very few studies on Sb that specifically address the influence of key environmental conditions on its associations in the solid and aqueous phase of soils as well as sediments. For some mine spoil-contaminated areas, past work on Pb has shown that elemental transport has occurred over distances of 10s of kilometres and subsequent deposition in lake sediments. There has been very little, if any research carried out on Sb behaviour upon transfer to aquatic sediments. Historical records

for Pb have been constructed using dated lake sediment profiles but this requires post-depositional immobility which although justifiable for Pb, may not be the case for Sb.

In areas remote from mining activities, ombrotrophic peat bogs have also been used to construct historical records of elemental emissions because: (i) they continually receive and accumulate nutrients and contaminants exclusively from the atmosphere; (ii) there is no post-depositional mobility of the contaminants. Much research in this respect has focused on Pb (Farmer *et al*, 1999, 2000, 2006; Shotyk *et al*., 2002; Cloy *et al.*, 2005, 2009) with only a few studies including records for Sb, e.g. two studies in Scotland (MacKenzie *et al*., 1998a; Cloy *et al*., 2009) and three elsewhere (Shotyk *et al*., 1996; Allan *et al*., 2013; Kuwae *et al*., 2013).

1.2. Aims and objectives

The main aim of this PhD was to investigate the behaviour and fate of key environmental contaminants (Sb, Pb, As, PAHs) which have predominantly originated from similar sources. Especial focus was on Sb since least is known about its behaviour and fate in both urban and rural environments.

The specific objectives were to:

- Determine the concentrations of Sb, Pb, Cu, Zn and PAHs in street dusts from Glasgow and Edinburgh, two cities which have similarly high vehicle numbers but have very different industrial histories, and establish the relative importance of current (vehicular) and past (old industrial) sources of these contaminants in urban settings.
- Determine concentrations and associations of Sb, As and Pb in soil, porewater and surface water, in order to elucidate both elemental retention and transport processes occurring in the vicinity of a former Sb mine in a rural area of SW Scotland. Use

the knowledge about elemental associations to predict conditions which would increase elemental mobility and increase the impact on receiving waters.

- Develop new analytical methods to determine the concentrations of Sb(III) and Sb(V) in soil-water systems. Apply the methodology to investigate the impact of the redox environment on Sb speciation and develop an improved understanding of the processes controlling Sb retention and mobility in mine spoil-impacted soils.
- Determine concentrations of Sb, Pb, As and redox-active elements, Mn and Fe in sediments from Loch Tay, ~25 km downstream from the Tyndrum Pb mine and investigate the effect of redox cycling on the vertical distribution of Sb and, subject to no post-depositional mobility, establish the contribution perturbations of mining activities had on records of atmospheric emissions of Sb in Loch Tay sediment.
- Establish atmospheric Sb and Pb deposition chronologies using two dated ombrotrophic peat cores from Scotland, and compare these to deposition records constructed from Loch Tay sediment and from previously published literature.
- Compare anthropogenic Sb/Pb ratios from urban dusts with those obtained for surficial loch sediment and peat samples to assess the extent to which increases in Sb emissions over the past few decades are being picked up in the archival records.

Chapter 2 Chalcophilic elements and PAHs as environmental contaminants

2.1 Introduction

This chapter examines the chalcophilic elements antimony (Sb), lead (Pb), arsenic (As), copper (Cu) and zinc (Zn) as environmental contaminants. It details elemental properties, occurrence, behaviour, impact to human health, environmental regulation, and subsequent emissions from historic and current anthropogenic activities. Often occurring from similar anthropogenic activities, 16 polycyclic aromatic hydrocarbon (PAHs) priority pollutants are also examined and are evaluated similarly to the previously mentioned chalcophilic elements. It furthermore gives detail on source apportioning techniques used for Pb and PAH analysis, through the use of Pb isotopic ratios and PAH molecular structure, respectively.

2.2 Antimony

2.2.1 Elemental properties and occurrence

Antimony is a group 15 metalloid with the atomic number 51 and an atomic weight of 121.8. It can exist in four oxidative states (-III, 0, +III and +V), although in environmental systems it is generally found in the +III and +V states (Krupka and Serne, 2002). There are two isotopes of Sb, ^{121}Sb and ^{123}Sb, with relative abundances of 57% and 43%, respectively (Rouxel *et al*., 2003). Often described as a soft, silvery, lustrous grey metalloid, Sb is commonly found in the presence of other elements such as sulfur (S) and oxygen (O), and in ores of Cu, silver (Ag) and Pb (Filella *et al*., 2002a). Although crustal abundance of Sb varies regionally, a mean crustal abundance of 0.2 mg kg^{-1} has been estimated globally (Taylor, 1964; Aherns, 1965; Mason, 1966; Wedepohl, 1968).

2.2.2 Antimony in the environment

2.2.2.1 Mineral forms, weathering processes and solution chemistry

Chalcophilic elements such as Sb, have a low affinity for O and prefer to bond with S as sulfites or sulfosalts (Goldschmidt, 1937). Antimony is commonly found in association with pyrites (FeS_2), often found in deposits of fossil fuels such as coal (Filella *et al*., 2002a). The most commonly found Sb ores are stibnite (Sb_2S_3) and the tetradredrite-tennantite series ($Cu_{12}Sb_4S_{13}$-$Cu_{12}As_4S_{13}$) (Roper *et al*., 2012), where the latter consists of differing compositions of Cu, Au, As and Zn substituting into the lattice to varying extents (De Bendetto *et al*., 2002; Roper *et al*., 2012). Other less common ores are pyrargyrite (Ag_3SbS_3), Zinkenite ($Pb_9Sb_{22}S_{42}$) and boulangerite ($Pb_5Sb_4S_{11}$). The effect of weathering and the subsequent oxidation of primary ores found in surface or near-surface environments can result in the formation of secondary ores (Equation 2.1), e.g. valentinite (ortho-rhombic Sb_2O_3), senarmontite (cubic Sb_2O_3), and the sulfosalt kermesite (Sb_2S_2O). Secondary ores formed from the weathering process, are slightly soluble in aerobic conditions, and can undergo dissolution into an aqueous phase (Equation 2.2) (Roper *et al*., 2012). Under standard temperature and pressure, Biver and Shotyk (2013) reported senarmonitie solubility of ~1.3 mg of Sb L^{-1}, whilst a study near an Sb mine by Sh *et al*. (2012) reported that 0.70-1.63% of total Sb was dissolution by the weathering process.

$$Sb_2S_3(s) + 15H_2O \rightarrow Sb_2O_3\,(s) + 3SO_4^{2-}\,(aq) + 30H^+\,(aq) \qquad \textbf{Equation 2.1}$$

$$Sb_2O_3(s) + 3H_2O \rightarrow 2Sb(OH)_3\,(aq) \qquad \textbf{Equation 2.2}$$

Under aerobic conditions, Sb is very soluble in aqueous systems, where, in accordance to thermodynamic predictions, it exists in mildly acidic, neutral and alkaline aqueous systems as the anionic Sb(V) species, $Sb(OH)_6^-$ (Brintzinger, 1948; Souchay and Peschanski, 1948; Pitman *et al*., 1957; Ricca and D'Amore, 1965; Filella *et al*., 2002b; Krupka and Serne,

2002). Only under very acidic conditions (pH <2) will Sb(III) exist as $Sb(OH)_2^+$ (Filella *et al*., 2002b; Krupka and Serne, 2002). Although the dominant Sb species present at this pH is confirmed by the Pourbaix diagram shown in Figure 2.1, it is worth noting however, that these diagrams are based purely on thermodynamics, and as a result represent the equilibrium state. In practice, many systems are not in equilibrium, which can result in differing theoretical and practical dominant species observed. This may be the case for the dominant Sb(III) and (V) aqueous species in anaerobic aqueous systems (E_h <0 at pH~6), where the role of kinetic stabilisation may explain the presence of Sb(V) under specific conditions. A study by Cutter (1991) observed Sb(V) as the dominant species below 200 m in the Black Sea, and other studies by Bertine and Lee (1983), and Andreae *et al*. (1984) have also reported Sb(V) in anaerobic conditions. It is believed that these results may be related to the sinking of detritus specifically in deep waters, formation of thiocomplexes, or the transport of surface waters containing high concentrations of $Sb(OH)_6^-$, all under slow rates of reduction. These mechanisms were postulated by Filella *et al*. (2002b), and whilst conceivable, more research is required to elucidate the presence of both Sb(III) and Sb(V) in particular systems. Taking this into consideration, this study aims to complement existing research on Sb speciation in soil-water systems, by developing the capabilities to quantify Sb species present in environmental samples.

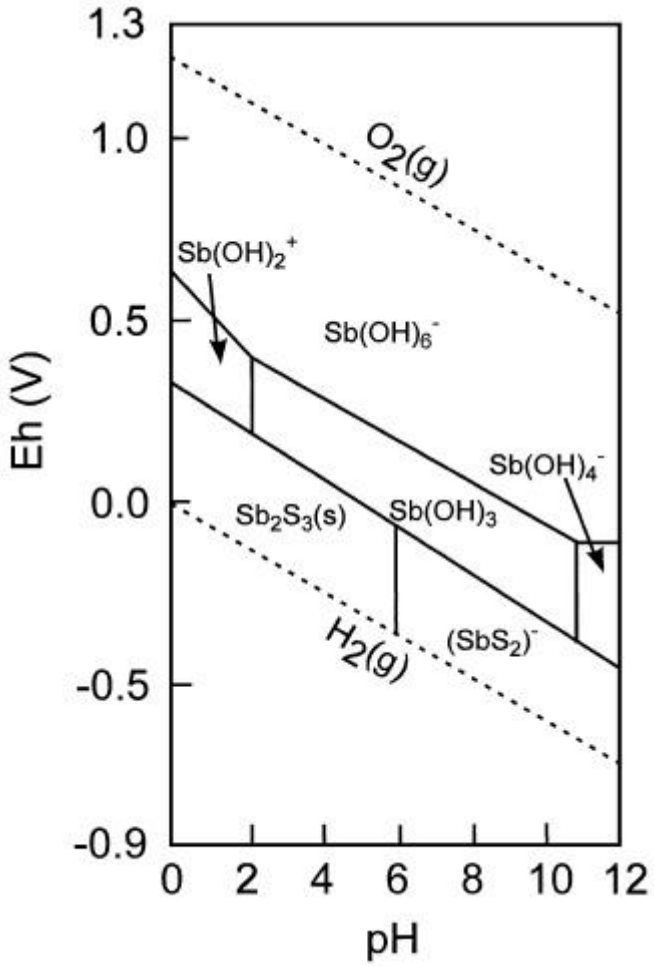

Figure 2.1: E_h-pH diagram for a Sb-S-H_2O system at a dissolved Sb concentration of 10^{-8} mol L^{-1} and a dissolved S concentration of 10^{-3} mol L^{-1} (25°C at 1 atm) (Filella *et a*l.,2002b).

2.2.2.2 The behaviour of Sb in the soil environment

The binding and mobility of elements in soil is often influenced by key variables such as organic matter, the abundance of major secondary minerals such as hydrous iron (Fe), manganese (Mn) and aluminium (Al) oxides (including oxides, hydroxides and oxyhyroxides), a change in redox conditions, pH and clay content. Of these variables, the most influential are organic matter, secondary minerals and a change in redox conditions, which are discussed in turn in the section below. Understanding how Sb binds to soil can be challenging, as organic matter is a complex mixture of poly-functional structures, including humic substances (HS) generally derived from humic and fulvic acids (Tella *et al*., 2012).

Whilst organic matter is often the most influential property for trace element retention in soil, only limited research exists in isolating mechanisms for complex formation with HS. Tella *et al*. (2012) completed a study investigating Sb(V) complexation using in situ potentiometry and X-ray absorption spectroscopy to examine binding with aqueous organic ligands, including carboxyl, alcoholic, hydroxyl, aliphatic and aromatic hydroxyl groups typically found in organic matter. This demonstrated that Sb(V) can form stable complexes with poly-functional carboxylic and hydroxyl groups in natural water through organic ligands, with complex co-ordination strongest at ~pH 4 (pH range studied was from 3-9). At near-neutral pH however, the affinity of Sb(III) to complex with organic matter was dominant, where the binding functional groups remained similar to Sb(V), but coordination and geometry changed to a pyramidal from an octahedral structure. This was consistent with Buschmann and Sigg (2004), who also identified increased binding of Sb(III) to carboxylic and phenolic groups at near-neutral pH. In contrast, other studies have questioned the importance of organic matter for retention in soil. For example, Filella and Williams (2012) stated that Sb(V) (in the form of $Sb(OH)_6^-$) has limited affinity for negatively charged humic and fulvic acids (at common environmental pH values), and indicated the retention of Sb in soil was influenced more by the presence of abundant mineral phases such as those containing Fe, Mn and Al.

Filella *et al.* (2002b) concluded that hydrous Fe oxides were effective in limiting Sb soil mobility, whilst Chen *et al*. (2003), Thanabalasingam and Pickering (1990) reported the retention of Sb by hydrous Mn and Al oxides. At pH $\geq$ 3, $Sb(OH)_6^-$ complex formation with hydrous oxide groups takes place via an inner-sphere surface interaction, e.g. via the formation of Fe-O-Sb bonds (McComb *et al*., 2007); the readiness of this occurring decreased towards near neutral pH due to the limited Fe binding sites available (Filella and William, 2012). Although hydrous Fe, Mn and Al oxides are major natural sorbents for Sb

(Johnson *et al*., 2005; Mitsunobu *et al*., 2010; Wilson *et al*., 2010; Okkenhaug *et al*., 2011), other factors such as redox conditions and pH are particularly important with respect to redox cycling of Fe. For example, a change from dry to waterlogged conditions is often accompanied with a transition from aerobic to anaerobic conditions and may promote reductive dissolution of Fe(III) solid phases. As a consequence, previously bound Sb will be released along with Fe(II) into the soil porewater increasing Sb mobility. This is consistent with a recent study by Hockman *et al*. (2014), which demonstrated the mobility of Sb under Fe-reducing conditions in contaminated shooting range soil, and found a correlation of Sb(III) with Fe(II) (R^2=0.86, $p<0.01$).

From the above summary of the literature, it is clear that associations with organic matter and/or mineral phases can either mobilise or immobilise Sb concentrations within soils. Although there may be some site-specific variability, further research however, is required to fully define the processes controlling Sb mobility in soil environments. This would help address the contrasting views on the extent of organic matter influence on Sb mobility.

2.2.3 Toxicity and human health exposure

Antimony is a nonessential element for plant and animal growth (Filella *et al*., 2007), and has potentially toxic and cumulative poisonous effects (Qi *et al*., 2011). Its chemico-toxicological characteristics are similar to As, and vary depending on its chemical form and oxidation state. The toxicological differences in Sb(III) and Sb(V) are well-known, with the +III state being around 10 times more toxic than the +V state (Smichowski, 2008). Whilst toxicological data on some chemical forms of Sb are limited, the International Agency for Research on Cancer (IARC) has classified antimony (III) trioxide (Sb_2O_3) as a potential carcinogen (IARC, 1989). In addition, its uptake by the human body can cause a number of other physical responses, e.g. it has been reported to irritate the respiratory tract, cause damage to skin and the mucous membrane of the alimentary canal, and even result in pulmonary edema, inflammation of the lungs, chronic bronchitis, and chronic emphysema (Qi *et al*., 2011).

Human exposure to Sb through ingestion, inhalation and, to a certain extent, dermal contact, is a growing concern, particularly in China, where high environmental concentrations of Sb exist as a consequence of anthropogenic activities (Wu *et al*., 2011). Although ingestion and inhalation are primary exposure routes affecting human health, the proportion of Sb exposure from each route can depend on local factors. For example, the occurrence and analysis of PM10 found in air samples collected in the mining and smelting town, Dachang, southern China, found concentrations greater than 575 mg m^{-3} and resulted in the exposure of local residents to high ambient air concentrations of Sb. Other residents however, may be affected more so by their diet, through the consumption of contaminated drinking water and food.

Table 2.1: Average Sb concentrations in contaminated water and food near Xikuangshan Sb mine. Adapted from Wu *et al*., 2011).

Sample media	N	Mean Sb concentration and range	Units
Drinking water	51	54 (8.1-152)	μg L^{-1}
Rice	7	470 (160-930)	μg kg^{-1} (dry weight)
Corn	8	300 (90-720)	μg kg^{-1} (dry weight)
Vegetable	70	379 (30-1660)	μg kg^{-1} (wet weight)
Meat and poultry	73	25 (1.8-144)	μg kg^{-1} (wet weight)

A study near Xikuangshan (XKS) Sb mine, Hunan province, China, by Wu *et al*. (2011), highlighted the impact of mining contaminants on the local water and food supply (Table 2.1). The atmospheric emissions of Sb originating from metal smelting onto surface water and soils, and subsequent uptake by plants and animals was a great concern. Residents from the vicinity of the mine were found to be consuming total Sb concentrations ~1.5 times greater (554 μg kg^{-1} d^{-1} for 60 kg body weight adult) than the World Health Organisation (WHO) tolerable daily intake (TDI) of 360 μg day (Figure 2.2) (WHO, 2008).

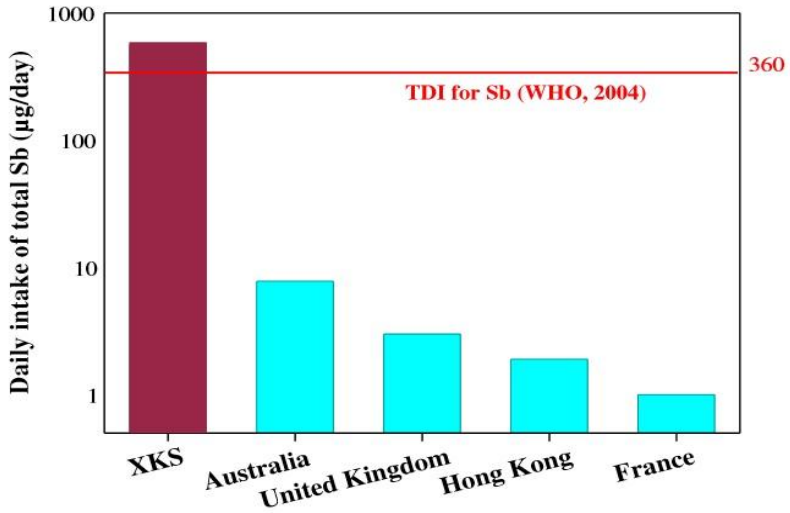

Figure 2.2: Daily intake of Sb for residents near XKS with global context (Wu *et al*., 2011).

For Europe, Sb exposure is generally via inhalation, where typical European ambient air concentrations of Sb in urban and rural areas are in the ranges 7-36 ng m^{-3} and 0.008-7 ng m^{-3}, respectively. The higher urban concentrations are attributed to human activity such as energy production and vehicle use (Schroeder *et al*., 1987). Globally, anthropogenic activities can account for about 74% of total atmospheric Sb concentrations (Filella *et al*., 2002a) contributing significantly to human exposure.

2.2.4 Environmental quality standards

The WHO has assigned an acceptable value of 20 µg L^{-1} for Sb concentration in drinking water (Fu *et al*., 2011), while the EU has imposed a maximum allowable concentration of 5 µg L^{-1} (Filella *et al*., 2002a). No freshwater environmental quality standard (EQS) has been set globally or in the UK but natural unpolluted water systems generally have Sb concentrations of around 1 µg L^{-1} (Filella *et al*., 2002b). Moreover, at the time of writing, there is no UK soil guideline value (SGV) for Sb nor have the Department for Environment, Food and Rural Affairs (DEFRA) and Environment Agency completed a Contaminant Land Exposure Assessment (CLEA) for Sb. Based on the Contaminated Land applications in real environment (CL:aire) assessment criteria, however, Sb is assigned a maximum soil

concentration of 550 mg kg^{-1} for residential soil (CL:aire, 2010), which is notably higher than the Canadian Government threshold of 20 mg kg^{-1} for residential and agricultural soil (CCME, 2007). Although the derivation models used for calculating Sb soil standards may account for some difference in setting Sb residential soil values, the considerable difference observed above demonstrates contrasting opinions on the toxicity and mobility of Sb in soil, with the mobility of Sb citically evaluated in this study.

2.2.5 Antimony production, use and emissions

2.2.5.1 Global Sb demand and use

Antimony production is dominated by China, (Figure 2.3), which supplies ~84% of global demand, with Australian, Bolivia, Canada and Turkey making up the remaining amount (Fu *et al*., 2010; He *et al*., 2012). Antimony ore extraction and production has increased significantly since the early 20th century, where Sb production equated to around 30 000 t in the early 20th century, contrasting to recent years, where production topped 170 000 t per year (Butterman and Carlin 2004; USGS, 2013). To meet global demand, it was reported that in 2012, China had 114 Sb mines in operation, across 18 provinces or autonomous regions. Environmental issues such as those described in section 2.2.3 however, has resulted in the closure of some mines in 2013 (USGS 2013).

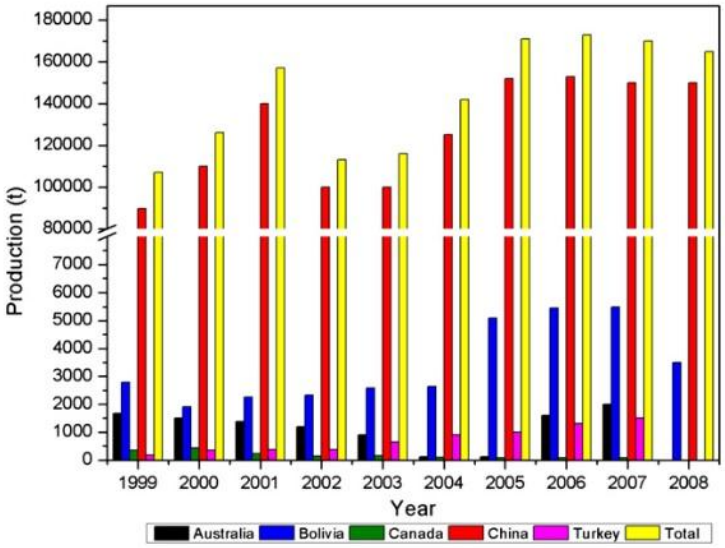

Figure 2.3: Global Sb production between 1999 and 2008 (He *et al*., 2012)

The primary global use of Sb is for flame retardants; it accounts for 60-70% of primary Sb production, and 90% of Sb trioxide (Sb_2O_3) production (Butterman and Carlin 2004, He *et al*., 2012). Although Sb or Sb_2O_3 in itself is not regarded as a flame retardant, it acts as a synergist along with halogenated flame retardants, and is often added to plastics and polypropylene found in packaging material, textiles and automotive components to comply with safety legislation and flammability standards. Furthermore, it is viewed as a more environmentally friendly additive to flame retardants, as it reduces the production and release of toxic halogenated flame retardants to the environment (Li *et al.*, 2012). Antimony trioxide is also key to the synthesis of polyethylene terephthalate (PET), where it is used as a catalyst, and is considered the most important part of PET production (Krachler *et al*., 2009; Bach *et al*., 2012). The use of Sb_2O_3 for the production of PET has also been observed in bottled drinking water, where trace concentrations of Sb have been reported to leach from the PET bottle, to its contents (Krachler *et al*., 2009).

The automotive industry utilise Sb for brake-linings, where Sb trisulfide (Sb_2S_3) is added to enhance the friction constancy and reduce braking vibration by acting as a lubricant (Ceriotti and Amarasiriwardena, 2009). Once released from the brake-linings, Sb_2S_3 readily oxidises in air to form the most toxic form of Sb, Sb_2O_3. Although brake-lining composition varies with manufacturer, car braking represents a significant diffuse source of Sb to the urban environment (Von Uexkull *et al*., 2005).

2.2.5.2 Global atmospheric Sb emissions

There are five main sources of atmospheric Sb emissions; fossil fuel combustion, nonferrous metal production, waste incineration, automotive brake wear and pig iron and steel production (Table 2.2), and these will be discussed in turn in the section below.

Fossil fuel combustion contributes the largest amount to global Sb emissions, and although trace amounts are present in petrol and natural gas, the burning of coal accounts for ~56% of global Sb emissions to the environment (Tian *et al.*, 2014). Not all Sb however, is released to

the atmosphere during the combustion process, with a proportion partitioned into a solid residue (He *et al*., 2012). For countries with a heavy reliance on coal, the proportion of Sb emissions occurring from this source can be considerably greater than the global average. This is especially true in China, where 70% of the national power originates from coal combustion, and where coal sourced and used from Guizhou and Mongolia is particularly rich in Sb (~2-3 times higher in Sb than the national Chinese average of ~2.0 mg kg^{-1}) (Zhao *et al*., 2002; He *et al*., 2012).

Table 2.2: Composition of global anthropogenic emission of Sb in 2010 (in tonnes). Adapted from Tian *et al*., (2014).

Continents	**FC**	**NMP**	**PISP**	**WI**	**BW**	**Total**
Africa	42	7	0	0	3	52
Asia	625	173	173	194	80	1079
Oceania	2	6	6	0	6	14
Europe (including Russia)	114	45	45	177	111	448
South America	8	68	68	0	16	93
North America	11	21	21	83	100	216
Total	**803**	**320**	**320**	**455**	**318**	**1094**

FC: Fuel combustion, NMP: Nonferrous metals production, PISP: Pig iron and steel production, WI: Waste incineration, BW: Brake wear

Metal production, ferrous or nonferrous, can use a number of different processes such as volatilisation roasting, blast furnace smelting and liquation to extract and purify the metal of interest (Butterman and Carlin 2004). These processes are predominantly used for Cu, Zn and Pb production but Sb is often present as an impurity and the smelting process releases Sb either in gaseous form or in the slag. Waste incineration and the subsequent release of Sb from flame retardant packaging accounts for ~26% of global Sb emissions (Tian *et al.*, 2014). Although brake wear is the second smallest contributor to global Sb emissions, it is of most concern in the urban environment. The growing global population, expanding

economic wealth of developing countries and wider affordability of cars will see Sb emissions continually increase from this source unless manufacturers are enforced to use ceramic replacements (Le Vine *et al*., 2012; Zhu *et al*., 2012; World Business Council for Sustainable Development, 2014). For example, UK road traffic has doubled since the mid-1970s through increased car and van use (le Vine *et al*., 2012). Ceriotti and Amarasiriwardena (2009) found Sb concentrations in brake-linings reaching 13,900 mg kg^{-1}, and Furuta *et al*. (2005) reported the release of 1.24 g of Sb per car per year in Japan. Brake wear and the subsequent release of Sb is greatest in urban areas where population density is highest placing a greater risk to human health through inhalation (Section 2.2.3).

For Sb, and indeed most other elements, current and past atmospheric emissions have been studied by sampling cores from environmental media such as peat bogs, lake sediments and ice. The release of Sb into the atmosphere and the subsequent wet and dry deposition, along with ^{210}Pb dating analysis (section 3.3.17), enables reconstruction of long-term Sb deposition rates over time. This technique allows pre-industrial atmospheric Sb emissions to be assessed relative to current anthropogenic emissions. As future chapters in this study will focus on peat and sediment cores, this section will examine these environmental media to establish Sb deposition chronologies in Scotland.

Records of atmospheric elemental contaminants have been obtained in ombrotrophic peat bogs and lake sediment cores in both heavily populated and remote regions in Scotland (Farmer *et al* 1996, 1997, 2005, 2006, 2015; Eades *et al* 1998, 2002; Cloy *et al*., 2005). Ombrotrophic peat bog cores provide a good record of past pollution because as they receive all their pollution directly from atmospheric deposition. Remote lake sediments similarly receive pollution directly from atmospheric deposition but in addition, also receive inputs from the lake catchment. Either system can be used for contaminant archives but a prerequisite is that the media accumulate elements over time with no physical mixing or post-depositional mobility. Although Sb deposition inventories are limited, the impact of anthropogenic activity since the industrial revolution can be observed in ombrotrophic peat

cores around the world. A comprehensive account of Sb deposition from 1400–2000 was completed by Allan *et al*. (2013) using peat cores from Misten, Belgium, which showed the clear impact of anthropogenic activities. The pre-industrial 1750 anthropogenic flux (0.003 mg m^{-2} yr^{-1}) was a factor of 50 lower than the fluxes spanning from 1983 - 1991 (~2 mg m^{-2} yr^{-1}). Kuwae *et al.* (2013) observed similar results in sediment cores from Japanese alpine lakes, where a notable increase in Sb enrichment was observed from 1930 onwards, increasing by a factor of 4.5.

2.2.5.3 Atmospheric Sb emissions from Scotland and the United Kingdom

Although no sediment core inventories for Sb deposition in Scotland have been published, a few recent published studies using ombrotrophic peat bogs in Scotland have. Cores from four ombrotrophic peat bogs across Scotland were collected by Cloy *et al*. (2009), enabling Sb deposition from the late 19th to 21st century to be studied. In general, Sb peat concentrations were low; however a 60 fold increase in concentrations were observed across all sites during the industrial period, where Sb fluxes ranged from 0.27 – 1.33 mg m^{-2} yr^{-1}. Thereafter (approximately 1970-1980), Sb deposition rates decreased to levels similar to the pre-industrial period. This was in agreement with Mackenzie *et al*. (1998a), where a peat core from west-central Scotland displayed similar Sb enrichment factors in the mid-20th century with a contemporary decline. Whilst both studies by Cloy *et al*. (2009) and Mackenzie *et al*. (1998a) showed similar results to research undertaken elsewhere (Shotyk *et al*., 1996; Allan *et al*., 2013), it is worth noting that contemporary decline in Sb deposition rates was not observed in Japan, where a marked increase was seen in the 1980s, correlating with the increase coal production and burning from China (Kuwae *et al*., 2013). For Scotland however, current Sb emissions from anthropogenic activity is low; industrial processes produced only 75 kg of Sb in 2012 (SEPA, SPRI, 2015) (including coal combustion plants), whilst 95% of municipal waste was landfilled for the year 2010-2011,

indicating little emissions from waste incineration. This places a greater importance on limiting vehicle emissions of Sb, as it remains the dominant source of Sb to the Scottish environment.

2.3 Lead

2.3.1 Elemental properties and occurrence

Lead (Pb) is a group 14 metal with atomic number 82 and an atomic weight of 207.2. It can exist in three oxidative states (0, +II and +IV), and is generally found in environmental systems as Pb (+II). Lead (+IV) is only present in extremely oxidising conditions and whilst Pb (0) can exist in nature, its occurrence is rare (Abadin *et al*., 2007). There are four stable isotopes of Pb; ^{208}Pb, ^{206}Pb, ^{207}Pb and ^{204}Pb, each of which are discussed in detail in the next section. Metallic Pb is a dull silvery colour; it has a high density (11.3 g cm^{-3}), is malleable and has a relatively low melting point (327^{o}C). It is a moderately good conductor of electricity and heat, and it is often added to make alloys, particularly for electrical items such as batteries and circuitry. Although crustal abundance of Pb varies globally, it is estimated to be in the range 10-16 mg kg^{-1} (Wedepohl, 1968; Nriagu, 1978).

2.3.2 Lead isotopes

2.3.2.1 Naturally occurring stable isotopes

The four stable isotopes ^{208}Pb, ^{206}Pb, ^{207}Pb and ^{204}Pb have natural abundances of 52%, 24%, 23% and 1%, respectively. Only ^{204}Pb is primordial whilst ^{206}Pb, ^{207}Pb, ^{208}Pb are radiogenic, and products of the radioactive decay of ^{238}U, ^{235}U and ^{232}Th, respectively (Figure 2.4) (Komarek *et al*., 2008). The abundance of each parent nuclei and its unique half-life (^{238}U:4.466 x 10^{9} y, ^{235}U:0.704 x 10^{9} y and ^{232}Th:14.01 x 10^{9} y), results in discrete differences in Pb geochemical signatures, enabling the origin of Pb to be apportioned. For example, the short half-life of ^{235}U has resulted in the environmental abundance of ^{207}Pb remaining relatively stable over time, as most of the radioactive decay has already taken place. This is not the case for ^{208}Pb and ^{206}Pb, where the longer half-lives of ^{232}Th and ^{238}U gives a greater degree of variation in environmental abundance. As a result, the varying abundance of ^{208}Pb

and ^{206}Pb isotopes relative to ^{207}Pb, can provide an isotopic ratio that is indicative of geological bodies. In general, the Pb isotopic ratio can effectively determine the age of the Pb ore deposit; older deposits were formed before the influence of U and Th decay giving, for an example, a typical ^{206}Pb/^{207}Pb ratio of ≤1.10. Whereas, younger Pb ore radiogenic deposits often have ^{206}Pb/^{207}Pb isotopic signature of ≥1.18 (Bacon, 2002).

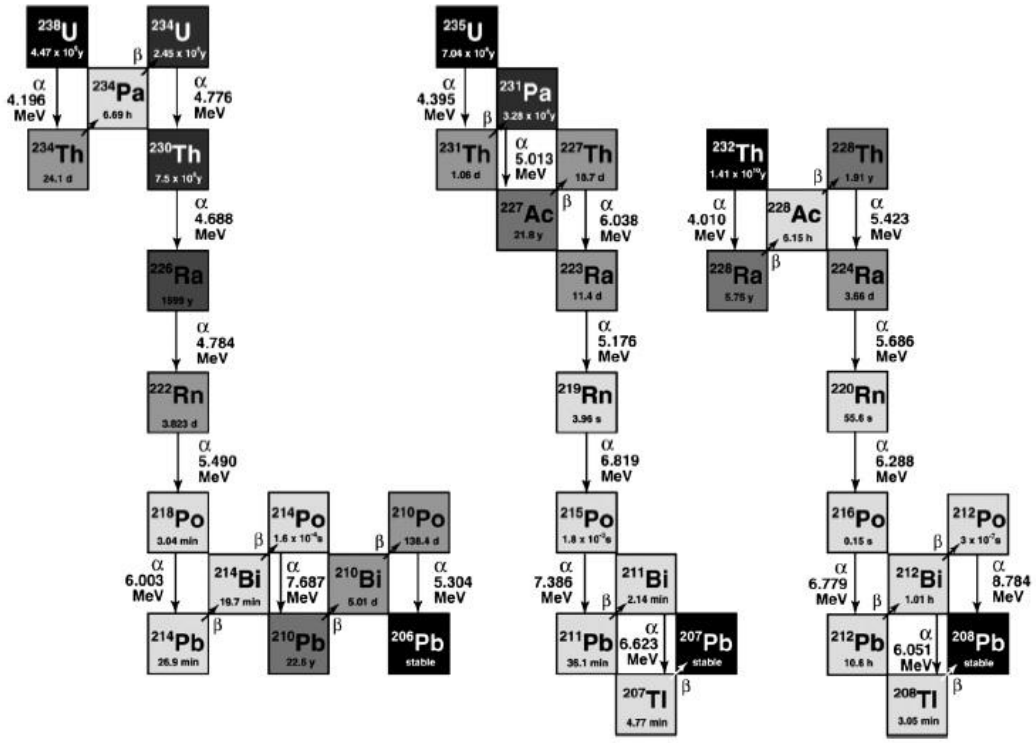

Figure 2.4: Decay chains of the naturally occurring radionuclide's ^{238}U, ^{235}U and ^{232}Th with, as respective final products, the stable isotopes ^{206}Pb, ^{207}Pb and ^{208}Pb (Vanhaecke *et al*., 2009).

2.3.2.2 Radioactive Pb isotopes

Of the ~30 radioactive isotopes, the most important is ^{210}Pb ($t_{½}$ =22.3 y), because it can be used to derive chronologies for peat, sediment and ice systems. It is a member of the ^{238}U radioactive decay series (Figure 2.4); decayed ^{226}Ra ($t_{½}$ =3.831 d) releases ^{222}Rn into the atmosphere at a constant rate, where it decays, via a number of subsidiaries, to ^{210}Pb, and is subsequently deposited onto surface soils directly, or indirectly through the water column. The ^{210}Pb deposited is defined as unsupported which means that the nuclide is immobile and

undisturbed upon deposition onto soil or peat. Over time, the accumulation and burial of ^{210}Pb allows a vertical distribution in soil systems, where ^{210}Pb decreases exponentially with depth (MacKenzie *et al*., 2011). The application of unsupported ^{210}Pb dating may not always be appropriate. For example, areas that have naturally high occurring concentration of U and Th can cause elevated background interference affecting the dating accuracy (Farmer *et al.*, 2015). In addition, other local factors such as elevated concentrations of ^{222}Rn and mineral weathering may also affect ^{210}Pb dating (Shirahata *et al*., 1980; Card and Bell., 1985; Erel *et al*., 1994). In such instances, supported ^{210}Pb dating should be used to take into account of background interferences. Using the ^{238}U series, the radioactive decay from ^{226}Ra to ^{210}Pb is determined (as opposed to ^{222}Rn) since these radionuclide's are at secular equilibrium, with final activity subtracted from the total ^{210}Pb.

2.3.3 Lead in the environment

2.3.3.1 Mineral forms, weathering processes and solution chemistry

Similar to Sb, metallic Pb is found in sulfidic ores, and is associated with pyrites present in coal (and at trace levels in petroleum). During the formation of coal, mineral matter is often mixed with the initial coal forming material (organic matter), resulting in their presence in coal. Although Pb concentrations in coal, and indeed other elements, is often regionally dependent, the average Pb content for Scottish coal is 23.9 mg kg^{-1} (Farmer *et al*., 1999).

Lead is often found in ores along with Zn, Cu, Au and Ag, with the most abundant Pb ore galena (PbS) bound to sulfur through simple Pb (II) Lewis acid-base electron sharing. The chemical weathering / oxidation of primary ores such as galena (Equation 2.3) to secondary ores, can result in the formation of cerussite ($PbCO_3$) (Equation 2.4) and anglesite ($PbSO_4$) (Pirajno *et al*., 2010). These are the most abundant ores observed from chemical weathering, but others include platterite (PbO_2), pyromorphite ($Pb_5(PO_4)_3Cl$) and plumbogummite ($PbAl_3(PO_4)_2(OH)_5H_2O$. The dissolution and subsequent mobility of Pb from mineral surfaces by chemical weathering is influenced by pH, as under oxidising conditions Pb is soluble, and at a higher pH, Pb precipitates to form Pb-bearing carbonates or oxides (Figure

2.5) (Drever, 1997; Ettler and John, 2014). In aqueous systems, Pb is usually found as Pb(II), as Pb(0) is insoluble, and Pb(IV) is predominantly fixed in inorganic complexes (Manceau *et al.*, 1996). Time is also an influential factor in the dissolution process as demonstrated by Ettler and John (2014), where a long-term leachate study on Pb mining slag showed a greater rate of Pb leachate was observed over a one year period, when compared to 1 and 7 day durations.

$PbS_{(S)} + 2H^{+} \leftrightarrow Pb^{2+} + H_2S_{(aq)}$ **Equation 2.3**

$Pb^{2+}{}_{(S)} + H_2CO_3 \leftrightarrow PbCO_3 + 2H^{+}$ **Equation 2.4**

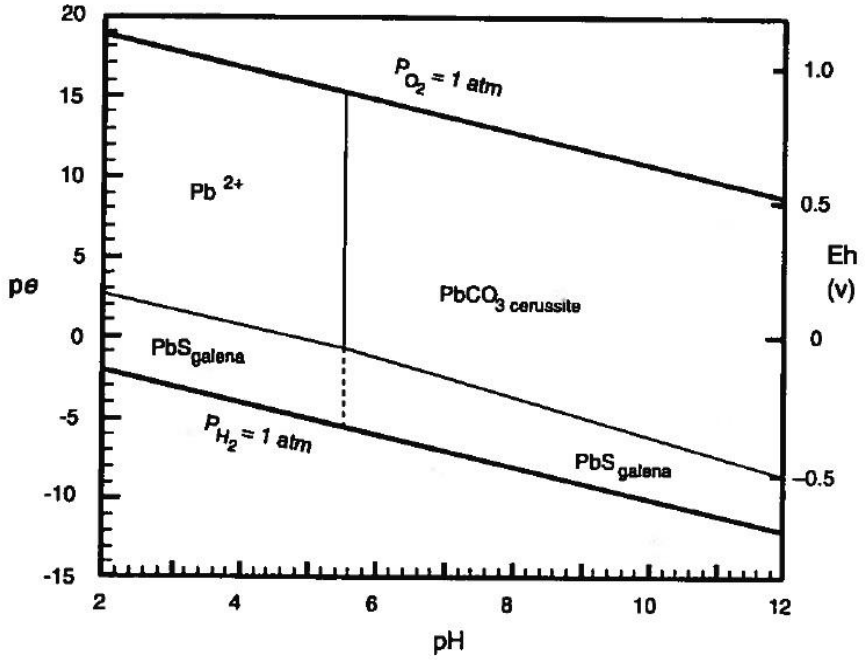

Figure 2.5: Pe-pH diagram for a Pb-CO_3-S-O-H_2O system (25°C at 1 atm). Solubility is defined as a dissolved Pb concentration of 10^{-6} mol L^{-1} and a dissolved S concentration of 10^{-3} mol L^{-1} (Drever, 1997).

As discussed and under specific conditions, Pb can be mobile in mineral aqueous systems. This however, is generally not the case, as the acidic pH required is not typically observed in environmental systems. In addition, at pH >6, Pb has a strong tendency to form phosphates and carbonates, indeed, these are often labelled as Pb controlling phases (Ettler and John, 2014) rendering it largely immobile.

2.3.3.2 The behaviour of Pb in the soil environment

Lead is renowned for being largely immobile in soil systems (McLean and Bledsoe 1992; Drever, 1997; Farmer *et al*., 1997; MacKenzie *et al.*, 1998b; Shotyk *et al*., 2002) and it has been found in association with hydrous Fe, Mn and Al oxides, clays, phosphates, sulfates, carbonates and organic matter (McLean and Bledsoe 1992; Drever, 1997). Indeed, McLean and Bledsoe (1992), compared the relative affinity of transition metals to Pb (Table 2.3) in a variety of environmental media and showed that Pb sorption was generally strongest.

Table 2.3: Relative affinity of metals for soils and soil constituents (McLean and Bledsoe 1992).

Soil or soil constituent	Relative order of sorption	Reference
Goethite	Cu>Pb>Zn>Co>Cd	Forbes *et al*. (1976)
Hydrous Fe oxide	Pb>Cu>Zn>Cd	Benjamin and Leckie (1981)
Soils	Pb>Cu>Zn>Cd>Ni	Biddappa *et al*. (1981)
Organic soils	Pb>Cu>Cd>Zn	Elliott *et al*. (1986)

Lead retention is controlled by its adsorption onto hydrous metal oxides such as Fe, Mn and Al in slightly acidic soils (~pH 4-6), and by clays in neutral soils (McLean and Bledsoe 1992; MacKenzie *et al.*, 1998b; Scheetz and Rimstidt, 2008). The mobility of Pb(II) is influenced by the permanent positive charge present on hydrous metal oxides, the high surface area of hydrous oxides (typically surface area in the order of 200 m^2 g), and at lower pHs, where a greater adsorption occurs (McLean and Bledsoe 1992; Drever, 1997). Binding is thought to occur via surface oxygen functional groups through bidentate outer-sphere or inner-sphere mechanisms for hydrous Fe and Mn oxides, and for clays (Figure 2.6). For outer sphere complexes, Pb is hydrated by water molecules, where it accumulates at surface binding sites causing binding to occur via electrostatic forces between the adsorption surface

and water; these are generally weakly bound. The binding strength of inner sphere complexation is far greater than outer, as no water is involved, and bonding with adsorption surface is directly with Pb by ionic or covalent character (McLean and Bledsoe, 1992).

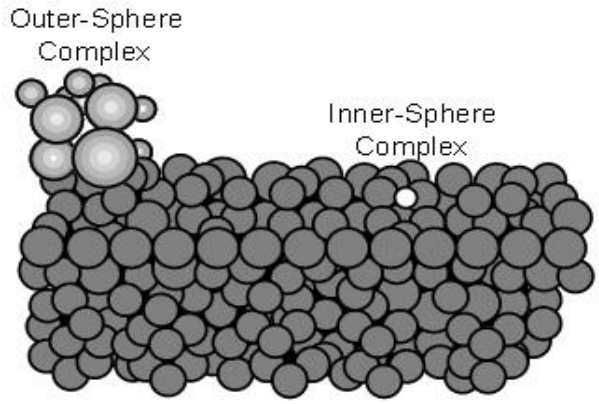

Figure 2.6: Two mechanisms for Pb adsorption onto a clay surface. Adapted from McLean and Bledsoe, (1992).

Although Pb is chalcophilic, the adsorption of Pb by S present in organic matter binding sites does not readily occur under environmental conditions. Chemical weathering of S significantly reduces its abundance in organic matter, while any remaining sulfur present is generally inaccessible to bind with. As a result, the adsorption of Pb by organic matter, or more specifically, HS is thought to occur through ionic or electrostatic interactions with anionic functional groups, primarily carboxylic and phenolic groups (Tipping, 2002). Although definitive agreement for the type of ligand bonding mechanism has not been reached, most studies have shown bidentate interactions with carboxylic and phenolic groups (Xia *et al*., 1997; Orsetti *et al*., 2013) (Figure 2.7), whilst other studies have observed mono-dentate interactions (Gondar *et al*., 2005).

Whilst Pb is largely immobile in soil systems, under certain conditions, a small proportion of Pb can become mobile in slightly acidic soils, where available hydrous Fe or Mn oxides or carbonate binding sites are low. A good example of this is observed in Pb contaminated soils from mining and shooting range sites, where the application of limestone to land was used to increase the soil pH and provide additional binding sites for Pb (Scheetz and Rimstidt, 2008;

Munksgaard and Lottermoser, 2012). In addition, the composition of organic matter present is also important, as the amount of fulvic and humic acids found in soil can influence Pb mobility. Fulvic acids are believed to form more soluble metal complexes, whilst humic acids generally form insoluble metal complexes (Gondar *et al*., 2005). Although other functional groups (amino groups) are present in organic matter and can form Pb sorption sites, most research addresses the interaction with C and O present in humic and fulvic acids due to their relative abundance in soil systems (McLean and Bledsoe, 1992).

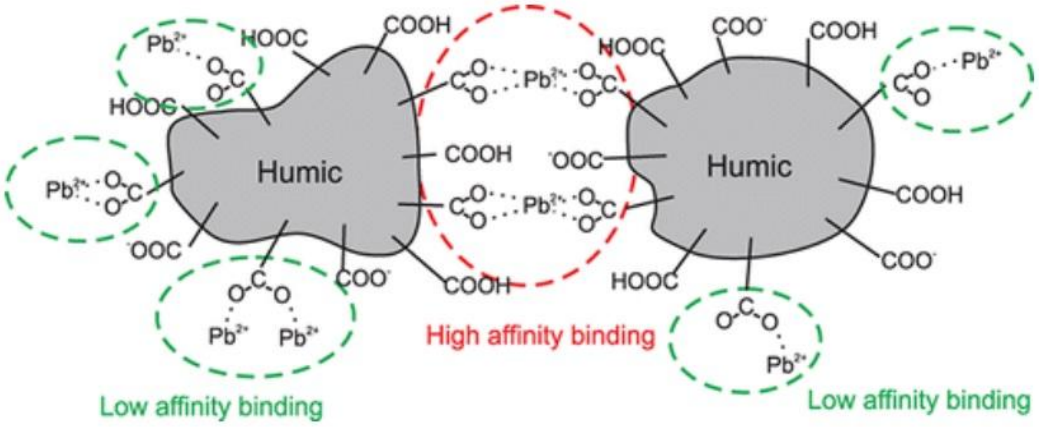

Figure 2.7: Schematic of postulated Pb adsorption by humic acids present in soil (Orsetti *et al*., 2013).

2.3.4 Toxicity and human health exposure

Lead is a nonessential element for plant and animal growth (Komarek *et al*., 2008). It is toxic and has cumulative properties that can affect a number of biological processes such as haemoglobin production, peripheral and central nervous systems, kidneys, blood pressure and can eventually cause death (Cheng and Hu, 2010). The human body cannot distinguish between Pb and Ca and as a result, the uptake of Pb results in its accumulation into bones and hair (Rabinowitz *et al*., 1991). Under physiological stress, Pb can be re-mobilised into the blood stream from bones, exacerbating the above causing health effects (Gulson, 2008).

The human uptake of Pb is primarily through the consumption of contaminated food and water, and the inhalation of contaminated air (Cheng and Hu, 2010). The potential for human bioaccumulation is dependent on the exposure route to the body. For example, Pb is

absorbed more effectively by the human body when in water, rather than food, and water can account for 20% of the daily intake (Baird, 1998). Although the assimilation of Pb into the body is greater from drinking fluid, the consumption of food can still represent a major exposure route. A number of studies of have shown elevated Pb content in rice, where Pb is readily accumulated by the plant and rice grain harvested (Lui *et al*., 2003;Yang *et al*, 2003; Ok *et al*., 2011). Yang *et al*. (2003) completed a study examining Pb uptake of rice near a Pb/Zn mine in Guangdong, China, where mean Pb concentrations in rice roots and rice grain were 419 mg kg^{-1} and 4.67 mg kg^{-1}, respectively. Based on the average daily intake of rice for the Guangdong population, the study concluded that local adults and children were consuming 5.9 and 2.7 times more than the assigned tolerable daily intake for Pb (429 μg kg^{-1} d^{-1}) (WHO 1978; Ali *et al* 2014).

Although the inhalation of atmospheric Pb is a current concern in continents such as Asia, this is less a concern in Europe, where European environmental regulation has resulted in a decline in Pb emissions, particularly since the ban of vehicular leaded petrol. Delves and Campbell, (1993) reported that leaded petrol contributed 30-40% of total Pb uptake for residents of inner London, whilst Tera *et al*. (1985) suggested it could account for up to 57% of Pb found in blood from residents of Washington. Blood Pb concentration is especially important for the neurological development of children, and numerous research studies have reported that a decline in IQ was associated with elevated blood Pb concentrations (Needleman *et al*., 1979; Winneke *et al*., 1983, 1988; Davis and Svendgard, 1987; Fulton *et al*., 1987; Hatzakis *et al*., 1989). Bierkens *et al*. (2011) reported a significant correlation in ambient air and blood Pb concentrations across Europe between 1978 and 2007. Over this 29 year period, a decline in ambient Pb concentrations from 0.31 μg m^3 to 0.045 μg m^3 was observed and there was a corresponding 48 and 57% decrease in blood Pb concentrations in adult women and men (+ 18 y), respectively. Whilst the mean daily intake of Pb for residents in Europe have declined significantly to a mean of 35.7 μg d since the ban of vehicular

leaded petrol (Bierkens *et al*., 2011), countries such as China and India have not experienced a similar drop in blood Pb concentrations. A review by Chang *et al*. (2010) observed only a slight drop in ambient air Pb concentrations in China since 2000, and although Gupta *et al*. (2010) reported a drop of ~10 ng m^{-3} y^{-1} in India from 1998 to 2008, ambient air concentrations were still in excess of the EU air quality guideline limit of 500 ng m^{-3} (EEA, 2013).

The analysis of blood has proven to be a useful tool for assessing current exposure to Pb, but the analysis of teeth and bone is also an effective means of looking at Pb exposure. The accumulative properties of Pb in the human body, enables the impact of anthropogenic activity to be monitored over time. A study by Farmer *et al*. (2006) compared human teeth (crown and root) originating from the 19th and 20th century, and showed Pb concentrations from 1990 had reduced by at least an order of magnitude, when compared to those from the 19th century and early 20th century. Keinonen, (1992) demonstrated the use of bone, as well as other environmental media such as soil and lake sediment to identify the impact to residents from local incinerators and Pb smelters in Helsinki, Finland. The high concentration of Pb accumulated in bone specifically in Helsinki residents, and the particular Pb isotopic ratio identified this process (discussed later) as the point source.

2.3.5 Environmental quality standards

The use of Pb is heavily restricted within the EU and North America due to its toxicity and human health effects. Within the EU, Pb falls under both the Restriction of Hazardous Substances (RoHS) Directive (E.C., 2008) and the WFD as a list I priority hazardous substance (E.C., 2000). As a result, the European freshwater environmental quality standard is 1.3 μg L^{-1} (EC, 2013), with a higher drinking water limit of 10 μg L^{-1} implemented by the WHO (WHO, 2011). For soil, DEFRA and Environment Agency have assigned a Pb SGV of 450 mg kg^{-1} and 750 mg kg^{-1} for residential and commercial soil, respectively (DEFRA, 2002).

2.3.6 Lead production, use and emissions

2.3.6.1 Historic and current Pb demand and use

Due to its malleability, Pb has a long history of use by humans dating back to pre-Roman times. In ancient Greece, it was used for coinage and drinking vessels, whereas the Romans added sweet lead salts to overly acidic wine to improve the flavour (Baird, 1998). The utilisation of Pb for items such as water pipes and cooking vessels meant that ore smelting activities increased significantly during the Roman times. Indeed, it was estimated that ~80 000 tonnes of Pb were produced per year over a 400 year period during the Roman Empire (Hong *et al*., 1994). Following its collapse however, there was a sharp decline in Pb production, with pre-collapse levels only exceeded by the industrial period observed in the UK and Western Europe in the mid-19th to 20th century (Cloy *et al*., 2009). Although Pb was used extensively for mechanical engineering and infrastructure during the industrial period, the large scale use of leaded petrol became the most dominant use of lead from its introduction in 1920, until the end of the 20th century (Kropschot and Doebirch, 2011). Despite the known health effects from Pb exposure and the subsequent strict regulation in use and emissions, current Pb production is increasing, with a rise of ~20% from 1984-2003, and a forecast rise from 6.8 in 2003, to 10 million tonnes a year by 2050 (Backman, 2008). Current use of Pb is dominated by its application in lead-acid batteries for the automotive industry and emergency power supplies for utilities. Although this can make up to 85% of Pb consumption, it is still frequently used for roof flashings, cladding for buildings and with Zn, for electroplating and soldering circuit boards.

2.3.6.2 Global atmospheric Pb emissions

As Pb and Sb co-exist, the resultant emissions from smelting and the combustion of coal, and subsequent deposition show similar temporal trends. Deposition chronologies for Pb however, are more distinctive than Sb, since it is present at greater concentrations in sulfidic minerals and coal than observed for Sb. For example, Sb concentrations in coal generally

range from 1-3 mg kg^{-1}, which is considerable less than the range of 10-1900 mg kg^{-1} for Pb (Kabata-Pendias and Szteke, 2015). The difference in atmospheric Sb and Pb concentrations can also be observed in dated flux profiles from peat and sediment cores, where past atmospheric Pb emissions from the industrial revolution and the decline towards the 21st century are generally a factor of 50-100 more than Sb. A good example of this is observed in the previously mentioned study by Cloy *et al*. (2009) (section 2.2.5.3), where the dates of peak Pb and Sb fluxes coincide, and originate from anthropogenic emissions during industrial periods in Scotland (Figure 2.8).

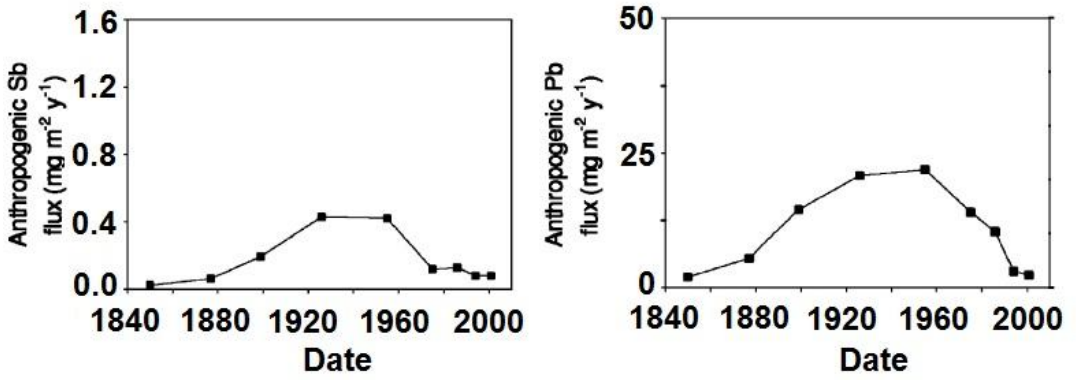

Figure 2.8: Calculated atmospheric depositional fluxes (mg m^{-2} y^{-1}) of anthropogenic Sb and Pb for Flanders Moss peat bog. Adapted from Cloy *et al*. (2009).

Elevated atmospheric concentrations of Pb in the 20th century were primarily from industry emissions, whilst 21st century was greatly influenced by leaded petrol emissions. The addition of tetraethyl-Pb to petrol as an anti-knocking agent increased vehicle performance and economy by raising the engine combustion temperature. At the time, these mechanical properties were internationally welcomed, with leaded petrol emissions only declining in the UK as a result of it being phased out from 1986, with its eventual ban in Europe in 2000. For Europe, leaded petrol contributed a significant proportion towards total atmospheric Pb concentrations (Figure 2.9), where the phase out and subsequent ban on leaded petrol use, along with improved regulation of Pb emitting industries, significantly reduced European

atmospheric Pb concentrations. At its peak in ~1975, European Pb emissions were estimated to be 160 000 t y^{-1}, with a decline by ~70% to 10 000 t y^{-1} in 2005 (Figure 2.9).

Whilst a major positive step in reducing Pb emissions has occurred, improvements in current Pb emissions are still required, and although the name suggests otherwise, unleaded petrol still contains Pb, albeit at a lower concentration of ~0.013 g L^{-1} (CONCAWE, 1992; Oudijk, 2010). Aviation gas (avgas) is often an overlooked source of Pb to the environment, and contains approximately 2.12g of Pb per gallon (ASTM International, 2005) and is regarded as the biggest single source of atmospheric Pb in the United States (Carr *et al.*, 2011). In addition, the over reliance of Pb batteries for electrical applications (Backman, 2008) and the emergence of Pb recycling plants across Europe also contribute to Pb emissions globally. Pacyna and Pacyna, (2001) created an inventory of global Pb emissions from 1995 data, and whilst the data was not compiled on recent figures, Asia still contributed the most to global Pb emissions (44293 t), followed by Europe (19507 t) and North America (15780 t).

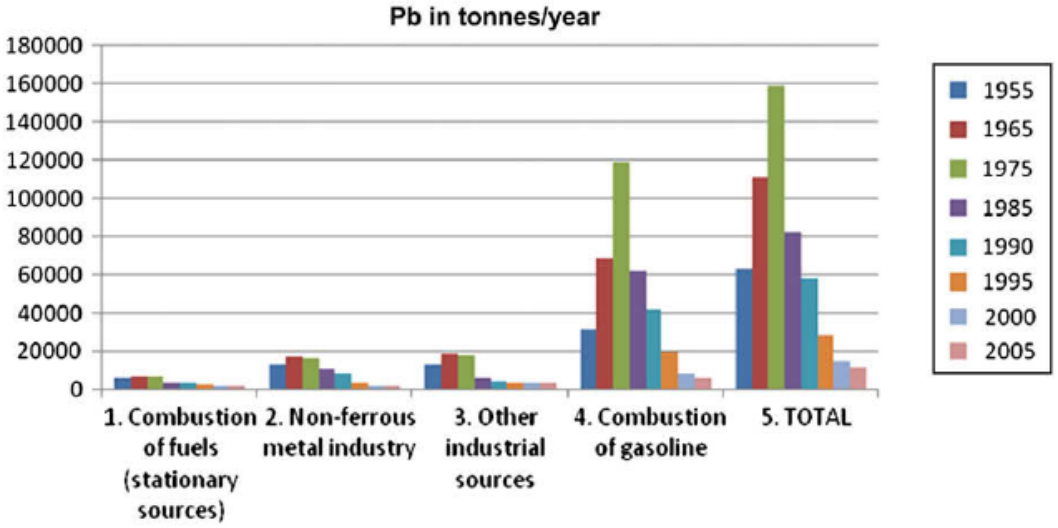

Figure 2.9: Change of atmospheric emissions of Pb in Europe in the period from 1955 – 2005 (Pacyna *et al.*, 2009).

Looking more specifically at UK Pb emissions, a significant reduction has occurred from 1986 to 2011, where total Pb emissions have dropped from ~8200 t yr^{-1} to just under 60 t yr^{-1} (Figure 2.10) (Dore *et al.*, 2014). The contribution of each Pb emission source over the same

duration has also changed. The previously dominant contribution towards total Pb emissions from leaded petrol (road transport) significantly reduced during the phasing out period (1986), and subsequent ban in use in 2000. In addition, improved technology used for stationary combustion such as particulate recovery systems, and the elimination of major mining and ore refineries in the UK also accounted for the significant reduction for UK Pb emissions.

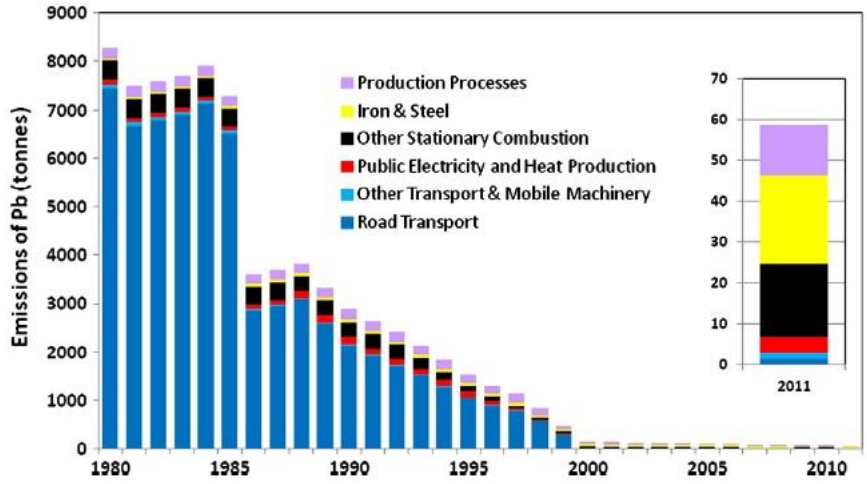

Figure 2.10: Trend in Pb emissions from the UK (Dore *et al*., 2014).

2.3.7 Applications of Pb isotopic ratios

The application of Pb isotope ratios to apportion its source in the environment has been applied in many previous studies (MacKenzie *et al*., 1998b; Shotyk *et al*., 2002; Farmer *et al*., 2005, 2006, 2010; Cloy *et al*., 2008; Robbins *et al*., 2010; MacKinnon *et al*., 2011). The identification of geological bodies is commonly expressed as isotopic ratios; $^{206}Pb/^{207}Pb$, $^{208}Pb/^{207}Pb$ and $^{206}Pb/^{204}Pb$, with particular importance to the $^{206}Pb/^{207}Pb$ ratio (section 2.3.2.1). The $^{206}Pb/^{207}Pb$ isotope ratio is regionally dependent and can vary within a country. A good example of this can be found in Scotland, where the $^{206}Pb/^{207}Pb$ isotopic ratio of Pb ore from Wanlockhead is 1.170 ± 0.003, distinctively different from the 1.144 ± 0.004 ratio observed at Tyndrum Pb ore (Moorbath, 1962; Farmer *et al*., 1999; MacKenzie and Pulford, 2002).

Table 2.4: Examples of $^{206}Pb/^{207}Pb$ isotopic ratios in leaded petrol, coal and Pb ore from various locations.

Sample	Location	$^{206}Pb/^{207}Pb$		References
		Range	Mean SD	
Leaded petrol	UK	1.059 - 1.079	1.067 ± 0.007	Monna *et al*. (1997)
Leaded petrol	France	1.060 - 1.100	1.083 ± 0.015	Monna *et al*. (1997)
Coal	Scotland	1.159 - 1.213	1.181 ± 0.011	Farmer *et al*. (1999)
Coal	Poland	-	1.177 ± 0.026	Farmer *et al*. (1999)
Scottish Pb Ore	Tyndrum	-	1.144	Moorbath (1962)
Scottish Pb Ore	Wanlockhead	1.170 – 1.178	1.170 ± 0.003	Farmer *et al*. (1999)
Australian Ore	Broken Hill	-	1.040	Cooper (1969)

The apportionment of Pb was particularly useful for assessing the global impact of leaded petrol emissions to the environment. Using this as an example, the leaded petrol $^{206}Pb/^{207}Pb$ isotopic ratios were distinctly different from indigenous $^{206}Pb/^{207}Pb$ isotopic ratios for Scotland. The Pb additive used for UK leaded petrol comprised mainly of Australian Pb ore (Broken Hill), and had an extremely low $^{206}Pb/^{207}Pb$ isotopic ratio (1.04). The addition of Australian Pb ore to leaded petrol, along with the lesser presence of naturally occurring Pb from petroleum, resulted in a leaded petrol $^{206}Pb/^{207}Pb$ isotopic ratio of ~ 1.06-1.09 (Table 2.4) (Monna *et al*., 1997). The low $^{206}Pb/^{207}Pb$ isotopic ratio of leaded petrol was easily distinguishable from $^{206}Pb/^{207}Pb$ ratios originating from industrial Pb emissions in Scotland during the 20th century. For this period of time, Pb emissions were largely from coal combustion and the smelting of Wanlockhead Pb ore, where $^{206}Pb/^{207}Pb$ isotopic ratios were 1.181 and 1.170, respectively (Moorbath, 1962; Farmer *et al*., 1999). The contrast in $^{206}Pb/^{207}Pb$ isotopic ratios observed in leaded petrol, when compared to those originating from coal combustion and the smelting of Wanlockhead Pb ore, allowed the contribution of

leaded petrol to total Pb atmospheric concentrations to be established. A study by Farmer *et al.* (2005) demonstrated this very point, where the atmospheric deposition of Pb and its $^{206}Pb/^{207}Pb$ isotopic ratios were determined for a soil core from Glensaugh, Scotland (Figure 2.11). The vertical concentration profile of Pb peaked in 1961, which corresponded with a significant decline in $^{206}Pb/^{207}Pb$ isotopic ratios thereafter, as a result of Pb originating from leaded petrol emissions.

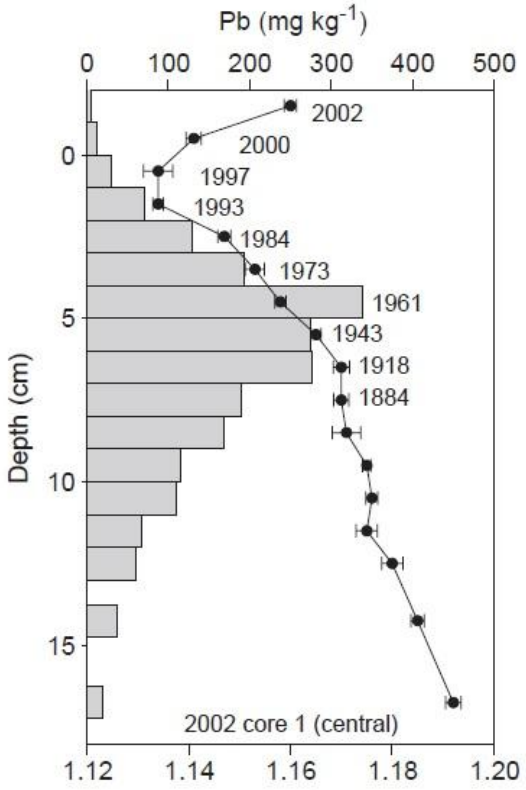

Figure 2.11: Profiles of Pb concentration (bars) and $^{206}Pb/^{207}Pb$ ratio (●) versus section depth, with the ^{210}Pb-derived date added for themed-point of each section (Farmer *et al*., 2005).

The apportionment of Pb emissions from coal combustion using $^{206}Pb/^{207}Pb$ isotopic ratios is notably different than leaded petrol, with isotopic ratios from coal combustion in Europe ranging between 1.16-1.21, depending on the local geology (Table 2.4) (Farmer *et al*., 1999). Coal combustion was a primary source of Pb emissions to the environment prior to leaded petrol, and has been confirmed by studies using $^{206}Pb/^{207}Pb$ isotopic ratio analysis (Vile *et*

al., 2000; Novak *et al*., 2003; Komarek *et al*., 2008). Over the last decade however, the application of $^{206}Pb/^{207}Pb$ isotopic ratios to apportion atmospheric Pb emissions resulting from coal have been largely unsuccessful, as $^{206}Pb/^{207}Pb$ isotopic ratios for coal and metal smelting across Europe are similar, and Pb apportionment requires a significant difference in isotopic ratios (Table 2.4) (Komarek *et al*., 2008).

2.4 Arsenic

2.4.1 Elemental properties and occurrence

Arsenic (As), like Sb, is a group 15 metalloid and can exist in four oxidative states (-III, 0, +III and +V); it is, however, commonly found in environmental systems in the +III and +V oxidation states. It has an atomic number of 33, an atomic weight of 74.9 and is monoisotopic. In its metalloid state, it is bright, silvery grey and brittle, but as it is usually found in minerals, its appearance can vary. Its crustal abundance can range from 0.01 to over 600 mg kg^{-1} with a mean abundance of ~ 2 mg kg^{-1} (Matschullat, 2000; Hughes *et al*., 2011).

2.4.2 Arsenic in the environment and its similarities to Sb

Since As and Sb share the same s^2 p^3 electron arrangement, they share a number of properties in environmental systems and affinity towards particular elements (Wilson *et al*., 2010). Indeed, the commonality of As and Sb has been crucial in establishing a starting point for assessing the geochemical behaviour of Sb. Both elements frequently co-exist in the environment in ores, primarily as sulfides and sulfosalts, as well as oxides, such as richelsdorfite ($Ca_2Cu_5Sb(AsO_4)_4(OH)_6Cl \cdot 6H_2O$) (31% As / 12% Sb) and sernarmonitie (7% As / 20-30% Sb) (Pauwels *et al*., 2010; Wilson *et al*., 2010). Arsenopyrite ($FeAsS_2$) is the most common ore of arsenic, with other ores being niccolite (NiAs) and cobalite (CoAsS) (Allard, 1995; Reimann and Caritat, 1998; Matchullat *et al*., 2000). Commercially, As-bearing ores following the M(II)AsS structure, where M(II) represents Fe, Ni and Co, are viewed as the most important ores (Matschullat *et al*., 2000). Arsenic can undergo dissolution from mineral ores at a greater rate than observed for Sb. Indeed, this is in part

responsible for the contamination of groundwater discussed further in the next section. For example, Casiot *et al*. (2007) examined surface water concentrations of As and Sb near an abandoned Sb mine in France, where As concentrations were ~2.5 times greater than those of Sb.

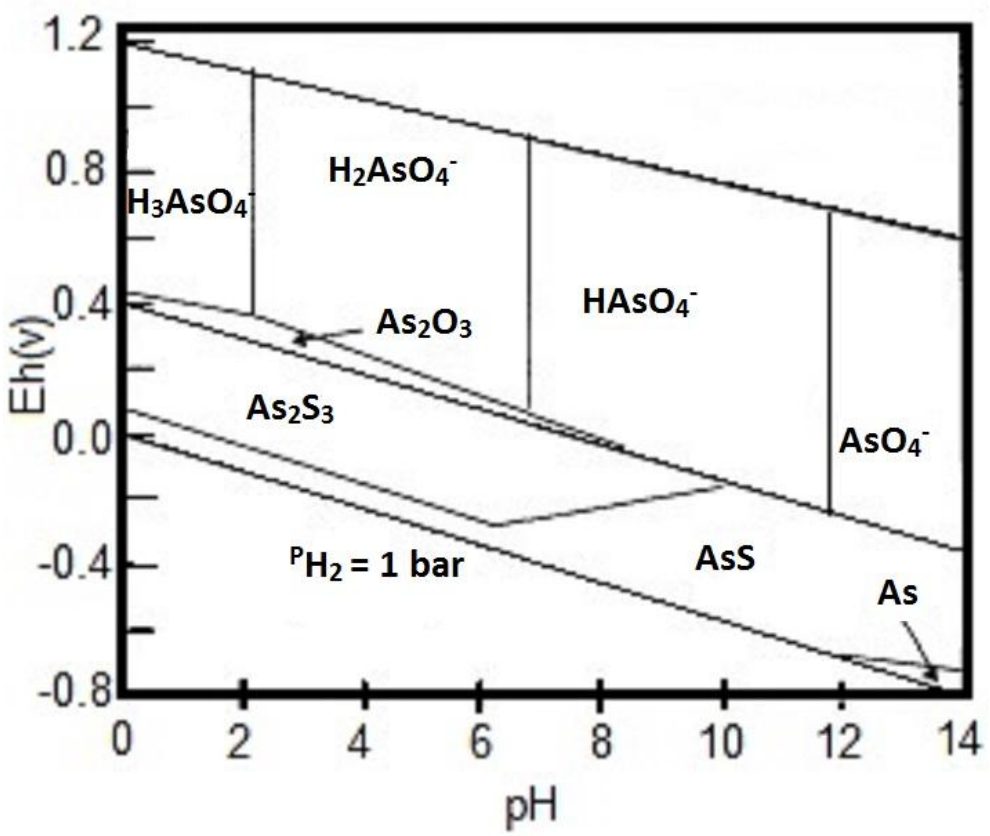

Figure 2.12: E_h-pH diagram for an As-S-H_2O system (25°C at 1 atm). Solubility is defined as a dissolved As concentration of 10^{-6} mol L^{-1} and a dissolved S concentration of 10^{-3} mol L^{-1}. Adapted from Bradl, (2005).

In the aqueous phase, As occurs as an anion ($H_2AsO_4^-$), or a neutral species ($H_3AsO_3^0$) rather than a cation (Figure 2.12)(Drever, 1997). The negative charge present in the As(V) state results in reduced mobility in the environment when compared with the neutral As(III) state. Under aerobic conditions, As(V) is the dominant oxidation state whilst As(III) is present under reducing conditions. Due to the large surface areas, high adsorption capacities and abundance of hydrous iron oxides in soil, arsenate species ($H_2AsO_4^-$) can readily bind with hydrous iron oxides to form monodentate and bidentate inner-sphere complexes at near-neutral pH (Figure 2.13) with adsorption decreasing with increasing pH (Drever, 1997;

Mitsunobu *et al*., 2006; Wang and Mulligan, 2008). In typical environmental conditions, As(III) however, is unable to form inner-sphere surface complexes at oxide surfaces due to its neutral charge, and is thus not adsorbed at any pH (Drever, 1997).

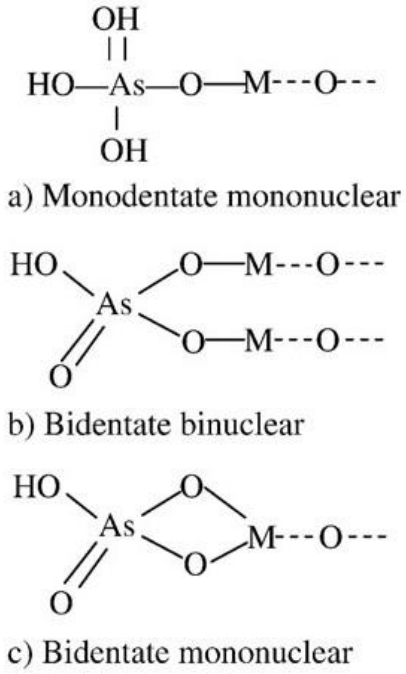

Figure 2.13: Schematic configuration of As (V) inner-sphere surface complexes (M=Al, Fe). Adapted from Wang and Mulligan (2008).

The precise binding structure of inorganic As species to organic matter is still under investigation, partly due to the negatively charged properties of humic acids in water. Research so far, have shown that the negatively charged As(V) anion can bind to carboxylic, phenolic and amine functional groups in humic acids to form a negatively charged complex stabilised by donor characteristics, with chelation by other functional groups, and H-bridges (Buschmann *et al*., 2006; Fakour and Lin, 2014). This is in agreement with a number of other studies demonstrating the potential complexation of As with organic matter (Anawar *et al.*, 2003; McArthur *et al*., 2004; Chen *et al*., 2008), with the charge present in As(V) allowing for stronger complexation than As(III). In addition, it has also been postulated that the presence of other metals in soil can also contribute to As-humic binding via ternary complexation, i.e. the binding of three different molecules (Tongesayi *et al*., 2007). For both

instances, and similarly to hydrous iron oxides, As(III) will have greater mobility in the environment due to the net zero charge whereas As(V) will be largely immobile.

2.4.3 Toxicity and regulation

Although some evidence has suggested the intake of As plays an essential physiological role for human health at very low doses (RSC, 2015), it is considered toxic and fatal if ingested at mg concentrations (Hughes *et al*., 2011). Its toxicity is very dependent on its oxidation state and its chemical form. For example, greater toxicity has been observed where As is in the +III rather than the +V state, and this is observed in some of the organic chemical forms as well (Smith *et al*., 1999; Abedin *et al*., 2002a, 2002b; Dobran *et al*., 2006). Methylated As forms such as monomethylarsonic acid (MMA) and dimethylarsinic acid (DMA) can occur as minor components of As in soil (Huang and Matzner, 2006) with their acute toxicity classification suggested by Singh *et al*. (2015) as the following; MMA(III) > As(III) > As(V) > DMA(V) > MMA(V). Arsenic and As-containing compounds are well-known human carcinogens (Tchounwou *et al*., 2015). Both oxidation states of As impair tissue respiration in biological systems. Arsenic(III) binds to sulfhydryl groups disrupting critical enzyme functions, while As(V) is substituted into biochemical reactions involving phosphorous (P), lowering the stability of high energy phosphate bonds and affecting the production of ATP (Hughes *et al*., 2011). Arsenic can also impair a range of biological organs, for example, the enlargement of liver, kidneys and spleen, as well as skin defects and ultimately cancerous tumours of the skin, lung and bladder (Gray *et al*., 2005).

Arsenic is categorised as a list II pollution reduction substance under the EU WFD. As a result, a freshwater EQS of 50 µg L^{-1} has been set (EC, 2000), with the WHO placing a 10 µg L^{-1} limit for drinking water (Bibi *et al*., 2015). For soil, DEFRA and the Environment Agency have assigned concentrations of As for SGV at 32 mg kg^{-1} and 640 mg kg^{-1} in residential and commercial soil, respectively. At a European level, ambient air quality concentration target limits have been assigned as 6 ng m^{-3} (EEA, 2013).

In Europe, the dominant human exposure route of As is through inhalation, where, like Sb and Pb, As is released from anthropogenic processes such as the combustion of fossil fuels, mining and smelting (Singh *et al*., 2015). Relative to atmospheric concentrations of Pb, As concentrations are a magnitude lower, and emissions are generally on the decline. A recent report on air quality across Europe (2013), showed that for 90% of 631 monitoring stations found ambient As concentrations were <2.4 ng m^3, with only 15 monitoring stations exceeding the 6 ng m^3 EU limit. The risk of arsenic exposure in Asia, North and South America is significantly higher, where the ingestion of contaminated drinking water, groundwater and food can occur from the dissolution of As from arsenic-rich soils or As containing ores (Matschullat, 2000; Choong *et al*., 2007; Singh *et al*., 2015). The abundance of As for these continents can be high due to their natural geology (Table 2.5). Indeed, a number of studies have demonstrated the uptake of As contaminated water by rice and vegetables, while elevated concentrations have also been observed in meat and milk from grazing mammals (EFSA, 2009; Mondal *et al*., 2010; Zhao *et al*., 2010; Fu *et al*., 2011; Rahman and Hasegawa, 2011; WHO, 2011; Bhattacharya *et al*., 2012 and Singh *et al*., 2015). Research by Ravenscroft *et al*. (2009) found that As contaminated drinking water was a health risk to more than 150 million people, with approximately 110 million people from South and South-East Asia the most affected (Brammer, 2008).

Table 2.5: Range of As concentrations in soil and groundwater from Asia, North and South America.

Environmental media	Location	Arsenic concentration	References
Soil	U.K.	7.03 mg kg^{-1} *	Salminen *et al*. (2005)
Soil	Brazil	200 – 860 mg kg^{-1}	Bundschuh *et al*. (2012)
Soil	Mexico	2215 – 2675 mg g^{-1}	Nriagu *et al*. (2007)
Soil	India	16 – 417 mg kg^{-1}	Das *et al*. (2013)
Freshwater	U.K.	0.63 µg L^{-1} **	Salminen *et al*. (2005)
Groundwater	China	1 – 2400 µg L^{-1}	Guo *et al*. (2001)
Groundwater	India	3 – 3700 µg L^{-1}	Das *et al*. (1996)
Groundwater	Chile	470 – 770 µg L^{-1}	United Nations (2001)

*Median value used, n=840, **Median value used, n=807.

2.4.4 Arsenic use and emissions

Throughout history, As has had a wide range of uses. For example, it was used in 1600 BC as an additive to bronze to improve its rigidity, and, in Victorian times, as a beauty product to make skin paler. In the early 20th century it was used as a pesticide, e.g. Pb arsenate ($HAsO_4Pb$), to treat gypsy moth infestations of orchards and its current application as chromated copper arsenate (CCA) as a wood preservative, accounts for up to 90% of global arsenic production. Although CCA was banned in the UK in September 2006 with voluntary bans by manufacturers in USA and Canada (Hughes *et al*., 2011; Netregs, 2015), a number of exceptions exists, and it is still frequently used in many countries for the construction of public buildings, agricultural sheds and bridges. Arsenic is additionally used in pharmaceutical products, the production of glass in the form of arsenic acid, and increasingly

for mobile phones and other wireless applications in the form of gallium arsenide (USGS, 2013).

Arsenic is frequently released to the atmosphere through the combustion of fossil fuels, and as mining and smelting by-products for the extraction of Cu, Au, Pb, Ni, and the production of iron and steel (Hughes *et al*., 2011). The similarities in chemical compartments of Sb, Pb and As can be observed in their historic and current anthropogenic emissions. For example, the study by Cloy *et al*. (2009) showed As enrichment from coal combustion during industrial periods in the mid-20th century in cores taken at four ombrotrophic peat bogs across Scotland. This was in agreement with Sb and Pb enrichments at these sites, and furthermore, agreed with other As chronologies from Scotland and Europe (Shotyk *et al.*, 1996; Küttner *et al*., 2014). In general, As fluxes were two magnitudes lower than those for Pb, and were more similar to those for Sb.

2.5 Copper

2.5.1 Elemental properties and occurrence

Copper is a group 11 transition metal with the atomic number of 29, an atomic weight of 63.5 and a mean crustal abundance of 55 mg kg^{-1} (Taylor, 1964). It is most stable in environmental systems in the +II oxidation state, but can also exist as 0 and +I. Some +III complexes have also been reported (Abu-El-Wafa *et al*., 1985). Copper has two isotopes, ^{63}Cu and ^{65}Cu, with relative abundances of 69% and 31%, respectively (RSC, 2015). Reddish-orange in colour, Cu is a ductile metal which possesses high thermal and electrical conductivity and as such it is often used in electrical wiring and cables. In addition, it is added to less conductive metals such as aluminium (Al) to improve overall conductance.

2.5.2 Copper in the environment

Copper occurs in a number of sulfidic minerals including chalcopyrite ($CuFeS_2$), bornite (Cu_5FeS_4), chalcocite (Cu_2S) and the low grade but highly economically mined porphyry Cu deposits. Porphyry is formed by hydrothermal solutions containing variable concentrations

of Cu, molybdenum (Mo), Au, silver (Ag), barium (Ba), Pb, Zn, As, Sb and tellurium (Te), and is recognised as the main source of both Cu and Mo globally (Dold and Fontbote, 2001; Khorasanipour *et al*., 2011). The chemical weathering effects on Cu minerals can lead to the formation of secondary minerals, such as malachite ($CuCO_3.Cu(OH)_2$), cuprite (Cu_2O) and tenorite (CuO), and under certain conditions, complete dissolution can also occur. The later has been observed in a number of studies, particularly at mining sites where a lowering of pH, often from the dissolution of minerals such as pyrite, or from secondary Fe^{2+}, Mn^{2+}, Fe^{3+} and Al^{3+} sulfate salts (e.g. pyrite, jarosite), can lead to the release of H^+ and metals such as Cu into the aqueous phase (Cravotta, 1994; Plumlee, 1999; Nordstrom and Alpers, 1999; Dold and Fontbote, 2001; Hansen, 2005; Khorasanipour *et al*., 2011). For aqueous systems Cu is found as $Cu(H_2O)_6^{2+}$ or as a complex such as $Cu_2(OH)_2CO_3$ (Cotton *et al.*, 1995; Drever, 1997). Once in the aqueous phase, the transport of Cu in soil is dependent on the surrounding minerals and soil pH, e.g. clay minerals have been postulated as a sink for Cu in noncalcareous soils, and for calcareous soils, Cu adsorption onto carbonate is said to control concentrations in solution (Cavallero and McBride, 1978; McLean and Bedsoe, 1992). Copper retention by soil is strongest where pH>7, as adsorption decreases with a declining pH (McLean and Bedsoe, 1992).

It is also well known that Cu can bind strongly to organic matter in soil, with binding mechanisms including complexation, ion-exchange and physical interactions (McLean and Bedsoe, 1992; Gezici *et al*., 2007). The extent to which binding to organic matter takes place is influenced by soil pH, as studies have shown that Cu binds to humic and fulvic acids more effectively at near neutral pH (Christl *et al.*, 2001; Gondar *et al.*, 2006). Other studies have demonstrated that Cu(II) can form strong complexes with key functional groups present in organic matter such as carboxylic and phenolic (Christl *et al*., 2000, 2001; Gondar *et al*., 2006) forming monodentate and bidentate complexes (Christl *et al.*, 2001; Gondar *et al*., 2006a, 2006b). In addition, humic acids are recognised as having stronger bonding sites for Cu(II) than fulvic, with the presence of aromatic systems containing carboxylic functional

groups preferred to aliphatic carbon backbones seen in fulvic acids (Murray and Linder, 1984; Gondar *et al*., 2006a, 2006b). In solution, Cu and dissolved organic matter is readily complexed via soluble organic ligands, which has often been identified as a major factor controlling total dissolved Cu concentrations in terrestrial systems (McLean and Bedsoe, 1992).

2.5.3 Toxicity and regulation

Copper is an essential trace element that is vital for the health of all living organisms; it contributes to biological processes such as respiration, connective tissue formation, peptide hormone maturation and antioxidant defence systems (Nordberg, 2007). Exposure to Cu in excess, however, can have significant negative biological effects; some reports have even considered copper as a human carcinogen, although this still remains to be sufficiently proven. It is not regarded as a carcinogen by the WHO (Denier van der Gon *et al*., 2007) but excessive intake of Cu can cause the development of liver cirrhosis, damage to the renal tubules and brain function, and detrimental effects to other human organs (Gaetke and Chow, 2003). The properties of Cu has led to its classification as a reactive oxygen species (ROS), catalysing the formation of hydroxyl radicals and causing oxidative damage to most biological systems (Gaetke and Chow, 2003). To this ends, the provisional tolerable daily intake value of 30 mg d^{-1} for the average adult body weight of 60 kg has been assigned to Cu by the Joint Expert Committee on Food Additives (JECFA, 1982).

In accordance with the EU WFD, Cu is a list II specific pollutant and has been assigned an EQS for dissolved Cu at 5 µg L^{-1}. The provisional drinking water limit of 2 mg L^{-1} set by the WHO (2003) is much higher than the freshwater EQS, as this takes into account the required intake of Cu for human health purposes, unlike the freshwater limit, where the EQS was assigned to protect aquatic organisms. A definitive SGV for Cu has not been determined nor has a Contaminant Land Exposure Assessment (CLEA) been implemented by the DEFRA or the EA. Using the generic assessment criteria, however Land Quality Management published

residential guidance values of 110 mg kg^{-1} and 2330 mg kg^{-1} using 1st and 2nd revisions of the derivation criteria (LQM, 2012).

Human exposure and uptake of Cu is often related to local geology or anthropogenic activities. Food and water is the main source of Cu intake for residents in developed countries (WHO, 2003), with inhalation and skin contact contributing to a lesser extent. A large proportion of the recommended daily intake of Cu can be attained by the consumption of impaired drinking water from the deterioration of Cu water pipes, particularly where water is naturally acidic. Although the uptake of Cu into plants, fish and mammals is well known, and necessary for biological growth, the range of concentrations assimilated could be a concern in respect to tolerable daily intake (TDI). A study by Cherfi *et al*. (2014) compared Cu concentrations in fruits and vegetables grown in Algeria, to those in similar products grown in Egypt, China and Saudi Arabia (Figure 2.14). The study showed that although Cu concentrations in the fruits and vegetables, particularly potatoes and cucumbers could contribute 500 μg kg^{-1} d^{-1} to the TDI, residents were unlikely to exceed the provisional TDI (global estimated daily intake of 12.2 μg kg^{-1} d^{-1} (FAO/WHO, 2001; Cherfi *et al*., 2014) unless they consumed large quantities of these. Other studies looking at Cu concentrations in fish from China (Ip *et al*., 2005), the Mediterranean Sea (Kalogeropoulos *at el*., 2012; Olemdo *et al*., 2013,), Scotland (Dean *et al*., 2007) and India (Sanker *et al*., 2006) were found to have similar Cu concentrations (between 0.5-2.0 mg kg^{-1} wet weight) making up around 13% of the Cu recommended daily allowance (Olmedo *et al*., 2013).

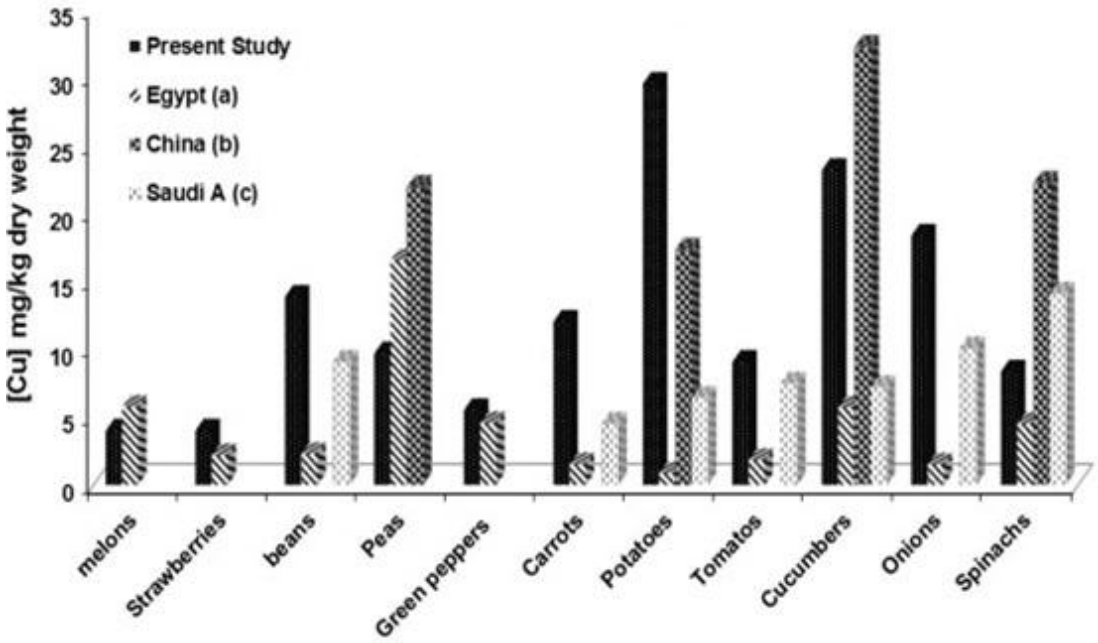

Figure 2.14: Copper concentrations in fruits and vegetables from Algeria, Egypt, China and Saudi Arabia (Cherfi *et al*., 2014).

2.5.4 Copper use and emissions

The discovery and use of Cu around 3300 BC led to the Bronze Age, where Cu and tin (Sn) was mined and combined to form the alloy bronze which was then used to form pots, utensils and coins. Additionally, similar tools were made from brass, which is also a Cu alloy containing Zn. The use of Cu was eventually reduced when Fe was discovered. Currently, Cu is used extensively in electronics, where its electrical and heat conductivity are exploited for applications such as wiring and circuit boards. As society has become more and more dependent on electrical goods, the demand for copper has significantly increased in recent years. This, along with building and construction (Figure 2.15), is expected to increase global production to 23,000 metric tonnes annually by 2050 (Backman, 2008).

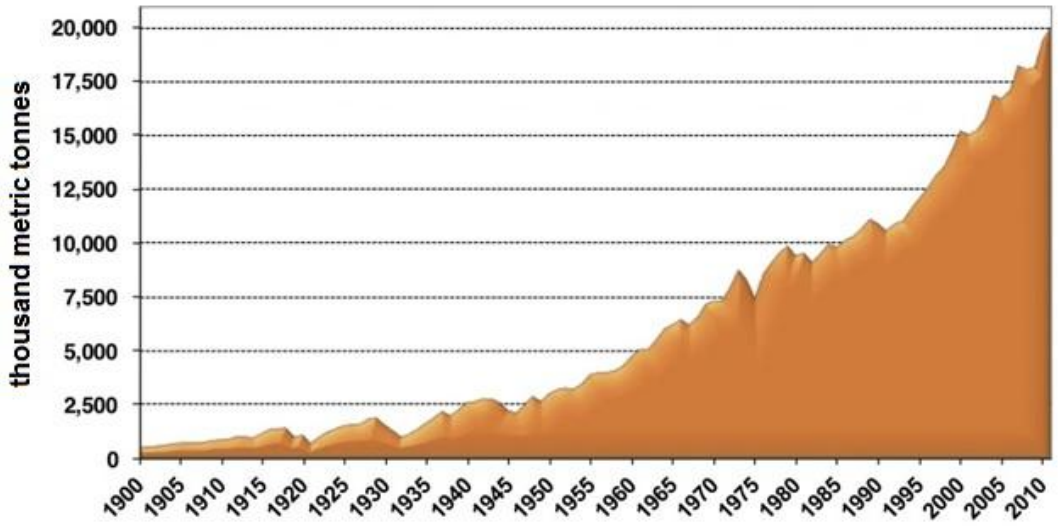

Figure 2.15: World refined copper usage, 1900 – 2011 (ICSG World Copper Fact Book, 2012).

The atmospheric emissions and subsequent deposition of Cu since the beginning of the 20th century is largely similar to that of other elements discussed in chapter 2, with peak Cu enrichment observed in European peat and sediment cores occurring around the industrial revolution (Olid *et al*., 2010; Allan *et al*, 2013; Vallius, 2014). Interestingly, these studies all show a steady decline in Cu fluxes from ~1990's, where Cu concentrations dropped by ~50%, which is in contrast to the increased Cu production observed in (Figure 2.15).

2.6 Zinc

2.6.1 Elemental properties and occurrence

Zinc is a transition metal with the atomic number 30, and an atomic mass of 65.4. It can exist as metallic Zn or as the (+II) oxidation state, and has five stable isotopes, ^{64}Zn (48%), ^{66}Zn (28%), ^{68}Zn (19%), ^{67}Zn (4.1%) and ^{70}Zn (0.62%) (Nordberg, 2007). It is a silvery-white metal with a blue tinge that tarnishes under aerobic conditions. Zinc is the 24th most abundant crustal element, with a mean crustal abundance of 79 mg kg^{-1} (Taylor, 1964).

2.6.2 Zinc in the environment

Zinc is a chalcophile and thus has a great affinity to bond with sulfur, primarily as sphalerite (ZnS), the most commonly occurring and mined ore (Stephan *et al*., 2008). As with most sulfidic ores, it is susceptible to weathering resulting in the formation of secondary ores such as smithsonite ($ZnCO_3$), hemimorphite ($Zn_4(Si_2O_7)(OH)_2H_2O$ and hydrozincite ($Zn_5(CO_3)_2(OH)_6$. Under oxidising conditions, Zn can undergo dissolution from minerals, and form one of the most mobile and soluble divalent trace metal cations (Stephan *et al*., 2008). Although the chemistry of Zn(II) is similar to that of Pb(II) and Cu(II), i.e. solubility increases under acidic conditions and decreases under reducing conditions, it is considered more mobile, as Zn(II) is stable over a large pH range (pH 1-7), and has a weaker binding strength than Pb and Cu to hydrous iron oxides and organic matter (Drever, 1997). A number of studies have investigated the dissolution of Zn from ores, by examining surface water downstream of current and former mining sites, and the sequential extraction of surrounding mining soil (Cappuyns *et al*., 2005; Li *et al*., 2013, 2015; Ettler and Johan, 2014). These studies showed that Zn could easily undergo dissolution from ores, and was very mobile in aqueous systems, since it was unlikely to precipitate out as a carbonate, which was in contrast to Pb.

For soil systems, Zn can be readily absorbed by clay minerals, carbonates, hydrous Fe, Mn and Al oxides present in soil and sediment (Tessier *et al*., 1980; Hickey and Kittrick, 1984; Mclean and Bledcoe, 1992; Shikazono *et al*., 2007). A good example of this was observed by Shikazono *et al*. (2007), where high concentrations of Zn were observed in sediments with high cation exchange capacities such as chlorite ($(Mg,Fe)_3(Si,Al)_4O_{10}(OH)_2\cdot(Mg,Fe)_3(OH)_6$), while sediments with low clay mineral content exhibited higher aqueous Zn concentrations.

2.6.3 Toxicity and regulation

The intake of Zn through cereals, red meat and dairy products is essential for a healthy diet and a minimum of ~1.4 mg kg^{-1} d^{-1} is advised (WHO, 1996). An estimated 20% of the global

population is deficient in Zn (Nordberg, 2007), with commonly observed health effects including growth retardation, behavioural problems, a delay in physical maturation and diarrhoea (WHO, 1996). Excessive exposure to Zn causes nausea, vomiting, diarrhoea and fever, but this is less frequently encountered (WHO, 1996; Nordberg, 2007). Clinical studies have shown, however, that Zn can interfere with the utilisation of Cu in the body, where even 50 mg d^{-1} to an average 60 kg adult can result in a decline in Cu levels in plasma and other functions (WHO, 1996). As a consequence, the WHO placed a maximum intake of 60 mg kg^{-1} d^{-1} (WHO, 1996).

Zinc is categorised as a list II pollution reduction substance and falls under Annex VIII of the WFD. The current freshwater EQS for Zn is set at 75 μg L^{-1} (UKTAG, 2008). This, however, is likely to change in the near future to incorporate bioavailability and influence of water hardness ($CaCO_3$); the new EQS may be as low as 8 μg L^{-1} (UKTAG, 2010). For soil, DEFRA and the EA have not assigned a Zn SGV or completed a CLEA as Zn is not considered to be sufficiently toxic. Using the generic assessment criteria of CLEA, Land Quality Management derived a residential guidance value of 3750 mg kg^{-1} (LQM, 2012), whilst the Dutch intervention value is lower at 720 mg kg^{-1} (VROM, 2000).

The greatest contribution to human Zn intake is primarily through diet, with the consumption of Zn by UK residents averaging 9.7 mg d^{-1} for an average 60 kg adult (n=2100) (Gregory *et al*., 1990). Although the uptake of Zn and its incorporation into vegetables and fruits will vary globally, their consumption is unlikely to cause any health effects. For example, a study by Rowell *et al*. (2014) looked at Zn concentrations present in rice from Sri Lanka, India, Pakistan, Egypt, Australia, Thailand, Italy, USA and Vietnam, each of which, only contributed a small proportion to the maximum intake of 60 mg kg^{-1} d^{-1} for an average 60 kg adult (mean Zn content in rice is ~13 mg kg^{-1}). For polluted environments, human occupation and residency can play an important role in determining the exposure to Zn,

where the consumption of contaminated food and water, and the inhalation of poor quality air can contribute significant amounts to the maximum daily intake of Zn. This is especially evident near mines and smelting sites as observed by Li *et al*. (2015) in China. This study examined Zn soil concentrations, mobility and bioavailability near a 60-year-old Pb/Zn smelter which was still in operation. Indeed, results showed that Zn soil concentrations were extremely high (max 8078 mg kg^{-1}), and exceeded the Chinese soil maximum allowable concentration for agricultural soil. In addition, the soil concentrations of Zn declined, as the distance from the Pb/Zn smelter increased, demonstarting the impact smelting activity had on the surrounding soils (Figure 2.16). Li *et al.* (2015) highlighted concern for the local population where the consumption of vegetables and grain grown in the surrounding mining area may be contaminated.

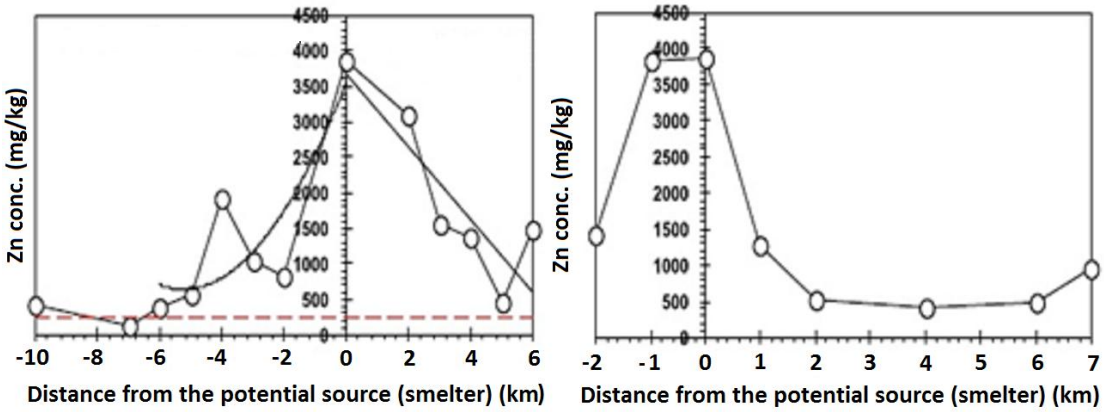

Figure 2.16: Declining Zn soil concentrations with distance from Pb/Zn smelter located in Zhehai, China (Li *et al*., 2015).

2.6.4 Zinc use and emissions

The dominant use of Zn historically was for the production of brass, where even before metallic Zn was discovered, ores were mixed with Cu to produce brass for utensils, ornaments, weapons and coins. Recent decades have used the noncorrosive properties of Zn for the construction industry, where it is used in protective coatings for metals and alloys and in addition, the automotive industry for brake linings, tyre rubber and dry cell batteries.

Atmospheric emissions from anthropogenic activities such as mining, metal smelting, Zn production, brass works, coal combustion, refuse incineration, and iron and steel works are the primary release of Zn to the environment (Ragaini *et al*., 1977; ATSDR, 2016). Nriagu and Pacyna, (1988) estimated a range of 50–70% of global Zn emissions were from the nonferrous metal industry equating to 462–1380 million kg of Zn per year. Using an ombrotropic peat core taken from Belgium (previously mentioned in section 2.2.5.2), fluxes from the 1400s onwards have steadily increased from 2 mg m^{-2} yr^{-1} to a maximum of 90 mg m^{-2} yr^{-1} observed between 1991–1996 (Allan *et al*., 2013). More recently (up to 2008), however, there has been a marked decrease in Zn emissions despite production increasing by 2.4% per annum (Backman, 2008). A reduction of 68% was observed in Belgium by Allan *et al*. (2013), which was in agreement with Steinnes *et al*. (2011), who also reported a 70% reduction from 1980–2005 at atmospheric monitoring sites in Norway. The WHO, (2001) reported a similar trend, with the reduction in coal combustion along with improved facilities for metal and Zn production reducing contemporary emissions of Zn (Allan *et al*., 2013). It is worth noting however, that natural Zn atmospheric emissions are significantly higher than all other elements in this study, with Nriagu (1989), estimating natural Zn emissions of 45 million t, notably higher than Cu (27.7 million t) and Pb (12 million t).

2.7 Polycyclic aromatic hydrocarbons (PAHs)

2.7.1 Introduction

PAHs consist of carbon and hydrogen atoms fused together typically forming 2–6 membered aromatic rings; these either occur naturally, or as by-products from the incomplete combustion of fossil fuels (Baird, 1998). They are categorised as persistent organic pollutants (POPs) due to their resistance to degradation, their toxicity to the environment and human health, and their potential to bioaccumulate and biomagnify in the food chain (Maliszewska-Kordybach, 1999). Whilst ~660 different PAHs exist (Sander and Wise, 1997; Hitzel *et al*., 2013), this study will focus predominantly on PAHs that commonly arise from

the burning of fossil fuels and those that are classed as Priority Hazardous Substances (PHS) or Priority Substances (PS) under the WFD (2000/60/EC). This group consists of 16 PAHs (Figure 2.17), often referred as EPA 16 PAHs or 16 PAH priority pollutants, and include naphthalene, acenaphthene, acenaphthylene, fluorene, phenanthrene, anthracene, fluoranthene, pyrene, benzo(a)anthracene, chrysene, benzo(b)fluoranthene, benzo(k)fluoranthene, benzo(a)pyrene, dibenzo(a,h,)anthracene, indeno(1,2,3-c,d)pyrene and benzo(g,h,i)perylene.

2.7.2 Toxicity and regulation of 16 PAH priority pollutants with respect to human health and the environment

Although the toxicity of PAHs is structurally dependent, the 16 PAHs studied here all (Figure 2.17), to a certain degree, have mutagenic and carcinogenic effects which have been well documented in recent years (IARC, 1987, 2010; Bostrom *et al*., 2002; Kim *et al*., 2013; Hitzel, 2013). PAHs are known to bind with DNA adducts in human biological systems causing gene mutations and reproductive defects (Perara *et al*., 2002). Increased inhalation leads to a greater risk in developing lung, bladder and urinary cancer (Gaertner and Theriault, 2002; Bosetti *et al*., 2007) and other symptoms such as liver damage, jaundice, inflammation of the skin and cardiopulmonary mortality have also been reported (Kim *et al*., 2013).

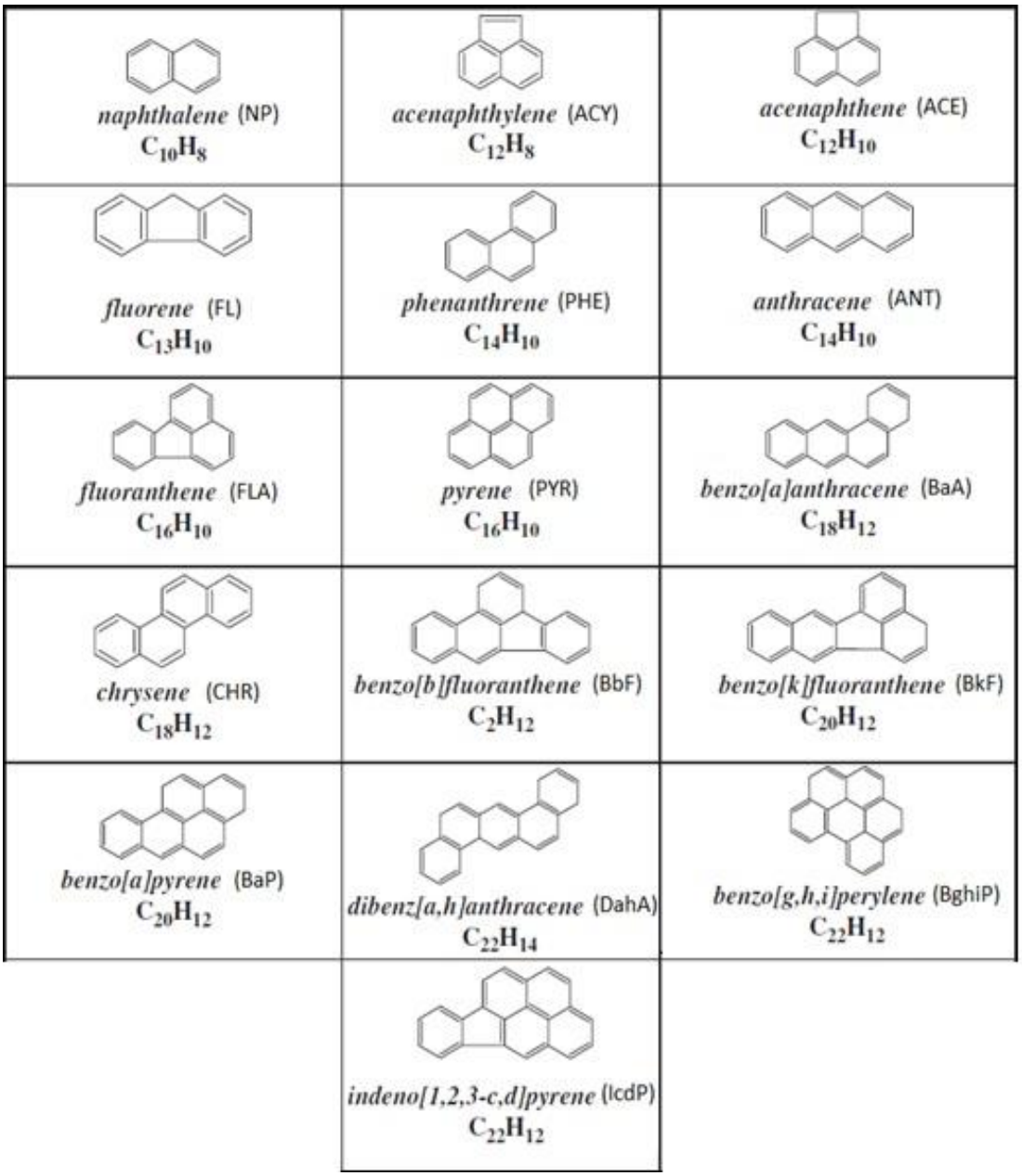

Figure 2.17: Chemical structure, formula and abbreviations of the 16 PAH priority pollutants. Adapted from Ravindra *et al*, (2008).

Due to PAH inherent toxicity, aqueous, soil, ambient and food PAH concentrations are heavily regulated, where Σ16PAHs, and for some instances, specific PAHs have been assigned European limits. There are 6 PAHs that are classed as priority hazardous substances (anthracene, benzo(a)pyrene, benzo(b)fluoranthene, benzo(g,h,i)perylene, benzo(k)fluoranthene and indeno(1,2,3-c,d)pyrene), with a further two identified as priority substances (naphthalene and fluoranthene) (Table 2.6) (2000/60/EC; SEPA, 2007). Limits

set for each criteria will vary depending on individual PAH structure, toxicity, chemical properties and proportion released to the environment from anthropogenic activity, for example, benzo(a)pyrene (one of the most toxic PAHs) is used as a relative indictor for the presence of PAH in air, and until recently food (Hitzel *et al*., 2013). Other PAHs such as acenaphthylene and fluorene are deemed less critical, and do not have a regulatory limit imposed on them.

Table 2.6: Key PAH regulatory limits for concentrations in aqueous, soil, ambient and food media.

PAH	*Class.	Freshwater EQS[a] ($\mu g\ L^{-1}$)	Soil guideline value[b] ($mg\ kg^{-1}$)	Ambient ($ng\ m^{-3}$)[c]	Food guidance value[d] ($\mu g\ kg^{-1}$)
Naphthalene	PS	1.2	40.0	0.25	30.0
Anthracene	PHS	0.1			
Fluoranthene	PS	0.1			
Benzo (b) Fluoranthene	PHS	Σ 0.03			
Benzo (k) Fluoranthene	PHS				
Benzo (a) Pyrene	PHS	0.05	1.0		
Benzo (g,h,i) Perylene	PHS	Σ 0.002	40.0		
Indeno (1,2,3-c,d) Pyrene	PHS				

* Classification: Priority Substance (PS), and Priority Hazadous Substance (PHS)
[a] from SEPA, 2008, [b] from Topsoil CLEA 2007, [c] from Defra, 2007, [d] from FSA, 2012.

Whilst regional factors may influence human exposure differently, the dominant exposure route of PAHs to the UK and European population is through food consumption (Kim *et al*., 2013), where Skupinska *et al*. (2004) suggested this could contribute up to 70% of human PAH intake. The Food Standard Agency (FSA) (2012) commissioned a report studying cereals, cereal products, vegetables, vegetable products and traditionally smoked foods, in which, all cereal and vegetable related products showed very little PAH content. This was in agreement with a report by Su and Zhu (2007) where PAH uptake by rice from contaminated soil was low. Smoked food, however, has been shown to contribute a large proportion of

PAHs to the body, particularly in smoked fish (Essumang *et al*., 2013; Hitzel *et al*., 2013). Within the same FSA report, 4 out of 73 samples exceeded the PAH concentration guidelines, with smoked fish and shellfish products a factor of ~17 higher than cereal and vegetable related products. Whilst the smoking process contributes large proportions of PAHs to seafood for consumption, during the lifetime of shellfish, and for some fish, PAHs can also accumulate in fatty tissue contributing to total PAH concentrations ingested. Indeed, mussels are often used as bio-indicators for monitoring water quality in respect to POPs due to the effectiveness of PAH accumulation (Webster *et al*., 2008). Due to the hydrophobic nature of PAHs in aqueous systems, PAHs are generally bound to suspended particulate matter rather than in a truly dissolved state, and thus human exposure and intake through water is low, unless originating from contaminated areas.

Although human exposure through inhalation is not the primary intake route for western Europe, for countries such as China and India, the inhalation of air of poor quality accounts for a large proportion of PAH intake (Kim *et al*., 2013; Kamal *et al*., 2014). Figure 2.18 depicts excessive use of biofuels and coal for electricity, and at a local level, high traffic volume, with China and India contributing just under 40% of global PAH 16 emissions (Zheng and Tao, 2009; Kamal *et al*., 2014). Atmospheric PAH concentrations are often found bound to Particulate Matter (PM), where their inhalation can greatly increase the risk of lung cancer (Wu *et al*., 2014).

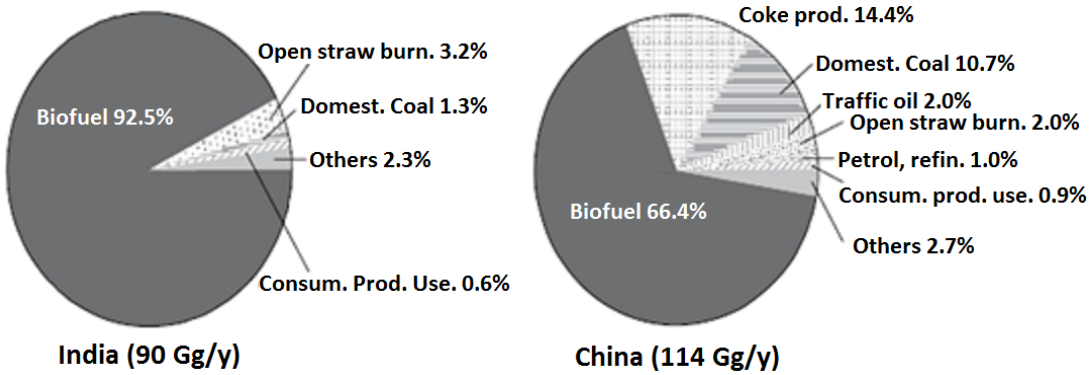

Figure 2.18: Relative distribution of priority 16 PAHs emissions from India and China (Zheng and Tao, 2009).

2.7.3 PAH emissions and source apportionment

Emissions of petrogenic PAHs are generally caused from environmental processes such as volcanic eruptions and the slow maturation of organic material (diagenesis)(Tobiszewski and Namiesnik, 2012) however, anthropogenic sources like diesel spills can also contribute to petrogenic PAH emissions. Although petrogenic emissions have largely remained the same over the last century, pyrogenic sources have not. A marked increase in pyrogenic PAH emissions were reported at the end of the 19th century; the rising demand for power was eased by the increased combustion of coal, diesel and petroleum. This is still the case for many rapidly developing countries such as China, where coal combustion accounts for approximately 75% of total energy production. In 2003, an estimated 1.16 x10^{5} tonnes of PAHs were released as a result of coal combustion (Liu *et al*., 2009). Although Zhang and Tao (2009) reported current PAH emissions had stabilised globally, the continual demand for power and the difficulty in documenting PAH source emissions globally can provide uncertainty in final calculations.

2.7.3.1 Source apportionment using diagnostic ratios

PAH emission profiles for specific anthropogenic processes can be established by examining the petrogenic and pyrogenic molecular structures, as summarised in Table 2.7.

Petrogenic: The structure of petrogenic PAHs frequently contain alkylated substituents on the fused benzene rings. Petrogenic PAHs are generally of low molecular weight, such as naphthalene and fluorene (two or three ringed molecular structure) shown in Figure 2.17.

Pyrogenic: These are found with very few alkylated substituent's present, and contain higher molecular weights such as benzo(a)pyrene and indeno(1,2,3-cd) pyrene (four or five ringed molecular structure) shown in Figure 2.17.

Key variables such as the original combustible material and the temperature of the burning process will result in a distinctive PAH ratio that can identify the source. Tobiszewski and

Namiesnik (2012) documented diagnostic PAH ratios from research carried out over the period 2002 to 2011 (Table 2.7).

Table 2.7: 16 PAH priority pollutant diagnostic ratios. Adapted from Tobiszewski and Namiesnik, 2012.

PAH Ratio	Value range	Source
Σ 2-3 ringed PAH / Σ 4-5 ringed PAH	< 1	Pyrogenic
	> 1	Petrogenic
FL / (FL + PYR)	<0.5	Petrol emissions
	>0.5	Diesel emissions
ANT / (ANT + PHE)	<0.1	Petrogenic
	>0.1	Pyrogenic
FLA / (FLA + PYR)	<0.4	Petrogenic
	0.4 – 0.5	Fossil fuel combustion
	>0.5	Grass, wood, coal
BaA / (BaA + CHR)	0.2 – 0.35	Coal combustion
	>0.35	Vehicular emissions
	<0.2	Petrogenic
	>0.35	Combustion
IcdP / (IcdP + BghiP)	<0.2	Petrogenic
	0.2 – 0.5	Petroleum combustion
	>0.5	Grass, wood and coal
BaP / BghiP	<0.6	Non-traffic emissions
	>0.6	Traffic emissions

KEY: (FL) Fluorene, (PHE) Phenanthrene, (ANT) Anthracene, (FLA) Fluoranthene, (PYR) Pyrene, (BaA) Benzo(a)anthracene, (CHR) Chrysene, (IcdP) Indeno(1,2,3-cd)pyrene, (BghiP) Benzo(g,h,i) perylene, (BaP) Benzo(a)pyrene.

2.7.4 PAHs in the environment

As previously stated, PAHs are hydrophobic compounds, and are only slightly soluble in water. The extent of solubility is dependent on each individual PAH, with PAH solubility decreasing as the molecular weight increases. For example, the two-ringed PAH naphthalene, has a solubility of 31 mg L^{-1}, which is considerably more than the 5-ringed benzo(a)pyrene solubility of 0.0038 mg L^{-1} (Wick *et al*., 2011). Additionally, the PAH structural arrangement can also influence solubility, where a linear structure is generally less soluble than those with an angular structure e.g. anthracene is less soluble than phenanthrene

(Figure 2.17). Although PAHs prefer to partition into sediment or biota in aqueous systems, they are still found within the water column, bound to suspended particulate matter (Macgregor *et al*., 2011).

Given the hydrophobicity of PAHs, the binding process in soils is different to elements, where PAHs are often held within cavities of organic matter, or between mineral surfaces, and not bound to carboxylic or phenolic groups. The affinity for PAHs to organic matter and their environmental persistence is influenced by key parameters such as chemical structure and properties, pH, soil type and redox conditions. For example, naphthalene, relative to other PAHs, has a low molecular weight and high vapour pressure, which indicates a greater mobility in the environment where it can readily evaporate and condense back to a solid state. In contrast, benzo(a)pyrene, a larger molecule, is less mobile and more likely to bind to sediment and soil, or be stored in biota. PAH volatilisation is additionally influenced by soil porosity and drainage, where greater soil retention occurs when soils are dry and with variable pore size (Wick *et al.*, 2011).

2.8 Chapter summary

The elements Sb, Pb, As, Cu and Zn discussed in this chapter are all chalcophilic, meaning they have a greater affinity to bind to S than to O, and are commonly found associated with pyrites and fossil fuels such as coal. The elemental toxicity to human health and the environment vary, with forms of Sb, Pb and As strictly regulated due their harmful effects, whilst Cu and Zn, in moderation, are essential for biological systems. Copper and Zn are most abundant in soils, with many forms commonly found associated with Sb, Pb and As in ores such as tennantite ($(Cu, Ag, Zn, Fe)_{12}As_4S_{13}$), the tetradredrite-tennantite Sb ore series ($Cu_{12}Sb_4S_{13}$-$Cu_{12}As_4S_{13}$) and Zinkenite ($Pb_9Sb_{22}S_{42}$). The dissolution and transport of elements from minerals into the environment are greatest for Zn, As and Cu, where, over a wide pH range, these elements can leach from ores and dissolve into surface waters. In contrast, under neutral conditions, Sb and Pb do not readily undergo dissolution from their

ores, where in most cases, < 3% of total Sb is released from stibnite to surface water, whilst Pb generally has a preference to precipitate into Pb-bearing carbonates. A similar trend is observed in the soil retention of elements, where Pb and Cu are retained by humic and fulvic acids reducing their mobility, whilst Sb, As and Zn are retained less and can become mobile in soil systems. Although Sb, Pb, As, Cu and Zn are chalcophilic, their retention in soil is heavily influenced by oxygen bearing organic matter since the availability of S is low, and elemental binding to carboxylic and phenolic groups can occur to form single or multi-dentate ligands.

Anthropogenic activities such as the combustion of fossil fuels, mining and smelting, waste incineration and automotive brake wear can release Sb, Pb, As, Cu and Zn to both the urban and rural environment. Using ombrotropic peat and sediment cores, historic deposition rates and trends from previous centuries can be observed globally, allowing chronologies of elemental atmospheric concentrations to be established. As these elements co-occur in sulfidic minerals and coal, trends in historic deposition rates are broadly similar, with increasing concentrations observed in the industrial and post industrial revolution, followed by a gradual decline from ~1950s to current day. Deposition chronologies for Pb differed when compared to other chalcophilic elements, where leaded petrol emissions from 1923 to 2000, significantly increased atmospheric Pb concentrations for that period of time. Although current atmospheric elemental concentrations are lower than previous decades, the increasing production and demand of Sb, Pb, As, Cu and Zn for modern applications is a growing concern, particularly for Sb where current production has increased by a factor of ~10 since the early 20th century. Whilst better environmental regulation has successfully limited elemental emissions from current industrial sources, other sources exist, such as diffuse pollution from transport, and abandoned former Sb and Pb mining sites. It is therefore important to assess the extent of elemental pollution in the urban and rural environment and gain a greater understanding on elemental transport in terrestrial systems.

This is indeed also true for PAHs, where a large proportion of atmospheric PAH concentrations are the result of similar anthropogenic activities seen for Sb, Pb, As, Cu and Zn, although some congeners are naturally occurring. The mutagenic and carcinogenic properties of PAHs are well known, their persistence and potential to accumulate in biological systems has led to strict regulations limiting PAH concentration in air, water, soil and food, highlighting the importance of PAH monitoring to minimise impact to human health and the environment. Although PAHs have been the subject of numerous past studies, recent studies addressing current PAH concentrations in the urban environment have been limited, with a greater need to understand contemporary emissions and concentrations present in densely populated areas.

Chapter 3 Sample collection and methodology

3.1 Introduction

This chapter gives details relating to sample collection including background information about the sampling sites as well as the number, nature and locations of samples collected. It also describes all sample preservation, preparation and analytical methods and gives a brief outline of the underlying principles of each method used in this study. The quality control data for these methods are also presented in this chapter.

3.2 Sample collection

3.2.1 Overarching sampling strategy

This section gives an overview of the experimental plan for environmental samples that were collected from Scotland to assess the release, mobility and fate of contaminants from current and past anthropogenic activity originating in urban cities such as Glasgow and Edinburgh, and from rural parts of Scotland. In addition, cores from two ombrotrophic peat bogs were also sampled, where past and current anthropogenic emissions of Sb and Pb, and their subsequent deposition was examined over several centuries and compared to results observed in the urban and rural setting. Emissions from urban and rural anthropogenic processes, and their subsequent deposition onto sediment and ombrotophic peat bogs is depicted in Figure 3.1, with the connectivity of sample preparation and analysis shown in Figure 3.2. More specific detail on each sample site and sampling methodology used for this study is detailed in section 3.2.3.

For the urban environment, the cities of Edinburgh and Glasgow were chosen to assess concentrations of contaminants in road dust and surface water in Scotland, as both cities experience a similar high volume of traffic although have contrasting industrial pasts. For each city, five roads with high traffic and five with low traffic were selected. In Glasgow, road dust was collected where available on each street and pooled together to form a

composite road dust sample, whilst in Edinburgh, specific distances of both 10 and 50 m from the junction were selected. A freedom-of-information request to Edinburgh city council (2012) yielded vehicle numbers for the high traffic locations (similar information not available for low traffic locations) and so the relationship between elemental or PAH concentrations and traffic volume could be assessed. In order to assess the mobility of elements after deposition on the road surface, a single set of road surface water samples were collected and analysed for contaminant concentrations; contaminant associations within the road dust and dust mineralogical composition were also investigated using sequential extraction spectroscopic techniques. Road dust samples were also collected in Edinburgh near initial sampling locations where elevated elemental road dust concentrations merited further investigation.

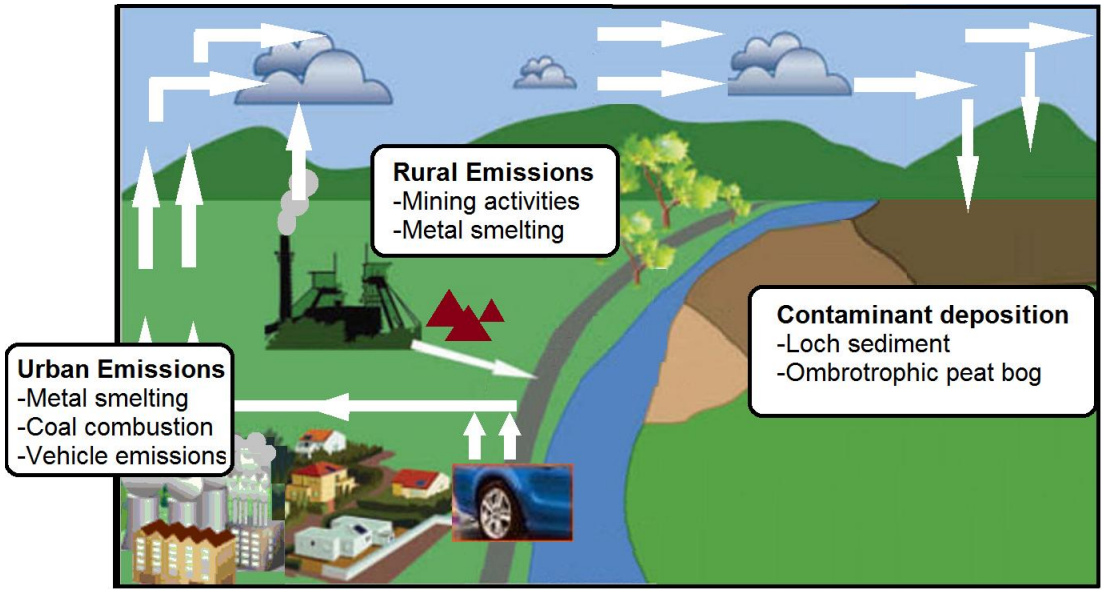

Figure 3.1: Underlying princples from past and current anthropogenic emissions, and their deposition in sediment and ombrotrophic peat bogs.

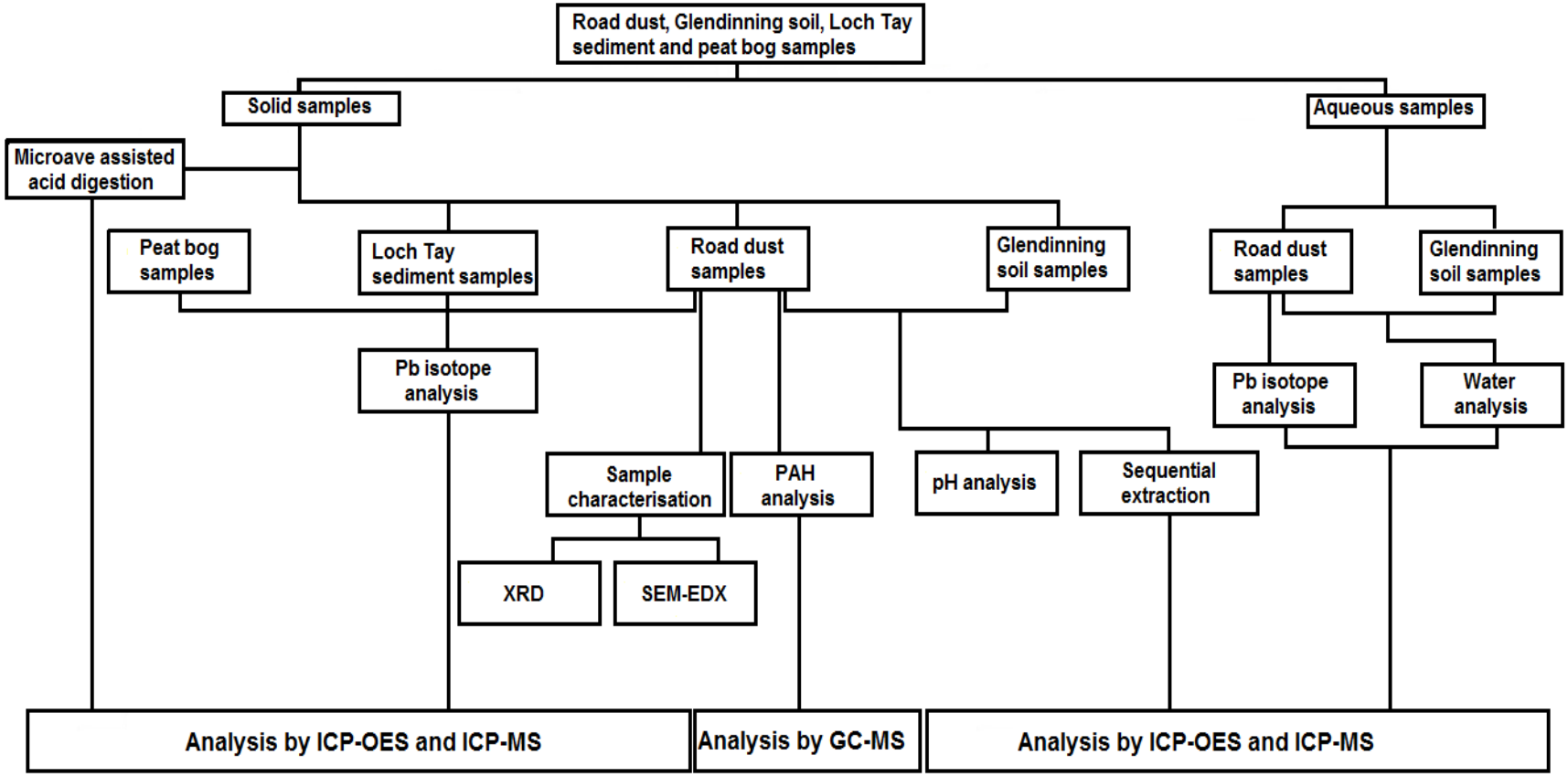

Figure 3.2: Sample analysis route map for road dust, Glendinning soil, Loch Tay sediment and peat bog samples collected for this project.

As identified in chapter 2, past industrial activity was the primary source of elemental contamination to the rural environment. Two former mining sites: Glendinning Sb mine in SW Scotland, and Tyndrum Pb mine in central Scotland, were chosen to focus on the release, transport and fate of Sb, Pb and As to the surrounding area. At Glendinning Sb mine, samples were collected from two spoil heaps and from soil cores (~12 cm deep; sampled down to bedrock) taken along transects running downslope from each spoil heap. Where they emerged, surface water samples were also taken along the same transects. Streamwater samples from Glenshanna Burn, located near Glendinning Sb mine, were sampled at up and downsteam points relative to the mine. Additionally, a soil core was sampled from a control site ~500 m uphill from Glendinning Sb mine and used as a soil reference for background elemental concentrations. Sampling at these locations allowed the elemental transport and fate from spoil dumps, downhill to soil and surface water to be examined. For the Tyndrum Pb mine, the transport and fate of elements were examined at a much larger scale, where contamination 25 km downstream to Loch Tay was assessed using two sediment cores. The vertical distribution of Sb in both sediment cores were examined to assess the effect of Mn and Fe redox cycling on the vertical concentrations of Sb. Once the sediment cores were dated, and subject to no post-depositional mobility of Sb, elemental chronologies were established to determine the impact of Tydrum Pb mine and other historic anthropogenic activities had to Loch Tay sediment.

The construction of atmospheric deposition chronologies for Sb and Pb were obtained from cores sampled from two Scottish ombrotrophic peat bogs; Great Moss, Cairngorms Mountains, and Auchencorth Moss, Midlothian. The deposition records for past centuries allowed the impact from current and historic anthropogenic activities to be observed, and enabled anthropogenic Sb/Pb ratios from urban dusts, surficial loch sediment and ombrotrophic peat samples to be assessed.

3.2.2 Preparation of sampling equipment

For solid environmental media, a spade, knife, nickel-silver alloy spatula and, where required, monolith and sediment corer, were thoroughly cleaned with 10% v/v Decon 90 solution (Fisher Scientific), rinsed with deionised water (18 MΏ) and dried overnight. After use, sampling equipment was also rinsed with deionised water (18 MΏ) and wiped clean. For aqueous samples, 250 mL polythene bottles were filled with 5% v/v Decon 90 solution, left overnight, and thereafter, thoroughly rinsed with deionised water (18 MΏ) and dried overnight. Cleanliness of sampling equipment was essential to ensure sample integrity.

3.2.3 Sampled sites

3.2.3.1 Urban environment - Edinburgh & Glasgow

3.2.3.1.1 Edinburgh & Glasgow sampling methodology

Since Edinburgh and Glasgow receive similar traffic volumes, the influence of vehicle emissions of target elemental and PAH concentrations found in road dust was best observed at these locations. The contrasting industrial history of both cities provided another means in which to assess urban road dust contaminants from Edinburgh and Glasgow. Heavy industrial activity in Edinburgh was relatively small when compared to Glasgow (Nenadic, 2011), where industrial activities such as textiles, ship buildings and other engineering works potentially released more contaminants to the surrounding area as compared with Edinburgh (Fordyce *et al*., 2013).

Taking this into consideration, five-high and low-traffic roads from Edinburgh were identified using Annual Average Daily Flow (AADF) data to give road vehicle count, and were sampled at; A90 (AADF: 46,435) Queen Street (AADF: 26,767), A8 (AADF: 22,013), A1 (AADF: 18,968) and A70 (AADF: 11,617) (Figure 3.3, Table 3.1). Low traffic roads were selected using residential roads within a 500 m distance of the high traffic roads and were; Hillpark Road, Thistle Street, Redhall Drive, Belmont Crescent and Cambusnethan Street (sampled March 2013). Supporting road dust sites at three specific areas in Edinburgh

which were likely to have been influenced by historic and current land use were also sampled (Table 3.2), and these locations were in the vicinity of Cambusnethan Street and Thistle Street, with a further seven locations in the vicinity of Edinburgh airport. Seven road locations were sampled within 2.5 km of Edinburgh airport as it was a suspected source of elemental pollution to the local area. Each of the locations were chosen to cover north, east, south and west of Edinburgh airport, as well as the average Edinburgh annual wind direction, which blows from south/south west and west/north west (sampled December 2014) (Windfinder, 2015). For Glasgow (Figure 3.4, Table 3.1), five high and low traffic roads were identified based on major routes in/out of Glasgow centre and by using AADF data from the Department for Transport, Scotland (2015). The five high traffic roads were; A8 of Glasgow (AADF: 19,811), A82 (AADF: 19,480), Broomielaw (AADF: 17,874), Baird Street (AADF: 8,917) and Hyndland Road (no AADF available), while the five low traffic roads were; Black Street, Goosedubbs, Leyden Street, Tradeston Street and West Princes Street (sampled May 2013).

The Edinburgh sample analysis route map is depicted in Figure 3.5, where duplicate road surface water samples were analysed for elemental concentrations and Pb isotope ratios, while duplicate road dust samples were analysed for: i) pH; ii) elemental and PAH concentrations; iii) Pb isotope ratios; iv) elemental mobility by sequential extraction; and v) mineral composition by X-ray diffraction and scanning electron microscopy with energy dispersive X-ray spectroscopy. Although road dust samples from Glasgow were not characterised to the same extent as those from Edinburgh, Glasgow road dust sites were still analysed for; pH, elemental and PAH concentrations, and Pb isotope ratios.

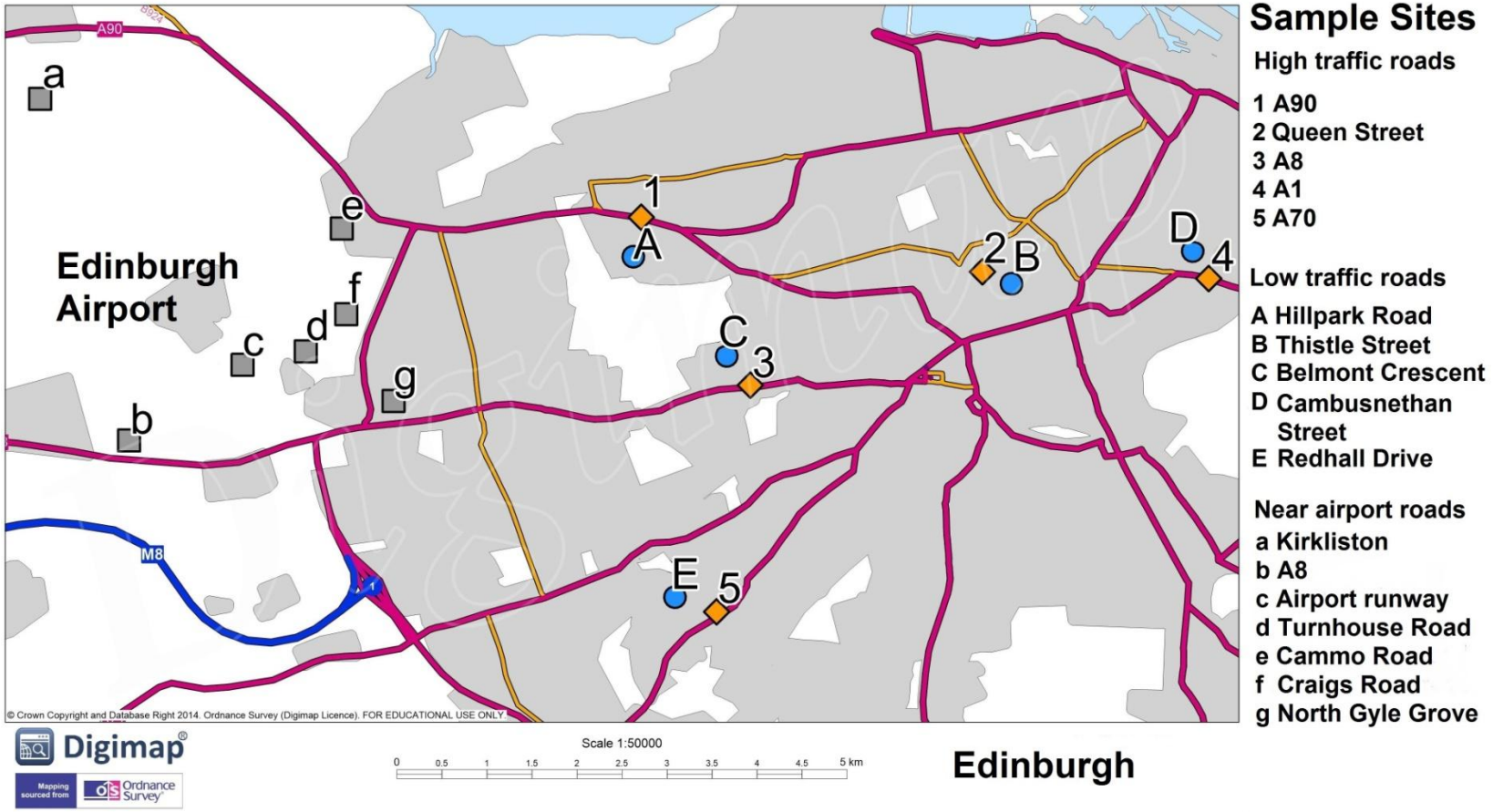

Figure 3.3: Edinburgh high-traffic, low-traffic and Edinburgh airport road dust sample sites.

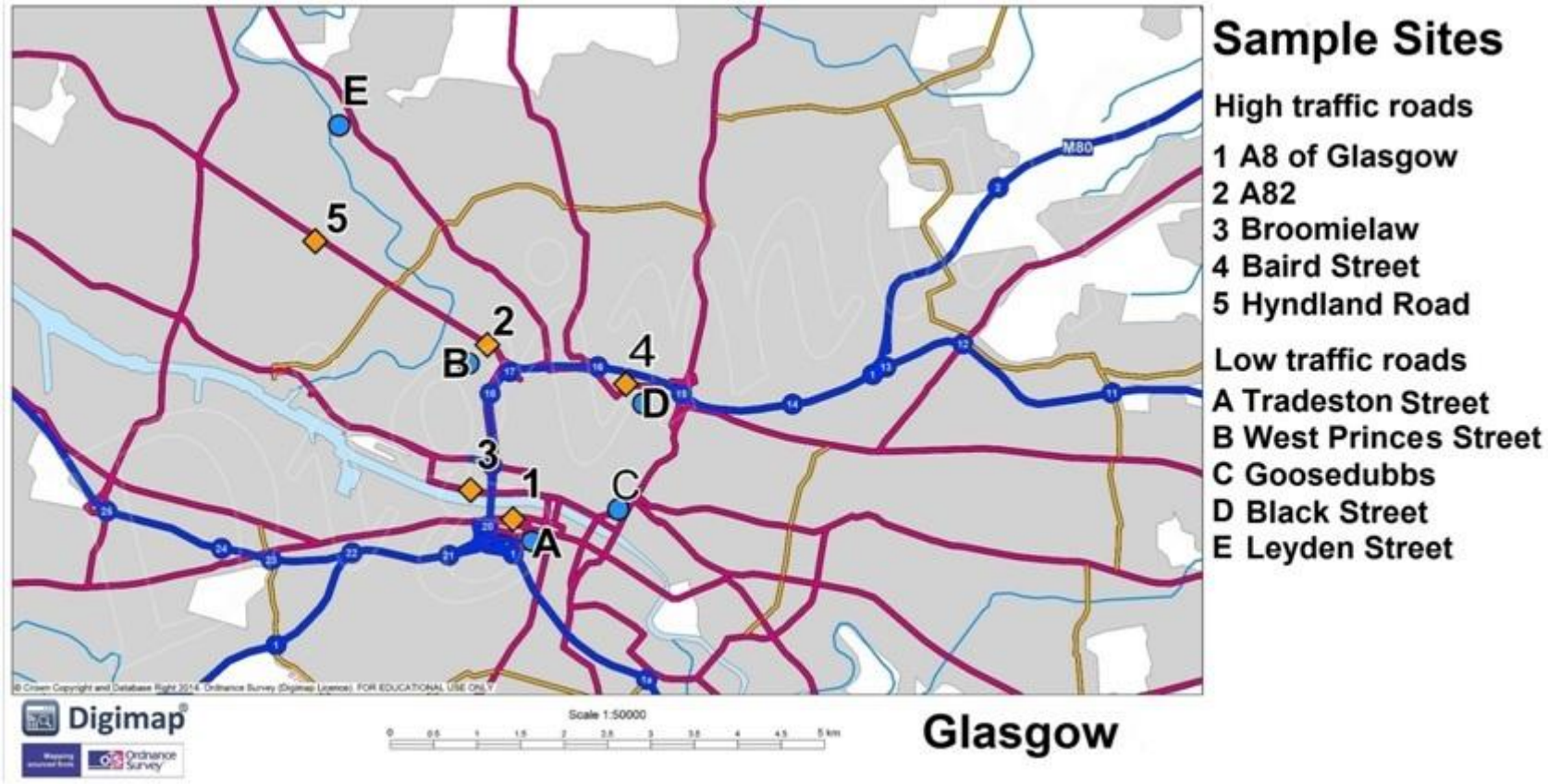

Figure 3.4: Glasgow high-traffic and low-traffic road dust sample sites.

Table 3.1: Summary of Edinburgh and Glasgow sampling location for high- and low-traffic sites.

Road dust Sites	AADF	Road lane count	Street cleaning frequency*	Site description
Edinburgh sites				
A90	46,400	4	Regularly	Main Edinburgh route to and from the forth road bridge. Exposed road with green spaces and residential housing at either side.
Queen Street	26,800	4	Regularly	Main route through the centre of Edinburgh. Part-exposed road with four storey tenement flats and green spaces at either side.
A8	22,000	4	Occasionally	Exposed road with green spaces and residential housing at either side.
A1	19,000	3	Fortnightly	Main road to the east of Edinburgh. Sheltered at either side by four storey tenement flats.
A70	11,600	4	Occasionally	Exposed road with green spaces and residential housing at either side.
Hillpark Drive	n.d.	2	Occasionally	Exposed residential housing estate with green spaces.
Thistle Street	n.d.	1	Regularly	Setted road, sheltered at either side by four storey tenement flats.
Belmont Crescent	n.d.	2	Occasionally	Exposed residential housing estate with green spaces.
Cambusnethan Street	n.d.	2	Occasionally	Sheltered road with residential parking and four storey tenement flats at either side.
Redhall Drive	n.d.	2	Occasionally	Exposed residential housing estate with green spaces.
Glasgow sites				
A8 of Glasgow	19,200	4	Rarely	Route to and from the centre of Glasgow. Exposed road with industrial buildings at either side.
A82	19,000	4	Rarely	Main route to Glasgow West End. Sheltered at either side by four storey tenement flats.
Broomielaw	17,900	6	Regularly	Main route beside the River Clyde. Part exposed road with multi-storey office buildings on one side.
Baird Street	8,680	4	Regularly	Main route to and from Glasgow centre. Exposed road with industrial buildings at either side.
Hyndland Road	n.d.	2	Regularly	Sheltered road with residential parking and four storey tenement flats at either side.
Tradeston Street	n.d.	2	Regularly	Part-exposed road with four storey tenement flats and waste ground at either side.
West Princes Street	n.d.	1	Regularly	Sheltered road with residential parking and four storey tenement flats at either side.
Goosedubbs	n.d.	2	Regularly	Setted road, sheltered by multi-storey buildings either side.
Black Street	n.d.	3	Regularly	Dead-end road with industrial buildings at either side.
Leydon Street	n.d.	2	Regularly	Sheltered road with residential parking and four storey tenement flats at either side.

n.d. indicates not determined. *Street cleaning frequency is defined as: Regularly: everyday or every other day, Occasionally: monthly, Fortnighly: every two weeks, Rarely: once or twice a year.

Table 3.2: Summary of Edinburgh sampling locations influenced by local historic and current land use.

Road dust Sites	Total number of road lanes	Site description
Road dust sites in the vicinity of Cambusnethan Street		
Carlyle Place	1	Sheltered dead-end road with residential parking at either side.
Dalgety Avenue	2	Sheltered cul-de-sac road with residential parking and four storey tenement flats at either side.
Dalgety Street	2	Sheltered road with residential parking and four storey tenement flats at either side.
Salmond Place	1	Sheltered dead-end road with residential parking at either side.
Road dust sites on Thistle Street		
West, Mid and East	1	Setted road, sheltered at either side by four storey tenement flats.
Road dust sites on the vicinity of Edinburgh airport		
Cammo Rd-North East	2	Exposed road within a residential housing estate with green spaces.
Turnhouse Rd-East	2	Exposed rural road
Craig Road-East	2	Exposed rural road
North Gyle Grove-East	2	Sheltered road with residential housing at either side
Glasgow Rd-South	4	Exposed dual carriageway
Kirkliston-West	2	Exposed road within a residential housing estate with green spaces.

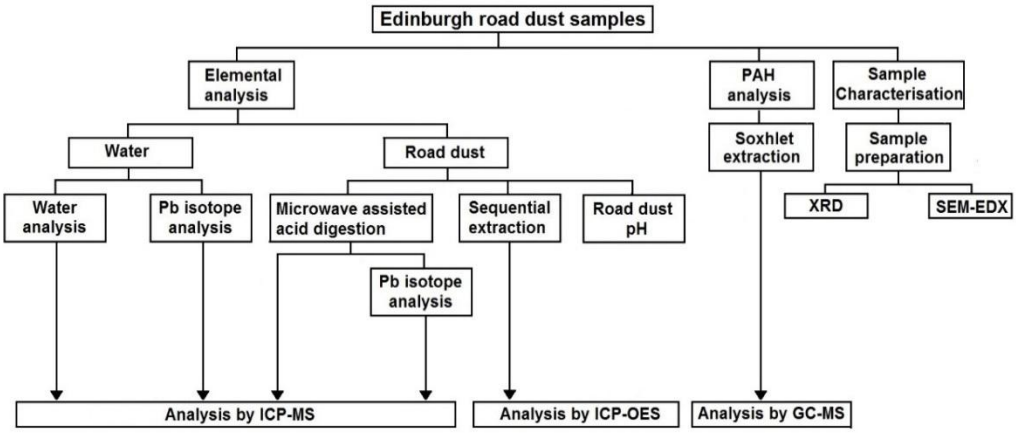

Figure 3.5: Edinburgh surface water, high- and low-traffic road dust analysis route map.

3.2.3.1.2 Edinburgh surface water sampling

Edinburgh road surface water samples were collected in March 2013, where 250 mL polythene bottles were used to collect samples during heavy rainfall just before the water entered the roadside drains. Due to the limited duration of the heavy rainfall, only one water sample was collected from each sample site. The water samples were labelled and then stored in a fridge at 4°C. The water sample pre-treatment was carried out as described in 3.3.3.

3.2.3.1.3 Edinburgh & Glasgow road dust sampling

The selected Edinburgh sample sites in Figure 3.3 were sampled using a nickel-silver alloy spatula to collect road dust from the road kerbside at 10 m and 50 m before the closest road junction (CRJ), e.g. before traffic lights or crossroads. Glasgow sample sites (Figure 3.4) were collected similarly using a nickel-silver alloy spatula, however, road dust was collected from any point on the street, and for each location, combined to form a composite sample. It was necessary to use composite Glasgow road dust samples since a limited amount of road dust was available from the road kerbside at 10 m and 50 m before the closest road junction (CRJ). Approximately 5 g of road dust was collected from each location in Edinburgh and

Glasgow and then placed in clean labelled polyethylene bags. Upon return to the laboratory, samples were air-dried, homogenised and placed in clean labelled polyethylene bags (section 3.3.2).

3.2.3.2 Rural environment – former mining sites

3.2.3.2.1 Site background and sampling methodology – Glendinning Sb mine

The former Glendinning Sb mine is located in Dumfries and Galloway, SW Scotland (Figure 3.6(a)-(b)), from which ~200 t of Sb ores were extracted during three main production periods, 1793-1798, 1888-1891 and 1919-1922 (Gallagher *et al*., 1983). Ore smelting took place at Jamestown, ~1 km downhill of the mine (Gallagher *et al*., 1983), with several spoil heaps in the vicinity of the mine still evident at the time of sampling. Sample collection focused on the lateral and vertical movement of Fe, Sb, As and Pb originating from the mineral-rich spoil heaps downhill to nearby soil and the Glenshanna Burn. A total of six ~12 cm deep intact soil cores were sampled (S1-S6); three of which were taken at an increasing distance from spoil heap 1 (SpH1), and the remaining three sampled at an increasing distance from spoil heap 2 (SpH2) (Figure 3.6(c)). The increasing distance of soil cores S1-S3, and S4-S6, relative to SpH2 and SpH1, respectively, enabled lateral elemental transport processes to be examined.

As shown in Figure 3.7, Glendinning Sb mine surface water and 2-cm depth soil core section samples were analysed for pH and elemental concentrations. Samples from selected soil depths also underwent sequential extraction and were chosen based on soil depths with the greatest elemental concentrations present and the soil core proximetry to SpH1. This was also the case for porewater samples, where they were extracted from soil cores S2-S5 and analysed for organic carbon content, and total, retentate (>3 kDa) and truly dissolved (<3 kDa) elemental concentrations present. Gel electrophoresis was carried out on retentate fractions obtained from porewater ultrafiltration.

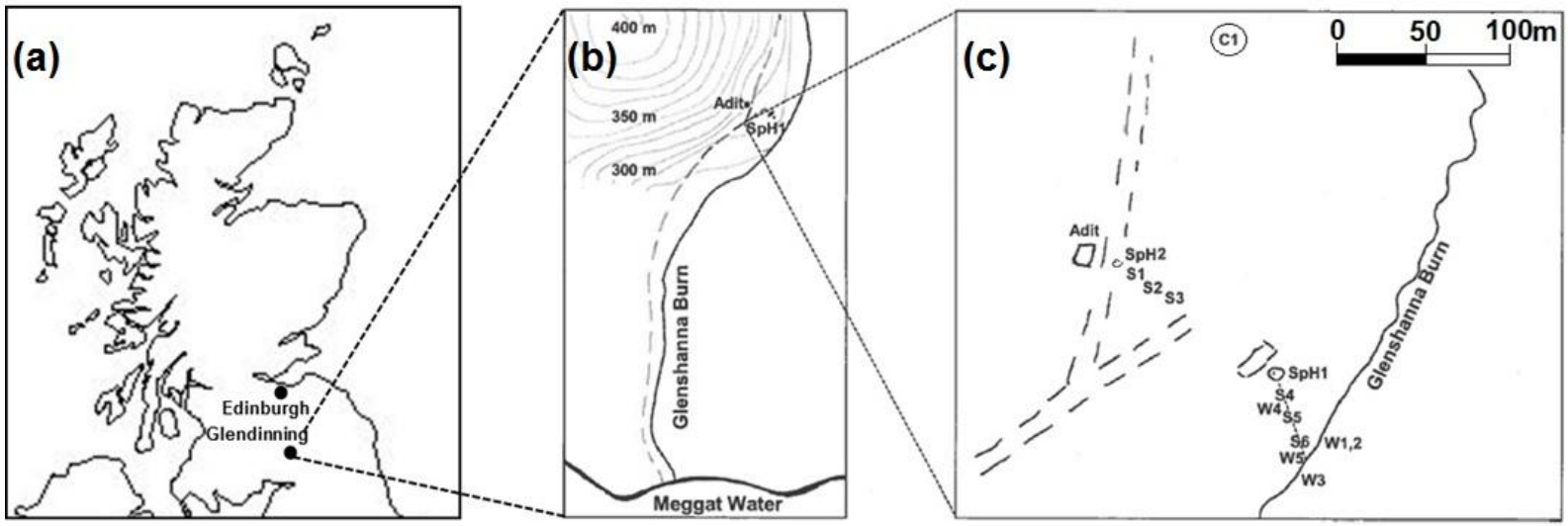

Figure 3.6: (a) Map of Scotland showing the location of Glendinning; (b) schematic of the Glendinning mining site showing the location of the adit and main spoil heap (SpH1); and (c) enlarged schematic showing the location of soil and water sampling sites in relation to the adit and SpH1.

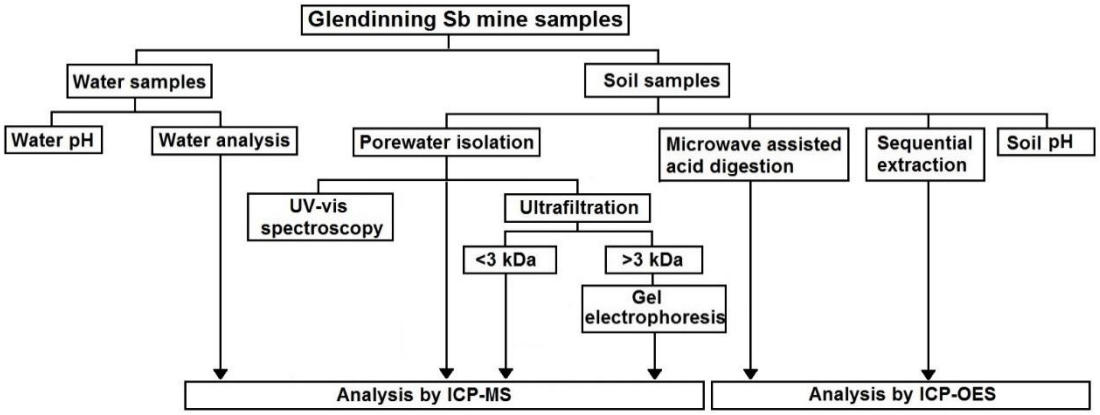

Figure 3.7: Glendinning surface water and soil analysis route map for samples taken on February 2013.

Although the sample analysis observed in Figure 3.7 enables elemental mobility and associations to be examined in the vicinity of the Glendinning Sb mine, very little was known about the lateral and vertical concentrations of Sb(III) and (V). The speciation of Sb present in soil-water systems has been highlighted as a potential factor that can influence the retention of Sb by soils, e.g. Mitsunobu *et al*. (2006) and Leuz *et al.* (2006). Taking this into consideration, soil cores were taken (S4A and S5A) from sampling locations near S4 and S5, where porewater concentrations of Sb were deemed sufficiently high to determine Sb(III) and (V) concentrations present. Eight selected depth sections were chosen for Sb speciation analysis (three from S4A, and five from S5A) to ensure the oxidation of Sb(III) during the sample processing stage was maintained.

3.2.3.2.2 Surface water sampling

To demonstrate connectivity between spoil heap 1 (SpH1) and the receiving water, the Glenshanna Burn, 250 mL water samples were collected in pre-cleaned polythene bottles from surface flows in the small gully leading steeply down from SpH1 towards the Burn and directly from the Burn itself. In February 2013, stream waters W1 and W2 were collected ~20 m upstream from SpH1, while W3 was collected ~2 m downstream of SpH1. The two surface flows collected at the same time were designated W4 and 5 (Figure 3.6(c)). Sampling

was repeated in October 2014 at W1, W3, W4 and W5. All stream water samples were collected in the centre of the stream at a depth of ~5 cm. The samples taken were clearly labelled after sampling and stored in a fridge at 4°C to await analysis (section 3.3.3). It was not necessary to use field blank water samples since the cleaning and preparation of sampling bottles was robust (detailed further in section 3.3.1.1).

3.2.3.2.3 Spoil heap and soil core sampling

Using a pre-cleaned spade, composite surface (0-5 cm; SpH1-surface) and sub-surface (30-35 cm; SpH1-deep) spoil samples were collected in February 2013 and placed in clean labelled polyethylene bags. The surface and sub-surface samples were each collected from three spoil heap sampling points until ~1 kg weight was achieved, and then combined to form their respective composite samples (SpH1-surface and SpH1-deep). Upon return to the laboratory, samples were air-dried, homogenised and placed in labelled clean polyethylene bags (section 3.3.2).

Depending upon soil depth, ≤12 cm-deep soil cores were excavated during February 2013 using a pre-cleaned spade and placed in clean labelled polyethylene bags. These were collected at: (i) three locations (S1-3) along a 30-m transect from spoil heap 2 (SpH2) which was near the mine entrance (adit shown in Figure 3.6(c)); (ii) three locations (S4-6) along a 50-m transect down-gully from SpH1 towards the Glenshanna Burn; and (iii) a control site (C1) approximately 500 m further up the Glenshanna valley (Figure 3.6(c)). Soil core dimensions were ~20 cm x 20 cm x ~12 cm depth and each core was sliced into 2-cm depth sections, air-dried, homogenised and placed in clean labelled polyethylene bags (section 3.3.2).

3.2.3.2.4 Soil core sampling for Sb speciation analysis

Depending upon soil depth, 16 cm-deep soil cores (S4A and S5A) were excavated using a precleaned spade during December 2014 at sites near S4 and S5; these locations were chosen since they were in close proximerty to SpH1 and were more likely to have greater

concentrations of Sb present. Each soil core was then sliced into 2-cm depth sections using a knife with each depth section placed into a polyethylene bag, filled with helium, sealed with tape and double bagged. The outer bag was labelled with sample depth, location and sampling date. These sites were both selected due to their close proximetry to SpH1

To preserve Sb oxidation state, it was crucial to remove each soil core and process samples promptly to minimise expose to air, or more specially, oxygen. Each soil core was excavated, sliced and bagged within a 10 minute period.

3.2.3.2.5 Site background and sampling methodology – Tyndrum Pb mine

The Tyndrum Pb mine is located in the Central Highlands of Scotland, 25 km west of Loch Tay (Figure 3.8(a) and (b)), and is found on the Dalradian Belt, which is renowned for having mineral rich deposits (Farmer *et al*., 1997). The mine was in operation from 1741 to 1921, where Pb ore extracted, predominately in the form of galena and sphalerite, totalled ~8000 tons over the operational duration (Hall, 1999). The transport and subsequent deposition of Pb from Tyndrum Pb mine downstream to Loch Tay has been previously noted by Farmer *et al.* (1997), where elevated concentrations of Pb in dated Loch Tay sediment was observed soon after Pb mining began. Further, more recent studies, also identified Tyndrum Pb mine as a source of Pb pollution to Loch Tay sediment, where the transport of particulate Pb waste from Tyndrum downstream to Loch Tay was thought to occur through fluvial transport and the dissolution of easily accessible Pb in upstream sediment (MacKenzie and Pulford, 2003; Pulford *et al*., 2009). Although a number of past studies examine the impact of Pb pollution originating from Tyndrum Pb mine (Farmer *et al*., 1997; MacKenzie and Pulford, 2002; Mansor, 2008; Pulford *et al*., 2009; Mills *et al*., 2014), no studies focus on the transport of Sb. The analysis of two sediment cores sampled from Loch Tay aims to address this, where historic and contemporary Sb concentrations are established,

as well as contemporary Pb concentrations and $^{206}Pb/^{207}Pb$ isotopic ratios not detailed by Farmer *et al*. (1997).

3.2.3.2.6 Sediment sampling

Sediment core sampling and the preparation of each depth section sample was carried out in 1992 by Farmer *et al*. (1997). Before sampling occurred, cone shaped polyethylene bags were made using polythene bags and a heat sealer, and labelled with sample depth, location and sampling date. A 90-cm sediment core was collected in November 1992 using a mini-Mackereth piston corer (Mackereth, 1969) at a water depth of 48 m. The sampling location was in the centre of the loch and about 3 km from the western end. The core was sliced into 1-cm sections to 20 cm depth, then 2-cm sections to 40 cm depth and 5-cm sections to 90 cm depth. The depth sections were air-dried, homogenised and placed in clean labelled polyethylene bags (section 3.3.2). Each depth section had been previously analysed for Mn, Fe, As and Pb concentrations by flame atomic absorption spectroscopy. Arsenic concentrations were determined by hydride generation AAS and stable lead isotope ratios ($^{206}Pb/^{207}Pb$) were determined by ICP-MS (Farmer *et al*., 1997). In this study, Sb concentrations in each depth section were determined by ICP-MS.

At the time of sampling the mini-Mackereth sediment core, a 19-cm Jenkin sediment core was also sampled within 10 m of where the mini-Mackereth sediment core was taken, and sliced into 1-cm sections (Farmer *et al*., 1997). All sediment depth sections were air-dried, homogenised and placed in clean labelled polyethylene bags (section 3.3.2). In this study, each archived depth section underwent quantification using ICP-MS analysis for Mn, Fe, As, Sb and Pb, as well as the determination of $^{206}Pb/^{207}Pb$ isotope ratio analysis.

Since the mini-Mackereth and Jenkin sediment cores collected in November 1992 were unable to give atmospheric deposition chronologies for the early 21st century, the top five 1-cm depth sections from two other Loch Tay sediment cores (core #1, core #2) sampled in 2003 at the same location were used to assess trends in the atmospheric deposition of Mn,

Fe, As, Sb, Pb, and $^{206}Pb/^{207}Pb$ isotope ratios from 1990-2003. This allowed a more recent account of elemental deposition for Loch Tay sediment to be established. In addition, the period of time between 1990 to 2003 was particularly important, as it spanned the years before and after the ban in leaded petrol use. After sampling, both sediment cores were sliced into 1-cm depth sections, air-dried, homogenised and placed into clean labelled polyethylene bags (section 3.3.2). The depth sections were ^{210}Pb dated at SUERC, and in this study, the top five depth sections underwent quantification using ICP-MS analysis for Mn, Fe, As, Sb and Pb, as well as the determination of $^{206}Pb/^{207}Pb$ isotope ratio analysis.

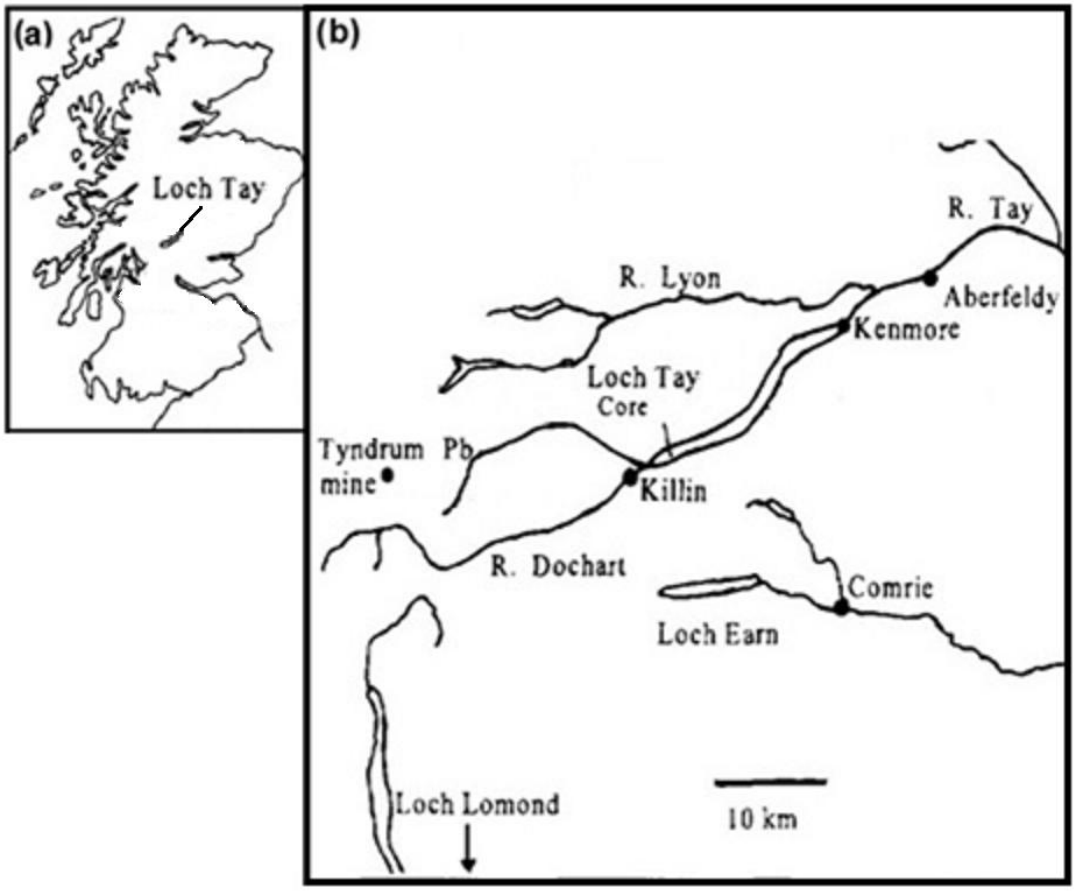

Figure 3.8: (a) Map of Scotland showing the location of Loch Tay and (b) map of Loch Tay area showing location of sediment core sampling site. Adapted from Farmer *et al*. (1997).

3.2.3.3 Ombrotrophic peat environment – Great Moss and Auchencorth Moss

3.2.3.3.1 Site background and sample methodology - Great Moss

The Great Moss, also known as the *Moine Mhor*, is located in the Cairngorm Mountains, Scotland, south of Loch Einich at an altitude of 900-945 m (Figure 3.9). The large peat blanket sits on a metamorphosed Dalradian sandstone and siltstone base, and is surrounded by Cairngorm Granite. The Great Moss provided a northern location in which to determine historic and contemporary atmospheric elemental deposition chronologies. It had been reliably ^{210}Pb dated in a past study e.g. Farmer *et al.* (2015), allowing an accurate archive of deposition records to be obtained over several centuries. For this study, a 50-cm peat core was collected at this location in June 2012 using a monolith tin, and sliced into 2-cm sections (see section 3.2.3.3.3). The depth sections were air-dried, homogenised and placed in clean labelled polyethylene bags (section 3.3.2). The peat core underwent ^{210}Pb dating at SUERC for the study by Farmer *et al.*, 2015, and for this study, was digested using microwave-assisted digestion and determined for Mn, Fe, Ti, Sb and Pb, as well as Pb isotope ratios by ICP-MS.

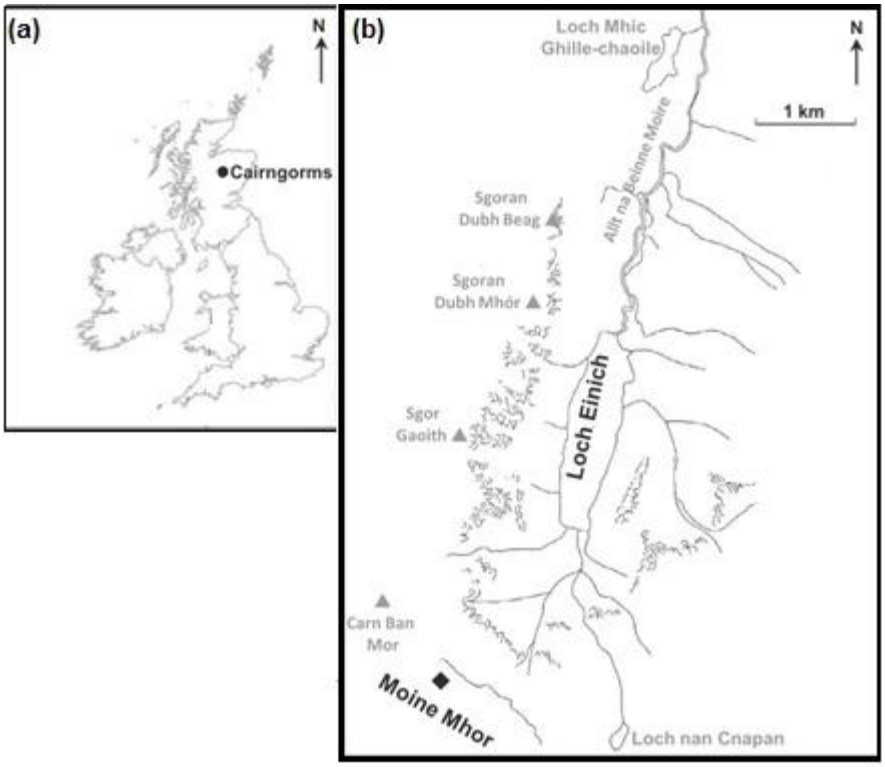

Figure 3.9: (a) Map showing location of Cairngorm Mountains in the UK and (b) sampling site of Great Moss and locations of other Lochs and mountain peaks nearby. Adapted from Farmer *et al*. (2015).

3.2.3.3.2 Site background and sample methodology - Auchencorth Moss

Auchencorth Moss is located in the southern uplands, Scotland, approximately 2.5 km south of Penicuik (Figure 3.10). Due to its rural location, air quality in Scotland is frequently monitored at Auchencorth Moss by the Centre for Ecology and Hydrology (CEH), which contributes to the UK air quality network managed by the DEFRA. Since Auchencorth Moss is used as an official background station for the UK air quality network, this site provided an excellent location in southern Scotland in which to construct atmospheric elemental deposition archives. It furthermore, along with Great Moss, gave spatial coverage of atmospheric elemental deposition across Scotland and allowed both peat bog chronologies to be compared. On April 2011, peat cores were taken from this location using a monolith tin, with one 40-cm peat core made available for this study (see section 3.2.3.3.3). The peat core

was sliced into 2-cm depth increments, air-dried and homogenised. Each depth section was ^{210}Pb dated, digested using microwave-assisted digestion and determined for Mn, Fe, Ti, Sb and Pb, as well as Pb isotope ratios by ICP-MS.

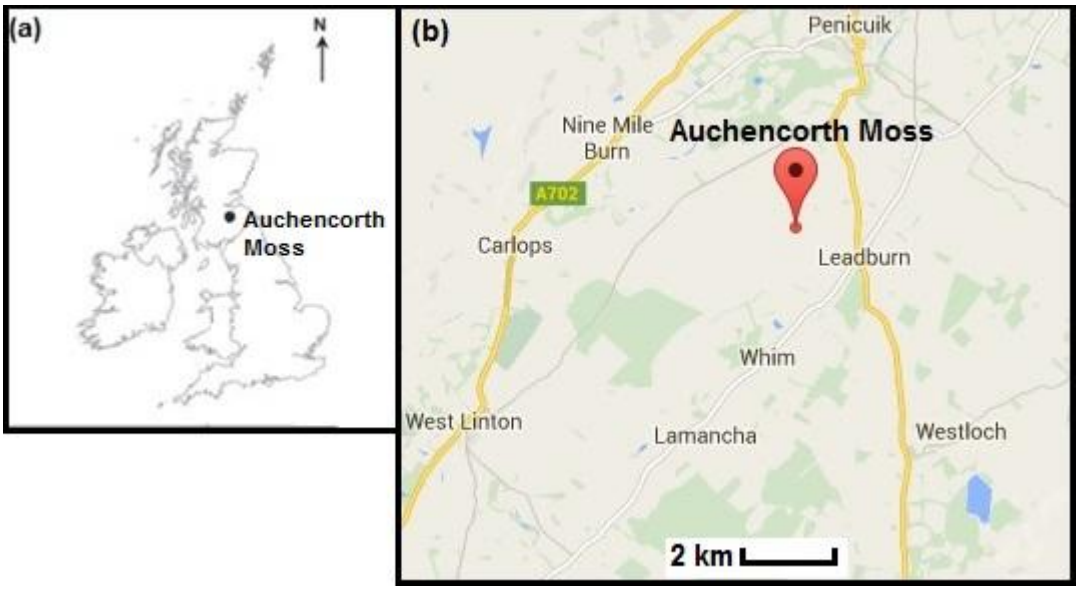

Figure 3.10: (a) Map showing location of Auchencorth Moss in the UK and (b) map of Auchencorth area in Scotland.

3.2.3.3.3 Great Moss and Auchencorth Moss peat core sampling

Using a monolith tin (50 x 15 x 7.5 cm), peat cores were collected by firstly excavating a trench (50 x 30 x 30 cm) using a spade and then pushing the monolith vertically into the trench wall. A spade and knife was then used to remove the monolith containing the peat core from the ground, where it was later laid horizontally for processing. The exact core dimensions were noted and used later for calculating deposition inventories and fluxes. Each depth sections was cut at 2-cm intervals ensuring the knife was thoroughly cleaned after each interval and placed in a clean labelled polyethylene bag with sample depth, location and sampling date.

3.3 Sample preparation and analysis

3.3.1 Glass and plasticware cleaning preparation

3.3.1.1 Elemental analysis

Before sample preparation and analysis occurred, glassware was submerged in a 5 mol L^{-1} Analar nitric acid bath, and boiled for 3 hours on a hotplate. After cooling, the glassware was removed, rinsed with deionised water and transferred to a deionised water bath which was then boiled for 3 hours on a hotplate. After cooling, glassware was removed, rinsed with fresh deionised water and transferred to a regularly cleaned drying cupboard. Plasticware was pre-cleaned by submerging in a 5% v/v Analar nitric acid bath for 24 hours, after which it was removed, rinsed with deionised water, and placed in a regularly cleaned drying cupboard.

3.3.1.2 PAH analysis

Since PAHs are organic, the glassware preparation is different from the inorganic procedure detailed above. Glassware was prepared by soaking in a 10% v/v Decon 90 solution (Fisher Scientific) bath for 24 hours. After this, the glassware was removed, rinsed with tap water, followed by acetone (glass distilled grade, Fisher), and placed in a regularly cleaned drying cabinet overnight.

3.3.2 Preparation of road dust, soil, spoil heap, sediment and peat samples before analysis

Samples were removed from their polyethylene bags, weighed tray (OHAUS, Pioneer PA214C) and air-dried at 20°C for ~20 days; the mild drying step allow the volatile contaminants to be retained by the sample during the drying process. Once a stable weight was achieved and noted, samples were then passed through a <2 mm sieve, and homogenised using a mortar and pestle until a fine homogeneous powder was achieved. The sample powder was then transferred to a clean labelled polyethylene bag and stored at room temperature.

3.3.3 Surface water pre-treatment

Samples were removed from the fridge and filtered through a 1 μm filter paper (Fisher Scientific, Whatman cellulose nitrate membrane filter) using a Büchner filter and flask. Using a clean pre-weighed 250 mL beaker, a sub-sample of 200 mL was taken, spiked with 100 μl of concentrated nitric acid (VWR, ARISTAR grade, 69% w/v) and the weight recorded. The beaker contents were reduced in volume to ~20 mL (45-60 min) at a temperature of ~60°C, removed from the hotplate, allowed to cool, and then re-weighed so that a sample concentration factor could be applied. The final solution was transferred to a sterilin tube (Thermo Scientific, Scientific Laboratory Supplies) and placed in a fridge at 4°C. Process blanks (deionised water; 18 MΏ) were prepared along with the surface water samples for quality control purposes. All samples underwent pre-treatment within 24 h of sampling and were analysed within one week.

3.3.4 Porewater extraction and ultrafiltration methodology

3.3.4.1 Porewater extraction

Porewater extracts were isolated by packing a 50 mL polypropylene tube (Fisher Scientific, Fisherbrand) with fresh soil and centrifuging at 8873 x gravity for ~10 min. The supernatant was removed using a plastic syringe (Fisher Scientific, BD Plastiplak) and filtered through a 0.2 μm hydrophilic membrane (VWR, Millex) into a sterilin tube (Thermo Scientific, Scientific Laboratory Supplies) before analysis. Samples were stored in a fridge at 4°C and analysed by ICP-MS within a week.

3.3.4.2 Principles of ultrafiltration

Ultrafiltration uses centrifugal forces to separate colloidal fractions through a semi-permeable membrane present in a cell (Figure 3.11). For the purposes of this study, Vivaspin 20 units (Sartorious) were used in conjunction with a Heraeus Instruments Biofuge Primo centrifuge and the fractionation process results in two samples:

Retentate: found in the top half of the unit and contains colloidal molecules that are too large to pass through the filter (Figure 3.11(a));

Filtrate: found in the lower half of the unit and contains colloidal and/or truly dissolved components of the sample which are small enough to pass through the filter (Figure 3.11(b)).

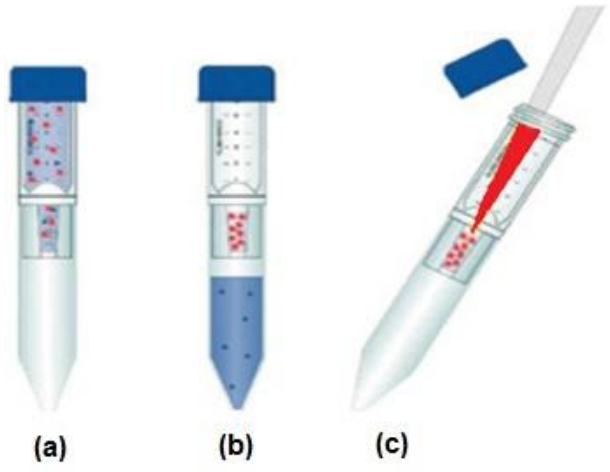

Figure 3.11: Colloidal fractionation using centrifugal ultrafiltration: (a) retentate, (b) filtrate, (c) retentate removal. Adapted from Sartorius, (2015).

The solution containing both colloidal and truly dissolved fractions is determined by the molecular weight cut off (MWCO) value of the membrane. The Vivaspin units used in this study contain a 3 kDa MWCO polyethersulfone membrane to separate colloidal from truly dissolved components of each sample. Although the use of ultrafiltration requires minimal equipment and operator skills, its use to isolate colloidal fractions does have limitations. For example, resulting fractionation may be influenced by the operator and/or equipment used, moreover, colloidal components and truly dissolved phases may overlap the 3 kaDa MWCO resulting in poor fractionation (Graham *et al.,* 2008)

3.3.4.3 Ultrafiltration method

A 20 mL porewater sample was weighed into an ultrafiltration unit (Sartorious, Vivaspin 20), placed in the centrifuge (Heraeus Instruments Biofuge Primo centrifuge) and spun at 6655 x g for 60 minutes. The bottom of ultrafiltration cell was removed, the filtrate was

transferred to a sterilin tube (Thermo Scientific, Scientific Laboratory Supplies) and its weight was recorded. The retentate was weighed and quantitatively removed from the membrane filter into a plastic test tube in two steps. Using a plastic pipette sliced in half at the tip, the retentate was first agitated and gently removed. This was followed by a filter rinse with 1-2 mL of deionised water which was then combined with the initial retentate extract and weighed. Samples were stored in a fridge at 4°C and analysed by ICP-MS within a week.

3.3.5 Gel electrophoresis

3.3.5.1 Principles of gel electrophoresis

Whilst ultrafiltration can be used to isolate the entire colloidal component from a water sample, gel electrophoresis is a technique which can be used to fractionate this component on the basis of size and charge.

As shown in Figure 3.12, flat bed gel electrophoresis consists of a gel bed, e.g. agarose, which is submerged in a low ionic strength buffer solution, e.g. Tris-borate. Platinum electrodes are submerged in the buffer and an electric current is applied, e.g. 20 mA. Charged colloidal components migrate towards either the positive or negative charged terminal depending on their overall charge, size and shape. There are several factors which influence the extent of migration across the gel; (i) concentration of the gel; (ii) the pH, ionic strength and composition of the buffer; and (iii) the applied current and length of the experiment. In general, small and highly charged colloids migrate faster than larger hydrophobic ones. The gel electrophoresis methodology used for this study had been previously published by Graham *et al.* (2008), and provided optimised conditions for electrophoretic separation.

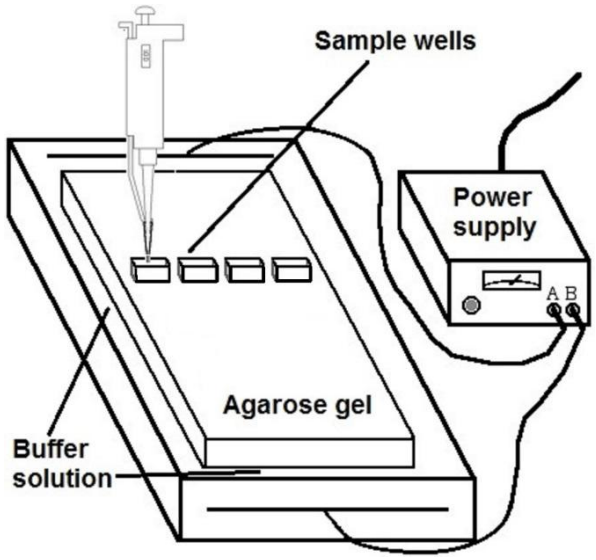

Figure 3.12: Gel electrophoresis diagram.

3.3.5.2 Gel electrophoresis method

A 0.045 mol L^{-1} Tris(trimethylsilyl)borate buffer solution was prepared in a 1 L volumetric flask by dissolving 5.4 g of 2-amino-2-hydroxymethyl-propane-1,3-diol and 2.75 g of orthoboric acid, and diluting to the mark using deionised water. A 1% w/v agarose gel (genetic analysis grade, Fisher Scientific; pore size ca. 100 nm) was prepared using the freshly prepared 0.045 M Tris-borate, and poured into the gel electrophoresis tray (Fisher Gel Electrophoresis tray 13 x 14 x 2 cm, CONSORT E863 power supply), well comb added, and left to solidify for 30 minutes.

The sample well comb was removed and filled with 500 μl of selected porewater retentate, and 0.045 M Tris-borate running buffer solution added to gel electrophoresis reservoir. Electrophoretic separation was achieved using a constant current of 20 mA over a period of 0.5 h. The gel was cut into 0.5 cm sections and placed under a UV light recording any florescence observed. Each 0.5 cm section was labelled and digested on a hotplate with 10 mL of 2 % (v/v) HNO_3 (VWR international Ltd, ARISTAR grade, 69% w/v). The gel dissolves in the acid and the volume was reduced to 0.5–1.0 mL, at which point, it was quantitatively removed by pasteur pipette and made up to approximately 5 mL in a sterilin tube (Thermo Scientific, Scientific Laboratory Supplies). Each batch of samples was

accompanied by process blanks, where gel was prepared using the same reagents and analysed for elemental impurities. The samples were then stored in a fridge at 4°C and analysed by ICP-MS within one week.

3.3.6 UV-visible absorption spectroscopic measurement as a proxy for dissolved organic carbon (DOC) in porewater

Using porewaters extracted from six soil cores sampled at Glendinning Sb mine, a 1 mL aliquot was taken from each depth section and transferred to a 1 cm quartz spectroscopy cell. The porewater absorbance was determined at 252 nm using a Varian 50 SCAN UV-Vis spectrometer set at a path length of 1.0 cm. The amount of dissolved organic carbon present in the porewater solution was directly proportional to the absorbance at this wavelength (Dobbs *et al*., 1972; Banoub, 1973; Farmer *et al*., 2002; Graham *et al*., 2008). The chemical group present in DOC that influences the absorption of UV-visible light is called the chromophore, where electrons present in multiple bond groups such as C=C and C=O are promoted from the ground state, to an excited state, by the absorption of UV-visible light. Providing minimal interference from other chemical components present, e.g. ionic irons, nitrites and nitrates, and in accordance to Beer Lambert Law (Equation 3.1), absorption at 252 nm was used as a proxy for dissolved organic carbon concentration.

Equation 3.1: $$A = \varepsilon \times l \times c$$

A = absorbance of cell
ε = molar absorption coefficient
l = length of path light travelled through a cuvette
c = cell concentration

3.3.7 Soil organic matter content by loss of ignition

Loss on ignition allows the organic content of a dried sample to be calculated by destroying and evaporating the organics present in a sample at high temperature. This is usually expressed as a percentage of total weight. Duplicate ~0.25 g aliquots of homogenised sample (section 3.3.2) were accurately weighed into clean beakers and placed in an oven (Gallenkamp) overnight at 105°C. The beakers were then removed, placed in a desiccator to cool, re-weighed, and then transferred to a muffle furnace (Carbolite) at 450°C for 4 hours. Each beaker position was carefully noted before the furnace was turned on as beaker labelling was also removed during this process. Once cooled, the beakers were removed from the furnace, re-labelled and the ash weighed.

3.3.8 Measurement of pH in surface water, soil, spoil and road dust samples

3.3.8.1 Surface water and porewater samples

No sample preparation was required prior to determining the pH of aqueous samples. Before and after use, the pH meter was calibrated using pH 4 and 7 buffer solutions prepared by dissolving a pH tablet into 100 mL of deionised water (Fisher, pH 4 phthalate buffer tablets; Fisher pH 7 phosphate buffer tablets).

3.3.8.2 Road dust, spoil and soil samples

Samples were prepared by weighing 5 g of homogenised air-dried soil, spoil or road dust solid (section 3.3.2) into a 50 mL centrifuge tube and adding 25 mL of 0.01 mol L^{-1} calcium chloride (Fisher, Laboratory grade reagent >99%). Once the centrifuge cap was securely tightened, the solution was mechanically shaken for 15 minutes (Stuart Scientific) and allowed to stand for 15 minutes. Once the pH probe was calibrated as detailed in section 3.3.8.1, the pH of each sample solution was measured, with a further calibration completed after sample analysis.

3.3.9 Microwave-assisted acid digestion of soil, spoil, road dust, sediment samples

3.3.9.1 Principle of microwave-assisted digestion

The aim of this procedure is to fully dissolve the solid sample via microwave-assisted acid digestion. Samples are suspended in concentrated acid (e.g. nitric/hydrofluoric acids), placed in sealed pressurised vessels and subjected to microwave energy causing an exothermic process under elevated pressure. This results in the dissociation of elements present in the solid phase and their transfer into the acid phase. After appropriate dilution, this permits elemental concentrations to be quantified by Inductively Coupled Plasma-Optical Emission Spectroscopy (ICP-OES) (section 3.3.11), or, Inductively Coupled Plasma-Mass Spectroscopy (ICP-MS) (section 3.3.12). Microwave-assisted digestion has a number of advantages over more conventional digestion methods: (i) sample digestion times are significantly faster; (ii) lower volumes of strong acids are required; (iii) reproducibility is improved; and (iv) and increased safety through the use of sealed sample vessels.

For this study, a CEM Microwave Accelerated Reaction System 6 (MARS6) was used for acid digestion of solid phase samples. This system incorporates a carousel containing 14 HP500 CEM microwave digestion vessels, which includes a reference vessel to monitor real-time pressure and temperature.

3.3.9.2 Microwave procedure

Solid phase samples were completed in duplicate and used the modified US-EPA 3052 method published by Yafa *et al*. (2006). The modification to the US-EPA 3052 method was the inclusion of a loss of ignition step prior to microwave-assisted acid digestion. Approximately 0.25 g of sample was placed in a beaker, oven-dried overnight at 105°C (Gallenkamp), and then ashed by loss of ignition (see section 3.3.7) to remove organic matter. The beaker contents were quantitatively transferred to the microwave digestion vessels using 10 mL of concentrated HNO_3 (VWR international Ltd, ARISTAR grade, 69%

w/v). This was followed by the addition of 1 mL concentrated hydrofluoric acid (Fisher Scientific, Trace metal grade). The microwave digestion vessel lid was put in place and the safety membrane cap was screwed on tightly. The closed vessels were transferred to the microwave carousel ensuring that the reference vessel temperature and pressure probe was fitted. The microwave was set up and operated using the method conditions shown in Table 3.3.

Table 3.3: MARS6 digestion method parameters.

MARS Microwave Parameter Function	Value
Name of standardised method	EPA3052
Power	900W
Initial temperature	20°C
Final temperature	180°C
Temperature ramp duration	6 minutes
Final temperature hold time	9 min
Initial pressure	0 psi
Final pressure	350 psi

Once completed and cooled, the contents were quantitatively transferred to a 100 mL teflon beaker using 2−4 mL of 2% v/v nitric acid (VWR international Ltd, ARISTAR grade, 69% w/v) and reduced on a hotplate (Nickel Electro Ltd, Clifton hotplate) until 1−2 mL remained. The remaining solution was quantitatively transferred to a 25 mL plastic volumetric flask (using 2% v/v nitric acid to wash the beaker), made up to the mark using 2% v/v nitric acid, and filtered through hardened ashless filter paper (Fisher Scientific, Whatman 40) into a labelled sterilin tube (Thermo Scientific, Scientific Laboratory Supplies). Each batch of samples were accompanied by two process blank and two certified reference material samples for quality control purposes (section 3.3.13). Samples were stored in a fridge at 4°C and analysed within a week.

3.3.9.3 Certified reference material (CRM)

The certified reference material used for each microwave-assisted acid digestion sample batch was selected to best match the environmental samples analysed, i.e. a peat reference material was digested along with organic rich soil samples and quantified by ICP-OES (section 3.3.11) and/or ICP-MS (section 3.3.12). The concentrations attained were compared to the certified values to assess the efficiency of the acid digestion of each CRM sample. Certified reference values and digestion efficiency for all CRM materials have been tabulated in section 3.3.13.3 (Tables 3.10-12).

Soil samples: Duplicate peat reference NIMT/UOE/FM/001 (Yafa *et al*., 2004) samples were digested and analysed with each batch of soil and spoil samples.

Sediment samples: Duplicate fresh water sediment reference samples (RTC:CNS392-50G) were digested and analysed with each batch of sediment samples.

Road dust samples: One peat reference material NIMT/UOE/FM/001 (Yafa *et al*., 2004) and one light sandy soil CRM 7002 (Analytika Co, Ltd, Czech Republic) were digested and analysed with each batch of road dust samples.

3.3.10 Sequential extraction

3.3.10.1 Principles of sequential extraction

Whilst many variants of sequential extraction procedures exist (Tessier *et al*., 1979; Ure *et al*., 1993; Hall *et al*., 1996; Maiz *et al*., 2000), the procedure used for this study was the EC Standards, Measurements and Testing Programme (formerly European Communities Bureau (BCR)) three stage and residual process extraction, as detailed by Davidson *et al*. (1998). Sequential extractions can improve the understanding of elemental-solid phase associations within environmental samples such as soil and road dust, and can contribute, amongst other techniques (XANES), to assessing elemental remobilisation from a change in environmental conditions (Bacon and Davidson, 2008; Sutherland, 2010). This involves exposing the sample to a series of specific reagents, collecting each solution extract, and determining

elemental concentrations dissolved in each extract. The first step, termed the acid soluble or exchangeable fraction, is where elemental mobility is potentially the greatest. A mild acetic acid solution is used to dissolve carbonates present in the soil, releasing associated elements that are either, bound to the mineral surface, or present as part of carbonate precipitate, into solution. The second step, which is denoted the reducible fraction, uses hydroxylammonium chloride to dissolve Fe and Mn oxides, along with elements associated with these phases. Whilst elements found in step 2 are not as mobile as step 1, they are considered mobile in terrestrial systems under certain conditions; step 2 simulates naturally occurring redox cycling that often leads to the mobilisation of elements under reducing conditions. The oxidisable fraction is extracted during step 3, and consists of two reagent solutions, hydrogen peroxide to destroy organic matter and oxidises sulfides present, and the addition of ammonium acetate to dissolve all released elements into solution. Elements found in this fraction are generally inaccessible under normal environmental conditions, as adsorption between the elements and organic matter is strong, particularly when compared to steps 1 and 2 (Davidson *et al*., 1998). In addition, a residual digestion is carried out on the remaining sample; here, elements incorporated into mineral structures are dissolved into solution using strong acids, such as aqua-regia (a mixture of concentrated hydrochloric and nitric acids). Elements released in this step are considered to be immobile under most environmental conditions.

Davidson *et al.* (1998) successfully developed and applied this method, and it has subsequently been adopted as a valuable tool to assess the likely elemental mobilisation under changing environmental soil conditions. Whilst the results from sequential extraction procedures are considered to be useful, such methods do have limitations. Lack of specificity in elemental removal, re-adsorption and subsequent redistribution have been identified as fundamental limitations (Davidson *et al*., 1998; Sutherland, 2010). In addition, the range of different reagents used for sequential extracts can vary considerably from the original

method, often causing difficulties for study comparisons. For the purpose of this study, the methodology published by Davidson *et al.* (1998) was used to keep continuity with past studies.

3.3.10.2 Sequential extraction methodology

BCR1: Using a 50 mL polypropylene tube (Fisher Scientific, Fisherbrand), 1 g of air-dried soil was mixed with 40 mL of 0.11 mol L^{-1} acetic acid (Fisher Scientific, laboratory reagent grade). The suspension was mechanically shaken for 16 h (Stuart Scientific) and centrifuged at 6673 x g for 15 mins. The resultant supernatant was filtered through 0.2 µm hydrophilic membrane (VWR international Ltd, Millex) via a plastic syringe (Fisher Scientific, BD Plastiplak), transferred to a sterilin tube (Thermo Scientific, Scientific Laboratory Supplies) and placed in the fridge at 4°C ready for analysis within one week. The remaining soil residue was shaken with 20 mL of distilled water (0.25 h), centrifuged, washings discarded and placed in the fridge at 4°C ready for the next sequential extraction step.

BCR2: Using 0.1 mol L^{-1} hyroxylammonium chloride (Fisher Scientific, laboratory reagent grade), 40 mL was added to the soil residue from step 1, suspension mechanically shaken for 16 h (Stuart Scientific) and centrifuged at 6673 x g for 15 mins. The resultant supernatant was filtered through 0.2 µm hydrophilic membrane (VWR international Ltd, Millex) via a plastic syringe (Fisher Scientific, BD Plastiplak), transferred to a sterilin tube (Thermo Scientific, Scientific Laboratory Supplies) and placed in the fridge at 4°C ready for analysis within one week. The remaining soil residue was shaken with 20 mL of distilled water (0.25 h), centrifuged, washings discarded and placed in the fridge at 4°C ready for the next sequential extraction step.

BCR 3: Using 8.8 mol L^{-1} hydrogen peroxide (Fisher Scientific, laboratory reagent grade), 10 mL was added to the soil residue from step 2, and sample covered and digested at 25°C for 1 h. The volume of the suspended solution was then reduced to 1-2 mL using a water

bath set at 85°C. This step was repeated, followed by the addition of 40 mL of 1.0 mol L^{-1} ammonium acetate (Fisher Scientific, laboratory reagent grade) to the polypropylene tube (Fisher Scientific, Fisherbrand), with the suspension mechanically shaken for 16 h (Stuart Scientific) and centrifuged at 6673 x g for 15 mins. The resultant supernatant was filtered through 0.2 µm hydrophilic membrane (VWR international Ltd, Millex) via a plastic syringe (Fisher Scientific, BD Plastiplak), transferred to a sterilin tube (Thermo Scientific, Scientific Laboratory Supplies) and placed in the fridge at 4°C ready for analysis within one week. The remaining soil residue was shaken with 20 mL of distilled water (0.25 h), centrifuged, washings discarded and placed in the fridge at 4°C ready for the residual step.

Residual: A hotplate digestion was carried out on the remaining sample residue using concentrated aqua regia (3:1 v/v c.HCl:cHNO_3) (VWR international Ltd, NORMATOM trace analysis HCl, 34%, ARISTAR HNO_3 grade, 69% w/v). The remaining sample was transferred to a clean beaker and 30 mL of aqua regia acid was added. A watch glass was placed on the beaker and it was transferred to a hotplate (Nickel ELectro Ltd, Clifton hotplate) to reflux for 2 h. The beaker was removed from the hotplate, quantitatively filtered using hardened ashless filter paper (Fisher Scientific, Whatman 40) and concentrated down to 1-2 mL using the hotplate. Using a 25 mL volumetric flask, the extract was made up to 25 mL using 2% v/v nitric acid (VWR international Ltd, ARISTAR grade, 69% w/v) and stored in a fridge at 4°C ready for analysis within one week. Elemental concentrations were determined by ICP-OES using calibration standards that were match-matched to sample solutions. For quality control purposes, sample reagents were analysed and impurities monitored to allow the blank correction of sample results.

3.3.11 Determination of elemental concentrations in sample digestion solutions by Inductively Coupled Plasma-Optical Emission Spectroscopy (ICP-OES)

3.3.11.1 Principles of ICP-OES

ICP-OES is a technique used to quantify elemental concentrations present in sample solutions by monitoring photon emissions released after atom excitation. The sample solution is introduced to the ICP-OES via a nebuliser, where a fast stream of argon gas converts the liquid to a fine aerosol (Figure 3.13). Only a small amount of this aerosol is transported into the plasma torch where it undergoes desolvation (transfer of solids to gas phase with atomisation). Argon fuel is accelerated in a cyclic movement up the torch inlet tubes through three radio frequency (RF) coils at the top of the torch. This results in the transfer of energy to gas through the collision of atoms (Harris, 1991). The plasma created is extremely hot (typically 6000-10000 K), and relies on argon coolant to protect the quartz torch. The process results in the ionisation of elements present, promoting them to a higher energy state, typically +1 state (Harris, 1991). Once excited, the ions return to their original energy state emitting characteristic photons for each particular ionised element. The wavelength of photons emitted is specific for each individual element, allowing elemental identification to take place. Furthermore, the number of photons emitted, or the intensity of light from this process, is proportional to the concentration present in the sample solution.

The photons released are collected and focused by a concave lens onto a polychromator detector, where it is converted from light to an electrical signal to achieve quantitative results. As ICP-OES can monitor several characteristic photon emissions at once, it allows the best spectra to be selected for quantification avoiding spectra with inferences present. Although ICP-OES may not be as sensitive as ICP-MS, it has good linearity, typically over 4–6 orders of magnitude.

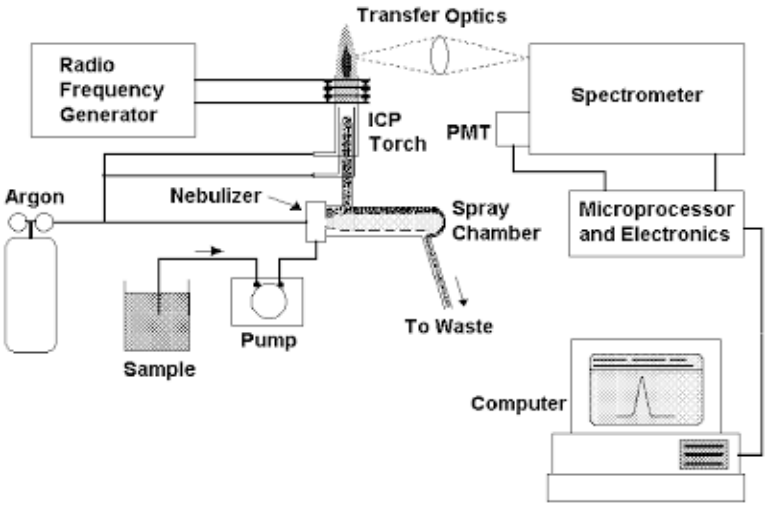

Figure 3.13: Key components of an ICP-OES. Taken from Analytical Instruments (2015).

3.3.11.2 ICP-OES methodology

3.3.11.2.1 Preparation of calibration standards

For each batch of sample solutions, a fresh set of calibration standards were prepared using M4 1000 ppm stock solution (Merck; ICP multielement standard solution IV in nitric acid) and a single element Sb stock solution at a concentration of 1000 ppm (Fisher; Sb solution in hydrochloric acid). Using an adjustable 5 mL and 0.5 mL pipette, calibration working standards were prepared in 2% (v/v) nitric acid (VWR international Ltd, ARISTAR grade, 69% w/v) at the following concentrations: 0.01, 0.1, 1.0, 10, 100, 200, 300 ppm.

For the determination of elemental concentrations found in sequential extraction sample solutions, calibration working standards were matrix-matched, and therefore prepared using 0.11 mol L^{-1} acetic acid, 0.1 mol L^{-1} hyroxylammonium chloride and 1.0 mol L^{-1} ammonium acetate, for sample solutions from fractions BCR1, BCR2 and BCR3, respectively.

3.3.11.2.2 Sample analysis using ICP-OES

The ICP-OES analysis used for this study was a Perkin-Elmer Optima 5300DV fitted with a peristaltic pump, Gem Tip cross-flow nebuliser and Scott-type spray chamber (Table 3.4). The instrument was run in axial mode with argon flow rates for plasma, auxiliary and

nebuliser at 15, 0.2 and 0.8 L min^{-1}, respectively (Table 3.4). The ICP-OES set up and sample processing was run in accordance to the manufacturer's instructions, with selected elements and their emission wavelengths monitored shown in Table 3.5.

Table 3.4: ICP-OES operating conditions.

Parameter		Value
RF power		1400 W
Nebuliser		Gem Tip cross-flow
Spray chamber		Scott-type
Argon Flow	Plasma	15 L min^{-1}
	Auxiliary	0.2 L min^{-1}
	Nebuliser	0.8 L min^{-1}
Pump flow rate		1.5 L min^{-1}
Plasma mode		Axial

Instrument detection limits were calculated by analysing ten blank solutions and adding one standard deviation on the mean (Currie, 1968; Gabriels, 1970). From this, the instrument detection limits were determined and shown in Table 3.5.

Table 3.5: Wavelengths monitored and limit of detection for ICP-OES elemental analysis.

Element	Spectral peak wavelengths (nm)†	Manufacturer's detection (µg L^{-1})*	Limit of detection (µg L^{-1})
As	**228.812**, 188.979, 193.696	2.0	2
Cu	224.700, 327.393, **324.752**	0.4	7
Fe	238.204, **239.562**, 259.939	0.1	8
Pb	**220.353**, 261.418	1.0	5
Sb	**206.836**, 231.146, 217.582	2.0	20
Zn	206.200, **202.548**, 334.501	0.2	16

† Spectral peak wavelengths in bold were used for sample quantification, whilst remaining wavelengths were only used for confirmatory purpose.
* Taken from Perkin Elmer, 2005

3.3.12 Determination of elemental concentrations in sample digestion solutions by Inductively Coupled Plasma-Mass Spectrometry (ICP-MS)

3.3.12.1 Principles of ICP-MS

ICP-MS is a sensitive technique that enables multi-elemental analysis of sample solutions by separating elements based on their mass-to-charge ratio (Taylor, 2001). Similarly to the ICP-OES, it has an inductively coupled plasma torch to introduce the sample into the mass spectrometer (Figure 3.14). Through the use of a peristaltic pump, the sample solution is pumped via the nebuliser where it is converted to an aerosol, atomised by the plasma torch (Taylor, 2001), then immediately ionised via collisions with argon atoms in a Radio Frequency (RF) field. The ICP-MS used for this study had an octapole reaction system installed, which reduced interference by removing unwanted polyatomic ions that formed in the plasma break up, allowing separation to occur by the quadrupole mass analyser.

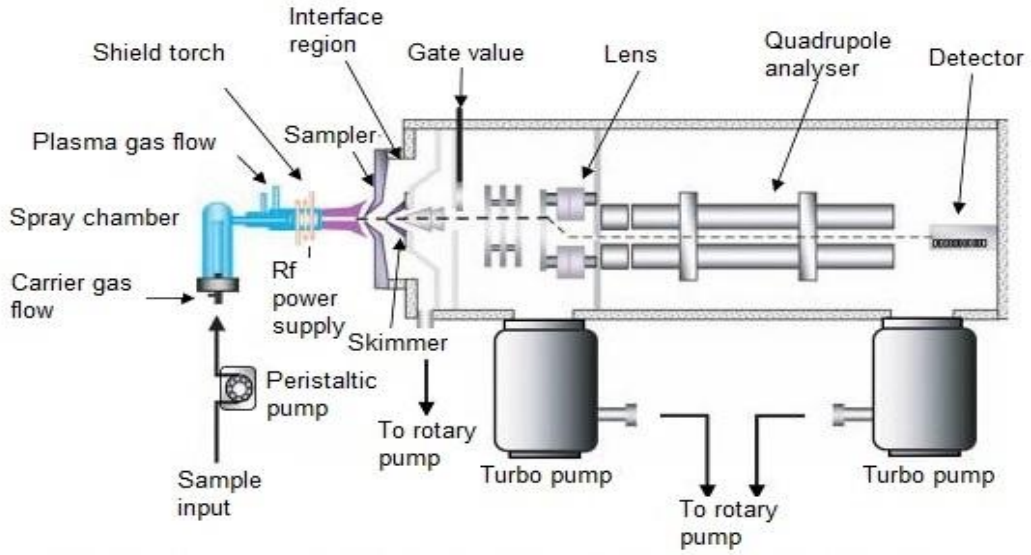

Figure 3.14: ICP-MS schematic and key components, depicted without octapole reaction system (Becker, 2008).

To prevent collisions with gas and interfering molecules, the mass spectrometer is under vacuum, where the sample ions are forced down a series of lenses to focus the ion beam prior to the quadrupole mass analyser. The quadrupole consists of four parallel steel rods that

have a radio frequency (RF) and direct current (DC) applied. Although the ratio of RF and DC remains approximately constant, together, these components vary to allow only the selected ions to progress while eliminating elements of differing atomic mass. The instrument resolution is approximately 1 amu. As the ions exit the mass spectrometer, generally as singular ions, they strike the active surface of the detector called the dynode, which multiplies the signal strength to allow final quantification.

The application of ICP-MS for the quantification of elements in environmental samples brings advantages over conventional ICP-OES. It is easily hyphenated to make more selective instrumentation such as HPLC-ICP-MS, and additionally, can detect elements at very low concentrations (ppt-ppb). The ICP-OES however, has a larger linear response range, as the ICP-MS is ~4 orders of magnitude.

3.3.12.2 ICP-MS methodology

3.3.12.2.1 Preparation of calibration standards

Calibration standards were prepared similarly to those in section 3.3.11.2.1. Since elemental concentrations determined using ICP-MS were lower than those of the ICP-OES, additional dilutions were required on stock solutions to reflect the lower concentrations quantified. Using M6 10 ppm stock solution (Merck, ICP multielement standard solution VI in nitric acid) and a single element Sb stock solution at a concentration of 1000 ppm (Fisher; Sb solution in hydrochloric acid), calibration working standards were prepared in 2% (v/v) nitric acid (VWR international Ltd, ARISTAR grade, 69% w/v) at the following concentrations: 0.1, 0.5, 1.0, 5, 10, 50, 100, 500, 1000 ppb.

3.3.12.2.2 Sample analysis using ICP-MS

The ICP-MS used for this study was an Agilent 7500ce quadrupole mass analyser fitted with Ni cones, a micro mist nebuliser, Scott-type spray glass chamber (Table 3.6) and a standard Agilent octapole reaction system.

Detection limits were calculated similarly to the ICP-OES outlined in section 3.3.11.2.2, and are given in Table 3.7.

Table 3.5: ICP-MS operating conditions.

Instrument	Parameter
RF power	1540 W
Reflected power	1 W
Argon gas carrier flow	0.82 L min^{-1}
Argon gas make-up flow	0.21 L min^{-1}
Nebuliser type	Micro mist
Nebuliser up-take rate	0.02 mL min^{-1}
Analyser pressure (Vacuum)	$3x10^{-6}$ Pa
Spray chamber	Glass Scott-type
IF/BK pressure (vacuum)	$8.5x10^{-1}$ Pa
Rinse speed (rinse vial)	0.3 rps
Between sample rinse time, rinse vial	40 seconds
Rinse speed	0.1 rps

Table 3.7: ICP-MS elemental detection limits.

Element	Amu monitored	Limit of detection (µg L^{-1})
As	75	0.001
Cu	63	0.003
Cd	111	0.001
Fe	56	0.2
Pb	208	0.002
Sb	121	0.0002
Zn	66	0.01

3.3.12.3 ICP-MS methodology for Pb isotope ratio analysis

Using the ICP-MS and instrument conditions detailed in section 3.3.12.2 the determination of Pb isotope ratios ($^{206}Pb/^{207}Pb$, $^{208}Pb/^{206}Pb$ and $^{208}Pb/^{207}Pb$) were completed using the

isotope analysis acquisition mode. Five data points at integration times of 2 s per point for ^{206}Pb and ^{207}Pb, and 1 s per point for ^{208}Pb were taken.

Where necessary, samples were diluted to fall within the ICP-MS pulsed dynamic range (5 - 30 μg L^{-1}), and isotopic standards (0.1-50.0 μg L^{-1}) were prepared using certified reference material, NIST SRM 981, to correct for mass bias.

3.3.13 Quality control

With every batch of samples run on the ICP-OES and ICP-MS, calibration drift standards were prepared similarly to instrument calibration standards and run at frequent intervals throughout analysis; a minimum of 1 in every 10 samples. These were monitored to assess the integrity of the instrument calibration for each element, where, in the event of excessive instrument calibration drift, instrument maintenance was carried out and samples re-run. In addition, independent checks on the calibration standard concentrations were carried out using certified stock solutions and standard reference materials (SRM) sourced from different stocks to those used for the calibration standards.

3.3.13.1 ICP-OES

This section gives detail on the instrument quality control data for ICP-OES analysis. All quantification was completed using calibration graphs where the R^2 coefficients were greater than 0.995.

Table 3.8: ICP-OES independent check standard results.

Element	ICP M6 certified value (mg L^{-1})	N	Mean instrument concentration (mg L^{-1})	S.D. (mg L^{-1})	% RSD
As	10.0	12	10.8	0.08	7.41
Cu	1.00	14	1.00	0.07	7.05
Fe	10.0	14	9.82	0.58	5.93
Pb	1.00	14	0.97	0.08	7.99
Zn	10.0	14	10.01	0.89	8.86

Mean concentrations for independent check standards (Table 3.8) were in good agreement with the certified values. The %RSD was typically <10%, and there was generally good agreement between mean and certified values.

Table 3.9: ICP-OES national Institute of Standards and Technology (NIST) Standard Reference Material (SRM) 1643e Trace Elements in Water results

Element	NIST certified reference value (µg L^{-1})	N	Mean instrument concentration (µg L^{-1})	S.D. (mg L^{-1})	% RSD
Cu	22.7	8	21.7	1.00	4.63
Fe	98.1	9	100	6.14	6.13
Pb	19.6	8	20.7	2.56	12.3
Sb	58.3	6	57.5	3.14	5.46
Zn	78.5	9	72.7	4.51	6.13

With the exception of Zn, where mean concentrations were 5.8 mg L^{-1} lower than the certified reference value, all other elemental mean concentrations for NIST SRM 1643e were in good agreement, and generally within 1 µg L^{-1} (Table 3.9). As the %RSD for Zn was acceptable and showed consistent results, Zn concentrations obtained were only used providing further quality control checks were passed e.g. independent check standards and certified reference material. Although the %RSD was typically low (<7%), the Pb value was higher than expected at 12.3%. Taking this into account, all Pb data was acquired from ICP-MS analysis.

3.3.13.2 ICP-MS

This section gives detail of the instrument quality control data for ICP-MS analysis. All quantification was completed using calibration graphs where the R^2 coefficients were greater than 0.995. The certified reference solutions for ICP-MS analysis were NIST SRM 1643e and 1640a solutions.

Table 3.10: ICP-MS National Institute of Standards and Technology (NIST) Standard Reference Material (SRM) 1643e Trace Elements in Water results.

Element	NIST certified reference value (µg L^{-1})	N	Mean instrument concentration (µg L^{-1})	S.D. (mg L^{-1})	% RSD
As	64.3	11	59.8	4.1	6.89
Cu	22.7	10	23.0	2.46	10.5
Pb	19.6	10	20.3	1.05	5.17
Sb	58.3	10	53.6	1.97	3.67
Zn	78.5	10	78.2	3.15	9.40

For NIST SRM 1643e (Table 3.10), mean instrument concentrations were generally in good agreement with the certified reference values (within 5 µg L^{-1}). The %RSD for As, Pb and Sb showed little variation, while %RSD for Cu and Zn was greater.

Table 3.11: ICP-MS National Institute of Standards and Technology (NIST) Standard Reference Material (SRM) 1640a Trace Elements in Water results.

Element	NIST certified reference value (µg L^{-1})	N	Mean instrument concentration (µg L^{-1})	S.D. (mg L^{-1})	% RSD
Cu	85.1	4	92.8	5.14	5.54
Pb	12.0	7	10.4	0.46	4.47
Sb	5.06	7	4.99	0.43	9.10

For NIST SRM 1640a (Table 3.11), mean instrument concentrations for Cu were 7.7 µg L^{-1} higher than the certified reference values. Acceptable agreement was observed for mean concentrations of Pb and Sb when compared to the reference value. The %RSD for Cu, Pb and Sb was reasonable at <10%. The use of NIST SRM 1640a as a quality control check was limited, and was only used in the absence of NIST SRM 1643e (Table 3.10). The low number of data points obtained for Cu using the NIST SRM 1640a may account for the differences observed between mean and reference concentrations.

3.3.13.3 Certified reference material

This section details results obtained from three CRMs that were present in each sample batch of analysis. Although CRMs were selected to match the environmental samples analysed, the certification of elements present in the CRM was also considered (section 3.3.9.3).

Table 3.12: NIMT/UoE/FM/001 Peat certified reference material results.

Element	Certified reference Value (mg kg $^{-1}$)	S.D. (mg kg $^{-1}$)	N	Mean (mg kg $^{-1}$)	S.D. (mg kg $^{-1}$)	%RSD
As	3.63	0.58	18	2.64	0.62	23.7
Cu	5.28	1.04	50	5.24	0.80	15.2
Fe	839	84.0	28	835	104	12.4
Mn	7.52	0.41	18	7.27	1.01	13.9
Pb	174	8.00	50	175	19.3	11.0
Sb*	2.37	0.34	50	2.13	0.39	18.1
Ti	357	18.0	10	341	27.4	8.00
Zn	28.6	1.90	50	29.0	5.75	19.8

*information only

Whilst As mean concentration results fell comfortably within 2 S.D. of the NIMT/UoE/FM/001 peat reference material, all other elemental concentrations fell within 1 S.D. of the certified reference value (Table 3.12). The data showed good precision and accuracy, and gave good reliable analytical results reported for this study. As the number of data points obtained for NIMT/UoE/FM/001 peat reference material was much greater than other certified reference materials used for this study, the elemental variation observed for the peat reference material was greater. In addition, the data points collected for NIMT/UoE/FM/001 peat reference material was collected over a three year period, which would incorporate other sources of variation not observed in reference material collected over a shorter period of time. For example, the replacement of ICP-MS parts such as the

detector can influence instrument sensitivity and performance, as well as annual maintenance on mass spectrometer components such as ion lens and quadrupoles.

Table 3.13: CNS392-50G Freshwater sediment certified reference material results.

Element	Certified reference Value (mg kg $^{-1}$)	S.D. (mg kg $^{-1}$)	N	Mean (mg kg $^{-1}$)	S.D. (mg kg $^{-1}$)	%RSD
As	6.5	3.21	8	10.7	0.79	7.85
Cu	146	6.30	8	142	4.26	2.99
Fe	7880	867	8	6590	334	5.06
Pb	121	8.17	8	135	8.31	6.14
Mn	6604	679	6	3602	344	9.55
Sb	12.0	3.17	24	14.8	1.16	7.85
Zn	81.7	6.63	8	71.3	1.71	2.4

The results observed from the analysis of CNS392-50G showed that Cu and Sb were all within 1 S.D., whilst As, Fe, Pb and Zn were within 2 S.D. of the certified reference values (Table 3.13). Concentrations of Mn were outwith 2 S.D. of the certified reference value, and were used for indication only. With the exception of Mn, these values are considered to be good. Variation was acceptable, with S.D. and %RSD below 8.3 mg kg $^{-1}$ and 7.85%, respectively.

Table 3.14: Czech Metrology Institute (CMI) 7002 Sandy loam certified reference material results.

Element	Certified reference Value (mg kg $^{-1}$)	S.D. (mg kg $^{-1}$)	N	Mean (mg kg $^{-1}$)	S.D. (mg kg $^{-1}$)	%RSD
Cu	29.3	0.6	10	29.1	1.2	4.3
Pb	58.9	4.9	10	63.9	6.2	9.7
Zn	69.0	7.7	10	71.0	17.7	26.4

Mean concentrations of Cu, Pb and Zn were in good agreement with the certified values assigned to reference material CMI 7002. The %RSD for Cu and Pb showed little variation, whilst Zn showed considerable more variation where a %RSD of 26.4 was observed.

3.3.13.4 Pb isotope ratio quality control

To ensure reliable Pb isotope ratio results, ICP-MSTop software was configured to perform five replicate measurements of each Pb isotope present in the standard or sample solution. This provided a Pb isotope mean value (n=5), and allowed instrument performance to be assessed for drift in isotopic abundances and ratios. Variation across the five data points were typically ± 0.1%, 0.1% and ± 0.05%, for $^{206}Pb/^{207}Pb$, $^{208}Pb/^{206}Pb$ and $^{208}Pb/^{207}Pb$ respectively.

The determination of Pb isotopic ratios were completed using a series of standards by diluting the certified reference material NIST SRM 981 to concentrations of 1, 5, 10 and 20 µg L^{-1}. The prepared standards were run before, and after, each sample batch to assess isotopic ratio measurements that may have suffered mass bias effects from instrument drift. Lead concentration standards were also run alongside isotope ratio standards. In addition, a 10 µg L^{-1} NIST SRM 981 standard was used periodically to bracket every five samples throughout an analysis batch, and were always proceeded by a rinse sample of 2% (v/v) ARISTAR nitric acidic to prevent carry-over contamination. By monitoring isotopic ratios throughout a sample batch, drift corrections could be made where instrument performance had deteriorated throughout the run, i.e. loss in sensitivity. Where standards prepared from the certified reference material NIST SRM 981 had indicated Pb isotope ratios had drifted during a sample batch, the samples analysed after the last acceptable 10 µg L^{-1} NIST SRM 981 standard were repeated.

3.3.14 Determination of Sb speciation in porewaters using High Performance Liquid Chromatography−Inductively Coupled Plasma-Mass Spectroscopy (HPLC-ICP-MS)

This section gives the analytical detail for the quantification of Sb(V) and Sb(III), but a full account of the underlying theory, method development carried out, and the consideration and implementation of quality control is given in Chapter 4.

On return to the laboratory after fieldwork, an Atmosbag (Sigma Aldrich), was purged three times with nitrogen (N) to remove O, and the helium-filled sample bags were placed in it (section 3.2.3.2.4). Once filled and sealed with N, the soils were removed from their sample bags, packed into 50 mL polypropylene tubes (Fisher Scientific, Fisherbrand), which were then capped and taped securely. The tubes were then removed from the atmos bag, centrifuged at 8873 x g for ~10 min, and returned to the Atmosbag which was again purged with N. Once in a sealed N atmosphere, the soil porewaters were removed from the 50 mL polypropylene tubes via plastic syringe (Fisher Scientific, BD Plastiplak). These were filtered through 0.2 μm hydrophilic membrane (VWR, Millex) into sterilin tubes (Thermo Scientific, Scientific Laboratory Supplies), and were capped and taped before being stored at 4°C, ready for analysis within 24 hours.

Prior to HPLC-ICP-MS analysis, fresh Sb(III) and Sb(V) standards were prepared from potassium antimonyl tartrate trihydrate ($C_8H_{14}K_2O_{12}Sb_2$) and potassium hexahydroxyantimonate ($KSb(OH)_6$, respectively, giving stock solutions of 1000 ppm. The diluent used for Sb(III) was nitrogen-purged HPLC mobile phase; 20 mol L^{-1} EDTA / 1 mol L^{-1} phthalic acid, whilst limited solubility of Sb(V) in the HPLC mobile required the use of N-purged deionised water instead.

For the Sb(III) stock solution, 0.2748 g potassium antimonyl tartrate trihydrate, was weighed into a polyethylene volumetric flask and diluted to the mark using N-purged HPLC mobile phase to give a final concentration of 1000 ppm. A secondary Sb(III) standard was prepared

by pipetting 100 µl of Sb(III) stock solution, into a 100 mL polyethylene volumetric flask, and diluting to the mark using HPLC mobile phase to give a standard concentration of 1 ppm. For the Sb(V) stock solution, 0.2159 g of potassium hexahydroxyantimonate was weighed into a polyethylene volumetric flask and diluted to the mark using N-purged deionised water to give a final concentration of 1000 ppm. A secondary Sb(V) standard was prepared by pipetting 100 µl of Sb(V) stock solution into a 100 mL polyethylene volumetric flask, and diluting to the mark using HPLC mobile phase to give a standard concentration of 1 ppm. Calibration standards were prepared in 25 mL polyethylene volumetric flasks using the volumes detailed in Table 3.15, and diluted to the mark using N-purged HPLC mobile phase. Standards and soil porewater samples were transferred to 1 mL glass amber vials by pasteur pipette and analysed under the conditions given in Table 3.14.

Table 3.15:HPLC-ICP-MS Sb speciation calibration working standard concentration range.

	0 ppb	**15 ppb**	**25 ppb**	**50 ppb**	**75 ppb**	**100 ppb**
Volume of secondary Sb(III) and Sb(V) to dispense (µl) into 25 mL volumetric flask	0	375	625	1250	1875	2500

Table 3.16: HPLC-ICP-MS Sb speciation instrument conditions.

HPLC	Agilent 1200
Injection conditions	100 µl injection/sample loop with PEEK tubing
Anion exchange columns	Hamilton PRP-X100 (150 X 4.6 mm, 10 µm)
Mobile Phase	20 mmol L^{-1} EDTA + 1 mmol L^{-1} phthalic acid
Pump Pressure	50 bar
pH Target	pH 4.5 ± 0.5
Gradient Program	Isocratic
Flow rate	1.0 L min^{-1}
Temperature	25°C
ICP-MS	Agilent 7500ce
RF Power	1540 W
Plasma gas flow	15 L min^{-1}
Reflected power	1 W
Argon gas carrier flow	0.82 L min^{-1}
Argon gas make-up flow	0.21 L min^{-1}
Nebuliser type	Micro mist
Nebuliser gas flow	1.1-1.4 L min^{-1}
Ions monitored	121 Sb , 123 Sb

The ICP-MS instrument count obtained for Sb(III) and (V) calibration working standards were plotted using Microsoft Excel, and gave calibration graphs where R^2 coefficients were typically greater than 0.995. Using the instrument count obtained for Sb(III) and (V) soil porewater samples, concentrations were obtained using the calibration graph and the straight line equation y=mx+c (further details are given in section 4.4.2.2).

3.3.15 X-ray diffraction spectroscopy

The principle of XRD analysis is based on targeting an X-ray beam onto a sample and detecting the emission of scattered waves. The diffraction that occurs is described by Bragg's law (Figure 3.15), where at an atomic level, the X-ray beam is uniquely diffracted, with the diffraction intensities dependent on the abundance of the atom. This allows the identification of crystalline minerals and concentrations present at quantitative / qualitative level.

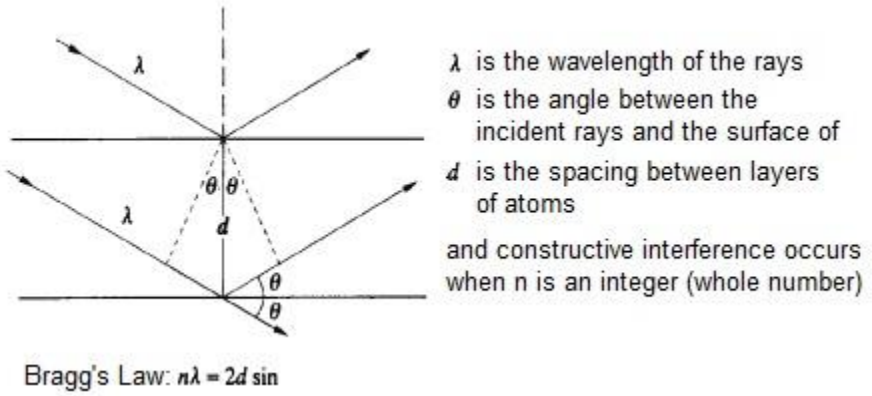

Figure 3.15: Bragg's law. Adapted from Meyers, (2003).

For Edinburgh road dust samples prepared in section 3.3.2, samples were ground to <125 μm by mortar and pestle and analysed by a Bruker D8-Advance X-ray Diffractometer (Bruker, Coventry, UK), employing a Cu-anode X-ray tube set at 40 KeV with a tube current of 40 mA. The samples were scanned in 2Θ from 2 - 60° at a scan step of 0.01°, with instrument detection limits of 1 mg kg $^{-1}$ attained. The data acquired by the NaI detector was processed using Bruker Diffrac.EVA software in conjunction with International Centre for Diffraction Data (ICDD) database.

3.3.16 Scanning electron microscope-energy dispersive spectroscopy (SEM-EDX)

SEM-EDX is a technique that allows elemental concentrations and morphology to be acquired on a micro-to-nanometre scale by using a high energy electron beam under vacuum. The interaction of the electron beam on the sample surface results in the emission of electromagnetic radiation in the form of low energy secondary electrons, backscattered electrons and X-rays. Both the low energy secondary and backscattered electrons are used for SEM, where the signal from low energy secondary electrons emitted is converted to an image giving detail on the surface topography, while heavier elements backscatter more efficiently and thus appear brighter than lighter elements. The emission of X-rays from the sample surface is used to gain the spectral abundance of elements found at each selected site. The EDX monitors the energy and intensity of each element specific X-ray emitted by electron shell-to-shell transitions; this allows information about elemental composition to be acquired.

Approximately 0.001g of Edinburgh road dust previously ground to <125 μm (section 3.3.15) was placed on a sticky aluminium tab and coated with a gold/palladium alloy using a Polaron SC7640 high resolution sputter coater. Using a Philips/FEI XL30 ESEM (Philips Innovation Services, Eindhoven, Netherlands) with Oxford Instruments INCA Energy 250 EDX system (Oxford Instruments NanoAnalysis, Buckinghamshire, UK), samples were analysed by tungsten filament at an acceleration voltage of 25 keV under a vacuum pressure of 3.0 $x10^{-5}$ bar. Road dust surface images were acquired by manual scanning, where regions of interest were identified and magnified in the range of 10x - 40,000x.

3.3.17 Gamma spectroscopy ^{210}Pb dating of sediment and peat samples

3.3.17.1 Principles of gamma spectroscopy

Gamma spectroscopy is used to detect and quantify the emission of γ rays caused by the radioactive decay of a gamma emitting parent radionuclide. The instability of a parent radionuclide results in the emission of radioactive energy to a stable lower energy state. This process is specific, and characteristic γ rays emitted from a particular decay series can be monitored, enabling the identification of the original parent radionuclide to take place.

For this study, the decay series of ^{238}U was used for dating the peat and sediment core using one of the decay intermediates, ^{210}Pb. ^{238}U is a naturally occurring crustal radioisotope, and its radioactive decay results in the emission of ^{222}Rn, a gaseous daughter nuclide. The physical state of ^{222}Rn is of particular importance as it naturally occurs in gaseous form. Consequently, it escapes to the atmosphere through a number of short half-life intermediaries, decaying to ^{210}Pb. The ^{210}Pb may be deposited directly onto soil and plants, or indirectly, through its adsorption onto particulate matter present in air and surface water with its eventual deposition onto soil and sediment. For direct and indirect deposition, radioactive decay and burial of ^{210}Pb will result in a vertical distribution of ^{210}Pb, where ^{210}Pb concentrations decrease exponentially with depth (assuming accumulation occurs at a constant rate) (MacKenzie *et al*., 2011). This provides a deposition distribution through time, where it is known as the "unsupported" form of ^{210}Pb. Conversely, the "supported" form of ^{210}Pb relates to the background concentrations of ^{238}U minerals in soil that have decayed, and will continue to do so, to give ^{210}Pb. If soil composition remains constant throughout a core, supported ^{210}Pb generally remains constant through depth. In practice, total ^{210}Pb activities are measured and the unsupported component calculated by subtraction of the measured supported component. The quantification of both total ^{210}Pb and the supported component (estimated by measurement of the ^{226}Ra activity from daughters ^{214}Pb and ^{214}Bi) require the

use of a high purity germanium (Ge) gamma photon detector monitoring the following isotopes at the following energies of 46.5 keV for ^{210}Pb, 295 and 352 keV for ^{214}Pb, and 609 keV for ^{214}Bi.

Two models can be applied to the unsupported ^{210}Pb data for the purpose of ^{210}Pb dating. The first of which is the Constant Initial Concentration (CIC) model, which assumes that soil and sediment has a constant accumulation rate of "unsupported" ^{210}Pb (Robbins, 1975). The second model, Constant Rate of Supply (CRS), assumes a constant ^{210}Pb flux but allows for a variable sedimentation rate, improving the accuracy of ^{210}Pb dating (Appleby and Oldfield, 1978). For CIC and CRS models to be applied correctly, they assume a constant rate of supply of unsupported ^{210}Pb occurs, and that accumulation is not affected by post deposition mobility, mixing, or anthropogenic activities such as the production of fertilisers (Carvalho, 1995).

For the purpose of this thesis, all ^{210}Pb dating was taken from previous studies (Farmer *et al*., 1997, 2015) and unpublished work from the University of Edinburgh, Geosciences. No dating was specifically undertaken for this PhD and is included for information only. All studies used the CRS model for ^{210}Pb dating (Equation 3.2).

Equation 3.2: $$t = \frac{1}{\lambda} \ln \frac{I_t}{I_i}$$

where:

t	= age (y) of ith layer
I_t	= total inventory of unsupported ^{210}Pb (Bq m^{-2})
I_i	= inventory of unsupported ^{210}Pb below the ith layer (Bq m^{-2}) and
λ	= ^{210}Pb decay constant (y^{-1}).

3.3.17.2 Gamma spectroscopy methodology

Gamma spectroscopy was used to provide the unsupported ^{210}Pb date which was used to date two sediment cores and two peat cores detailed in Table 3.17. Sub-samples weighing 5 g, 10 g, 15 g or 20 g of each dried homogenised sediment or peat depth section were taken, weight recorded and pressed into 4 cm diameter disk using a hydraulic press and stainless steel template block. Each disk was placed into a 5 cm diameter transparent plastic container, and sealed with an epoxy adhesive resin. The sealed containers were left for ~3 weeks prior to analysis, allowing internal atmospheric radon to reach equilibrium. For quality control, detection efficiencies were established using standards prepared by adding known activities of the radionuclides of interest from certified radionuclide standard solutions, such as ^{210}Pb (Amersham primary standard solution), ^{214}Pb and ^{214}Bi (Harwell primary standard solution), to peat of an age that no unsupported ^{210}Pb or anthropogenic radionuclides were present. The geometry of each peat gamma reference standard was closely matched to the geometry of the unknown samples analysed, i.e. 20 g standard was used for a 20 g sample. The peat gamma reference standards were analysed at the start and/or end of each sample batch, and results processed at SUERC.

Table 3.17: List of dated sediment and peat cores used for this study

Location	Dated core matrix	Core sampler	Length of core sampled (cm)	Depth section interval (cm)	Dated by
Loch Tay	Sediment	Mini-Mackereth	90	1	Farmer *et al.* (1997)
Loch Tay	Sediment	Jenkin	19	1	Farmer *et al.* (1997)
Great Moss	Peat	Monolith tin	50	2	Farmer *et al.* (2015)
Auchencorth Moss	Peat	Monolith tin	38	2	University of Edinburgh (SUERC, 2013)

The detectors used for gamma spectroscopy were low background, co-axial n-type high purity Ge gamma photon detectors (Tennelec and Ortec). Background count rates were reduced by housing the detector in a 10 cm Pb shield with a Cd-Cu lining to reduce X-ray background. The detector itself was also placed on 10 cm of Pb to further reduce background. Specific activities were determined using EG & G Ortec multichannel buffer and analysis software, with further manual calculation (Equation 3.2). Analysis times of up to 168 hours were used to obtain counting statistics uncertainties of less than 5%. As the CRS model was used for dating all sediment and peat cores for this study, the specific activities of ^{210}Pb at 46.5 keV was counted, as well as ^{214}Pb at 295 and 352 keV and ^{214}Bi at 609 keV since these were adopted as proxies for supported ^{210}Pb activity.

3.4 The Soxhlet extraction of 16 Polycyclic Aromatic Hydrocarbons (PAHs) from road dust samples

3.4.1 Soxhlet extraction

PAHs can be extracted from solid phase samples using a number of different techniques, such as accelerated solvent extraction, microwave and Soxhlet extraction. Whilst Soxhlet extraction is more time intensive, it is easier to use than the other techniques, and in addition, has no reliance on instrument availability and operation. The extraction process is based on the continual reflux of an organic solvent through a solid phase sample; solvent is heated, evaporated and then condensed. For this instance, the molecular structure of PAHs, which consists of C and H, have a greater affinity for the polarity of the solvent (also containing C and H), which results in their removal from the solid phase to the refluxed solvent phase.

Prior to extraction, cellulose extraction thimbles (Whatman, Fisher) were pre-cleaned to remove possible interferences by refluxing 120 mL of 2:1 hexane:acetone mixture (HPLC grade, Fisher) for 6 hours. A 3 g sub-sample of air-dried road dust (section 3.3.2) was weighed into a pre-cleaned cellulose thimble and placed into a Soxhlet extractor. Approximately 120 mL of 2:1 hexane:acetone mixture was added to the round bottom flask,

placed on the heating mantle, connected to the Soxhlet extractor and a water-cooled condenser, and refluxed for 12 hours overnight.

The solvent extract was concentrated down to 1-2 mL via a rotatory evaporator and cleaned-up using a 6 g 10% w/w deactivated alumina adsorption chromatography column (MERCK 1097, standardised (Activity II-III) particle size 0.063-0.200 mm, VWR) and eluted with 60 mL of hexane (HPLC grade, Fisher). The eluent was collected and concentrated down to 1-2 mL via a rotatory evaporator. The process was then repeated but using a 3 g silica gel chromatography column (0.035-0.070 mm, 60A, Fisher) and eluted with 60 mL of hexane (HPLC grade, Fisher). Before every sample concentration step, 2 mL of toluene (HPLC grade, Fisher) was added as a keeper to minimise PAH loss through evaporation. The samples were then spiked with 100 µl of 1 mg L^{-1} p-terphenyl internal standard and stored in a fridge at 4°C, ready for GC-MS analysis.

3.4.2 The determination of 16 PAHs using Gas Chromatography-Mass Spectrometry (GC-MS)

3.4.2.1 Principles of GC-MS

The sample extract is injected into the gas chromatograph where it is volatilised and swept down the capillary column by the helium (He) carrier gas; separation occurs based on the compounds affinity for the stationary phase (typically a DB-5) and its boiling point. The separation is necessary to eliminate organic interferences that may affect the final quantification, and where present, separate molecular isomers, e.g. phenanthrene and anthracene, before they enter the mass spectrometer. Upon exit from the capillary column, the gaseous mixture is bombarded with high energy electrons resulting in the fragmentation of PAH molecules. The fragments are then repelled down the mass spectrometer where they are separated based on their mass-to-charge ratio. This results in a small electrical signal which is collected and amplified by the photomultiplier tube. The selectivity of GC-MS analysis enables most interferences to be removed from final quantification, particularly in

Selective Ion Monitoring (SIM) mode, where only specific mass fragments related to PAHs were collected.

3.4.2.2 GC-MS methodology

3.4.2.2.1 Preparation of instrument standards

Prior to GC-MS analysis, PAH calibration, independent and internal standards were prepared using volumes and concentrations detailed in Table 3.18, 3.19 and 3.20, respectively. The preparation of standards was a two stage process, where volumes were dispensed using calibrated automatic pipettes and diluted with solvent in a 10 mL volumetric flask. Each standard was stored at 4°C and used within a three month duration.

Table 3.18: Standard dilution and volumes for the preparation of PAH calibration standard from a custom mix stock solution.

Compound	Supplier of compound	Concentration of custom mix primary standard ($mg\ L^{-1}$)	Volume of primary standard required 10 mL (µL)	Concentration of secondary standard ($mg\ L^{-1}$)
Naphthalene	Accu-Standard	500	1000	50
Acenaphthylene		500	1000	50
Acenaphthene		500	1000	50
Fluorene		500	1000	50
Phenanthrene		500	1000	50
Anthracene		500	1000	50
Fluoranthene		500	1000	50
Pyrene		500	1000	50
Benzo (a) anthracene		500	1000	50
Chrysene		500	1000	50
Benzo (b) fluoranthene		500	1000	50
Benzo (k) fluoranthene		500	1000	50
Benzo (a) pyrene		500	1000	50
Indeno (1,2,3-cd) pyrene		500	1000	50
Dibenzo (a,h) anthracene		500	1000	50
Benzo (g,h,I) perylene		500	1000	50

Calibration standards were prepared by taking 1000 µl of 500 mg L^{-1} Accustandard custom mix solution and dispensing into a 10 mL volumetric flask, and diluting to the mark with toluene (HPLC grade, Fisher).

Table 3.19: Standard dilution and volumes for the preparation of PAH independent standard from individual solid stocks.

Compound	Supplier of individual compound	Weight of solid stock used (g)	Primary standard concentration in 10 mL (mg L^{-1})	Volume of primary standard required in 10 mL (µL)	Secondary standard concentration in (mg L^{-1})
Naphthalene	Greyhound	0.00285	285	351	10
Acenaphthylene	Greyhound	0.00295	295	339	10
Acenaphthene	Greyhound	0.00255	255	392	10
Fluorene	Greyhound	0.00305	305	328	10
Phenanthrene	QmX	0.00265	265	377	10
Anthracene	QmX	0.00275	275	364	10
Fluoranthene	Greyhound	0.00255	255	392	10
Pyrene	Greyhound	0.00250	250	400	10
Benzo (a) Anthracene	Greyhound	0.00280	280	357	10
Chrysene	Greyhound	0.00235	235	426	10
Benzo (b) Fluoranthene	QmX	0.00270	270	370	10
Benzo (k) Fluoranthene	Greyhound	0.00260	260	385	10
Benzo (a) Pyrene	Greyhound	0.00300	300	333	10
Indeno (1,2,3-cd) Pyrene	Greyhound	0.00230	230	435	10
Dibenzo (a,h) Anthracene	Greyhound	0.00255	255	392	10
Benzo (g,h,I) Perylene	QmX	0.00250	250	400	10

Independent standards were prepared by weighing out approximately 0.0025 g of PAH solid stock material into a 10 mL volumetric flask and diluting to the mark with methanol (HPLC grade, Fisher). This gave a primary standard concentration of approximately 250 mg L^{-1}

(Table 3.18). Approximately 400 µl was then dispensed into a 10 mL volumetric flask, and made up to the mark using toluene (HPLC grade, Fisher). This gave a secondary standard concentration of 10 mg L^{-1} (Table 3.19). The internal standard was similarly prepared (Table 3.20).

Table 3.20: Standard dilution and volumes for the preparation of PAH internal standard from individual solid stocks.

Compound	Supplier of individual compound	Weight of solid stock used (g)	Primary standard concentration in 10 mL (mg L^{-1})	Volume of primary standard required in 10 mL (µL)	Secondary standard concentration in (mg L^{-1})
P-Terphenyl	Sigma-Aldrich	0.00285	285	351	10

Calibration working standards were prepared in 2 mL glass amber vials using the calibration and internal standards, quantitative syringes and the volumes detailed in Table 3.21. Each standard had a total volume of 1 mL and was screw-capped and sealed with a PTFE septum.

Table 3.21: Preparation volumes for calibration working standards for GC-MS quantification.

Concentration (mg L^{-1})	0	0.1*	0.5*	1.0*	5.0	10	30
Calibration standard used	n/a	3°	3°	3°	2°	2°	2°
Amount of secondary calibration standard to dispense (µl)	0	20	100	200	100	200	600
Volume of diluent (µl) (iso-octane)	750	730	650	550	650	550	150
Volume of internal standard to add (µl)	250						

* Concentrations require the preparation of a tertiary calibration standard (3°). This was prepared by diluting 100 µl of secondary calibration standard (2°) with 900 µl of toluene (HPLC grade, Fisher) in a 2 mL glass amber vial.

3.4.2.2.2 Sample analysis by GC-MS

A Shimadzu Gas Chromatograph Mass Spectrometer GCMS-QP2010S was used for the quantification of road dust samples. Operator conditions were in accordance to the manufacturer's instructions, and specific instrument variables detailed in Table 3.22. The instrument was run in selective ion monitoring mode (SIM) with atomic mass units (amu) given in Table 3.23.

Table 3.22: GC-MS instrument parameters for the quantification of 16 PAHs.

PARAMETER	SET POINT
Initial Oven Temperature	50 °C
Hold Time	1.00 min
Ramp Rate	12°C /min
Final Oven Temperature	100 °C
Ramp Rate	7.0°C /min
Final Oven Temperature	220 °C
Ramp Rate	2.5 °C /min
Final Oven Temperature	325 °C
Hold Time	2.00 min
Total Program Time	66.31 min
Column	DB-5MS 60 m x 0.25 mm x 0.25 µm
Constant Column Flow	1.5 mL min^{-1}
Injector	On-column
Injector Temperature	280 °C
Injector Hold Time	66.31 min
Injector type	Manual
Injection Volume	1 µL
Ion source temperature	250 °C
Transfer line temperature	325 °C

Table 3.23: GC-MS instrument acquisition parameters for the quantification of 16 PAHs.

Acquisition Segment	Retention Time	Compound	PAH (m/z)	Product (m/z)
1	10.667	Naphthalene	127	77
2	21.008	Acenaphthylene	152	76
	21.789	Acenaphthene	154	76
3	23.884	Fluorene	166	115
4	27.270	Phenanthrene	178	127
	27458	Anthracene	178	127
5	31.611	Fluoranthene	202	151
	32.578	Pyrene	202	151
6	33.744	p-Terphenyl	230	230
7	39.356	Benzo (a) anthracene	228	200
	39.573	Chrysene	228	200
8	46.800	Benzo (b) fluoranthene	252	225
	46.992	Benzo (k) fluoranthene	252	225
	49.002	Benzo (a) pyrene	252	225
9	56.599	Indeno (1,2,3-cd) pyrene	276	249
	56.963	Dibenzo (a,h) anthracene	278	250
	58.189	Benzo (g,h,I) perylene	276	249

3.4.2.3 Quality control for GC-MS analysis

This section gives detail on the instrument quality control data for GC-MS analysis.

All quantification was completed on calibration graphs with R^2 coefficients greater than 0.995. An independent standard was analysed at the beginning of every sample batch, and calibration drift standards analysed after every 10 samples to ensure no deterioration of instrument performance occurred throughout sample analysis. Due to limited instrument availability, instrument detection limits were calculated by using the lowest calibration standard divided by the extracted sample weight used e.g. 0.1 mg L^{-1} / 3 g= 0.033 mg L^{-1}.

Table 3.24: GC-MS instrument independent standard results.

PAH component	N	Mean (mg L^{-1})	S.D. (mg L^{-1})	%RSD	Target
Naphthalene	3	4.14	0.97	23.3	5.00
Acenaphthylene	3	5.33	0.88	16.4	5.00
Acenaphthene	3	3.71	0.69	18.5	5.00
Fluorene	3	4.37	0.81	18.5	5.00
Phenanthrene	3	4.13	0.65	15.8	5.00
Anthracene	3	4.16	0.60	14.4	5.00
Fluoranthene	3	4.75	0.16	3.3	5.00
Pyrene	3	4.45	0.16	3.6	5.00
Benzo(a)anthracene	3	5.54	0.91	16.5	5.00
Chrysene	3	4.52	0.15	3.3	5.00
Benzo(b)fluoanthene	3	5.13	1.50	6.7	5.00
Benzo(k)fluoanthene	3	4.24	0.92	5.6	5.00
Benzo (a)pyrene	3	4.80	1.47	7.2	5.00
Indeno(123cd)pyrene	3	5.30	2.03	5.9	5.00
Dibenzo(ah)anthracene	3	5.97	2.22	3.5	5.00
Benzo(ghi)perylene	3	4.78	1.28	9.3	5.00

As shown in Table 3.24, mean independent standard concentrations were generally in agreement with the calibration standards, with acenaphthene showing the greatest concentration difference (3.71 mg L^{-1}) and Benzo(b)fluoranthene the least (5.13 mg L^{-1}) to the assigned 5 mg L^{-1} concentration target. Although mean calibration and independent standard concentration showed some variation, this was expected, due to the preparation of the independent standard from solid stocks.

With every batch of samples, two CRM122-100G RTC certified reference materials were extracted and quantified as part of quality control (Table 3.25). Due to poor recoveries most likely attributable to low concentrations and volatility, naphthalene and acenaphthylene will

not be discussed further. All other PAH component concentrations were similar to the certified reference material and were within 2 S.D., or at worst 3 S.D. of the certified value.

Table 3.25: CRM122-100G RTC certified reference material results for PAH analysis.

PAH component	N	Mean (mg kg $^{-1}$)	S.D. (mg kg $^{-1}$)	%RSD	% recovery	Certified reference value (mg kg $^{-1}$)	S.D. (mg kg $^{-1}$)
Naphthalene	10	1.71	19.7	55.0	35.7	4.78	0.48
Acenaphthylene	10	0.613	17.0	9.1	186	0.329	0.03
Acenaphthene	10	0.331	4.9	6.3	77.8	0.425	0.07
Fluorene	10	3.63	12.9	20.1	64.1	5.67	0.50
Phenanthrene	10	4.95	15.0	20.4	73.7	6.72	0.57
Anthracene	10	0.993	10.6	8.1	130	0.759	0.12
Fluoranthene	10	5.46	9.2	10.4	88.1	6.2	0.48
Pyrene	10	1.55	8.4	8.4	99.7	1.55	0.16
Benzo(a) Anthracene	10	5.67	11.4	12.4	91.8	6.18	0.50
Chrysene	10	6.30	16.3	19.6	83.1	7.57	0.50
Benzo(b) fluoanthene	10	4.93	17.9	15.2	117	4.16	0.26
Benzo(k) fluoanthene	10	5.88	12.3	13.1	93.9	6.24	0.40
Benzo (a) Pyrene	10	1.83	9.3	9.7	96.0	1.89	0.28
Indeno(123cd) Pyrene	10	6.20	21.2	21.7	97.9	6.34	0.61
Dibenzo(ah) Anthracene	10	7.47	19.2	17.0	113	6.61	0.61
Benzo(ghi) Perylene	10	6.79	13.9	14.9	93.3	7.27	0.68

3.5 Statistical analysis

For some instances, sample results can be summarised more effectively using statistical analysis. In this project, statistics have been used to determine the significance of two sample populations (p and t test) and to demonstrate an association between two variables (regression analysis). The significance is measured to determine whether the difference of two sample populations can be explained by the presence of random errors obtained by the measurement process, or, a difference in sample population means, where the sample population has been influenced by other factors rather than random error. For example, if the p-value obtained from the statistical analysis of two sample populations is <0.05, there is a 1 in 20 chance that the difference observed can be attributed to random error, when in fact it is not. For the purpose of this project, statistical significance was used to identify the chemical and environmental factors that may have influenced the final sample results. The use of regression analysis allowed the relationship between two variables (a dependent and an independent varaible) to be determined to help understand how the dependent variable influences the independent variable. Regresssion analysis was important to predict and explain sample results, particualrly for chemical associations in the environment, e.g. the retention of Sb by OM.

All statistical analysis was completed using data analysis in Microsoft Excel, with each data output listed in Appendix 7. Since analytical results were generated from duplicate analysis, statistical values were based using pseudo-replications.

Chapter 4 Method development and quantification of Sb(III) and Sb(V)

4.1 Introduction

Whilst analytical speciation methods for elements such as As, Hg and Se are well-established, it has only been since the late 1990s that methods to quantify Sb species have been explored (Miravet *et al*., 2010), in response to growing concern about the environmental fate and toxicity of Sb(III) and Sb(V). This chapter outlines the challenges in quantifying Sb species in environmental media, and the optimisation and application of methodology used in this study.

4.2 Quantification challenges for Sb speciation

There are several challenges in quantifying Sb(III) and Sb(V) species but perhaps the most important stems from the stability of each species. In aerobic conditions, Sb(III) is readily oxidised to Sb(V); indeed this process has been reported to occur under ambient conditions in distilled water within a few hours (Kracher *et al.,* 2001), whilst a laboratory study examining the photo-oxidation of Sb(III) in seawater reported full oxidation in only 10 minutes (Quentel and Filella, 2002). The readiness with which oxidation occurs means that preserving sample integrity is paramount. Taking this into consideration, samples must be stored and prepared in an O-free atmosphere (section 3.2.3.2.4), and in addition, reagent solutions should be thoroughly purged with N before use. Samples should also be processed and analysed within 48 hours of sampling, and where possible, sunlight exposure minimised by use of amber tinted containers to prevent any photo-induced oxidation of Sb(III) (Fan *et al*., 2014). In contrast to the oxidation described above, thermodynamic considerations suggest that the reduction of Sb(V) to Sb(III) in environmental samples does not readily occur, except under very acidic conditions (pH <2) (Krupka *et al*., 2002). Therefore, the preservation of Sb oxidation state is principally aimed at avoiding the conversion of Sb(III) to Sb(V) in both porewater and soil samples.

Due to stability issues, no commercially available analytical standards exist for either Sb(III) and Sb(V); consequently standard preparation for analysis involves the dissolution of solid materials (Table 4.1), specifically potassium antimonyl tartrate ($C_8H_{14}K_2O_{12}Sb_2$) and potassium hexahydroxyantimonate ($KSb(OH)_6$) for Sb(III) and Sb(V), respectively. Standards are prepared from a series of dilutions in volumetric flasks using a nitrogen purged solution of 20 mmol L^{-1} Ethylenediaminetetraacetic acid (EDTA) and 1 mmol L^{-1} phthalic acid. These reagents are used partly because they are also used as the HPLC mobile phase for separating Sb(III) and Sb(V) species. However, each one has an additional purpose: EDTA as a complexing agent helps preserve Sb oxidation state, whilst the use of phthalic acid helps to reduce peak broadening during chromatographic separation (Lintschinger *et al*., 1997; Zheng *et al*., 2000; Krachler *et al*., 2001; 2010; Miravet *et al*., 2010). The preparation of Sb(III) stock solution uses HPLC mobile phase (20 mmol L^{-1} EDTA and 1 mmol L^{-1} phthalic acid) to dissolve 0.2748 g of potassium antimonyl tartrate in a 100 mL volumetric flask giving a final concentration of 1000 mg L^{-1}. For Sb(V), 0.2159 g of potassium hexahydroxyantimonate was dissolved in nitrogen-purged deionised water as opposed to HPLC mobile phase; potassium hexahydroxyantimonate has low solubility in the HPLC mobile phase. All further dilutions to prepare standard solutions and calibration standards using either Sb(III) or Sb(V) stock solutions were carried out using the HPLC mobile phase (section 3.3.14). It was important that standards for each oxidation state were prepared and analysed individually, e.g. Sb(III) and Sb(V) standards were not combined to give a single set of standard solutions. This allowed any changes from Sb(III) to Sb(V) to be monitored throughout sample analysis.

Table 4.1: Prepared standard definition, concentration and use.

Standard name	Sb(III) and Sb(V) concentration	Use
Stock standard Solution	1000 mg L^{-1}	Preparation of Sb(III) and Sb(V) stock solutions from potassium antimonyl tartrate and potassium hexahydroxyantimonate solid materials.
Standard solution	1 mg L^{-1}	Intermediate standard to dilute stock solutions by a factor of 100.
Calibration standard	0-100 µg L^{-1}	Standards prepared for instrument calibration for the quantification of unknown samples.
Spike standard	1 mg L^{-1}	To assess % recovery of Sb(III) and Sb(V) for soil samples.

The instability of Sb oxidation states has also meant that no certified reference materials are commercially available for either Sb(III) and Sb(V) in environmental samples (Krachler *et al*., 2001). As a result, measured sample concentrations for Sb(III) and Sb(V) must be combined to give total Sb concentrations, which are compared to certified Sb reference values (discussed further in section 4.4.3.2).

Another issue relating more generally to accurate determination of Sb concentrations is the widespread use of Sb in industrial processes (section 2.2.5.1), since common laboratory materials may contain trace amounts of Sb which may then lead to sample contamination. For example, the production of polyethylene terephthalate (PET) uses antimony trioxide (Sb_2O_3) as a catalyst (Nishioka *et al*., 2002), while, in the production of glassware, Sb_2O_3 is added as a clarifying agent (Krachler *et al*., 2000). Contact of samples with PET and glass surfaces should be limited, or better still avoided by using different materials such as polyethylene (PE). Although contamination of samples from contact with these surfaces can occur, detectable concentrations are generally only encountered when there had been a long contact period. For example, Shotyk and Krachler (2007) reported a 19% increase in Sb concentrations for PET bottled drinking water that had been stored at room temperature for 6 months. Taking this into consideration, surface water and porewater samples were collected

in PE sample bottles and centrifuge tubes, respectively, and were analysed within 48 hours of sampling.

4.3 Instrumentation selection

Traditionally, the concentration of Sb(V) species has been calculated by subtracting Sb(III) concentrations from total Sb concentrations. Total Sb concentrations were determined using ICP-OES or ICP-MS, whilst the production and analysis of volatile SbH_3 using hydride generation coupled to ICP-MS was used for Sb(III) quantification (Nash *et al*., 2000). This often gave results with high uncertainties, especially where Sb(III) concentrations were low. Over past decades, the development of other hyphenated instrumental techniques has given rise to a diverse selection of instruments that are capable of simultaneous quantification of Sb species in solution. Most of the recently developed instrumental methods have two interfaced components, a chromatographic system to separate Sb species, which is then efficiently transferred to a quantification system, usually a mass spectrometer. Although the application of gas chromatography (GC) has been reported in previous studies (Dodd *et al*., 1996; Andrewes *et al*., 1999), it is not particularly sensitive or selective for Sb species due to their low volatility and chemical similarities, and thus, is only successfully used for methylated Sb species (Crasher *et al*., 2001). The use of Capillary Electrophoresis (CE) has many advantages over other chromatographic separation techniques; its ease of use and great resolving power make it an obvious choice for the separation of Sb species (Krachler et *al*., 2001). It does, however, fall short on mass spectrometric detection and quantification of Sb species because the interfacing between chromatography system and detector is often poor and this gives rise to operating difficulties. Therefore, CE is generally coupled with a UV detector which unfortunately has poor sensitivity and selectivity. This was demonstrated in a review by Krachler *et al*. (2001), where typical method detection limits were stated as 64 µg L^{-1} and 147 µg L^{-1} for Sb(III) and Sb(V), respectively. The preferred technique used in this study for Sb speciation was High Performance Liquid Chromatography-Inductively Coupled

Plasma-Mass Spectroscopy (HPLC-ICP-MS). The solution chemistry of Sb compounds make ion chromatography ideally suited for the separation of Sb(III) and Sb(V), with a number of HPLC columns available (section 4.4.1) to resolve Sb species in solution (Nash *et al*., 2000; Krachler *et al*., 2001; Miravet *et al*., 2010). In addition, the preparation of analytical standards and sample analysis does not involve excessive cost or time to carry out, and the instrument selectivity and sensitivity ensure trace amounts of Sb can be quantified, with typical detection limits of ~1 μg L^{-1} (Nash *et al*., 2000). Due to these advantages, HPLC-ICP-MS is the most frequently used instrument for Sb speciation analysis, with a number of studies published providing a good starting point for method development.

4.4 Speciation using HPLC-ICP-MS

4.4.1 Instrument configuration

In this study, Sb species were separated using an Agilent 1200 HPLC system fitted with a Hamilton PRP-X100 strong anion exchange column under the conditions shown in Table 3.16 detailed in section 3.3.14. The sample solution is introduced to the HPLC via a 1 μ L sample loop, where it is pumped, along with 20 mmol L^{-1} EDTA / 1 mmol L^{-1} phthalic acid mobile phase, through the Hamilton PRP-X100 strong anion-exchange column at a pressure of 50 bar (Figure 4.1), where the differing affinities of Sb(III) and Sb(V) for the column stationary phase and mobile phase allowed separation to occur, i.e. Sb(III) is retained more than Sb(V) by the column stationary phase resulting in longer Sb(III) retention times. Although other anion-exchange columns have the potential to be used, e.g. Dionex AS4 and Waters IC-Pak, a review article by Michalski *et al*. (2012) demonstrated the popularity and user preference for the Hamilton PRP-X100. More specifically, Lintschinger *et al*., (1998) found the Hamilton PRP-X100 column to have better resolving power, and less interference issues when tested and compared with the Dionex AS4 column. Once the sample component is eluted from the column, it was directly fed into an Agilent 7500ce ICP-MS for final quantification using conditions detailed in Table 3.16. The HPLC-ICP-MS instrument

conditions were based on research published by Krachler *et a*l. (2001), Telford *et al*. (2008) and Ceriotti and Amarasiriwardena (2009).

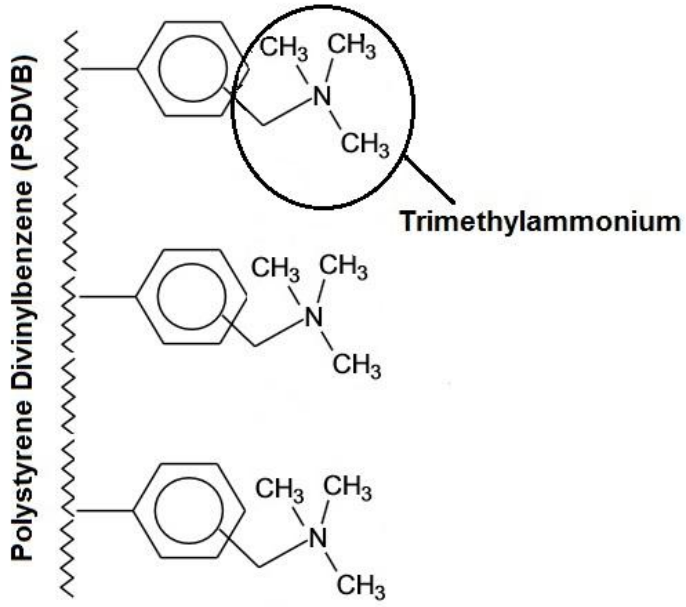

Figure 4.1: Stationary phase of the Hamilton PRP-X100 anion-exchange column.

4.4.2 Method optimisation

4.4.2.1 Separation of Sb(III) and Sb(V)

Mobile phase parameters were tested for optimal conditions using a 50 μg L^{-1} Sb(III) and Sb(V) calibration standard prepared as described in section 3.3.14. As shown in Table 4.2, a factorial design was used to assess the influence of the mobile phase composition examining variables: pH, EDTA and phthalic acid concentration. Whilst these parameters look largely similar, they were often the only variables that changed when published methods were compared, and it was essential to ascertain the impact these had on the separation of Sb(III) and Sb(V).

Table 4.2: Mobile phase composition test parameters.

Test Number	pH	EDTA Concentration (mmol L^{-1})	Phthalic acid (mmol L^{-1})
1	4.0	10	0.0
2	4.0	10	1.0
3	4.0	20	0.0
4	4.0	20	1.0
5	4.5	10	0.0
6	4.5	10	1.0
7	4.5	20	0.0
8	4.5	20	1.0
9	5.0	10	0.0
10	5.0	10	1.0
11	5.0	20	0.0
12	5.0	20	1.0

Results indicated that pH and EDTA concentration (Table 4.2) made little difference to optimising Sb(III) and Sb(V) separation, with both variables producing chromatograms which had similar peak retention times and gave similar sensitivity (Figure 4.2 and 4.3). Taking this into consideration, the target pH chosen for the mobile phase was 4.5 ± 0.5, since pH 4.0 and 5.0 made little difference to final quantification. For EDTA, the concentration of 20 mmol L^{-1} was selected, as although no difference was observed in the above tests, an excess of complexing agent should preserve oxidation states even for those samples with higher Sb concentrations.

A clear improvement however, was observed upon the addition of phthalic acid to the mobile phase. This had been cited to improve chromatographic peak shape by reducing peak tailing, which particularly affects late eluting peaks (Lintschinger *et al*., 1997; Zheng *et al*., 2000; Krachler *et al*., 2001; 2010; Miravet *et al*., 2010). Since the retention time of Sb(V) was 180 secs, the addition of phthalic acid had little effect on peak shape, as the occurrence of peak

tailing is typically low for early eluting species. In contrast, the later eluting Sb(III) peak (retention time 260 secs) was more susceptible to peak tailing, with the addition of phthalic acid reducing this by 20 secs. Calibration standard chromatograms for Sb(III) and Sb(V) at concentrations of 50 µg L^{-1} are shown in Figure 4.2 and 4.3.

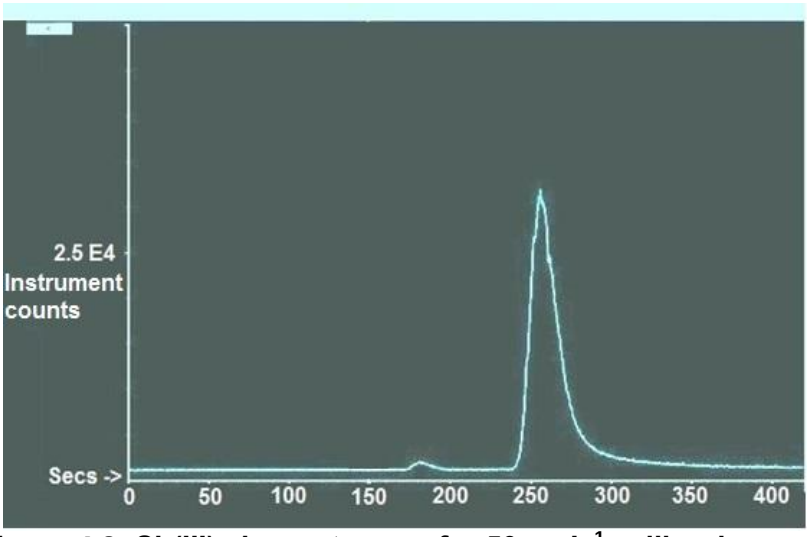

Figure 4.2: Sb(III) chromatogram for 50 µg L^{-1} calibration standard.

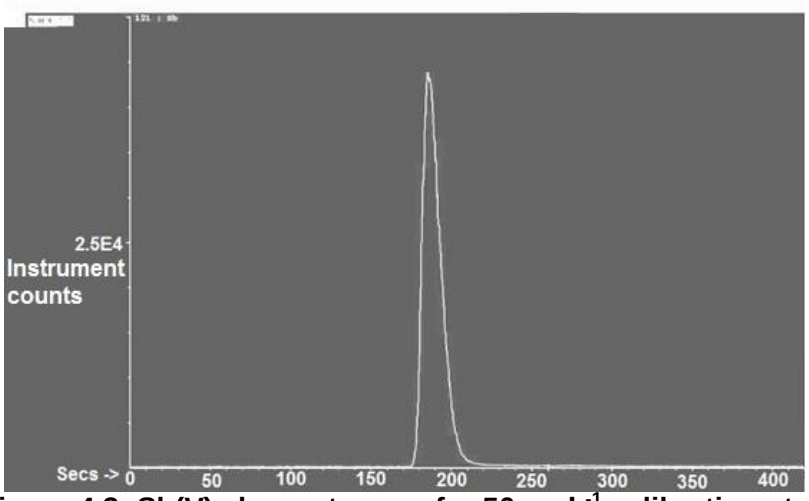

Figure 4.3: Sb(V) chromatogram for 50 µg L^{-1} calibration standard.

4.4.2.2 Data handling

Before data acquisition took place, a method to quantify Sb concentrations in standard and sample solutions had to be established as no peak integration function existed in the Agilent

ICP-MSTop software. The integration of Sb peaks were carried out manually, where instrument counts taken from the analysis of calibration standards were initially plotted and compared for accuracy using peak area and height. For peak area, three point Gaussian peaks were plotted using Sigmaplot, and compared to peak height plotted using Excel. The comparison of peak area and height calibration graphs was necessary to establish the most consistent and accurate way of quantifying unknown sample solutions with. This was done by quantifying standards at a known concentration using both peak area and height calibration graphs. Both approaches used a simple straight line calibration ($y = mx + c$) and were not considerably different for known and unknown sample solutions. Both graph displayed a good linear relationship with instrument counts and concentration, with R^2 correlations for calibration graphs routinely greater than 0.995. As quantification using Excel with peak height was more time efficient, all future quantification used peak height.

4.4.3 Quality control

4.4.3.1 Analytical standards

As stated in section 4.2, no certified standard solutions or reference materials exist for Sb(III) and Sb(V), and as a result, implementing quality control measures was not straightforward, as no independent concentration checks were available. The individual preparation and analysis of Sb(III) and Sb(V) calibration standards (section 3.3.14), and the analysis of Sb(III) and Sb(V) calibration drift standards were vital to monitor the potential conversion of Sb(III) to Sb(V) before and during a sample batch. The limited stability of Sb(III), and the subsequent conversion to Sb(V), even in the presence of the EDTA complexing agent resulted in prepared standards only lasting between 24-48 hours. Once concentrations of Sb(V) present in the Sb(III) calibration standard had exceeded the instrument limit of detection (section 4.4.4.2), new Sb(III) and Sb(V) calibration standards were prepared from fresh stock solutions. The standard reference material (SRM) 1643e from the National Institute of Standards and Technology (NIST) was used as an independent

concentration check standard for Sb(V). Although certification is for total Sb present in solution and not Sb(V), it is assumed all Sb will be present as (V), given the aerobic conditions of the water. Whilst no independent check standard for Sb(III) concentrations were possible, the periodic monitoring of Sb(III) calibration drift standards as well as the mass balance check detailed below, meant Sb(III) concentrations reported were reliable.

4.4.3.2 ICP-MS mass balance

Antimony(III) and Sb(V) concentrations from HPLC-ICP-MS analysis were summed, and then compared to total Sb concentrations attained from conventional ICP-MS analysis (section 3.3.12.2) (Figure 4.4). This provided an additional confirmation step, particularly in the absence of an Sb(III) independent check standard.

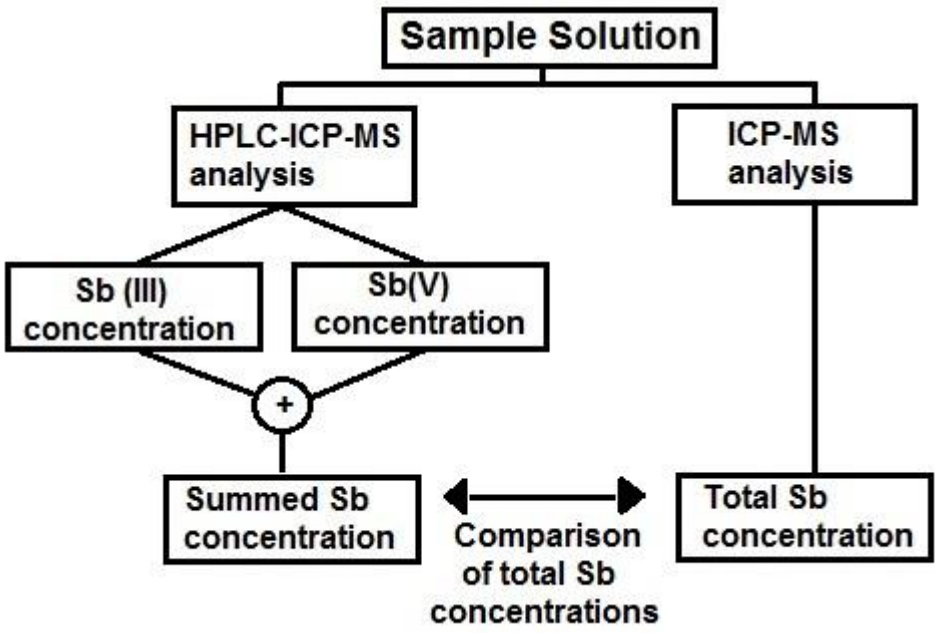

Figure 4.4: Diagram of Sb concentration mass balance from HPLC-ICP-MS and ICP-MS analysis.

4.4.4 HPLC-ICP-MS method validation

4.4.4.1 Validation set up

In order to ensure robust analysis of Sb speciation was achieved by HPLC-ICP-MS, method performance was established by quantifying a series of standards to establish precision, accuracy and instrument limit of detections (LOD). Six replicates of standards at concentrations of 15 μg L^{-1} and 50 μg L^{-1} were run, along with, six NIST 1643e reference solution replicates. Standards and reference material replicates were then analysed over the course of two analytical batches.

15 μg L^{-1} validation standards: These were prepared similarly to the lowest Sb(III) and Sb(V) calibration standards detailed in section 3.3.14. Based on methodology published by Agilent Technologies (2010), standards were run to attain instrument LOD, where instrument response was calculated by taking the standard deviation of concentration across six replicates and multiplying by three.

50 μg L^{-1} validation standard: These were prepared similarly to the mid Sb(III) and Sb(V) calibration standards detailed in section 3.3.14. The 50 μg L^{-1} validation standard was used to assess the HPLC-ICP-MS accuracy in quantifying Sb(III) and Sb(V) concentrations against the calibration graph, and in addition, the variability of standard concentration throughout a batch of samples.

SRM 1643e NIST: These were used as an independent concentration check for Sb(V) concentration.

4.4.4.2 Validation results

Instrument validation data is detailed in Tables 4.3 and 4.4, with typical calibration graphs shown in Figure 4.5 and 4.6.

Table 4.3: Sb(III) standard instrument validation data.

Standard Type	Replicate concentration (µg L^{-1})						Mean (µg L^{-1})	S.D. (µg L^{-1})	RSD (%)	LOD (µg L^{-1})
	1	2	3	4	5	6				
15 µg L^{-1} validation standard	18.3	15.5	17.3	15.8	16.1	17.4	16.7	1.09	6.6	3.3
50 µg L^{-1} validation Standard	50.4	48.6	49.6	53.6	53.6	55.8	51.9	2.81	5.4	

Table 4.4: Sb(V) standard instrument validation data.

Standard Type	Replicate concentration (µg L^{-1})						Mean (µg L^{-1})	S.D. (µg L^{-1})	RSD (%)	LOD (µg L^{-1})
	1	2	3	4	5	6				
15 µg L^{-1} validation standard	17.8	15.9	17.4	17.2	17.6	16.0	17.0	0.83	4.9	2.5
50 µg L^{-1} validation standard	52.2	49.9	51.3	51.6	52.6	53.4	51.8	1.20	2.3	
SRM 1643e NIST	63.1	62.8	61.7	62.0	61.7	56.5	61.3	2.42	4.0	

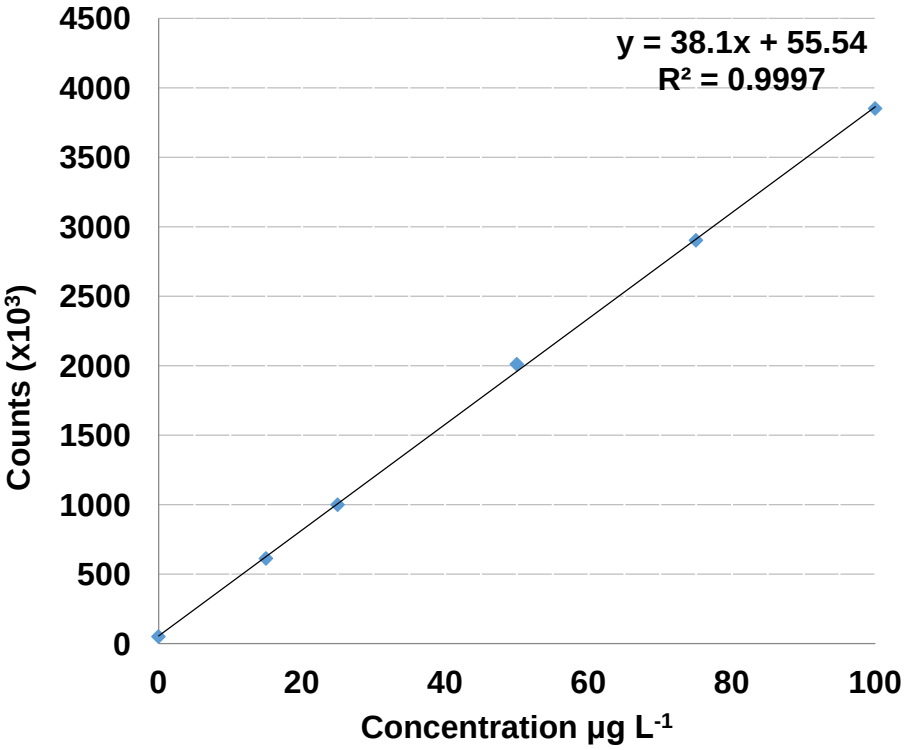

Figure 4.5 Sb(III) typical calibration graph attained by HPLC-ICP-MS.

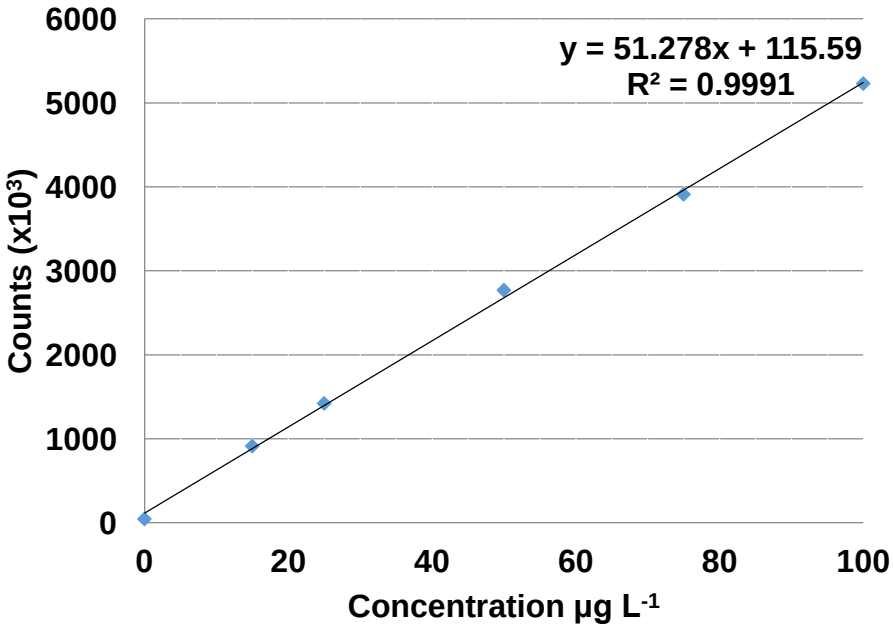

Figure 4.6 Sb(V) typical calibration graph attained by HPLC-ICP-MS.

Although mean validation concentrations for Sb(III) and Sb(V) were generally close to their target concentration, a positive bias (~1.7-2.0 μg L^{-1}) was observed for all validation standards. In future, this may be improved with the application of specific chromatographic software for data integration and processing. For example, the reproducibility of manual peak integration is lower than peaks integrated by software, and this may result in greater variation for both the calibration of the instrument and the quantification of samples.

The S.D. (<2.8 μg L^{-1}) and %RSD (<6.6) observed was good, particularly as validation data was acquired over two analysis batches increasing potential variation. Antimony(V) results from SRM 1643e NIST replicates (Table 4.4) showed good reproducibility (S.D. 2.4 μg L^{-1}, %RSD 4.0) and a mean validation concentration 3 μg L^{-1} higher than the certified value of 58.3 μg L^{-1}. Although a positive bias of 3 μg L^{-1} was observed, the quantification of the NIST reference solution was acceptable, particularly as variation was low.

4.5 The determination of Sb(III) and Sb(V) concentrations in soils by HPLC-ICP-MS

4.5.1 Introduction

The extraction of Sb from soil can be a challenge in itself. It is often difficult to achieve total dissolution of Sb from soil samples, as it is strongly retained by organic matter, Fe oxyhydroxides and clay minerals (Buschmann *et al*., 2005; Steely *et al.*, 2007; Sh *et al*., 2012). As a result, the quantification of Sb(III) and Sb(V) from soil samples is difficult, as it involves both efficient extraction and careful preservation of Sb species present during the sample preparation steps. Due to their low pH, aggressive reagents such as hydrofluoric, nitric and hydrochloric acid do not preserve oxidation states and will reduce Sb(V) to Sb(III) (detailed in section 4.2.) Conversely, too mild a reagent may not extract sufficient amounts of Sb from the soil matrix.

The type of extraction reagent depends on the solid phase sample that Sb speciation is to be determined in, e.g. biological samples generally require a solvent based approach involving

methanol or chloroform (Foster *et al*., 2005), whereas aqueous solutions are often adopted for soil samples. Although a few Sb speciation studies for soil samples have used N-purged EDTA (Zheng *et al.*, 2000) and deionised water (Steely *et al*., 2007; Ceriotto *et al*., 2009), 25 mmol L^{-1} of citric acid has been used more often as an extraction reagent (Zheng *et al*., 2001; Amereih *et al*., 2005; Telford *et al*., 2008). A study by Potin-Gautier *et al*. (2005) compared the effectiveness of citric acid, EDTA, oxalic acid, ascorbic acid and deionised water for the extraction of Sb species from spiked sediment at a concentration of 600 μg L^{-1}. Citric acid extraction gave the greatest recoveries for both Sb(III) and Sb(V) where it obtained recoveries of ~70%. This was similar to a study by Zheng *et al.* (2001), where Sb(III) and Sb(V) recoveries were 74 and 97%, respectively. It is important to note however, that spiked recovery tests are problematic, as the chemical form of added Sb(III) and Sb(V) is very different from that of Sb bound to soil. Consequently, extraction efficiency is usually better for spiked Sb recoveries, when compared to CRM recoveries (Table 4.5). Indeed, with the exception of the study by Zheng *et al.* (2001), CRM recoveries have generally been poor for Sb speciation studies (Lintschinger *et al*., 1997, 1998; Ulrich *et al*., 1998; Krachler and Emons 2000). Taking this into consideration and for this study, the extraction efficiency was assessed firstly, using NIMT/UOE/FM/001 CRM to determine the total Sb extracted by the speciation extraction reagent, and secondly, by spiking of NIMT/UOE/FM/001 CRM with a known concentration of Sb(III) and Sb(V) (Table 4.5). Due to the excessive cost involved in Sb speciation analysis by HPLC-ICP-MS (3-4 times more expensive than ICP-MS), extraction efficiency of total Sb was examined first before further tests were carried out.

Table 4.5: Extraction efficiency tests and purpose used to assess Sb speciation methods.

Extraction efficiency parameter	Sb form assessed	How test is prepared	Purpose
Sb CRM recovery	Total Sb	A CRM sample is prepared similarly to the Sb speciation method, but quantified using ICP-MS.	Since the Sb concentration present in the CRM is known, the recovery of Sb bound to the soil matrix can be assessed. The Sb speciation extraction reagent used is typically mild to preserve oxidation states, and it may not be aggressive enough to extract Sb bound to soil.
Sb spiked recoveries	Sb(III) and Sb(V)	A known concentration of Sb(III) or Sb(V) is spiked onto a soil matrix, and is treated as an unknown sample. The samples are then prepared and analysed using the Sb speciation method.	Since no Sb(III) and Sb(V) CRM exist, this remains the only way to assess the extraction efficiency of Sb species throughout an analytical procedure. Results from this technique can be artificially high. The extraction efficiency is based on recovering spiked Sb concentrations, which are more assessable to the extraction reagent than Sb bound to the soil matrix.

Three key Sb speciation methods were identified and used as a starting point to determine Sb(III) and Sb(V) concentrations in soils. Methods were chosen based on a range of sample preparation techniques, and where possible, the extraction efficiency obtained for Sb CRM and spiked recoveries. The first method was by Telford *et al*. (2001), where sample extraction occurred via a MARS6 unit, and published total Sb recoveries were between 47-78%. The second method was by Ceriotti and Amarasiriwardena (2009), where samples were extracted using sonication, but no extraction efficiency details were detailed for this method. The last method was by Zheng *et al*. (2001), where samples underwent mechanical shaking for 4 hours, and reported Sb CRM recoveries of ~100%, and spiked recoveries of Sb(III) and Sb(V) greater than 74%.

4.5.2 Methodology selected for Sb(III) and Sb(V) extraction from solid phase soil samples collected from the Glendinning Sb mining-impacted site in SW Scotland

4.5.2.1 Method 1 - microwave assisted digestion

This method was based on a method published by Telford *et al*. (2001). To a MARS6 digestion vessel, 0.5 g of soil sample and 10 mL of 25 mmol L^{-1} N-purged citric acid (Sigma Aldrich, ACS reagent ≥ 99.5%) was added, sealed and placed in the MARS6 oven ready for extraction. The MARS6 unit was set up and run using the settings shown in Table 4.6. Once cooled to room temperature, samples were transferred to a 50 mL polypropylene tube (Fisher Scientific, Fisherbrand), centrifuged at 6655 x g for 10 min (Heraeus Instruments Biofuge Primo centrifuge), filtered through a 0.45 μm hydrophilic membrane (VWR, Millex) using a plastic syringe (Fisher Scientific, BD Plastiplak) into a sterilin tube (Thermo Scientific, Scientific Laboratory Supplies) to await analysis. Samples were stored in a fridge at 4°C and analysed within 6 h.

Table 4.6: MARS6 speciation digestion method parameters.

MARS Microwave Parameter Function	Value
Ramp	6 min.
Temperature	90°C
Pressure	150 PSI
Hold time	20 min.
Power	900 W

4.5.2.2 Method 2 - hot water bath sonication

Method 2 combined components from two published Sb speciation studies, where sample sonication (Ceriotti and Amarasiriwardena, 2009) and citric acid (Telford *et al*., 2001) was used to extract Sb species from soil samples. The combination of sonication and citric acid was a mild extraction technique, and would help preserve Sb(III) and Sb(V), particularly as

citric acid was known to preserve Sb oxidation state (Zheng *et al*., 2001; Amereih *et al*., 2005; Potin-Gautier *et al*. 2005; Telford *et al*., 2008).

Approximately 0.4 g of soil was weighed in a 50 mL polypropylene tube (Fisher Scientific, Fisherbrand) and 10 mL of 25 mmol L^{-1} N-purged citric acid was added. The solution then underwent sonication (VWR Ultrasonic cleaner) for 60 min. at room temperature. Previous tests by Potin-Gautier *et al*. (2005) demonstrated that greater recoveries were observed using a 60 min sonication time rather than 20 or 120 min duration. Samples were then centrifuged at 6655 x g for 10 min (Heraeus Instruments Biofuge Primo centrifuge), filtered through a 0.45 μm hydrophilic membrane (VWR, Millex) using a plastic syringe (Fisher Scientific, BD Plastiplak) into a sterilin tube (Thermo Scientific, Scientific Laboratory Supplies) to await analysis. Samples were stored in a fridge at 4°C and analysed within 6 h.

4.5.2.3 Method 3 - mechanical agitation

This method was based on a method published by Zheng *et al*. (2000). Using a 50 mL polypropylene tube (Fisher Scientific, Fisherbrand), 0.3 g of soil sample and 6 mL of 20 mmol L^{-1} EDTA at pH 7 was added and mechanically shaken for 4 hours (Stuart Scientific). The solution was then centrifuged at 6665 x g for 10 min (Heraeus Instruments Biofuge Primo centrifuge), and resultant supernatant filtered through a 0.45 μm membrane (VWR international Ltd, Millex) using a plastic syringe (Fisher Scientific, BD Plastiplak), and into a sterilin tube (Thermo Scientific, Scientific Laboratory Supplies). Samples were stored in a fridge at 4°C and analysed within 6 h.

4.5.2.4 Initial results for total extractable Sb dissolution concentrations for Methods 1-3

Initial test results showed that Method 1 was the most efficient at extracting total Sb dissolution concentrations from NIMT/UOE/FM/001 CRM (~30% recovery), and in addition, variability was low (S.D. ± 2.5%) (Table 4.7). Method 3 was the least effective with a mean recovery of only 15% with respect to total Sb, and therefore was no longer considered an option for the determination of Sb(III) and Sb(V) in soil samples. Although

precision appeared good, and the application of a recovery correction factor could have been used, the low recovery of Sb would have contributed greatly to the uncertainty of final results. Indeed, this was a problem for Methods 1 and 2, but not to the same extent. For Method 2, it was worth noting that the Ceriotti and Amarasiriwardena (2009) method was only modified after the original method resulted in data <LOD. Both Methods 1 and 2 were selected for future method development tests.

Table 4.7: Recoveries for Methods 1-3 based on peat reference NIMT/UOE/FM/001 value.

Method number	Replicate number	% recovery of 2.37 mg kg $^{-1}$ CRM Value	Method S.D. (%)
1	1	33.6	2.5
1	2	29.0	
1	3	30.0	
2*	1	18.0	4.3
2*	2	24.1	
3	3	15.9	0.6
3	1	14.8	
3	2	15.9	

* Third replicate lost at sample preparation stage due to spill

4.5.2.5 Sb(III) and Sb(V) analysis using Methods 1 and 2

To assess the method performance for determining Sb species in soil samples, NIMT/UOE/FM/001 CRM samples were spiked prior to sample preparation steps and treated as unknown samples. The NIMT/UOE/FM/001 CRM was used for this purpose as it closely matched the soil matrix of future samples to undergo Sb speciation analysis. Since NIMT/UOE/FM/001 CRM was exposed to air, all Sb found in the material would be exclusively present as Sb(V), and would not provide an assessment for recovering Sb(III) concentrations. Therefore, 2 unspiked and 10 spiked matrix recoveries were used to reliably assess stability and % recovery of Sb(III) and Sb(V) for Methods 1 and 2. Mean results

obtained from the unspiked samples were subtracted from spiked results, to take into account Sb present in the NIMT/UOE/FM/001 CRM. The spiking of NIMT/UOE/FM/001 CRM was carried out with 1250 µl of 1 mg L^{-1} Sb(III) and Sb(V) spiking standard.

4.5.2.6 Spiked and unspiked matrix recoveries using Method 1

No detectable Sb(III) concentrations were attained for unspiked % recoveries, while for Sb(V), 10.8% was recovered based on the total Sb value present in the NIMT/UOE/FM/001 CRM (since NIMT/UOE/FM/001 CRM was exposed to air, it was most likely that Sb present would be present as the Sb(V) form). As shown in Table 4.8, spiked recoveries for Sb(V) were generally good, giving a mean % recovery of 76.7%, and a range between 68.6−87.4%. A S.D. of 3.18% and RSD of 10.4% was observed for Sb(V) recoveries across all 10 tests. For Sb(III), no recovery values were attained, as Sb(III) concentrations were all below the HPLC-ICP-MS limit of detection (3.3 µg L^{-1}). Whilst the application of citric acid as an extraction solution had been used to complex with Sb(III) and Sb(V) successfully in previous studies (Zheng *et al*., 2001; Amereih *et al*., 2005; Potin-Gautier *et al*. 2005; Telford *et al*., 2008), this was not the case for Method 1. The absence of Sb(III) was most likely attributed to its conversion to Sb(V) during the sample preparation stage, where the microwave assisted digestion temperature may have been too high to preserve the Sb speciation. If this was indeed the case, it would invalidate the Sb(V) recoveries obtained here. Other possible explanations are its evaporation or inefficient removal from the prepared sample. A study examining Sb(III) and Sb(V) stability in solution by Calle-Guntinas *et al*. (1992), identified temperature as a factor that could result in the oxidation of Sb(III) to Sb(V). This consisted of test water solutions stored between 0-4^{o}C and 25^{o}C and left over the duration of a day, a month, 3, 6 and 12 months, with results showing a reduced amount of Sb(III) present after 3 months when stored at 25^{o}C. This was in agreement with research by Lindemann *et al*. (2000), where temperature was also recognised to influence Sb(III) stability; up to 40% of Sb(III) was lost in a month when stored in water at -20^{o}C, while 3^{o}C was identified as the most stable storage temperature. Clearly temperature influences Sb(III)

stability within solution, albeit when left for long periods of time. Taking this into consideration, the impact temperature had on the microwave assisted digestion method was tested by lowering the digestion temperature to 70^{o}C and 80^{o}C (originally 90^{o}C). It was thought that the original microwave assisted digestion parameters were too aggressive to extract and maintain Sb oxidation states. The test results showed no improvement in Sb(III) recoveries and were all still <LOD, suggesting that 70^{o}C may still be too high a temperature to preserve Sb(III) in solution. As Telford *et al*. (2007) only reported ~36% of Sb(III) was converted to Sb(V), further differences in the application of methodologies used was investigated. One notable difference however, was for this study dried NIMT/UOE/FM/001 CRM was used to assess Sb spiked recoveries with, while Telford *et al.* (2007) used wet soil. Indeed, the NIMT/UOE/FM/001 CRM used in this study was not stored in an oxygen-free environment, and therefore, Sb(III) may be oxidised to Sb(V) after sample spiking. Future work determining Sb(III) and Sb(V) concentrations in CRM, or soil, should allow samples to equilibrate in a nitrogen-filled Atmos bag overnight, to eliminate trace levels of O present.

Although the recovery of total Sb dissolution concentrations were shown to be best for this method (section 4.5.2.1), it was unsuitable for the extraction of Sb(III) and Sb(V) species due to the poor stability and recovery of Sb(III). Therefore, Method 1 was no longer considered for the determination of Sb(III) and (V) in soils.

Table 4.8: Spiked Sb(III) and Sb(V) % recoveries attained from Method 1 and 2.

Test number	Method 1		Method 2	
	Sb(III) % recovery	Sb(V) % recovery	Sb(III) % recovery	Sb(V) % recovery
1	< LOD	68.8	29.4	101
2	< LOD	73.9	24.2	106
3	< LOD	68.6	28.3	94.9
4	< LOD	71.2	30.5	97.8
5	< LOD	87.4	35.5	97.3
6	< LOD	76.1	29.2	97.1
7	< LOD	84.5	32.5	100
8	< LOD	77.7	29.9	97.4
9	< LOD	75.8	32.8	97.9
10	< LOD	83.1	33.9	104
Mean	-	76.7	30.6	99.5
S.D.	-	6.54	3.18	3.54
RSD	-	8.5	10.4	3.6

4.5.2.7 Spiked and unspiked matrix recoveries using Method 2

Similar to Method 1, no detectable Sb(III) concentrations were attained for unspiked % recoveries, while for Sb(V), 17.9% was recovered based on the total Sb value present in the NIMT/UOE/FM/001 CRM (since NIMT/UOE/FM/001 CRM was exposed to air, it was most likely that Sb present would be as the Sb(V) form). Method 2 results showed a marked improvement over Method 1 for the recovery of spiked Sb(III) and Sb(V) (Table 4.8). For Sb(III), recoveries ranged between 28.3-35.3%, giving a mean recovery of ~31%, and a precision of S.D. ± 3.18% (Table 4.8). Spiked recoveries of Sb(V) ranged between ~97-104% giving a mean of 99.5%, and S.D. ± 3.5% (Table 4.8). As previously stated in section 4.5.2.2, Method 2 was developed based on methodology from two Sb speciation studies, Ceriotti and Amarasiriwardena (2009) and Telford *et al.* (2007), and were modified to incorporate citric acid and a sonication sample preparation step. The modifications looked to have improved the original sonication method by Ceriotti and Amarasiriwardena (2009), as Sb(III) spiked matrix tests reported very little Sb(III) recovered (~0.5 μg L^{-1}) using a similar

HPLC-ICP-MS method, whilst the modified method presented in this study recovered up to 36% of Sb(III) spiked onto the CRM reference material (concentration of 18 μg L^{-1}). Whilst the analytical performance of Method 2 was an improvement on Methods 1 and 3, further development is required to increase the stability of Sb(III) in solution, particularly as Sb(III) may be undergoing oxidation to Sb(V), which may result in high % recoveries for Sb(V). Further tests using 100 mmol L^{-1} of oxalic acid and the addition of ascorbic acid to an extraction solution as detailed by Potin-Gautier *et al*. (2005) was trialled, but was unsuccessful in preserving Sb(III) oxidation state giving unspiked and spiked % recoveries of 4.4 and 7.7%, respectively. As discussed for Method 1, future work should allow samples to equilibrate in a nitrogen-filled Atmos bag overnight, to help preserve Sb(III) oxidation state. Currently, Sb recoveries were too low to confidently accept results for soil samples, as spiked % recoveries for Sb(III) were not sufficiently recovered. Indeed, this was the case for several methods that extracted Sb(III) and Sb(V) from soil material reported in literature. A number of comprehensive reviews examining Sb speciation methodology (Guerin *et al*., 1999; Nash *et al*, 2000; Krachler *et al*., 2001; Michalski *et al*, 2011) all acknowledged the difficulty in extracting and maintaining Sb oxidation state from soil material.

4.6 Determination of Sb(III) and Sb(V) in porewater samples from the Glendinning Sb mining-impacted site in SW Scotland

Following the successful development of a method for determining Sb(III) and Sb(V) in water samples, an important next step was to analyse real aqueous phase samples in addition to standard solutions for the analysis of Sb(III) and Sb(V). Real samples can often cause problems for newly developed methods by adding new analysis variables such as sample matrix effects, and concentrations either above or below the developed instrument calibration range. These problems can potentially affect quantification and results, and in additional sample preparation time, highlighting the importance of trial analysis using real samples, before determining important samples.

The preparation of soil porewater samples for Sb speciation analysis required significantly less preparation than that of solid phase samples, as only minimal sample pre-treatment was required before instrument analysis. As detailed in section 3.2.3.2.4, two soil cores (S4A and S5A) were sampled at sites near S4 and S5 (Figure 3.6), and immediately sliced into 2-cm depth sections using a knife, placed and sealed into two He polyethylene bags. Upon arrival at the lab, the soil depth sections were placed in a N-filled Atmos bag, where approximately 60 g of fresh soil solid phase sample was transferred to a 50 mL polypropylene tube, securely sealed, removed from the Atmos. bag and centrifuged at 8873 x g for 10 minutes to separate porewater from soil. Once completed, the 50 mL polypropylene tube was returned to the Atmos. bag where supernatants were removed using a 0.45 μm membrane filter via plastic syringe and eluted into a N-filled sterilin tube (see section 3.3.14).

4.6.1 Initial results for Sb(III) and Sb(V) in soil porewater

Trial porewater samples were prepared and analysed in duplicate, as shown in section 3.3.14, with results described in Table 4.9. Where samples exceeded instrument calibration range, they were diluted by a factor of 10 using the HPLC mobile phase.

Table 4.9: Soil core Sb(III) and Sb(V) concentrations from both HPLC-ICP-MS and ICP-MS analysis.

Sample name & depth	Concentrations (μg L^{-1})		Total Sb concentration HPLC-ICP-MS (μg L^{-1})	Total Sb concentration ICP-MS (μg L^{-1})	Mass balance as % difference
	Sb (III)	Sb (V)			
S4A 4-6 cm	51.6 ± 1.7	916 ± 320	968	2290	42.3
S4A 8-10 cm	20.4 ± 5.5	96 ± 7.3	116	156	25.6
S4A 12-14 cm	16.8 ± 3.4	1136 ± 152	1150	1005	13.4
S5A 2-4 cm	3.68 ± 0.8	18 ± 5.6	21.6	121	82.1
S5A 6-8 cm	5.51 ± 1.8	108 ± 4.3	114	175	35.1
S5A 14-16 cm	56.0 ± 0.3	980 ± 1.6	1040	1610	35.6

Notable variation was observed for measured concentrations of Sb(III) in duplicate analysis of porewater samples. Variation was worse for samples from S5A 6-8 cm and S4A 8-10 cm, where they differed by 32.6% and 27.0%, respectively, while the remaining samples varied by <22%. For Sb(V) concentrations, the variation observed for duplicate analysis was similar, where samples S4A 4-6 cm and S5A 2-4 cm differed by 34.9% and 31.1%, with all other samples showing <13% variation. Although not exclusively, the increased variation seen in Sb(V) concentrations may be influenced by greater sample concentrations present, where sample dilutions were necessary for quantification within the instrument calibration range. The mass balance of total Sb concentrations obtained from HPLC-ICP-MS and ICP-MS were generally not in agreement with each other, with the difference in Sb concentrations ranging from 13.4% (S4A 12-14 cm) to 42.3% (S4A 4-6 cm). Results from S4A 12-14 cm was the only sample where there was a reasonable mass balance based on the sum of the values for Sb(III) and Sb(V) in comparison with measured total Sb concentrations (13.4%).

Overall, the data obtained from trial porewater analysis showed considerable variation for duplicate speciation analysis, and for the mass balance of total Sb concentrations obtained from HPLC-ICP-MS and ICP-MS analysis.

4.6.2 Optimisation of porewater analysis

A clear difference in reliable quantification was observed between the analysis of a water reference solution (SRM 1643e NIST) (Table 4.4), to that of porewater samples, where porewater analysis results were inconsistent and inaccurate (Table 4.9). In order to elucidate the problems observed in the previous section, both instrument and sample preparation steps required investigation to resolve sample matrix problems.

4.6.2.1 Instrument corrective action-Sb(V) retention times

Upon greater examination of the Sb chromatograms, the analysis of porewater samples showed a retention time drift of 7 seconds for Sb(V) when compared to the calibration

standards, i.e. Sb(V) retention time for porewater samples were 187 s, while calibration standards eluted at 180 s. The longer retention of Sb(V) was attributed to the different chemical composition of the porewater samples in comparison with the calibration standards. Thus it was hypothesised that the absence of HPLC mobile phase in porewater samples was most likely responsible for the retention time drift. This was confirmed when porewater samples were diluted using HPLC mobile phase, where no retention time drift was observed. In contrast with Sb(V), no retention time drift was observed for Sb(III), but it is suggested that the longer retention times and the resulting broader chromatographic peaks may have masked any sample matrix effects. Although retention time drift for Sb(V) was only 7 seconds, the drift in retention time was considered for data processing, where the time of the data acquisition window was increased by 10 s to prevent the under reporting of Sb(V) concentrations.

4.6.2.2 Sample preparation corrective action-sample dilutions and filtration

Further improvements to porewater sample preparation steps were required to reduce variation detailed in section 4.6.1, and included the preparation of sample dilutions and filtration. The first of these was the preparation of porewater sample dilutions, as many samples exceeded Sb concentrations for instrument calibration. Originally, x10 dilutions were prepared in 1 mL aliquots, where 100 µl of sample was diluted into 900 µl of HPLC mobile phase. This was later compared to larger volume x10 dilutions, where 500 µl of sample was diluted with 4500 µl of HPLC mobile phase. The comparison of both, to undiluted samples, showed accuracy improved when x10 dilutions were carried out using larger volumes, and fell within 1% of expected values (Table 4.10). Although all pipettes used for dilutions were calibrated before use and serviced annually, larger volume dilutions were used from this point onwards. The second potential source of variability identified in the preparation of porewater samples was the removal of suspended particulates through the use of a filtration membrane. Similarly to sample dilutions, this was a necessary step that the

water reference solution (SRM 1643e NIST) did not undergo. The filtration step was tested by filtering two porewater samples through a 0.22 μm hydrophilic membrane and a further two porewater samples through a 0.45 μm hydrophilic membrane, with all replicates analysed as described in section 3.3.14. Test results showed that filter size made no difference to variation in Sb(III) and Sb(V) porewater concentrations.

Table 4.10: Porewater concentration reproducibility comparison table with x10 dilution samples prepared by 100μl and 1000μl pipette using HPLC mobile phase.

Test number	Target concentration of porewater sample ($\mu g\ L^{-1}$)*	Calculated porewater X10 dilution concentration using 100μl pipette ($\mu g\ L^{-1}$)	% difference in target 100μl pipette concentration ($\mu g\ L^{-1}$)	Calculated porewater X10 dilution concentration using 1000μl pipette ($\mu g\ L^{-1}$)	% difference in target 1000μl pipette concentration ($\mu g\ L^{-1}$)
1	408	359	**13.7**	417	**-2.3**
2	408	356	**14.4**	403	**1.1**
3	410	356	**15.3**	401	**2.3**
4	409	359	**14.0**	410	**-0.2**
5	379	338	**12.2**	368	**2.9**
6	365	328	**11.2**	356	**2.3**
Mean % difference from target concentrations			**13.5**		**1.0**

* Target concentration attained using total Sb concentrations from ICP-MS analysis of porewater samples.

4.6.2.3 Optimisation summary

Following the examination of initial instrument analysis set-up and sample preparation, Sb(V) retention time drift and sample dilution steps were the root cause of variation observed for Sb(III) and Sb(V) concentrations. Corrective action for both issues were as follows:

Sb(V) retention time drift: Data acquisition windows were expanded by 10 s to take into account the drift in the Sb(V) peak observed for porewater samples.

Porewater sample dilutions: On the occasion that a sample dilution is required, x10 sample dilutions were completed using 500 µl of sample and diluted with 4500 µl of HPLC mobile phase.

4.6.3 Optimised porewater analysis

As a result of the findings detailed in the previous section, the corrective actions from data acquisition windows and porewater sample dilutions were implemented before the analysis of another two soil cores (S4A & S5A) from Glendinning Sb mine. The method detailed in section 3.3.14 was used and results are presented in Table 4.11.

Table 4.11: Porewater sample results from optimised Sb speciation methodology.

Sample name & depth	Concentrations (µg L^{-1})		Total Sb conc. HPLC-ICP-MS (µg L^{-1})	Total Sb conc. ICP-MS (µg L^{-1})	Mass balance as % Difference
	Sb(III)	Sb(V)			
S4A 2-4 cm	37.1 ± 0.9	1660 ± 36	1700	1710	0.6
S4A 6-8 cm	16.2 ± 1.0	896 ± 34	912	940	3.0
S4A 12-14 cm	14.0 ± 0.7	405 ± 13	419	455	7.9
S5A 2-4 cm	3.20 ± 0.1	27.7 ± 0.5	30.9	40.6	23.9
S5A 4-6 cm	2.74 ± 2.0	76.4 ± 0.2	79.1	92.3	14.3
S5A 6-8 cm	3.24 ± 0.1	24.3 ± 0.2	27.6	39.1	29.4
S5A 8-10 cm	3.30 ± 0.6	44.6 ± 0.3	47.9	62.7	23.6
S5A 14-16 cm	7.91 ± 0.4	243 ± 0.4	251	268	6.3

A marked improvement was seen in method performance since implementing the optimisation steps detailed in section 4.6.2.3. Variation was significantly reduced for duplicate sample concentrations, where optimised analysis reduced variation by a factor of ~10 compared to initial analysis. A reasonable mass balance was also achieved for total Sb porewater concentrations attained from HPLC-ICP-MS and ICP-MS analysis, ranging from

0.6 to 29.4% with a mean of 13.6%. The largest % difference between total Sb porewater concentrations in HPLC-ICP-MS and ICP-MS analysis were for profiles S5A 2-4 cm, 6-8 cm and 8-10 cm, and were most likely attributed to the lower Sb concentrations present for these porewater samples (three lowest total Sb concentrations present).

4.6.4 Porewater quality control data

Quality control measures implemented for porewater analysis are detailed in section 4.4.3, and results shown Table 4.12. The mean concentration for the 50 μg L^{-1} standard for Sb(III) and Sb(V) was 51.3 and 52.4 μg L^{-1}, respectively. Acceptable reproducibility was observed for Sb(III) (S.D. 3.25 μg L^{-1}, %RSD 6.3) and Sb(V) (S.D. 1.48 μg L^{-1}, %RSD 2.8), although it is worth noting, there were only three sample batches. Mean SRM 1643e NIST concentrations were also acceptable (58.6 μg L^{-1}), with reproducibility (S.D. 3.18 μg L^{-1}, %RSD 5.4) similar to that observed in section 4.4.4.2.

Table 4.12: Porewater quality control data for Sb(III) and Sb(V) standard.

Standard Type	Standard sample batch conc. (μg L^{-1})						Mean (μg L^{-1})	S.D. (μg L^{-1})	RSD (%)
	1A	1B	2A	2B	3A	3B			
Sb (III) Calibration 50 μg L^{-1} standard	46.6	50.9	50.7	56.5	50.7	52.5	51.3	3.25	6.3
Sb (V) Calibration 50 μg L^{-1} standard	52.4	53.9	54.2	52.5	50.6	50.9	52.4	1.48	2.8
SRM 1643e NIST	56.5		57.0		62.3		58.6	3.18	5.4

4.7 Chapter summary

An instrument method for determining Sb(III) and Sb(V) concentrations in standards and in certified reference water (SRM 1643e) was successfully developed and validated giving good analytical performance. Although the analysis of 15 and 50 μg L^{-1} replicate standards indicated a small positive bias of ~1.8 μg L^{-1} for mean concentrations, variation during analysis was low, with S.D. < 2.8 μg L^{-1}. The developed instrument method was then used to

attempt the quantification of Sb(III) and Sb(V) concentrations in NIMT/UOE/FM/001 CRM, and for porewaters from two soil cores sampled in the vicinity Glendinning Sb mine.

For the determination of Sb species in soil samples, it was necessary to combine key sample preparation parameters published in methods by Telford *et al.* (2001) and Ceriotti and Amarasiriwardena (2009). These included the use of 25 mmol L^{-1} N-purged citric acid as an extraction reagent, and sonication as a sample preparation technique. Together, both parameters were identified as steps that could improve the preservation of Sb species throughout sample preparation. Although spiked Sb(V) recoveries of ~100% were observed, Sb(III) was not sufficiently recovered (mean 30.6%, n=10). This indicated that Sb(III) was undergoing oxidation to Sb(V), and would also account for the ~100% recovery for Sb(V). Whilst the instrument quantification of samples using HPLC-ICP-MS was fit for purpose, the sample preparation steps did not preserve Sb(III) oxidation state effectively. In addition, total Sb concentrations extracted from the NIMT/UOE/FM/001 CRM using the 25 mmol L^{-1} N-purged citric acid extraction reagent was significantly less than the certified value (~20% recovery), and gave a great deal of uncertainty to final results. Despite testing a number of alternative extraction reagents; distilled water, EDTA, citric acid, oxalic acid and ascorbic acid, all fell short of preserving Sb(III) concentrations. For future work, one improvement identified was to allow the CRM, or soil sample, to equilibrate in the N-filled Atmos. bag overnight. This would decrease trace levels of O present, and potentially increase Sb(III) stability during sample preparation. Overall, this methodology will need to be improved before reliable results can be obtained, where Sb stability during sample preparation, and the low extraction efficiency of Sb from soil matrix will need addressed.

More success was achieved in developing and validating methodology to determine Sb(III) and Sb(V) concentrations in soil porewater. Trial analysis of porewater samples highlighted improvements required to original methodology, and these included a more efficient sample dilution step, and the adjustment of data acquisition windows for real environmental samples. Once optimised, the method was used to quantify Sb species present in two soil

cores sampled in the vicinity Glendinning Sb mine. Reliable porewater results were achieved, with 80% of duplicate Sb(III) and Sb(V) samples agreeing within 1 μg L^{-1}, as well as good agreement for ICP-MS mass balance analysis (mean difference 13.6%, n=8). In addition, quality control measures showed little variation throughout the analysis batch (S.D. <3.25 μg L^{-1}, %RSD <6.3) indicting good reproducibility. Porewater results for Sb(III) concentrations were highest at S4A, ranging from 14.0–37.1 μg L^{-1}, while Sb(V) was detected as the dominant species, making up ~ 94% of total Sb concentrations present.

Chapter 5 Urban Environment

5.1 Introduction

This chapter gives an account of elemental (Sb, Pb, Cu and Zn) and polycyclic aromatic hydrocarbon (PAH) concentrations found in road dust, and where sampled, surface water in the urban environment, with a specific focus on vehicle emissions, industrial activity and previous land use as influential sources. Where applicable, source apportionment was achieved through Pb isotopic analysis and PAH diagnostic ratios, and for inner city Edinburgh, road dust composition was further characterised using chemical (sequential extraction) and spectroscopic (X-ray diffraction, SEM-EDX) methods.

5.2 Anthropogenic processes occurring in the urban environment

5.2.1 Vehicle-related emissions of Sb, Pb, Cu, Zn and PAHs

Over the last decade, a growing number of studies examining road dust from the urban environment have reported increased concentrations of Sb (Von Uexkull *et al*., 2005; Ceriotti and Amarasiriwardena, 2009; Kukutschova *et al*, 2009; Varrica *et al*., 2013). The addition of Sb to brake-linings to enhance the friction constancy and reduce braking vibration is discussed in section 2.2.5.1. Furthermore, the release of Cu and Zn from vehicular brake-linings also remains a major source of these metals to the urban environment. Although the composition of brake linings varies with supplier, metallic Cu, tenorite (CuO), covellite (CuS), chalcopyrite ($CuFeS_2$) and sphalerite (ZnS) have all been reported as key components (Kukutschova *et al*., 2009; Amato *et al*., 2012). The ban on asbestos, a previous major component of brake linings, has also given rise to an increase of up to 40% in Cu used in brake lining (Denier van der Gon *et al*., 2007; Kukutschova *et al*., 2009). Additionally, zincite (ZnO) is often used as a rubber filler in tyres and can similarly contribute to vehicular emissions, (Blok, 2005, Kukutschova *et al*., 2009; Amato *et al*., 2012), along with oil loss, albeit to a lesser extent (Blok, 2005). Although historic, the release of Pb from leaded petrol emissions during the 20th century continues to have a

significant impact on the environment today (section 2.3.4). Previously deposited Pb from leaded petrol, and from past industrial activity, is often re-suspended in the urban environment, along with Pb emissions from vehicle tyre wear and engine components (MacKinnon *et al*., 2011). Despite increasing restrictions on vehicle emissions for hydrocarbons (of which a proportion will be in the form of PAHs), fuel combustion from road transport remains the largest source of hydrocarbon emissions in the UK, contributing 61% of total emissions in 2006 (Dore *et al*., 2008). Whilst this is a significant emission contribution, the implementation of the European emission standards in 1993 (Euro 1), which was periodically revised up until 2014 (Euro 6), did result in ~80% reduction in UK 16PAH road traffic emissions over the 19 year duration (91/441/EEC; 715/2007/EC 2007; Dore *et al*., 2008).

5.2.2 Non-vehicle emissions

Historically, non-vehicle related contaminant emissions for the UK originated from past industrial activities such as coal combustion and the production of metal. Whilst emissions from previous anthropogenic sources have considerably declined in recent decades, they have since been replaced by contemporary sources. Commercial air travel is a good example of this, where its increasing use has resulted in significant emissions of elements and PAHs from the combustion of aviation and jet fuel (Kumar *et al*, 2013). The demolition and construction of buildings was also identified as another contemporary source of contaminants to the environment (Charlesworth *et al*., 2011). The release of Zn and Cd from galvanised structures such as roofs, balconies and window ledges were highlighted as potential sources, along with the release of Pb from paint flakes and deteriorating walls. Whilst a UK reduction of ~90% has been observed in PAH emissions from domestic heating and the burning of biomass since the 1990s (Dore *et al*, 2008), this trend is not global, and nearly 3 billion people still rely on this method for cooking and warmth (Kumar *et al*., 2013). With the exception of commercial air travel, the contribution and impact of non-vehicle related emissions on the urban environment is largely unknown. It should, however, be

considered when assessing road surface water and road dust contaminant concentrations. For this study, source apportionment techniques such Pb isotopic analysis and PAH diagnostic ratios will be used on road surface water and road dust samples, allowing non-vehicle, and vehicle emissions to the urban environment to be distinguished.

5.3 Road dust and road surface water sampling locations and analysis for Edinburgh and Glasgow sites

The cities of Edinburgh and Glasgow were selected as the urban areas in which to assess concentrations of elements (Sb, Pb, Cu and Zn) and PAHs in road dust and surface water samples. Of all cities in Scotland, Edinburgh and Glasgow have the greatest volume of traffic on a daily basis (Department of Transport, 2015). Edinburgh and Glasgow have, however, contrasting industrial histories. While industrial activity did occur in Edinburgh, it was relatively small as compared to Glasgow, and Edinburgh was regarded more for its administrative and commercial activities, along with its brewing and distilleries (Nenadic, 2011). Glasgow, however, became a centre for heavy industrial activity during the industrial revolution, with textiles, ship buildings and other engineering works all releasing contaminants to the local area (Farmer *et al*., 2011; Fordyce *et al*., 2013). By selecting Edinburgh and Glasgow, the impact of contrasting past, and similar contemporary anthropogenic activity for these locations upon current contaminant concentrations in road dust could be assessed.

This section gives a brief account of road dust and road surface water sampling locations and analysis in Edinburgh and Glasgow. More detail can be found in section 3.2.3.1.

5.3.1 Road dust and surface water sampling locations in Edinburgh

Road dust locations were selected at five high- and five low-traffic roads in Edinburgh, and are shown in Table 3.1 and Figure 3.3 (section 3.2.3.1). The high-traffic road sites were selected following a freedom of information request to Edinburgh City Council (2012) where sites were identified using Annual Average Daily Flow (AADF) data to give road vehicle

count. The high-traffic sites were the A90, Queen Street, A8, A1 and A70. Low-traffic sites were then selected using residential roads within a 500 m distance of the high traffic roads, namely, Hillpark Road, Thistle Street, Belmont Crescent, Cambusnethan Street and Redhall Drive (sampled March 2013). Each Edinburgh location was sampled using a nickel-silver alloy spatula to collect road dust from the road kerbside at 10 m and 50 m before the closest road junction (CRJ) to investigate the effect of vehicle braking on elemental concentrations in road dusts. In addition, road surface water spot samples were collected on each street using a pre-cleaned 250 mL polythene bottle (sampled March 2013).

Upon analysis and results from initial road dust samples listed in Table 3.1, additional road dust sites were selected at three specific areas believed to be influenced from historic and current land use (Table 3.2, section 3.2.3.1). These locations were in the vicinity of Cambusnethan Street, Thistle Street and near Edinburgh airport. More detail on road dust site selection and sampling is found in section 3.2.3.1.1.

5.3.2 Road dust sampling locations in Glasgow

Similarly for Glasgow (Table 3.1, Figure 3.4, section 3.2.3.1), five high- and five low-traffic roads were identified through the Department for Transport, Scotland (2014). The five high-traffic roads were A8 of Glasgow, A82, Broomielaw, Baird Street and Hyndland Road, while the five low-traffic roads were Tradeston Street, West Princes Street, Goosedubbs, Black Street and Leyden Street. Since only a limited quantity of road dust was available for each Glasgow location, road dust was collected the length of the road using a nickel-silver alloy spatula to give a composite road dust sample at each location (sampled May 2013).

5.3.3 Road dust and surface water analysis

Although road dust samples from Glasgow were not characterised to the same extent as those from Edinburgh, the contrast in high industrial with low industrial activity could still be examined. The Edinburgh sample analysis route map is shown in Figure 3.5, where duplicate road surface water samples were determined for Sb, Pb, Cu and Zn concentrations and Pb isotope ratios.

Duplicate road dust samples from Edinburgh were determined for: i) pH; ii) Sb, Pb, Cu, Zn and priority 16PAH concentrations; iii) Pb isotope ratios; iv) elemental mobility by sequential extraction; and v) mineral composition by X-ray diffraction and scanning electron microscopy with energy dispersive X-ray spectroscopy. Duplicate road dust samples from Glasgow were determined for; pH, and Sb, Pb, Cu, Zn and priority 16PAH concentrations and Pb isotope ratios.

5.4 Elemental and PAH concentrations in road dust samples from Edinburgh and Glasgow

5.4.1 Elemental road dust samples from Edinburgh

Sampling at 10 m and 50 m from road junctions was carried out to investigate the effect of vehicle braking on elemental concentrations in road dusts. Since there was no consistent trend in concentrations of any of the four elements ($t>0.36$, $p>0.37$, appendix 7, output 1), the data at both sampling locations will be described together for each element.

For the high-traffic locations, mean and range concentrations of Sb in road dust was 5.2 ± 2.8 mg kg^{-1} and 1.9-10.2 mg kg^{-1}, respectively (Table 5.1). Concentrations of Pb were much greater than Sb, with maximum concentrations observed at Queen Street (312 mg kg^{-1}) and lowest at the A70 (19.3 ± 1.1 mg kg^{-1}), with a mean concentration of 96.0 ± 97 mg kg^{-1}. Road dust Cu concentrations were notably lower than those for Pb, ranging from 38.8-168 mg kg^{-1}. Maximum concentrations were found in samples from the A1 (168 mg kg^{-1}) and lowest in those from the A8 (Edinburgh) (38.8 ± 4.3 mg kg^{-1}). The mean concentration of Zn was 215 mg kg^{-1}, with values for most locations in the range ~100-300 mg kg^{-1}. Concentrations of Zn were greatest in the sample from the A90 (348 mg kg^{-1}) and lowest in that from the A8 (Edinburgh) (59.8 ± 8.7 mg kg^{-1}). For Edinburgh high-traffic locations, there were no statistical significant trends ($P>0.36$, $R^2<0.28$ $n=20$, appendix 7, output 2) for

elemental concentrations in road dust and traffic volume, with maximum and minimum elemental concentrations appearing to be randomly distributed across all sites.

For Edinburgh low-traffic locations, concentrations of elements in road dust were generally greater than those of high-traffic sites. Mean concentrations of Sb were 5.4 ± 3.0 mg kg^{-1}, with the greatest concentrations observed at Cambusnethan Street (9.6 ± 1.6 mg kg^{-1}), and lowest at Belmont Crescent (1.8 ± 0.6 mg kg^{-1}). For Pb, concentrations were much greater than those observed for Sb, where concentrations reached 410 ± 34 mg kg^{-1} at Cambusnethan Street and 297 ± 59 mg kg^{-1} at Thistle Street, with an overall mean Pb concentration for low-traffic sites of 172 ± 150 mg kg^{-1}. Cambusnethan Street was also the location where Cu road dust concentrations were greatest (151 ± 19 mg kg^{-1}), while Belmont Crescent had the lowest (37.6 ± 1.2 mg kg^{-1}), with mean concentrations of 80.3 ± 38 mg kg^{-1} observed. Zinc concentrations were generally higher than those for Cu with most being in the range ~100-400 mg kg^{-1}. Again the greatest concentrations were obtained for Cambusnethan Street (606 mg kg^{-1}) and Thistle Street (310 ± 9.5 mg kg^{-1}) samples, with lowest values occurring in the samples obtained at Hillpark Drive (104 ± 25 mg kg^{-1}). The concentration of elements present in road dust from low-traffic locations showed a consistent trend for four 10 m and 50 m locations, with Cambusnethan Street and Thistle Street showing significantly high concentrations of elements present, while Belmont Crescent and Hillpark Drive showed the least.

Table 5.1: Elemental concentrations and Pb isotope ratios for Edinburgh road dust sampled at high- and low-traffic roads, at 10 and 50 m from the closest road junction (CRJ).

Road dust sites	CRJ	pH	% OM	Sb (mg kg^{-1}) ± 1SD	Pb (mg kg^{-1}) ± 1SD	Cu (mg kg^{-1}) ± 1SD	Zn (mg kg^{-1}) ± 1SD	$^{206}Pb/^{207}Pb$ ± 1SD	$^{208}Pb/^{207}Pb$ ± 1SD	$^{208}Pb/^{206}Pb$ ± 1SD
High traffic										
A90	10 m	7.5	4.3	6.6 ± 1.7	30.4 ± 6.5	83.4 ± 5.6	233 ± 6.3	1.145±0.002	2.428±0.002	2.123±0.003
	50 m	7.2	7.6	1.9 ± 0.3	20.9 ± 2.5	63.8*	348*			
Queen Street	10 m	7.4	9.4	8.6 ± 1.3	88.3 ± 17	158 ± 28	335 ± 21	1.151±0.001	2.432±0.005	2.115±0.005
	50 m	7.3	10.1	3.9 ± 0.2	312*	107 ± 41	251 ± 56			
A8	10 m	7.6	8.8	2.7 ± 0.5	29.1 ± 3.3	38.8 ± 4.3	59.8± 8.7	1.140±0.002	2.425±0.004	2.130±0.007
	50 m	7.1	14.4	4.4 ± 0.0	35.5 ± 3.6	62.9 ± 1.3	135 ± 3			
A1	10 m	7.0	5.8	5.0 ± 0.2	65.6 ± 0.8	72.1 ± 0.1	198 ± 46	1.145±0.002	2.414±0.006	2.109±0.003
	50 m	6.8	6.8	10.2± 0.3	161 ± 7.5	168*	285 ± 56			
A70	10 m	7.0	13.1	2.3 ± 0.2	19.3 ± 1.1	48.5 ± 2.7	84.0± 2.3	1.140±0.002	2.416±0.002	2.121±0.004
	50 m	7.1	11.1	6.9 ± 2.6	94*	100 ± 5.3	218 ± 12			
Low traffic										
Hillpark Drive	10 m	6.9	7.1	2.6 ± 1.0	60.6 ± 4.7	46.4 ± 3.1	169 ± 0.2	1.148±0.004	2.427±0.006	2.117±0.001
	50 m	7.2	1.7	9.1 ± 3.2	30.0 ± 4.6	53.6*	104 ± 25			
Thistle Street	10 m	8.1	6.2	8.2 ± 0.3	297 ± 59	113 ± 4.4	310 ± 9.5	1.146±0.004	2.414±0.005	2.111±0.008
	50 m	8.0	4.7	4.3 ± 0.6	288 ± 54	69.0 ± 4.1	294 ± 19			
Belmont Crescent	10 m	6.9	5.5	4.2 ± 0.3	39.9 ± 5.7	70.6 ± 30	166 ± 7.7	1.134±0.002	2.416±0.001	2.128±0.005
	50 m	7.5	6.9	1.8 ± 0.6	107 ± 39	37.6 ± 1.2	126 ± 5.2			
Cambusnethan Street	10 m	7.0	9.0	8.0 ± 0.0	372 ± 1.5	137 ± 12	495 ± 5.0	1.140±0.006	2.422±0.007	2.125±0.005
	50 m	6.0	7.9	9.6 ± 1.6	410 ± 34	151 ± 19	606*			
Redhall Drive	10 m	6.8	8.0	2.8 ± 0.2	84.5 ± 4.2	47.1*	191 ± 10	1.116±0.002	2.393±0.004	2.143±0.006
	50 m	6.8	10.0	3.5 ± 0.5	54.1 ± 0.2	77.8 ± 1.0	293 ± 28			

*Indicates single analysis entry

Table 5.2: Elemental concentrations and Pb isotope ratios of Edinburgh road dust sites affected by local historic and current land use, and runway dust.

Road dust sites	pH	% OM	Sb (mg kg^{-1}) ± 1SD	Pb (mg kg^{-1}) ± 1SD	Cu (mg kg^{-1}) ± 1SD	Zn (mg kg^{-1}) ± 1SD	$^{206}Pb/^{207}Pb$ ± 1SD	$^{208}Pb/^{207}Pb$ ± 1SD	$^{208}Pb/^{206}Pb$ ± 1SD
Road dust sites in the vicinity of Cambusnethan Street									
Carlyle Place	6.3	6.0	2.7±0.1	100±3.9	50.7±7.2	241±0.9	1.154±0.001	2.437±0.008	2.115±0.001
Dalgety Avenue	6.5	5.8	3.1±0.4	90.4±8.9	65.9±3.3	272±60	1.138±0.008	2.419±0.009	2.125±0.005
Dalgety Street	6.6	14.0	2.8±0.6	195*	57.3±3.3	267±26	1.142±0.006	2.418±0.005	2.124±0.004
Salmond Place	6.7	9.9	4.0±2.6	157*	40.4±2.2	203±3.6	1.148±0.001	2.425±0.001	2.114±0.004
Road dust sites on Thistle Street									
West	8.0	7.6	17.2±0.1	917±64.8	292±46	650±7.5	1.147±0.002	2.433±0.001	2.121±0.001
Mid	8.1	4.9	4.6±1.8	718*	182±7.2	440±57	1.152±0.006	2.418±0.001	2.101±0.001
East	8.0	15.2	13.6±8.5	472±8.2	116±7.1	350±5.9	1.146±0.001	2.424±0.005	2.113±0.005
Road dust sites in the vicinity of Edinburgh airport									
Cammo Rd-North East	6.0	16.3	3.0±0.5	40.1±3.0	65.8±8.7	289±15	1.154±0.004	2.429±0.002	2.102±0.004
Turnhouse Rd-East	6.6	5.8	3.9±0.2	311±8.7	83.8±12	297±26	1.116±0.006	2.387±0.001	2.136±0.001
Craig Road-East	6.7	2.5	1.6±0.1	44.6±1.5	146±12	58.9±0.8	1.121±0.004	2.398±0.006	2.141±0.002
North Gyle Grove-East	6.5	6.3	2.2±0.1	44.5±0.3	200±22	120±52	1.102±0.003	2.377±0.009	2.159±0.004
Glasgow Rd-South	6.8	5.9	2.6±0.2	51.3±22	112±5.6	296*	1.162±0.001	2.441±0.002	2.104±0.001
Kirkliston-West	7.0	4.2	7.6±1.4	113±12.4	218±63	455±13	1.161±0.003	2.431±0.007	2.094±0.006
Edinburgh airport runway	7.3	14.9	1.5±0.3	1750±6.3	55.9±25.3	150±1.8	1.158±0.003	2.433±0.001	2.102±0.005

*Indicates single analysis entry

Table 5.3: PAH concentrations in road dust from Edinburgh high- and low-traffic roads, at 10 m from the closest road junction.

Road dust sites	ACE	Fl	PHE	ANT	FLA	PYR	BaA	CHR	BbF	BkF	BaP	IcdP	DahA	BghiP	Σ PAH
	in µg kg^{-1} ± 1SD														in µg kg^{-1}
High traffic-*Edinburgh sites*															
A90	37.4 ± 4.4	73.0 ± 11	192 ± 52	61.0 ± 2.4	344 ± 38	292 ± 20	303 ± 17	307 ± 2.8	307 ± 44	255 ± 13	252 ± 38	213 ± 38	75.0 ± 19	239 ± 43	2950
Queen Street	62.1 ± 6.1	122 ± 37	611 ± 179	51.0 ± 23	811 ± 152	694 ± 113	419 ± 87	674 ± 94	830 ± 138	289 ± 58	741 ± 127	625 ± 43	164 ± 4.2	686 ± 91	6780
A8	<33.0	93.8 ± 62	698 ± 92	37.1 ± 9.1	1180 ± 30	933 ± 37	459 ± 174	675 ± 91	566 ± 13	200 ± 101	532 ± 3.8	409 ± 22	64.7 ± 40	480 ± 224	6330
A1	43.0 ± 3.6	75.4 ± 15	339 ± 107	73.0 ± 9.2	674 ± 153	529 ± 115	389 ± 53	516 ± 86	472 ± 70	308 ± 27	373 ± 62	345 ± 64	111 ± 13	398 ± 71	4640
A70	<33.0	<33.0	202 ± 6.1	<33.0	321 ± 39	275 ± 44	149 ± 35	228 ± 60	204 ± 52	67.8 ± 21	225 ± 18	271 ± 18	<33.0	346 ± 33	2350
Low traffic-*Edinburgh sites*															
Hillpark Drive	51.2 ± 3	75.2 ± 22	706 ± 118	96.6 ± 1.8	2000 ± 333	1420 ± 195	1140 ± 5.1	1100 ± 25	1150 ± 4.0	492 ± 15	1080 ± 15	994 ± 4.9	245 ± 79	944 ± 60	11500
Thistle Street	<33.0	<33.0	435 ±59	<33.0	435 ± 117	348 ± 68	137 ± 40	307 ± 38	224 ± 121	81.7 ± 15	194 ± 130	56.2 ±10	<33.0	121 ± 64	2400
Belmont Crescent	40.0 ± 0.7	75.7 ± 4.2	219 ± 3.9	61.9 ± 1.1	528 ± 2.7	424 ± 10	395 ± 16	446 ± 4.9	486 ± 30	322 ± 9.3	413 ± 22	344 ± 12	113 ± 4.2	365 ± 31	4230
Cambusnethan Street	<33.0	75.4 ± 29	437 ± 32	<33.0	246 ± 9.8	196 ± 13	<33.0	195 ± 38	107 ± 27	<33.0	76.6 ± 15	<33.0	<33.0	82.5 ± 38	1520
Redhall Drive	<33.0	68.9 ± 3.6	326 ± 9.3	109 ± 3.1	364 ± 14	329 ± 13	281 ± 16	408 ± 29	294 ± 27	230 ± 14	320 ± 31	414 ± 19	247 ± 15	512 ± 30	3920

NOTE: (ACE) Acenaphthene, (Fl) Fluorene, (PHE) Phenanthrene, (ANT) Anthracene, (FLA) Fluoranthene, (PYR) Pyrene, (BaA) Benzo (a) anthracene, (CHR) Chrysene, (BbF) Benzo (b) fluoranthene, (BkF) Benzo (k) fluoranthene, (BaP) Benzo (a) pyrene, (IcdP) Indeno (1,2,3-cd) pyrene, (DahA) Dibenzo (a,h) anthracene, (BghiP) Benzo (g,h,i) perylene. Limit of Detection (LOD) was calculated by using lowest calibration standard /weight of road dust sample extracted (3g). Where values were below LOD, PAH congener was assigned value of 16.5 µg kg^{-1} (half LOD).

Following elemental concentrations determined in road dust from five high- and low-traffic locations, three specific areas were chosen for further sampling and analysis where high elemental concentrations were found. This was carried out to establish whether or not the levels of contamination found at these locations were representative of surrounding roads for each area (Table 3.2). The first of these had especially elevated concentrations of Pb and Zn. The set of roads in the vicinity of Cambusnethan Street had mean concentrations of Sb, Pb, Cu and Zn of 3.1 ± 0.6, 136 ± 49, 53.6 ± 11 and 247 ± 32 mg kg^{-1}, respectively. More specifically, road dust concentrations of Pb and Zn were greatest at Dalgety Street (195 mg kg^{-1}) and Dalgety Avenue (272 ± 60 mg kg^{-1}), respectively. For both locations, concentrations of Pb and Zn were approximately half of those observed at Cambusnethan Street, but were still considered high, given the location and the expected low traffic flow for these locations (Table 3.2). The second area selected for further sampling and analysis was Thistle Street, as initial road dust analysis had shown elevated mean concentrations of Sb (6.2 ± 2.8 mg kg^{-1}), Pb (293 ± 6.4 mg kg^{-1}), Cu (91.0 ± 31 mg kg^{-1}) and Zn (302 ± 11 mg kg^{-1}) present for this location. When initial road dust results were compared to further samples collected at west, mid and east points of Thistle Street, mean concentrations of Sb (11.8 ± 6.5 mg kg^{-1}), Pb (702 ± 223 mg kg^{-1}), Cu (197 ± 89 mg kg^{-1}) and Zn (480 ± 154 mg kg^{-1}), were all greater than initially observed, and exceeded concentrations of elements found in road dust sampled at all Edinburgh locations (Table 5.1). Road dust sites in the vicinity of Edinburgh airport were the last specific location where additional samples were collected. The sites detailed in Table 3.2 were chosen to determine whether elemental road dust concentrations were influenced by aviation emissions from Edinburgh airport. In general, elemental concentrations were within the same concentration range as high- and low-traffic roads. Some sites did, however, show elemental concentrations that were elevated, such as Turnhouse Road-East for Pb (311 ± 8.7 mg kg^{-1}), North Gyle Grove-East for Cu (200 ± 22 mg kg-1) and Kirklisten-West for Cu (218 ± 63 mg kg^{-1}) and Zn (455 ± 13 mg kg^{-1}).

5.4.2 PAH road dust samples from Edinburgh

In contrast to elemental concentrations and for all Edinburgh road dust sites, Cambusnethan Street had the lowest Σ16PAH concentrations observed at 1520 μg kg^{-1}, with maximum concentrations found at Hillpark Drive (11500 μg kg^{-1}) (Table 5.3). With the exception of Hillpark Drive, mean concentrations of Σ16PAHs were greater at high-traffic roads (4610 ± 1970 μg kg^{-1}) than at low traffic roads (3018 ± 1280 μg kg^{-1}). Although individual PAH concentrations varied at each sampled site, pyrogenic PAHs contributed the most to Σ16PAH road dust concentrations, where fluoranthene and pyrene were dominant with mean contributions of 14.4 and 11.6 %, respectively. High PAH concentrations were also observed for, phenanthrene, benzo(b)fluoranthene, benzo(g,h,i)perylene and benzo(a)pyrene contributing a mean % of ΣPAH concentrations of 10.8, 9.6, 8.6 and 8.9%, respectively. The least prevalent PAHs for all Edinburgh sites were acenaphthene and fluorene.

5.4.3 Elemental road dust samples from Glasgow

Similarly, to Edinburgh, concentrations of elements in road dust from Glasgow high-traffic sites were generally lower than those of low-traffic sites (Table 5.4). For high-traffic sites, mean concentrations of Sb were 3.5 ± 1.8 mg kg^{-1}, ranging from 1.9 ± 0.2 mg kg^{-1} at Hyndland Road, to 6.1 ± 2.0 mg kg^{-1} at A8 of Glasgow. The sample from the A8 of Glasgow also had the greatest concentration of Pb at 312 ± 38 mg kg^{-1}, with the Baird Street sample having the lowest, at 20.3 ± 4.9 mg kg^{-1}. Mean concentrations of Pb and Cu at high-traffic locations were comparable at 112 ± 115 mg kg^{-1} and 93 ± 51 mg kg^{-1}, respectively. Concentrations of Cu at three locations were generally similar at ~125 mg kg^{-1}, with both A82 and again, Hyndland Road considerably lower at 35 ± 6.5 mg kg^{-1} and 44.8 ± 7.4 mg kg^{-1}, respectively. The most abundant element present in the Glasgow road dust was Zn, where mean concentrations were 230 ± 160 mg kg^{-1}, which was two orders of magnitude higher than Sb, and more than double of Pb and Cu. Similar to other elements, concentrations of Zn at the A8 (Glasgow) were greatest (450 ± 50 mg kg^{-1}) and lowest at

Baird Street (124 ± 2.7 mgkg^{-1}). For Glasgow high-traffic locations, there was no statistical significant trends (P >0.4, R^2<0.67 n=20, appendix 7, output 3) for concentrations of elements in road dust and traffic volume, with maximum and minimum elemental concentrations appearing to be randomly distributed across all sites.

For low traffic sites, concentrations of Sb and Cu were ~35% greater than high traffic sites, with Pb and Zn a further 70% higher. Antimony road dust concentrations ranged from 3.7 ± 0.2 mg kg^{-1} at Black Street, to 8.3 ± 3.5 mg kg^{-1} at Leydon Street, with a mean value of 5.5 ± 2.1 mg kg^{-1}. Mean concentrations of Pb were ~2 orders of magnitude greater than Sb at 389 ± 345 mg kg^{-1}, and ranged considerably across all low-traffic locations. For example, mean road dust concentrations of Pb at Black Street and West Princes Street were 776 ± 280 mg kg^{-1} and 711 ± 102 mg kg^{-1}, respectively, whilst the sample from Tradeston Street had a considerably lower value of 53.5 ± 23 mg kg^{-1}. The mean Cu concentrations were 93 ± 51 mg kg^{-1}, with Goosedubbs samples having somewhat higher values than all other road dust sites at 288 ± 23 mg kg^{-1}, while Leydon Street samples had the lowest values at 78.5 ± 26 mg kg^{-1}. Both Goosedubbs and Leydon Street were also found to be where concentrations were greatest, and lowest for Zn, where a remarkable 2550 ± 360 mg kg^{-1} and 254 ± 40 mg kg^{-1} were observed, respectively.

5.4.4 PAH road dust samples from Glasgow

The trend of higher contaminant concentrations observed at low-traffic sites, compared with high-traffic sites, was also evident from Σ16PAH road dust concentrations, where low-traffic sites had a mean concentration of 46100 μg kg^{-1}, compared with the high traffic mean of 6220 μg kg^{-1}. For the low traffic sites, Σ16PAH concentrations ranged considerably from the lowest at Leyden Street (3250 μg kg^{-1}), to the greatest at Black Street (192000 μg kg^{-1}). Goosedubbs had the second greatest Σ16PAH concentrations (13800 μg kg^{-1}) present, but was still considerably less than values observed at Black Street, with Σ16PAH concentrations at Black Street most likely due to its location in an industrial estate. For high

traffic locations, Σ16PAH concentrations were greatest in Broomielaw road dust (11300 μg kg^{-1}), and lowest at the A82 (2030 μg kg^{-1}).

Of the 16 PAHS that were analysed, fluoranthene and pyrene concentrations were highest in each of the samples, ranging between 359-40700 μg kg^{-1} and 271-32100 μg kg^{-1}, respectively. Thus fluoranthene and pyrene contributed 18.2 ± 2.0% and 14.0 ± 1.6%, respectively, to mean Σ16PAH concentrations observed at Glasgow locations, while chrysene also made a notable contribution (9.1 ± 1.6%) to mean concentrations observed.

Table 5.4: Elemental concentrations and Pb isotope ratios for Glasgow road dust sampled at high- and low-traffic roads.

Road dust sites	pH	% OM	Sb (mg kg^{-1}) ± 1SD	Pb (mg kg^{-1}) ± 1SD	Cu (mg kg^{-1}) ± 1SD	Zn (mg kg^{-1}) ± 1SD	$^{206}Pb/^{207}Pb$ ± 1SD	$^{208}Pb/^{207}Pb$ ± 1SD	$^{208}Pb/^{206}Pb$ ± 1SD
High traffic-*Glasgow sites*									
A8 of Glasgow	7.4	8.9	6.1±2.0	312±38	106±13	450±50	1.149±0.002	2.439±0.004	2.079±0.004
A82	7.5	0.9	3.5±2.7	72.8±8.6	35.1±6.5	90.1±14	1.166±0.002	2.441±0.003	2.093±0.004
Broomielaw	7.7	4.5	4.4±0.2	99.2±23	150±0.3	348±28	1.148±0.003	2.427±0.004	2.114±0.003
Baird Street	7.4	2.2	1.8±0.5	20.3±4.9	110*	124±2.7	1.160±0.001	2.442±0.005	2.109±0.003
Hyndland Road	7.6	2.2	1.9±0.2	59.4±19	44.8±7.4	139±41	1.169±0.005	2.450±0.005	2.097±0.001
Low traffic-*Glasgow sites*									
Tradeston Street	7.4	5.6	3.3±0.3	53.5±23	90.8±16	321±21	1.150±0.003	2.434±0.002	2.122±0.004
West Princes Street	6.5	5.9	6.5±3.9	711±102	91.6±11	510±46	1.151±0.003	2.429±0.002	2.113±0.001
Goosedubbs	6.6	7.3	5.6±2.2	345±13	288±267	2550±360	1.160±0.001	2.440±0.002	2.101±0.002
Black Street	6.1	20.1	3.7±0.2	776±280	152±13	312±9.0	1.174±0.003	2.433±0.002	2.076±0.002
Leydon Street	7.0	4.2	8.3±3.5	60.2±17	78.5±26	254±40	1.140±0.002	2.433±0.006	2.094±0.008

***** Indicates single analysis entry

Table 5.5: PAH concentrations in road dust from Glasgow high- and low-traffic roads.

Road dust sites	ACE	Fl	PHE	ANT	FLA	PYR	BaA	CHR	BbF	BkF	BaP	IcdP	DahA	BghiP	Σ PAH
	in µg kg^{-1} ± 1SD														in µg kg^{-1}
High traffic-*Glasgow sites*															
A8 of Glasgow	301 ± 66	352 ± 37	1730 ± 165	232 ± 9.3	1880 ± 168	1460 ± 107	507 ± 1.2	870 ± 80	554 ± 0.2	273 ± 11	460 ± 0.4	309 ± 11	80.5 ± 4.6	465 ± 35	9470
A82	48.5 ± 3.6	71.6 ± 1.0	214 ± 3.3	<33.0	359 ± 13	271 ± 7.8	125 ± 0.8	182 ± 2.5	196 ± 3.2	45.1 ± 4.3	96.0 ± 3.5	179 ± 0.1	<33.0	206 ± 0.4	2030
Broomie-law	224 ± 14	273 ± 5.4	1680 ± 60	227 ± 16	1940 ± 195	1560 ± 176	626 ± 222	852 ± 241	637 ± 300	321 ± 165	660 ± 16.5	856 ± 43	296 ± 34	1180 ± 120	11300
Baird Street	101 ± 33	163 ± 48	569 ± 53	81.3 ± 15	715 ± 32	506 ± 16	234 ± 5.0	268 ± 11	296 ± 22	95.2 ± 4.3	144 ± 22	260 ± 118	<33.0	283 ± 39	3730
Hyndland Road	167 ± 49	229 ± 70	827 ± 165	120 ± 36	822 ± 78	627 ± 39	243 ± 24	358 ± 43	253 ± 6.2	127 ± 9.7	240 ± 21	184 ± 20	107 ± 22	245 ± 9.2	4550
Low traffic-*Glasgow sites*															
Tradeston Street	301 ± 28	355 ± 55	2150 ± 51	235 ± 2.8	2140 ± 84	1740 ± 45	648 ± 64	1000 ± 114	666 ± 57	256 ± 93	575 ± 93	221 ± 68	<33.0	403 ± 105	10700
West Princes Street	263 ± 14	257 ± 11	1890 ± 85	205 ± 29	2100 ± 157	1570 ± 69	766 ± 20	875 ± 44	766 ± 195	263 ± 91	576 ± 180	544 ± 188	<33.0	597 ± 204	10700
Goose-dubbs*	242	284	2270	240	2760	2050	884	1420	1170	576	1070	338	<33.0	489	13800
Black Street	983 ± 175	1770 ± 244	19200 ± 1170	3090 ± 212	40700 ± 273	32100 ± 221	20700 ± 1070	20800 ± 486	13600 ± 2180	7200 ± 1200	13700 ± 196	7210 ± 676	1900 ± 97	8600 ± 162	192000
Leyden Street	49.0 ± 8.9	82.8 ± 22	290 ± 53	38.1 ± 7.1	444 ± 6.4	354 ± 13	177 ± 18	371 ± 52	358 ± 45	99 ± 5.2	168 ± 22	352 ± 4.0	<33.0	450 ± 6.5	3250

NOTE: (ACE) Acenaphthene, (Fl) Fluorene, (PHE) Phenanthrene, (ANT) Anthracene, (FLA) Fluoranthene, (PYR) Pyrene, (BaA) Benzo (a) anthracene, (CHR) Chrysene, (BbF) Benzo (b) fluoranthene, (BkF) Benzo (k) fluoranthene, (BaP) Benzo (a) pyrene, (IcdP) Indeno (1,2,3-cd) pyrene, (DahA) Dibenzo (a,h) anthracene, (BghiP) Benzo (g,h,i) perylene. Limit of Detection (LOD) was calculated by using lowest calibration standard /weight of road dust sample extracted (3g). Where values were below LOD, PAH congener was assigned value of 16.5 µg kg^{-1} (half LOD).*Indicates single analysis entry

5.4.5 Comparison of contaminant concentrations found in road dust from Edinburgh and Glasgow

The comparison of Edinburgh and Glasgow contaminant road dust concentrations made in this section does not include Edinburgh sites affected by historic and current land use (Table 3.2) because the inclusion of this data would distort the Edinburgh data in favour of the three areas where intensive sampling had been carried out; instead this data will be discussed in sections 5.7 and 5.10.

Mean concentrations of Sb, Pb, Cu and Zn in road dust from Edinburgh (Sb 5.3 ± 2.8 mg kg^{-1}, Pb 135 ± 129 mg kg^{-1} , Cu 91.4 ± 48 mg kg^{-1}, Zn 248 ± 144 mg kg^{-1}) and Glasgow (Sb 4.5 ± 2.1 mg kg^{-1}, Pb 250 ± 282 mg kg^{-1}, Cu 114 ± 71 mg kg^{-1}, Zn 283 ± 146 mg kg^{-1}) were statistically indistinguishable by t test (two-sample assuming unequal variances, Sb and Cu: t=0.9, p=0.37, n=30; Pb: t=1.2, p=0.24 n=30; Zn: t=1.1, p=0.29, n=30, appendix 7, output 4). Although the selected road dust sites for Edinburgh high-traffic locations had greater AADF than high-traffic locations in Glasgow, the greater vehicle emissions observed for Edinburgh sites were not reflected in greater Edinburgh road dust elemental concentrations. This could be the result of a number of factors, such as a more effective street cleaning network, and differing rainfall for each location (mean rainfall for 1981-2010; Glasgow 1124 mm, Edinburgh 704 mm, Met Office, 2015). Although AADF data for Edinburgh road dust locations were generally higher than those of Glasgow, the greater traffic numbers experienced citywide for Glasgow (~30% more than Edinburgh citywide), and the legacy of Glasgow's industrial past would account for the higher concentrations of Pb and Σ16PAH observed here.

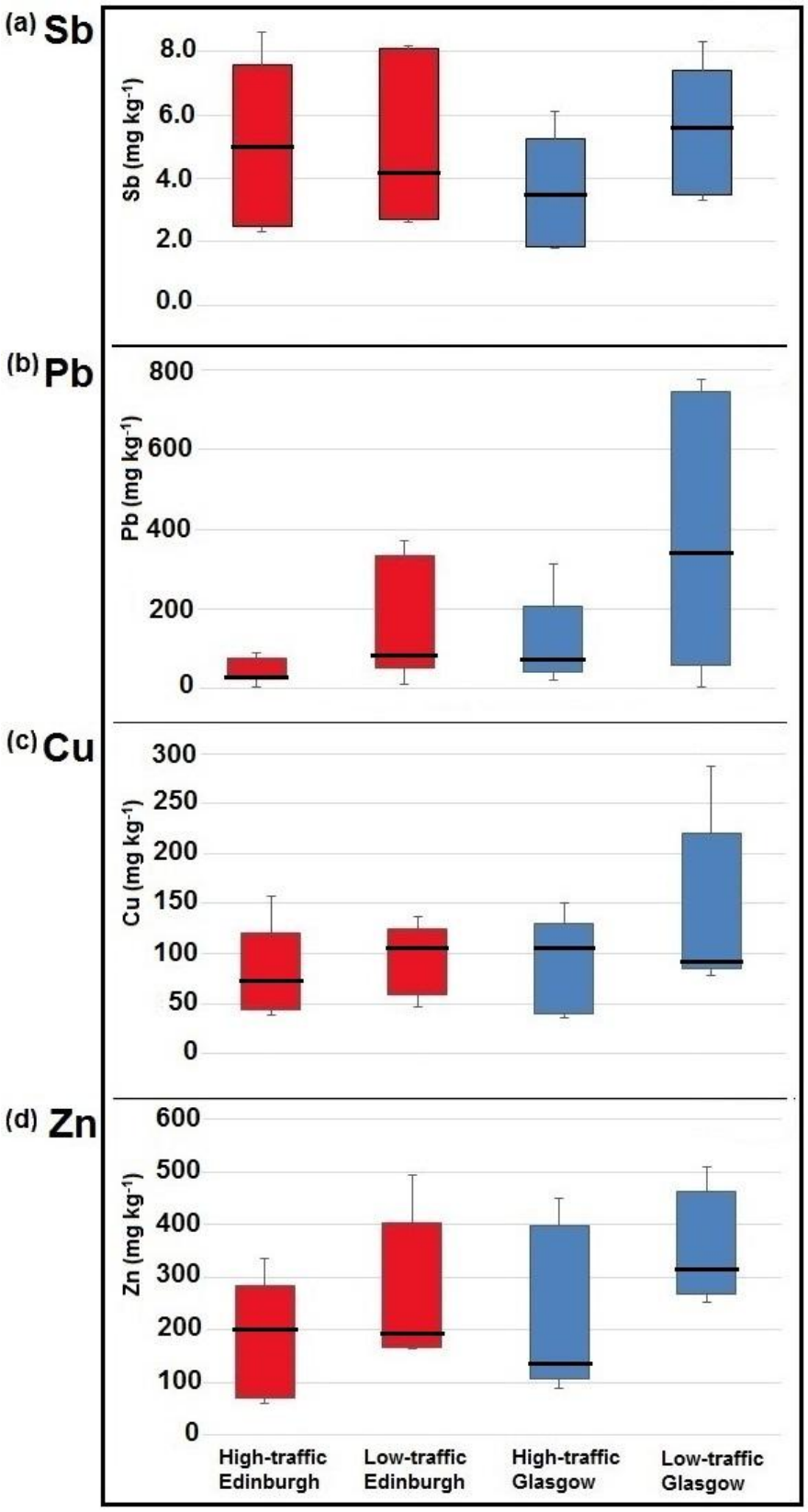

Figure 5.1: Comparison of Edinburgh and Glasgow high- and low-traffic road dust samples using median, 25th and 75th percentile, minimum and maximum concentrations for: (a) Sb, (b) Pb, (c) Cu and, (d) Zn.

Mean and median elemental concentrations for each element found in road dust from Edinburgh and Glasgow were generally similar, although mean road dust concentrations from Glasgow for Zn, and Edinburgh for Pb, were ~50% and ~60% higher than the respective medians. Figure 5.1(a)-(d) demonstrates the comparable median concentrations for each element in road dust from Edinburgh 10 m locations and all Glasgow locations (n=20). The one exception to this was for Pb, where median concentrations in Glasgow road dust were over double those observed in Edinburgh, and were most likely attributed to the past emissions of Pb from former metal works, heavy engineering, shipbuilding and marine engineering industries, as well as coal combustion used to power local industry. The maximum concentrations for each element were obtained at the low traffic sites; this was particularly evident for Pb, where a marked difference in the minimum and maximum Pb concentrations obtained for low and high traffic sites were observed. For both Edinburgh and Glasgow sites, the minimum Pb concentrations were fairly similar (~30 mg kg^{-1}) but the maximum values for low-traffic locations were ~2-3 times greater than their respective high-traffic locations. For Zn, maximum concentrations for dusts from both cities were found at the low-traffic sites but, in contrast with Pb, the minimum values were also higher at these sites; for the Glasgow road dust samples, the range of values were actually narrower for the low traffic sites. The trend in road dust concentrations for Pb and Zn was, to some extent, similar to data for Sb and Cu, but the differences between low and high traffic sites were not as pronounced (especially for the Edinburgh samples).

As for PTEs, the mean Σ16PAH concentrations in dust samples from Edinburgh and Glasgow were statistically indistinguishable by t test (two-sample assuming equal variances, t=1.189, p=0.25, n=20, appendix 7, output 5). Although there was no statistically significant difference, the mean value for Edinburgh road dust (4700 ± 2940 mg kg^{-1}) was ~two-thirds that for Glasgow (7730 ± 4320 mg kg^{-1}) (Black Street Σ16PAH concentrations were excluded from Glasgow mean value). As the dominant source of PAHs to the urban environment is through vehicle emissions (Dore *et al*., 2008; Shen *et al*., 2010), the higher

concentrations observed at Glasgow reflects the greater amount of traffic it experiences city wide. Using total traffic count (TTC) data for Edinburgh and Glasgow as an example, Edinburgh experienced just under a third less road traffic than Glasgow at the time of sampling. Indeed, the trend of greater traffic numbers in Glasgow was observed every year since records began in 2000 (Department of Transport, 2015) and would help account for the greater Σ16PAH concentrations observed in Glasgow, when compared to Edinburgh road dust locations.

5.4.6 Comparison of Scottish and global contaminant concentrations found in road dust

There are few studies of Sb concentrations in road dusts but the mean value of 5.3 ± 2.8 mg kg^{-1} and 4.5 ± 2.1 mg kg^{-1} recorded in this study for Edinburgh and Glasgow, respectively (Table 5.1 and 5.4), was similar to mean road dust concentrations reported by De Miguel *et al*. (1997) from 16 sites in Oslo, Norway (6.0 ± 0.5 mg kg^{-1}). Other studies collecting dust samples from Jeddah City, Saudi Arabia (Kadi, 2009) and from highways in Massachusetts, US (Ceriotti and Amarasiriwardena, 2009), observed maximum concentrations of 2.76 mg kg^{-1} and 0.024 mg kg^{-1}, respectively. It is worth noting, however, that the Massachusetts road dust was not sampled from the urban environment, which would account for the lower concentrations observed here, when compared with city values from Edinburgh and Glasgow.

There have been numerous studies of Pb concentrations in urban areas in the UK and around the world. Road dust studies by Farmer and Lyon (1977) and Sugden *et al.* (1993) showed Pb concentrations in Glasgow and Edinburgh reaching 2300 mg kg^{-1} and 1194 mg kg^{-1}, respectively, for the late 20^{th} century before the European ban on leaded petrol. More recently, Farmer *et al*. (2011) sampled 27 urban soils in and around Glasgow and determined Pb concentrations to be in the range of 126-2160 mg kg^{-1}, while Mitchell *et al.* (2014) examined 54 gardens in New York, US, and found that 44% of them exceeded the 400 mg

kg^{-1} garden soil guidance value set by the New York State's Environmental Remediation Program. In general, elevated Pb concentrations are a legacy of past industrial activity and the use of lead additives in petrol. From a global review by Charlesworth *et al.* (2011), Pb concentrations in road dust and urban soils from 26 worldwide cities were compared, and showed 70% of reported road dust concentrations of Pb were ≤300 mg kg^{-1}. For this study, most road dust samples had Pb concentrations of ~20-300 mg kg^{-1}, which was in good agreement with the global review by Charlesworth *et al*. (2011). Lead concentrations at a total of six road dust sites exceeded 300 mg kg^{-1} where the values ranged from 312-776 mg kg^{-1}. The specific locations were Thistle Street, Cambusnethan Street in Edinburgh, and the A8, Goosedubbs, West Princes Street and Black Street in Glasgow (Table 5.1 and 5.4).

Mean Cu concentrations in Edinburgh and Glasgow road dust were 91.4 ± 48 mg kg^{-1} and 114 ± 72 mg kg^{-1}, respectively, and these were notably lower than at other locations in the UK. A study in Birmingham by Charlesworth *et al*. (2003) reported a mean Cu concentration in road dust of 467 ± 99 mg kg^{-1}, whilst Wang *et al.* (1998) reported 300 mg kg^{-1} present in road dust from London. Since the decline of heavy industry in city centres, the deposition of Cu from traffic-related sources, particularly brake linings, is the primary source of Cu deposited in urban areas (Charlesworth *et al*., 2003). Although TTC data was not available for the year road dust from Birmingham was sampled, TTC data from 2000 to 2014 showed Birmingham had up to one third more road traffic annually than Edinburgh and Glasgow, which would partly account for the higher Cu road dust concentrations found at this location (Department of Transport, 2015). In addition, past industry activity was also identified to have increased Cu road dust concentrations in Birmingham, where values were enriched near former metal work sites and a brass foundry (Charlesworth *et al*., 2003). Since road traffic in London (TTC 81,000) was considerably lower than Birmingham, Edinburgh and Glasgow (Department of Transport, 2015), past industrial activity would also account for elevated concentrations of Cu observed in road dust. For example, in London during early to mid-20^{th} century, large quantities of elements were emitted to the urban environment from coal

combustion, which led to the London smog of 1952 (Brimblecombe, 1987; Laskin, 2006). For some instances, past anthropogenic activity can have a greater influence on elemental concentrations in road dust than road traffic emissions, with factors such as historic land use, construction, domestic heating and natural deposition all contributing to elemental concentrations in road dust (Charlesworth *et al*., 2003). For Edinburgh and Glasgow, road dust Cu concentrations were more comparable with mean results recorded from much smaller cities such as Mieres, Spain (122 mg kg^{-1}) (Ordóñez *et al*., 2003) and Taejon, South Korea (57 mg kg^{-1}) (Kim *et al*., 1998), and indicated Cu concentrations in road dust from Edinburgh and Glasgow were relatively low.

Similar to Cu, vehicle emissions have become a major source of Zn in road dust since the decline of metal smelting during the 20th century. A study by Napier *et al.* (2008), quantified the amount of Zn released from passenger car components in the UK including: tyre erosion (990 t), brake wear (44 t), oil losses (2.3 t) and exhaust emissions (1.0 t). Again, past industrial activities can also influence Zn road dust concentrations, where previously deposited elements can often be incorporated into road dust. With the exception of Goosedubbs (2550 ± 360 mg kg^{-1}), mean Zn concentrations for Edinburgh and Glasgow were 237 ± 48 mg kg^{-1} and 283 ± 146 mg kg^{-1}, respectively, and lower than the mean road dust concentrations from the previously mentioned cities Birmingham (534 mg kg^{-1}) and London (1866 mg kg^{-1}). Whilst the greater traffic numbers observed in Birmingham when compared to Edinburgh and Glasgow, would account for the higher Zn concentrations present in road dust, past industrial activities would have also increased road dust concentrations in Birmingham, and specifically for London (Wang *et al*., 1998; Charlesworth *et al*., 2003). Road dust concentrations of Zn from Glasgow and Edinburgh were more comparable to mean concentrations observed at much smaller cities, such as Oslo (412 mg kg^{-1}) (De Miguel *et al*., 1997) and Taejon, South Korea (214 mg kg^{-1}) (Kim *et al*.,

1998), indicating Zn road dust concentrations from Edinburgh and Glasgow were relatively low.

Vehicle exhaust emissions, oil losses and tyre wear contribute significant amounts of PAHs to road dust concentrations (Napier *et al*., 2008). The mean Σ16PAH road dust concentrations for Edinburgh and Glasgow samples were 4700 ± 2940 μg kg^{-1} and 7730 ± 4320 μg kg^{-1}, respectively. These values were lower than those reported by Lorenzi *et al*. (2011) in Newcastle road dust, where Σ16PAH concentrations were generally in the range of 15600−22500 μg kg^{-1}. For 2014, TTC for Newcastle was 558,000, which was approximately half the TTC observed for Edinburgh, and a third less for Glasgow, yet Σ16PAH concentrations were much greater. Lorenzi *et al*. (2011) concluded that Σ16PAH concentrations in Newcastle road dust were a result of vehicle emissions, yet for this study, both Edinburgh and Glasgow had greater city vehicle numbers and lower concentrations of Σ16PAH in road dust. For this instance, it is more likely that elemental concentrations observed in Newcastle road dust were considerably influenced from past emissions of industrial activities; Newcastle was renowned for its ship building, heavy engineering and coal trade during the 19^{th} and 20^{th} century (Johnson, 2015). For Birmingham, Σ16PAHs concentrations found in road dust reflected the greater traffic numbers experienced there, when compared to Edinburgh and Glasgow (~33% higher). Road dust collected from a busy road location on Bristol Road, Birmingham, was considerably higher (28500 μg kg^{-1}) than values found at Edinburgh and Glasgow (Smith *et al*., 1995). In comparison with dusts from cities outside the UK, the mean Σ16PAH road dust concentrations for Edinburgh and Glasgow were lower than larger more densely populated international cities, such as Shangai, China (14,098 μg kg^{-1}) (Lui *et al.*, 2007), and Ulsan, South Korea (45800 μg kg^{-1}) (Dong and Lee, 2009).

As individual PAHs present in the priority 16 vary in terms of toxicity and source, benzo(a)pyrene is often used as an indicator for atmospheric PAH concentrations (Table

2.6). It is considered one of the most toxic isomers due to its carcinogenic properties, and is well-known to originate from the incomplete combustion of fuels from vehicles, and from rubber tyre wear (EEA, 2013). In accordance with the Contaminated Land Exposure Assessment (CLEA) implemented by the Environment Agency, the 1000 μg kg^{-1} acceptable benzo(a)pyrene limit for domestic garden topsoil was marginally exceeded in Edinburgh at Hillpark Drive (1080 μg kg^{-1}) and in Glasgow at Goosedubbs (1070 μg kg^{-1}), and values were over a magnitude higher at Black Street, Glasgow (13700 μg kg^{-1}). The inhalation of PAHs associated with re-suspended road dust particulates represents a potential human health risk for these three road dust locations.

5.5 Urban road dust and surface water $^{206}Pb/^{207}Pb$ isotopic ratios

5.5.1 Road dust and surface water $^{206}Pb/^{207}Pb$ isotopic ratio results

Lead isotope ratio analysis ($^{206}Pb/^{207}Pb$, $^{208}Pb/^{207}Pb$, $^{208}Pb/^{206}Pb$) was completed on Edinburgh road surface water (Table 5.6), Edinburgh 10 m road dust sites, three specific road dust areas chosen in Edinburgh (Table 5.1 and 5.2), and Glasgow road dust sites (Table 5.4). Mean $^{206}Pb/^{207}Pb$ isotope ratios in Edinburgh road surface water were 1.143 ± 0.008, and ranged from 1.130 ± 0.002 at the A70, to 1.156 ± 0.003 at Thistle Street. For road dust, broadly similar isotope ratios were obtained from Edinburgh 10 m sites (1.141 ± 0.01), although considerable more variation was observed ranging from 1.116 ± 0.002 at Redhall Drive, to 1.151 ± 0.001 at Queen Street. Further road dust sampled from three additional areas in Edinburgh, such as the nearby roads to Cambusnethan Street and at locations on Thistle Street, had comparable $^{206}Pb/^{207}Pb$ isotope ratios to Edinburgh 10m road dust sites, at 1.146 ± 0.007 and 1.148 ± 0.003, respectively. There was however, a significant difference in isotope ratios obtained within 5 km east, south east, of Edinburgh airport ($t=6.9$, $p=0.002$, $n=17$, appendix 7, output 6), where North Gyle Grove (1.102 ± 0.003), Turnhouse Road (1.116 ± 0.006) and Craig Road (1.121 ± 0.004) all had notably low $^{206}Pb/^{207}Pb$ isotope ratios, and were in agreement with low ratios obtained at Redhall Drive, which was similarly

located near Edinburgh airport. All other road dust sites near Edinburgh airport had the highest $^{206}Pb/^{207}Pb$ isotope ratios observed in Edinburgh ranging from 1.154 ± 0.004 at Cammo Road, to 1.162 ± 0.001 at Glasgow Road.

The mean $^{206}Pb/^{207}Pb$ isotope ratios recorded in Glasgow road dust sites were significantly higher than Edinburgh, with a mean ratio of 1.157 ± 0.01, and range from 1.140 ± 0.002 at Leydon Street, to 1.174 ± 0.003 at Black Street. No spatial trend in $^{206}Pb/^{207}Pb$ isotope ratios was observed across Glasgow.

5.5.2 Road dust and surface water $^{206}Pb/^{207}Pb$ isotopic ratio discussion

As discussed in section 2.3.7, the use of Pb isotope ratios $^{206}Pb/^{207}Pb$ and $^{208}Pb/^{207}Pb$ for assessing the impact of leaded petrol on water and soil has been applied in numerous historic and contemporary studies (MacKenzie *et al*., 1998; Shotyk *et al*., 2002; Farmer *et al*., 2005, 2006, 2010; Cloy *et al*., 2008; Robbins *et al*., 2010; MacKinnon *et al*., 2011). Source apportionment using Pb isotope ratios can be carried out assuming sample values lie on a mixing line between two main end points: the $^{206}Pb/^{207}Pb$ ratio found in UK coal (1.182 ± 0.009)(Farmer *et al*., 1999) or indigenous Pb ore from Wanlockhead (1.172 ± 0.003) (Cloy *et al*., 2005), and the low $^{206}Pb/^{207}Pb$ isotope ratio of tetra alkyl Pb present in UK leaded petrol (~1.08) (Farmer *et al*., 2000) of which Australian Pb ore ($^{206}Pb/^{207}Pb$ ~1.04) was a major component (Cooper *et al.*, 1969). The $^{206}Pb/^{207}Pb$ and $^{208}Pb/^{207}Pb$ isotopic ratios for Edinburgh surface water samples, Edinburgh road dust, and isotopic ratios from UK leaded petrol, Petrostock aviation gas (avgas) from Switzerland (Chiaradia and Cupelin, 2000), Wanlockhead ore (Cloy *et al*., 2005) and UK coal (Farmer *et al*., 1999) have been plotted in Figure 5.2.

Table 5.6: Duplicate analysis results for concentrations of Sb, Pb, Cu, Zn, and Pb isotope ratios for Edinburgh high- and low-traffic road surface water samples collected 1 m before entering the roadside drain.

Road dust sites	Sb ($\mu g\ L^{-1}$) ± 1SD	Pb ($\mu g\ L^{-1}$) ± 1SD	Cu ($\mu g\ L^{-1}$) ± 1SD	Zn ($\mu g\ L^{-1}$) ± 1SD	$^{206}Pb/^{207}Pb$ ± 1SD	$^{208}Pb/^{207}Pb$ ± 1SD	$^{208}Pb/^{206}Pb$ ± 1SD
High traffic							
A90	1.04 ± 0.07	0.58 ± 0.03	16.4 ± 2.20	43.1 ± 9.92	1.139±0.004	2.412±0.007	2.119±0.004
Queen Street	1.02 ± 0.01	1.47 ± 0.09	12.7 ± 1.50	46.2 ± 2.76	1.146±0.004	2.412±0.001	2.107±0.006
A8 of Edinburgh	1.29 ± 0.06	0.17 ± 0.06	21.7 ± 3.37	42.1 ± 4.11	1.148±0.001	2.428±0.005	2.113±0.004
A1	0.76 ± 0.02	1.06 ± 0.07	9.93 ± 0.20	44.5 ± 4.15	1.147±0.005	2.427±0.006	2.110±0.010
A70	0.17 ± 0.00	0.37 ± 0.02	4.18 ± 0.10	16.4 ± 1.85	1.130±0.002	2.396±0.004	2.136±0.012
Low traffic							
Hillpark Drive	0.10 ± 0.00	1.86 ± 0.39	45.9 ± 1.18	1550 ± 245	1.140±0.003	2.402±0.005	2.110±0.002
Thistle Street	1.12 ± 0.02	3.6 ± 0.36	15.6 ± 0.43	40.6 ± 11.5	1.156±0.003	2.426±0.004	2.098±0.003
Belmont Crescent	0.34 ± 0.03	0.57 ± 0.07	5.94 ± 0.65	259 ± 21.2	1.131±0.004	2.403±0.006	2.122±0.003
Cambusnethan Street	0.42 ± 0.08	1.89 ± 0.04	14.7 ± 0.87	33.7 ± 0.50	1.147±0.003	2.420±0.001	2.109±0.007
Redhall Drive	0.17*	0.48*	38.4*	227*	1.146±0.001	2.418±0.001	2.109±0.003

*Indicates single analysis entry

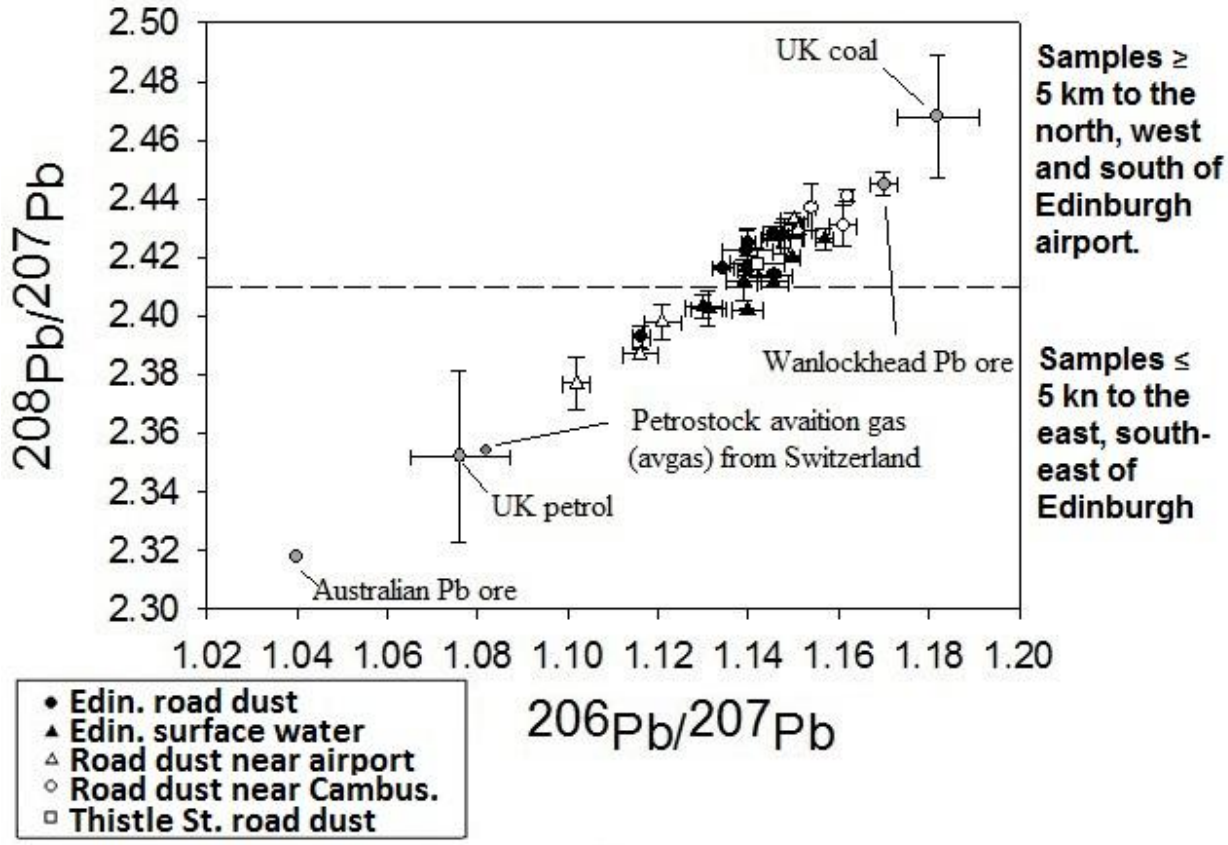

Figure 5.2: Three-isotope ($^{208}Pb/^{207}Pb$ vs $^{206}Pb/^{207}Pb$) plot (±1SD) of values taken from Edinburgh road dust sites, Edinburgh surface water sites compared with Australian Pb ore (Cooper *et al*., 1969), UK leaded petrol (1989-1998) (Farmer *et al*., 2000), Petrostock aviation gas from Switzerland (Chiaradia and Cupelin, 2000), Pb ore from Wanlockhead (Cloy *et al*., 2005) and UK coal (Farmer *et al*., 1999).

The mean $^{206}Pb/^{207}Pb$ isotopic ratio for road dust from Glasgow was 1.157 ± 0.011, and ranged from 1.140-1.174, which contrasted with road dust values from Edinburgh, where mean (1.141 ± 0.010) and range (1.116-1.151) isotopic ratios were much lower. Past road dust and soil studies from Glasgow showed similar isotopic ratios to this study, e.g. MacKinnon *et al*. (2011) observed $^{206}Pb/^{207}Pb$ ratios in road dust sampled in 2010 at four locations ranging from 1.132 to 1.162, while Farmer *et al.* (2011) reported $^{206}Pb/^{207}Pb$ ratios ranging from 1.057 to 1.175 at 27 soil sites, with 80% of the sites above 1.13. Thus, a clear difference in $^{206}Pb/^{207}Pb$ isotopic ratios found in Glasgow road dust was observed for this and, previous studies when compared with Edinburgh. This was attributed to Glasgow's industrial past, where coal power was heavily used for shipbuilding, metal works and textiles (Farmer *et al*., 2011; Fordyce *et al*., 2013), resulting in the emission and deposition of indigenous Pb being more dominant here, than in Edinburgh. Indeed, this was in agreement with the higher mean concentrations of Pb in Glasgow road dust (250 ± 282 mg kg^{-1}) when compared to Edinburgh concentrations (135 ± 129 mg kg^{-1}).

The mean $^{206}Pb/^{207}Pb$ isotope ratios observed in Edinburgh road surface water samples (1.143 ± 0.008) were notably higher than past values determined in rainwater from northern Scotland in 1990 (~1.10-1.13)(Sugden *et al.,* 1993). The considerable increase in isotope ratios since the 1990s, demonstrates the reduction in Pb emissions originating from the combustion of leaded petrol since its European ban in 2000. More recently, isotope ratios observed in rainwater from Glensaugh, Scotland showed higher values than those from Edinburgh road surface water; Vinogradoff *et al.* (2005) reported values of 1.153 ± 0.007 and 1.158 ± 0.008 from two sampling sites in 2002, and Farmer *et al*. (2010) also obtained values of 1.154 ± 0.018 and 1.145 ± 0.014 for rainwaters collected in 2006 and 2007, respectively. The difference in isotope ratios for Edinburgh and Glensaugh are most likely attributable to the difference in urban and rural sampling locations.

For Edinburgh road dust locations to the east of Edinburgh airport, $^{206}Pb/^{207}Pb$ isotopic ratios were typically lower within a ~5 km distance to Edinburgh airport (Table 5.1 and 5.2). In particular, Redhall Drive (1.116 ± 0.002), and additional sites closer (within 2 km) such as Turnhouse Rd, Craighouse Rd and North Gyle Grove, where low $^{206}Pb/^{207}Pb$ ratios were observed (mean 1.113 ± 0.008). The low isotope ratios found in road dust for these sites had been greatly influenced by past emissions occurring upwind from their location by local anthropogenic activities. The average wind direction for Eastern Scotland/Edinburgh blows from the south or south west, but as the depression moves away, the wind direction will also change, where it blows from the west or north west (Met Office, 2016; Weather Online, 2016). Taking into account the wind blowing from south/south west direction, and the close northern proximetry (~2 km) of Turnhouse Rd, Craighouse Rd and North Gyle Grove to major road routes in/out of Edinburgh (M8, Glasgow Road and the Edinburgh Bypass), it is most likely that Pb isotope ratios in road dust for these locations were considerably influenced by past vehicle emission from leaded petrol. Although vehicle emissions of leaded petrol were expected to be the dominant source of Pb to road dust for these particular sites, another potential emission source of Pb was identified when the wind direction of Edinburgh changed and blew from the west/north west. Since Turnhouse Rd, Craighouse Rd, North Gyle Grove and Redhall Drive are situated easterly and in close proximetry to Edinburgh airport, it is most likely that the lower $^{206}Pb/^{207}Pb$ isotopic ratios observed in road dust for these locations were also partly influenced from past emissions of avgas originating from Edinburgh airport. Chiaradia and Cupelin (2000) determined $^{206}Pb/^{207}Pb$ ratios for Petrostock aviation fuel used in Switzerland in 1997 as 1.0812, and whilst small national differences may occur as observed in leaded petrol ($^{206}Pb/^{207}Pb$ ratios for petrol from Scotland (1989-1998) and France (1980-1995) ranged ~1.06-1.09 (Farmer *et al*., 2000) and 1.06-1.10 (Veron *et al.,* 1999), respectively), the specific fuel used at Edinburgh airport would have had a similarly low $^{206}Pb/^{207}Pb$ ratio present. As previously mentioned (section 2.3.6.2), avgas can contain up to 0.56 g of Pb per litre (ASTM International, 2005), and due

to the low $^{206}Pb/^{207}Pb$ isotopic ratio present in the fuel (Figure 5.2), its emission can be similarly apportioned but not distinguished from leaded petrol emissions. Whilst current avgas use is typically <0.1% of total air traffic at Edinburgh airport, its previous use was high. Due to runway crosswinds, the construction and use of a new runway in Edinburgh airport was completed in 1977. This signalled a change in use for the previous runway, where it is currently used for the organisation and parking of aeroplanes. As detailed in Table 5.2, the $^{206}Pb/^{207}Pb$ isotopic signature for dust sampled from the old runway was higher than expected (1.158 ± 0.003), and was believed to be a result of Pb released from a combination of past avgas use, and from current use of jet fuel. As current avgas use is very low, jet fuel is used almost exclusively for all aviation travel, and although Pb content is typically lower than avgas, ranging between 0.11 and ~100 μg L^{-1} (Shumway, 2000; Moses, 2008), the high volumes used have resulted in a change in $^{206}Pb/^{207}Pb$ isotopic signature observed in the dust sample. Moreover, Pb observed in runway dust originating from jet fuel has an indigenous $^{206}Pb/^{207}Pb$ isotopic signature; in 2004, up to 80% of jet fuel was sourced from the North Sea crude oil (UKpia, 2015). It is believed that the $^{206}Pb/^{207}Pb$ isotopic signature observed in dust from the old runway was influenced by emissions of jet fuel occurring from the organisation of aeroplanes at ground level, over several decades. This would also agree with the very high Pb runway dust concentrations observed at the old runway (1750 mg kg^{-1}).

5.6 PAH source apportionment

5.6.1 Criteria

In order to gain insight to the origin of PAHs found in Edinburgh and Glasgow road dust, isomeric ratios were used to try and identify petrogenic and pyrogenic sources through diagnostics detailed by Yunker *et al*. (2002) and later used by Vane *et al*. (2011, 2014) for Glasgow river sediment. Essentially, the diagnostic approach uses relative thermodynamic stability of isomer PAH pairs, to identify and draw a cross-plot of PAH source emissions (Yunker *et al*., 2002). The criterion are detailed in Table 5.7.

Table 5.7: PAH isomeric diagnostic ratios used for road dust apportionment (Yunker *et al*., 2002).

PAH Isomers	Isomeric ratio formula	Diagnostic criteria	Source Category
Anthracene: Phenanthrene	[ANT]/ ([ANT]+[PHE])	0.0-0.1 Petroleum	Petrogenic
		0.1-0.7 Combustion	Pyrogenic
Fluoranthene: Pyrene	[FLA]/ ([FLA]+[PYR])	0.1-0.4 Petroleum	Petrogenic
		0.4-0.5 Petroleum combustion	Pyrogenic
		0.5-0.7 Grass/wood/coal combustion	Pyrogenic
Benzo (a) anthracene: Chrysene	[BaA]/ ([BaA]+[CHR])	0.0-0.2 Petroleum	Petrogenic
		0.2-0.35 Mixed sources	Pathogenic/ Pyrogenic
		0.35-0.7 Combustion	Pyrogenic
Indeno (1,2,3-cd) pyrene: Benzo (g,h,i) perylene	[IcdP]/ ([IcdP]+[BghiP])	0.0-0.2 Petroleum	Petrogenic
		0.2-0.5 Petroleum combustion	Pyrogenic
		0.5-0.7 Grass/wood/coal combustion	Pyrogenic

KEY: (PHE) Phenanthrene, (ANT) Anthracene, (FLA) Fluoranthene, (PYR) Pyrene, (BaA) Benzo (a) anthracene, (CHR) Chrysene, (IcdP) Indeno (1,2,3-cd) pyrene, (BghiP) Benzo (g,h,i) perylene

5.6.2 Discussion

Upon examination of the PAH cross-plot shown in Figure 5.3(a), (b) and (c), PAH's present in road dust can be apportioned to their source using diagnostic ratio values. For example, PAHs in road dust identified as petroleum, are likely to have originated from fuel or oil leaks, whereas those identified as combustion, are a result of the burning of hydrocarbons. In some instances, diagnostic ratios are also able to distinguish between the types of hydrocarbons undergoing combustion, such as petroleum combustion, or grass, wood and coal combustion as seen for the [anthracene:phenanthrene] diagnostic ratio.

Starting with isomeric ratios present on the y axis, [anthracene:phenanthrene] road dust ratios appeared to straddle both petroleum and combustion diagnostic criteria, with four locations (Redhall Drive, A90, Belmont Crescent and A1) indicating a very distinct isomeric combustion ratio when compared to all other sites (Figure 5.3(a)). Glasgow road dust sites were also tightly grouped together unlike Edinburgh, where a greater spread of [anthracene:phenanthrene] diagnostic ratios were found. For [benzo(a)anthracene:chrysene] diagnostic ratios (Figure 5.3(b)), most road dust sites indicated PAHs originating from combustion emissions, while three locations signified other sources. Both Leydon and

Thistle Street were marginally out with the combustion criteria where they were both present as mixed sources; this was in contrast to Cambusnethan Street, where a clear isomeric petroleum signature was found. The origin of PAHs found at Cambusnethan Street was also in agreement with [indeno(1,2,3-cd)pyrene/benzo(g,h,i)perylene] diagnostics ratios (Figure 5.3(c)), where again a distinct petroleum signature was seen at this site. With the exception of Hillpark Street which fell marginally within grass, wood and coal combustion criteria, all other sites showed isomeric ratios typical for a petroleum combustion source. Plots taken from x axis diagnostic ratios [fluoranthene/pyrene] (Figure 5.3(a)-(c)), showed all road dust sites originated from the combustion of grass, wood and coal, although it is worth noting that diagnostic ratios were close to the petroleum combustion value of 0.5.

Whilst diagnostic ratios provide a good indication of where PAH emissions have originated from, ratios should not be viewed as definitive, as they are unable to calculate the contribution each PAH source makes to the final PAH concentrations present. For example, in this study, no or very few road dust sites observed the diagnostic criteria for petroleum, even though it is very likely that PAHs from this source were present. Diagnostic ratios can only indicate what the dominant source is, i.e. combustion, which masks any smaller contribution such as petroleum to final PAH concentrations (Vane *et al*., 2011).

In general, the dominant emission source of PAHs present in road dust from Edinburgh and Glasgow was from the combustion of petroleum, and grass, wood and coal. Road dust PAH diagnostic ratios were heavily influenced by vehicle emissions, and was in agreement with a study by Dore *et al*. (2008), where vehicle emissions were identified as the biggest source of PAHs to the UK. Emissions from the burning of fuel such as wood and coal also proved to be influential to road dust diagnostic ratios for this study, where the release of PAHs at a local, and global level through long-range atmospheric transportation were also prominent.

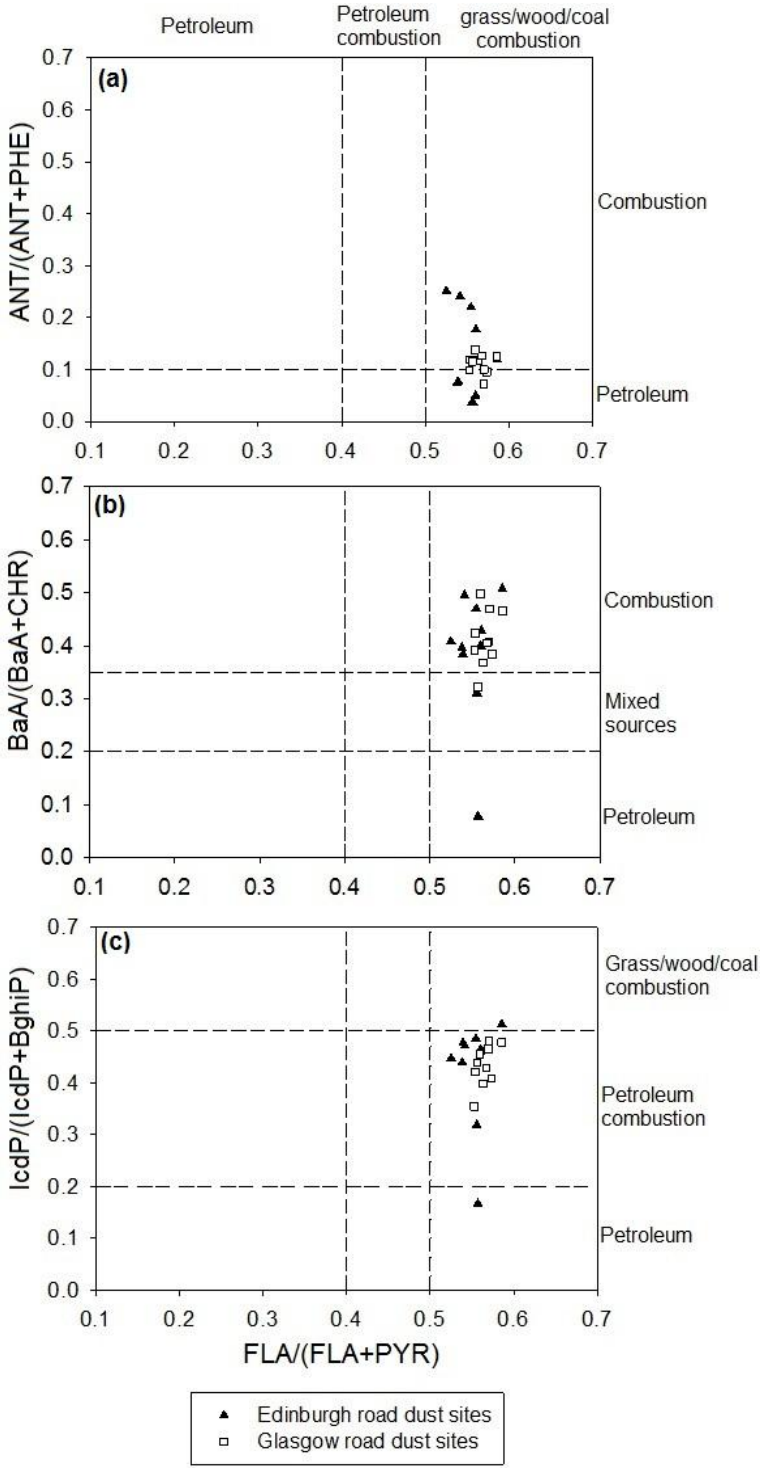

Figure 5.3: PAH isomeric cross-plot for road dust sites from Glasgow and Edinburgh using x-axis for Fluoranthene (FLA):Pyrene (PYR) diagnostic ratios and y-axis diagnostic ratios for: (a) Anthracene (ANT):Phenanthrene (PHE); (b) Benzo(a)anthracene (BaA): Chrysene (CHR); and (c) Indeno(1,2,3-cd)pyrene (IcdP):Benzo(g,h,i)perylene (BghiP).

The results for this study were largely in agreement with a study in Glasgow river sediment by Vane *et al*. (2011), where a strong petroleum, grass, wood and coal combustion signature was also reported. There was however, one road dust sample that did not exhibit a pyrogenic signature, and that was Cambusnethan Street, Edinburgh, where a petrogenic signature was observed. The unique diagnostic ratio for Cambusnethan Street from [benzo(a)anthracene/ chrysene](Figure 5.3(b)), [indeno(1,2,3-cd)pyrene/ benzo(g,h,i)perylene] (Figure5.3(c)), and to a lesser extent [anthracene/phenanthrene] (Figure 5.3(a)) (lowest diagnostic ratio plotted) displayed a strong petroleum source. A signature of this characteristic is often related to an oil or fuel spillage, and by taking into consideration the high number of residential parked cars at this location, it is most likely to have originated from a vehicle oil or fuel leak. Indeed, vehicle oil losses can contribute large amounts to PAH emissions in the UK, albeit from localised point sources. A study by Napier *et al*. (2008), estimated annual oil losses during 2003 for all UK road traffic to be 320 metric tonnes, which is considerable more than estimated exhaust emissions from UK passenger cars (HGV emissions not included) at 130 metric tonnes and tyre wear at 21.7 metric tonnes (Napier *et al*., 2008).

When PAH source and concentrations were compared to elemental results and road traffic count for Edinburgh and Glasgow, two notable trends were observed, and these were for Glasgow road dust sites. For Glasgow locations, an association with concentrations of Σ16PAH and Zn was observed ($P < 0.01$, $R^2=0.96$, n=10, appendix 7, output 7a), and to a lesser extent, Cu ($P<0.01$, $R^2=0.71$, n=10, appendix 7, output 7b). Both relationships indicate road dust concentrations were influenced by a similar source. The identification of the source is very difficult to ascertain, as each site has varying amounts of traffic, street cleaning, historic and current local emissions nearby, e.g. industrial units found near Black Street. One common emission source for Σ16PAH, Zn and Cu however, is their presence together in tyre erosion (Napier *et al*., 2008), which could be an important factor when considering the Σ16PAH, Zn and Cu relationships. No statistical relationship was observed for road dust

concentrations in Sb and Pb, even though both elements are known to be influenced by vehicle emissions. This is most likely attributed to the greater contribution past industrial emissions make to road dust concentrations of Sb and Pb, when compared with emissions originating from vehicles.

5.7 The influence that urban areas have on contaminant concentrations found in road dust

Contaminant concentrations observed at each road dust location are influenced, to a varying degree, by site-specific variables such as street cleaning, local weather, road topography, construction, surrounding buildings, and traffic count. These can play an important role in explaining the occurrence of contaminants and their concentrations for each road dust site. Just over half the streets in this study were routinely cleaned by mechanical sweepers (A90, Queen Street, A1, Thistle Street, Baird Street, Broomielaw, Hyndland Road, Black Street, Goosedubbs, Leyden Street, Tradeston Street and West Prince's Street) (Table 3.1), yet no significant reduction in elemental road dust concentrations were noted for these locations, indeed most of these sites were found to be at the higher end of the contaminant concentration range. Past studies examining the effectiveness of mechanical sweepers at lowering elemental and PAHs concentrations present in road dust were reported as being highly variable (Bris *et al.*, 1999; AIRUSE, 2013), and for this study, no notable decline was observed. Other factors such as parked cars can also reduce the effectiveness of mechanical sweepers, allowing road dust and deposited contaminants to accumulate in areas not accessible by the mechanical sweeper; this may account for the high elemental concentrations observed at West Princes Street, and to an extent, Cambusnethan Street (Table 5.2 and 5.5).

Specific local factors were observed at low-traffic roads Cambusnethan, Black Street, Thistle Street and Goosedubbs, where elemental concentrations in road dust samples were notably higher. Cambusnethan Street to the east of Edinburgh, is situated beside two historic

industrial locations, a large metal foundry (Miller and Co) used from 1867-1991, and St Margaret's railway depot which was operational until the late 1960's. Elements released from metal smelting and coal combustion, primarily as impurities present in metal ore and coal, will have resulted in their emission and deposition to the surrounding area. From the results of this study, it is clear that the legacy of previous land use is still having an impact today. Four locations (Carlyle Place, Dalgety Avenue, Dalgety Street and Salmond Place) near Cambusnethan Street (Table 3.2) all showed elevated concentrations of Pb, Cu and Zn, and since these locations are not thoroughfare roads, traffic flow was expected to be low for these sites (Table 3.2) (Carlyle Street and Salmond Place both single tracked dead-end roads, and Dalgety Avenue and Street are two-lane roads leading to a cul-de-sac). The impact of historic land use is in good agreement with a study from Oslo, where Pb road dust concentrations were highest near a former smelter site, which demonstrated the potential redistribution of local soil particles into road dust (Miguel *et al.*, 1997). Whilst historic land use has contributed to total elemental concentrations observed in road dust from Cambusnethan Street, current factors also play an important role in influencing elemental concentrations. For example, Cambusnethan Street was identified as a short-cut to a near-by retail park (Table 3.1), and with the high sided buildings either side, natural wind distribution (Chen, 2004) can be minimised providing ideal conditions for deposited contaminants to accumulate. In this instance, the mean annual wind direction for Edinburgh blows from the south or south west, a 90 degree difference to the road entrance at Cambusnethan Street; the limited wind flow would severely restrict road dust mobility through re-suspension. This is in agreement with local authority data observed at Haymarket, Edinburgh, where PM10 particles had less mobility when the wind and road direction were not aligned (Edinburgh Council, 2004). Other local factors that could account for elevated elemental concentrations in road dust were also observed at Black Street and Goosedubbs in Glasgow, and Thistle Street in Edinburgh. For Black Street, elevated concentrations of Pb, Cu and Zn found in

road dust were most likely attributed to the sampling locations close proximity to industrial units. Enhanced vehicle wear from the uneven granite sett surface at Goosedubbs and Thistle Street would in part, explain the elevated elemental concentrations observed here. Indeed, this was in agreement with past studies where road surface was identified as particularly important when considering non-exhaust emissions from vehicles (Omstedt *et al.,* 2005; Amato *et al.,* 2011; Pant and Harrison, 2013). Since no appreciable concentrations of Sb, Pb, Cu and Zn are found in Scottish granite (Harrison, 1988), the vehicle wear of setts, along with gravel and sand jointing, were not expected to contribute to road dust concentrations of Sb, Pb, Cu and Zn. In addition, the deterioration of setts and jointing road structure since its completion ~19th century (EWH and BGS, 2005; Wilson *et al.,* 2005) may also contribute to the accumulation of contaminants over time. Although routinely cleaned, setts have the potential to accumulate deposited elements in hollows and sett joints that are difficult for the mechanical sweeper to access. Further analysis at three locations on Thistle Street confirmed elevated elemental road dust concentrations (see Table 5.2), with mean Sb, Pb, Cu and Zn concentrations of 11.8 mg kg^{-1}, 702 mg kg^{-1}, 197 mg kg^{-1} and 480 mg kg^{-1}, respectively.

5.8 Elemental road dust characterisation and dissolution

5.8.1 Sequential extraction results

Moving on from elemental concentrations in road dust, this section aims to address the chemical form of elements present and potential for mobility under different conditions. Using the BCR sequential extraction as detailed by Davidson *et al*. (1998), road dust samples from Edinburgh 10 m sites were selected and analysed in duplicate to assess the potential for elements to undergo dissolution (Figure 5.4 and 5.5, Appendix 3). For quality control purposes, concentrations obtained from each sequential extraction step were totalled, and compared to elemental road dust concentrations obtained from aqua regia digestions. Typical overall recoveries for Sb, Pb, Cu and Zn were 85-110%, with results from Queen Street omitted due to unacceptable variation seen for recovery values. With exception of the A8 sample, the sequential extraction results suggested that Sb was the least available element for

most sites, with maximum of 3% in each of the BCR1 (exchangeable) and BCR2 (reducible fractions), and the greatest amount (60-96%) present in the residual phase. The proportion of total Sb concentrations in the BCR3 (oxidisable) fraction varied from 3-19%, with the three highest values coming from the low-traffic roads. At all sites, the greatest proportion (46-75%) of Pb was found in the residual fraction but there was up to 21% in the BCR1 fraction and 2-22% and 3-27% in each of the BCR2 and BCR3 fractions, respectively. There was no obvious difference between high- and low-traffic roads. For Cu, there was a clear difference in the proportion found in BCR1 for high (~22-54%) and low (~7-22%) traffic roads ($t=3.0$, $p=0.02$, $n=9$, appendix 7, output 8) (discussed further in section 5.10). Less than 7% was found in the BCR2 fraction while ~6-47% was present in the BCR3 fraction. The proportion in the residual fraction was generally lower for the high traffic roads (38-55%), compared with the low traffic roads (44-68%). There was no obvious association between Cu distribution and either %OM or total Cu concentration. In comparison with the other elements, a much higher proportion (37-63%) of Zn was present in the BCR1 fraction. The values for low traffic roads were consistently towards the lower end (37-50%) of this range. Approximately 4-19% of Zn was in the BCR2 fraction with a further 8-25% in the BCR3 fraction. The samples with the lowest BCR1 Zn concentrations often had the greatest proportion in the residual phase. Although overall elemental mobility decreased in the order of Zn>Cu>Pb>Sb, both Pb and Sb were considerably less mobile than Zn and Cu.

.

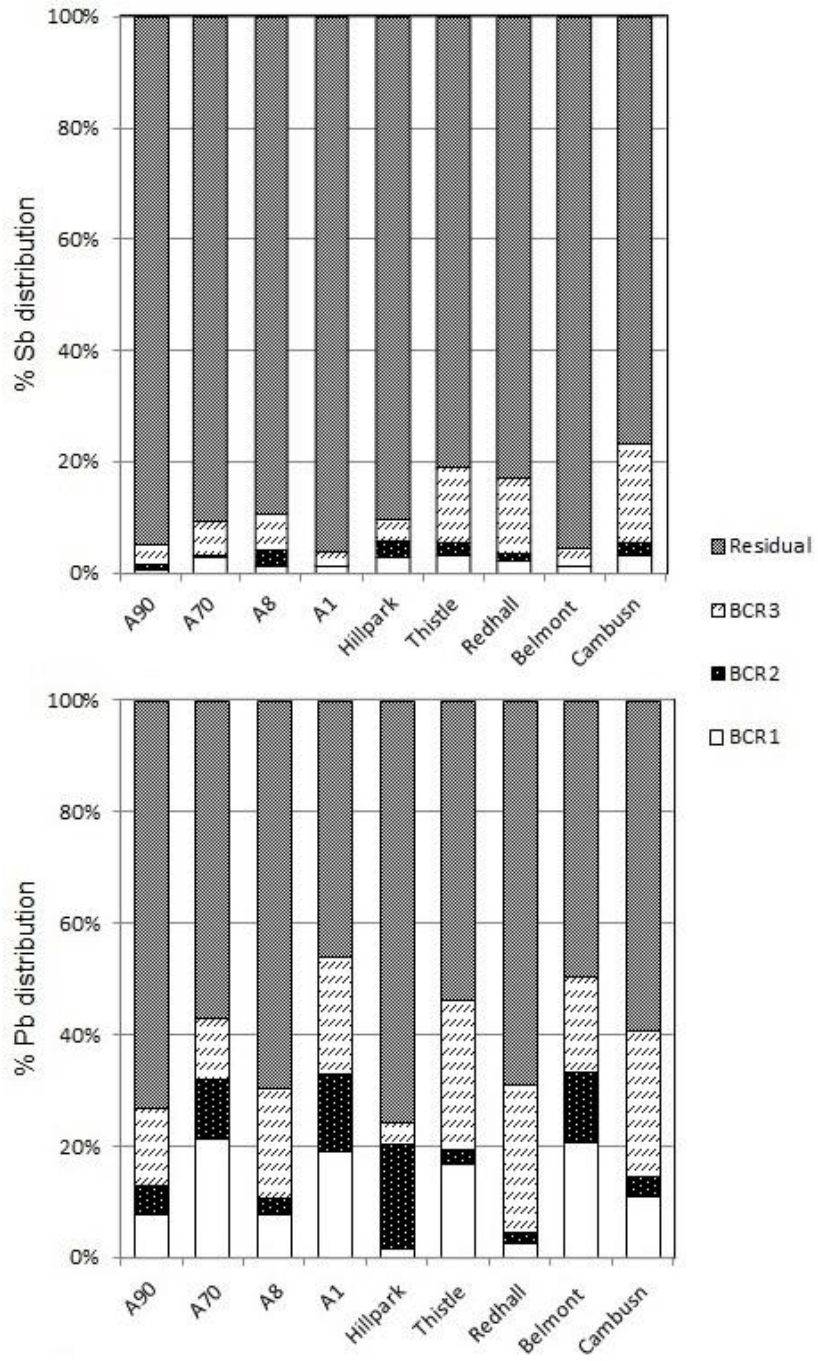

Figure 5.4: Distribution of Sb and Pb amongst BCR fractions (BCR1, BCR2, BCR3) and the residual phase of Edinburgh road dust sites.

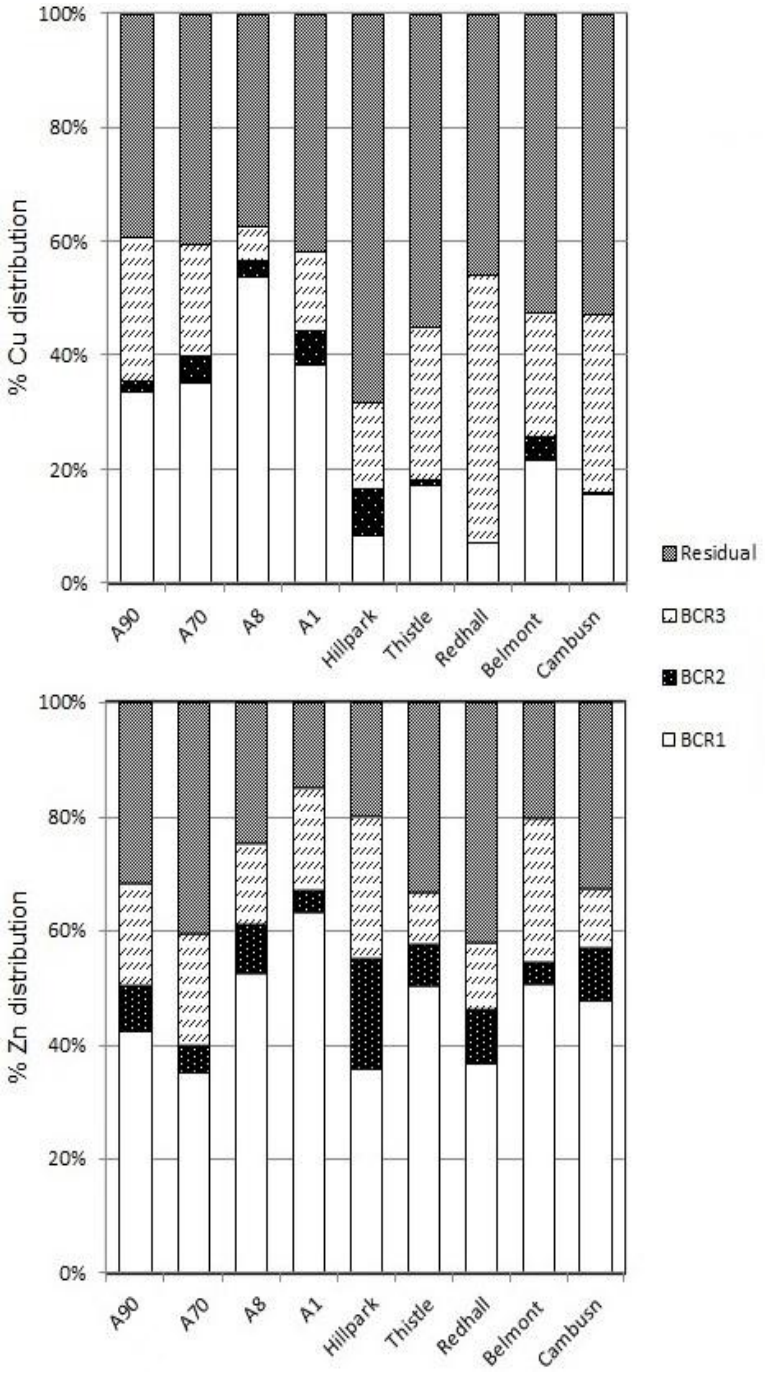

Figure 5.5: Distribution of Cu and Zn amongst BCR fractions (BCR1, BCR2, BCR3) and the residual phase of Edinburgh road dust sites.

5.8.2 Edinburgh Road dust composition using XRD and SEM-EDX

Mineral constituents present in road dust play an important role in predicting the behaviour of elements present, such as the retention and ease in which elements undergo dissolution into the aqueous phase. Although the limit of detection for XRD and SEM-EDX analysis is generally not sensitive enough to quantify concentrations of Sb, Pb, Cu and Zn present in road dust, both techniques will give information on the amount and type of minerals present. To this ends, Edinburgh 10 m road dust samples were characterised, and data was used to assess the retention of elements to mineral components found in road dust.

XRD analysis on Edinburgh 10 m road dust sites showed that the mineral composition of each site was generally similar. Quartz was the dominant mineral present (Figure 5.6), with a mean of ~54%, and a range from 43% at Cambusnethan Street to 67% at A8. Feldspars made up the greatest proportion of the remaining mineral content, with albite and anorthite contributing ~12 and 8%, whilst orthoclase and miscrocline each made up ~5%. The dominant clays were illite, kaolinite and chlorite each contributing ~2% to total composition. Although calcite was found at a similar abundance to clay, other carbonates such as dolomite and siderite were generally found at trace levels. With regard to carbonates, three exceptions were observed: samples from Thistle Street and the A1 were found to contain 8 and 4% calcite, respectively, with 4% dolomite found in the Belmont Crescent sample. Goethite and pyrite were only detected at trace levels, contributing ~1% to road dust composition, while typical brake-linings constituents, tenorite, sphalerite, chalcopyrite and zincite were identified but below the instrument LOQ (<1.0 mg kg^{-1}).

A total of six samples, three from high-traffic locations (A8, A90 and A70), and three from low-traffic locations (Thistle Street, Cambusnethan Street and Redhall Drive), were selected as exemplar road dust for SEM-EDX analysis. Images and spectra from four road dust locations (A8, A90, Thistle Street and Cambusnethan) are shown in Figures 5.6 - 5.8.

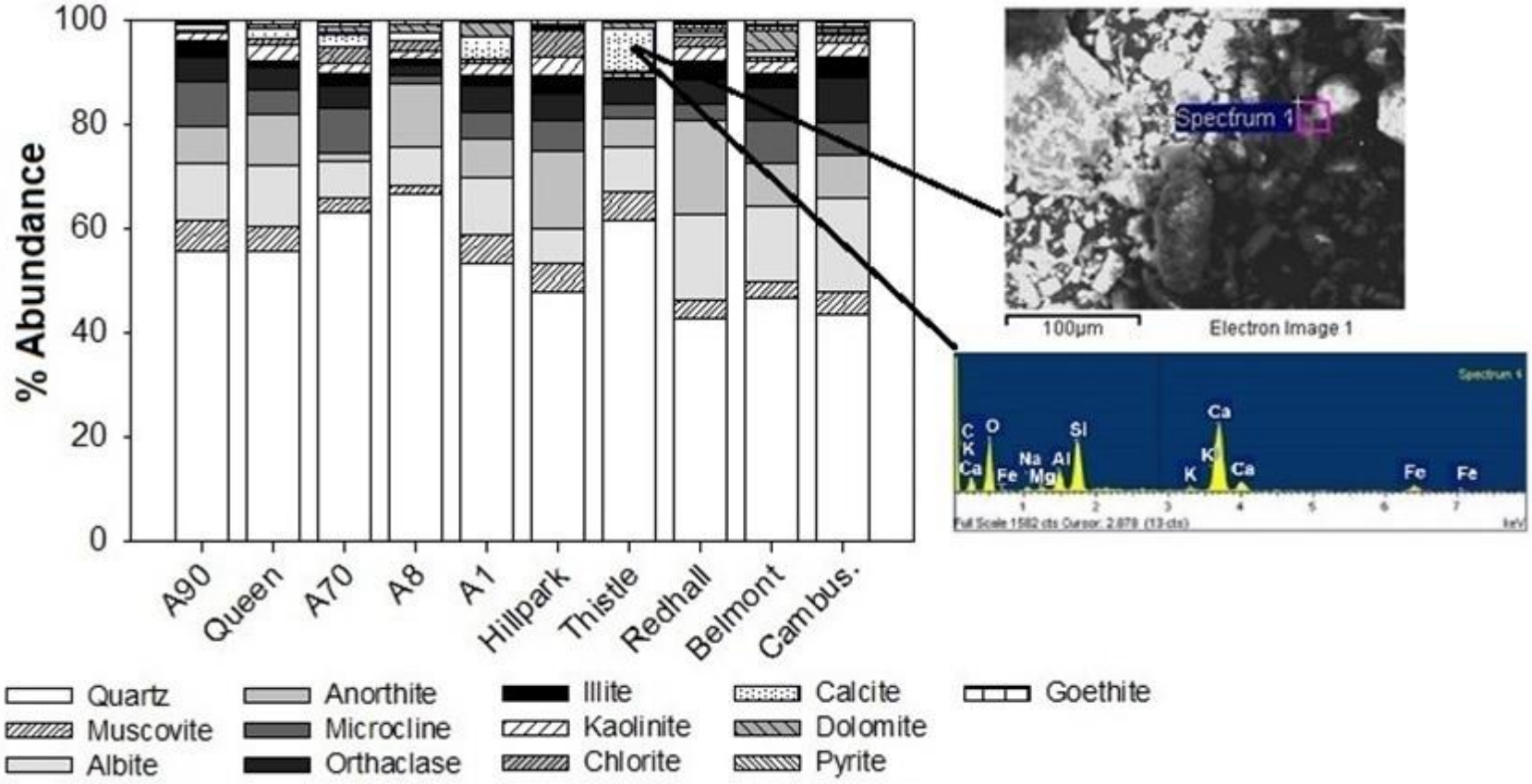

Figure 5.6: XRD and SEM-EDX mineral road dust composition from Edinburgh 10 m sample site.

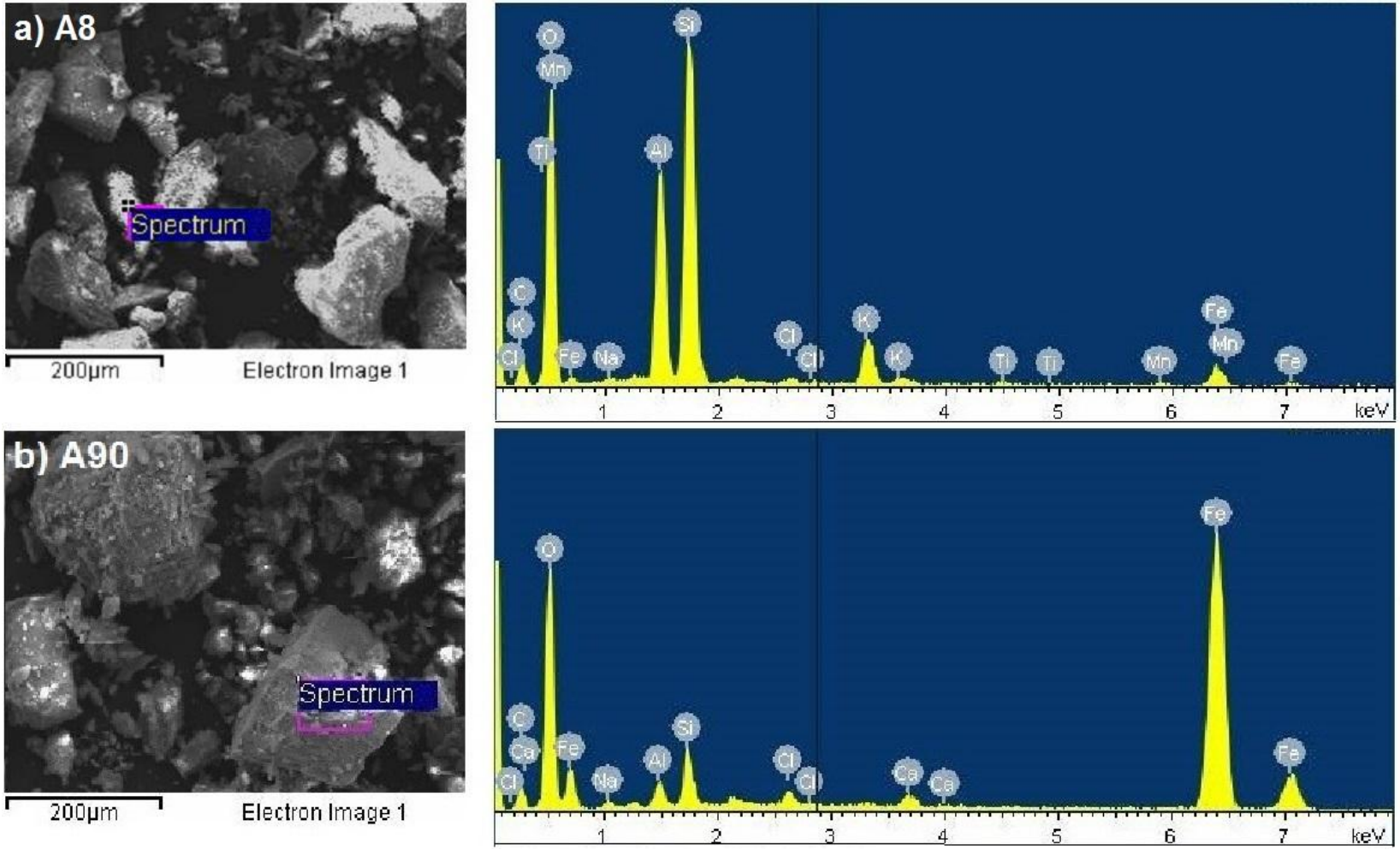

Figure 5.7: SEM images and EDX spectra for road dust sampled from high-traffic locations: a) A8 of Edinburgh and, b) A90.

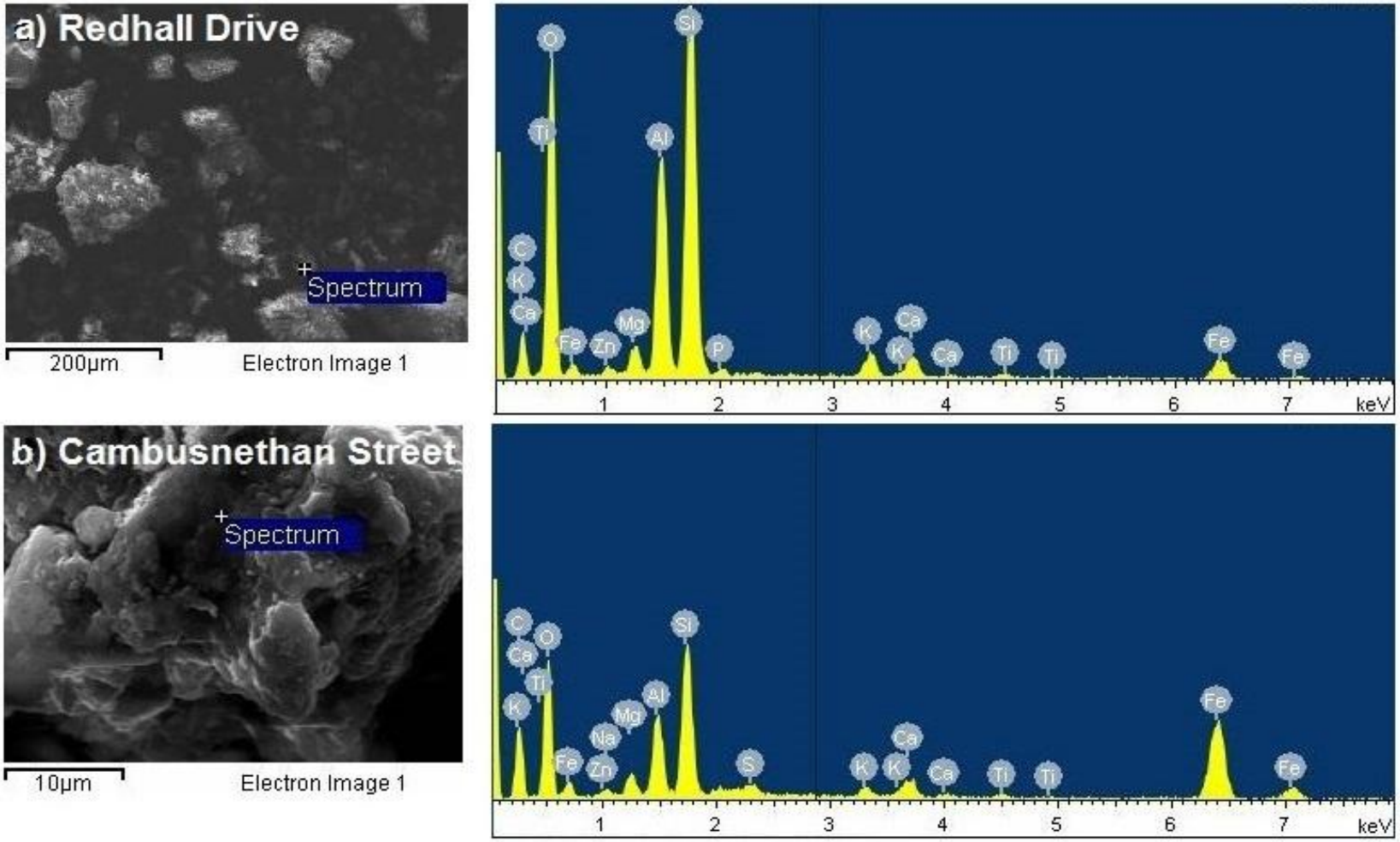

Figure 5.8: SEM images and EDX spectra for road dust sampled from low-traffic locations: a) Redhall Drive and, b) Cambusnethan Street.

Elements determined in road dust using SEM-EDX were largely similar for all six road dust samples, where Si, O, Ca, Mn, C, Ti, K and Fe were all detected and consistent with road dust characterised in other studies (Kreider *et al.,* 2010; Gunawardana *et al.,* 2012; Swietlik *et al*., 2015). Silicon and O were the most abundant elements present, which agreed with previous XRD results, where ~54% of road dust mineral composition was made up from quartz (SiO_2). The occurrence, albeit to a lesser extent, of Al, Ca and Na was also consistent with feldspars, albite ($NaAlSiO_8$) and anorthite ($CaAl_2Si_2O_8$), also previously identified by XRD. Studies by Swietlik *et al*. (2015) and Mummullage *et al.* (2016) postulated the source of a number of elements observed in road dust: Si and O was believed to originate from the use of traction sand, Ca from carbonate rock mineral filler, whilst asphalt was recognised as the source of Na and Ti. The occurrence of hydrous Fe oxides (FeOOH) is clearly shown in road dust from the A90 (Figure 5.7), with Fe most likely to originate from vehicle exhaust emissions and, along with Al, in vehicle component rust and brake-lining material (Gunawardana *et al.,* 2012; Swietlik *et al.,* 2015).

5.9 Elemental concentrations in road surface water samples from Edinburgh

In general, the aqueous phase Sb concentrations were greatest for the high-traffic roads (Table 5.6), where concentrations ranged from 0.1-1.3 µg L^{-1}, with most low-traffic road concentrations <0.42 µg L^{-1}. Mean Pb concentrations for high traffic roads (0.73 ± 0.5 µg L^{-1}) were lower than low traffic roads (1.68 ± 1.2 µg L^{-1}) with concentrations an order of magnitude higher than those of Sb. Similarly, mean road dust concentrations of Cu were higher at low-traffic sites (24.1 ± 17 µg L^{-1}) than high-traffic sites (13.0 ± 6.6 µg L^{-1}) where maximum concentrations of 45.9 µg L^{-1} and 38.4 µg L^{-1} were obtained at Hillpark Drive and Redhall Drive, respectively. Although aqueous phase Zn concentrations were typically in the range 16.4-46.2 µg L^{-1}, significantly higher concentrations were again found at the low-traffic roads, Hillpark Drive (1550 µg L^{-1}), Belmont Crescent (259 µg L^{-1}) and Redhall Drive (227 µg L^{-1}).

5.10 Discussion of road dust and road surface water elemental concentrations in respect to their retention and mobilisation in the urban environment

The concentration of elements found in road surface water is influenced by both the accumulation of atmospheric elements in rainwater and the dissolution of elements from road dust to the aqueous phase. Whilst road dust concentrations of Sb were too low to be characterise by XRD and SEM-EDX, it is largely accepted that Sb in road dust will be present as Sb_2O_3 (Ceriotti and Amarasiriwardena, 2009; Quiroz *et al*., 2013; Douthwaite *et al.*, 2014). Past studies have documented ~3% of total Sb can leach from mineral rich deposits (Filella *et al*., 2009; Biver and Shotyk, 2013), and although the sample matrices for these studies differs from road dust, road surface water is most likely to have been influenced more so by atmospheric concentrations of Sb. This was consistent with mean Sb/Pb ratios found in Edinburgh road surface water (1.28) and road dust (0.0793), where ratios were considerably different. Since the Sb/Pb ratios for road surface water and road dust did not match, this indicated Sb released from road dust into the aqueous phase contributed little to total Sb surface water concentrations. Antimony concentrations for road surface water exceeded the typical <1 μg L^{-1} found in non-polluted waters at four locations, and were closer to values obtained for urbanised rivers in the UK, such as the River Thames (1.9 μg L^{-1}) (Filella *et al.*, 2002). Since no European Sb freshwater EQS exists, and road surface water concentrations were in the range of 1 μg L^{-1}, road surface water run-off into river systems via roadside drains and diffuse pollution was not expected to be a concern for water quality.

As Pb is strongly retained in soil by OM and specific mineral phases such as Fe oxyhydroxides (Mclean and Bledsoe, 1992; Graham *et al*., 2006; Garrido and Helmhart, 2012), it was important to examine the retention of Pb in road dust, particularly as the low OM content present (~10%) may increase Pb mobility. This was seen at Thistle Street,

Edinburgh, where % mass of calcite (8.51%) was ~4 times greater than any other site (Figure 5.6). It also corresponded with the greatest surface water concentrations of Pb found in this study, where concentrations found at Thistle Street (3.6 μg L^{-1}) were approximately double that found at Cambusnethan Street (1.89 μg L^{-1}); the next highest Pb surface water concentrations observed. In addition, Thistle Street road dust had a pH ~8, similar to calcerous soils, and contrasting with pH ~7 at all other sites. In this instance, and in accordance to E_h-pH diagram for Pb-CO_3-H_2O systems, two possible forms of Pb carbonate will be present in road dust; cerussite ($PbCO_3$) at pH 7, and for Thistle Street, hydrocerussite $Pb_3(CO_3)_2(OH)_2$ at pH 8. Once in contact with the acidic rainwater observed in Edinburgh (pH ~5.7, appendix 2), Pb bound carbonate would undergo dissolution resulting in elevated Pb concentrations in road surface water. Any dissolution of Pb from road dust into road surface water should also be reflected in Sb/Pb ratio values present. For example, and with the exception of Thistle Street, mean Sb/Pb ratios for road surface water (1.38) and road dust (0.086) were considerably different from each other, and suggested that atmospheric Pb made the greatest the contribution to road surface water concentrations. For Thistle Street however, a closer match for Sb/Pb ratios were obtained between road dust (0.021) and road surface water (0.311), and suggested that the dissolution of Pb from road dust into road surface water made a greater contribution towards total Pb surface water concentrations at Thistle Street, when compared to all other sites. This would account for both greater Pb concentrations present in surface water and BCR1 fraction from the sequential extraction. Whilst no environmental standard exists to regulate urban surface water run-off, the Scottish freshwater EQS for Pb is 1.2 μg L^{-1} (EC, 2013), and indicted road surface water run-off from Thistle Street would have a detrimental impact to the aquatic environment should it enter a river system. All other road surface water locations had Pb concentrations either below or near the EQS, and were not considered to cause any significant determination to nearby rivers.

For Cu, BCR results for high-traffic locations showed that ~20% more Cu was available, i.e. extracted in the BCR1 sequential extraction fraction, when compared to the low-traffic sites ($t=3.0$, $p=0.02$, $n=9$). The difference is most likely attributed to the form of Cu mineral present in road dust. Although metallic Cu, tenorite (CuO), sphalerite (CuS) and chalcopyrite ($CuFeS_2$) (Kukutschová *et al*., 2009; Amato *et al*., 2012) are all present in brake-linings, metallic Cu and CuO are the dominant forms released, while organo-Cu was also found to be present in road dust (Hur *et al*., 2003; Kukutschová *et al*., 2009). It is difficult to identify the Cu forms in road dust that leads to increased Cu mobility for high-traffic sites, particularly as other Cu sources such as exhaust emissions, tyre erosion and oil losses exist. One explanation could be related to the vehicle type using the high- and low-traffic roads. For example, vehicles that require high performance braking requirements (ambulances, police cars) use metallic brake-linings, unlike passenger cars, where they are more likely to use low or semi-metallic brake-linings (Grigoratos and Martini, 2015). A detailed investigation of the Cu content in brake-linings used just in passenger cars by Hulskotte *et al*. (2014) revealed considerable differences in the amount of Cu found in 65 brake-linings, ranging from 0.11 to 17.8% (w/w). The proportion of emitted Cu, and the chemical form present that readily undergoes dissolution, is likely to be different for each type of brake-lining. Hur *et al*. (2003) postulated that surface area was also particularly important in explaining Cu dissolution rates. With the exception of the A70, all road surface water concentrations exceed the 5.0 μg L^{-1} freshwater EQS for Cu, and would potentially have a negative impact on water quality if road surface water entered river systems.

For Zn, the dominant chemical forms present in road dust have been reported by Swietlik *et al*. (2015) as Zn, ZnO and Zn-FeOOH. The greater solubility of Zn forms relative to Sb, Pb and Cu, was reflected in Zn concentrations observed in road surface water samples and BCR1 sequential extraction fractions (Figure 5.5). Exceptionally high Zn concentrations were observed in road surface water at Hillpark Drive (1550 μg L^{-1}), and were most likely

influenced by construction work occurring in close proximity to the water sampling site. Although elevated Zn concentrations were not observed in road dust sampled for this location, studies by Charlesworth *et al.* (2011) and Fergusson and Kim (1991), both identified construction work as a potential source of Zn to the urban environment. Road surface water concentrations at Hillpark Drive were similar to those determined in water affected by anthropogenic activity, e.g. Bambic *et al.* (2006) and Ning *et al.* (2011) both reported Zn water concentrations of ~1000 μg L^{-1} near mining sites for Cu and gold, respectively. With the exception of Hillpark Drive, Belmont Crescent and Redhall Drive, road surface water concentrations of Zn were lower, or in the range of the freshwater EQS (40 μg L^{-1}), with road run-off not likely to be a concern to nearby river water quality.

5.11 Urban area remedial measures to limit past and current contaminant emissions

The main contaminants, both elements (Sb, Pb, Cu, Zn) and priority 16PAHs, were investigated in Edinburgh and Glasgow road dust, and showed concentrations that were influenced by historic and current land use in the urban environment. The influence of Scotland's industrial past is still being observed today, particularly for the elements, as once deposited they are not broken down by environmental processes and will remain present for many years after. Through time, contaminants will cycle through re-suspension and deposition in the urban environment, with eventual deposition in the aquatic environment through roadside drains and diffuse pollution (Zhao *et al*., 2006; Kukutschová *et al*., 2009; Charlesworth *et al*., 2011). As discussed in chapter 2, the industrial revolution resulted in considerable emissions of elements and PAHs from coal combustion, shipbuilding, metal works and textiles to the urban environment. With the gradual decline of heavy industry in Scotland over recent decades, the contribution it makes to urban contaminants has significantly reduced, with road traffic emissions now being the single largest source (Beasley and Kneale. 2002; Dore *et al*., 2008).

To address the impact from traffic emissions, tighter regulation and management of vehicles in the UK and Europe has been implemented in recent decades. The introduction of vehicle emission limits in 1992, and their periodic revision up to Euro 6 standard has resulted in the eventual ban of leaded petrol, and decline in vehicle hydrocarbon emissions (amongst other contaminants) (EC No 715/2007). The European End of Life Vehicle (ELV) directive (2000/53/EC) implemented in 2000 also limits vehicles environmental impact by preventing the use of heavy metals such as Pb and Cr during vehicle construction, placing recycling targets on ELV, and ensuring the safe disposal of vehicle fluids and components. This, however, does not address the use and subsequent deposition of elements from vehicle brake-linings, and although a reduction programme is underway in a number of states in America, no EU or UK regulation exists to govern these emissions (Lee and Filip, 2013). For example, emissions from vehicle braking can be reduced by using ceramic linings instead of Cu based equivalents, particularly when brake performance is comparable (Napier *et al*., 2008).

Vehicle regulation however, can only reduce emissions, with the release of elemental and PAH contaminants always likely to occur. For this instance, traffic flow management and sustainable urban drainage (SUDS) can help limit the impact of deposited contaminants on the urban environment. Roads can be constructed to limit traffic speed whilst also reducing the frequency of braking; stop start traffic significantly increases brake-lining and exhaust emissions (a total hydrocarbons increase of 148%) (Lim *et al*., 1999; Napier *et al*., 2008). The application of SUDS to capture contaminant deposition by filtration and sedimentation processes are very effective at preventing contaminant transport into the aquatic environment (Napier *et al*., 2009).

5.12 Chapter conclusions

Elemental (Sb, Pb, Cu, Zn) and priority 16 PAH concentrations were determined in road dust sampled from five high- and five low-traffic locations in Edinburgh, where road dust from each location was collected at distances of 10 and 50 m from the closest road junction.

Results showed that there was no significant difference between the elemental concentrations in the samples from the 10 m and those from the 50 m locations ($t>0.36$, $p>0.37$), nor was there any difference between contaminant concentrations in samples from roads that were mechanically cleaned and those that were not. Taking the contaminant concentrations determined in road dust from both five high- and five low-traffic roads sampled at 10 and 50 m from the CRJ, mean concentrations for Sb, Cu and Zn were 5.3 ± 2.8 mg kg^{-1}, 91.4 ± 48 mg kg^{-1} and 237 ± 144 mg kg^{-1}, respectively, and were similar to road dust sampled from five high- and five low-traffic locations in Glasgow (Sb 4.5 ± 2.1 mg kg^{-1}; Cu 117 ± 71.9 mg kg^{-1}; Zn: 283 ± 146 mg kg^{-1}). This was in contrast to mean concentrations for Pb and Σ16PAHs obtained from Glasgow (Pb 250 ± 283 mg kg^{-1}, Σ16PAH 7.7 ± 4.3 mg kg^{-1}) where values were approximately double and two-thirds greater than those found in Edinburgh (Pb 135 ± 129 mg kg^{-1}, Σ16PAH 4.7 ± 2.9 mg kg^{-1}), respectively. Although AADF data for Edinburgh road dust locations were generally higher than those of Glasgow, the greater traffic numbers experienced citywide for Glasgow (~30% more than Edinburgh citywide), and the legacy of Glasgow's industrial past would account for the higher concentrations of Pb and Σ16PAH observed here.

The source of priority 16 PAHs and Pb to road dust concentrations was apportioned using PAH diagnostic and Pb isotopic ratios. Diagnostic ratio analysis indicated that PAHs present in dust samples originated from the combustion of petroleum, and grass, wood and coal. These results are not unexpected since it is well known that road traffic emissions are a dominant source of PAHs in urban areas of the UK (Dore *et al.,* 2008) and combustion of wood and then coal was an intrinsic part of past industrial activities (Lohmann *et al.,* 2000). The range of $^{206}Pb/^{207}Pb$ isotopic ratios in road dust from Edinburgh (1.116-1.151) were notably lower than the range observed in dusts from Glasgow (1.140-1.169). Since recent rainwater has $^{206}Pb/^{207}Pb$ ratio values of ~1.15-1.16, the low values in Edinburgh dust samples strongly suggest that the influence of leaded petrol is persisting some 15 years after the ban in its use. A significant trend was also found at three road dust locations ~2 km north

of major road routes in/out of Edinburgh (M8, Glasgow Road and the Edinburgh Bypass) ($t=6.9$, $p=0.002$, $n=17$), where the road dust isotopic ratios were notably lower than all other sites in this study (1.102-1.121). These locations were considerably influenced by past emissions from leaded petrol, and to a lesser degree, emissions from avgas, and was consistent with the mean annual wind direction for Edinburgh. Although combustion emissions from leaded fuels also influenced Pb isotope ratios observed in Glasgow road dust, there was a greater influence from indigenous Pb sources, attributable to continued impact of emissions from past industrial activities such as metal smelting, engineering works and coal combustion, e.g. via remobilisation of contaminated soil, weathered urban materials from old industrial sites. This was particularly evident at two locations in Glasgow (Black Street, Goosedubbs) and two from Edinburgh (Cambusnethan Street, Thistle Street). For Black Street, situated in a Glasgow industrial estate, elevated road dust concentrations of Pb and Σ16PAHs were most likely a result of local emissions originating from nearby industrial units. The impact of historic land use on road dust was also observed at Cambusnethan Street and four locations in the surrounding area. Elevated elemental concentrations in road dust from these locations were associated with past industrial activity that occurred in the vicinity, such as a metal foundry (Miller and Co) used from 1867-1991, and St Margaret's railway depot which was operational until the late 1960s. Elevated contaminant concentrations observed at Goosedubbs and Thistle Street were attributed to the difference in the road surface (setted vs tarmac), where enhanced vehicle wear from the uneven setted road and the accumulation of deposited contaminants between cracks and jointing of the setts would account for the contaminant concentrations observed here.

The retention of elements by road dust and their potential to become mobile into the aqueous phase was determined by road surface water analysis, sequential extraction analysis of road dust, and the analysis of road dust composition via XRD and SEM-EDX. Edinburgh road surface water samples collected from each high- and low-traffic location showed mean

concentrations of Sb and Pb of 0.64 ± 0.45 µg L^{-1} and 1.25 ± 1.02 µg L^{-1}, respectively. Higher concentrations were observed for Cu (18.6 ± 14 µg L^{-1}) and Zn (84.0 ± 91 µg L^{-1}). Sequential extraction results indicated that a high proportion of Zn had the potential to be mobilised into the aqueous phase (~37-63% of total Zn present in BCR1), followed by Cu (~22-54% of total Cu present in BCR1), with Pb and Sb showing very little of total concentrations available in BCR1, and were highest at 21% and 3%, respectively. This was in agreement with surface water results, where surface water concentrations were greatest for the elements that showed a greater potential to be mobilised in the BCR1 fraction, and were distributed as Zn>Cu>Pb>Sb. The composition of road dust was investigated using XRD and SEM-EDX, and revealed that quartz comprised ~54% of the road dust samples, with smaller contributions from albite and anorthite at ~12 and 8%, respectively. Although Pb bound to carbonates, such as calcite at Thistle Street may increase Pb mobility, Sb and Pb were largely retained by road dust, whilst Zn and Cu showed a greater potential to become mobilised into the aqueous phase.

Chapter 6 Former mining sites in a rural environment

6.1 Introduction

This chapter examines the behaviour and fate of elemental pollution originating from two former mining sites, an Sb mine at Glendinning, SW Scotland, and a Pb mine at Tyndrum in central Scotland. The specific elements of interest were Sb, As, Pb and Fe, and the chapter focuses on their release, transport and fate in the surrounding area. The first part of this chapter concerns the Louisa mine, a small Sb mine, where spoil heap material had been dumped onto the surrounding organic-rich soil. Analysis of spoil heap material, soil samples, soil porewater and surface water samples was used to reveal the extent of elemental contamination in the vicinity of the mine, while the nature of elemental association within the soil and soil porewater were determined using sequential extraction, porewater isolation and gel electrophoresis techniques. The second part of this chapter examines the fate of elements at a much larger scale, where historical contamination from Tydrum Pb mine 25 km downstream at Loch Tay was assessed using two sediment cores. Analysis of sediment for elemental and Pb isotope concentrations, as well as the use of ^{210}Pb dating allowed the relative impact of Tydrum Pb mining and other historic anthropogenic activities had on Loch Tay sediments to be assessed by the construction of deposition chronologies.

6.2 Assessing environmental impact from historic mining activities

The release of Sb, As, Pb and Fe, from mining waste material is still observed in the 21st century, despite the closure of mines during the mid-20th century (Flynn *et al*., 2003; Gál *et al*., 2007; Shepherd *et al*., 2009; Chenery *et al*., 2012). Although the economic viability was the primary reason for the closure of mines in Scotland, particularly for Glendinning and Tyndrum mines, other factors such as a shortage of labour and fatalities also contributed to their closure (Wilson *et al*., 1921; Gallagher *et al*., 1983). This often resulted in mines being abandoned, and excavated mineral-rich soil dumped on the nearby surface soil with no attempt to restore the former landscape.

The use of soil and sediment cores to examine the historic impact from mining and smelting activities has been successfully applied in a number of publications (section 2.2.5.2) (Merrington and Alloway, 1994; Farmer *et al*., 1997; Audry *et al*., 2004; Cappuyns *et al*., 2006; Thevenon *et al*., 2011; Xu *et al*., 2011). For both Glendinnning Sb mine and Tyndrum Pb mine, previous studies exist, which provided a good, albeit limited, starting point for further research at these locations. For example, studies by Flynn *et al*. (2003) and Gal *et al*. (2007) focusing on Glendinning Sb mine demonstrated that the Sb soil concentrations were considerably elevated above background levels for that area, but little attempt was made to address the geochemical associations, lateral and vertical elemental mobility and transport mechanisms. The first half of this chapter addresses this, by using soil cores, typically 12 cm deep, sampled in the vicinity of Glendinning Sb mine. Elemental contamination resulting from Tyndrum Pb mine, a much larger mining site, is discussed in the second half of this chapter, using two Loch Tay sediment cores (mini Mackereth: 0-90 cm and Jenkin 0-19 cm). The elemental data obtained from the acid-digestion of sediment core depth sections, along with the ^{210}Pb dating of each depth section, enables a chronology of elemental deposition in the sediment core to be established. Using Pb isotope ratio analysis and Sb/Pb ratios, the influence of Pb mining at Tydrum on total elemental concentrations found in Loch Tay sediment, and the contribution of other anthropogenic sources can be ascertained. Although a past study by Farmer *et al*. (1997) tried to establish the extent of Pb pollution from Tyndrum Pb mine to Loch Tay sediment, no pollution inventory for Sb was determined and there was therefore, no Sb/Pb ratio data which could help to delineate the contaminant source. This chapter addresses this, and gives an account of contemporary Pb concentrations and ^{206}Pb/^{207}Pb isotopic ratios not detailed by Farmer *et al*. (1997).

6.3 Glendinning Sb mine

This section gives a brief overview of Glendinning Sb mining site, along with samples collected. Full details are given see section 3.2.3.2.1.

Glendinning Sb mine is located in Dumfries and Galloway, SW Scotland (Figure 3.4(a)-(b)), from which ~200 t of Sb ores were extracted over the period 1793-1922 (Gallagher *et al*., 1983). The excavation of Sb primarily occurred via an underground shaft that ran from the mine adit to SpH1 (Gallagher *et al*., 1983) (Figure 3.6(b)–(c)). Ore smelting took place at Jamestown, ~1 km downhill of the mine (Gallagher *et al*., 1983), with several spoil heaps in the vicinity of the mine still evident today.

A total of 6 soil cores (S1-6), surface (SpH1-surface) and sub-surface (SpH1-deep) spoil material, and surface water samples were collected in the vicinity of Glendinning Sb mine. Soil cores S2 and S3 were identified as being water-logged whilst all remaining soil cores were not. A control site core (C1) was also sampled 500 m further up the Glenshanna valley (Figure 3.6(c)).

6.4 Glendinning Sb mine results

The full dataset, upon which the tables and figures shown in this section are based, is contained in Appendix 4.

6.4.1 Glendinning Sb mine control site (C1)

6.4.1.1 Soil pH and organic matter content

There was little variation in soil pH with increasing depth at the control site (C1). The pH values were low and ranged from 3.9-4.1 (Figure 6.1(a)). Organic matter (OM) content for C1 soils was in the range of ~15–95% w/w (on a dry weight basis) and highest in the top 0–5 cm sections (Figure 6.1(b)).

Organic matter largely comprises of humic and fulvic acids which contain carboxylic and other weakly acidic functional groups, and their presence will naturally lower soil pH. Conversely, the natural abundance of mineral components such as sodium carbonate

(Na_2CO_3) and sodium bicarbonate (Na_2HCO_3) will increase soil pH (Baird, 1998). The balance of mineral and organic components will determine the overall soil pH. The exceptionally high OM content, especially in the top sections (Figure 6.1(b)), most likely accounts for the low pH of the C1 soils (Figure 6.1(a)).

6.4.1.2 Vertical soil concentration profiles for Fe, Sb, As and Pb

Elemental concentrations observed at the control site (C1) were largely similar to the geochemical baseline obtained at Glendinning, Scotland, as part of the Forum of European Geochemical Surveys (FOREGS; now Euro Surveys) and published by Salminen *et al.* (2005) (Table 6.1). Very good agreement was observed in duplicate analysis of each 2-cm depth section profile, where typical soil concentrations were within 0.1% for Fe, and 0.2, 0.1 and 0.9 mg kg^{-1} for Sb, As and Pb, respectively. The vertial soil concentration for Fe increases with increasing depth (Figure 6.1(c)), and was inversely related to OM content (corr. coeff. -0.92) (Figure 6.1(b)). Little variation in Sb and As concentrations with depth were observed (Figure 6.1(d)-(e)), with concentrations of Sb in soil comparable to those attained by the FOREGS top soil study, whilst soil concentrations of As were a magnitude lower (Table 6.1, Appendix 4) (Salminen *et al*., 2005). This indicated that no, or very little, impact from anthropogenic activity was observed for Sb and As at C1. Concentrations of Pb below a depth of 4 cm were ~35.0 mg kg^{-1}, with a notable decline to ~5.0 mg kg^{-1} observed near the soil surface (Figure 6.1(f)). Lead concentrations were, however, higher than expected based on its crustal abundance (~12–15 mg kg^{-1}) (Taylor, 1964; Wedepohl, 1995), and showed evidence of past anthropogenic activity. Concentrations of up to 57 mg kg^{-1} were attributed to atmospheric deposition of Pb emissions from coal combustion, smelting and leaded gasoline in the industrial and post-industrial periods (Salminen *et al*., 2005; Cloy *et al*., 2009; Farmer *et al*., 2010).

Table 6.1: Elemental concentration range for control site (C1) and homogenised top soil reported by FOREGS at sampling locations within a 2 km distance of C1 (Salminen *et al*., 2005).

Element	Fe (%)	Sb (mg kg^{-1})	As (mg kg^{-1})	Pb (mg kg^{-1})
C1 soil core elemental concentration range	0.11-3.35	0.41-1.18	0.43-0.91	3.07-57.1
FOREGS concentration Range	2.77-3.51	0.60-1.05	4.30-9.60	29.0-33.0

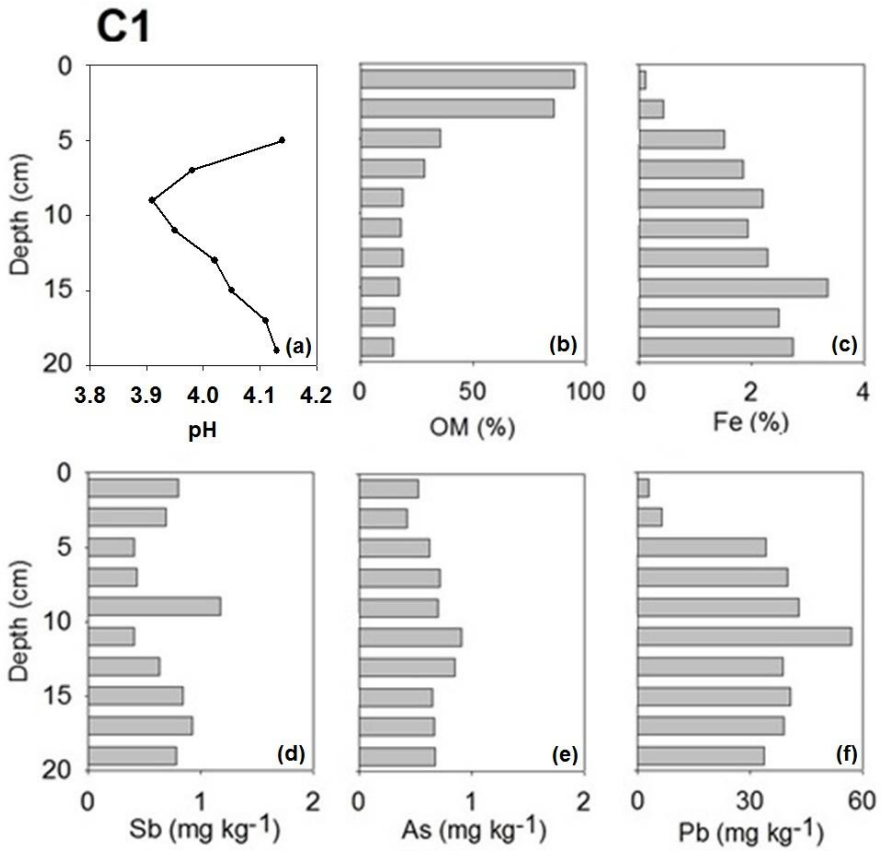

Figure 6.1: Vertical variations in the concentrations of (a) pH, (b) OM, (c) Fe, (d) Sb, (e) As and (f) Pb in solid phase soils from Glendinning control site (C1).
NOTE: Associated errors for data have been omitted for visual reasons, and values can be found in Appendix 4.

6.4.2 Soil and porewater results from the vicinity of Glendinning Sb mine

6.4.2.1 Soil pH and organic matter results

Although the lowest pH values were obtained at C1, low pH values were also obtained for S4 (4.7–4.9) and S1 (4.4–5.2), i.e. those closest to the spoil heaps, SpH1 and SpH2, respectively (Section 3.2.3.2.1, Figure 3.6). The pH values for the soils at S2, S3, S5 and S6 were slightly less acidic and ranged from 5.4–6.3 (Figure 6.2). With the exception of S2 which had a maximum value of ~77%, peak OM content for S1–6 soils was typically ~39–54% w/w (Table 6.3, Figure 6.3). The vertical OM profiles for S1–6 all showed similar trends, decreasing from the surface towards the bottom of the cores (Figure 6.3), and had consistently lower OM content than C1. This feature, along with the low pH of soils at S1 and S4, was a result of exposure to acid mine drainage water, where sulphur-bearing minerals, such as pyrite (FeS_2), stibnite (Sb_2S_3) and galena (PbS), are exposed to water, which results in the formation of sulphuric acid (Johnson and Hallberg, 2005). The acidic run-off from SpH1 and SpH2, to the surrounding soils, causes the degradation of organic matter through the depletion of nutrients, trace elements and microbial activity.

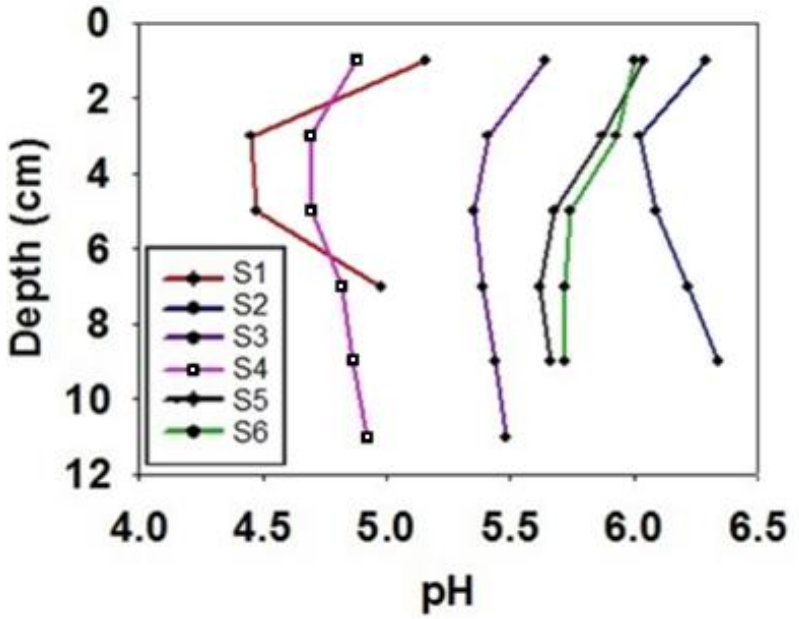

Figure 6.2: Vertical pH values from Glendinning Sb mine soil cores (S1-S6).

6.4.2.2 Absorbance of porewater depth profiles using 252 nm as a proxy for humic acid content.

The porewaters extracted from the soils were pale brown-coloured, indicating the presence of dissolved humic substances. With the exception of S5, where absorbance values at 252 nm (a measure of colour and proxy for DOM (Edzwald *et al*., 1985)) remained approximately constant, the maximum absorbance occurred at depths of 5–8 cm in each core. This was ~5 cm below the maximum solid phase OM content (Figure 6.3(a)), similar to results observed in many other studies (e.g. Michalzik and Matzner, 1999). The DOM profile shape is the result of production and leaching in the upper layers and removal via adsorption in the deeper layers (Kalbitz *et al*., 2000; Kalbitz and Kaiser, 2008).

6.4.2.3 Vertical soil concentration profiles for Fe, Sb, As, and Pb

6.4.2.3.1 Iron

The Fe concentrations at S1–6 were higher than C1, and ranged from ~0.2–6.3% w/w (Figure 6.1(c), Figure 6.3, Table 6.2, Appendix 4), with highest values occurring in the soils closest to SpH1 and SpH2. In contrast with the OM content and in agreement with C1, vertical profiles for Fe showed very low concentrations in the top sections and then a general trend of increasing concentration with increasing depth, reflecting the transition from the peaty surface layer to mineral-rich material. Porewater Fe concentrations were also typically greater at depth than at the surface but there was no strong relationship with solid phase Fe concentration. Consistent with a transition to reducing conditions, for S2, S4 and S5 there was a clear subsurface maximum at ~5–10 cm and, for S3, the Fe concentration continued to increase to the bottom of the core. Highest porewater concentrations of ~80 mg L^{-1} were obtained for the deeper sections of S3 and S5 (Figure 6.3(b)).

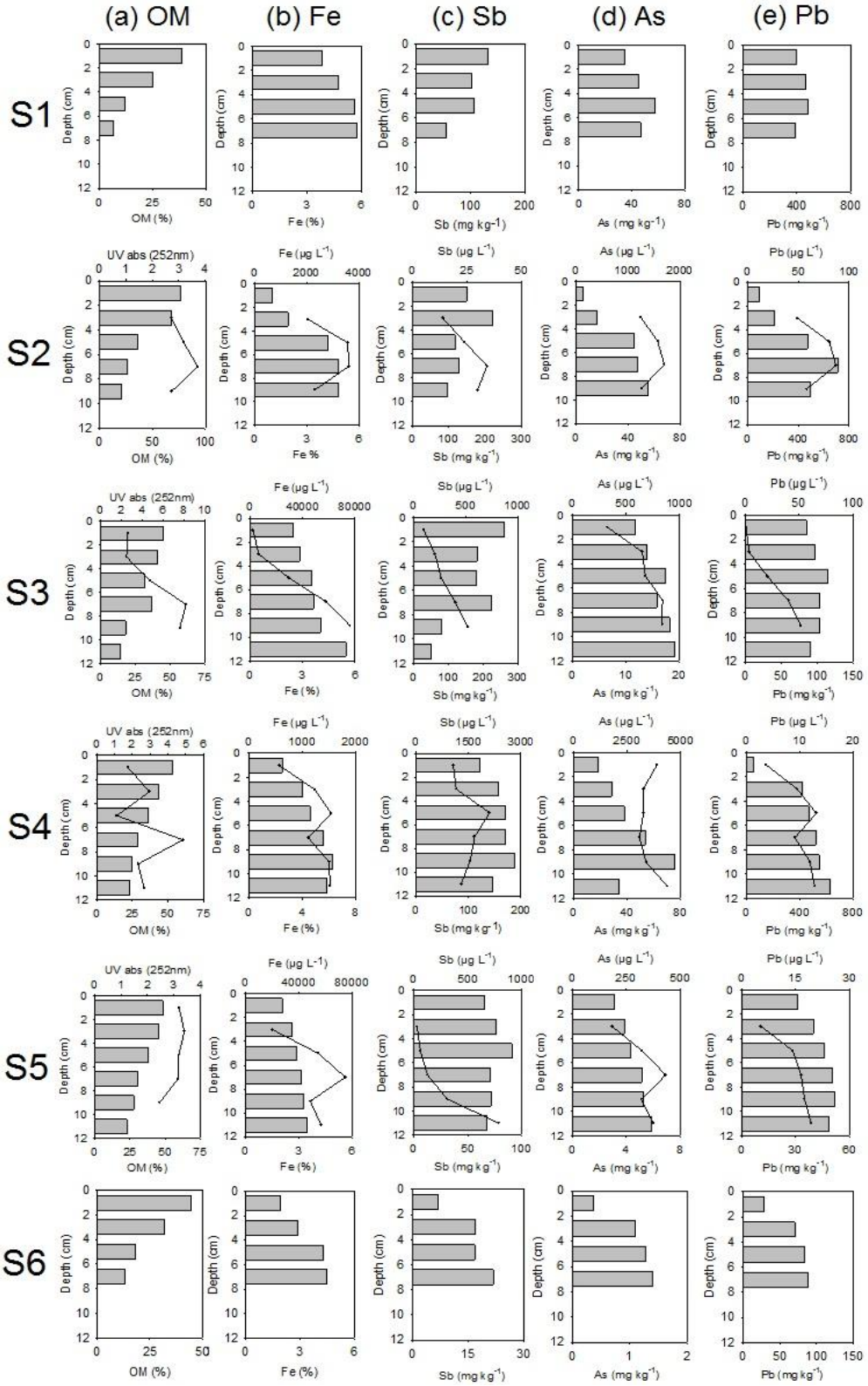

Figure 6.3: Vertical variations in the concentrations of (a) OM, (b) Fe, (c) Sb, (d) As and (e) Pb in solid phase soils displayed as solid bars (S1-6) and their respective porewaters displayed as solid lines (S2-5). NOTE: Associated errors for data have been omitted for visual reasons, and values can be found in Appendix 4.

Table 6.2: Elemental concentration range found in control soil (C1), spoil (SpH1), soil profile (S1-6) samples taken in the vicinity of Glendinning antimony mine.

Samples collected	pH	%OM	Fe %	Sb mg kg^{-1}	As mg kg^{-1}	Pb mg kg^{-1}
FOREGS*	n.r.	n.r.	2.77 – 3.51	0.60 – 1.05	4.03 – 9.60	29.0 – 33.0
C1*	3.9 – 4.1	14.8 – 95.3	0.11 – 3.35	0.41 – 1.18	0.43 – 0.91	3.07 – 57.1
SpH1-surface†	5.0	7.31 – 10.9	3.98 – 5.26	174 – 302	74.0 – 85.0	873 – 1020
SpH1-deep†	6.6	2.82 – 3.77	4.02 – 4.46	300 – 541	104 – 170	421 – 621
S1	4.4 – 5.2	6.60 – 38.6	3.83 – 5.80	55.4 – 132	34.9 – 57.2	390 – 486
S2	6.0 – 6.3	21.0 – 77.2	0.21 – 4.86	95.5 – 222	5.68 – 55.6	91.6 – 710
S3	5.4 – 5.6	14.3 – 44.9	2.45 – 5.48	50.7 – 261	13.9 – 19.1	90.9 – 114
S4	4.7 – 4.9	23.2 – 53.6	2.51 – 6.28	120 – 188	18.4 – 75.3	52.2 – 632
S5	5.6 – 6.0	22.8 – 48.4	2.08 – 3.46	65.9 – 91.2	3.87 – 5.92	40.2 – 52.1
S6	5.7 – 6.0	13.0 – 44.6	1.94 – 4.50	6.77 – 21.7	0.36 – 1.40	27.9 – 88.6

*Results taken from Table 6.1, n.r. not reported, † 6 sub-samples of spoil.

NOTE: A full list of individual results for each soil core profile is shown in Appendix 4.

6.4.2.3.2 Antimony

Antimony concentrations in S1–6 soils were several orders of magnitude higher than in the control soil (C1). Maximum values of ~260 mg kg^{-1} were found in S3 soils and, for S4–6, there was a clear trend of decreasing concentration with increasing distance downslope from SpH1 (Figure 6.3(c), Table 6.2, Appendix 4). The porewater Sb concentrations for S4 and S5 also reflected this trend with distance from SpH1 (Figure 6.3(c)). Regression analysis showed that there was a strong relationship between solid phase OM content and Sb concentrations at S3 ($P < 0.01$, $R^2 = 0.95$, appendix 7, output 9a). Although the porewater Sb and solid phase Sb profiles for S2–5 appeared to be unrelated, there were strong correlations between the porewater concentration profiles of Sb and DOM (e.g. S3: $P < 0.01$, $R^2=0.95$, appendix 7, output 9b) and of Sb and Fe (e.g. S3: $P < 0.01$, $R^2=0.98$, appendix 7, output 9c). An exception was S5, however, where the Sb porewater profile was distinctly different from those of both Fe and DOM (Figure 6.3(a)-(c)).

6.4.2.3.3 Arsenic

Concentrations of As in soils from S6 (<1.4 mg kg^{-1}) were similar to C1 (Figure 6.1(e) and Table 6.1), for all other sites at least an order of magnitude higher for S1–5 (Figure 6.3(d), Table 6.2, Appendix 4). The highest As concentration of ~75 mg kg^{-1} was obtained at S4, the site closest to SpH1, and, as for Sb, As concentrations decreased with increasing distance downslope from SpH1. In agreement with the vertical Fe concentration profiles, however, As concentrations showed a general increase with increasing soil depth. For S2 and S5, there was also a strong relationship between porewater As and Fe concentrations, suggesting concomitant release from the soil solid phase.

6.4.2.3.4 Lead

Considerably higher values (up to 710 mg kg^{-1}) were observed for S1–4, compared with those observed at C1 and S5–6 (Figures 6.1(f) and 6.3(e), Tables 6.1 and 6.2, Appendix 4), consistent with the additional contribution of mining-derived Pb to these soils. The vertical concentration profiles for S1 and S3 had slight sub-surface maxima at ~5 cm depth whilst

there was a general increase towards the bottom of each of the other cores. Highest concentrations of ~600–700 mg kg^{-1} were observed towards the bottom of S2 and S4. Akin to Sb and As, porewater Pb profiles bore little resemblance to the respective solid phase profiles. There was a statistical significant relationship between the vertical porewater profiles of Fe and Pb ($t>2.4$, $P<0.02$, $n=20$, appendix 7, output 10) (Figures 6.3(b) and (e)).

6.4.3 Glendinning spoil heap material (SpH1 and SpH2)

6.4.3.1 Spoil heap pH and organic matter

The pH measured at SpH1-surface and deep was 5.0 and 6.6, respectively (Table 6.2; Appendix 4). The lower pH found at the SpH1-surface was in agreement with earlier findings, where the chemical weathering of sulfide minerals had resulted in a lower pH observed on the spoil heap surface and for soil in the spoil heap vicinity. As expected, the spoil samples had lower OM content than the surrounding soils (Table 6.2). There was, however, a thin coverage of soil-like material supporting heathers and mosses and this was reflected in an OM content of ~7–11% w/w for SpH1-surface, i.e. the top 2-cm of the spoil heap. With less soil present at depth, the OM content for SpH1-deep dropped to ~3–4% w/w.

6.4.3.2 Spoil heap concentrations of Fe, Sb, As, and Pb

The ore material at Glendinning comprised stibnite (Sb_2S_3) and semseyite ($Pb_9Sb_8S_{21}$) in association with a stratiform arsenopyrite (FeAsS) and pyrite (FeS_2) mineralisation (Gallagher *et al*., 1983), and SpH1 samples contained elevated concentrations of Sb, As, Pb and Fe when compared with the surrounding soil. These samples were difficult to homogenise and the composition of the spoil was not uniform (See section 3.3.2). The range of values reflects the analysis of six aliquots of these samples (See Appendix 4). Higher Sb and As concentrations of ~300–540 mg kg^{-1} and ~100–170 mg kg^{-1}, respectively, were obtained for SpH1-deep (Table 6.2). In contrast, SpH1-surface had higher Pb concentrations of ~870–1020 mg kg^{-1}. The median Fe concentrations were 5.1% w/w and 4.2% w/w for SpH1-surface and SpH1-deep, respectively, and the range of Fe concentrations was also

greater for the surface sample, , i.e. the top 2-cm of the spoil heap (Table 6.2). The variation in composition may be attributable to changes in the nature of weathering processes operating at the surface and at greater depth within the spoil (discussed further in section 6.4.8.1).

6.4.4 Surface water elemental concentrations

For samples collected in February 2013, aqueous phase Sb concentrations were ~0.1 μg L^{-1} at W1–2 (upstream of the gully) but ~5.9 μg L^{-1} at W3 (downstream of the gully) (Table 6.3). Similar results of ~0.3 μg L^{-1} at W1 and 7.5 μg L^{-1} at W3 were obtained in October 2014, demonstrating that the waters flowing down the gully from SpH1 were transferring measurable Sb concentrations to the Glenshanna Burn. The W3 values were, however, ~100-fold lower than the values of ~780 μg L^{-1} (02/2013) and ~670 μg L^{-1} (10/2014) obtained at W5 (surface flow furthest down-gully from SpH1) (Table 6.3) and so considerable dilution had taken place upon entering the Burn. Similar to Sb, As concentrations were also lower at the upstream sites (~0.9–1.0 μg L^{-1}) than the values of ~13.2 ± 1.1 μg L^{-1} (02/2013) and 20.2 μg L^{-1} (10/2014) at the downstream site. Again, since the As concentrations at W5 were ~1770 μg L^{-1} (02/2013) and ~1480 μg L^{-1} (10/2014) the dilution upon entering the Burn was, to a first approximation, ~100-fold. Lead concentrations were close to detectable limits (0.06–0.08 μg L^{-1}) with no difference between upstream and downstream waters seen, nor was there any elevation in the surface flow, W5. Iron concentrations in stream waters W1–3 were higher than in W4-5 and, in contrast with the other elements, Fe concentration in the downstream sample, W3, was slightly lower than in the upstream samples (W1-2).

Table 6.3: Elemental concentration range found in water (W1-5) samples taken in the vicinity of Glendinning antimony mine.

Water Sites	Date of sampling	Fe µg L^{-1}	Sb µg L^{-1}	As µg L^{-1}	Pb µg L^{-1}
W1*	02/13 10/14	32.8 ± 0.04	0.10 0.26	1.13 ± 0.09 0.89	0.08 ± 0.03 0.38
W2*		32.0 ± 0.09	0.11	1.00 ± 0.01	0.08 ± 0.00
W3*	02/13 10/14	22.2 ± 3.79	5.88 ± 0.29 7.53	13.2 ± 1.14 20.2	0.07 ± 0.03 0.68
W4*		4.95 ± 2.69	83.8 ± 0.90	181 ± 26.4	0.55 ± 0.68
W5	02/13 10/14	5.31	783 6.74	1770 1480	0.06 0.21

* Mean from duplicate analysis.

6.4.5 Sequential extraction for selected soil samples from S2-S5

Performing a sequential extraction on selected soil profiles allows a better understanding of elemental associations and potential for mobilisation caused by a change in soil chemistry. Careful consideration however, should be taken when choosing the sequential extraction methodology to use, where methods are often modified to improve the performance for particular elements. For example, a number of modified BCR methods for Sb and As exist, where each study attempts to improve on existing methodologies by considering specific chemical and physical factors such as elemental speciation and the environmental media of sample used (Tessier *et al*., 1979; Nirel *et al*., 1990; Keon *et al*., 2001; Fuentes *et al*., 2004; Hudson-Edwards *et al*., 2004). There is however, no real agreement in the best solution to account for these factors (Bacon and Davidson, 2008). To this ends, the original BCR methodology was employed for this study, as the chemical properties of each selected element differed, and prevented the use of a more selective methodology. Moreover, and detailed in an extensive review by Bacon and Davidson (2008), continuity with previous studies is crucial particularly for the interpretation of data and comparison to other studies. A sequential extraction procedure involves suspending each soil sample in a sequence of three increasingly aggressive solutions, where each suspension is shaken for 16 hours, and where resulting solution was centrifuged, filtered and analysed for elemental concentrations. The

three extractants were used on selected soil samples to assess the exchangeable/acid-soluble (BCR1), reducible (e.g. hydrous Fe/Mn oxides) (BCR2), and oxidisable (e.g. organic matter, sulphide) (BCR3) fractions. The residual soil underwent a hotplate digestion to release elements from the "non-extractable" phases. Samples from 2–4 cm or 4–6 cm for each of S2–5 and from 6–8 cm and 8–10 cm for S2 and S4, respectively, were selected as exemplar near-surface and deeper sections (Figures 6.4, 6.5 and Appendix 4). These samples and depths were selected because: (i) total element concentrations were sufficiently high to ensure that those in the sequential fractions would most likely be above limits of detection; (ii) the importance of Fe redox cycling on elemental associations could be assessed; and (iii) the effect of organic matter degradation on elemental associations could be assessed.

When considering sequential extraction results, it is important to treat data with caution, as there is a potential for Sb, As, Pb and Fe bound to solid phases to re-adsorb post-extraction onto soil, which may result in low elemental recoveries (Davidson *et al*., 1998; Bacon and Davidson, 2008; Sutherland, 2010). This however, was generally not observed in this study, where typical recoveries for Sb, As and Pb were ~80–100% whilst those for Fe were ~60%, with the latter being attributable to the use of aqua regia, a mixture of concentrated HCl/HNO_3, rather than concentrated HNO_3/HF for the digestion of the residual phase. Whilst HF is considered a weak acid due to its low dissociation constant (K_a), in a concentrated form, it has the ability to homoassociate which significantly increases its acidity. Often used in conjunction with HNO_3, its ability to dissolve silicates in addition as most oxides means that it can be used to dissolve rock samples as well as effecting total dissolution of soil samples. Thus concentrated HNO_3/HF is more powerful reagent mixture compared with aqua regia. The results for Sb showed that very little was extracted in BCR1 and 2 (<5% in total) from any of the samples. Approximately 66% was extracted in BCR3 from S2 2–4 cm which had ~70% w/w OM whilst ~15–20% was extracted from the other near surface samples which had ~45–55% OM. The two samples from the deeper sections of S2 and S4 had lower OM contents and <10% Sb was extracted in BCR3. For As, ~5–18% was extracted in BCR1

from the samples taken from S2 and S3 whilst <3% was found in the same fraction for samples from S4 and S5. About 3–24% was extracted in BCR2 with the greater proportions being extracted from the samples from the deeper sections of S2 and S4, and especially the S5 4–6 cm section. As for Sb, the greatest proportion of As (~65%) extracted in BCR3 was for the sample which had the highest OM content, S2 2–4 cm. The lowest proportions extracted in this fraction were again for the deeper sections of S2 and S4. In these samples and in S4 4–6 cm, the greatest proportion (60– ~80%) of As was in the residual phase. For Pb, <1% was extracted in BCR1 and 2 from each of the samples. Approximately 65% Pb was in BCR3 for S2 2–4 cm whilst in all other samples, ~18–39% was extracted in this fraction. Thus the majority of Pb was present in the residual fraction in all samples except the highly organic S2 2–4 cm sample. For Fe the pattern was quite similar to that for Pb but with up to 12% in BCR2, 10–55% in BCR3 and the remainder in the residual phase. Although the overall extractability (sum of BCR1–3) increased in the order Sb < Fe < Pb < As, the between-site and "with-depth" trends were quite similar for all four elements.

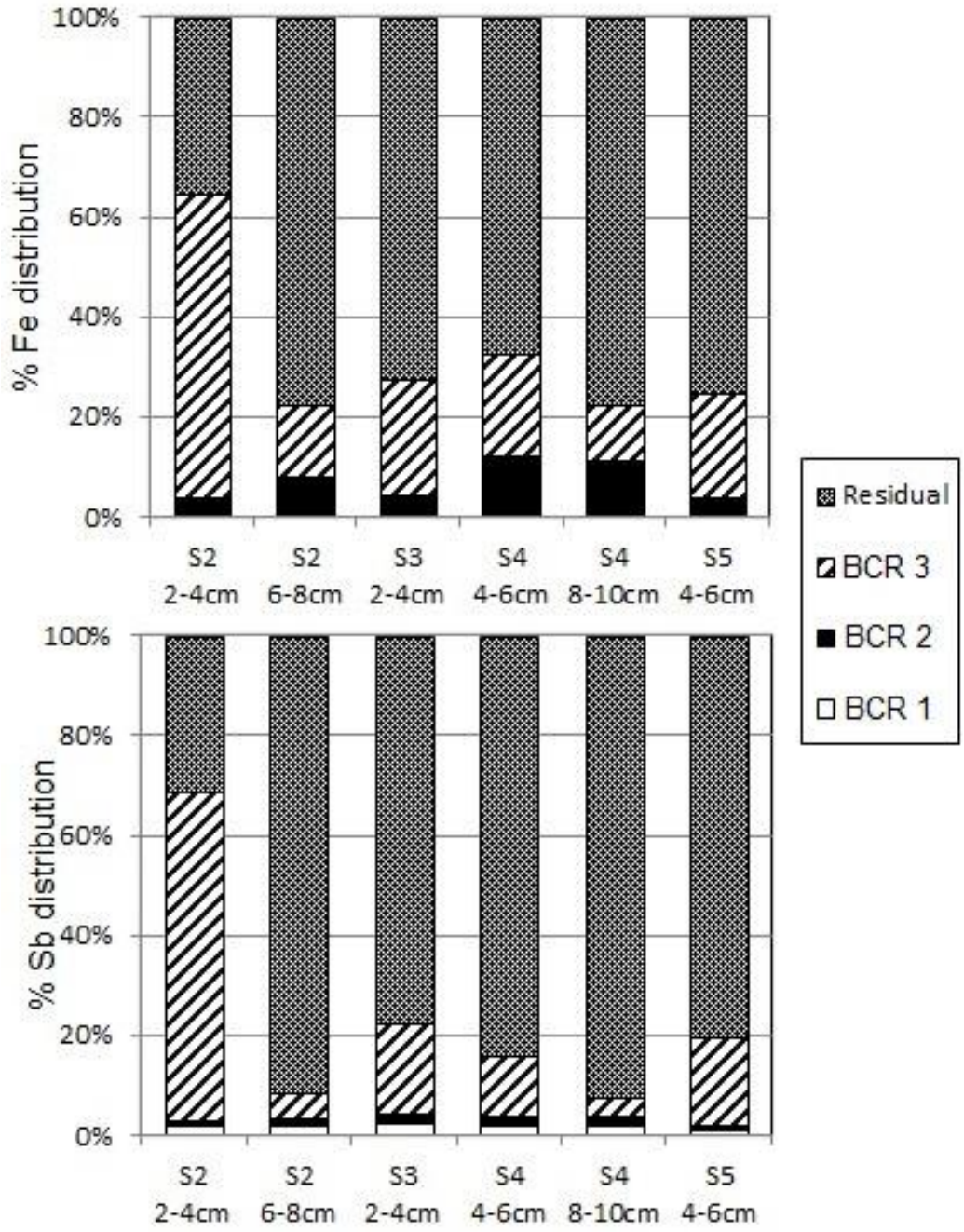

Figure 6.4: Distribution of Fe and Sb amongst BCR fractions (BCR1, BCR2, BCR3) and the residual phase of selected soil samples from S2-S5.

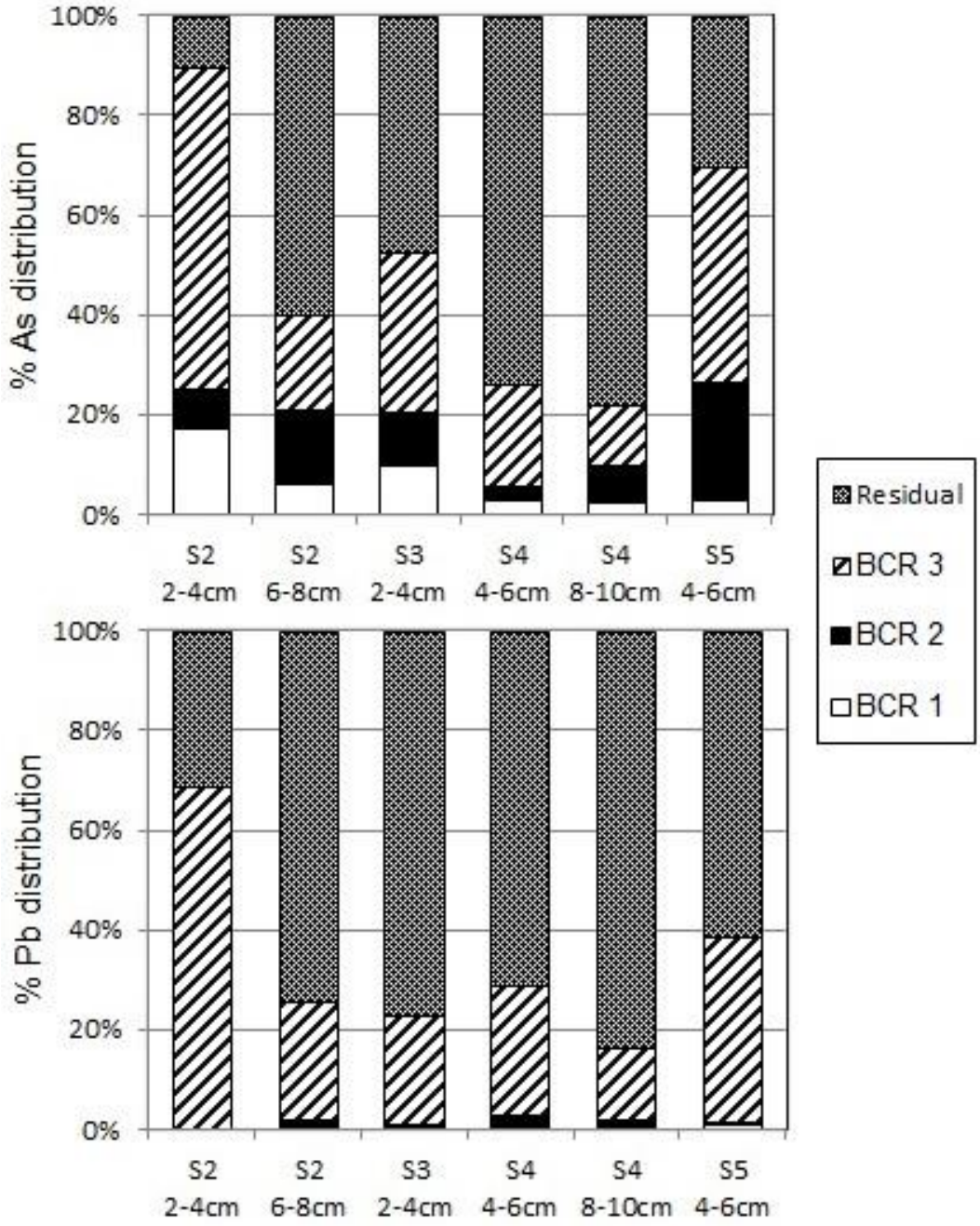

Figure 6.5: Distribution of As and Pb amongst BCR fractions (BCR1, BCR2, BCR3) and the residual phase of selected soil samples from S2-S5.

6.4.6 Colloidal and dissolved fractions of porewater from S2-S5

The analysis of soil porewaters (the water found in the spaces between soil particles) is particularly important when examining elemental transport in soils, as porewater concentrations can indicate how strongly bound elements are to a solid phase substrate, or whether a change in soil chemistry has occurred. In addition, the fractionation of porewaters using ultrafiltration also allows elemental associations between organic colloids and truly dissolved fractions to be examined. Theoretically colloids range between 1 to 1000 nm, however in practice, and for this study, colloids were fractionated between 3 kDa (2-3 nm) and 200 nm. Since 1 kDa centrifugal ultrafilters are no longer available, porewaters were fractionated using 3 kDa centrifugal ultrafilters for the low molecular weight cut-off, whilst the removal of particulate matter and bacteria using 0.2 μm hydrophilic membrane filters (200 nm) was used for the high molecular weight cut-off. The application of porewater fractionation will help to construct an idea of what processes are occurring in the vicinity of the spoil heaps and assist in the explanation of elemental transport from the spoil heaps to the surrounding soils and Glenshanna burn.

In general, the proportion of each element in the colloidal fraction increased in the order Sb ≤ As ≤ Pb ≤ Fe (Figure 6.6) but there were considerable variations with depth for both Sb and As. At S2, there was ~65-70% colloidal Sb in the near-surface porewaters which decreased to ~30% towards the bottom of the core. At S5, values ranged from 6-55% but at S3 and S4 there was <25% Sb in the colloidal fraction of the porewaters. The distribution of As between colloidal and truly dissolved forms was similar to Sb in the S4 porewaters ($t>4.5$, $p<0.01$) but, for S2, S3 and S5 there were distinct differences despite no statistical significance observed, e.g. there was an increase from ~20% to ~80% As in the colloidal fraction of S3 porewaters with increasing depth whilst the amount of colloidal Sb remained <20%. Similar associations were evident for the S5 porewaters, and it was clear that there were site-specific differences between the porewater distributions of Sb and As. With the

exception of Pb in the porewaters of S3 and the bottom section of S5, both Pb and Fe were almost exclusively present in the colloidal fraction.

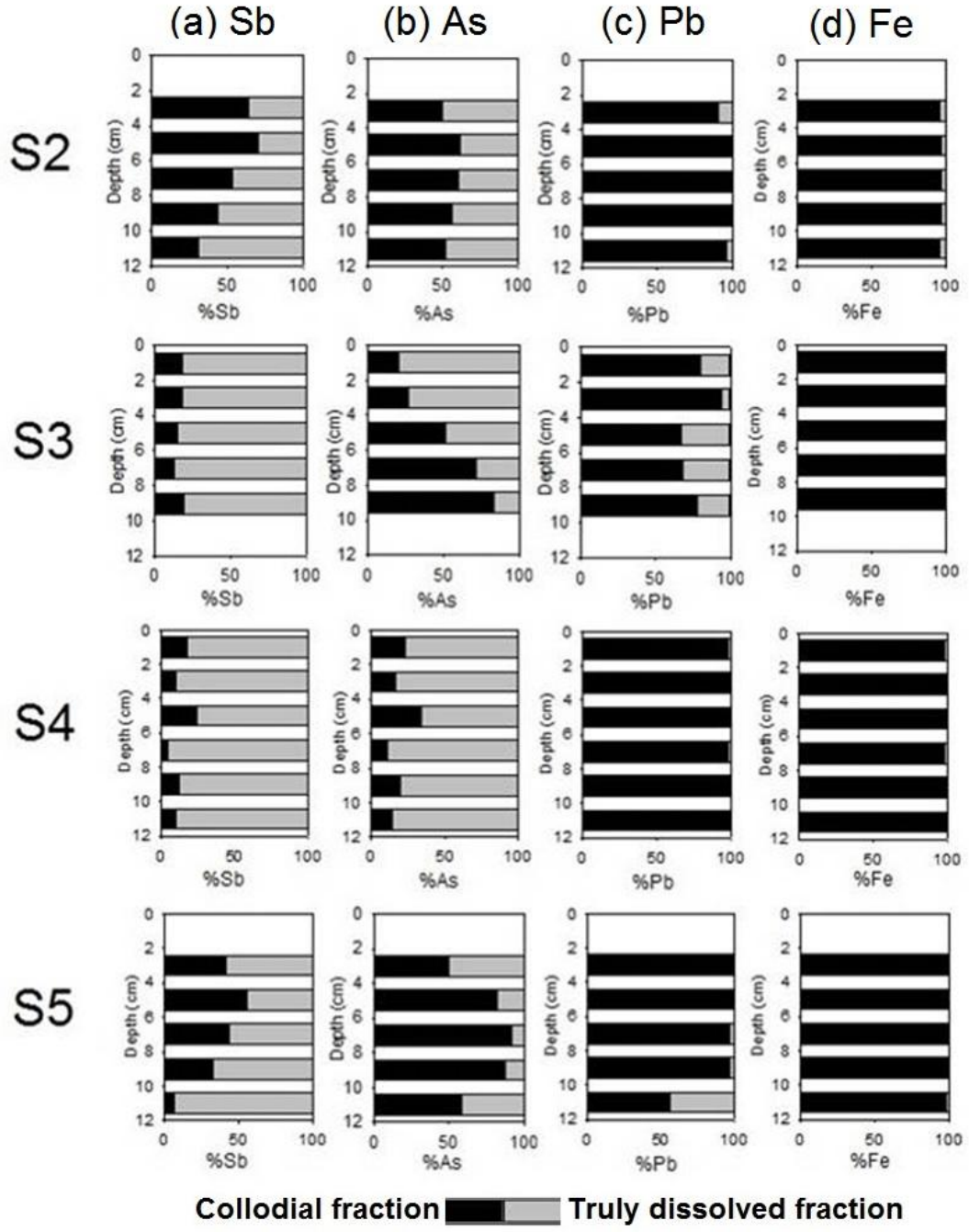

Figure 6.6: Vertical variations in the distribution of (a) Sb, (b) As, (c) Pb and (d) Fe amongst colloidal (3 kDa-0.2 µm) and dissolved fractions (< 3kDa) of the porewaters from S2-S5.

6.4.7 Gel electrophoretic fractionation of colloids from S2-S5

To complement data attained from ultrafiltration analysis, the application of gel electrophoresis allows colloids to be fractionated based on size and charge. The determination of each fraction for elemental concentrations by ICP-MS provides greater detail on colloidal composition and elemental association. As elemental concentrations were sufficiently high, and depth typical of a change in soil chemistry, the 4–6 cm 3 kDa-ultrafilter retentates from S2 to S5 were separated into 8 fractions (F1 - low electrophoretic mobility=large size/low charge; F8 - high electrophoretic mobility=small size/high charge) and analysed (section 3.3.5).

The highest concentrations of Sb, As and Fe were typically found in the fractions closest to the gel well i.e. F1 (Figure 6.7). Previous work has demonstrated that the separation is largely based on size (Graham *et al*., 2008), and thus Sb and As were associated with large Fe-rich humic colloids. In comparison, for the 4-6 cm samples from S3 and S4, Sb and As were associated with smaller organic colloids. The distribution of Pb was similar to that of Fe at S2 and S3 but, at both S4 and S5, Pb was predominantly associated with small organic colloids and there was little correlation between the distribution of Pb and those of Sb or Fe (Figure 6.7).

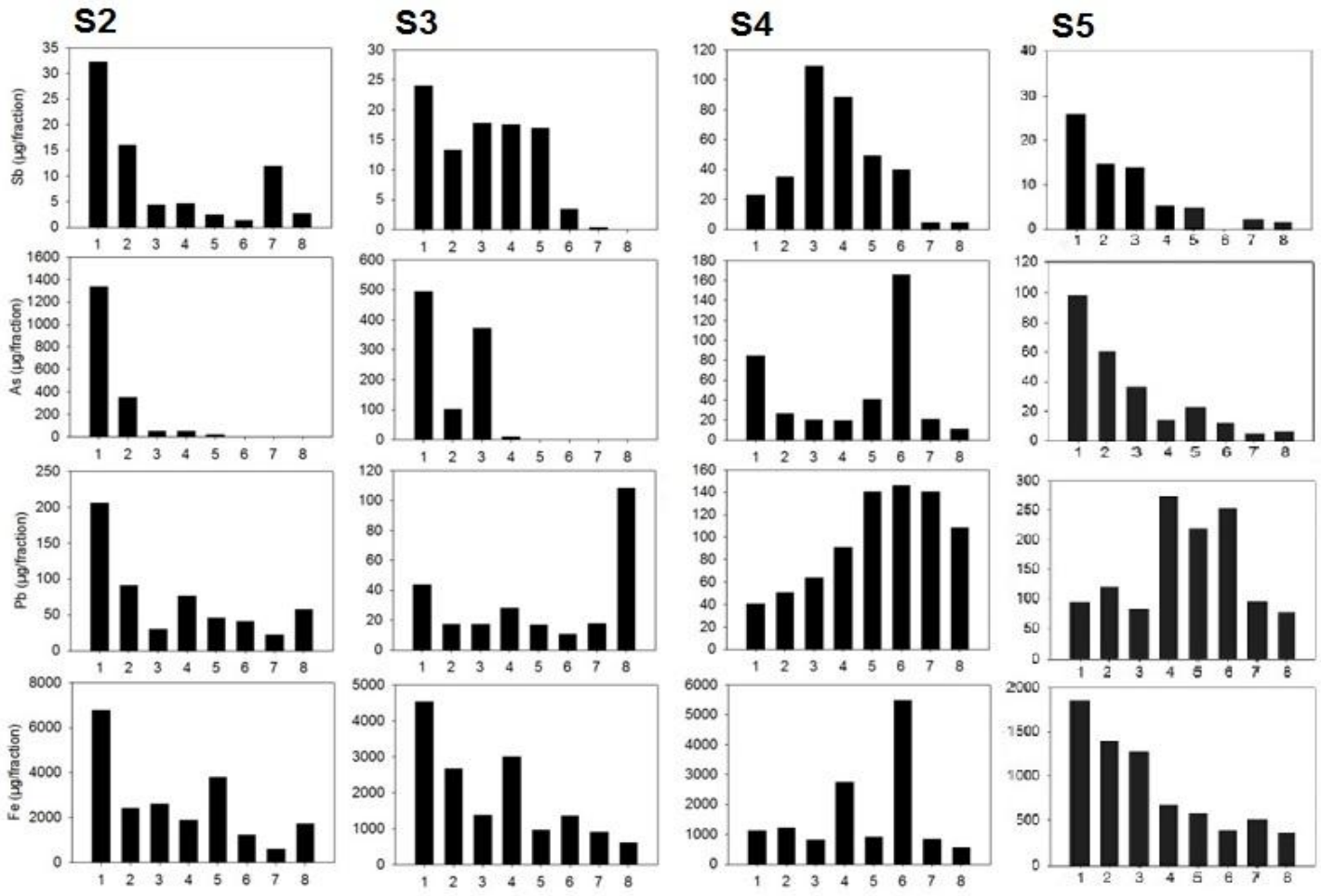

Figure 6.7: Distribution of Sb, As, Pb and Fe across gel electrophoretic fractions obtained for the colloid fraction (3 kDa-0.2 µm) isolated from S2-S5 porewaters.

6.4.8 Discussion

6.4.8.1 Spoil heap (SpH1) elemental concentrations

Antimony, As and Pb concentrations in the spoil material from SpH1 were typically greater than those in all six soil cores (S1–6) and the control soil (C1) (Table 6.1 and 6.2). Excavation of the lower mining area (Gallagher *et al*., 1983), which ran underground from the adit to a shaft near SpH1 (Figure 3.6(b)–(c)), resulted in spoil with high mineral content (stibnite (Sb_2S_3), arsenopyrite (FeAsS) and galena (PbS)) being deposited on the surrounding land and this has subsequently been exposed to the atmosphere and subject to infiltration of rainwater. Biver and Shotyk (2012) studied the kinetics of Sb release from stibnite and showed that higher rates of dissolution occurred as pH decreased from 5.1 to 1.1 and also with increasing dissolved oxygen concentrations from 0.05 to 0.8 atm (Equation 6.1). The presence of Fe^{3+} was also found to help catalyse the dissolution and accelerate the dissolution rate by an order of magnitude through the oxidation of sulfide to elemental sulphur (Equation 6.2). A follow up study examining senarmonitie (Sb_2O_3) and valentinite (Sb_2O_3), the dominant secondary ores from chemical weathering, reported a higher dissolution rate than stibnite; at least half an order of magnitude greater (Biver and Shotyk, 2013). The dissolution of secondary ores was found to be a surface-controlled process (Biver and Shotyk, 2013), which was in agreement with the results in this study, where lower concentrations of Sb in the surface spoil (SpH1-surface) was most likely a consequence of greater Sb ore weathering rates on the surface of the spoil.

$$Sb_2S_3(s) + 6O_2 + 6H_2O \rightarrow 2Sb(OH)_3(aq) + 3H_2SO_4\,(aq) \qquad \textbf{Equation 6.1}$$

$$Sb_2S_3(s) + Fe^{3+} + 15H_2O \rightarrow 2Sb(OH)_3(aq) + Fe^{2+} + 3SO_4^{2-} + 27H^+ \qquad \textbf{Equation 6.2}$$

$$4FeAsS + 11O_2 + 6H_2O \rightarrow 4Fe^{2+} + 4H_3AsO_3 + 4SO_4^{2-} \qquad \textbf{Equation 6.3}$$

$$4Fe^{2+} + O_2 + 10H_2O \rightarrow 4Fe(OH)_3 + 8H^+ \qquad \textbf{Equation 6.4}$$

Oxidative dissolution of arsenopyrite also releases As and Fe into solution (Equation 6.3), but the latter tends to hydrolyse and precipitate in the form of hydrous Fe oxides (Equation 6.4) (e.g. Walker *et al*., 2006). Walker *et al*. (2006) postulated that the dissolution of

arsenopyrite occurred through the slow reduction of water on the ore surface, and this was identified as the rate determining step. Moreover, coatings on the surface of Sb-containing munitions have been shown to be enriched in both Fe and Pb (Ackermann *et al*., 2009). Thus at Glendinning, it is proposed that oxidative dissolution processes lead to the loss of Sb (Biver and Shotyk, 2012) and As (Walker *et al*., 2006) whilst precipitation favours the enrichment of Fe and Pb in surface spoil. At depth, reductive dissolution of hydrous Fe oxides favours the loss of both Fe and Pb from surface coatings, accounting for the lower concentrations of these elements in SpH1-deep. While the hypothesis is in general agreement with a number of previous published studies, there are others which reach different conclusions. For example, Asta *et al*. (2010) reported the precipitation of hydrous Fe oxides and subsequent coating of arsenopyrite surfaces as the rate determining step, as this prevented the dissolution of arsenopyrite by surface water and suggested a lower mobility for As. Although the results obtained were consistent with high As mobility in the vicinity of the spoil heap to surface soils and water, further analysis using XRD and SEM-EDX could help characterise the surface of arsenopyrite and determine the extent of hydrous Fe oxide precipitation.

6.4.9 Processes controlling the spatial distribution of Sb, As, Pb and Fe in soils at Glendinning Sb mine

6.4.9.1 Downslope from the adit

Core S1 was situated below SpH2 on a shallow slope leading down from the adit whilst S2–3 were in a water-logged area at the base of this slope (Figure 3.6(b)–(c)). Antimony concentrations consistently decreased with increasing soil depth whilst the profiles for As, Pb and Fe showed either increased or near-constant concentrations with increasing depth. Based on the similarity of their vertical profiles, Sb may be strongly retained by OM in the near-surface sections of S1–3. This would be consistent with results for shooting range soils which attributed strong retention in surface organic layers to Sb (V) binding by humic acids

(Steely *et al*., 2007). A study in Norway by Reimann *et al*. (2007) also reported significant Sb retention in highly organic-rich soils sampled over a 120 km transect, where a 7-fold increase in median values from the soil C-horizon (consists of broken up bedrock material) to the O-horizon (consists of partially decomposed organic material) was observed. Moreover, the importance of OM to the retention of Sb was in agreement with numerous other studies reporting similar findings (Buschmann and Sigg, 2004; Tighe *et al*., 2005; Clemente *et al.*, 2008; Ceriotti and Amarasiri, 2009; Tella and Pokrovski, 2009; Reimann *et al.*, 2010; Wilson *et al*., 2010). The correlation of Sb concentrations with OM and the sequential extraction results for soil from Glendinning, as well as the previously mentioned research, highlights the importance and influence of OM on the retention of Sb in soils. This conflicts with conclusions postulated in a review by Filella and Williams (2012), where organic matter was reported to have little influence, and was almost exclusively related to mineral phases (hydrous Fe oxides) present in the soil (section 2.2.2.2).

The soil concentrations of Sb increased along the transect from S1 to S3 but this trend was not observed for As and Pb (Table 6.2 and Figure 6.3). Thus, although originating from the same source material, the processes controlling not only vertical but also lateral mobility have affected Sb differently from As and Pb. There was little variation in pH with increasing soil depth (Figure 6.2, Table 6.1) nor was there an obvious relationship between pH and elemental concentration with distance downslope from SpH2 (pH: $P>0.01$, $R^2=0.1$, elemental concentration: $P>0.3$, $R^2=0.16$). The profiles of As and Pb generally followed the trend for Fe at each of S1-3 and so sequential extraction was expected to reveal a major difference between the solid phase associations of Sb and those of As and Pb. In contrast with the anticipated results, all four elements behaved similarly. For example, the majority of each was associated with OM at S2 (2-4 cm) whilst at S3 (2-4 cm) the majority of Sb, Pb, Fe and ~50% As was in the residual phase. Comparison of the data for the 2–4 cm and 6–8 cm sections for the S2 core also revealed a consistent change for all four elements with increasing depth: the proportion associated with OM decreased markedly, resulting in a

concomitant increase in the percentage present in the residual fraction (Figure 6.4 and 6.5). This is fitting for typical soil horizons, where OM or humic acids are enriched at the soil surface and decrease with depth. Overall, the solid phase associations *per se* do not explain the observed differences in vertical and lateral distribution of Sb in comparison with As and Pb (Figure 6.3).

For porewater profiles, an increasing trend with depth from 3 to 7 cm, followed by a decline at 9 cm, was observed at S2 and S3 for Sb, As and Pb, which were very similar to each other and, in each case, similar to those of both DOM and Fe (Figure 6.3). However, when the distribution between colloidal and truly dissolved forms was considered (Figure 6.6), there was a considerable difference between the distributions of Sb and As and those of Pb and Fe. Moreover, the colloidal fraction had a strong brown colour indicating that humic substances, the main component of DOM, had been retained, although the limited colloidal sample volume prevented this from being quantified. For Pb and Fe, the vast majority (70–100%) was present in the colloidal fraction whilst up to ~90% Sb and up to ~80% As were present in the truly dissolved fraction. Furthermore, for S2, there was a major change from colloidal Sb in the near-surface sections to truly dissolved forms at depth whilst, at S3, the proportion in the truly dissolved phase remained almost constant with depth. At both locations, this strongly contrasted with the distribution of As at S2, where there was little change with depth whilst at S3, the proportion of colloidal As increased with increasing depth and thus the behaviour of As became more similar to that of Pb, Fe and OM. It is proposed that lateral transport promotes the removal of truly dissolved Sb species from deeper sections of the soil whilst association of As and Pb with large Fe-rich/organic colloids favours their retention.

For S2 4-6 cm, where the solid phase associations indicated that large proportions of Sb, As, Pb and Fe were associated with OM, more than 50% of each element was in colloidal forms within the porewater. Gel electrophoresis confirmed a strong association of Sb, As and Pb with very large Fe-rich organic colloids which have low mobility. For S3 4-6 cm, where the

solid phase association with OM was lower, Sb was mainly in the truly dissolved fraction and gel electrophoresis showed that, within the colloidal fraction, the greater proportion of As was again associated with very large Fe-rich colloids. Overall, the results of both ultrafiltration and gel electrophoresis point to differences in associations, which may start to explain the differences in the vertical distribution of Sb compared with As, Pb and Fe.

6.4.9.2 Down-gully from SpH1

There were ~2-fold and ~9-fold decreases in the maximum Sb concentration in the solid phase soils between S4 and S5 and S4 and S6, respectively (Table 6.2). Arsenic and Pb concentrations decreased much more rapidly between S4 and S5 (Table 6.2), suggesting that mobilised Sb may be transported over longer distances than both As and Pb before being attenuated by the gully soils. Mitsunobu *et al*. (2006) found that, where Sb and As behaved differently in soil, Sb was almost exclusively present in its oxidised form Sb(V) whilst As was present as a mixture of As(III) and As(V), indicative of the greater stability of Sb(V) in soil-water systems. Indeed, this was in agreement with Sb speciation results from porewaters extracted from two soil cores, S4A and S5A, sampled near the location of S4 and S5, respectively (discussed in section 4.6.3; Table 4.11). Porewater concentrations of Sb(V) were dominant in both S4A and S5A soil cores, and contributed on average to ~94% of total Sb concentrations present for these samples. Porewater concentrations for Sb(III) were low, ranging between 2.74– 37.1 μg L^{-1}, and appeared unaffected by reducing conditions observed at lower depths in both soil cores. In addition to the greater stability of Sb(V) in soil porewaters (Mitsunobu *et al*., 2006), Sb(V) sorbs less strongly to Fe oxides than As(V) in a pH range of 6.0 to 8.4 (pH range of S5 and S6, 5.6-6.0) (Leuz *et al*., 2006). In this study, there was a distinct change in solid phase associations of As with distance down-gully. The sequential extraction data for S5 soils showed that, in contrast with Sb, the majority of solid phase As was associated with Fe oxides and with OM, which may also be intimately associated with Fe oxides. This was in agreement with a Bauer and Blodau (2004), where dissolved OM and iron oxides increased As mobility by up to 53.3% by targeting the weakly

sorbed sites, with the competition of As and organic anions identified as the primary mechanism occurring (Bauer and Blodau, 2004). Moreover, the porewater profile of As was very similar to that of Fe, the majority of this As was in the colloidal fraction and, from the gel electrophoresis, As was mainly associated with large Fe-rich organic colloids. Although Sb was also associated with the same type of colloids, a greater proportion was present in truly dissolved forms. Thus the extent of sorption to Fe oxides may at least in part explain the observed trends with distance down-gully from SpH1.

As for the results for S3 soils, sequential extraction data for 4–6 cm samples from both S4 and S5 revealed that ~80% Sb was present in the residual phase. At 8–10 cm in S4, there was a decrease in association with OM and the percentage in the residual phase had increased to >90%. The distributions of As and Pb were similar to that of Sb at both 4-6 cm and 8-10 cm in S4, which suggests a very low potential for remobilisation of all three elements at this location. At S5, however, because As was almost evenly distribute amongst the iron oxide, organic matter and residual phases and could thus be more susceptible to redox-related remobilisation and loss from the soils should prevailing conditions change in the future.

The Sb concentrations in the porewaters at S4 were ~2-4 times greater than at S3, whilst the S4 solid phase concentrations were only slightly higher than those at S3. Since the sequential extraction data showed very little difference in the solid phase associations of Sb, and the pH of the S4 soils (~4.7-4.9) was similar to that of the surface spoil (~4.8), the higher S4 porewater Sb concentrations are attributed to rainwater-induced leaching from the spoil, which was ~5 m upslope. Moreover, the much higher solid phase Pb concentrations at S4 in comparison with S3 were not reflected in higher porewater concentrations, suggesting a lower leachability of Pb from the spoil in comparison with Sb. This is consistent with the data for the spoil which, as discussed above, indicated preferential loss of Sb (and As) from SpH1-surface samples (Table 6.3). In the S4 porewaters, both Sb and As were predominantly present in truly dissolved form. The small amount of Sb present in colloidal forms was

associated with smaller organic colloids which had a low Fe content. In contrast, the small amount of colloidal As at S4 was mainly associated with larger Fe-rich colloids, providing an additional explanation for its more rapid removal to the solid phase during its down-gully transport.

Comparing S4 and S5 porewaters, the maximum Sb concentration decreased by a factor of ~2 whilst that of As decreased by ~10. Thus for Sb and As, this trend mirrored that described above for the solid phase, providing further support for the poorer attenuation of Sb by the gully soils. One potential anomaly, however, was that the distributions of Pb and As at S5 were similar and, although the solid phase Pb concentration had decreased by a factor of ~15, porewater Pb concentrations were similar to those at S4. In the porewaters of both S4 and S5, Pb, Fe and DOM (colour retention) were almost exclusively found in the colloidal fraction whilst >~50% Sb and ≤70% As was present in the truly dissolved fraction. Gel electrophoretic fractionation of the colloid fraction of porewaters from the 4–6 cm section of S5 then revealed further important differences in elemental speciation. Antimony and As present within the colloidal fraction were both associated with large Fe-rich organic colloids whilst Pb was associated with smaller organic colloids which contained low concentrations of Fe (Figure 6.6). In agreement with Graham *et al*. (2011) and Crançon *et al*. (2010), who showed that association with small Fe-poor organic colloids inhibited the removal of depleted uranium (DU) from firing range soils, small organic-colloidal association of Pb inhibits its removal from the porewaters to the solid phase of the S5 gully soils.

6.4.10 Impact upon receiving water

The Sb concentrations of ~6–8 μg L^{-1} and ~84 μg L^{-1} for W3 (downstream of gully) and W4 (surface flow closest to SpH1), respectively, were in reasonable agreement with those previously reported for downstream (14.3 μg L^{-1}) and spoil heap drainage (60.4 μg L^{-1}) samples (Mohammad *et al*., 1990). The Sb concentrations at W3 were more than an order of magnitude higher than the value of 0.11 μg L^{-1} in the upstream waters (W1–2). The latter

was in line with those published in an extensive review by Filella *et al*. (2002b) where concentrations ranged from 0.17 μg L^{-1} in pristine water at Loch Ewe, Scotland, to 1.9 μg L^{-1} in the urbanised River Trent (Apte and Howard, 1986; Jarvie *et al*., 2000; Filella *et al*., 2002b). For As, water concentrations can be more variable due to local mineralogy, with natural concentrations ranging between 1 and 10 μg L^{-1} (Jarvie *et al*., 2000). The values of ~1–1.1 μg L^{-1} for W1–2 fell within this range whilst that for W3 (~13–20 μg L^{-1}) only slightly exceeded the natural concentration range and was much lower than concentrations of ≤283 μg L^{-1} found downstream of an abandoned Slovakian Sb mine (Hiller *et al*., 2012). Nevertheless, the water from W4 and W5 exceeded the 50.0 μg L^{-1} As freshwater Environmental Quality Standard (EQS) (SEPA, 2013). The implications of mining and the subsequent release of elements downstream has also been observed at other mining sites in Scotland such as Tyndrum Pb mine.

6.5 Historic trends in Sb, Pb and $^{206}Pb/^{207}Pb$ isotopic ratio concentrations at Loch Tay using ^{210}Pb dating

6.5.1 Introduction

A significant body of work has focused on the use of Scottish loch sediments to construct historic trends in Pb deposition over several centuries (Farmer *et al*., 1986; 1996; 1997; 2015; Eades *et al*., 1998; 2002). Particular attention has been paid to Loch Tay because of its direct hydrological connectivity to a historic Pb mine at Tyndrum. The effects of the mining activities, starting in the 1740s, expanding through the 1800s, diminishing and then ceasing in the early 1900s, on the surrounding landscape and the resultant elemental transport and deposition of Pb in Loch Tay sediments has been investigated by several research groups (MacKenzie and Pulford, 2002; Mansor, 2008; Pulford *et al*., 2009; Mills *et al*., 2014). There is no historic record, however, for Sb which is known to be present as an impurity in Pb ores which were extracted at Tyndrum. This chapter gives an initial brief historical account of the mining activities and past research focused on the spoil in the vicinity of the mine.

Thereafter, the historical records for Sb obtained for both the mini-Mackereth and Jenkin sediment cores will be established and interpreted, compared with those for Pb and then set in the context of records obtained for peat cores in Scotland.

6.5.2 Brief historical account of activities at the Tyndrum Pb mine over the period 1740-1920

Located in the Central Highlands of Scotland, Tyndrum Pb mine is situated 25 km west of Loch Tay (Figure 3.8(a) and (b)) where, during 1741 to 1921, a total of ~8000 tons of Pb ore was extracted and transported off-site, usually to Glasgow for smelting (Wilson, 1921; Mills *et al*., 2014). The discovery of Pb ore and subsequent extraction in the earlier years from 1740-1790 were the most productive period at the mine (~7700 ore produced), where the abundance and accessibility of high purity Pb ore resulted in a profitable period from mining activities (Wilson, 1921; Mills *et al.*, 2014). As easily obtained Pb ore began to dwindle, it became apparent that the transport costs to and from such a remote location was unsustainable, with the mine eventually abandoned in 1790 (Wilson, 1921; Mills *et al.*, 2014). In 1838, the mine was re-opened for a second period, and although the mining facilities were improved, there was still no on-site smelter. With the productivity of Pb ore extraction remaining low, the mine was closed again in 1865 (Wilson, 1921; Mills *et al.*, 2014). This was largely due to the complexity of the ore mineralisation left, which made Pb separation from its ore difficult and expensive. The Tyndrum Lead and Zinc Company oversaw the final period of mining activity from 1916 to 1928, where Pb ore extraction in underground workings and large processing dumps were utilised to yield ~330 tonnes of Pb ore before its final closure (Mills *et al.*, 2014).

6.5.3 Key findings from past research focused on the spoil in the vicinity of the Tyndrum Pb mine

A number of past studies detailing the history of the Tyndrum Pb mine and the local geology of the area (Wilson, 1921; Pattrick, 1985; Hall, 1999; Mills *et al*., 2014) has helped assess the impact of Pb mining in the vicinity of Tyndrum and its transport downstream to Loch

Tay. For this chapter, the most important study to date was completed by Farmer *et al*. (1997), where sediment cores were sampled from Loch Tay, quantified for Pb concentrations, and dated using ^{210}Pb. The results showed considerably elevated Pb concentrations present in the sections of the sediment cores which coincided with dates of when the mine was still in operation. This was confirmed using ^{206}Pb/^{207}Pb isotopic ratios, where the lower ^{206}Pb/^{207}Pb isotopic signature found for Tyndrum Pb ore (1.144), when compared to Pb ore from Wanlockhead (1.170 ± 0.003) and Scottish coal (1.181 ± 0.011) (Moorbath, 1962; Farmer *et al.,* 1999), was observed in Loch Tay sediment dating between 1741 to 1928. Further research by MacKenzie and Pulford (2002), focused on Pb contamination in the vicinity of Tydrum Pb mine and its transport downstream. The results showed significantly greater Pb contamination in the vicinity of the mine (up to 21% Pb), along the riverbanks (up to 5.22% Pb), and also demonstrated that Pb transport from Tyndrum to Loch Tay occurred via fluvial transport of particulate matter fractions with size <53μm. The transport of Pb from Tyndrum Pb mine to Loch Tay, was in agreement with Farmer *et al*. (1997), and was also observed in studies by Mansor (2008) and Pulford *et al*. (2009).

The above studies provide an excellent starting point for understanding Pb contamination caused by mining activity in Tyndrum and its subsequent transport downstream to Loch Tay. Whilst useful, no previous studies focusing on Sb concentrations in Loch Tay sediment exist, and this will be addressed in this chapter.

6.6 Results and Discussion: Historical record of Sb deposition obtained from dated mini-Mackereth sediment core from Loch Tay

In this section the previously published ^{210}Pb dates for a sediment core collected in 1992 (Farmer *et al*., 1997) are used to construct a historical record of Sb deposition in Loch Tay using the concentration data obtained in this study. This will be compared with the previously published record for Pb.

A full account of sampling and analytical methods is given in section 3.2.3.2.5 and 3.2.3.2.6 but, in brief, a 90-cm sediment core was collected in November 1992 using a mini-Mackereth piston corer (Mackereth, 1969) at a water depth of 48 m. The sampling location was in the centre of the loch and about 3 km from the western end (Figure 3.8(b)). The core was sliced into 1-cm sections to 20 cm depth, then 2-cm sections to 40 cm depth and 5-cm sections to 90 cm depth. The sections were dried and homogenised and Mn, Fe, As and Pb concentrations had previously been determined by flame atomic absorption spectroscopy. Arsenic concentrations were determined by hydride generation AAS and stable Pb isotope ratios ($^{206}Pb/^{207}Pb$) were determined by ICP-MS (Farmer *et al*., 1997). In this study, Sb concentrations were determined by ICP-MS.

6.6.1 Sb concentration profile – evidence for post-depositional immobility within the sediment

Table 6.4 shows the total Sb concentrations obtained for duplicate digestions (see section 3.3.9) of each section of the mini-Mackereth core (1991). The values ranged from 0.39-1.80 mg kg^{-1} and there was generally good agreement between the values for duplicates (mean S.D. of 0.03). The values (14.8 ± 1.2 mg kg^{-1}, n=24) obtained for sediment reference material, RTC:CNS392-50G, were in good agreement with the certified value of 12.0 ± 3.2 mg kg^{-1}.

Figure 6.8(a)-(f) shows the vertical concentration profile for Sb obtained in this study set against the previously published data for Mn, Fe, As, Pb and $^{206}Pb/^{207}Pb$ isotope ratios. The Mn and Fe profiles shown in Figure 6.8(a)-(b) are typical of those found in many lochs; there is clear evidence of diagenetic enrichment of both elements in the upper sections of the core with a solid phase maximum for Mn (~2.4% w/w) occurring in the top 0-1 cm section and one for Fe (~7.3% w/w) in the 1-3 cm sections. With the exception of peaks for both elements at the sediment-water interface, the concentrations of both elements decrease over the top sections until near-constant values of ~0.2% w/w and ~4.9% w/w (below 24 cm) are

reached for Mn and Fe, respectively. Significantly, the vertical concentration profile for As, a redox-sensitive element, shows a very similar pattern to that for Fe (Figure 6.8(b)-(c)) and strongly suggests that the profile for As has been modified as a consequence of diagenetic cycling of Fe. Indeed, the association of Fe and As was also observed at Glendinning Sb mine for soil and porewater samples seen earlier in this chapter (section 6.4.9).

Table 6.4: Concentrations of Sb in each section profile from Loch Tay mini-Mackereth sediment core.

Depth (cm)	Sb concentration ($mg\ kg^{-1}$)	Depth (cm)	Sb concentration ($mg\ kg^{-1}$)
0-1	0.66 ± 0.11	**20-22**	1.29 ± 0.03
1-2	0.75 ± 0.01	**22-24**	0.93 ± 0.01
2-3	0.85 ± 0.02	**24-26**	0.86 ± 0.02
3-4	0.95 ± 0.03	**26-28**	0.64 ± 0.02
4-5	1.38 ± 0.04	**28-30**	0.62 ± 0.02
5-6	1.39 ± 0.02	**30-32**	0.54 ± 0.02
6-7	1.50 ± 0.02	**32-34**	0.58 ± 0.07
7-8	1.37 ± 0.04	**34-36**	0.61 ± 0.01
8-9	1.28 ± 0.02	**36-38**	0.58 ± 0.03
9-10	1.42 ± 0.02	**38-40**	0.60 ± 0.02
10-11	1.59 ± 0.04	**40-45**	0.45 ± 0.03
11-12	1.61 ± 0.01	**45-50**	0.47 ± 0.01
12-13	1.65 ± 0.04	**50-55**	0.51 ± 0.01
13-14	1.68 ± 0.05	**55-60**	0.46 ± 0.01
14-15	1.80 ± 0.05	**60-65**	0.44 ± 0.03
15-16	1.65 ± 0.06	**65-70**	0.45 ± 0.03
16-17	1.55 ± 0.01	**70-75**	0.41 ± 0.02
17-18	1.37 ± 0.01	**75-80**	0.42 ± 0.02
18-19	1.32 ± 0.02	**80-85**	0.40 ± 0.03
19-20	1.38 ± 0.08	**85-90**	0.39 ± 0.02

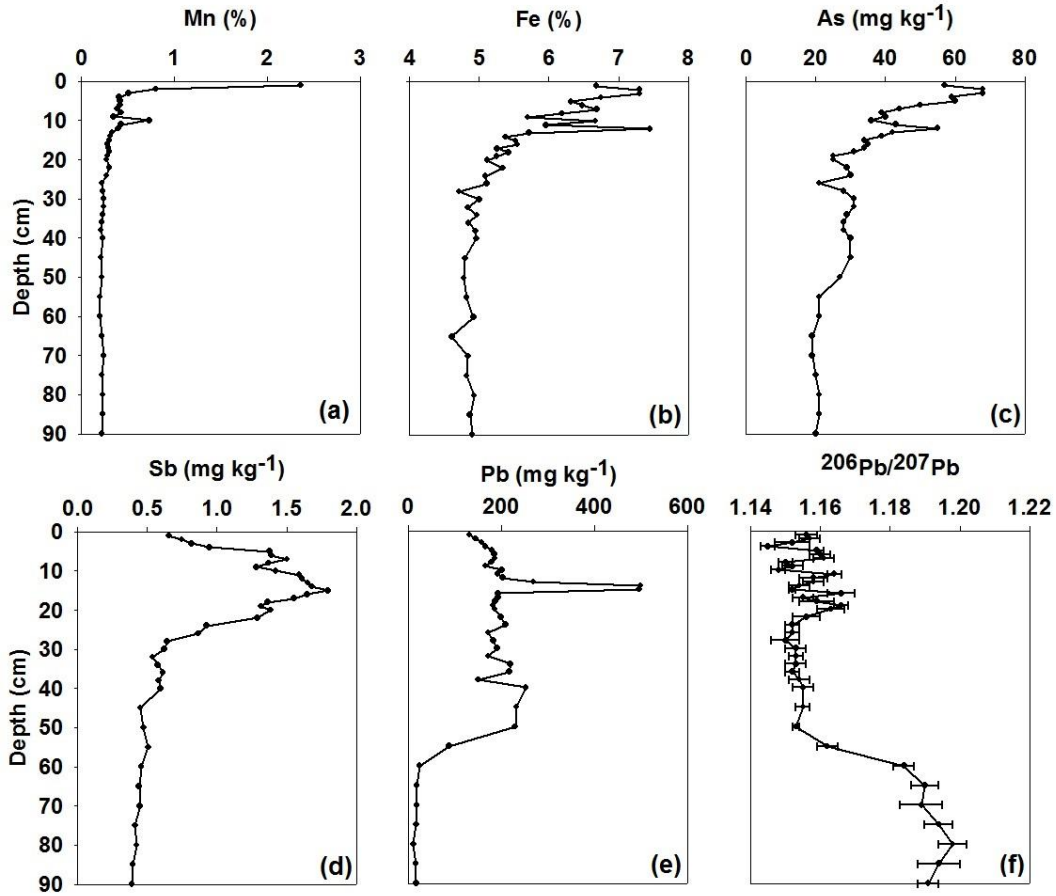

Figure 6.8: Vertical concentrations of (a) Mn, (b) Fe, (c) As, (d) Sb, (e) Pb and (f) $^{206}Pb/^{207}Pb$ isotopic ratios plotted with depth from Loch Tay mini-Mackereth sediment core. Adapted from Farmer *et al*. (1997).

The diagenetic mobilisation of elements throughout a sediment core is particularly important for understanding the fate of elements deposited. A change in environmental conditions (E_h-pH), generally occurring in the near-surface sediment, can result in the transport of elements after deposition through redox cycling and prevents deposition chronologies for elements in sediment cores being established. For the mini-Mackereth core, this was observed for Mn, Fe and As, and was in agreement with a number of previous sediment core studies (Bryant *et al*., 1997; Lee and Cundy, 2001; Spencer *et al*., 2003; Yang and Rose, 2005). Using Mn as an example, the reduction of Mn oxides/oxyhydroxides to Mn^{2+} results in its release to the sediment porewaters, where diffusion can occur either upwards or downwards from this

point of maximum concentration. Upwards diffusion will lead to the oxidation and precipitation of Mn as an oxide or oxyhydroxide, whilst downwards diffusion will result in equilibrium with carbonates and sulphides (Bryant *et al*., 1997). The depths that this occurs is governed by the redox potential (Bryant *et al*., 1997; Spencer *et al*., 2002), which is determined by factors such as biological activity, OM content and concentration of dissolved oxygen present (Spencer *et al*., 2003). In addition, Mn released to the sediment porewaters can also be present as an organically complexed ion (Elderfield, 1981), and once in an oxidised state, are also known to be present with other elements such as Na, K and Zn (Burdige, 1993). Under these conditions, the chemical behaviour of Fe and As is similar to Mn, but not to the same magnitude. Since Mn is more sensitive under a change in redox conditions, sub-surface concentration peaks of Fe and As are generally smaller and occur at greater depths.

The profiles for Sb and Pb were notably different from those of Mn, Fe and As. Importantly, there was no evidence of near-surface enrichment and thus no evidence for post-depositional mobility of either element within the sediment. This is in strong agreement with the vast body of published work on Pb in both peat and sediment cores (Farmer *et al.*, 1996, 1997, 2005, 2006, 2015; Eades *et al.*, 1998, 2002; Cloy *et al*., 2005) and adds to the smaller number of such studies which have also concluded that Sb is immobile (Shotyk *et al*., 1996; Mackenzie *et al*., 1998; Cloy *et al*., 2009; Allan *et al*., 2013).

The profiles for Sb and Pb were also different from each other. At depths of greater than 55 cm, Sb concentrations were in the range 0.39-0.46 mg kg^{-1} (mean 0.43 ± 0.03 mg kg^{-1}) whilst those at depths of 28-55 cm were only very slightly higher (range: 0.45-0.62 mg kg^{-1}; mean 0.55 ± 0.06 mg kg^{-1}). Above this there was a rapid increase to 1.8 mg kg^{-1} at a 14-15 cm depth and, from 8-9 cm (1.28 mg kg^{-1}) towards the sediment surface, this was followed by a marked decline to 0.66 mg kg^{-1}. For Pb, concentrations of ~17 mg kg^{-1} were observed

between the depths of 60-90 cm but a considerable increase began at ~55 cm depth, and values in the range ~150-255 mg kg^{1} were obtained over the depth range 15-50 cm. At 13-15 cm, there was a dramatic spike in Pb concentrations (497-500 mg kg^{-1}) above which Pb concentrations returned to ~200 mg kg^{-1} before decreasing over the top 0-5 cm sections to 132 mg kg^{-1} at the sediment surface. To a certain extent, the vertical Pb concentration profile was reflected in the observed changes in the $^{206}Pb/^{207}Pb$ isotopic ratios: at depths greater than 60 cm, the mean $^{206}Pb/^{207}Pb$ ratio was 1.191 ± 0.003, with a range of 1.184-1.198. Where the Pb concentrations increased over the 50-60 cm sections, the $^{206}Pb/^{207}Pb$ ratio dropped considerably and a mean value $^{206}Pb/^{207}Pb$ ratio of 1.153 ± 0.002 was obtained for the 22-50 cm sections. After this point $^{206}Pb/^{207}Pb$ ratios increased to 1.166 ± 0.002 and, towards the sediment surface, $^{206}Pb/^{207}Pb$ ratios fluctuated between 1.145 and 1.166. The value for the 0-1 cm depth section was 1.156 ± 0.003, and that for 13-15 cm depth sections where the position of the dramatic increase in Pb concentration was 1.152 ± 0.002. Further discussion on the Pb isotope ratio data from the mini-Mackereth sediment core is detailed in section 6.6.2.2.

6.6.2 Historic trends in Sb and Pb concentrations, $^{206}Pb/^{207}Pb$ isotopic ratios and anthropogenic Sb/Pb ratios for mini-Mackereth sediment core from the western basin of Loch Tay

6.6.2.1 Comparison of dated Sb and Pb concentrations

Having established that there was no evidence of post-depositional mobility for Sb, previously published ^{210}Pb-derived dates by Farmer *et al*. (1997) were used to construct a historical record of anthropogenic input to Loch Tay (Figure 6.9). This was done by deriving the sedimentation rate (28.3 mg cm^{-2} y^{-1}) using the sample and section weight, along with the activity of ^{210}Pb throughout the sediment core. The dating was then cross-checked by using radiocaesium activity, where dates from nuclear weapons testing (1963) and the Chernobyl accident (1986) helped to validate the dates attained from ^{210}Pb analysis. Although the

sedimentation rate allowed the calculation of deposition dates for Sb and Pb (Appendix 6), it was noted by Farmer *et al*. (1997) that due to a change in local land use, i.e. deforestation, the sedimentation rates were believed to be ~2.5 times higher during the 18th and 19th century, when compared to the 20th century. It is important to recognise that accurate dates can only be obtained over the ~150 years prior to collection of the core. This corresponds to ~7 half-lives for ^{210}Pb ($t_{½}$ = 22.3 y) and means that dating of the core is potentially unreliable before ~1850 due to the low levels of radioactivity in the deeper sediment sections (Farmer *et al*., 1997). As a result, Figure 6.9 shows dates from 1852 onwards and historical records of mining and other industrial activities will be used to facilitate data interpretation prior to 1850.

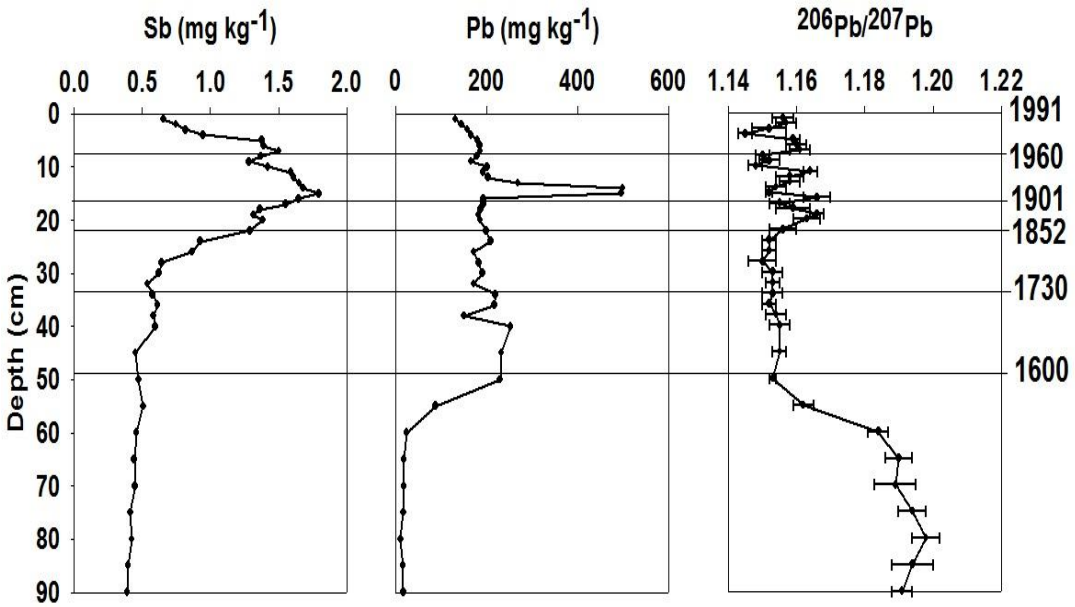

Figure 6.9: Loch Tay mini-Mackereth sediment core vertical concentrations of Sb, plotted beside Pb and associated ^{206}Pb/^{207}Pb isotopic ratios taken from Farmer *et al*. (1997), verses depth and ^{210}Pb dates. NOTE: Associated errors for Sb data have been omitted to present data similarly to Farmer *et al*., 1997.

From Figure 6.9, it is immediately evident that there are clear differences between the chronologies for Sb and Pb. Specifically, before ~1850, Sb concentrations were very low and there was only a slight increase in Sb concentrations most likely in the first part of the 19th

century. The rapid increase at ~1850 corresponded to the onset of the Industrial Revolution in UK cities, e.g. Manchester, N England, and Glasgow, W Scotland, and the associated major expansion of mining and smelting activities and a concomitant increase in coal combustion within this "industrial belt". This rapid increase in Sb concentrations, however, occurred considerably later than the increase in Pb concentrations. The latter was dated at ~1600, but was more likely to be ~1740s-1760s, the period when commercial Pb mining activities at Tyndrum were first documented. At this time, estimates suggest that ~400 tonnes of Pb ore per year were being produced (Mills *et al.*, 2014).

A further contrasting feature was the broad maximum in Sb concentrations which coincided with the period of maximum coal combustion (~1950s) whilst, with the exception of a large spike at ~1916, Pb concentrations remained approximately constant until ~mid-1980s. The observed large spike in Pb concentrations (~500 mg kg^{-1}) was in good agreement with the period of redevelopment of the Tyndrum Pb mine when large Pb ore dumps were reprocessed (Wilson, 1921).

The concentrations of Sb declined rapidly from the 1960s to the date of core collection whilst that of Pb decreased only to a limited extent, e.g. ~30% decrease. The former is most likely attributable to the continued decrease in contribution of emissions from coal combustion.

6.6.2.2 Comparison of dated Sb concentration profiles with $^{206}Pb/^{207}Pb$ isotopic ratio profile

From 1740 to the onset of the Industrial Revolution (~1850), $^{206}Pb/^{207}Pb$ isotopic ratios changed significantly from the geological background ratio of ~1.192 (Farmer *et al*., 1997), to a mean of 1.154 ± 0.003 (Figure 6.9). Although Pb released into the atmosphere through coal combustion and smelting activities will influence Pb concentrations found in Loch Tay sediment, its contribution to total Pb concentrations observed is secondary to the impact of the Tyndrum Pb mine. This can be established through the use of $^{206}Pb/^{207}Pb$ isotopic ratios,

because coal and Tyndrum Pb ore have different $^{206}Pb/^{207}Pb$ signatures. For example, Tyndrum Pb ore has a distinctive $^{206}Pb/^{207}Pb$ ratio of 1.144 ± 0.004 (Moorbath, 1962), notably different from both Scottish coal average ($^{206}Pb/^{207}Pb$: 1.181 ± 0.011) and the signature for Pb deposited from the atmosphere as a result of industrial activities ($^{206}Pb/^{207}Pb$: 1.170) (Sugden *et al*., 1991a,b; Farmer *et al*., 1997, 1999; MacKenzie and Pulford, 2002). The lowering of $^{206}Pb/^{207}Pb$ ratios values, along with the increase in mean Pb concentrations by at least a factor 10 (24.0 to 253 mg kg^{-1}), provided strong evidence that Tyndrum Pb mine was indeed the dominant source of elevated Pb concentrations found in Loch Tay sediment. This however, was in contrast to Sb, where concentrations in sediment from 1740 to 1850 only increased by ~25% from 0.46 to 0.61 mg kg^{-1}, indicating that mining activity in Tyndrum had no, or very little, impact on concentrations observed in Loch Tay sediment. Indeed, the marginal increase in Sb sediment concentrations is most likely attributable to coal combustion.

From 1850 to 1990, $^{206}Pb/^{207}Pb$ isotopic ratios fluctuate between ~1.14–1.17, and are increasingly influenced by atmospheric deposition originating from coal combustion and smelting activity during the Industrial Revolution, and latterly, from the use of leaded petrol. Up until 1940, mean $^{206}Pb/^{207}Pb$ isotopic ratios increased to 1.159 ± 0.005, where the $^{206}Pb/^{207}Pb$ signature of indigenous sources such as coal combustion (1.181 ± 0.011) and smelting of Wanlochhead Pb ore (1.170 ± 0.003) were dominant. At this point, the production of Pb ore from Tyndrum Pb mine was significantly less (~330 tonnes produced from 1850 to 1928) (Mills, 2014). Therefore the associated $^{206}Pb/^{207}Pb$ isotopic signature from Tyndrum Pb ore (1.144 ± 0.004) contributed less and the high ratio values were consistent with greater contribution from coal combustion and the smelting of Wanlockhead ore from the central belt. Between 1905 and 1913, a large spike in Pb sediment concentrations was observed (~500 mg kg^{-1}), which coincided with the redevelopment of the Tyndrum Pb mine, where Pb ore extraction in underground workings and large processing

dumps were utilised (Wilson, 1921). This was confirmed by a change in $^{206}Pb/^{207}Pb$ isotope ratios for that period, where ratios dipped from 1.166 ± 0.004 to a minimum of 1.152 ± 0.001, and increased thereafter to 1.158 ± 0.003. This reflected the impact and contribution Tyndrum Pb ore had on sediment Pb concentrations at Loch Tay, as the unusually low $^{206}Pb/^{207}Pb$ ratio for Tyndrum Pb ore (1.144 ± 0.004) (Moorbath, 1962) resulted in a decline in $^{206}Pb/^{207}Pb$ ratio over the same period of time. In contrast, and as expected, no large spike in Sb concentrations were observed between 1905 and 1913, since Tyndrum Pb mine does not influence Sb sediment concentrations. There were, however, other influential anthropogenic activities occurring at the time, such as coal combustion and the smelting of Wanlockhead Pb ore, which resulted in a broad maximum peak spanning the mid-19th to 20th century. This broad Sb peak was similarly observed in peat deposition studies by Shotyk *et al*. (1996) and Cloy *et al*. (2005; 2009). From 1940 onwards, the influence of coal combustion and the smelting of Wanlockhead Pb ore on Sb and Pb concentrations in Loch Tay sediment reduced. Whilst Sb emissions were on the decline, the combustion from leaded petrol became a different source of Pb emissions, particularly between 1960-1975 when leaded petrol emissions peaked (Robbins *et al.,* 2010). The addition of Australian sourced Pb, to leaded petrol, resulted in leaded petrol having a $^{206}Pb/^{207}Pb$ isotopic ratio of ~1.06-1.09 (Farmer *et al*., 2000). The impact of the low $^{206}Pb/^{207}Pb$ isotopic ratio for leaded petrol was consistent with the low $^{206}Pb/^{207}Pb$ isotopic ratios observed in Loch Tay sediment for this time period, where values reduced to a minimum of 1.143 ± 0.002, with a mean value of 1.154 ± 0.005 (1940-1990).

6.6.2.3 Anthropogenic Sb/Pb ratio

As discussed in chapter 2, Sb and Pb (as well as As) are often found together in sulfidic minerals and ores, and so anthropogenic activities such as mining, smelting and coal combustion generally release both Sb and Pb into the environment. Since impurities such as Sb will be present at different amounts, Sb/Pb ratios in coal and Pb ores have been quantified and subsequently used to distinguish between difference sources within archival materials

including sediments and peats cores (Cloy *et al*., 2005; 2009; Xu *et al*., 2011). Table 6.5 shows previously determined Sb/Pb ratios for British coal (0.036 ± 0.032) and Wanlockhead Pb ore (0.0056 ± 0.0004), along with the extremely low Sb/Pb ratio for Tyndrum Pb ore (0.0003).

Table 6.5: Sb/Pb ratios and $^{206}Pb/^{207}Pb$ isotopic ratios in a selection of environmental samples.

Environmental Sample	Sb/Pb Ratio	$^{206}Pb/^{207}Pb$ isotope ratio	Reference
Upper Continental Crust	0.018	n.a.	Wedepohl, 1995
Tyndrum Pb ore, Scotland	0.0003 n.a.	n.a. 1.144 ± 0.004	Cloy, thesis Moorbath, 1962
Wanlockhead Pb ore, Scotland	0.0056 ± 0.0004	1.170 ± 0.003	Cloy *et al*., 2005
British coal	0.036 ± 0.032	1.182 ± 0.009	Farmer *et al*., 1999
Flanders moss peat (71-102 cm depth), Scotland	0.010 ± 0.004	1.176 ± 0.003	Cloy *et al*., 2005
Atmospheric deposited Pb from industrial activity	n.a.	1.170	Farmer *et al*., 1997

The subtraction of Sb and Pb geological background concentrations from total Sb and Pb concentrations in each section of the sediment core, enables the impact of anthropogenic activity *per se* to be assessed. In this instance, the mean concentrations of Sb and Pb at depths of >60 cm (pre-dating known mine activity) were 0.42 and 17 mg kg^{-1}, respectively, and after these values had been subtracted, the anthropogenic Sb/Pb ratio was calculated for each section of the core (Figure 6.10). These values were deemed reliable, as calculated Sb/Pb ratios for Loch Tay background (0.025) were similar to the Upper Continental Crust Sb/Pb ratio of 0.018 (Wedepohl, 1995).

Before commercial mining began in Tyndrum (pre-18^{th} century), mean Sb/Pb ratios of ~0.0015 and a range of 0.0003 to 0.0012 was observed in Loch Tay sediment. This suggested that Tyndrum Pb ore had been worked on in the past, as Sb/Pb ratios were similar to ratios found in Tyndrum Pb ore (Table 6.5). Indeed, this was confirmed using $^{206}Pb/^{207}Pb$

isotopic ratios over the same period of time, where the $^{206}Pb/^{207}Pb$ geological background value of 1.192 (Farmer *et al.*, 1997) had declined to ~1.154, reflecting the influence of Tyndrum Pb ore had on $^{206}Pb/^{207}Pb$ isotopic ratios. Moreover, it also agreed with a historic account of the mine by Mills *et al.* (2014), where early evidence had suggested Pb ore workings occurred in the 15th century.

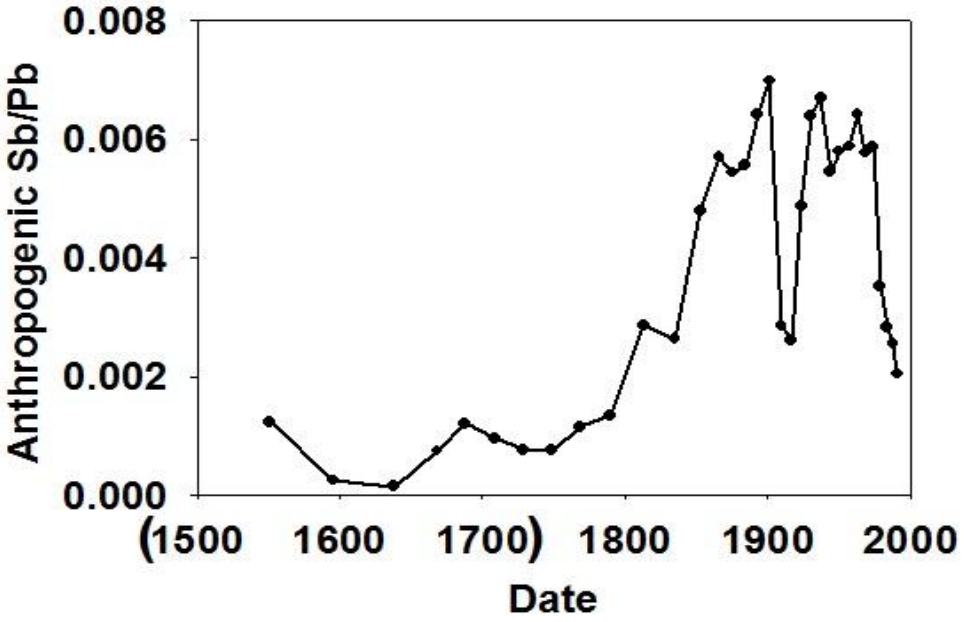

Figure 6.10: Temporal variations in anthropogenic Sb/Pb ratios from Loch Tay mini-Mackereth sediment core

During the 18th century, when Tyndrum Pb mine began commercial operations, Sb/Pb ratios observed in Loch Tay sediment were generally stable at 0.001 ± 0.0003, and were notably higher than the expected Sb/Pb ratio of 0.0003 for Tyndrum Pb ore (Table 6.5). Although no significant change in $^{206}Pb/^{207}Pb$ ratios was observed over this period, the higher Sb/Pb ratio found in sediment, when compared to the Tyndrum Pb ore, represents the beginning of emissions from other industrial activities. Emissions of Sb and Pb from the combustion of coal and smelting of Wanlockhead Pb ore had resulted in elevated Sb/Pb ratios present in the Loch Tay sediment. The increasing trend for Sb/Pb ratios intensifies throughout the 19th century, where it reaches a value of ~0.006 during the Industrial Revolution. At this point, significant amounts of Sb and Pb are released to the atmosphere and deposited from the

combustion of coal and the smelting of Pb ore. This signifies a change in the dominant source influencing Sb and Pb concentrations found in Loch Tay sediment. This was reflected in the different mean $^{206}Pb/^{207}Pb$ ratios observed for the 18th century (1.152 ± 0.001) and 19th century (1.159 ± 0.006), where the upwards shift was indicative of a greater influence from coal combustion (1.181 ± 0.011) and smelting of Wanlochhead Pb ore (1.170 ± 0.003).

The final years of commercial activity at Tyndrum Pb mine occurred in the early 20th century. As discussed in section 6.5.2, a large spike in sediment concentrations for Pb occurred ~1916, which coincided with the redevelopment of the Tyndrum Pb mine. As a result, a significant dip in Sb/Pb ratios occurs for this period, where Pb released from mining activity is transported downstream, whilst the low Sb content present in Tyndrum Pb ore meant that sediment concentrations of Sb remained the same (Table 6.5). This was again reflected by a change in $^{206}Pb/^{207}Pb$ isotope ratios for that period, where ratios dipped from 1.166 ± 0.004 to a low of 1.152 ± 0.001, and increased thereafter to 1.158 ± 0.003, consistent with a greater influence of $^{206}Pb/^{207}Pb$ ratios originating from Tyndrum Pb ore (1.144 ± 0.004) (Moorbath, 1962). Upon the closure of Tyndrum Pb mine (1928), Sb/Pb ratios increased to ~0.0067, where the input of Sb and Pb concentrations to Loch Tay sediment was exclusively from coal combustion and the smelting of Wanlockhead Pb ore. From ~1940 to 1980, Sb/Pb ratios remain steady, and thereafter, decline as a result of reducing emissions of Sb from industrial sources, and Pb, from the phasing out of leaded petrol in 1986. This was in agreement with mean $^{206}Pb/^{207}Pb$ ratios, where ratios observed from 1940 to 1980 were lower (1.155 ± 0.006) than those from 50 years earlier (1.158 ± 0.005), and clearly influenced by the low $^{206}Pb/^{207}Pb$ signature of leaded petrol (~ 1.06-1.09) (Farmer *et al*., 2000). In addition, the decline in Sb/Pb ratios at the end of the 20th century has been similarly observed in a number of other ombrotrophic peat cores (Shotyk *et al*., 2004; Cloy *et al*., 2005; 2009).

The above gives an account and explanation of Sb/Pb ratios observed in the mini-Mackereth sediment core over specific time periods. The Sb/Pb ratio values over the entirety of the sediment core, however, merits further consideration, particularly in respect to apportioning the contribution Pb sources make to total sediment concentrations found. Using data from Farmer *et al*. (1997) (Table 6.6), it is estimated that pre-1862, Tyndrum Pb mine provided ~12.7 g m^{-2} of Pb to Loch Tay, while industrial emissions contributed much less at 3.81 g m^{-2}. This, however, changed between 1862-1928, where mining activity at Tyndrum contributed less Pb (2.64 g m^{-2}) to Loch Tay sediment, and was more comparable to the Pb contribution by industrial emissions (2.01 g m^{-2}). Whilst the Pb apportionment reported by Farmer *et al*. (1997) gave a good estimation of the contribution Tyndrum Pb mine and industrial emissions had on total Pb concentrations found in Loch Tay sediment before 1862, it does not, however, fully account for the Sb/Pb ratios observed post-1862 for this study. For example, Pb concentrations in sediments dating from 1862-1928 comprised a ~60:40 mixture of Tyndrum Pb mine and industrial emissions, respectively. Taking into consideration the higher Sb/Pb ratio found in industrial emissions such as coal combustion (Sb/Pb ratio: 0.036 ± 0.032) and ore smelting (Sb/Pb ratio: 0.0056 ± 0.0004) relative to Tyndrum Pb ore (Sb/Pb ratio: 0.0003), the Sb/Pb ratios observed from 1862 onwards should be much higher (~0.022) than the maximum of 0.0067 observed. The Sb/Pb ratios suggest that Pb (and Sb) emissions from ore smelting from 1862 onwards were the dominant source of Pb to Loch Tay sediment. In addition, further studies by MacKenzie and Pulford, (2003), and Pulford *et al*. (2009) also identified Pb from Tyndrum as a source of Pb to Loch Tay sediment, despite the decline in Pb ore production from 1862-1928. The studies highlighted large mine dumps and waste situated on floodplains as a potential source of Pb to Loch Tay sediment. Both Pb ore smelting and the transport of Pb from Tyndrum would account for the Sb/Pb ratio of 0.0067 observed in Loch Tay between 1862-1928, while the contribution of coal combustion emissions to Pb in Loch Tay sediment is expected to be low since the Sb/Pb ratio was 0.036 ± 0.032.

Table 6.6: Anthropogenic Pb apportionment from Loch Tay and Loch sediment cores (Farmer *et al*., 1997).

Period	Loch Tay			Loch Lomond
	Total ($g\ m^{-2}$)	Mining [a] ($g\ m^{-2}$)	Industrial [b] ($g\ m^{-2}$)	Total ($g\ m^{-2}$)
1928-1992	2.99			2.29
1906-1928	2.50	1.73	0.77	0.77
1862-1906	2.15	0.91	1.24	1.44
pre-1862	16.50	12.69	3.81	1.85
Total	24.14			6.35

[a] Based on $^{206}Pb/^{207}Pb$ ratio of Tyndrum mine Pb as 1.144 (Moorbath, 1962).
[b] Based on $^{206}Pb/^{207}Pb$ ratio of industrial Pb as 1.170 (Sugden *et al*., 1991a.b; Farmer *et al*., 1993, 1996
[c] to which petrol Pb has contributed 24-53%, based on $^{206}Pb/^{207}Pb$ ratio of petrol as 1.06-1.12 (Farmer *et al*., 1996).

6.6.2.4 Anthropogenic Sb flux for a mini-Mackereth sediment core from the western basin of Loch Tay

The calculation of anthropogenic Sb flux allows the deposition rate of Sb to be determined over time. As detailed in section 6.6.2.3, Sb background concentrations were established (0.42 mg kg^{-1}), to which total Sb concentrations for each profile section were deducted to give anthropogenic-only input to Loch Tay. Once attained, the Sb flux was determined using the Sb inventory (a calculation using anthropogenic Sb concentration), sample weight and corer area, multiplied by the number of years in each profile section. The equation and calculated data used to plot Figure 6.11 can be found in Appendix 5 and 6.

The Sb flux observed before commercial mining activities began was very low (~0.15 mg $m^{-2}\ y^{-1}$), which compared well to the moderate Pb flux found (20 mg $m^{-2}\ y^{-1}$) for the same period of time (Figure 6.12). This, however, changed for Pb, where fluxes began to increase during ~1740s-1760s, while no increase in Sb flux occurred until ~1800. Although this was expected given the Sb/Pb ratio of Tyndrum Pb ore, it was also in agreement with local smelting and industrial activities found near Tyndrum at the time. For example, a

historical account of Tyndrum Pb mine by Mills *et al*. (2014) highlighted that only early Tyndrum Pb ore was smelted near to the mine (~3 km) with most smelting occurring in Glasgow, Alloa and the north of Wales. This is particularly important, as it indicates that only limited coal combustion took place at Tyndrum and that Sb released from coal combustion was very low, and in agreement with the Sb flux for the 18th century. Indeed, this was one of several reasons why Tyndrum Pb mine closed, as obtaining enough coal for smelting activities in such a rural part of Scotland was difficult, and there have been suggestions that early smelting activities used wood, and not coal (Mills *et al.*, 2014).

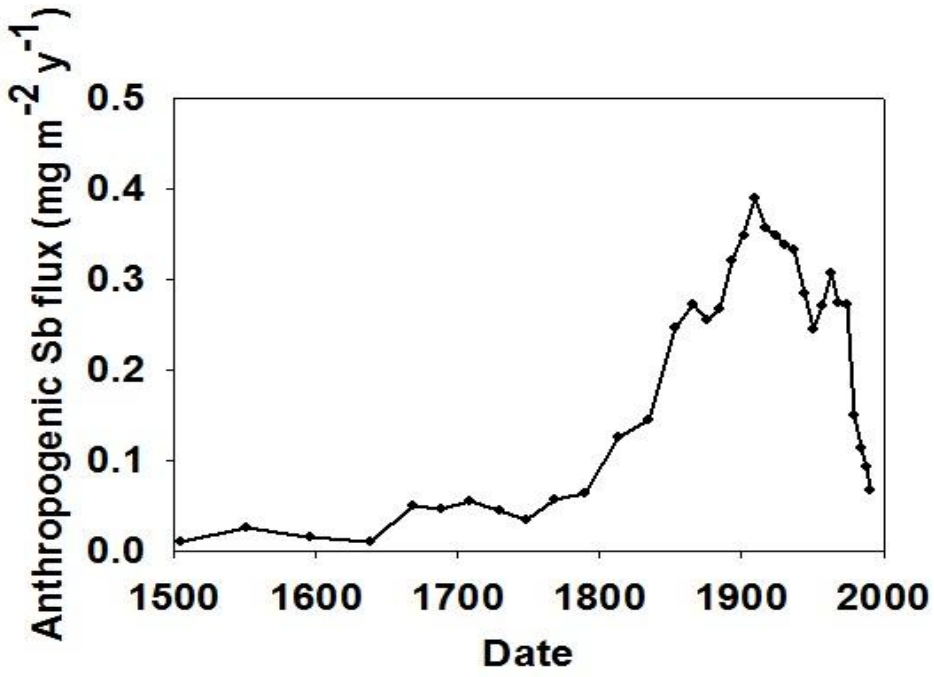

Figure 6.11: Temporal variations in anthropogenic Sb flux from Loch Tay mini-Mackereth sediment core.

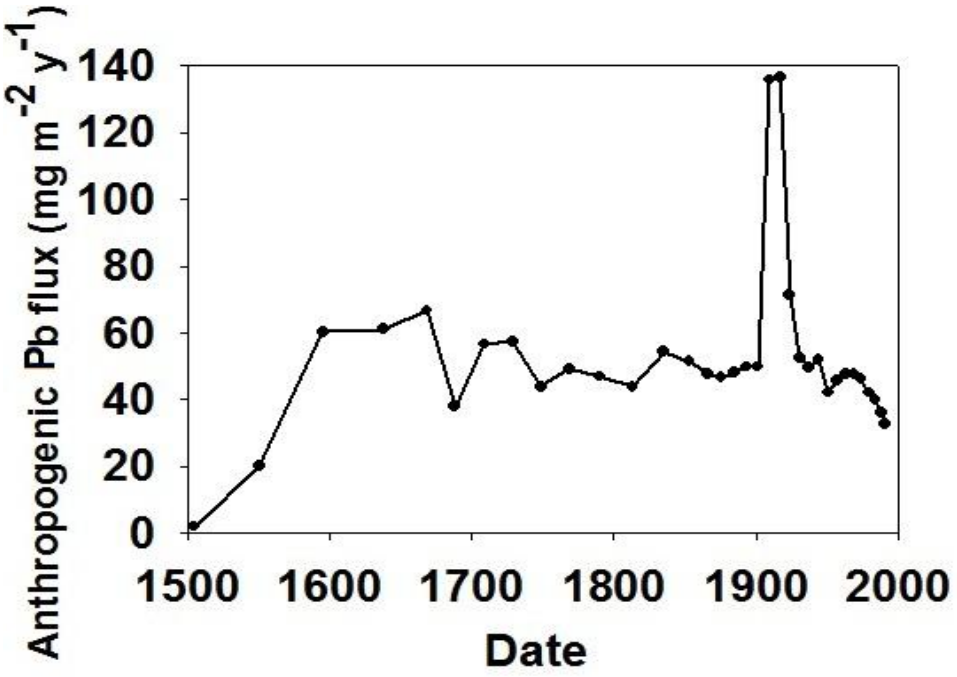

Figure 6.12: Temporal variations in anthropogenic Pb flux from Loch Tay mini-Mackereth sediment core. Taken from Farmer *et al*. (1997).

Taking the limited access to coal into consideration, the sharp increase in Sb fluxes during the 19th century, where Pb fluxes remained generally stable, were very likely to have originated from the atmospheric emissions from the central belt of Scotland and the industrial belt of northern England. From ~1860, mining activity at Tyndrum ends, whilst a rapid increase in industrial activities requiring coal combustion occurs during the main industrialisation period in the UK. This is not marked by a change in Pb flux (as this was already elevated due to the mining activities) but is denoted by a change in the $^{206}Pb/^{207}Pb$ isotope ratios which increases to ~1.16, where the dominant source originates from industrial Pb, with Tyndrum Pb ore still contributing to total Pb concentrations, albeit to a lesser extent. The $^{206}Pb/^{207}Pb$ ratios remain similar until ~1930s-1940s, where a general decreasing trend occurs to ~1.14-1.15 near the sediment core surface, reflecting the increase in the contribution of leaded petrol and a concomitant decrease in the importance of Pb originating from smelting and coal combustion. The fluctuations over the entire period most likely indicate that there has been change in the contribution of Tyndrum-derived material. The documented reworking of the slag in the early 1900s resulted in a massive increase in

anthropogenic Pb flux and a clear decline in the $^{206}Pb/^{207}Pb$ isotope ratio. From the mid-20th century onwards, Sb fluxes typically decline, as large mining operations at Leadhills and Wanlockhead had already closed (~1930s) (Wilson 1921; Elliott *et al*., 1937; Cloy *et al*., 2005), and improved technology and regulation had helped reduce Sb emissions from coal combustion by significantly reducing the release of ash particles. The reduction in Pb flux however, occurs ~20 years later than observed for the Sb, and is largely a result of Pb emissions from leaded petrol. The introduction of leaded petrol in the 1920s, and its increased use throughout the 20th century, gave rise to significant atmospheric concentrations of Pb originating from transport emissions. This would also account for the $^{206}Pb/^{207}Pb$ isotope ratios during the mid to late-20th century, where ratios were ~1.15, and only began to increase after 1986 when leaded petrol was phased out (Figure 2.10).

6.6.3 Results and Discussion: Historical record of Sb deposition obtained from a dated Jenkin sediment core from Loch Tay

At the time of collecting the mini-Mackereth sediment core (1992) detailed in the section 6.6, a Jenkin sediment core was also collected from Loch Tay at the same sampling location, i.e. the centre of the loch, about 3 km from the western basin end. By using two sediment cores to construct a historical record of Sb deposition in Loch Tay, it allowed a more definitive record to be established. Since sediment can accumulate at different rates on the Loch bed, it was important to reproduce elemental deposition chronologies obtained from the mini-Mackereth sediment core.

Sections 3.2.3.2.5 and 3.2.3.2.6 give a full account of sampling and methodologies used on the Jenkin core sediment samples but, to summarise, the 19 cm Jenkin sediment core was sliced into 1-cm sections, dried and homogenised. Each section underwent quantification using ICP-MS analysis for Mn, Fe, As, Sb and Pb, as well as the determination of $^{206}Pb/^{207}Pb$ isotope ratio analysis. Since the Jenkin core was sampled at the same time and location as the mini-Mackereth core, the previously published ^{210}Pb data and calculated sedimentation rate (28.3 mg cm^{-2} y^{-1}) by Farmer *et al*. (1997) were used to date the Jenkin core sections.

6.6.4 Historic trends in Sb and Pb concentrations, $^{206}Pb/^{207}Pb$ isotopic ratios and anthropogenic Sb/Pb ratios for Jenkin sediment core from the western basin of Loch Tay

6.6.4.1 Jenkin sediment core Mn, Fe, As, Sb and Pb concentrations, and $^{206}Pb/^{207}Pb$ isotope ratio profile- confirmation of Sb and Pb immobility within sediment

The elemental concentrations from the Jenkin sediment core for Mn, Fe, As, Sb and Pb, and associated $^{206}Pb/^{207}Pb$ isotope ratios are shown in Table 6.7 and Figure 6.13 (a)-(f). There was good agreement between duplicate sediment sample analysis values for Fe, As, Sb and Pb (Fe 6590 ± 334, As 10.7 ± 0.8, Sb 15.3 ± 0.5 and Pb 135 ± 8.3, all in mg kg^{-1}) (see section 3.3.13.3), and the respective values for the certified reference material RTC:CNS392-50G concentrations (Fe 7880 ± 867, As 6.5 ± 3.2, Sb 12.0 ± 3.2 and Pb 121 ± 8.2, all in mg kg^{-1}). Duplicate sediment sample analysis values for Mn were low (Mn 3602 ± 344), when compared to the certified reference value (6604 ± 679), and were used for indication only.

The near-surface enrichment observed for both Mn (1.83 ± 0.01%) and Fe (8.5 ± 0.01%) profiles shown in Figure 6.13(a)-(b) is clear evidence of diagenetic mobilisation within the sediment core (Bryant *et al.,* 1997; Farmer *et al.,* 1997; Yang and Rose 2005). At depths below 1 cm, Mn concentrations were generally stable (0.29 ± 0.05%), while Fe concentrations steadily declined from a depth of 3 cm (7.1 ± 0.4%) to 19 cm (5.2 ± 0.1%). This is typical behaviour for redox-active elements (Farmer and Lovell, 1986; Yang and Rose, 2005), and was in agreement with results obtained from the mini-Mackereth core discussed earlier (section 6.6.1). Notably, vertical concentrations for As in the Jenkin core were only marginally influenced by diagenetic mobilisation, where only a small sub-surface peak was found in the 11-12 cm section (53.8 ± 3.3 mg kg^{-1}), which was unlike the more distinctive sub-surface peak seen in the mini-Mackereth core. With the exception of a decline in As concentrations from 5 cm (61.5 ± 4.9 mg kg^{-1}) towards the sediment surface

(32.9 ± 2.2 mg kg^{-1}), As concentrations fluctuate with depth, with a general decline towards the 18-19 cm section (40.4 ± 1.1 mg kg^{-1}).

Table 6.7: Loch Tay Jenkin sediment core Mn, Fe, As, Sb, Pb concentrations (mg kg-1) and $^{206}Pb/^{207}Pb$ isotopic ratios for each 1-cm section.

Depth (cm)	Mn (%)	Fe (%)	As (mg kg^{-1})	Sb (mg kg^{-1})	Pb (mg kg^{-1})	$^{206}Pb/^{207}Pb$
0-1	1.83 ± 0.01	8.84 ± 0.1	32.9 ± 2.2	1.06 ± 0.02	209 ± 1.0	1.154 ± 0.001
1-2	0.41 ± 0.01	8.33 ± 0.6	42.2 ± 1.2	0.94 ± 0.05	195 ± 2.5	1.153 ± 0.003
2-3	0.37 ± 0.02	7.12 ± 0.4	47.4 ± 3.4	1.07 ± 0.07	197 ± 0.6	1.156 ± 0.005
3-4	0.32 ± 0.01	6.57 ± 0.8	57.3 ± 1.4	1.02 ± 0.02	187 ± 19	1.148 ± 0.001
4-5	0.33 ± 0.01	7.02 ± 0.2	61.5 ± 4.7	1.28 ± 0.01	218 ± 2.9	1.153 ± 0.003
5-6	0.31 ± 0.01	6.30 ± 0.2	52.4 ± 0.2	1.42 ± 0.01	220 ± 2.6	1.147 ± 0.004
6-7	0.32 ± 0.01	6.46 ± 0.2	59.0 ± 0.8	1.44 ± 0.03	231 ± 1.7	1.145 ± 0.001
7-8	0.31 ± 0.01	6.00 ± 0.1	59.9 ± 0.8	1.48 ± 0.02	217 ± 0.8	1.148 ± 0.002
8-9	0.28 ± 0.01	6.05 ± 0.2	47.9 ± 0.3	1.44 ± 0.07	212 ± 4.7	1.154 ± 0.002
9-10	0.31 ± 0.01	5.95 ± 0.4	35.8 ± 0.8	1.27 ± 0.02	192 ± 7.2	1.155 ± 0.003
10-11	0.27 ± 0.01	6.48 ± 0.2	45.4 ± 1.6	1.30 ± 0.06	231 ± 13	1.158 ± 0.003
11-12	0.27 ± 0.01	5.82 ± 0.1	53.8 ± 3.3	1.47 ± 0.01	212 ± 3.1	1.156 ± 0.004
13-14	0.22 ± 0.01	5.30 ± 0.4	48.6 ± 4.0	1.38 ± 0.10	258 ± 10	1.155 ± 0.001
14-15	0.24 ± 0.01	5.39 ± 0.1	49.5 ± 0.8	1.68 ± 0.01	630 ± 8.1	1.147 ± 0.002
15-16	0.23 ±0.01	5.11 ± 0.1	41.7 ± 0.5	1.78 ± 0.01	292 ± 0.7	1.157 ± 0.006
16-17	0.25 ± 0.01	5.46 ± 0.1	39.6 ± 1.1	1.57 ± 0.03	244 ± 18	1.158 ± 0.005
17-18	0.25 ± 0.02	5.55 ± 0.1	42.3 ± 1.3	1.45 ± 0.06	230 ± 6.2	1.161 ± 0.001
18-19	0.25 ± 0.01	5.17 ± 0.1	40.4 ± 1.1	1.31 ± 0.11	229 ± 19	1.162 ± 0.002

NOTE: No results for the 12-13 cm section exist as no sample material was available.

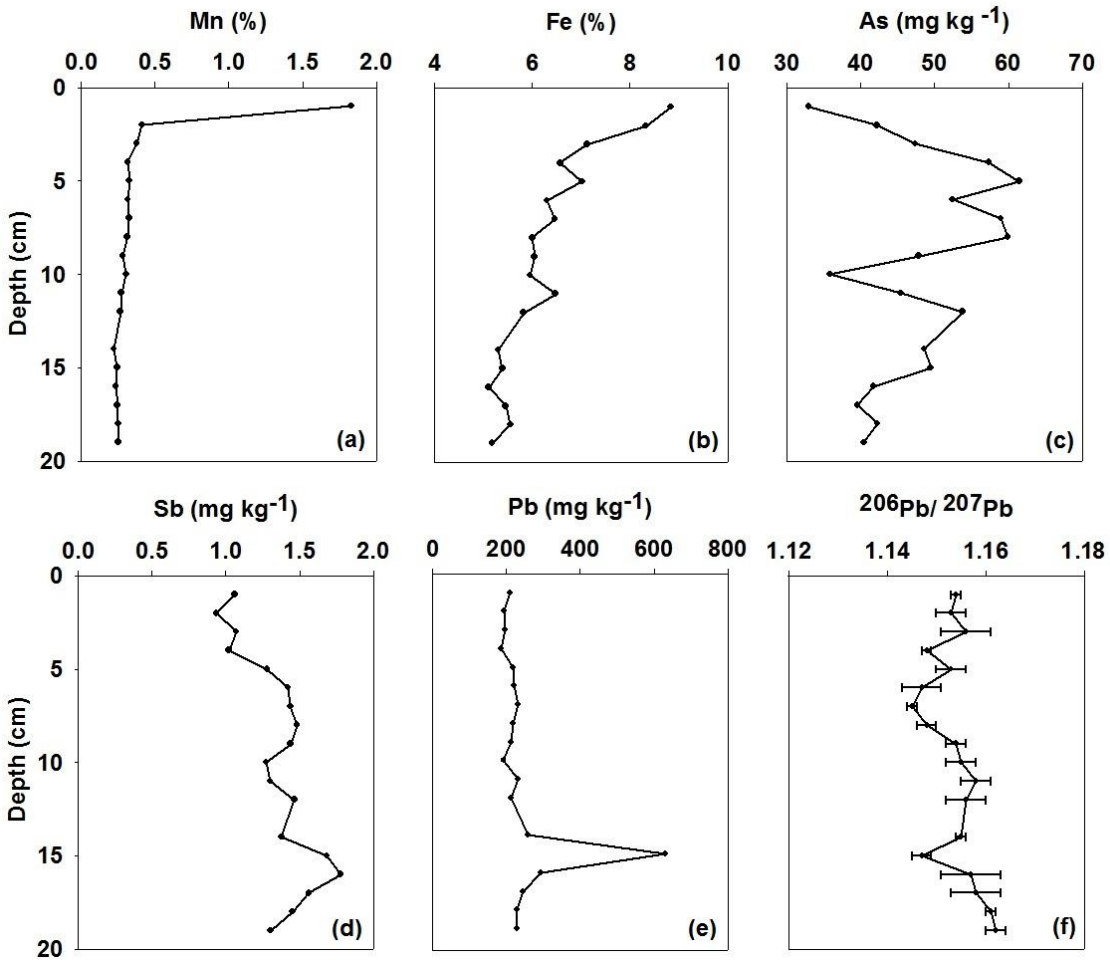

Figure 6.13: Vertical concentrations of (a) Mn, (b) Fe, (c) As, (d) Sb, (e) Pb and (f) $^{206}Pb/^{207}Pb$ isotopic ratios plotted with depth from Loch Tay Jenkin sediment core. NOTE: With excepiton of $^{206}Pb/^{207}Pb$ isotopic ratios, associated errors for data have been omitted for visual reasons, and values can be found in Table 6.7.

Unlike Mn, Fe and As, vertical concentration profiles for Sb and Pb showed that they were unaffected by diagenetic mobilisation, as no evidence of near-surface enrichment was found in Figure 6.13(d)-(e). The absence of post-depositional mobility for Sb and Pb was expected, as this was similarly observed in the mini-Mackereth core, and in agreement with other published Sb and Pb archival chronologies (Shotyk *et al*., 1996; Farmer *et al* 1996, 1997, 2005, 2006, 2015; Eades *et al* 1998, 2002; Mackenzie *et al*., 1998; Cloy *et al*., 2005; 2009; Allan *et al*., 2013).

Although Sb and Pb were both immobile in sediment, their vertical profile concentrations were again notably different from each other. In general, concentrations of Sb throughout the Jenkin sediment core were broadly similar. With exception of a small peak in Sb concentrations occurring in the 15-16 cm section (1.78 ± 0.5 mg kg^{-1}), mean concentrations at depths greater than 5 cm were comparable (1.46 ± 0.2 mg kg^{-1}), while in the top 5 sections, a small decline in concentrations to ~1.0 mg kg^{-1} was observed. For Pb, three distinct regions were observed over the length of the core. At depths greater than 15 cm, concentrations of Pb were generally stable at ~248 mg kg^{-1}, after which, a significant peak in concentrations to 630 ± 8.1 mg kg^{-1} was seen at a 14-15 cm depth. From this point towards the sediment surface, Pb concentrations were broadly stable, with a mean concentration of 214 mg kg^{-1} and range of 187–219 mg kg^{-1}. The depth profile for $^{206}Pb/^{207}Pb$ isotopic ratios fluctuated considerably throughout the sediment core, where a general lowering of the isotopic ratio value occurred towards the sediment surface. For the bottom 15-19 cm sections, isotopic ratios were briefly stable at ~1.160, and thereafter, a considerable dip to 1.147 ± 0.002 occurred in the 14-15 cm section, coinciding with the significant peak in Pb concentrations mentioned earlier. At this point, isotopic ratios were briefly stable for sections 8-14 cm, with a mean $^{206}Pb/^{207}Pb$ ratio of 1.155 ± 0.002, followed by another drop in values to a minimum of 1.145 ± 0.001, at a 5-8 cm depth. From this point towards the sediment surface, $^{206}Pb/^{207}Pb$ ratios increased to a mean value of 1.153 ± 0.003.

6.6.4.2 Comparison of dated Sb and Pb concentration profile

In the absence of post-depositional mobility for Sb and Pb, a historical record of Sb and Pb deposition in Loch Tay sediment could be obtained using the previously published ^{210}Pb-derived data from Farmer *et al*. (1997) (Figure 6.14). This was calculated similarly to the previous mini-Mackereth sediment core detailed in section 6.6.2.1 where by using the same derived sedimentation rate of 28.3 mg cm^{-2} y^{-1} for dating, an accurate comparison of elemental deposition for each sediment core over time was achieved. As the Jenkin core was

short in length (0-19 cm), the ^{210}Pb dating attained was over a shorter period of time, from 1900 to 1991.

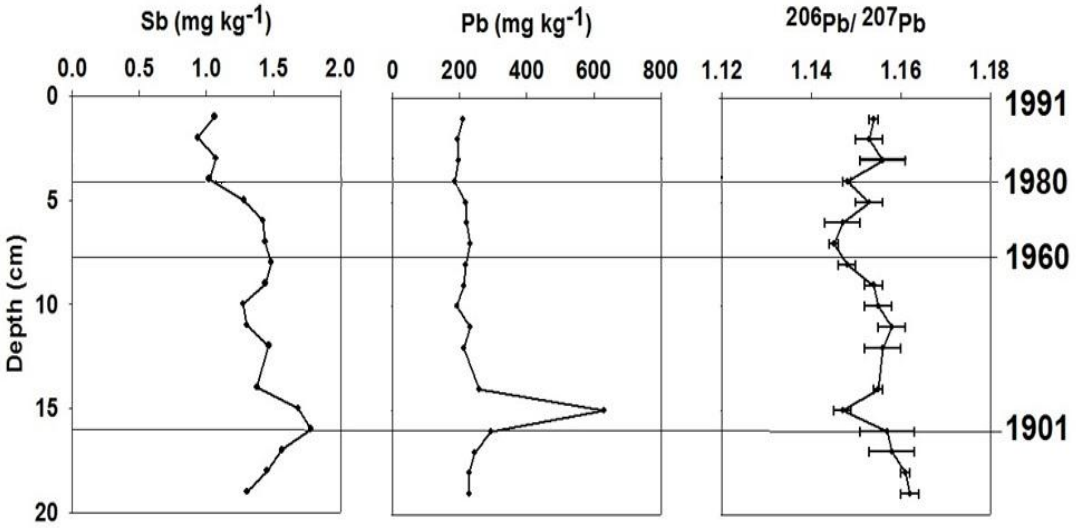

Figure 6.14: Loch Tay Jenkin sediment core vertical concentrations of Sb, Pb and associated ^{206}Pb/^{207}Pb isotopic ratios plotted with depth and ^{210}Pb dates. NOTE: With excepiton of ^{206}Pb/^{207}Pb isotopic ratios, associated errors for data have been omitted for visual reasons, and values can be found in Table 6.7.

Upon examination of Figure 6.14, a contrast in Sb and Pb chronologies during the 20th century was clearly evident. Whilst sediment concentrations of Sb in the 20th century were generally similar, a small peak in concentrations was observed ~1900, which was ~15 years before the redevelopment of Tyndrum Pb mine where underground workings and old mining dumps were reprocessed (Wilson, 1921). The small increase in Sb concentrations ~1900 was also observed in the mini-Mackereth sediment core, and is most likely a result of elevated atmospheric emissions of Sb from the combustion of coal for that period of time. The increased mining activity at Tyndrum was, however, recorded in the sediment Pb concentrations, where a significant peak occurred (630 ± 0.2 mg kg^{-1}) ~1910, which coincided with the extraction of Pb ore, and resulted in the fluvial transport of Pb downstream to Loch Tay (MacKenzie and Pulford, 2002). Indeed, this was consistent with a notable drop in ^{206}Pb/^{207}Pb isotopic ratios; the value before 1910 was 1.157 ± 0.007 and then

dropped to 1.147 ± 0.002. Further differences in dated vertical concentration profiles for Sb and Pb, were also observed from the mid to end of the 20th century. For example, concentrations of Sb began to decline in ~1960s, and from 1980 onwards, remained fairly stable to the top of the core at a mean concentration of 1.07 ± 0.1 mg kg^{-1}. This was similarly observed in the mini-Mackereth sediment core, and is attributed to the declining atmospheric emissions of Sb caused by the improved regulation of emissions originating from the combustion of coal in the UK. For Pb however, only a marginal decline was observed in mean concentrations when compared to those between 1930−1975 (216 ± 12 mg kg^{-1}), and 1980−1990 (196 ± 9.3 mg kg^{-1}), where the decline occurred ~20 years later than what was observed for Sb. Although the reduction in sediment concentrations for Pb were more distinctive in the mini-Mackereth core, both sediment cores showed a decline in Pb concentrations during the same time period, where emissions from the use of leaded petrol resulted in a much later decline in sediment concentrations of Pb, than observed for Sb. The general agreement with deposition chronologies for Sb and Pb in both the Jenkin and mini-Mackereth sediment cores added greater confidence to the initial results obtained by the mini-Mackereth core. As previously mentioned, sediment can accumulate at differing rates on the Loch bed which can introduce variability into deposition chronologies. In some past sediment studies, the analysis and interpretation of deposition chronologies based on a single sediment core have been criticised for this reason, and therefore, deposition chronologies based on two cores, like this study, give a more accurate account of elemental deposition over time.

6.6.4.3 Comparison of dated Jenkin sediment Sb concentrations with $^{206}Pb/^{207}Pb$ isotope ratio profile

At the start of the 20th century, a small peak in Sb sediment concentrations (1.78 ± 0.01) was observed, and was most likely caused by a minor increase in industrial activity resulting in greater emissions and subsequent atmospheric concentrations of Sb (Figure 6.14). This was consistent with the high $^{206}Pb/^{207}Pb$ isotopic ratio (1.157 ± 0.006) observed for that time,

where the higher isotopic signature of coal combustion (1.182 ± 0.009) and smelting of Wanlockhead Pb ore (1.170 ± 0.003) had a greater influence on the $^{206}Pb/^{207}Pb$ isotopic ratio, than from Tyndrum Pb ore (1.144 ± 0.004) (Moorbath, 1962; Farmer *et al*., 1999; Cloy *et al*., 2005). In addition, the rise in Pb concentrations from 244 ± 19 mg kg^{-1} to 292 ± 0.7 mg kg^{-1}, also reflected a minor increase in industrial emissions. Thereafter, ~1910, concentrations of Pb significantly increased to 630 ± 8.1 mg kg^{-1}, while Sb concentrations fell to 1.68 ± 0.1 mg kg^{-1}. This coincided with the redevelopment of Tyndrum Pb mine, where old dumps were reprocessed (Wilson, 1921), resulting in Pb transported downstream to Loch Tay (MacKenzie and Pulford, 2003). This was confirmed using the $^{206}Pb/^{207}Pb$ isotopic ratios, where a drop from 1.157 ± 0.006, to 1.147 ± 0.002 clearly demonstrated the influence of Tyndrum Pb ore on the isotopic ratio. Moreover, the absence of any increase in Sb concentrations suggest that it could only have come from Tyndrum Pb mine, as coal combustion and the smelting of Wanlockhead Pb ore would have resulted in a net increase in Sb concentrations.

From ~1910 to 1970 both Sb and Pb sediment concentrations were generally stable, yet a broad drop in $^{206}Pb/^{207}Pb$ isotopic ratios occurred between 1950 and 1970, with a minimum ratio occurring in 1960 (1.145 ± 0.001). This reflected a change in the dominant source of Sb and Pb atmospheric concentrations, where mining and smelting of Wanlockhead Pb ore had ceased, and emissions from coal combustion had declined, both resulted in a reduction in Sb sediment concentrations observed soon after. For Pb however, the 1960s was a period of growing importance for emissions originating from leaded petrol, as indicated by a lowering of $^{206}Pb/^{207}Pb$ isotopic ratios; the isotopic ratio signature of UK leaded petrol was ~1.06-1.09 (Farmer *et al*., 2000). Consequently, sediment concentrations of Pb declined later than Sb, with $^{206}Pb/^{207}Pb$ isotopic ratios gradually increasing towards the sediment surface (1.154 ± 0.001), where in 1986, leaded petrol began to be phased-out.

6.6.4.4 Anthropogenic Sb/Pb ratio from the Jenkin sediment core

The calculation of anthropogenic Sb/Pb ratios for the Jenkin sediment core was completed as shown for the mini-Mackereth sediment core in section 6.6.2.3.

Although the Jenkin sediment core Sb/Pb ratios observed in early 20th century agreed with results obtained from the mini-Mackereth sediment core (Figure 6.10), it did however, differ from a number of other deposition chronologies seen in peat (Cloy *et al.*, 2005; 2009). The significant dip in Sb/Pb ratios from 0.0049 to 0.0021 at ~1915 was unique to Loch Tay, and was generally not found elsewhere. This coincided with commercial activity occurring in Tyndrum Pb mine, where the release of Pb downstream to Loch Tay significantly increased sediment concentrations of Pb, while the low content of Sb present in Tyndrum Pb ore (Sb/Pb ratio: 0.0003) resulted in sediment concentrations of Sb remaining stable. This was confirmed by the $^{206}Pb/^{207}Pb$ isotope ratios, where before commercial activity occurred, isotope ratios were 1.157 ± 0.006, and latterly dropped to 1.147 ± 0.002, close to the isotopic signature of Tydrum Pb ore (1.144 ± 0.011). Although the Tyndrum Pb mine was abandoned soon after this time, the transport of Pb downstream to Loch Tay still occurred thereafter.

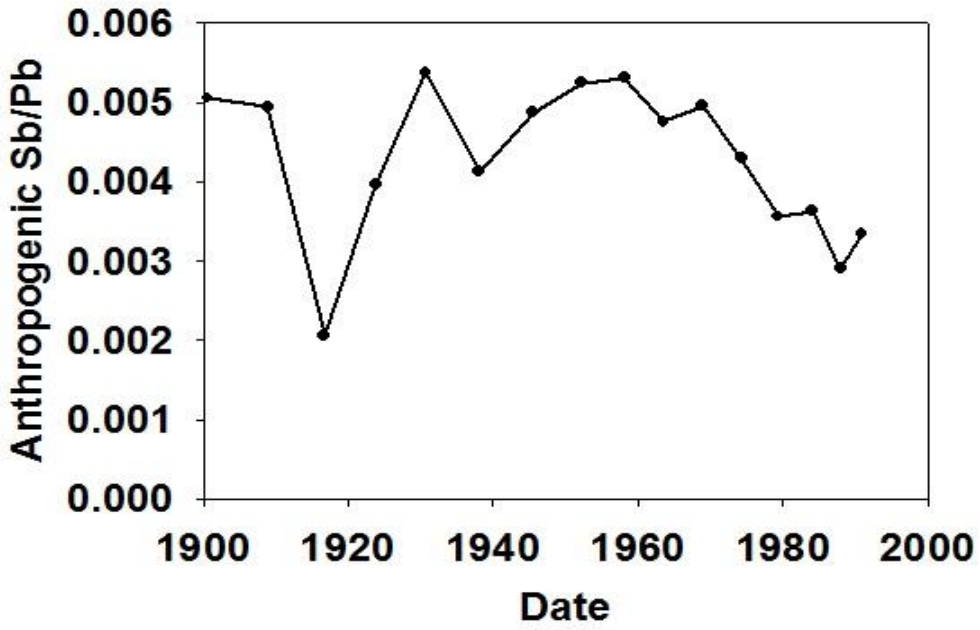

Figure 6.15: Temporal variations in anthropogenic Sb/Pb ratios from Loch Tay Jenkin sediment core.

As discussed in section 6.6.2.3, the leaching of Pb-rich mine dumps and waste, situated on floodplains, and beside contributory rivers for Loch Tay have been highlighted as potential sources for the release of Pb. Indeed, previous studies by MacKenzie and Pulford (2003) and Pulford *et al*. (2009) identified the local area as having considerably elevated Pb concentrations present, which may also, over time, be released downstream to Loch Tay. In the ~1930s, a small dip in Sb/Pb ratios from 0.0054 to 0.0041 was observed, and is most likely attributed to the closure of mining operations at Leadhills and Wanlockhead, where a change in the industrial sources contributing to Sb and Pb atmospheric concentrations occurred (Elliott *et al*., 1937; Cloy *et al*., 2005). This again, was consistent with a greater influence of coal combustion on $^{206}Pb/^{207}Pb$ isotope ratios (1.181 ± 0.011), where an increase from 1.156 ± 0.004 to 1.158 ± 0.003 was observed, while the contribution of isotopic ratios from the smelting Wanlockhead Pb ores (1.170 ± 0.003) ceased.

From 1940 to 1960, mean Sb/Pb isotopic ratios were 0.005 ± 0.0002, which denotes a relatively stable period of atmospheric concentrations for Sb and Pb. At this point however, a

change in the primary source of atmospheric concentrations of Pb took place, as emissions from the combustion of coal decreased, vehicle emissions from leaded petrol increased, which subsequently reduced $^{206}Pb/^{207}Pb$ isotope ratios from 1940 (1.158 ± 0.003) to 1960 to 1.145 ± 0.001). From ~1960 to 1987 (the top of the sediment core), Sb/Pb ratios began to decline, which reflected the reduced emissions of Sb from coal combustion, and the increased emissions of Pb from leaded petrol up until its gradual phase-out in 1986. Interestingly, a small increase in Sb/Pb ratio was found in 1991, where Sb/Pb ratios increased from 0.0029 (1987) to 0.033 (1991), and although no Sb/Pb ratio increase was found ~1990 for the mini-Mackereth sediment core, other studies had shown similar trends (Cloy *et al*., 2005; 2009; Iijima *et al*., 2008) . For example, a peat study at Flanders Moss by Cloy *et al*. (2005) discussed the importance of comparatively new sources of Sb, where Sb emissions from brake linings (see chapter 5) and flame retardants were likely to have increased Sb/Pb ratios at Flanders Moss. The increase in Sb/Pb ratios for Loch Tay sediment were also in agreement with other peat locations in Scotland, such as Turclossie Moss, Red Moss of Balerno and Carsegowan Moss (Cloy *et al*., 2009)

6.6.4.5 Anthropogenic Sb and Pb flux for a Jenkin sediment core from the western basin of Loch Tay

To assess the anthropogenic flux of Sb and Pb in the Jenkin sediment core over time, the anthropogenic-only Sb and Pb concentrations were calculated as shown in section 6.6.2.4. Once attained, the Sb and Pb flux was determined using the corresponding inventory (a calculation using anthropogenic Sb concentration), sample weight and corer area, multiplied by the number of years in each profile section. Further specific detail on the calculation and data used for Figure 6.16 and 6.17 can be found in Appendix 5 and 6.

Unlike results obtained by the mini-Mackereth sediment core, the earliest dates for elemental fluxes observed in the Jenkin core occur after the industrial revolution, at the beginning of the 20th century. This is particularly important, as emissions of Sb and Pb from former industrial activities such as the smelting of Pb ore and the combustion of coal are high at this

point. For example, Sb fluxes were highest ~1900, and with the exception of a prominent peak observed for Pb flux ~1910, Pb fluxes were also highest for this date. From the beginning to mid-20th century, Sb fluxes declined from 0.38 to 0.29 mg m^{-2} y^{-1}, which was in agreement with the mini-Mackereth sediment core, and a result from the reduction and eventual closure of Pb ore mining and smelting facilities in Scotland. This was in contrast with Pb over the same period of time, where a prominent peak in Pb flux (174 mg m^{-2} y^{-1}) occurred ~1910, coinciding with the approximate time of the redevelopment of Tyndrum Pb mine, and subsequent release of Pb downstream to Loch Tay. Thereafter, Pb fluxes remained stable to 1992 (54.5 ± 4.1 mg m^{-2} y^{-1}), as emission reductions originating from former industrial activities were replaced by increasing Pb emissions originating from leaded petrol. As Sb flux values were unaffected by leaded petrol emissions, fluxes continued to decline throughout the 20th century to a minimum of 0.15 mg m^{-2} y^{-1} until 1991, where a minor increase to 0.181 mg m^{-2} y^{-1} was observed. This in agreement with Sb/Pb ratios discussed in section 6.6.4.4, where Sb fluxes have shown an increase in deposition rates as a result of emerging Sb emission sources, such as the use of brake linings (chapter 5) and within flame retardants.

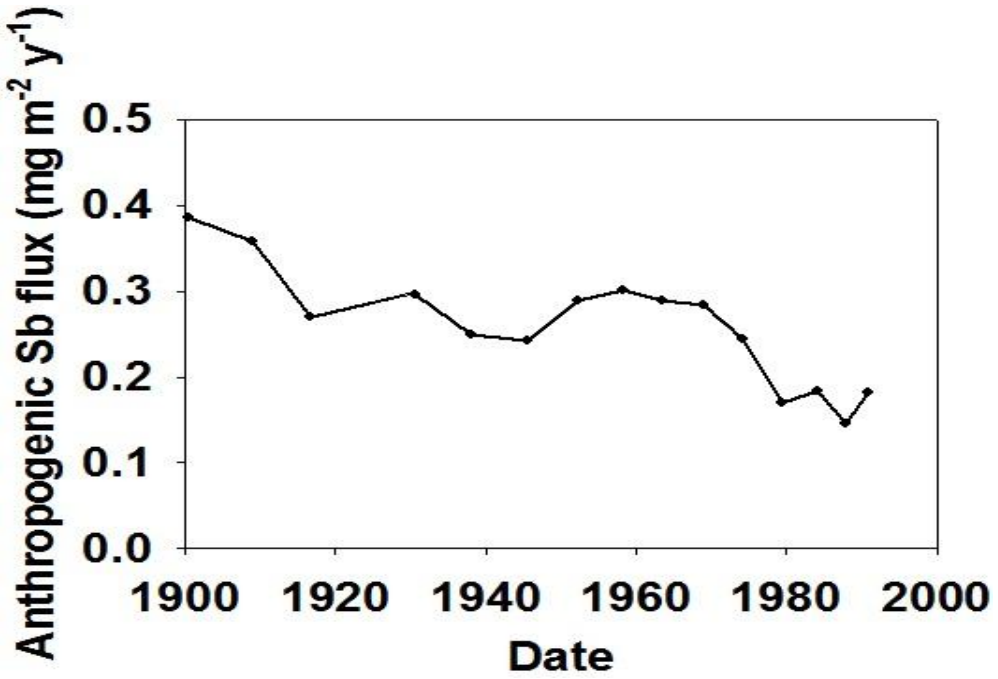

Figure 6.16: Temporal variations in anthropogenic Sb flux from Loch Tay Jenkin sediment core.

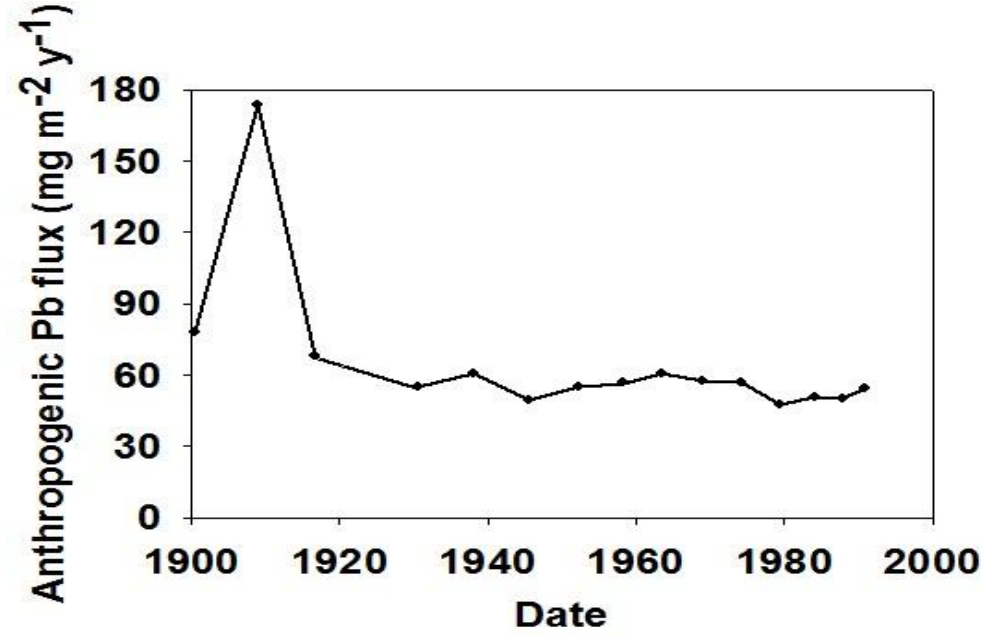

Figure 6.17: Temporal variations in anthropogenic Pb flux from Loch Tay Jenkin sediment core.

6.6.4.6 Mini-Mackereth and Jenkin sediment core comparison

In general, the mini-Mackereth and Jenkin sediment core vertical elemental profiles were in good agreement with each other and were statistically indistinguishable using by t test (two-sample assuming equal variances, $t>0.17$, $p>0.31$, $n=18$, appendix 7, output 11) (Figure 6.18). Both Mn profiles showed similar concentration enrichment at the sediment surface, followed by a sharp decline to ~0.35% w/w. A small difference in Mn concentrations was observed at a depth of ~10 cm, where the mini-Mackereth core showed a much larger sub-surface peak (40% enrichment in Mn concentrations when compared to 10-11cm depth section) than that of the Jenkin core (13% enrichment in Mn concentrations when compared to 10-11cm depth section). Similarly for Fe, both sediment cores were generally comparable, showing the same decreasing trend in concentrations with depth, and as observed for Mn, a smaller sub-surface peak for Fe was observed in the Jenkin core (11% enrichment in Fe concentrations when compared to 11-12 cm depth section) at a depth ~11 cm, when compared to the mini-Mackereth core (23% enrichment in Fe concentrations when compared to 12-13 cm depth section). Arsenic concentrations showed the greatest variability between the two sediment cores, and these differences may be a result of slight changes in the redox conditions and influence it has on As. Whilst both profiles were similar below ~11 cm, where comparable concentrations and similar sub-surface peaks occurred, the upper most part of the sediment cores were less comparable. This was consistent with a study by Farmer and Lovell (1986) from Loch Lomond, Scotland, where data from 13 sediment cores also showed a degree of variation in sub-surface enrichment of As, and was found to be closely associated with the redox cycling of Fe.

Vertical Sb concentration profiles were remarkably similar for mini-Mackereth and Jenkin sediment cores, where concentrations peaked during the early 20th century, and generally declined up until 1992 (Figure 6.18). Very good agreement was also observed for concentrations of Pb, where both profiles showed significant Pb enrichment at 1910, and

thereafter, a slight decline until 1992. The similarity of both elements in both sediment cores was confirmed by using anthropogenic Sb/Pb ratios, as shown in Figure 6.19. The comparability of $^{206}Pb/^{207}Pb$ isotopic ratios was limited for mini-Mackereth and Jenkin sediment core. Whilst major points, such as high (1900 and 1940) and low (1910 and 1980) $^{206}Pb/^{207}Pb$ ratios were in general agreement, fluctuations in between these points did not match exclusively.

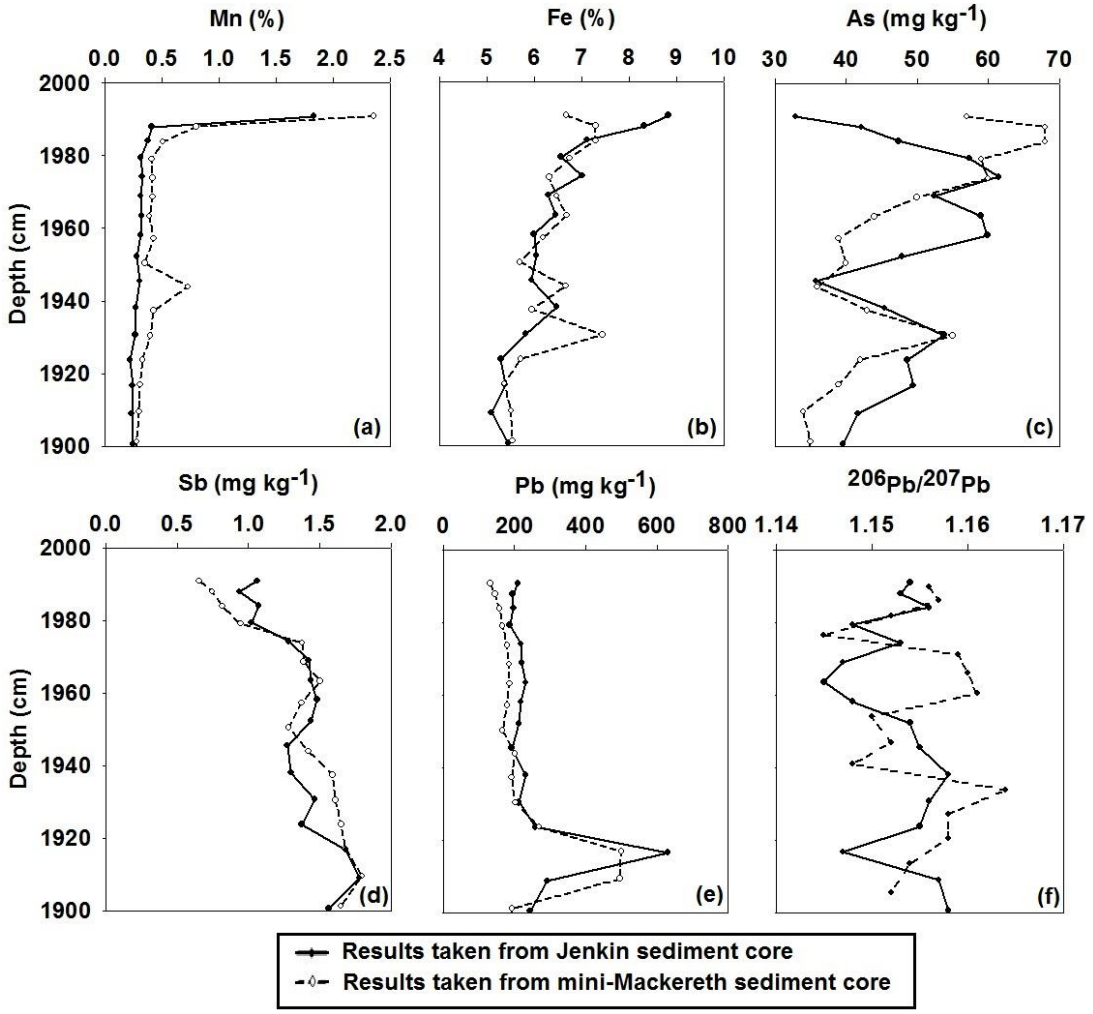

Figure 6.18: Comparison of mini-Mackereth and Jenkin sediment core vertical concentrations of (a) Mn, (b) Fe, (c) As, (d) Sb, (e) Pb and (f) $^{206}Pb/^{207}Pb$ isotopic ratios plotted with depth.

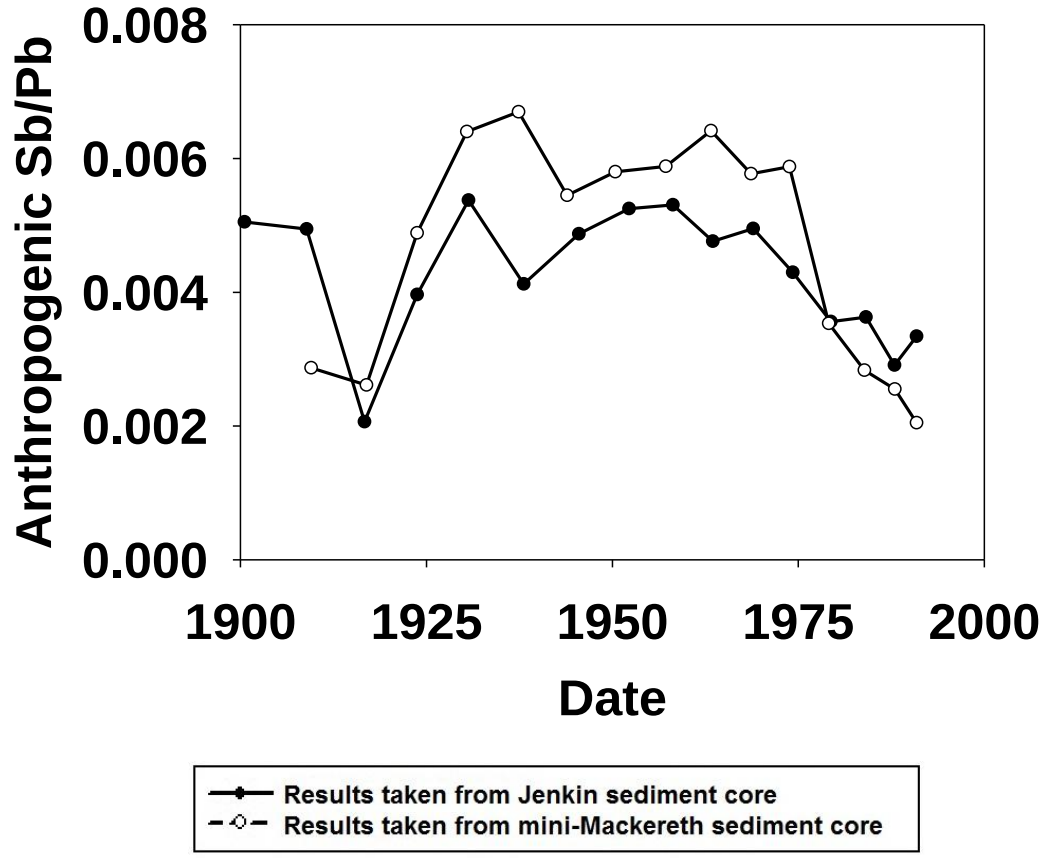

Figure 6.19: Comparison of anthropogenic Sb/Pb ratios from Loch Tay mini-Mackereth and Jenkin sediment core verses years.

6.6.5 Vertical profiles from contemporary sediment cores (1990-2003)

In order to study more recent deposition occurring in Loch Tay, it was necessary to examine the top five sections of more recently sampled sediments, core #1 and #2. Both sediment cores were ^{210}Pb dated by SUERC in 2005, and provided elemental concentrations deposited on Loch Tay sediment from 1990 to 2003. This was particularly important, as the mix of industrial emissions in the UK from 1990-2003 changed considerably; as previously noted, leaded petrol was banned in 2000, and improved emission controls for industrial activities including coal combustion were implemented. The inclusion of this data will help assess whether the change in practice has reduced atmospheric deposition of elements in Scottish loch sediments.

Elemental concentrations in both core #1 and #2 were in agreement with each other (Table 6.8 and 6.9), and generally corresponded with elemental concentrations and vertical depth profiles observed for the mini-Mackereth and Jenkin sediment cores. For example, sediment surface Mn and Fe enrichment also occurred for cores #1 and #2, with concentrations decreasing with depth. The concentrations of Mn and Fe obtained for samples from the 0-1 cm depth sections from core #1 (Mn 2.63 ± 0.03%; Fe 9.16 ± 0.2%) and from core #2 (Mn 1.98 ± 0.06%; Fe 8.26 ± 0.1%) were comparable to values obtained from depth section 0-1 cm for the mini-Mackereth (Mn 2.36%; Fe 6.68% (no S.D. data was published by Farmer *et al*. (1997)) and Jenkin sediment core (Mn 1.98 ± 0.01%; Fe 8.84 ± 0.1%). In addition, all sediment cores also showed a decline of ~85% for vertical Mn concentrations from depth section 0-1 cm to 4-5 cm, which demonstrated consistent post depositional behaviour for Mn in Loch Tay sediment. For Fe, the reduction of vertical concentrations from the sediment core surface to depth section 4-5 cm, was more variable than observed for Mn; a reduction of ~33% was found for core #1 and #2, whilst a decline of 21% and 5% was obtained for the Jenkin and mini-Mackereth sediment core, respectively. This indicated that the post-depositional mobility of Fe in Loch Tay sediment varied, and was most likely a result of differences in the down-core redox gradient. Vertical concentrations of As in core #1 and #2 were similar, with concentrations relatively stable at 53.1 ± 3.8 mg kg^{-1} over the 5 cm depth profile. The mini-Mackereth sediment core had greater As concentrations compared with core #1 and #2, where concentrations for depth section 0-1 cm were 57 mg kg^{-1}. Whilst this suggests a decline in the deposition of As into Loch Tay sediment had occurred from 1990 to 2003, As concentrations observed in the Jenkin core for depth section 0-1 cm (32.9 ± 2.2 mg kg^{-1}) were lower than those in core #1 and #2. Since As concentrations in depth section 0-1 cm for core #1 (56.4 ± 0.9 mg kg^{-1}) and #2 (50.7 ± 0.7 mg kg^{-1}) fell either side of As concentrations found at equivalent depths in the mini-Mackereth and Jenkin sediment core, it is unlikely that a reduction in As deposition in Loch Tay sediment has occurred from 1990 to 2003.

Table 6.8: Loch Tay sediment core #1 Mn, Fe, As, Sb, Pb concentrations (mg kg^{-1}) and $^{206}Pb/^{207}Pb$ isotopic ratios for each 1-cm section.

Depth (cm)	Mn (%)	Fe (%)	As (mg kg^{-1})	Sb (mg kg^{-1})	Pb (mg kg^{-1})	$^{206}Pb/^{207}Pb$
0-1	2.63 ± 0.03	9.16 ± 0.3	56.4 ± 0.9	0.98 ± 0.02	198 ± 2.1	1.153 ± 0.003
1-2	2.30 ± 0.01	9.24 ± 0.2	55.9 ± 2.1	0.98 ± 0.06	198 ± 0.5	1.155 ± 0.002
2-3	1.05 ± 0.01	9.38 ± 0.1	55.1 ± 0.1	1.01 ± 0.04	199 ± 5.0	1.158 ± 0.001
3-4	0.55 ± 0.03	7.92 ± 1.0	55.9 ± 3.0	1.10 ± 0.06	201 ± 6.8	1.156 ± 0.002
4-5	0.38 ± 0.01	6.08 ± 0.1	50.0 ± 1.3	1.14 ± 0.36	215 ± 8.5	1.154 ± 0.004

Table 6.9: Loch Tay sediment core #2 Mn, Fe, As, Sb, Pb concentrations (mg kg^{-1}) and $^{206}Pb/^{207}Pb$ isotopic ratios for each 1-cm section.

Depth (cm)	Mn (%)	Fe (%)	As (mg kg^{-1})	Sb (mg kg^{-1})	Pb (mg kg^{-1})	$^{206}Pb/^{207}Pb$
0-1	1.98 ± 0.06	8.26 ± 0.1	50.7 ± 0.7	0.91 ± 0.05	180 ± 4.3	1.157 ± 0.001
1-2	0.49 ± 0.01	8.33 ± 0.3	51.4 ± 1.7	0.95 ± 0.02	188 ± 5.7	1.157 ± 0.003
2-3	0.36 ± 0.02	6.34 ± 0.6	57.0± 2.3	0.93 ± 0.04	166 ± 13	1.155 ± 0.001
3-4	0.30 ± 0.01	5.96 ± 0.1	53.5 ± 1.8	0.97 ± 0.02	184 ± 1.9	1.154 ± 0.002
4-5	0..27 ± 0.01	5.59 ± 0.2	44.9 ± 0.2	1.03 ± 0.05	194 ± 0.7	1.152 ± 0.002

For the post-depositional immobile elements Sb and Pb, a general trend of reducing concentration with reducing depth for core #1 and #2 was observed. Concentrations of Sb in core #1 declined by 14% from depth section 4-5 cm (1.14 ± 0.36 mg kg^{-1}) to 0-1cm (0.98 ±

0.02 mg kg^{-1}), while a 12% decline was observed for core #2 from 4-5 cm (1.03 ± 0.05 mg kg^{-1}) to 0-1 cm (0.91 ± 0.05 mg kg^{-1}). This was consistent with a similar decline in Sb concentrations observed in the top 5 depth sections from the mini-Mackereth core; although Sb concentrations in sediment were lower for this core, i.e. the concentration of Sb in depth section 0-1 cm was 0.66 mg kg^{-1}. No steady decline in Sb concentrations were found in the top sediment sections from the Jenkin core, where concentrations observed in the sediment surface for this core were 1.06 ± 0.02 mg kg^{-1}, and lay either side of concentrations from the 4-5 cm depth sections from core#1 (1.14 ± 0.36 mg kg^{-1}) and core#2 (1.03 ± 0.05 mg kg^{-1}). For Pb, the concentrations in core #1 were generally 10% higher than those determined in core #2, and ranged between 198-215 mg kg^{-1} and 166-194 mg kg^{-1}, respectively. A decline of 8% in Pb concentrations was observed in both cores from the depth of 4-5 cm to the sediment surface. A similar decline for Pb concentrations was also found in the top five sections of the mini-Mackereth sediment core; although Pb concentrations were notably lower here, i.e. Pb concentration in depth section 0-1 cm was 132 mg kg^{-1}. Whilst no such decline for Pb concentrations were observed for the Jenkin core, the Pb concentration at the sediment surface (209 ± 1.0 mg kg^{-1}) lay either side of concentrations from the 4-5 cm depth sections from core#1 (215 ± 8.5 mg kg^{-1}) and core#2 (194 ± 0.7 mg kg^{-1}). No trend in $^{206}Pb/^{207}Pb$ isotope ratios were evident in core#1, with the values spanning the depth sections 0-5 cm largely the same (1.155 ± 0.002), whilst for core#2, a slight increasing trend for $^{206}Pb/^{207}Pb$ isotope ratios were observed from 4-5 cm (1.152 ± 0.002) to 0-1 cm (1.157 ± 0.001). No major difference in $^{206}Pb/^{207}Pb$ isotope ratios were found when core#1 and #2 were compared to the 0-1 cm depth section values obtained from the mini-Mackereth (1.156 ± 0.003) and Jenkin core (1.154 ± 0.001).

Overall, taking into account the sediment concentrations of Sb and Pb from core #1, #2, mini-Mackereth and Jenkin core, a small decline (~10%) in concentrations of Sb and Pb deposited on Loch Tay sediment has occurred from 1990 to 2003.

6.6.6 The comparison of elemental concentrations found in Loch Tay mini-Mackereth and Jenkin sediment cores with sediment cores sampled across the UK

Concentrations of As in Loch Tay were broadly similar to other freshwater lakes reported in the UK and elsewhere. A comprehensive study by Yang and Rose (2005) examined trace elements (including As and Pb) in 5 remote lakes and a reservoir spanning the UK (Table 6.10). Although no numeric values were published within this report, elemental concentrations could be attained from plotted figures to establish the extent of contamination to Loch Tay sediment from Tyndrum Pb mine. For Loch Tay sediment, concentrations of As ranged from 19-68 mg kg^{-1}, which were considerably lower than the range observed at Lliyn Llagi (40-800 mg kg^{-1}), Burnmoor Tarn (40-390 mg kg^{-1}), Loch Chon (20-190 mg kg^{-1}) and Loch Grannoch (10-190 mg kg^{-1}), and were more comparable to Lochnager (5-30 mg kg^{-1}) and Banbury Reservoir (7-15 mg kg^{-1}). The high elemental concentrations found in sediment by Yang and Rose (2005) at Burmoor Tarn, Loch Chon and Loch Grannoch were influenced, to various extent by, atmospheric deposition, differing sedimentation rates, and a change in surrounding land use such as afforestation and farming. Lliyn Llagi was the only site identified as being influenced directly from mining activity. Since the range of As concentrations found in Loch Tay sediment are considerably lower than sediment from four remote locations, three of which were not directly affected by mining activities, sediment concentrations of As are most likely attributed to atmospheric deposition, rather than mining Pb ore at Tyndrum. As discussed in section 2.4.4, As, like Sb and Pb, is often found co-existing together in coal, with emissions from coal combustion the primary source of As to the atmosphere, along with smaller contributions from Cu and Au smelting (Matschullat, 2000). Little influence from Pb mining at Tyndrum on Loch Tay sediment concentrations was also observed when sediment concentrations of As were compared to remote lakes outside the UK. The concentration range was similar to remote alpine lakes in Japan (5-90

mg kg^{-1}) (Kuwae *et al*., 2013), and slightly higher than lake sediment sampled from southern Norway (0.41-32.7 mg kg^{-1}) (Rogerud *et al*., 2000).

Table 6.10: Approximate mean As and Pb concentrations reported by Yang and Rose (2005) from 5 UK lakes and reservoir.

Loch or lake name	Region	Country	Approximate As concentration range (mg kg^{-1})		Approximate Pb concentration range (mg kg^{-1})	
			Minima	Maxima	Minima	Maxima
Lochnager	Grampians	Scotland	5	30	10	260
Loch Chon	Stirlingshire	Scotland	20	190	5	570
Loch Grannoch	Dumfries and Galloway	Scotland	10	190	110	400
Burnmoor Tarn	Cumbria	England	40	390	30	200
Llyn Llagi	Gwynedd	Wales	40	800	80	350
Banbury Reservoir	London	England	7	15	70	250

Loch Tay sediment concentrations of Pb ranged from 11-630 mg kg^{-1}, and were a great deal higher than those reported by Yang and Rose (2005) in sediments from Lochnagar (5-25 mg kg^{-1}), Loch Grannoch (110-400 mg kg^{-1}), Burnmoor Tarn (30-200 mg kg^{-1}), Llyn Lliagi (80-350 mg kg^{-1}) and Banbury Reservoir (70-250 mg kg^{-1}), and were comparable with Loch Chon (5-570 mg kg^{-1}). Loch Chon is situated 25 km south-west of Loch Tay, and a closer look at the vertical concentration profile for Pb reveals notable differences in the source of Pb to sediment concentrations. For example, mining activity in Tyndrum contributed considerable amounts of Pb to Loch Tay sediment before the 18th century. This, however, did not occur at Loch Chon (or at Lochnagar and Burnmoor) where sediment concentrations of Pb were influenced at the end of the 19th century by emissions from coal combustion and metal smelting during the Industrial Revolution. Emissions from these industries would have influenced Loch Chon sediment concentrations more, when compared with Loch Tay, since

Loch Chon is closer to central Scotland, or more specifically Glasgow, where a large proportion of Pb emissions were originating. The concentration range for Pb in Loch Tay sediment also appeared elevated when compared to other sediment cores sampled in remote locations in Europe. For example, lake sediment sampled from Lake Zurich, Switzerland and southern Norway had a concentration range of 57-150 mg kg^{-1} and 8.9-412 mg kg^{-1}, respectively (Von Gunten *et al.*, 1997; Rogerud *et al*., 2000). Further afield, the previously mentioned study on two remote Japanese alpine lakes observed sediment concentrations of Pb ranging between 20-220 mg kg^{-1} (Kuwae *et al*., 2013). More comparable concentrations of Pb were found in sediment influenced by local mining activity in Malter reservoir, Germany and Temple reservoir, France, where concentrations ranged from 200-740 mg kg^{-1} and 31-593 mg kg^{-1}, respectively (Muller *et al*., 2000; Audry *et al*., 2004). Overall, the impact of Pb ore mining at Tyndrum has contributed notable amounts of Pb to sediment in Loch Tay, with the resultant increase in Pb concentrations easily distinguishable from non-polluted lakes.

Unfortunately, very few chronologies of Sb in sediment cores exist. Indeed this was the primary reason for examining Sb deposition using sediment cores, as no such studies exist in Scotland and the UK, nor are there any in Europe, with only a handful of notable publications to date. One of which, is the previously mentioned study using sediment from two remote Japanese alpine lakes, where the sediment concentration of Sb ranged from 0.5-5.5 mg kg^{-1}, with a notable increase in concentrations occurring between the end of the 19th century and the beginning of the 21st (Kuwae *et al*., 2013). A second report using sediment from Lake Qinghai, China, found a greater range in Sb concentrations (3.5-9.0 mg kg^{-1}) than those observed in Japan, although the range from Loch Tay was lower (0.39-1.80 mg kg^{-1}). Fawcett *et al*. (2015) examined sediment concentrations of Sb near a large gold mine in Yellowknife, Canada, where sulfidic ores such as arsnopyrite (FeAsS), stibnite (Sb_2S_3) and chalcopyrite ($CuFeS_2$), as well as aurostibite ($AuSb_2$) were found in great abundance. Lake

sediment concentrations of Sb at three locations downstream of the mine ranged from 20-1100 mg kg^{-1}, considerably more than the values observed at Loch Tay. Despite an estimated total of ~8000 tonnes of Pb ore extracted from Tyndrum Pb mine, Sb contamination from the mine downstream to Loch Tay was marginal, as a result of its low content in Tydrum Pb ore.

6.7 Chapter conclusions

The impact of historic mining activities in rural Scotland is still observed today, where the release of elements from Glendinning Sb mine and Tyndrum Pb mine to the environment has resulted in the contamination of local aquatic and terrestrial systems. Although the type of ore extracted at both locations differs, the analysis of soil or sediment affected by mining activity provided the means to monitor the transport of Sb, Pb, As downstream to their eventual sink.

This chapter has shown that Sb, under specific conditions, can indeed be mobile or immobile in the environment. For example, the chemical weathering of stibnite found in spoil heaps at Glendinning Sb mine demonstrated that ~3% of total Sb can be mobilised during oxidative dissolution at a pH of 5.0 and 6.6. The dissolution and transport of Sb at Glendinning Sb mine was specifically shown to originate from a mineral-rich spoil heap, downhill into surrounding soils and the Glenshanna Burn. Once in the aqueous form, porewaters from soil cores (S1-S6) showed that Sb was largely present in the truly dissolved form (<3 kDa) and was not retained by soil to the same degree as As and Pb. Porewater speciation analysis for Sb using two soil cores (S4A and S5A) near the large spoil heap revealed that Sb was largely present as Sb(V), contributing ~94% towards total Sb concentrations present. Indeed, Sb speciation results for this study were in agreement with a study by Mitsunobu *et al*. (2006), and were indicative of a greater stability as Sb(V) in soil-water systems. In general, the porewater behaviour of Sb highlighted its loss from deeper sections of certain cores, and its transport over distances down steeper sections of the catchment. Where Sb was retained by soil, retention occurred near the surface in cores S1-S5, where Sb was found associated with organic matter and Fe oxides. Upon deposition, Sb retention and immobility was evident in

Loch Tay sediment, where a change in redox conditions in two sediment cores mobilised other deposited elements, such as Mn, Fe and As, but did not affect Sb. Here the immobility of Sb allowed deposition chronologies to be established, and there was excellent agreement between mini-Mackereth and Jenkin sediment cores chronologies. Both chronologies identified atmospheric deposition as the primary source of Sb to Loch Tay sediment, with little influence of Sb transported downstream from Tyndrum Pb mine. This was in agreement with the Sb/Pb ratio found in Tyndrum Pb ore (0.0003), which signified a low Sb content present in Tyndrum Pb ore, and indicated that emissions from coal combustion (Sb/Pb ratio:0.036 ± 0.032) and the smelting of Wanlockhead ore (Sb/Pb ratio:0.0056± 0.0004) were the primary source of Sb to Loch Tay sediment. Moreover, the atmospheric deposition chronology for Sb in Loch Tay sediment was similar to other peat chronologies observed during the 19th and 20th century (Cloy *et al*., 2009; Allan *et al.*, 2013).

The behaviour of Pb in the aquatic and terrestrial environment has been covered, to a certain extent, in previous studies. For Glendinning Sb mine, concentrations of Pb in soil (S2) reached 710 mg kg^{-1}, while aqueous concentrations downstream of the mine were low, consistent with its strong affinity for the soil solid phase. Although the vertical concentration profiles for Pb followed the trend for Fe in all soil cores, sequential extraction results suggested that this association was not exclusive, and that organic matter was also an influential factor for retaining Pb in the soil. The examination of porewaters from S2-S6 revealed that Pb and Fe were almost exclusively present in the colloidal fraction (70-100%) showing that Pb solubility is enhanced by association with both organic matter and Fe-rich colloids. The strong affinity of Pb for the solid phase was also observed in Loch Tay sediment, where upon deposition, Pb remained immobile and was not susceptible to redox cycling as observed for other elements. As shown for Sb, excellent agreement was found for constructed Pb deposition chronologies for both Loch Tay sediment cores, and indicated considerable Pb pollution had occurred from the release of Pb to Loch Tay, as a result of

upstream mining activities. This was consistent with a notable peak for sediment Pb concentrations and the change in associated Pb isotope ratios occurring ~1915, coinciding with the reprocessing of mining dumps prior to the closure of Tydrum Pb mine in 1928. Thereafter, the dominant input of Pb to Loch Tay sediment was from the combustion of coal and leaded petrol. A decline in Pb sediment concentrations began ~1980s, and continued towards the end of the 20th century, where improved technology and regulation for coal combustion and the phasing out of leaded petrol use in 1986 in the UK all reduced the atmospheric emissions of Pb. A continuing reduction in sediment Pb concentrations were also observed from 1990 to 2003 using sediment core#1 and #2.

In comparison with Sb and Pb, As had the greatest mobility at both mining sites. At the Glendinning Sb mine, As was also affected by chemical weathering on the two spoil heaps, and as observed for Sb, this resulted in its dissolution from the solid phase to the aqueous phase. Once in the aqueous phase, As was found present in both truly dissolved and colloidal fractions, where its association with large Fe-rich organic colloids favoured the retention its by the solid phase. The greater mobility of As, relative to Sb and Pb, was demonstrated in elemental concentrations observed in Glenshanna Burn, where considerably higher concentrations of As (13.2 ± 1.14 μg L^{-1}) were found in Glenshanna Burn when compared with Sb (5.88 ± 0.29 μg L^{-1}) and Pb (0.07 ± 0.03 μg L^{-1}). The greater mobility of As observed at Glendinning Sb mine was also evident in results obtained from Loch Tay sediment, where As was shown to have post-depositional mobility, along with the redox-active elements, Mn and Fe. Although more distinguishable in the As vertical concentration profile obtained in the mini-Mackereth sediment core than the Jenkin core, both cores revealed a sub-surface peak at a depth of ~11 cm for As concentrations. Vertical concentrations of Arsenic showed the greatest variability between the two sediment cores, and were most likely a result of slight changes in the redox conditions and influence this has on As.

Chapter 7 Establishing contaminant deposition chronologies using ombrotrophic peat bogs

7.1 Introduction

Ombrotrophic peat bogs provide an effective means to assess atmospheric deposition of contaminants over past centuries, as they continually accumulate and receive all their nutrients and contaminants exclusively by deposition from the atmosphere (Cloy *et al*., 2009). Chapter 7 examines the deposition archives of Sb and Pb in two Scottish peat cores: (i) Great Moss, Cairngorms Mountains, Scotland, and (ii) Auchencorth Moss, Midlothian, Scotland. It includes: (i) the Sb and Pb concentrations throughout each peat core; (ii) Sb and Pb deposition records for past centuries, with a specific focus on the component that has resulted from anthropogenic activities; and (iii) an examination of anthropogenic Sb/Pb ratios. It furthermore discusses contaminant chronologies obtained at both peat sites in relation to current and historic anthropogenic activities observed in urban and rural environments (Chapters 5 and 6).

7.2 The formation and environment of an ombrotrophic peat bog

Peat is categorised as a histosol, where the degradation of organic plant material, primarily *Sphagnum* moss, forms a deep organic soil with two distinct layers, the acrotelm and the catotelm (USDA, 1999; SNH, 2001). At general depths of up to 50 cm, the acrotelm is the upper layer which consists of largely living upright stems of *Sphagnum* moss (Figure 7.1) (Clymo, 1984; SNH, 2001). It is considered to be the aerobic layer, where water can move up and down freely. This movement is often seasonally related and affects the position of the water table in the peat bog (Qunity and Rochefort, 2003). The lower layer, the catotelm, is a much denser material, where plant stems from *Sphagnum* moss have collapsed under the weight of the acrotelm (Figure 7.1). Due to its higher bulk density, vertical water movement in the catotelm is very slow (<1 m per day), and consequently, most rainwater is stored here.

Under normal environmental conditions, the peat bog water-table does not drop into the catotelm as the porous acrotelm regulates water-table levels in response to high or low levels of rainfall (SNH, 2001).

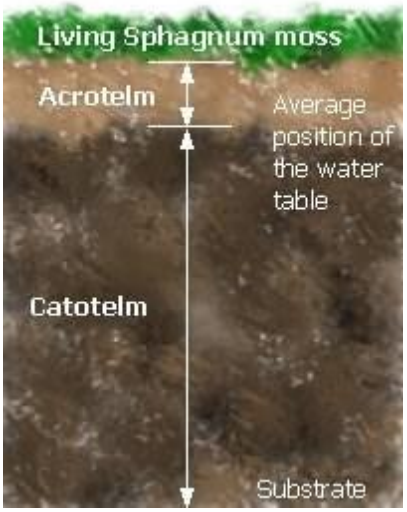

Figure 7.1:Cross-section of peat bog layers showing upper acrotelm and lower catotelm layers. Taken from Geocaching, (2015).

Peat bogs are formed when plant material, usually in wet areas, is inhibited from decaying fully by acidic and anaerobic conditions to form a peat blanket. Due to high rainfall and the presence of hollows and hummocks, the amount of peat grows blanketing the ground creating inhospitable conditions for plant life to grow. At this point, vegetation can no longer root in the mineral soils below, and in addition, a nutrient deficient zone is also created in the swamp, where available nutrients are soaked-up by surrounding plant life (SNH, 2001). With few nutrients available, and the excessive amount of water present, the environmental conditions are perfect for the growth of *Sphagnum* moss and other less abundant mosses such as ribbed bog moss (*Aulacomnium paluste*) and feather moss (*Pleurozium schreberi*). A Sphagnum carpet is then formed thereafter on top of a slowly accumulating layer of dead plant material (catotelm).

7.3 The application of ombrotrophic peat bogs as archives of elemental atmospheric deposition

When undisturbed, ombrotrophic peat bogs can act as a sink for atmospheric deposited elements, creating a chronology of deposited elemental. This however, is only the case where elements are immobile in the peat matrix, and not subject to post-deposition mobilisation. The rate at which peat bog layers accumulate can often be site specific and influenced by local climate, with typical surface mass accumulation rates of ~3.3 mm per year (Baker *et al*., 1972; Clymo, 1984). The atmospheric deposition of elements, and subsequent burial, represents a record of deposition for the duration of time the peat layer was accumulating. For example, atmospheric elements deposited in 2015 will be present at the peat surface; however in 2018, these will be present at a depth of ~10 mm, as additional peat layers will have accumulated on the peat surface over the three year duration. Numerous studies exist globally, where ombrotrophic peat cores have successfully been used to construct deposition chronologies through the analysis of elemental concentrations and ^{210}Pb activity to create atmospheric elemental deposition chronologies (Shotyk *et al*., 1996; Martinez-Cortizas *et al*., 1997; Benoit *et al*., 1998; MacKenzie *et al*., 1998; Nieminen *et al*., 2002; Farmer *et al*., 2005, 2009; Cloy *et al*., 2008, 2009). Redox active elements such as Mn and Fe were found to undergo post-deposition mobilisation by Cloy *et al.* (2009) at four ombrotrophic peat bogs in Scotland, and this can similarly be observed in other archival materials such as sediment (section 6.6.1 and 6.6.4.1). Each peat core is then dated using unsupported ^{210}Pb, which is deposited from the atmosphere and its decay and eventual burial within peat horizon allows deposition dates to be obtained. This has been discussed in detail in Chapter 3.3.17.

For this project, the elements chosen to establish atmospheric deposition chronologies for peat cores sampled from Great Moss and Auchencorth Moss were Ti, Sb and Pb. Both Mn and Fe were included as redox active elements, and therefore could potentially influence

elemental concentration distributions in the uppermost part of the peat core. The selection of Ti allowed atmospheric deposition concentrations to be adjusted for natural dust (non-anthropogenic) deposition and will be discussed further in section 7.4.2, while Sb and Pb were the primary elements of interest.

7.4 Ombrotrophic peat bog 1−The Great Moss (0-50 cm)

The Great Moss, or Moine Mhor, is located in the Cairngorm Mountains, Scotland, and is at an altitude of 900-945 m (Figure 3.9). A large blanket of peat sits on metamorphosed Dalradian sandstone and siltstone base, and is surrounded by the Cairngorm Granite. One peat core was taken from the site in June 2012, and was analysed for elemental concentrations, Pb isotope ratios and ^{210}Pb dating. Further sampling details are given in section 3.2.3.3.1.

7.4.1 Vertical concentration profiles of Mn, Fe, Ti, Sb and Pb and ^{206}Pb/^{207}Pb isotope ratios from Great Moss

Concentrations of Mn throughout the Great Moss peat core ranged from 0.4 to 79 mg kg^{-1} (Figure 7.2). At depths of greater than 20 cm, Mn solid phase concentrations were generally similar at ~2.0 mg kg^{-1}, and thereafter, a gradual increase from 5.9 mg kg^{-1} at 18-20 cm, to 12 mg kg^{-1} at 6-8 cm was observed. A considerable increase in Mn concentrations occurred in the top 0-6 cm, peaking at 79 mg kg^{-1}. At depths below 20 cm for Fe, considerable concentration fluctuations were observed (ranging between 93 mg kg^{-1} and 747 mg kg^{-1}), but concentrations were generally lower than in the rest of the core. Concentrations of Fe significantly increased thereafter; there was a broad peak and shoulder at depths of 10-12 cm (1400 mg kg^{-1}) and 12-14 cm (1200 mg kg^{-1}), respectively. From 10 cm towards the peat surface, Fe concentrations continually declined to reach a surface concentration of 454 mg kg^{-1}. The post-depositional mobility of redox-active elements such as Mn and Fe often results in surface and sub-surface peaks such as those described above. As discussed in Chapter 6, this may also affect the distribution of elements such as As.

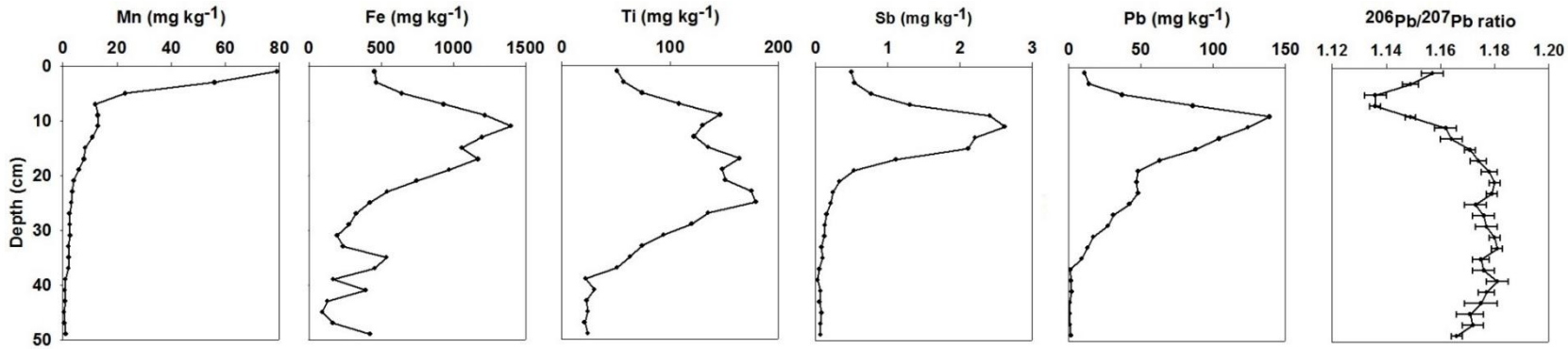

Figure 7.2: Profiles for elemental concentrations, and $^{206}Pb/^{207}Pb$ isotopic ratios versus depth for the Great Moss peat core. Adapted from Farmer *et al*. (2015). NOTE: Associated errors for Sb data have been omitted to present data similarly to Farmer *et al*., 2015.

For example, As adsorbed on the surface of Fe(III)-containing mineral phases can be released into the peat porewaters upon a change in the redox potential. This typically occurs in water-logged peat where anaerobic conditions previal. Once released, and depending on the specific elemental properties, elements may bind to decaying organic matter, or migrate upwards towards the peat surface, along with a large proportion of Mn and Fe to reprecipitate out as oxides or hydroxides. The surface enrichment of Mn at Great Moss may be attributable to redox cycling, but may also be influenced by plant cycling of nutrients from deeper sections of peat, to the peat surface (Cloy *et al*., 2009; Farmer *et al*., 2015). There was no evidence of perturbation of the other elemental profiles in the near-surface sections (Figure 7.2). The depth of the water table plays a key role in controlling the redox conditions in peat bogs and quite often the transition between Fe(III) and Fe(II) coincides with this. At the Great Moss, the water table occurred at a depth of ~8 cm based on the moisture content profile shown in Figure 7.3 (at the time of sampling). In the case of the Great Moss, there was no sub-surface peak at this depth which would indicate a transition to more reducing conditions and there was no obvious perturbation of the vertical concentration profiles of the other elements. Indeed, the major peaks in concentration for Fe, Ti, Sb and Pb were typically found below this depth, as observed by Cloy *et al.* (2009) at Flanders Moss and Red Moss and so these were concluded to be unaffected by redox-related elemental cycling and instead were a record of past atmospheric deposition. The profiles for each element are described in the following paragraphs.

Concentrations of Ti were low at depths greater than 38 cm (~24 mg kg^{-1}), above which, concentrations significantly increased forming a broad peak at depths between 4-32 cm, where the mean and range of concentrations were 130 mg kg^{-1} and 74-164 mg kg^{-1}, respectively. Titanium concentrations then declined to a concentration of 51 mg kg^{-1} in the 0-2 cm section.

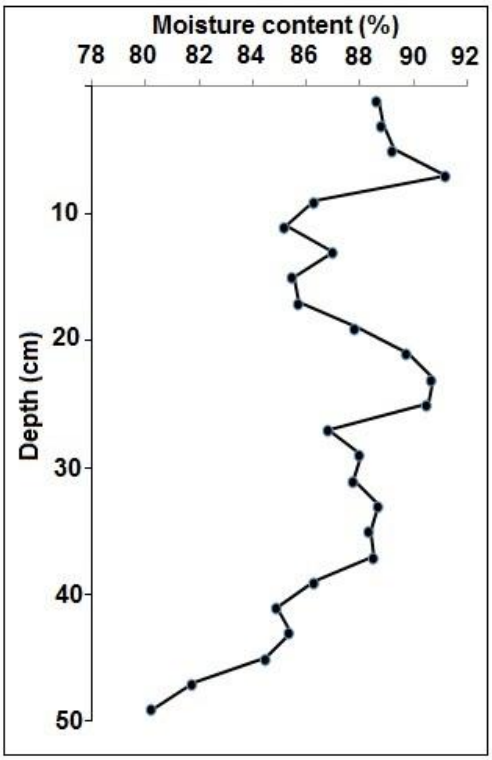

Figure 7.3: Great Moss solid phase profile for moisture content.

Antimony concentrations at depths of greater than 20 cm were generally stable, with a mean value and range of concentrations of 0.12 ± 0.08 mg kg^{-1} and 0.05-0.33 mg kg^{-1}, respectively (Figure 7.2). Between depths of 6 and 20 cm, considerable enrichment in Sb concentrations occurred, peaking at ~2.6 mg kg^{-1} (10-12 cm), and thereafter, concentrations declined towards the peat surface where a concentration of 0.49 mg kg^{-1} was observed. Little variation in concentrations of Pb was evident at depths greater than 36 cm (0.6 to 2.1 mg kg^{-1}), where mean concentrations were 1.21 ± 0.6 mg kg^{-1}. Above this, there was a gradual increase to a maximum concentration of 48 mg kg^{-1} 18-20 cm, followed by a significant increase to 139 mg kg^{-1} at a depth of 8-10 cm. From this point towards the peat surface, Pb concentrations decreased to a minimum of 11 mg kg^{-1} in the 0-2 cm section. The vertical profile for $^{206}Pb/^{207}Pb$ isotope ratios were, to some extent, inversely related to that for Pb concentrations, i.e. where Pb concentrations were high, $^{206}Pb/^{207}Pb$ ratios were low. At depths >20 cm, $^{206}Pb/^{207}Pb$ ratios were quite uniform, with a mean value of 1.176 ± 0.004

and a range of 1.166-1.180. From 20 cm depth towards the surface, $^{206}Pb/^{207}Pb$ isotopic ratios declined to a minimum value of 1.136 ± 0.004 between 4 and 8 cm. From this point upwards, $^{206}Pb/^{207}Pb$ ratios increased and a value of 1.157 ± 0.004 was attained for the 0-2 cm section.

7.4.2 Historic trends in Sb, Pb and $^{206}Pb/^{207}Pb$ isotopic concentrations from Great Moss

Applying the CRS model to obtain a dating chronology using ^{210}Pb activity in the peat core (Chapter 3.3.17), average annual total and anthropogenic Sb and Pb fluxes were calculated and plotted in Figure 7.4 (Appendix 7). For anthropogenic fluxes of Sb and Pb, data was calculated relative to Ti, where Sb/Ti and Pb/Ti ratios were used as shown in Equation 7.1; this adjusted results to account for natural atmospheric dust deposition.

$$[X]_{anthropogenic} = [X]_{peat} - [X]_{lithogenic}$$

where

$$[X]_{lithogenic} = [X]/[Ti]_{UCC} \times [Ti]_{peat}$$

$[X]_{peat}$: Sb or Pb concentration in peat section

$[X]_{lithogenic}$: Sb or Pb concentration of Upper Continental Crust*

$[Ti]_{peat}$: Ti concentration in peat section

$[Ti]_{UCC}$: Ti concentration of Upper Continental Crust*

Equation 7.1: Sb and Pb anthropogenic derivation formula taken from Cloy *et al*. (2009), with * indicating values taken from Wedepohl, (1995).

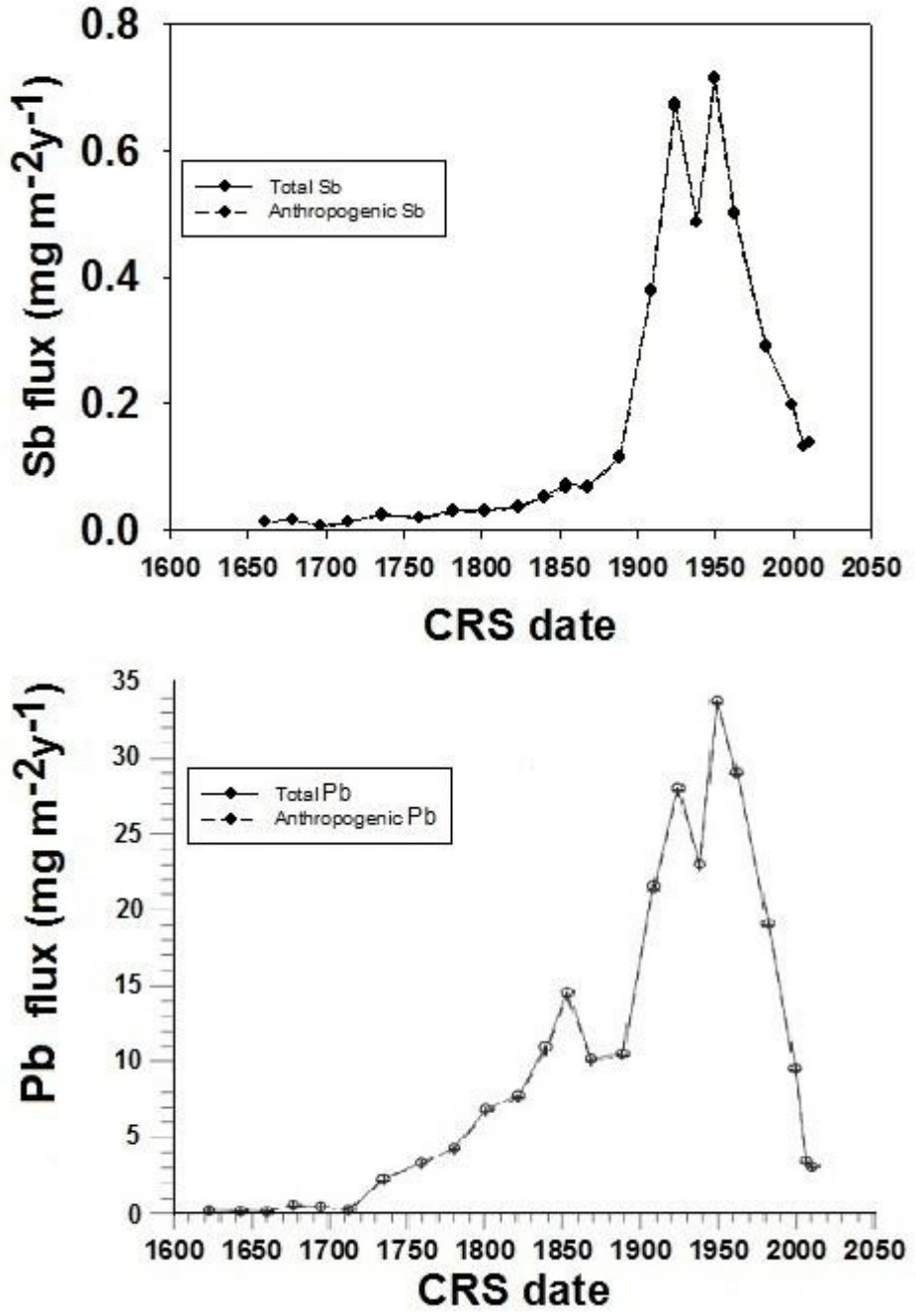

Figure 7.4: Average total and anthropogenic fluxes for Sb and Pb in CRS dated Great Moss peat core. Adapted from Farmer *et al*. (2015). NOTE: Associated errors for Sb data have been omitted to present data similarly to Farmer *et al*., 2015.

The trend in Sb and Pb flux from 1660 to 2011 was largely comparable (Figure 7.4), although differences were observed in absolute flux values, and the earlier date of Pb flux increase when compared with Sb. There was also very little difference between total and

anthropogenic fluxes, indicating that emissions of Sb and Pb from anthropogenic activities almost entirely contributed to total annual fluxes. Pre-Industrial Revolution (pre-1800), Pb flux values were already showing the impact of early anthropogenic activity, where between 1730 to 1800 a flux increase from ~1 mg cm^{-2} y^{-1} to ~5.0 mg cm^{-2} y^{-1} was observed. For the same period of time, flux values for Sb were consistently low and steady at ~0.03 mg cm^{-2} y^{-1}. The contrasting values found here signified the beginning of coal combustion, where the effect on Pb fluxes were observed before Sb, since Pb is present in coal at considerably higher concentrations (section 2.3.6.2). Significant increases in both Sb and Pb fluxes were observed from the mid-19th century onwards as coal combustion and mining and smelting activities intensified. Two notable peaks were observed for both Sb and Pb fluxes in 1924 and 1949. The maximum Sb and Pb fluxes for the first peak (1924) were ~0.6 and ~28 mg cm^{-2} y^{-1}, respectively, with fluxes increasing marginally for the second peak giving values of ~0.7 and ~33 mg cm^{-2} y^{-1}. The decline in Sb and Pb fluxes in 1938, was the result of an economic downturn from the inter-war period, where subsequent industrial activity for this duration was reduced (Farmer *et al*., 1997, 2015).

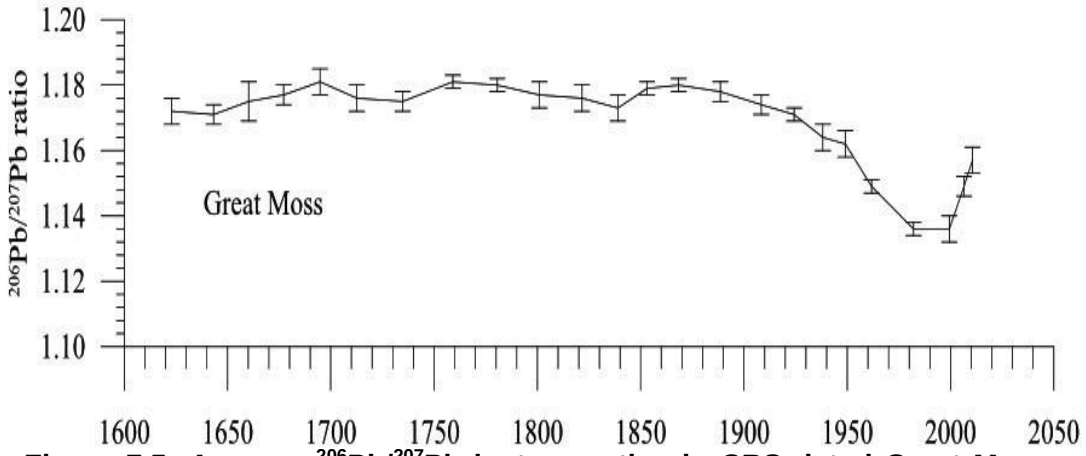

Figure 7.5: Average $^{206}Pb/^{207}Pb$ isotope ratios in CRS dated Great Moss peat core. Taken from Farmer *et al*. (2015).

Although maximum Sb and Pb fluxes at 1924 and 1949 look similar, the second Pb flux peak is proportionally larger than that of the Sb flux, which is most likely attributed to Pb emissions from leaded petrol. This is consistent with the $^{206}Pb/^{207}Pb$ isotope ratios (Figure

7.5), where ratios began to decline in 1924 (1.171 ± 0.002) to 1960 (1.149 ± 0.002), as Pb emissions were increasingly influenced by Australian sourced Pb contained in leaded petrol ($^{206}Pb/^{207}Pb$ ratio ~ 1.06-1.09) (Farmer *et al*., 2000). Indeed, this trend continued over the entire second half of the 20th century, where $^{206}Pb/^{207}Pb$ isotope ratios were lowest between 1980 and 2000 (1.136 ± 0.004), and thereafter, began to increase as leaded petrol was banned in the UK and indeed Europe in 2000. Antimony and Pb fluxes for the same period of time were significantly reduced, where in the early 21st century, values were ~0.14 and ~3.0 mg $cm^{-2}\,y^{-1}$, respectively.

7.4.3 Sb/Pb ratios from Great Moss

As discussed previously in Chapter 2 and 6, Sb and Pb are co-occurring elements in sulfidic minerals and coal, and their release into the environment can often be from the same anthropogenic sources (Mackenzie *et al*., 1998; Cloy *et al*., 2009). In some instances, this is not the case such as past emissions from leaded petrol, and the examination of Sb/Pb ratios can help clarify a change in emission point sources, e.g. Cloy *et al*., 2005, 2009.

As industrial activity and resultant emissions were low between 1750 and 1850, this was reflected in the low Sb/Pb ratios (~0.005) observed for this period of time (Figure 7.6). The onset of the Industrial Revolution in the second half of the 19th century resulted in a significant increase in ratio values, as emissions of Sb and Pb increased from the intensive use of coal combustion, and from mining and smelting activities. By 1924, Sb/Pb ratios had increased by a factor of 5 compared with the 1850's. Thereafter, Sb/Pb ratios began to decrease as a result of declining use of coal combustion, mining and smelting activities, and additionally, increased use of leaded petrol. The impact of Pb emissions from the use of leaded petrol was again confirmed by the $^{206}Pb/^{207}Pb$ ratios, where the values decreased from 1.171 ± 0.002 in 1924, to 1.136 ± 0.002 in 1980. Consequently, emissions of Sb decreased up until the 1980's, while a marked contrast was observed for Pb, causing the Sb/Pb ratios to decline to ~0.015. Since the ban on the use of leaded petrol, lower emissions of Pb from

2000 onwards marked a dramatic increase in Sb/Pb ratios. Moreover, the production and use of Sb over the last decade has increased by ~65% (He *et al*., 2012) potentially influencing atmospheric Sb concentrations. Both the decline in Pb emissions, and increase in Sb emissions have caused the rise in Sb/Pb ratios to ~0.045.

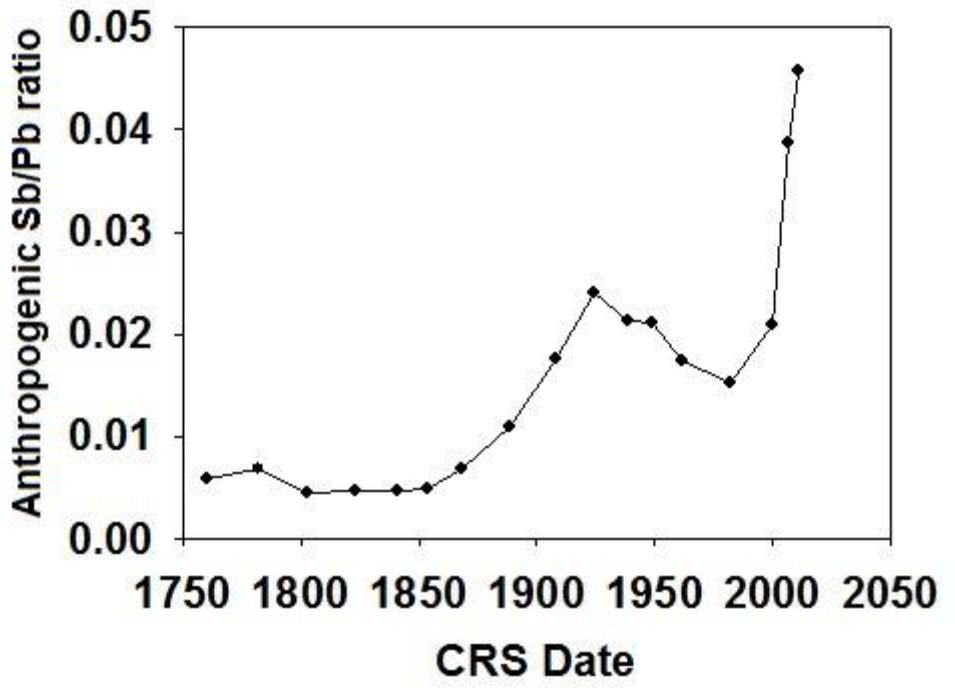

Figure 7.6: Anthropogenic Sb/Pb ratio in CRS dated Great Moss peat core.

7.5 Ombrotrophic peat bog 2-Auchencorth Moss (0-40 cm)

Auchencorth Moss is located in rural part of south east Scotland about 1.5 miles south of Penicuik and is used by the CEH as a monitoring site for rural air quality in southern Scotland (Figure 3.10). It is approximately 10 km^2, with a total peat bog depth of ~45 cm, and a vegetative layer depth of 15 cm, which consists mainly of *Sphagnum* moss, with patches of grasses and sedges also present (CEH, 2015). In April 2011, a 40 cm peat core (area 15 cm x 15 cm) was sampled using a monolith tin, sliced into 2-cm depth increments, air-dried and homogenised. Further details of the Auchencorth Moss sampling can be found in section 3.2.3.3.2. This peat core had been collected during a previous project (Table 7.1) and so sample collection, sample processing and moisture content determination were

completed by Blair (2014) and ^{210}Pb dating was carried out by the Scottish Universities Environmental Research Centre (SUERC) (2013). In this study, all elemental concentration determinations and ^{206}Pb/^{207}Pb isotopic ratio analysis, along with data interpretation were carried out exclusively for this project (Table 7.1).

Table 7.1: Traceability and ownership of Auchencorth Moss sample preparation, analysis and data interpretation.

Auchencorth Moss sample preparation, analysis and interpretation parameter	Completed by
Peat core sampling	Blair (2014)
Peat core sample preparation (including the slicing, air-drying and homogenisation of 2 cm peat core	Blair (2014)
Moisture content of the peat core depth increment	Blair (2014)
^{210}Pb dating of the peat core	SUERC (2013)
All elemental concentration analysis of 2 cm depth increments of peat core.	Macgregor (2015)
All ^{206}Pb/^{207}Pb isotopic ratio analysis of 2 cm depth increments of peat core.	Macgregor (2015)
Data calculations and review of elemental concentrations and ^{206}Pb/^{207}Pb isotopic ratios in each 2 cm depth increment of the peat	Macgregor (2015)
Data interpretation of historic trends in Sb, Pb and ^{206}Pb/^{207}Pb isotopic ratios using calculated fluxes.	Macgregor (2015)
Data calculation and interpretation of anthropogenic Sb/Pb ratios.	Macgregor (2015)

7.5.1 Vertical concentration profiles of Mn, Fe, Ti, Sb and Pb and ^{206}Pb/^{207}Pb isotope ratios from Auchencorth Moss

The elemental concentration profiles for the 40-cm peat core are shown in Figure 7.7. Concentrations of Mn at depths greater than 19 cm were very similar, with a mean of 43.2 ± 3.9 mg kg^{-1} and range of 37.1 to 50.9 mg kg^{-1}. From 19 cm to a depth of 5 cm, Mn concentrations began to increase reaching a value of 129 mg kg$^{-1.}$ Concentrations then increased markedly to a value of 377 mg kg^{-1} in the top section (0-2 cm). The Fe concentrations were in the range of 1500- 15600 mg kg^{-1} and the concentration maximum (15600 mg kg^{-1}) occurred at a depth of 10-12 cm, the mid-point of a broad sub-surface peak.

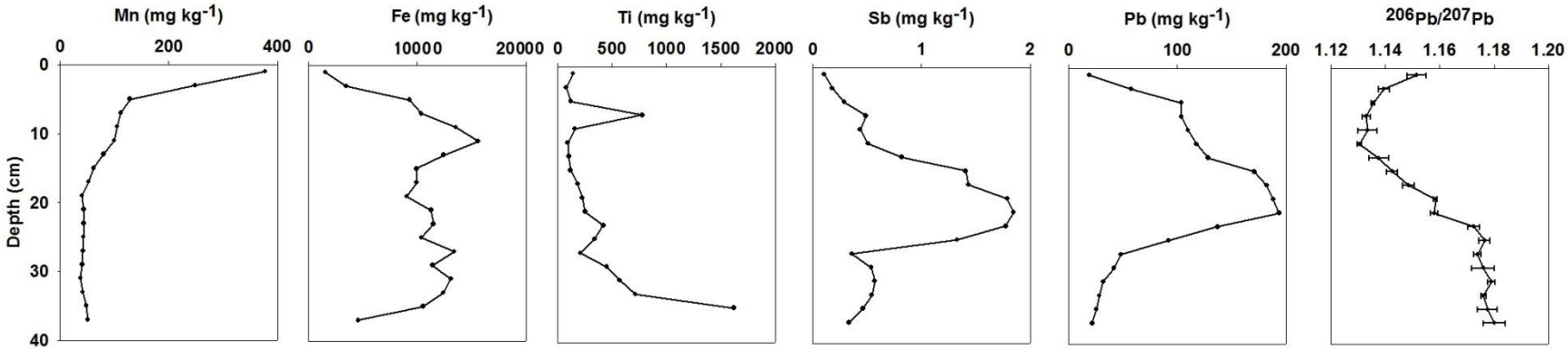

Figure 7.7: Profiles for elemental concentrations, and $^{206}Pb/^{207}Pb$ isotopic ratios versus depth for the Auchencorth Moss peat core. NOTE: with excepiton of $^{206}Pb/^{207}Pb$ isotopic ratios, associated errors for data have been omitted for visual reasons, and values can be found in appendix 6.

There was a clear decline in concentrations towards the peat surface (1500 mg kg^{-1}). The highest concentrations of Ti throughout the peat core were found in the bottom two sections, 36-38 cm (3940 mg kg^{-1}) and 34-36 cm (1621 mg kg^{-1}), and these were considerably higher than all other Ti results found; these points were omitted from Figure 7.7 to give a clearer visualisation of the trends in Ti concentration over the rest of the peat core. From a depth of 34 cm, Ti concentrations gradually declined towards the peat surface, where top sections of peat had typical concentrations of ~110 mg kg^{-1}. The one exception to this was a distinctive peak in Ti concentrations at a depth of 6-8 cm (776 mg kg^{-1}).

The mean Sb concentrations in the peat core were 0.80 ± 0.10 mg kg^{-1}, and the range was 0.10-1.85 mg kg^{-1}. Antimony concentrations at depths greater than 26 cm were near-constant at ~0.5 mg kg^{-1}, and were followed by a significant increase in concentrations to 1.85 mg kg^{-1} between depth sections 20-22 cm and 22-24 cm. Thereafter, a general decreasing trend in Sb concentrations with reducing depth occurred towards the peat surface where an Sb concentration of 0.1 mg kg^{-1} was observed. There was a prominent shoulder to the large Sb concentration peak at a depth between 6 and 12 cm; the highest concentration within this depth range occurred at a depth of 6-8 cm, coincident with the sub-surface peak for Ti. For Pb, the mean and range of concentrations were 94.8 ± 10 mg kg^{-1} and 19.0-194 mg kg^{-1}, respectively, and the depth profile was similar in shape to that of Sb. At depths greater than 24 cm, Pb concentrations were fairly stable at ~32 mg kg^{-1}; this was followed by a significant increase to 194 mg kg^{-1} between depths of 20-24 cm. From 20 cm towards the peat surface, concentrations of Pb generally declined to a minimum of ~30 mg kg^{-1}, and similarly to Sb, a prominent albeit broader shoulder was also observed between depths of 6-14 cm. The accompanying $^{206}Pb/^{207}Pb$ isotope ratios are also shown in Figure 7.7. At depths of greater than 22 cm, the $^{206}Pb/^{207}Pb$ ratios were very similar with a mean and isotope ratio range of 1.176 ± 0.002 and 1.173-1.180, respectively. A notable drop in $^{206}Pb/^{207}Pb$ ratios started at a depth of 20-22 cm (1.158 ± 0.001), which coincided with peak Sb and Pb

concentrations. The $^{206}Pb/^{207}Pb$ ratios continued to decline towards the peat surface reaching a minimum of 1.131 ± 0.001 at 10-12 cm, where ratios remained similar, until a near-surface increase at 4-6 cm (1.136 ± 0.001). This increase continued towards the peat surface where final $^{206}Pb/^{207}Pb$ ratios of 1.152 ± 0.004 was observed.

7.5.2 Evidence for limited post-depositional mobility for Mn, Fe, Ti, Sb and Pb and $^{206}Pb/^{207}Pb$ isotope ratios for Auchencorth Moss

As for the Great Moss core, there was a significant near-surface enrichment for Mn over the top 3 sections (0-6 cm) and a sub-surface enrichment for Fe centred in the 10-12 cm section. The position of the water table was ~6-7 cm, based on the moisture content profile; there was an increase in moisture content from 85% w/w at the surface to ~90% w/w at this depth and near-constant values to ~25 cm, below which the composition of the solid phase changed from peat to a more clay-rich substrate (Figure 7.8). The shoulders/peaks in the depth range 6-14 cm in the vertical profiles of Fe, Ti, Sb and Pb for the Auchencorth peat core were therefore situated at or just below the position of the water table. As such, these features may have arisen from post-depositional redox cycling. Since they occur above the position of the sub-surface Fe peak (10-12 cm), it is postulated that release upon reduction of Mn^{IV} (hydr)oxides (which may also contain small amounts of Fe) is followed by removal to the solid phase (i) via precipitation of Fe^{III} (hydr)oxides; (ii) adsorption onto Fe^{III} (hydr)oxides and/or (iii) sorption onto peat particles which form towards the bottom of the acrotelm. Further evidence would be required to substantiate the proposed mechanisms and to establish the reasons why this occurs at Auchencorth but not at other locations including the Great Moss. One factor might be that the vegetation layer at Auchencorth Moss is relatively deep (~15 cm), approximately 10 cm deeper than at Great Moss, and so the concentration perturbations of Ti, Sb and Pb all occur within the acrotelm rather than in the catotelm (as at the Great Moss). Moreover, Figure 7.9 shows comparable depth profiles for Sb, Pb and Ti obtained for a peat core from Flanders Moss, central Scotland, published by Cloy *et al.* (2009). Here there appear to be similar shoulders in the Ti, Sb and Pb profiles (red circles in

Figure 7.9). As at Auchencorth Moss, the redox cycling of Mn and Fe at Flanders Moss occurred in the acrotelm (shown as green in Figure 7.9). The water table was very close to the surface at the time of the Flanders Moss sampling (note – the broad minimum in the moisture content profile was attributable to mineral-rich material deposited during the Industrial Revolution, confirmed by the inverse relationship to the % ash profile) and the Mn and Fe enrichments almost coincident at the scale of core-sectioning. It is therefore difficult to distinguish between the potential roles of Mn and Fe cycling in perturbing the solid phase profiles of Ti, Sb and Pb.

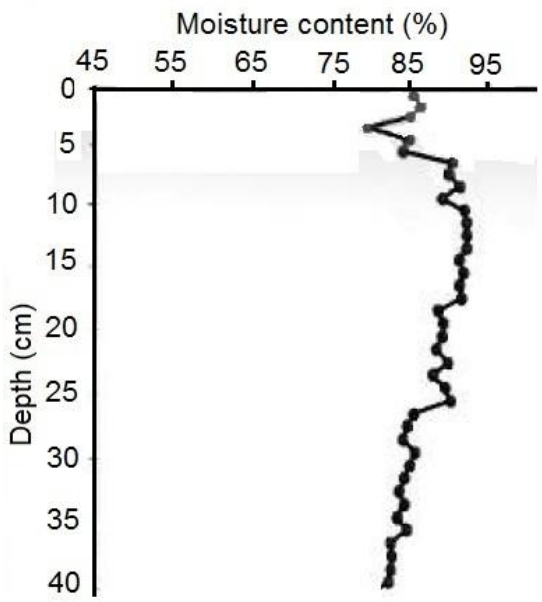

Figure 7.8: Auchencorth Moss solid phase profile for moisture content. Adapted from Blair (2014).

In terms of establishing historical records, it is important to note that the main peaks for Sb and Pb occur at ~20 cm depth, and that these are likely to be unaffected by the redox cycling of Mn and Fe described above. The $^{206}Pb/^{207}Pb$ isotope ratio profile exhibits the same characteristic shape observed for other cores, including that from Great Moss (MacKenzie *et al.*, 1997; Farmer *et al.*, 2006; Cloy *et al.*, 2009), with near-constant values of ~1.18 in the deeper sections and a marked transition to values of ~1.13 at a depth of 10-12 cm. There was

also a characteristic upturn in the uppermost sections to a value of ~1.15 in the 0-2 cm section. Thus, to a first approximation, the perturbations do not appear to have had a significant effect on the trends in isotope ratio. Although the finer details will be examined further in section 7.5.3, the reason for the limited effect might be that the released elements are quickly removed from the solution phase and so there is only limited scope for upwards/downwards diffusion.

Finally, on the basis of its conservative behaviour, Ti is an element that is often used to normalise the concentrations of contaminant elements such as Pb and Sb. Yet the results of this study suggest that Ti enrichments can occur as a result of elemental cycling. A past study by Bain (1976) did show evidence for limited Ti mobility in Ti-rich peaty podzols, where Ti-solubilisation occurred from the dissolution of cryptocrystalline anatase (TiO_2). Caution is therefore required before data normalisation is carried out, especially where perturbations occur close to the position of the water table.

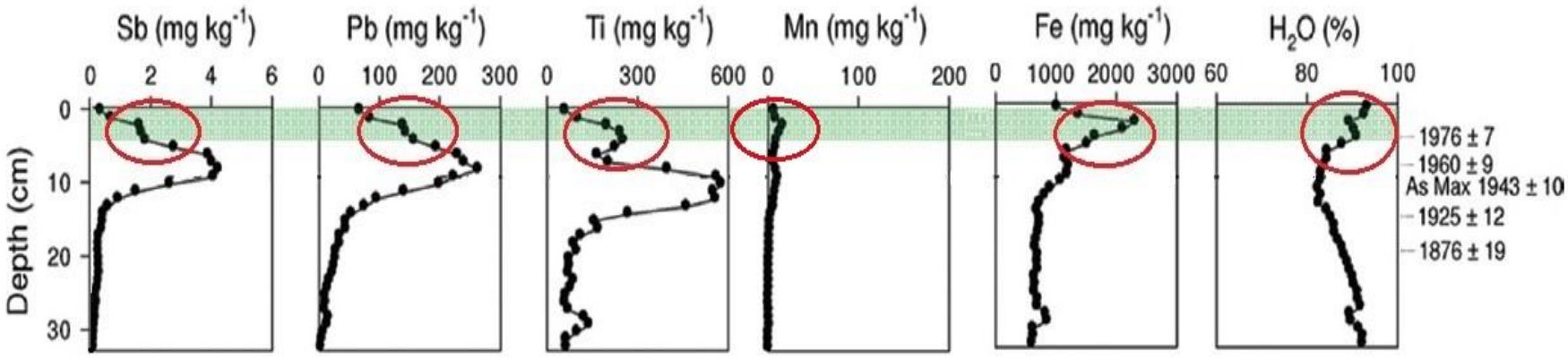

Figure 7.9: Vertical elemental concentration and moisture content profile obtained at Flanders Moss (FM01CM-1), Scotland. Shaded area indicates vegetation/litter to interface with peat. Adapted from Cloy *et al*., 2009. The potential zone of impact of redox cycling on Sb, Pb and Ti has been indicated using red circles.

7.5.3 Historic trends in Sb, Pb and $^{206}Pb/^{207}Pb$ isotopic concentrations from Auchencorth Moss

For comparability purposes, Great Moss and Auchencorth Moss data were calculated using the same techniques: dating was carried out using the CRS model and with anthropogenic fluxes calculated relative to Sb/Ti and Pb/Ti ratios using the Equation 7.1 detailed in section 7.4.2 (Appendix 7).

The similarity of total and anthropogenic fluxes shown in Figure 7.10 suggested that anthropogenic activity contributed to almost all total flux emissions of Sb and Pb over the time period 1900 to 2011 (core collection date). Anthropogenic Sb and Pb fluxes ranged from 0.03 - 0.21 mg cm^{-2} y^{-1} and 2.52 - 30.1 mg cm^{-2} y^{-1}, respectively. The early 20^{th} century was when a maximum Sb flux was seen (0.22 mg cm^{-2} y^{-1}), with the corresponding Pb flux showing moderate values (~16 mg cm^{-2} y^{-1}). The observed peak in Sb flux during the early 20^{th} century was attributed to the use of coal combustion, and resultant emissions from mining and smelting activities. This was confirmed by the high $^{206}Pb/^{207}Pb$ ratios shown in Figure 7.11 (1.174 ± 0.001), where typical $^{206}Pb/^{207}Pb$ ratios were similar to British coal 1.182 ± 0.009 and indigenous Pb ore 1.172 ± 0.003 (Famer *et al*., 1999; Cloy *et al*., 2005).

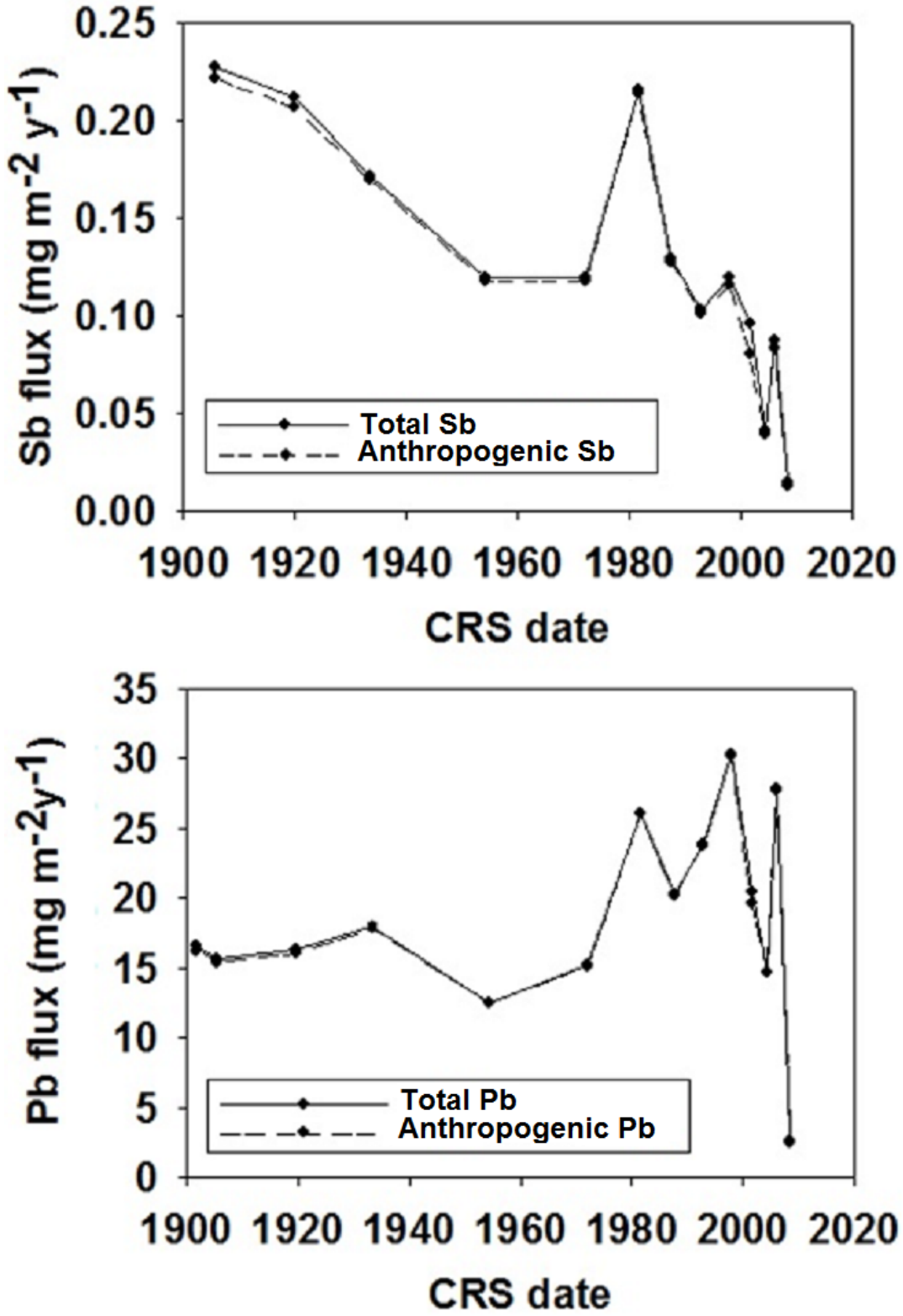

Figure 7.10: Average total and anthropogenic fluxes for Sb and Pb in CRS dated Auchencorth Moss peat core.

As coal combustion, and mining and smelting activities declined throughout the 20th century, so did Sb fluxes until the 1980s. Although only a small decline in Pb fluxes were observed between 1900 and 1980, a clear change in source emissions from anthropogenic activities was observed upon examination of $^{206}Pb/^{207}Pb$ isotope ratios, where $^{206}Pb/^{207}Pb$ ratios decreased from 1.174 ± 0.001 in 1901 to 1.143 ± 0.002 in 1981. From around the 1930s, Pb emissions from mining and smelting activities declined, whilst emissions from vehicular use of leaded petrol increased (Cloy *et al*., 2008, 2009), which in part, explains why Pb fluxes did not decline like Sb, over the same 80 year period.

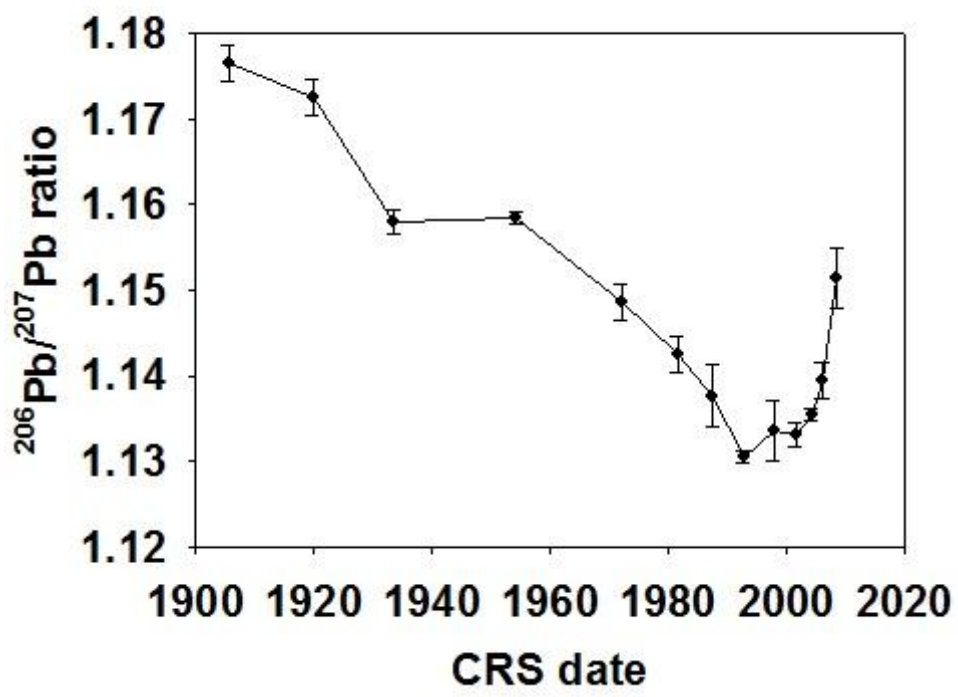

Figure 7.11: Average $^{206}Pb/^{207}Pb$ isotope ratios in CRS dated Auchencorth Moss peat core.

In 1980, a significant peak in Sb flux (0.21 mg cm^{-2} y^{-1}) was observed, which was followed by a general decline to 0.01 mg cm^{-2} y^{-1} in 2008. Although Pb fluxes were unusually variable between 1980 and 2008, an increase to 26 mg cm^{-2} y^{-1} was found in 1980 and the maximum Pb flux was observed in 1997 (30 mg cm^{-2} y^{-1}). It is very unlikely that the peaks for Sb and Pb fluxes occurring from 1980 to 1997 were a true reflection of atmospheric deposition, as

European Sb and Pb inventories had shown a significant decline over the same period of time (Pacyna, 1984; Pacyna *et al*., 2009; Tian *et al*., 2014). Moreover, it differed from previously published studies in Scotland, where maximum Sb and Pb fluxes occurred between 1900 and 1960 (Cloy *et al*., 2005, 2009; Farmer *et al*., 2005, 2015). This therefore indicated that depth profiles of Sb and Pb, along with Ti, were indeed being affected by the redox cycling of Mn and Fe in the near-surface vegetation of the peat core.

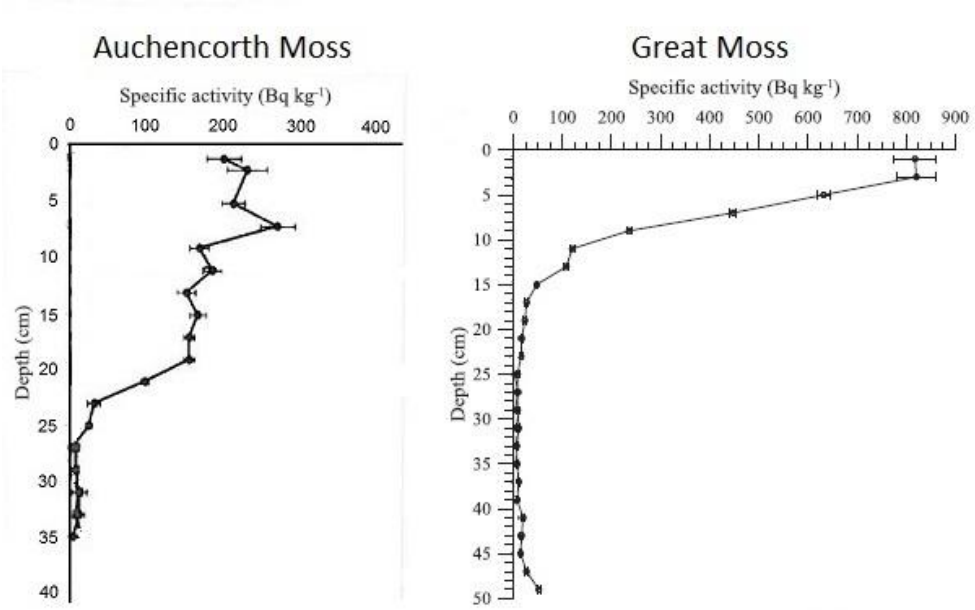

Figure 7.12: Comparison of typical ^{210}Pb activity profile at Auchencorth Moss and Great Moss. Adapted from Blair (2014) and Farmer *et al*. (2005).

Upon examination of the ^{210}Pb activity (Bq kg^{-1}) with depth, a very distinctive profile was observed, where ^{210}Pb activity was approximately constant over the top 0-20 cm sections (Figure 7.12). Moreover, a ^{210}Pb activity peak occurred at a depth of 7 cm which coincided with concentration peaks for Sb, Pb and Ti. This is a marked contrast from typical ^{210}Pb activity throughout a peat core, where the constant decay of ^{210}Pb activity exponentially declines with depth, as shown for the Great Moss (Figure 7.12). Clearly this is not occurring at Auchencorth Moss, where ^{210}Pb is retained in the vegetation layer, or the top 20 cm of the peat core. Indeed, the uptake and accumulation of Pb by moss has been the focus of a number of past studies; Ceburnis and Valiulis (1999) reported up to 63% of atmospheric

deposited Pb can be sequestered by moss, whilst Berg *et al.* (1995) reported 100%. For both instances, the accumulation of Pb by moss can represent an influential factor when considering ^{210}Pb activity profiles. Below the depth of 20 cm, where the transition from vegetation to clay-rich soil occurs, the ^{210}Pb activity profile was more comparable to that of Great Moss and is more likely to be accurate for ^{210}Pb dating.

This helps to explain why large Sb and Pb fluxes are found at Auchencorth Moss in the late 20th century, with flux peaks occurring in 1980 for Sb, and 1980 and 1997 for Pb. Upon comparison of Sb and Pb flux profiles with the concentration profile shown Figure 7.7, less distinctive features were observed for the concentration profile, where only peak shoulders were evident. The peat layers at Auchencorth Moss were generally low density and thus influenced by the deep layer of vegetation present which resulted in Sb and Pb fluxes influenced greatly by modest changes in concentrations.

7.5.4 Sb/Pb ratios from Auchencorth Moss

The Sb/Pb ratios shown in Figure 7.13 for the early 20th century were highest (0.0144) during the UK Industrial Revolution (~1850 to 1950), where Sb and Pb was both released from the combustion of coal, and from mining and smelting activities. This was in general agreement with ^{206}Pb/^{207}Pb isotopic ratios (1.176 ± 0.002) found at Auchencorth Moss where high indigenous ^{206}Pb/^{207}Pb ratios of 1.182 ± 0.009 were typically observed in the early 20th century (Farmer *et al.*, 1999). From this period forward, Auchencorth Moss Sb/Pb ratios began to decline throughout the 20th century to a minimum of 0.0027 in 2002, and thereafter, increased to 0.005 in 2010. The trend in Sb/Pb ratios observed at Auchencorth Moss during the 20th century and early 21st century were in agreement with previously published literature. During the 20th century, emissions from mining and smelting activities in the UK were on the decline, particularly in Scotland, where large Pb ore mining operations at Leadhills and Wanlockhead began to close in the 1930s (Wilson 1921; Elliott *et al.*, 1937; Cloy *et al.*, 2005). At this point, atmospheric Pb present in Scotland could be apportioned

into three sources: 46% originating from coal, 35% from smelting activities and the remaining 19% from the rest of the UK (Farmer *et al*., 1999; Cloy *et al*., 2005).

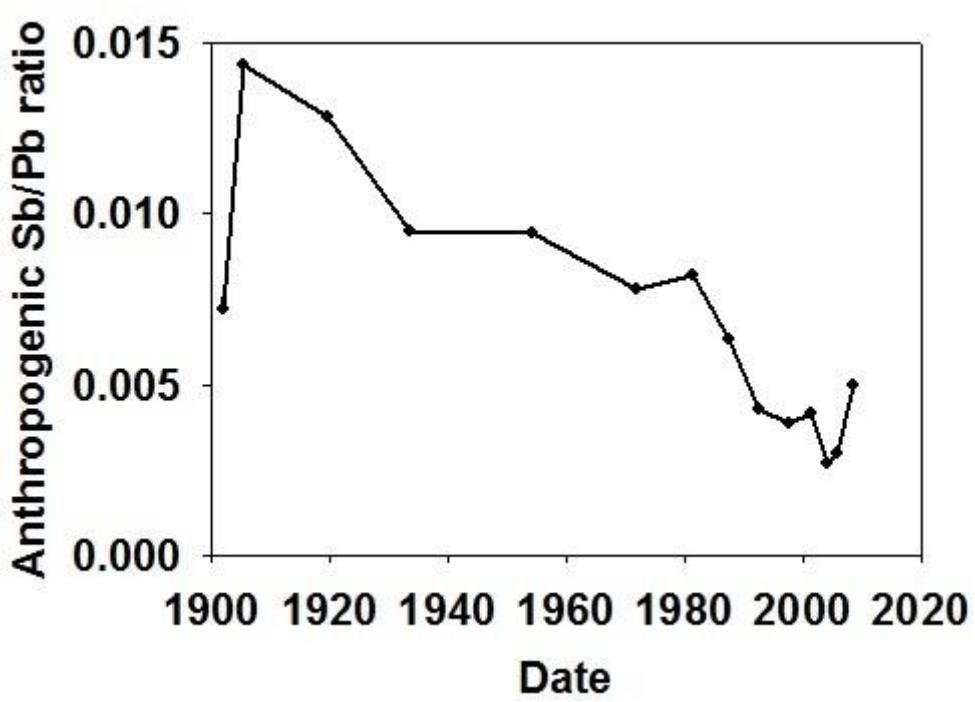

Figure 7.13: Anthropogenic Sb/Pb ratio in CRS dated Auchencorth Moss peat core.

The emergence of leaded petrol in 1923 resulted in a change in the atmospheric ratio of Sb and Pb, where Pb emissions from the combustion of leaded petrol became dominant duting the 20th century (Cloy *et al*., 2009). This significantly reduced the Sb/Pb ratios throughout the 20th century, where excessive amounts of Pb were released into the atmosphere through vehicle exhaust emissions, whilst Sb, not present in leaded petrol, began to decline along with the reduction of previous industrial activities.

The trend continued throughout the 20th century until the beginning of the 21st century, where a small increase in Sb/Pb ratio was observed in 2005. As a result of lower atmospheric Pb concentrations present, there is an increasing importance on other Pb sources such as waste incineration and the emergence of Pb recycling plants across Europe. In addition, the greater use of Sb in the 21st century for flame retardants, vehicle brake-linings and the

production of polyethylene terephthalate (PET) has also led to an increase in Sb/Pb ratios (Lijima *et al*., 2008; Cloy *et al*., 2009).

7.6 Sb and Pb inventories for Great Moss, Auchencorth Moss and other ombrotrophic peat bogs

The use of Sb and Pb deposition inventories provides a means of comparing spatial trends in elemental concentrations originating from atmospheric deposition within Scotland and elsewhere. These are calculated by using the weight, area and elemental concentration for each section to give the elemental concentration per unit area (g m^{-2}) (Table 7.2).

Table 7.2: Cumulative Sb and Pb inventories taken from peat bogs and Loch Tay sediment detailed for this study, and peat bogs studied by Cloy *et al.* (2009)

Peat bog or loch sediment site	Dated period		Total Sb inventory (g m^{-2})	Total Pb inventory (g m^{-2})
	From	To		
Auchencorth Moss	1900	2008	0.018	2.1
Great Moss	1900	2008	0.047	2.4
Great Moss	post-1800	2010	0.053	3.3
Turclossie Moss*	post-1800	2004	0.026	1.2
Flanders Moss*	post-1800	2001	0.035	2.1
Red Moss of Balerno*	post-1800	2000	0.045	4.3
Carsegown Moss*	post-1800	2003	0.056	5.0
Loch Tay -Mini-Mackereth	post-1800	1991	0.07	11.5
Loch Tay-Jenkin Core	1900	1991	0.03	6.6

*from Cloy *et al.* (2009)

Table 7.2 shows that the total Sb inventories obtained from peat cores around Scotland were in the range 0.026-0.056 g m^{-2} over the post-1800 to early 21st century time period. The variation of a factor of ~2 is partly attributable to location; Turclossie Moss, the most northerly peat bog shown in the table, and Carsegowan Moss, the most southerly bog, had the lowest and highest peat bog Sb inventories, respectively. The Great Moss, sampled in

this study and located only ~95 miles to the SW of Turclossie Moss, also had one of the highest of the peat bog Sb inventories. Indeed, from 1900 to 2008 the Sb inventory at the Great Moss (0.047 g m^{-2}) was approximately double that at Auchencorth Moss (0.018 g m^{-2}), which is located ~100 miles further south. This is contrary to what might be expected on the basis of proximity to the UK industrial belt, including cities such as Manchester and Glasgow. The key difference is that the Great Moss is situated at an altitude of ~600 m AOD and is subject to ~45% more rainfall (Met Office, 1981-2010) than Auchencorth Moss; importantly, increasing elemental deposition with increasing altitude has previously been documented (Smith *et al.*, 1997; Farmer *et al*., 2006; Farmer *et al*., 2015) and so greater inventories can be obtained at upland locations which are more distant from the pollution source.

The Sb inventory obtained for the mini-Mackereth sediment core from Loch Tay (0.07 g m^{-2}) was the highest of all those listed in Table 7.2. Since Sb/Pb ratio for the Tyndrum ore are extremely low (~0.0003), it is unlikely that this is the source of the additional Sb. Instead, it is more likely that Loch Tay sediments receive an input from the surrounding catchment (steep-sided hills with elevation up to ~600 m) and that catchment-to-loch transfer of previously deposited industrial belt-derived contaminants is the source of the additional Sb.

Total Pb inventories obtained from peat cores around Scotland were in the range 1.2 - 5.0 g m^{-2} over the post-1800 to early 21st century time period. Again, highest inventories were obtained in the south (Carsegowan Moss) and lowest values were obtained in the north (Turclossie Moss). As for Sb, the inventory at the Great Moss (3.3 g m^{-2}) was greater than that obtained at Turclossie Moss and was also ~50% higher than the comparable value of 2.1 g m^{-2} for Auchencorth Moss, again consistent with an altitude effect.

Comparison with both Loch Tay inventories dating from post-1800 to 1991 (mini-Mackereth), and from 1900-1991 (Jenkin core) reported in Chapter 6 (Table 7.2), demonstrates the impact of additional local anthropogenic activities on Pb inventories, where

Pb ore mining at Tyndrum significantly increased Pb inventories; over the period 1800-1991, the value for Loch Tay (11.0 g m^{-2}) was more than twice that obtained for Carsegowan Moss, SW Scotland.

There are very few global studies examining Sb inventories over several centuries but considerable research for Pb inventories has been published in recent decades. Rothwell *et al*. (2007) included a summary table (Table 7.3) to demonstrate the variation in Pb inventories found globally; they ranged from 1.0 g m^{-2} at Store Mosse, Sweden, for a dated period of 110 years (Bindler *et al*., 2004), to 7.43 ± 1.45 g m^{-2} at Glensaugh, Scotland, for a dated period of ~150 years (Farmer *et al*., 2005). A typical Pb inventory range of ~2-3 g m^{-2} for a 100 cm deep peat core was reported in several peat bogs from Switzerland (Mauntschas, Praz Rodet, Etang de la Gruere, La Tourbiere and Suossa) and Sweden (Bottnard, Norra Kvill, Hashult) by Shotyk *et al*. (2000) and Bindler *et al*. (1999), respectively. The one notable exception to this is Gola di Lago, Switzerland, where this site was heavily influenced by its close proximity to anthropogenic activity occurring in the north of Italy (Shotyk *et al*., 2000). Taking into account the Pb inventory range (1.1-3.2 g m^{-2}) for peat bogs in Switzerland and Sweden spanning between 1060 and 3630 years, Pb inventories found in Scottish peat bogs were generally higher, where they ranged between 1.2 - 5.0 g m^{-2} spanning 118-390 years.

Table 7.3: Selection of Pb inventories from UK and global monitoring sites. Adapted from Rothwell *et al*. (2007).

Location	Sampling depth (cm)	Time period represented by inventory (years)	Inventory type	Pb inventory ($g\ m^{-2}$)
Oberhauser Ried, Zurich, Switzerland	30	na	Anthropogenic	17.50
Samaru, Nigeria	100	na	Anthropogenic	12.50
Gola di Lago, Switzerland	100	3100	Anthropogenic	9.70
Thorter Hill, Glensaugh, Grampian Highlands, Scotland	~20	~150	Anthropogenic	7.43 ± 1.45
Indiana Dunes National Lakeshore Lake Michigan, USA	80	100	Anthropogenic	7.30 ± 3.10
Lehstenbach, Fichtelgebirge, Germany	60	na	Total	6.93
Vallatscha, Swiss National Park, Alps, Switzerland	20	na	Anthropogenic	5.38
Bílá Smědă, Czech Republic	40	100	Anthropogenic	4.40
Flanders Moss, Scotland	16	224	Anthropogenic	3.39
Suossa, Switzerland	100	1870	Anthropogenic	3.20
Häshult, Sweden	100	na	Anthropogenic	3.05
Regensdorf, Zurich, Switzerland	30	na	Anthropogenic	2.88
South Drumboy Hill, Scotland	20	na	Total	2.81
Flanders Moss, Scotland	30	333	Anthropogenic	2.44
La Tourbière des Genevez, Switzerland	100	1730	Anthropogenic	2.20
Etang de la Gruère, Switzerland	100	2110	Anthropogenic	2.10
Norra Kvill, Sweden	100	na	Anthropogenic	2.06
Mugdock Bog, Scotland	28	na	Total	2.05
Bottnard, Sweden	100	na	Anthropogenic	2.04
Praz Rodet, Switzerland	100	1060	Anthropogenic	2.00
Lochnagar, Scotland	~25	na	Anthropogenic	1.97 ± 0.92
Flanders Moss, Scotland	30	235	Anthropogenic	1.78
Lehstenbach, Fichtelgebirge, Germany	60	na	Total	1.75
Mauntschas, Switzerland	100	3630	Anthropogenic	1.10
Store Mosse, Sweden	75 and ~30	110	Anthropogenic	1.03 ± 0.33
James Mclean Oliver Ecological Centre, Ontario, Canada	10	na	Anthropogenic	0.78
Pod Jelení horou, Czech Republic	40	92	Total	0.5
Langmoos Bog, Mondsee, Austria	40	125	Total	~0.12

7.7 Comparison of Sb and Pb fluxes from Great Moss, Auchencorth Moss with previously published literature

7.7.1 Comparison of Great Moss and Auchencorth Moss Sb and Pb fluxes

Despite the post-depositional mobility of Sb and Pb caused by Mn and Fe redox cycling in the uppermost sections of the Auchencorth Moss core, comparisons of the Sb and Pb fluxes at Great Moss and at Auchencorth Moss can be made up until ~1970s (Figures 7.4 and 7.10). Antinomy fluxes at Great Moss were high between 1920 and 1950 (~0.67 mg cm^{-2} y^{-1}) and then declined towards the 1970s, whereas Auchencorth Moss were high in the early 20th century (~0.22 mg cm^{-2} y^{-1}) and declined towards ~1950s. For the Great Moss, Pb fluxes were generally stable from 1920 to 1960 where a mean Pb flux of ~28 ± 4.4 mg cm^{-2} y^{-1} was observed; this was almost double that for Auchencorth Moss (15 ± 1.8 mg cm^{-2} y^{-1}) during a similar stable flux period from 1900 to 1950. At the Great Moss however, a dip in Pb flux took place in 1938 as a result of the well-documented economic slump (Farmer *et al*., 2015). This was not observed at Auchencorth Moss, possibly suggesting areas to the south of Edinburgh were less affected by the economic downturn. After the 1970s, fluxes observed at both peat sites varied and were not comparable due to the post-depositional mobilisation of Sb and Pb arising from the redox cycling of Mn and Fe at Auchencorth Moss. As discussed above, redox cycling of Mn and Fe did not affect chronologies for Sb and Pb at Great Moss, since the depth of peak Fe enrichment was present in the catotelm layer, and not the acrotelm, as observed for Auchencorth Moss.

7.7.2 Comparison of Sb and Pb fluxes with previous published literature

7.7.2.1 Comparison of Sb fluxes

Although numerous studies examining elemental concentrations in ombrotrophic peat cores exist, very few specifically examine and establish chronologies for Sb. One such study that does fulfil these criteria is by Cloy *et al*. (2009), where Sb anthropogenic fluxes were calculated for four ombrotrophic peat bogs in Scotland: Flanders Moss, Red Moss of Balerno, Carsegowan Moss and Turclossie Moss (Figure 7.14).

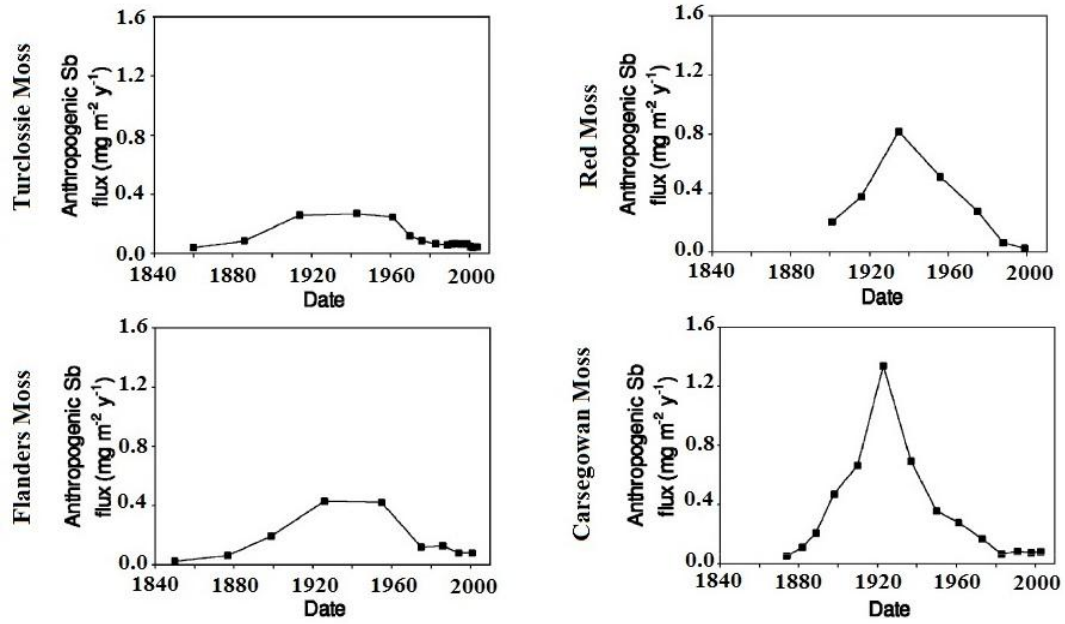

Figure 7.14: Anthropogenic Sb fluxes versus ^{210}Pb date for Turclossie Moss, Flanders Moss, Red Moss of Balerno and Carsegown Moss, Scotland. Adapted from Cloy *et al*. (2008)

For these four sites, maximum Sb fluxes were observed ranging from 0.3 to 1.3 mg cm^{-2} y^{-1} between the dates 1920 to 1960. The maximum anthropogenic Sb flux for Auchencorth Moss occurred in 1905 (0.22 mg cm^{-2} y^{-1}), 15 years earlier than observed for Carsegowan Moss, ~100 miles to the SW. In contrast, the temporal trends for the Great Moss, where maximum and sub-maximum anthropogenic Sb fluxes were seen in 1949 (0.71 mg cm^{-2} y^{-1}) and 1924 (0.67 mg cm^{-2} y^{-1}), respectively, were more similar to those for the central

(Flanders Moss, Red Moss of Balerno) and northern locations (Turclossie Moss). This confirmed that Great Moss maximum Sb flux concentrations were comparable with three other peat bog sites in Scotland, while those obtained from Auchencorth Moss appeared to be ~15 years earlier than all previously published data for Scotland. A study by Shotyk *et al*. (1996) examining anthropogenic Sb fluxes in an ombrotrophic peat bog near the Jura Mountains, Switzerland, is a good example of a site that showed maximum Sb fluxes in the early 20th century, similar to Auchencorth Moss. This demonstrated that the peak flux date can often vary depending on a number of factors such as location and local anthropogenic activities. Shotyk *et al.* (1996) attributed the peak in Sb (and Pb) flux in the early 20th century to the rapid increase in emissions from the combustion of coal. Farmer *et al.* (1999) showed the trends in consumption of coal for the UK over several centuries (Figure 7.15). Much of the early increase occurring from 1850-1900 must be attributable to use of coal in industrial processes because the earliest coal-fired power plants opened in the 1890s (a large proportion of these were in the Greater London region). Interestingly, there were 8 plants opening between 1890 and 1914 in NE England that closed by 1932. It is conceivable that this may have had a localised impact on the Sb fluxes observed at Auchencorth Moss. There were some coal-fired plants in NW England opened in the early 1900s and continuing to operate to the 1950s/60s and there have been no coal-fired plants in SE Scotland and indeed only 3 operating prior to 1950 (2 in Glasgow and 1 in Edinburgh). This may be part of an explanation for the variations observed in the Sb flux chronologies obtained from peat bog cores taken in different parts of Scotland and merits further investigation.

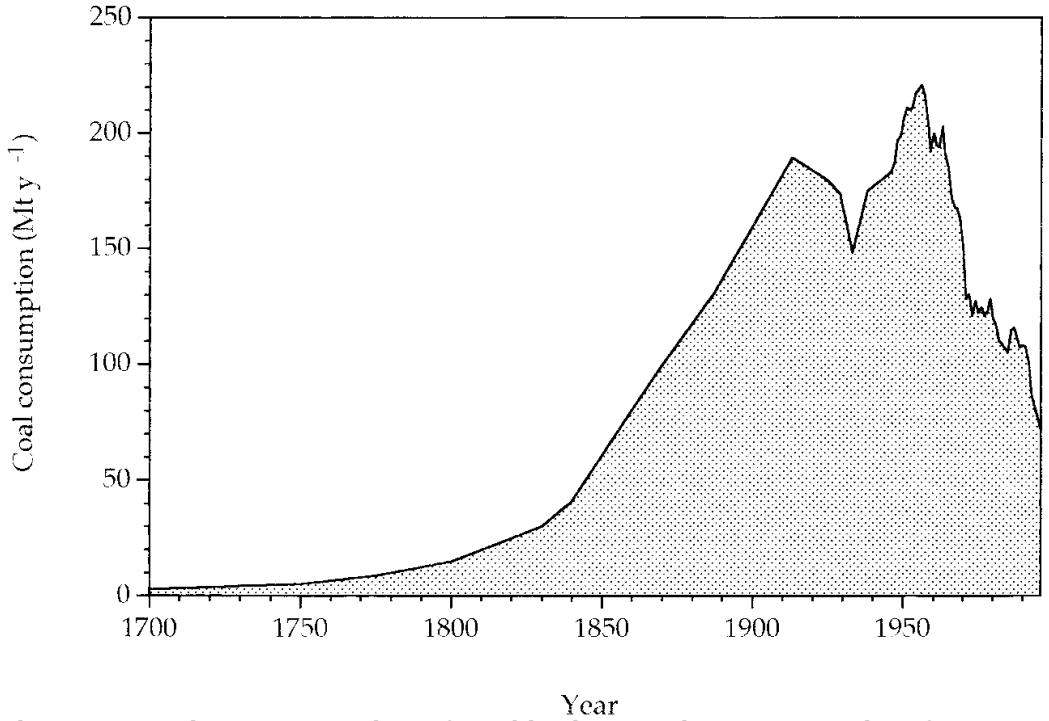

Figure 7.15: The consumption of coal in the UK since 1700. Taken from Farmer *et al.* (1999).

A more recent account of European Sb fluxes was given by Allan *et al*. (2013), where an ombrotrophic peat bog in Hautes-Fagnes, Belgium, was sampled and reported to have fluxes ranging from ~0.3 to 1.5 mg cm^{-2} y^{-1} for the 20th century. The Sb fluxes at Hautes-Fagnes were notably higher than what was reported at both Great Moss and Auchencorth Moss, but this was attributed to Pb-Zn ore deposits located 20 km from the peat bog. Whilst flux values were lower at the Great Moss, a similar trend in dated Sb flux profiles was seen at Hautes-Fagnes, where again a large broad peak and shoulder for Sb fluxes occurred throughout the 20th century, followed by a decline near the start of the 21st century. This decline was also observed in all of the Scottish ombrotrophic peat bogs for which Sb flux data is available; by the end of the 20th century fluxes had declined to <0.1 mg cm^{-2} y^{-1}.

7.7.2.2 Comparison of Pb fluxes

A considerable amount of published literature exists detailing Pb fluxes in ombrotrophic peat bogs in Scotland and Europe. A recent study by Farmer *et al*. (2015) compared dated anthropogenic Pb fluxes found at Great Moss to ombrotrophic peat bogs at Turclossie Moss

and Glensaugh, Scotland, with all three sites along with Auchencorth Moss anthropogenic Pb fluxes shown in Figure 7.16. Although maximum deposition Pb fluxes varied at Great Moss (~33 mg cm^{-2} y^{-1}), Glensaugh (~ 65 mg cm^{-2} y^{-1}) and Turclossie Moss (~12 mg cm^{-2} y^{-1}), all three peaked at very similar dates around the 1950s, where throughout the 20th century a large broad peak were observed. The good agreement between anthropogenic Pb fluxes at Great Moss, Turclossie Moss and Glensaugh, was only partly seen for Auchencorth Moss. Prior to 1970, the maximum Auchencorth Moss anthropogenic Pb flux appeared to be ~20 years earlier to those above (~15 mg cm^{-2} y^{-1}), before being affected by Fe redox cycling in the uppermost part of the core.

Turclossie Moss, Glensaugh, Great Moss and Auchencorth Moss anthropogenic Pb fluxes ranged between ~12 and 65 mg cm^{-2} y^{-1}, which indicated concentrations of Pb deposited can vary depending on location, with local factors such as peat bog altitude, annual rainfall, vegetation present and hydrology all influencing flux rates. Great Moss anthropogenic Pb fluxes were also in agreement with a past study by Cloy *et al*. (2005) at Flanders Moss, Scotland, where a similar broad large peak throughout the 20th century was observed ~1950 (22 mg cm^{-2} y^{-1}). When compared with Auchencorth Moss, maximum Pb flux occurred ~20 years earlier than Flanders Moss, with post-1970 fluxes affected by Fe redox cycling occurring in the uppermost part of the core.

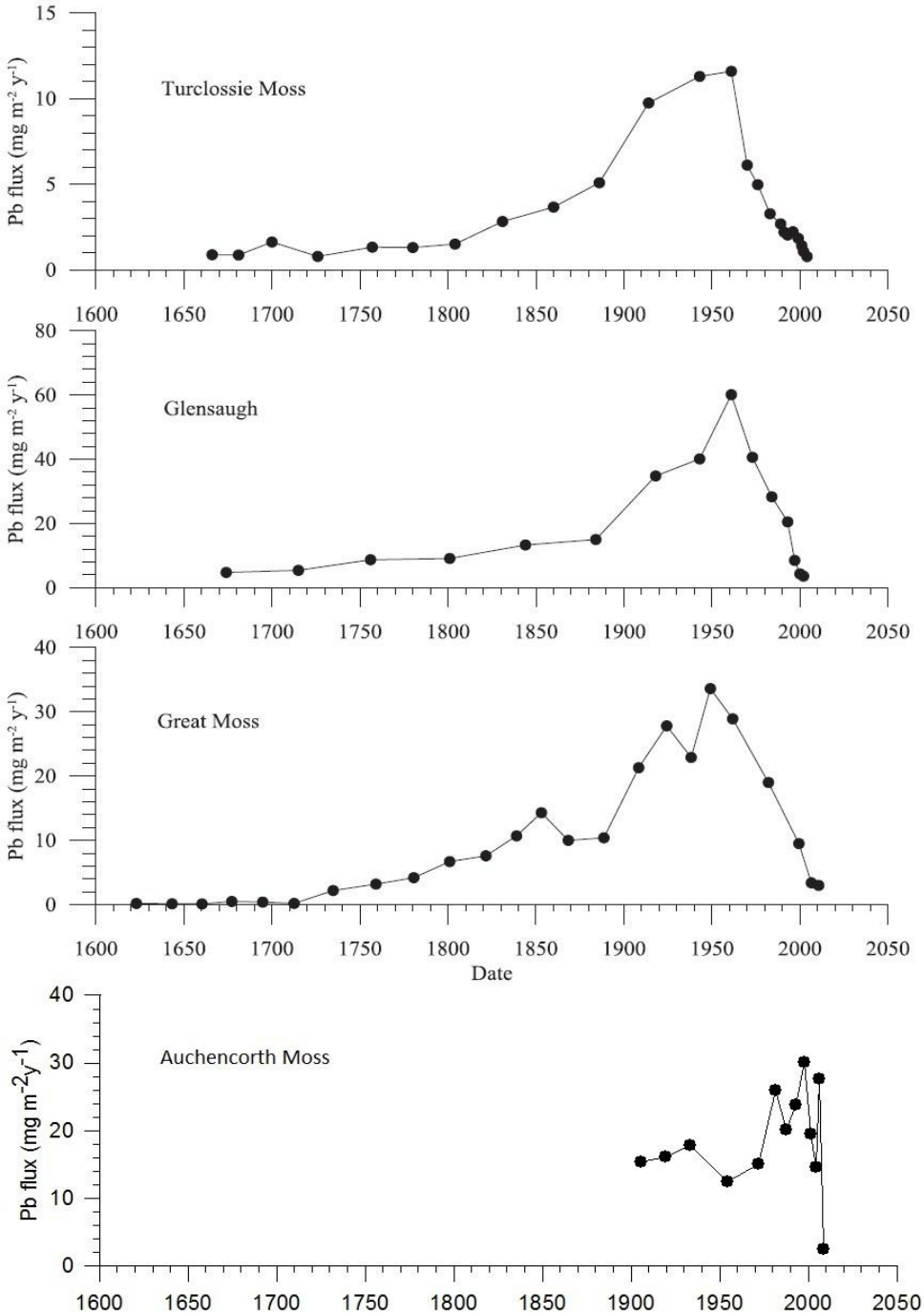

Figure 7.16: Comparison of temporal variations in anthropogenic Pb fluxes date for Great Moss, Auchencorth Moss peat, Turclossie Moss (Cloy *et al*., 2009) and Glensaugh peat (total Pb) (Farmer *et al*., 2005).

When Pb flux profiles from Great Moss and Auchencorth Moss were compared to those obtained from the peat bog in the Jura Mountain previously mentioned in section 7.7.2.1, only limited similarities to each peat bog location was evident. A maximum and sub-

maximum Pb flux for Jura Mountain was observed around the 1980's and 1905, respectively. Excluding Pb fluxes after 1970 due to Fe redox cycling, maximum Pb fluxes at Auchencorth Moss occurred at 1930, with Great Moss a further 20 years later. Whilst the dated maximum Pb fluxes did not match, similar flux trends were seen for Great Moss and Jura Mountains, where a large broad peak and shoulder was observed. This was also the case in peat bogs located in the Czech Republic by Zuna *et al*. (2011), where two peat bogs studied had maximum total Pb fluxes of ~40 mg cm^{-2} y^{-1} in 1980. There was, however, a greater similarity when dated maximum Pb fluxes of Great Moss and Auchencorth Moss were compared to the study in Hautes-Fagnes, Belgium, by Allan *et al*. (2013), where a maximum total Pb flux of ~50 mg cm^{-2} y^{-1} was seen in the mid-20^{th} century. Moreover, agreement was also observed by Olid *et al*. (2010) at four peat bog sites located in the Iberian Peninsula, Spain, where all maximum Pb fluxes peaked in ~1950, and were in the range of 15 - 42 mg cm^{-2} y^{-1}.

Maximum Pb flux dates observed during the 20^{th} century can vary in Scotland and Europe by two distinct periods. The early to mid- 20^{th} century, and ~1980 as given by Shotyk *et al*. (1996) and Zuna *et al*. (2011). The limited agreement observed can be attributed to location and source of Pb deposited on the peat bog. For example, peat bogs that have maximum Pb fluxes occurring early to mid- 20^{th} century were influenced more so by emissions from coal combustion and mining and smelting activities, rather than leaded petrol (Olid *et al*., 2010). This was in agreement with the Great Moss, where the maximum Pb flux occurred in 1950, coinciding with a $^{206}Pb/^{207}Pb$ isotope ratio of 1.162 ± 0.004. In contrast, maximum Pb fluxes occurring ~1980s are influenced more so by leaded petrol. A good example of this can be observed in the study by Shotyk *et al*. (1996) (Jura Mountains), where both dates of maximum Pb flux and lowest $^{206}Pb/^{207}Pb$ isotope ratio value (~1.13) occurred ~1980.

7.8 Comparison of Sb/Pb ratios from Great Moss and Auchencorth Moss with previous published literature

Despite differences in Sb and Pb flux profiles at Great Moss and Auchencorth Moss, similar trends were observed for anthropogenic Sb/Pb ratios plotted with ^{210}Pb dates (Figure 7.6 and 7.13). In the early 20th century, the Sb/Pb ratio was initially high, which was followed by a gradual decline throughout the century, and thereafter, an increase at the turn of the 21st century. The trend was in agreement with the Sb/Pb ratios reported by Cloy *et al*. (2009), at Turclossie Moss, Flanders Moss, and Carsegown Moss, Scotland (Table 7.4). The Sb/Pb ratio values attained from Great Moss were comparable to those reported by Cloy *et al*. (2009), where 20th century maximum and minimum values were between 0.02-0.03 and 0.008-17, respectively. There was also good agreement with the dates that maximum and minimum Sb/Pb ratio values were observed. The lower anthropogenic Sb concentrations at Auchencorth Moss resulted in Sb/Pb ratios that were notably lower than at other peat bog sites shown in Table 7.4, with maximum and minimum values occurring at 1905 and 1995, respectively. This is most likely attributed to the central location of Auchencorth Moss (~10 km south of Edinburgh) and a greater influence of Pb emissions originating from leaded petrol. One commonality across all peat bog sites was the considerable increase in Sb/Pb ratios found at the beginning of the 21st century (Table 7.4). This was a result of a declining Pb emissions since the ban in use of leaded petrol in 2000, but additionally by the increased use of Sb for flame retardants, vehicle brake-linings and the production of polyethylene terephthalate (PET) resulting in greater Sb/Pb ratios (Lijima *et al*., 2008; Cloy *et al*., 2009). With the exception of Auchencorth Moss, Sb/Pb ratio values attained at the beginning of the 21st century for the remaining four peat bogs were comparable, giving a mean and range of 0.045 and 0.037-0.052, respectively (Table 7.4). For Auchencorth Moss, Sb/Pb ratio values were notably different to the other peat bogs, and were most likely a result of greater anthropogenic Pb input at the beginning of the 21st century. For example, Pb inventories

from 2000 onwards for Auchencorth Moss (147 mg m^{-2}) were over double of those for Great Moss (61.0 mg m^{-2}), and was consistent with the proximity of Auchencorth Moss to anthropogenic emissions from central Scotland. Interestingly, this was very similar to mean Sb/Pb ratios attained from road dust sites sampled in 2013 discussed in Chapter 5. This showed that ratios of Sb/Pb were similar for urban and rural areas (Table 7.4), and suggested that there was no major difference between deposition sources for urban and rural environments. It moreover, demonstrates that road dust may provide a good indicator of current environmental Sb/Pb ratios either to replace or complement data obtained from ombrotrophic peat cores. The early 21st century Sb/Pb ratios obtained from Glendinning Sb mine (0.184) and Loch Tay (0.005) were considerably different from those in peat, and indicated that the major impact at these two locations was still from past mining activities.

Table 7.4: Anthropogenic Sb/Pb ratios from ombrotrophic peat samples, Loch Tay sediment and road dust from Scotland.

Environmental Sample	20th century				21st century	
	Date	Maximum Sb/Pb ratio	Date	Minimum Sb/Pb ratio	Date	Surface Sb/Pb ratio
Auchencorth Moss	1905	0.0144	1995	0.0038	2008	0.005
Great Moss	1924	0.0240	1982	0.0151	2010	0.046
Turclossie Moss*	1918	0.03	1980	0.017	2003	0.052
Flanders Moss*	1920	0.02	1975	0.008	2001	0.037
Carsegown Moss*	1930	0.03	1970	0.011	2000	0.044
Loch Tay	1930	0.0054	1987	0.0029	2003	0.005
Mean road dust	-		-		2013	0.036
Glendinning control site (C1)					2013	0.184

*Values taken from Cloy *et al*. (2009)

7.9 The comparison of atmospheric Sb and Pb deposition chronologies in peat cores from Great Moss and Auchencorth Moss, and sediment cores from Loch Tay, with long-term ice core chronologies

In this and the previous chapter, peat and sediment cores were used to establish a chronology of atmospheric Sb and Pb deposition in Scotland. However, ice cores sampled from remote locations such as the Greenland ice sheet and the Alps also provide an excellent archive of elemental atmospheric concentrations. The same assumptions used for peat and sediment cores, however, still apply: elemental deposition should occur through atmospheric input only, and once deposited, elements should remain immobile. A key study by Bindler, (2006) discussed later in this section, provides a good example of the synchronicity of elemental deposition to the long-term peat and sediment cores available, where the impact and influence of past industrial emissions were compared to pre-anthropogenic emissions over several millennia.

Murozumi *et al.* published the first deposition record for Pb in 1969 but comparable records for Sb were obtained much later in the 20th century (e.g. Van de Velde *et al.* 1999). To date, only a small number of ice core studies establish chronologies for atmospheric Sb deposition, with most ice cores being used for short-term studies (<200 years) (Van der Valde *et al*., 1999; Barbante *et al*., 2004). Exceptions to this are the studies by Krachler *et al.* (2005, 2008), where atmospheric Sb deposition over 16,000 years in Arctic ice and snow was determined. Using this chronology for the past 3000 years, the dated ice core concentrations for Sb showed enrichments by a factor of 5, 3 and 3 for the Medieval, Roman and Greek/Phoenician time, respectively, when compared with the natural background concentrations (~0.1 pg g^{-1}) (Krachler *et al.* (2008). More specifically, a closer look at the deposition profile in the ice core for Sb from 1840 to 2000 demonstrated good agreement with deposition chronologies established using peat cores at Great Moss and Auchencorth Moss (Figure 7.17), and Loch Tay sediment cores.

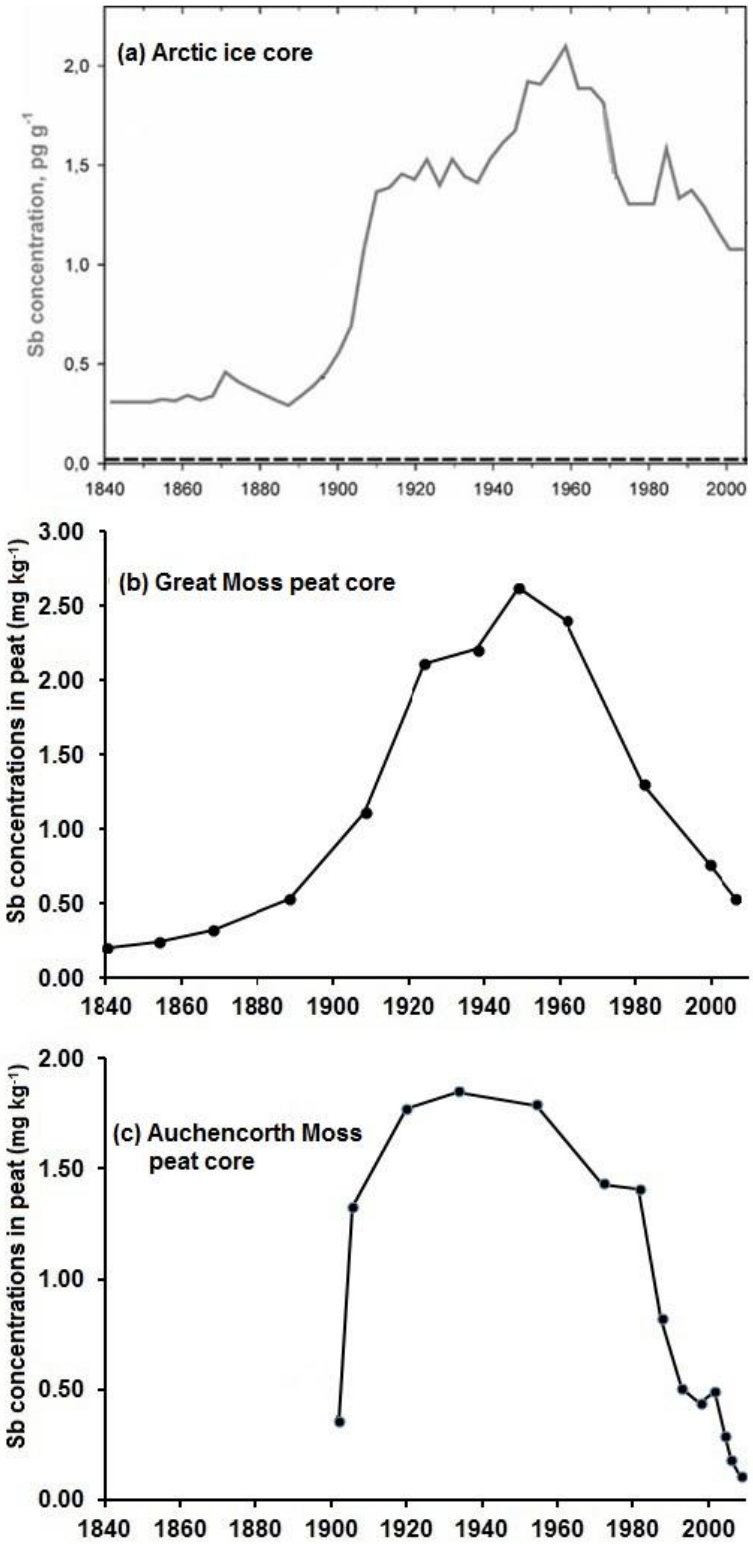

Figure 7.17: Comparison of temporal variations in Sb concentrations dated for: a) Devon Island Canadian arctic ice core (Kratchler *et al.,* 2005), b) Great Moss peat core and c) Auchencorth Moss peat core.

For example, a broad peak in Sb concentrations during the 20th century was observed in peat cores from Great Moss and Auchencorth Moss (Figure 7.17, Table 7.5), where maximum concentrations of Sb occurred in ~1950 and ~1933, respectively. A comparable broad peak in Sb concentrations during the 20th century was also observed in the dated ice core sampled from the Arctic, with Sb concentrations peaking in ~1955 (Krachler *et al.*, 2005). The good agreement observed from 1840 to 2000, and the date at which maximum Sb concentrations occurred, highlight the good synchronicity between ice and peat core chronologies. Moreover, and by using Sb concentrations taken from the bottom depth section of each dated core (the closest date for pre-Industrial Revolution Sb concentrations), an approximate peak enrichment for Sb at Auchencorth Moss was 5-fold, which was comparable to the 6-fold increase observed in the Arctic ice samples (Table 7.5). It is worth noting, however, that the Sb enrichment was greater at Great Moss (twelve-fold), although the general trend remained largely similar. Indeed, both peat cores were in good agreement with another dated ice core study sampled in the Pienne Alps by Van der Velde *et al*. (1999). For this ice core, a broad peak in Sb concentrations occurred from 1900 to 1990, where in ~1920, an 8-fold enrichment in Sb concentrations was observed when compared with values obtained from the bottom depth section of the dated core (~1850). Further agreement, albeit to a lesser extent, was also found when Sb chronologies were compared to a Swiss-Italian Alp ice core; a similar broad peak in Sb concentrations occurred throughout the 20th century with the maximum concentration in this core occurring later, at ~1970 (Barbante *et al.*, 2004).

Table 7.5: Comparison of Sb profiles of ^{210}Pb dated Sb concentrations, Sb enrichment periods, maximum Sb enrichment concentrations and enrichment factor for ice, peat and sediment cores.

Archive material	Location	Reference	Sb concentration taken from the bottom depth section of the dated core.		Beginning and end dates for broad peak in Sb concentrations		Date and maximum Sb concentration observed		Maximum Sb enrichment factor [d]
			Date	Concentration	From	To	Date	Concentration	
Ice	Arctic	Krachler *et al.* (2005)	1840	0.35 pg g^{-1}	1900	2000	1950	2.1 pg g^{-1}	X6
Ice	French-Italian Alps	Van der Valde *et al.* (1999)	1850	~5.0 pg g^{-1}	1910	1980	1920	~42 pg g^{-1}	X8
Ice	Swiss-Italian Alps	Barbante *et al.* (2004)	1840	~3.0 pg g^{-1}	1920	1990	1970	~45 pg g^{-1}	X15
Peat	Great Moss, Scotland	Macgregor, (2015)	1840	0.21 mg kg^{-1}	1870	1980	1950	2.62 mg kg^{-1}	X12
Peat	Auchencorth Moss, Scotland	Macgregor, (2015)	1840	0.33 mg kg^{-1}	1900[c]	1990	1933	1.85 mg kg^{-1}	X5
Sediment	Mini-Mackereth, Loch Tay, Scotland	Macgregor, (2015)	est. 1700[a]	0.42 mg kg^{-1}	1850	1990	1910	1.80 mg kg^{-1}	X5
Sediment	Jenkin, Loch Tay, Scotland	Macgregor, (2015)	est. 1700[b]	0.42 mg kg^{-1b}	1900[c]	1990	1900	1.78 mg kg^{-1}	X5

[a] Estimated ^{210}Pb date as a result of low activity observed at deeper sections of the sediment core (discussed previously in section 6.6.2.1), [b] Date and pre-industrial Sb concentration taken from the mini-Mackereth sediment core since the Jenkin core was not dated prior to 1900, and were both sampled at the same site on the same day, [c] The earliest date of when the peat or sediment core chronology began, [d] Maximum Sb enrichment factor = (maximum Sb concentration/ Sb concentration from the bottom depth section of the date core).

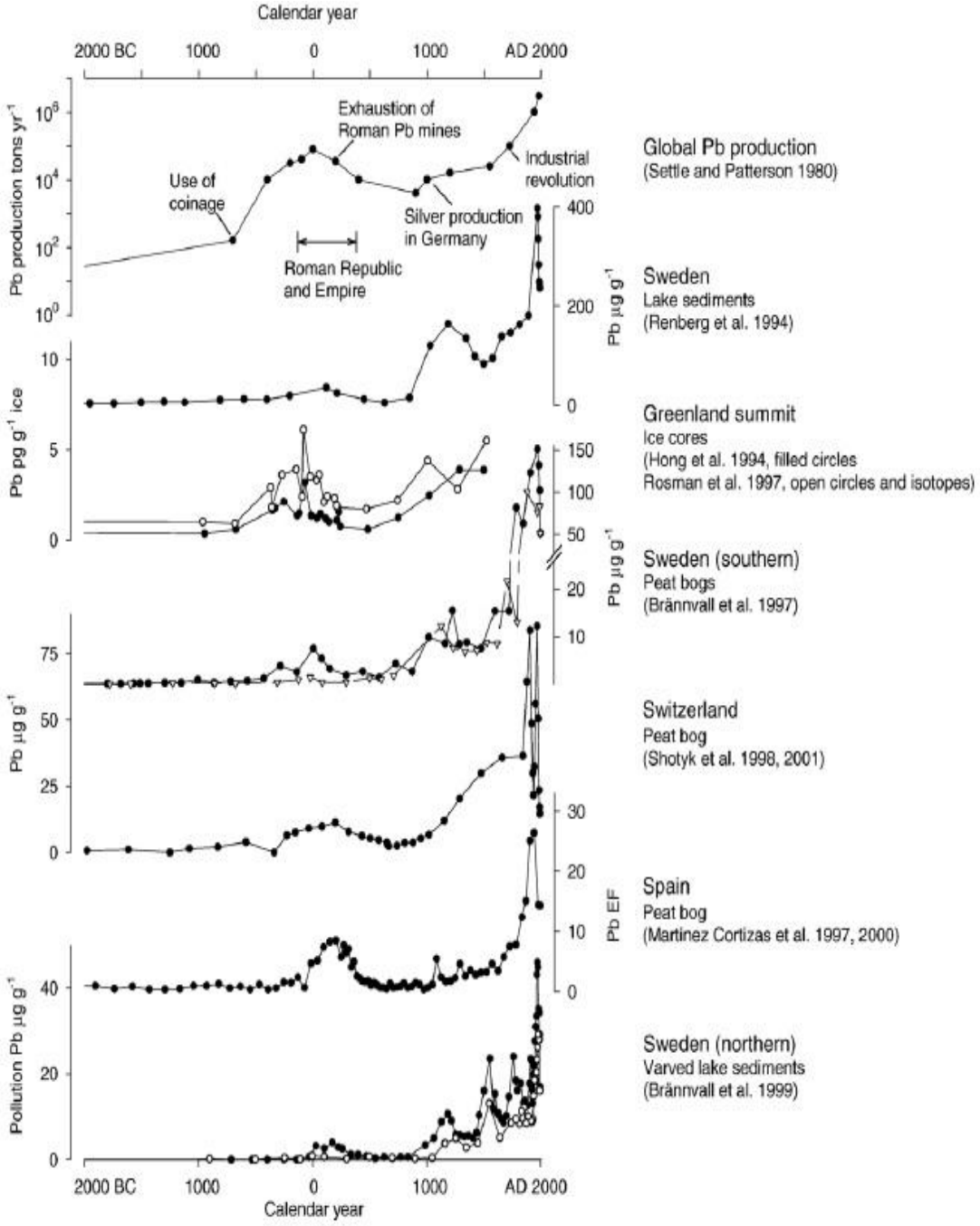

Figure 7.18: Comparisons of Pb chronological archives in glacial ice, peat cores and lake sediments (Bindler, 2006)

Whilst there was very good agreement for Sb deposition chronologies when peat cores from Great Moss and Auchencorth Moss were compared with ice cores, a slight difference in the date of Sb enrichment was observed for Loch Tay sediment cores (Table 7.5). For example, Loch Tay sediment Sb concentrations notably increased ~1850, which was ~20 years earlier

than a similar increase was observed in Great Moss and the ice cores (Table 7.5, Figures 6.9 and 6.14). Thereafter, all sediment and ice core concentrations declined towards the end of the 20th century. The difference for Sb enrichment dates for sediment and ice cores is most likely a result of local factors. As Loch Tay is located approximately 80 km north of Glasgow, early emissions from coal combustion and metal smelting from Glasgow during the 19th century would have greatly influenced Loch Tay sediment concentrations. Indeed, this was comparable with Pb data from Loch Lomond sediment by Eades *et al.*, (1999). Although the focus of this study was for Pb, emissions of Sb would have similarly occurred from the same industrial process of those for Pb. The slightly earlier date of increase for Sb deposition would not have been found in ice core chronologies, since no nearby source emissions exist, nor would it have been found in the Great Moss peat core, since no significant mid-19th century source emissions were nearby. Both sediment cores did, however, show a similar level of Sb enrichment to the ice cores (Table 7.5), where a 5-fold increase in Sb concentrations were observed when compared with Sb concentrations from ~1700.

In contrast to Sb, a considerably larger number of studies using ice cores to construct chronologies for Pb deposition exist (WHO, 1978; Needlemen *et al.*, 1979; Tera *et al.*, 1985; Sturges and Barrie, 1987; Delves and Campbell, 1993). Using the previously mentioned study by Bindler (2006) as a starting point (Figure 7.18), long-term atmospheric Pb deposition studies using ice cores have been shown to match not just peat and sediment cores sampled from remote locations, but the global Pb production throughout previous millennia. The comparison of dated Pb deposition profiles from Great Moss and Auchencorth Moss peat cores to the study by Binder (2006) and ice core studies detailed in Table 7.6, showed excellent agreement. For example, both peat cores showed a significant Pb enrichment beginning the early ~20th century, increasing significantly to ~1950s, and declining towards the end of the 20th century. The trend for Pb enrichment over time was comparable to results obtained from the previously mentioned ice core study from the Arctic (Figure 7.19)

(Krachler *et al.*, 2005). With respect to maximum Pb enrichment, however, both peat cores appeared to differ somewhat more to the Arctic ice core, where the Great Moss (eight-fold) and Auchencorth Moss (nine-fold) Pb enrichment was lower than the Arctic ice core (fifteen-fold). Differences such as these can often be related to climatic conditions, where high amounts of precipitation, as observed in the Arctic, can increase the rate of Pb deposition. More comparable Pb enrichment values to Great Moss and Auchencorth Moss were obtained from ice core studies from Nepal (X8) and Canada (X8) (Osterberg *et al.*, 2008; Lee *et al*., 2011) (Table 7.6). For these ice core studies however, concentrations of Pb peaked later than those observed in Great Moss and Auchencorth Moss; maximum concentrations of Pb in ice cores from Nepal and Canada occurred in 1997 and 1980, respectively.

Very few similarities were observed between Pb chronologies observed in Loch Tay sediment and ice core studies shown in Table 7.6. This was expected, given the significant influence of Pb mining at Tyndrum had on Loch Tay sediment concentrations of Pb. For instance, shortly after Pb mining at Tyndrum began ~1730, sediment concentrations of Pb increased by ~200 mg kg^{-1}, contrasting with ice core studies (and peat cores) for that time, where very little evidence of anthropogenic activity was observed. Additionally, no broad peak in Pb concentrations was observed throughout the 20th century for the Loch Tay sediment cores, which was inconsistent with the ice cores shown in Table 7.6. The influence of Tyndrum Pb mine was also observed in the maximum Pb enrichment factors, where up to a thirty-seven-fold increase in sediment concentrations of Pb were seen ~1915, when compared with early 18th century background concentrations. The one similarity observed between both archive materials was the decreasing trend of Pb concentrations towards the 21st century, where Pb mining had stopped, and improved technology and regulation had reduced Pb emissions from coal combustion. Clearly, the Loch Tay sediment chronologies for Pb were considerably influenced by local factors, which resulted in a different chronology when compared to those established in ice cores.

Table 7.6: Comparison of Pb profiles of ^{210}Pb dated Pb concentrations, Pb enrichment periods, maximum Pb concentrations and enrichment factor for ice, peat and sediment cores.

Archive material	Location	Reference	Pb concentration taken from the bottom depth section of the dated core.		Beginning and end of dates for broad peak in Pb concentrations		Date and maximum Pb concentration observed		Maximum Pb enrichment factor [d]
			Date	Concentration	from	To	Date	Concentration	
Ice	Arctic	Krachler *et al.* (2005)	1840	10.0 pg g^{-1}	1900	1995	1965	145 pg g^{-1}	X15
Ice	Nepal	Lee *et al*, (2011)	1865	61 pg g^{-1}	1900	2002	1997	504 pg g^{-1}	X8
Ice	Canada	Osterberg *et al*. (2008)	1730-1910	8.9 pg g^{-1}	1910	2000	1981-1998	68.9 pg g^{-1}	X8
Peat	Great Moss, Scotland	Farmer *et al*. (2015)	1782	17.0 mg kg^{-1}	1850	2000	1962	139 mg kg^{-1}	X8
Peat	Auchencorth Moss, Scotland	Macgregor, (2015)	~1850	21.7 mg kg^{-1}	1900 [c]	2006	1933	194 mg kg^{-1}	X9
Sediment	Mini-Mackereth, Loch Tay, Scotland	Macgregor, (2015)	est. 1700 [a]	17.0 mg kg^{-1}	1730	1990	1915	500 mg kg^{-1}	X30
Sediment	Jenkin, Loch Tay, Scotland	Macgregor, (2015)	est. 1700 [a]	17.0 mg kg^{-1} [b]	1900 [c]	1990	1910	630 mg kg^{-1}	X37

[a] Estimated ^{210}Pb date as a result of low activity observed at deeper sections of the sediment core (discussed previously in section 6.6.2.1), [b] Date and pre-industrial Sb concentration taken from the mini-Mackereth sediment core since the Jenkin core was not dated prior to 1900, and were both sampled at the same site on the same day, [c] The earliest date of when the peat or sediment core chronology began, [d] Maximum Sb enrichment factor = (maximum Sb concentration/ Sb concentration from the bottom depth section of the date core).

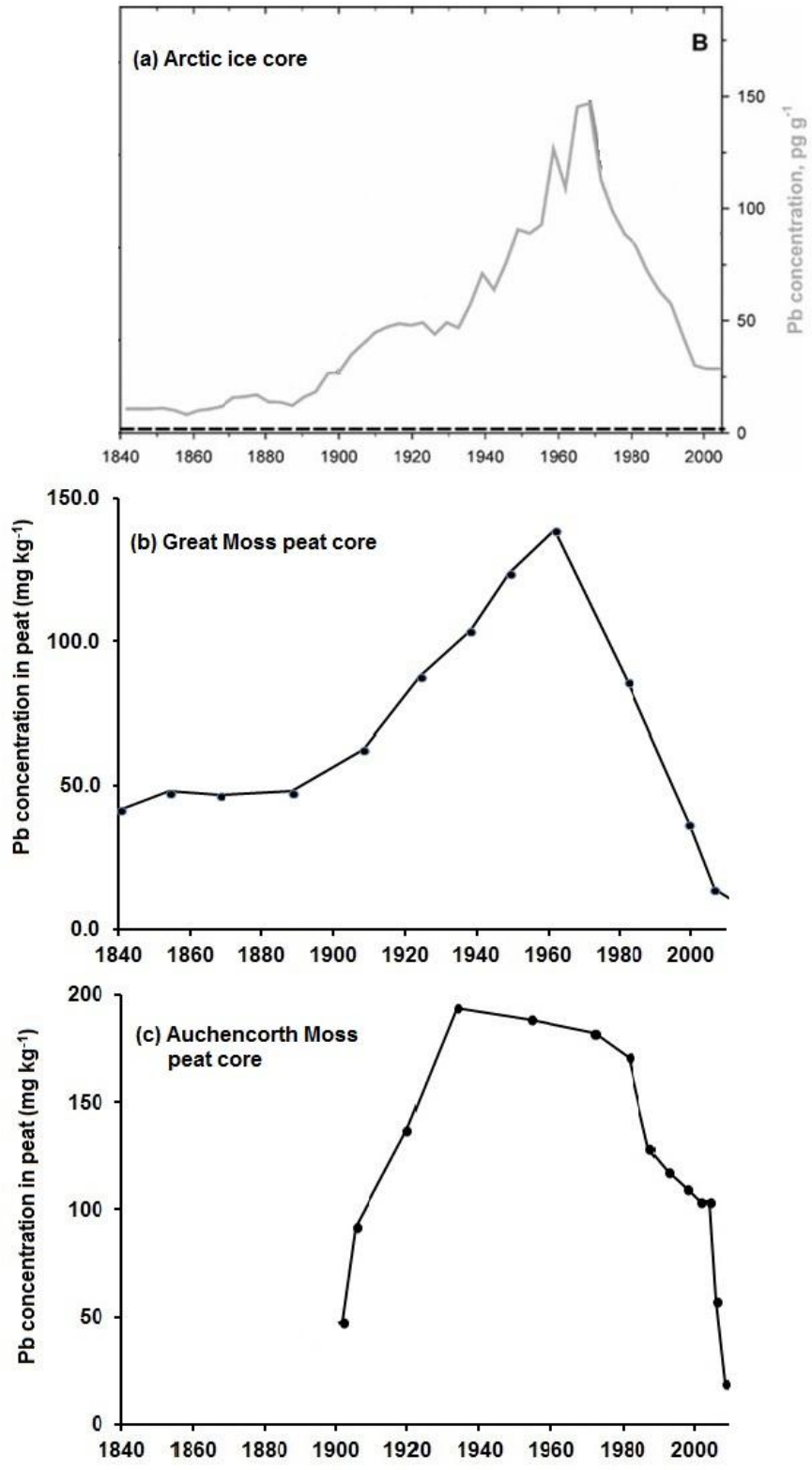

Figure 7.19: Comparison of temporal variations in Pb concentrations dated for: a) Devon Island Canadian arctic ice core (Kratchler *et al.,* 2005), b) Great Moss peat core and c) Auchencorth Moss peat core.

7.10 Chapter conclusions

Deposition records of Sb and Pb found at Great Moss were well-preserved and showed an accurate account of Sb and Pb fluxes from previous centuries. During the 19th century, Sb fluxes increased by a factor of 10 to 0.30 mg cm^{-2} y^{-1}, while an increase by a factor of 4 to 16 mg cm^{-2} y^{-1} was also observed for Pb fluxes at the start of the Industrial Revolution. The rise in both Sb and Pb fluxes continued into the 20th century, where large Sb and Pb flux peaks were observed at 1924 and 1950, respectively. For the early to mid-20th century, Sb fluxes rose to ~0.71 mg cm^{-2} y^{-1}, with corresponding Pb fluxes increasing to ~33 mg cm^{-2} y^{-1}. Thereafter, a considerable decline in Sb and Pb fluxes occurred towards 2011. This was in agreement with literature (Bindler *et al*., 2004; Farmer *et al*., 2005, 2015; Cloy *et al*., 2009; Allan *et al*., 2013), where Sb and Pb enrichment was the result of anthropogenic activities such as the combustion of coal, and from mining and smelting operations up until the mid-20th century. Latterly, Pb fluxes were greatly influenced by leaded petrol, where typically low ^{206}Pb/^{207}Pb isotopic ratios of 1.136 ± 0.004 in the 1980s indicated Australian Pb input from leaded petrol emissions.

At Auchencorth Moss, historic deposition records of Sb and Pb found in the peat core were unusual, as both elements, along with Ti, demonstrated perturbations in the vertical concentration profiles for the peat core that were consistent with post-depositional mobility. This was not typical behaviour for Sb, Pb and Ti, as they are not redox-sensitive elements and not renowned for post-depositional mobility in the peat environment. Upon examination of vertical concentrations of Mn and Fe, concentration enrichments for Mn occurred in the top 5 cm of the peat core, whilst a notable sub-surface peak for Fe occurred at the depth of ~10 cm. Both near surface and sub-surface peaks for Mn and Fe occurred at comparable depths observed for Ti, Sb and Pb sub-surface enrichments (7 cm). The redox cycling of Mn and Fe, and the subsequent release of previously bound elements to the porewater resulted in the mobilisation of Sb, Pb and Ti to upper sections of the core. The perturbations in vertical Mn, Fe, Sb, Pb and Ti concentrations all occurred in the vegetation layer, where they were

influenced by a change in environmental conditions as a result of vertical movement in the water-table. This was consistent with the depth of the water table at the time of sampling, where moisture content of peat layers indicated the water table rested at a depth of ~5-10 cm. Furthermore, uncharacteristic ^{210}Pb activity was also observed throughout the peat core. Typically, ^{210}Pb activity declines exponentially with depth, and his however, did not occur at Auchencorth Moss, where activity remained fairly stable in the top 20 cm of the core. Moreover, a ^{210}Pb activity peak occurred at a depth of 7 cm which coincided with concentration peaks for Sb, Pb and Ti. A similar vertical depth profile for Sb, Pb and Ti concentrations was observed at another ombrotrophic peat bog in Scotland, Flanders Moss (Cloy *et al*., 2009). Comparable concentration peaks were found in the top sections of the peat core, and demonstrated that under specific environmental conditions, Sb, Pb and Ti can become mobile in the peat environment.

Due to the post-depositional mobility of Sb and Pb at Auchencorth Moss, well preserved fluxes were only obtained from 1900 to ~1970. For this period, Sb fluxes in the early 20th-century peaked (0.22 mg cm^{-2} y^{-1}) and declined towards 1970, as emissions from coal combustion and mining and smelting activities decreased. Fluxes for Pb over the 70 year duration were generally stable (~15 mg cm^{-2} y^{-1}), with a small decline observed in mid-20th century (12 mg cm^{-2} y^{-1}). When Sb and Pb dated flux profiles were compared to other Scottish ombrotrophic peat bogs, it appeared that peak Sb and Pb enrichments from anthropogenic activity occurred ~20 years earlier than at other sites. This was similarly seen at other locations across Europe, such as the Jura Mountains in Switzerland (Shotyk *et al*., 1996).

Although values of Sb/Pb ratios at Great Moss were twice those found at Auchencorth Moss, both sites showed comparable trends over time spanning 1900 to 2008. The Sb/Pb dated profile was similar to previously published results from other Scottish peat bogs (Cloy *et al*., 2009). A contemporary Sb/Pb ratio range of 0.037-0.052 was observed at Great Moss and at

three other Scottish peat bogs (Cloy *et al*., 2009), which closely matched Sb/Pb ratios found in Edinburgh and Glasgow road dust (0.036). This comparison had not been made in previous research, and providing no evidence of post-depositional mobility has been observed for Sb, Pb and Pb isotopes, ombrotrophic peat bog cores provide a suitable environment to assess current atmospheric deposition for these elements.

Chapter 8 Conclusions

8.1 Project conclusions

8.1.1 The release and behaviour of Sb, Pb, Cu, Zn and PAHs from historic and contemporary sources in the urban environment

Elemental (Sb, Pb, Cu, Zn) and priority 16 PAH concentrations were determined in road dust sampled from five high- and five low-traffic locations in Edinburgh, where road dust from each location was collected at distances of 10 and 50 m from the closest road junction. Results showed that there was no significant difference between the elemental concentrations in the samples from the 10 m and those from the 50 m locations ($t>0.36$, $p>0.37$), nor was there any difference between contaminant concentrations in samples from roads that were mechanically cleaned and those that were not. Taking the contaminant concentrations determined in road dust from both five high- and five low-traffic roads sampled at 10 and 50 m from the CRJ, mean concentrations for Sb, Cu and Zn were 5.3 ± 2.8 mg kg^{-1}, 91.4 ± 48 mg kg^{-1} and 237 ± 144 mg kg^{-1}, respectively, and were similar to road dust sampled from five high- and five low-traffic locations in Glasgow (Sb 4.5 ± 2.1 mg kg^{-1}; Cu 117 ± 71.9 mg kg^{-1}; Zn: 283 ± 146 mg kg^{-1}). This was in contrast to mean concentrations for Pb and Σ16PAHs obtained from Glasgow (Pb 250 ± 283 mg kg^{-1}, Σ16PAH 7.7 ± 4.3 mg kg^{-1}) where the respective values were approximately double and two-thirds greater than those found in Edinburgh (Pb 135 ± 129 mg kg^{-1}, Σ16PAH 4.7 ± 2.9 mg kg^{-1}). Although annual average daily flow (AADF) data for Edinburgh road dust locations were generally higher than those of Glasgow, it was concluded that the greater traffic numbers experienced citywide for Glasgow (~30% more than Edinburgh citywide), and the legacy of Glasgow's industrial past accounted for the higher concentrations of Pb and Σ16PAH observed here.

The source of priority 16 PAHs and Pb to road dust concentrations was apportioned using PAH diagnostic and stable Pb isotopic ratios, respectively. Diagnostic ratio analysis indicated that PAHs present in dust samples originated from the combustion of petroleum,

and grass, wood and coal. These results was not unexpected since it is well-known that road traffic emissions are a dominant source of PAHs in urban areas of the UK (Dore *et al.*, 2008) and combustion of wood and then coal was an intrinsic part of past industrial activities (Lohmann *et al.*, 2000). The range of $^{206}Pb/^{207}Pb$ isotopic ratios in road dust from Edinburgh (~1.12-~1.15) were notably lower than the range observed in dusts from Glasgow (~1.14-~1.17). Since recent rainwater has $^{206}Pb/^{207}Pb$ ratio values of ~1.15-1.16, the low values in Edinburgh dust samples strongly suggest that the influence of leaded petrol has persisted some 15 years after the ban in its use. A significant trend was also found at three road dust locations ~2 km north of major road routes in/out of Edinburgh (M8, Glasgow Road and the Edinburgh Bypass) ($t=6.9$, $p=0.002$, $n=17$), where the road dust isotopic ratios were notably lower than all other sites in this study (1.102-1.121). These locations, close to the major motorway routes on the west of the city (M8 and M9), were especially influenced by past emissions from leaded petrol, and to a lesser degree, emissions from avgas, consistent with the mean annual wind direction for Edinburgh. Although combustion emissions from leaded fuels also influenced Pb isotope ratios observed in Glasgow road dust, there was a greater influence from indigenous Pb sources, attributable to continued impact of emissions from past industrial activities such as metal smelting, engineering works and coal combustion, e.g. via remobilisation of contaminated soil and weathered urban materials from old industrial sites. This was particularly evident at two locations in Glasgow (Black Street, Goosedubbs) and also at two in Edinburgh (Cambusnethan Street, Thistle Street). For Black Street, situated in a Glasgow industrial estate, elevated road dust concentrations of Pb and Σ16PAHs were most likely a result of local emissions originating from nearby industrial units. The impact of historic land use on road dust was also observed at Cambusnethan Street and four locations in the surrounding area. Elevated elemental concentrations in road dust from these locations were associated with past industrial activity that occurred in the vicinity, such as a metal foundry (Miller and Co) used from 1867-1991, and St Margaret's railway depot which was operational until the late 1960s. Elevated contaminant concentrations observed at

Goosedubbs and Thistle Street were attributed to the difference in the road surface (setted vs tarmac), where enhanced vehicle wear from the uneven setted road and the accumulation of deposited contaminants between cracks and jointing of the setts would account for the contaminant concentrations observed here.

The retention of elements by road dust and their potential to be transferred into the aqueous phase was determined by road surface water analysis, sequential extraction analysis of road dust, and the analysis of road dust composition via XRD and SEM-EDX. Edinburgh road surface water samples collected from each high- and low-traffic location showed mean concentrations of Sb and Pb of 0.64 ± 0.45 µg L^{-1} and 1.25 ± 1.02 µg L^{-1}, respectively. Higher concentrations were observed for Cu (18.6 ± 14 µg L^{-1}) and Zn (84.0 ± 91 µg L^{-1}). Sequential extraction results indicated that a high proportion of Zn had the potential to be mobilised into the aqueous phase (~37-63% of total Zn present in BCR1), followed by Cu (~22-54% of total Cu present in BCR1), with Pb and Sb showing very little of total concentrations available in BCR1, and were highest at 21% and 3%, respectively. This was in agreement with surface water results, where surface water concentrations were greatest for the elements that showed a greater potential to be mobilised in the BCR1 fraction; ease of mobilisation followed the order Zn>Cu>Pb>Sb. The composition of road dust was investigated using XRD and SEM-EDX, and revealed that quartz comprised ~54% of the road dust samples, with smaller contributions from albite and anorthite at ~12 and 8%, respectively. Although Pb bound to carbonates, such as calcite at Thistle Street may increase Pb mobility, Sb and Pb were largely retained by road dust, whilst Zn and Cu showed a greater potential to become mobilised into the aqueous phase.

8.1.2 The release and behaviour of Sb, Pb and As from former mining sites in the rural environment

The primary source of elemental contaminants to the rural environment was from past anthropogenic activity. Two examples of this were found at former mining sites, an Sb mine at Glendinning in southern Scotland and a Pb mine at Tyndrum in central Scotland, where upon closure, no remedial action was implemented to prevent the release of elements into the surrounding soil and aquatic environment. Although the nature of ore extracted at both locations differed, the analysis of soil or sediment affected by mining activity provided the means to monitor the transport and fate of all three main contaminants, Sb, Pb and As. At both mining sites, and under specific conditions, Sb was found to be both mobile and immobile in soil and sediment. For example, the chemical weathering of stibnite found in spoil heaps at Glendinning Sb mine demonstrated that ~3% of total Sb can be mobilised during oxidative dissolution at a pH of 5.0 and 6.6. The dissolution and transport of Sb at Glendinning Sb mine was specifically shown to originate from a mineral-rich spoil heap, downhill into surrounding soils and the Glenshanna Burn. Once in the aqueous form, porewaters from soil cores (S1-S6) showed that Sb was largely present in the truly dissolved form (<3 kDa) and was not retained by soil to the same degree as As and Pb. Porewater speciation analysis for Sb using two soil cores (S4A and S5A) near the large spoil heap revealed that Sb was largely present as Sb(V), contributing ~94% towards total Sb concentrations present. Indeed, Sb speciation results for this study were in agreement with a study by Mitsunobu *et al*. (2006), and were consistent with the greater stability as Sb(V) in soil-water systems. In general, the porewater behaviour of Sb highlighted its loss from deeper sections of certain cores, and its transport over distances of 50 m down steeper sections of the catchment to receiving waters. Where Sb was retained by soil, retention occurred near the surface in cores S1-S5, and Sb was found to be associated with organic matter and Fe oxides. At Loch Tay, in the vicinity of the Tyndrum Pb mining site, Sb retention and immobility was evident within the bottom sediments; a change in redox

conditions in two sediment cores mobilised other elements, such as Mn, Fe and As, but did not affect Sb. Here the immobility of Sb allowed deposition chronologies to be established, and there was excellent agreement between mini-Mackereth and Jenkin sediment core chronologies. Both chronologies identified atmospheric deposition as the primary source of Sb to Loch Tay sediment, with little influence of Sb transported downstream from the Pb mining site. This was in agreement with the Sb/Pb ratio found in Tyndrum Pb ore (0.0003), which signified an extremely low Sb content in the Tyndrum Pb ore, and instead indicated that emissions from coal combustion (Sb/Pb ratio: 0.036 ± 0.032) and the smelting of Wanlockhead ore (Sb/Pb ratio: 0.0056± 0.0004) were the primary source of Sb to Loch Tay sediment. Moreover, the atmospheric deposition chronology for Sb in Loch Tay sediment was similar to other peat chronologies observed during the 19th and 20th century (Cloy *et al*., 2009; Allan *et al.*, 2013).

The behaviour of Pb in the aquatic and terrestrial environment has been covered, to a certain extent, in previous studies. For Glendinning Sb mine, concentrations of Pb in soil (S2) reached 710 mg kg^{-1}, while aqueous concentrations downstream of the mine were low, consistent with its strong affinity for the soil solid phase. Although the vertical concentration profiles for Pb followed the trend for Fe in all soil cores, sequential extraction results suggested that this association was not exclusive, and that organic matter was also an influential factor for retaining Pb in the soil. The examination of porewaters from S2-S6 revealed that Pb and Fe were almost exclusively present in the colloidal fraction (70-100%) showing that Pb solubility is enhanced by association with both organic matter and Fe-rich colloids. The strong affinity of Pb for the solid phase was also observed in Loch Tay sediment, where upon deposition, Pb remained immobile and was not susceptible to redox cycling as observed for other elements. As shown for Sb, excellent agreement was found for constructed Pb deposition chronologies for both Loch Tay sediment cores, and indicated considerable Pb pollution had occurred from the release of Pb to Loch Tay, as a result of

upstream mining activities. This was consistent with a notable peak for sediment concentrations of Pb and a change in associated Pb isotope ratios occurring ~1915, coinciding with the reprocessing of mining dumps prior to the closure of Tydrum Pb mine in 1928. Thereafter, the dominant input of Pb to Loch Tay sediment was from the combustion of coal and leaded petrol. A decline in sediment concentrations of Pb began ~1980s, and continued towards the end of the 20th century, where improved technology and regulation for coal combustion and the phasing out of leaded petrol use in 1986 in the UK all reduced the atmospheric emissions of Pb. A continuing reduction in sediment concentrations of Pb was also observed from 1990 to 2003 (separate Jenkin cores denoted core#1 and #2).

In comparison with Sb and Pb, As had the greatest mobility at both mining sites. At the Glendinning Sb mine, As was also affected by chemical weathering on the two spoil heaps, and as observed for Sb, this resulted in its dissolution from the solid phase to the aqueous phase. Once in the aqueous phase, As was found present in both truly dissolved and colloidal fractions, where its association with large Fe-rich organic colloids favoured its retention by the solid phase. The greater mobility of As, relative to Sb and Pb, was demonstrated in elemental concentrations observed in Glenshanna Burn, where considerably higher concentrations of As (13.2 ± 1.14 μg L^{-1}) were found in Glenshanna Burn when compared with Sb (5.88 ± 0.29 μg L^{-1}) and Pb (0.07 ± 0.03 μg L^{-1}). The greater mobility of As observed at Glendinning Sb mine was also evident in results obtained from Loch Tay sediment, where As was shown to exhibit post-depositional mobility, along with the redox-active elements, Mn and Fe. Although more distinguishable in the As vertical concentration profile obtained in the mini-Mackereth sediment core than the Jenkin core, both cores revealed a sub-surface peak at a depth of ~11 cm for As concentrations. Vertical concentrations of Arsenic showed the greatest variability between the two sediment cores, and were most likely a result of slight changes in the redox conditions and influence it has on As.

8.1.3 The use of peat reference sites to establish atmospheric Sb and Pb deposition chronologies

Well-preserved historic records of Sb and Pb deposition over several centuries were established at Great Moss. During the 19th century, Sb fluxes increased by a factor of 10 to 0.30 mg cm^{-2} y^{-1}, while an increase by a factor of 4 to 16 mg cm^{-2} y^{-1} was observed for Pb fluxes at the start of the Industrial Revolution. The rise in both Sb and Pb fluxes continued into the 20th century, where large Sb and Pb flux peaks were observed at 1924 and 1950, respectively. For the early to mid-20th century, Sb fluxes rose to ~0.71 mg cm^{-2} y^{-1}, with corresponding Pb fluxes increasing to ~33 mg cm^{-2} y^{-1}. Thereafter, a significant drop in Sb and Pb fluxes occurred towards 2011. This was in agreement with literature (Bindler *et al*., 2004; Farmer *et al*., 2005, 2015; Cloy *et al*., 2009; Allan *et al*., 2013), where Sb and Pb enrichment was the result of anthropogenic activities such as the combustion of coal, and from mining and smelting operations up until the mid-20th century. Latterly, Pb fluxes were greatly influenced by leaded petrol, where typically low $^{206}Pb/^{207}Pb$ isotopic ratios of 1.136 ± 0.004 in the 1980s indicated Australian Pb input from leaded petrol emissions.

At Auchencorth Moss, historic deposition records of Sb and Pb found in the peat core were unusual, as both elements, along with Ti, demonstrated perturbations in the vertical concentration profiles for the peat core that were consistent with post-depositional mobility. This was not typical behaviour for Sb, Pb and Ti, as they are not redox-sensitive elements and not renowned for post-depositional mobility in the peat environment. Upon examination of vertical concentrations of Mn and Fe, concentration enrichments for Mn occurred in the top 5 cm of the peat core, whilst a notable sub-surface peak for Fe occurred at the depth of ~10 cm. Both near surface and sub-surface peaks for Mn and Fe occurred at comparable depths observed for Ti, Sb and Pb sub-surface enrichments (7 cm). The redox cycling of Mn and Fe, and the subsequent release of previously bound elements to the porewater resulted in the mobilisation of Sb, Pb and Ti to upper sections of the core. The perturbations in vertical

Mn, Fe, Sb, Pb and Ti concentrations all occurred in the vegetation layer, where they were influenced by a change in environmental conditions as a result of vertical movement in the water-table. This was consistent with the depth of the water table at the time of sampling, where moisture content of peat layers indicated that the water table rested at a depth of ~5-10 cm. Furthermore, uncharacteristic ^{210}Pb activity was also observed throughout the peat core. Typically, ^{210}Pb activity declines exponentially with depth, and this however, did not occur at Auchencorth Moss, where activity remained fairly stable in the top 20 cm of the core. Moreover, a ^{210}Pb activity peak occurred at a depth of 7 cm which coincided with concentration peaks for Sb, Pb and Ti. A similar vertical depth profile for Sb, Pb and Ti concentrations was observed at another ombrotrophic peat bog in Scotland, Flanders Moss (Cloy *et al*., 2009). Comparable concentration peaks were found in the top sections of the peat core (again in the vegetation layer), and demonstrated that under specific environmental conditions, Sb, Pb and Ti can become mobile in the peat environment.

Despite the post-depositional mobility of Sb and Pb at Auchencorth Moss, it was possible to establish deposition chronologies from 1900 to ~1970. Over the 70 year period, Sb fluxes peaked early in the 20th-century (0.22 mg cm^{-2} y^{-1}) and declined towards 1970, where emissions from coal combustion and mining and smelting activities decreased. Fluxes for Pb over the 70 year duration were generally stable (~15 mg cm^{-2} y^{-1}), with a small decline observed ~mid-20th century (12 mg cm^{-2} y^{-1}). Although the dated flux profile for Sb and Pb showed reasonable agreement to peat core chronologies from Turclossie Moss, Red Moss of Balerno, Flanders Moss and Carsegowan Moss (Cloy *et al.*, 2009), the date at which Sb and Pb peak flux occurred was ~20 years earlier.

Although values of Sb/Pb ratios at Great Moss were twice those found at Auchencorth Moss, both sites showed comparable trends over time spanning 1900 to 2008. The Sb/Pb dated profile was similar to previously published results from other Scottish peat bogs (Cloy *et al*., 2009). A contemporary Sb/Pb ratio range of 0.037-0.052 was observed at Great Moss and at three other Scottish peat bogs (Cloy *et al*., 2009), which closely matched Sb/Pb ratios found

in Edinburgh and Glasgow road dust (0.036). This comparison had not been made in previous research, and where there is no evidence of post-depositional mobility Sb and Pb, ombrotrophic peat bog cores provide a suitable environment to assess current atmospheric deposition for these elements.

8.1.4 Closing summary

The well-preserved historic records for contaminant deposition in Loch Tay sediment and the Great Moss ombrotrophic peat bog provided an accurate account of current and past contaminant release from anthropogenic activity. The release of contaminants from mining and smelting activities is still observed in rural and urban parts of Scotland today, such as soil and water from Glendinning Sb mine, and road dust from Edinburgh and Glasgow. More recent anthropogenic processes, i.e. vehicular transport, was also identified to have released considerable quantities of contaminants to the environment, specifically Pb and Sb. Whilst this study examined the release and deposition of a range of contaminants (Sb, Pb, As, Cu, Zn and PAHs) in urban and rural parts of Scotland, there was a specific focus on Sb, and its occurrence with Pb.

Understanding the retention and transport of Sb and Pb in the soil-water environment from their deposition, or from their natural occurrence, is important for predicting environmental conditions that would increase their mobility and therefore impact on receiving waters. Under specific conditions, Sb was found to be both mobile and immobile in the environment; mobility was demonstrated in the chemical weathering of Sb-containing minerals, whereas OM and Fe oxides present in soil were identified to retained Sb. Further examination of soil porewaters revealed that Sb present was found largely as Sb(V), which contributed to ~94% of total porewater concentrations. While Sb demonstrated greater mobility in the soil-water environment than Pb, both were generally immobile in sediment and peat, which allowed their atmospheric deposition profiles to be established as shown in Loch Tay sediment and Great Moss peat. One exception to these findings, however, was identified in a peat core

sampled from Auchencorth Moss, where Sb and Pb, as well as Mn, Fe and Ti exhibited post-depositional mobility. The upwards migration of elements via redox cycling was a result of an uncharacteristic deep vegetation layer, where the vertical movement of the water table caused a change in the environmental conditions.

8.1.5 Further research directions and challenges

Whilst this study addresses a number of questions raised by results obtained in this research, there are however, areas that could benefit from future work.

For Glendinning Sb mine, a greater understanding of As speciation present at sampling sites S4-6 would elucidate differences observed in Sb and As speciation in soil porewater, and add to current data indicating a difference in mobility for these locations. Method development would be required to determine As species present in soil porewaters; however, the same instrumentation and ion exchange column used for Sb speciation could also determine concentrations of As species present. In addition, further refinement of soil porewater sampling for Sb speciation analysis should be considered. The preservation of oxygen sensitive species such as Sb(III) and As(III) may be controlled more effectively by using a hyporheic zone multilevel sampler. Traditionally, the application of multilevel samplers were for the extraction of porewaters from sediment but its use to extract porewater from waterlogged organic soil, as observed at Glendinning Sb mine, would improve method performance.

Further research at Auchencorth Moss should be carried out to understand the geochemical processes that influence the behaviour of Sb and Pb for this location. The research should delineate the principle factors causing Sb and Pb mobility at Auchencorth Moss, and should consider Mn and Fe redox cycling, as well as plant nutrient cycling. This would incorporate the sampling and elemental analysis of peat cores and respective porewaters for several spatially targeted peat cores across Auchencorth Moss, while elemental associations in the

peat should be determined using sequential extraction, porewater isolation and gel electrophoresis techniques.

References and bibliography

Abadin, H., Ashizawa, A., Stevens, Y.-W., Llados, F., Diamond, G., Sage, G., Citra, M., Quinones, A., Bosch, S.J., Swarts, S.G., 2007. Toxicological Profile for Lead, Agency for Toxic Substances and Disease Registry (ATSDR) Toxicological Profiles. Agency for Toxic Substances and Disease Registry (US), Atlanta (GA).

Abedin, M.J., Howells, J.C., and Meharg, A.A., 2002a, Arsenic uptake and accumulation in rice (Oryza sativa L.) irrigated with contaminated water. Plant and Soil, 240, 311–319.

Abedin, M.J., Feldmann, J., and Meharg, A.A., 2002b, Uptake kinetics of arsenic species in rice plants. Plant Physiology, 128, 1120-1128.

Abu-El-Wafa, S.M., Issa, R.M., McAuliffe, C.A., 1985. Unusual Cu(III) Schiff's base complexes. Inorganica Chimica Acta 99, 103–106. doi:10.1016/S0020-1693(00)86056-9.

Ackermann, S., Gieré, R., Newville, M., Majzlan, J., 2009. Antimony sinks in the weathering crust of bullets from Swiss shooting ranges. Science of the Total Environment 407, 1669–1682. doi:10.1016/j.scitotenv.2008.10.059.

Agency for Toxic Substances and Disease Registry. Toxicological profiles for zinc, p 139, http://www.atsdr.cdc.gov/toxprofiles/tp60-c6.pdf (accessed 20/02/2016).

AIRUSE. 2013. Scientific basis of streeting cleaning activities as road dust mitigation measure. LIFE 1 ENV/ES/584.

Amato, F., Pandolfi, M., Moreno, T., Furger, M., Pey, J., Alastuey, A., Bukowiecki, N., Prevot, A.S.H., Baltensperger, U., Querol, X., 2011. Sources and variability of inhalable road dust particles in three European cities. Atmospheric Environment 45, 6777–6787. doi:10.1016/j.atmosenv.2011.06.003.

Amato, F., Font, O., Moreno, N., Alatuey, A., Querol, X., 2012. Mineralogy and elemental composition of brake pads. SEM/SEA, no16.

Analytical Instruments. http://analyticalprofessional.blogspot.co.uk/p/oil.html (accessed 27th of March 2015).

Anawar, A.H., Akai,J., Komaki, K., Terao, H., Yoshioka, T., Ishizuka, T., Safiul-lah, S., Kato, K. 2003. Geochemical occurrence of arsenic in groundwater of Bangladesh: sources and mobilization processes, Journal of Geochemical Exploration. 77, 109–131.

Ahrens, L.H., 1965. Distribution of the Elements in Our Planet. McGraw-Hill, New York. Mason, B., 1966. Principles of Geochemistry. 3rd edn. Wiley, New York.

Ali, M., Choudhury, T.R., Hossain, B., Ali, M.P., 2014. Determination of traces of molybdenum and lead in foods by x-ray fluorescence spectrometry. SpringerPlus 3, 341. doi:10.1186/2193-1801-3-341.

Allen, J.R.L., Rae, J.E., Zanin, P.E., 1990. Metal speciation (Cu, Zn, Pb) and organic matter in an oxic salt marsh, Severn Estuary, southwest Britain. Marine Pollution Bulletin 21, 574–580. doi:10.1016/0025-326X(90)90606-9.

Allan, M., Le Roux, G., De Vleeschouwer, F., Bindler, R., Blaauw, M., Piotrowska, N., Sikorski, J., Fagel, N., 2013. High-resolution reconstruction of atmospheric deposition of trace metals and metalloids since AD 1400 recorded by ombrotrophic peat cores in Hautes-Fagnes, Belgium. Environmental Pollution 178, 381–394. doi:10.1016/j.envpol.2013.03.018.

Amato, F., Pandolfi, M., Moreno, T., Furger, M., Pey, J., Alastuey, A., Bukowiecki, N., Prevot, A.S.H., Baltensperger, U., Querol, X., 2011. Sources and variability of inhalable road dust particles in three European cities. Atmospheric Environment 45, 6777–6787. doi:10.1016/j.atmosenv.2011.06.003.

Amereih, S., Meisel, T., Kahr, E., Wegscheider, W., 2005. Speciation analysis of inorganic antimony in soil using HPLC-ID-ICP-MS. Analytical and Bioanalytical Chemistry 383, 1052–1059. doi:10.1007/s00216-005-0049-y.

Amouroux, D.,Anschutz, P., Jouanneau, J., Gilbert, F., Rabouille, C., *et al*.. Biogeochemical and contaminant cycling in sediments from a human-impacted coastal lagoona - Introduction and summary. Estuarine, Coastal and Shelf Science, Elsevier, 2007, vol. 72, pp. 387-392.<10.1016/j.ecss.2006.11.022>.<hal-00780252>.

Andreae, M.O., Byrd, J.T., Froelich, P.N., 1983. Arsenic, antimony, germanium, and tin in the Tejo Estuary, Portugal: Modelling a polluted estuary. Environmental Science & Technology. 17, 731–737.

Andrewes, P., Cullen, W.R., Feldmann, J., Koch, I., Polishchuk, E., 1999. Methylantimony compound formation in the medium of Scopulariopsis brevicaulis cultures: 13CD3-L-methionine as a source of the methyl group. Applied Organometallic Chemistry. 13, 681–687. doi:10.1002/(SICI)1099-0739(199910)13:10<681::AID-AOC911>3.0.CO;2-X.

Apte, S.C., Howard, A.G., 1986. Determination of dissolved inorganic antimony (V) and antimony (III) species in natural waters by hydride generation atomic absorption spectrometry. Journal of Analytical Atomic Spectrometry 1, 221–225.

Asta, M.P., Cama, J., Ayora, C., Acero, P., de Giudici, G., 2010. Arsenopyrite dissolution rates in O_2-bearing solutions. Chemical Geology 273, 272–285. doi:10.1016/j.chemgeo.2010.03.002.

ASTM International, 2005. Annual Book of ASTM Standards Section 5: Petroleum Products, Lubricants, and Fossil Fuels, vol. 05.01, Petroleum Products and Lubricants (I):pp. D 56- D 3230.

ATDSR, 1992, Toxicological profile for antimony and compounds.US. Public Health Service.

Audry, S., Schäfer, J., Blanc, G., Jouanneau, J.-M., 2004. Fifty-year sedimentary record of heavy metal pollution (Cd, Zn, Cu, Pb) in the Lot River reservoirs (France). Environmental Pollution 132, 413–426. doi:10.1016/j.envpol.2004.05.025.

Bach, C., Dauchy, X., Chagnon, M. C., Etienne, S., 2012. Chemical compounds and toxicological assessments of drinking water stored in polyethylene terephthalate (PET) bottles: A source of controversy reviewed. Water Research 46, 571–583. doi:10.1016/j.watres.2011.11.062.

Backman, C.M., 2008. Global supply and demand of metals in the future. Journal of Toxicology and Environmental Health, Part A 71, 1244–1253. doi:10.1080/15287390802209582.

Bacon, J.R., 2002. Isotopic characterisation of lead deposited 1989–2001 at two upland Scottish locations. Journal of Environmental Monitoring. 4, 291–299. doi:10.1039/B109731H.

Bacon, J.R., Davidson, C.M., 2007. Is there a future for sequential chemical extraction? Analyst 133, 25–46. doi:10.1039/B711896A.

Bain, D.C., 1976. A titanium-rich soil clay. Journal of Soil Science 27, 68–70. doi:10.1111/j.1365-2389.1976.tb01976.x.

Baird, C. 1998. Environmental chemistry. W.H.Freeman and Company. October, 1998.

Baker, J . H. 1972 The rate of production and decomposition of Chorisodontiumaci phylum (Hook. f. & Wils.) Broth. British Antarctic Survey Bulletin. 27, 123-129.

Bambic, D.G., Alpers, C.N., Green, P.G., Fanelli, E., Silk, W.K., 2006. Seasonal and spatial patterns of metals at a restored copper mine site. I. Stream copper and zinc. Environmental Pollution 144, 774–782.

Banoub, M.W., 1973. Ultra violet absorption as a measure of organic matter in natural waters in Bodensee. Archiv fur Hydrobiologie 71, 159-165.

Barbante, C., Schwikowski, M., Döring, T., Gäggeler, H.W., Schotterer, U., Tobler, L., Van de Velde, K., Ferrari, C., Cozzi, G., Turetta, A., Rosman, K., Bolshov, M., Capodaglio, G., Cescon, P., Boutron, C., 2004. Historical Record of European Emissions of Heavy Metals to the Atmosphere Since the 1650s from Alpine Snow/Ice Cores Drilled near Monte Rosa. Environmental Science & Technology. 38, 4085–4090. doi:10.1021/es049759r.

Bauer, M., Blodau, C., 2006. Mobilization of arsenic by dissolved organic matter from iron oxides, soils and sediments. Science of the Total Environment 354, 179–190. doi:10.1016/j.scitotenv.2005.01.027.

Beasley, G., Kneale, P., 2002. Reviewing the impact of metals and PAHs on macroinvertebrates in urban watercourses. Progress in Physical Geography 26, 236–270. doi:10.1191/0309133302pp334ra.

Beavington, F., Cawse, P.A., Wakenshaw, A., 2004. Comparative studies of atmospheric trace elements: improvements in air quality near a copper smelter. Science of the Total Environment 332, 39–49. doi:10.1016/j.scitotenv.2004.04.016.

Becker, S., 2008. Inorganic Mass Spectrometry: Principles and Applications. John Wiley & Sons.

Benjamin, M. M. and J. O. Leckie. 1981. Multiple-site adsorption of Cd, Zn, and Pb on amorphous iron oxyhydroxide. Journal of Colloid Interface Science. 79:209-221.

Benoit, J.M., Fitzgerald, W.F., Damman, A.W.H., 1998. The Biogeochemistry of an ombrotrophic bog: Evaluation of use as an Archive of Atmospheric Mercury Deposition. Environmental Research 78, 118–133. doi:10.1006/enrs.1998.3850.

Berg, T., Røyset, O., Steinnes, E., 1995. Moss (Hylocomium splendens) used as biomonitor of atmospheric trace element deposition: Estimation of uptake efficiencies. Atmospheric Environment 29, 353–360. doi:10.1016/1352-2310(94)00259-N.

Bertine, K.K., Lee, D.S., 1983. Antimony content and speciation in the water column and interstitial waters of Saanich Inlet. In: Wong, C.S., Boyle, E., Bruland, K.W., Burton, J.D., Goldberg, E.D. (Eds.), Trace Metals in Sea Water NATO Advanced Research Institute Plenum Press, New York, pp. 21–38.

Berrow, M.L., Wilson, M.J., Reaves, G.A., 1978. Origin of extractable titanium and vanadium in the a horizons of scottish podzols. Geoderma 21, 89–103. doi:10.1016/0016-7061(78)90019-8.

Bhattacharya, S.J., 1996. Surfactant enhanced electrokinetic remediation of gasoline contaminated soils (Ph.D. thesis) The University of Wyoming, USA.

Bibi, M., Hashmi, M.Z., Malik, R.N., 2015. Human exposure to arsenic in groundwater from Lahore district, Pakistan. Environmental Toxicology and Pharmacology 39, 42–52. doi:10.1016/j.etap.2014.10.020.

Biddappa, C.C., Chino, M., Kumazavra, K., 1981. Adsorption, desorption, potential and selective distribution op heavy metals in selected soils of japan. Journal of Environmental Science and Health, Part B 16, 511–528. doi:10.1080/03601238109372275.

Bierkens, J., Smolders, R., Van Holderbeke, M., Cornelis, C., 2011. Predicting blood lead levels from current and past environmental data in Europe. Science of the Total Environment 409, 5101–5110. doi:10.1016/j.scitotenv.2011.08.034.

Bindler, R., Klarqvist, M., Klaminder, J., Forster, J., 2004. Does within-bog spatial variability of mercury and lead constrain reconstructions of absolute deposition rates from single peat records? The example of Store Mosse, Sweden. Global Biogeochemical Cycles 18, issue 3.

Bindler, R., 2006. Mired in the past — looking to the future: Geochemistry of peat and the analysis of past environmental changes. Global and Planetary Change, Peatlands: records of global environmental changes 53, 209–221. doi:10.1016/j.gloplacha.2006.03.004.

Biver M., Shotyk, W. 2012. Stibnite (Sb_2S_3) oxidative dissolution kinetics from pH 1 to 11. Geochimica et Cosmochimica Acta 79, 127–139.

Biver, M., Shotyk, W., 2013. Stibiconite (Sb_3O_6OH), senarmontite (Sb_2O_3) and valentinite (Sb_2O_3): Dissolution rates at pH 2–11 and isoelectric points. Geochimica et Cosmochimica Acta 109, 268–279.

Blair D.S.H. 2014. Carbon and contaminant trace metal biogeochemistry in surficial organic-rich terrestrial systems. PhD. thesis, University of Edinburgh.

Blok, J., 2005. Environmental exposure of road borders to zinc. Science of the Total Environment 348, 173–190. doi:10.1016/j.scitotenv.2004.12.073.

Bosetti, C., Boffetta, P., Vecchia, C.L., 2007. Occupational exposures to polycyclic aromatic hydrocarbons, and respiratory and urinary tract cancers: a quantitative review to 2005. Annals Oncology 18, 431–446.

Boström C.E, Gerde, P., Hanberg, A., Jernström, B., Johansson, C., Kyrklund, T., *et al*. 2002. Cancer risk assessment, indicators and guidelines for polycyclic aromatic hydrocarbons in ambient air. Environmental Health Perspective, 110:451–89.

Bradl, H., 2005. Heavy Metals in the Environment: Origin, Interaction and Remediation: Origin, Interaction and Remediation. Academic Press.

Brannon, J.M., Patrick Jr., W.H., 1985. Fixation and mobilization of antimony in sediments. Environmental Pollution Series B, Chemical and Physical 9, 107–126. doi:10.1016/0143-148X(85)90027-8.

Brännvall, M.L., Bindler, R., Emteryd, O., Nilsson, M., Renberg, I., 1997. Stable Isotope and Concentration Records of Atmospheric Lead Pollution in Peat and Lake Sediments in Sweden. Water, Air, & Soil Pollution 100, 243–252. doi:10.1023/A:1018360106350.

Brännvall, M.L., Bindler, R., Renberg, I., Emteryd, O., Bartnicki, J., Billström, K., 1999. The Medieval Metal Industry Was the Cradle of Modern Large-Scale Atmospheric Lead Pollution in Northern Europe. Environmental Science & Technology. 33, 4391–4395. doi:10.1021/es990279n.

Brintzinger, H., Rausch, F., Backhausen, M., 1948. Eine Methode zur Wolframbestimmung. Zeitschrift fur anorganishe und allgemeine Chemie. 255, 323–324. doi:10.1002/zaac.19482550604

Bris F.J., Garnuad S., Apperry N., Gonzalez A., Mouchel J.M., Chebbo G., Thévenot D.R., 1999. A street deposit sampling method for metal and hydrocarbon contamination assessment. Science of the Total Environment, 235, 211-220.

Brown, R.J.C., Yardley, R.E., Muhunthan, D., Butterfield, D.M., Williams, M., Woods, P.T., Brown, A.S., Goddard, S.L., 2007. Twenty-five years of nationwide ambient metals measurement in the

United Kingdom: concentration levels and trends. Environmental Monitoring Assessment 142, 127–140. doi:10.1007/s10661-007-9914-9.
Bryant, C.L., Farmer, J.G., MacKenzie, A.B., Bailey-Watts, A.E., Kirika, A., 1997. Manganese behavior in the sediments of diverse Scottish freshwater lochs. Limnology and Oceanography. 42, 918–929. doi:10.4319/lo.1997.42.5.0918.
Bundschuh, J., Litter, M.I., Parvez, F., Roman-Ross, G., Nicolli, H.B., Jean, J.S., Liu,C.W., Lopez, D., Armienta, M.A., Guilherme, L.R.G., Cuevas, A.G., Cornejo, L., Cumbal, L., Toujaque, 2012. One century of arsenic exposure in Latin America: a review of history and occurrence from 14 countries. Science of the Total Environment .429,2–35.
Buschmann, J., Sigg, L., 2004. Antimony (III) binding to humic substances: influence of pH and type of humic acid. Environmental Science & Technology. 38, 4535–4541.
Buschmann, J., Kappeler, A., Lindauer,U., Kistler, D., Berg, M., Sigg, L. 2006. Arsenite and arsenate binding to dissolved humic acids: influence of pH, type of humic acid, and aluminium. Environmental Science & Technology. 40 6015–6020.
Butterman, W.C., Carlin, J.F., 2004. Mineral commodity profiles-Antimony. U.S. Department of the Interior, U.S. Geological Survey. Open-file report 03-019.
Calle-Guntiñas, M.B. de la, Madrid, Y., Cámara, C., 1992. Stability study of total antimony, Sb(III) and Sb(V) at the trace level. Fresenius Journal of Analytical Chemistry 344, 27–29. doi:10.1007/BF00324836.
Canadian Council of Ministers of the Environment. 2007. Canadian soil quality guidelines for the protection of environmental and human health: Summary tables. Updated September, 2007. In: Canadian environmental quality guidelines, 1999, Canadian Council of Ministers of the Environment, Winnipeg.
Cappuyns, V., Swennen, R., Vandamme, A., Niclaes, M., 2006. Environmental impact of the former Pb–Zn mining and smelting in East Belgium. Journal of Geochemical Exploration, Extended Abstracts presented at the 7th Symposium on the Geochemistry of the Earth's Surface (GES-7) 7th Symposium the Geochemistry of the Earth's Surface 88, 6–9. doi:10.1016/j.gexplo.2005.08.005.
Card, J.W., Bell, K., 1985. The relationship of soil ^{210}Po and ^{210}Pb geochemical dispersion patterns to uranium mineralization. Journal of Geochemical Exploration 23, 101–115. doi:10.1016/0375-6742(85)90021-4.
Carr, E., Lee, M., Marin, K., Holder, C., Hoyer, M., Pedde, M., Cook, R., Touma, J., 2011. Development and evaluation of an air quality modeling approach to assess near-field impacts of lead emissions from piston-engine aircraft operating on leaded aviation gasoline. Atmospheric Environment 45, 5795–5804. doi:10.1016/j.atmosenv.2011.07.017.
Casiot, C., Ujevic, M., Munoz, M., Seidel, J.L., Elbaz-Poulichet, F., 2007. Antimony and arsenic mobility in a creek draining an antimony mine abandoned 85 years ago (upper Orb basin, France). Applied Geochemistry 22, 788–798. doi:10.1016/j.apgeochem.2006.11.007.
Cavallaro, N. and M. B. McBride. 1978. Copper and cadmium adsorption characteristics of selected acid and calcareous soils. Soil Science Society of America Journal. 42:550-556.
Carvalho, F.P., 1995. ^{210}Pb and ^{210}Po in sediments and suspended matter in the Tagus estuary, Portugal. Local enhancement of natural levels by wastes from phosphate ore processing industry. Science of The Total Environment 159, 201–214. doi:10.1016/0048-9697(95)04332-U.
Ceburnis, D., Valiulis, D., 1999. Investigation of absolute metal uptake efficiency from precipitation in moss. Science of the Total Environment. 226, 247–253.
Centre for Ecology and Hydrology. 2015. Auchencorth Moss: and atmospheric observatory. http://www.ceh.ac.uk/our-science/monitoring-site/auchencorth-moss-atmospheric-observatory (accessed 3rd of September 2015).
Ceriotti, G., Amarasiriwardena, D., 2009. A study of antimony complexed to soil-derived humic acids and inorganic antimony species along a Massachusetts highway. Microchemical Journal 91, 85–93. doi:10.1016/j.microc.2008.08.010.
Charlesworth, S., Miguel, E.D., Ordóñez, A., 2011. A review of the distribution of particulate trace elements in urban terrestrial environments and its application to considerations of risk. Environmental Geochemistry Health 33, 103–123.
Chen, Q.Y., 2004. Using computational tools to factor wind into architectural environment design. Energy and Buildings, Energy and Environment of Residential Buildings in China 36, 1197–1209. doi:10.1016/j.enbuild.2003.10.013.

Chen, Y.W., Deng, T.L., Filella, M., Belzile, N., 2003. Distribution and Early Diagenesis of Antimony Species in Sediments and Porewaters of Freshwater Lakes. Environmental Science & Technology. 37, 1163–1168. doi:10.1021/es025931k.

Chen, Z., Cai, Y., Liu, G., Solo-Gabriele, H., Snyder, G.H., Cisar, J.L., 2008. Role of soil-derived dissolved substances in arsenic transport and transformation in laboratory experiments, Science of the Total Environment. 406, 180–189.

Chenery, S.R., Izquierdo, M., Marzouk, E., Klinck, B., Palumbo-Roe, B., Tye, A.M., 2012. Soil–plant interactions and the uptake of Pb at abandoned mining sites in the Rookhope catchment of the N. Pennines, UK-A Pb isotope study. Science of the Total Environment 433, 547–560. doi:10.1016/j.scitotenv.2012.03.004.

Cheng, H., Hu, Y., 2010. Lead (Pb) isotopic fingerprinting and its applications in lead pollution studies in China: A review. Environmental Pollution 158, 1134–1146. doi:10.1016/j.envpol.2009.12.028.

Cherfi, A., Abdoun, S., Gaci, O., 2014. Food survey: Levels and potential health risks of chromium, lead, zinc and copper content in fruits and vegetables consumed in Algeria. Food and Chemical Toxicology 70, 48–53. doi:10.1016/j.fct.2014.04.044.

Chiaradia M, Cupelin F., 2000. Behaviour of airborne lead and temporal variations of its source effects in Geneva (Switzerland): comparison of anthropogenic versus natural processes. Atmospheric Environment 34, 959–71.

Choong, T.S.Y., Chuah, T.G., Robiah, Y., Gregory Koay, F.L., Azni, I., 2007. Arsenic toxicity, health hazards and removal techniques from water: an overview. Desalination 217, 139–166. doi:10.1016/j.desal.2007.01.015.

Christl, I., Knicker, H., Kögel-Knabner, I., Kretzschmar, R., 2000. Chemical heterogeneity of humic substances: characterization of size fractions obtained by hollow-fibre ultrafiltration. European Journal of Soil Science 51, 617–625. doi:10.1111/j.1365-2389.2000.00352.x.

Christl, I., Kretzschmar, R., 2001. Interaction of copper and fulvic acid at the hematite-water interface. Geochimica et Cosmochimica Acta 65, 3435–3442. doi:10.1016/S0016-7037(01)00695-0.

City of Edinburgh Council Environmental and Consumer Services Department, 2004. Detailed Assessment Report (Local Air Quality Management Round 2).

CL:AIRE.2010. Soil generic assessment criteria for human health risk assessment contaminated land: applications in real environments London.

Clemente, R., Dickinson, N.M., Lepp, N.W., 2008. Mobility of metals and metalloids in a multi-element contaminated soil 20 years after cessation of the pollution source activity. Environmental Pollution 155, 254–261. doi:10.1016/j.envpol.2007.11.024.

Cloy, J.M. 2005. Chemical records of environmental pollution in ombrotrophic peat bogs. PhD Thesis. University of Edinburgh. Table 3.8.

Cloy, J., Farmer, J.G., Graham, M.C., MacKenzie, A.B. and Cook, G.T., 2005. A comparison of antimony and lead profiles over the past 2,500 years in Flanders Moss ombrotrophic peat bog, Scotland, Journal of Environmental Monitoring 7(12) p.1137-1147.

Cloy, J.M., Farmer, J.G., Graham, M.C., MacKenzie, A.B., Cook, G.T., 2008. Historical records of atmospheric Pb deposition in four Scottish ombrotrophic peat bogs: An isotopic comparison with other records from western Europe and Greenland. Global Biogeochemical Cycles 22 (GB2016). doi: 10.1029/2007GB003059

Cloy, J.M., Farmer, J.G., Graham, M.C., MacKenzie, A.B., 2009. Retention of As and Sb in Ombrotrophic Peat Bogs: Records of As, Sb, and Pb Deposition at Four Scottish Sites. Environmental Science & Technology. 43, 1756–1762. doi:10.1021/es802573e.

Clymo, R.S., 1984. The Limits to Peat Bog Growth. Philosophical Transactions of the Royal Society of London B: Biological Sciences 303, 605–654. doi:10.1098/rstb.1984.0002.

Cooper JA, Reynolds PH, Richards JR. 1969. Double-spike calibration of the Broken Hill Standard Lead. Earth Planet Science Letters 6, 467–78.

CONCAWE. 1992. Gasolines. Publication number. 92/103, Brussels, Belgium, http://www.concawe.be/ (accessed June, 2015).

Council of the European Union, 1998. Council Directive 98/83/EC of 3 November 1998 on the quality of water intended for human consumption. Official Journal L 330, 05/12/1998, pp. 32–54.

Crançon, P., Pili, E., Charlet, L., 2010. Uranium facilitated transport by water-dispersible colloids in field and soil columns. Science of the Total Environment 408, 2118–2128.

Currie, L.A., 1968. Limits for qualitative detection and quantitative determination. Application to radiochemistry. Analytical Chemistry 40, 586–593. doi:10.1021/ac60259a007.
Cutter, G.A., 1991. Dissolved arsenic and antimony in the Black Sea. Deep-Sea Research. 38, S825–S843.
Das, D., Samanta, G., Mandal, B.K., Chowdhury, T.R., Chanda, C.R., Chowdhury, P.P., Basu, G.K., Chakraborti, D., 1996. Arsenic in groundwater in six districts of West Bengal, India. Environ Geochem Health 18, 5–15. doi:10.1007/BF01757214.
Das, S., Jean,J.S., Kar,S., 2013. Bioaccessibility and health risk assessment of arsenic in arsenic enriched soils, Central India. Ecotoxicology and Environmental Safety.92,252–257.
Davidson, C.M., Duncan, A.L., Littlejohn, D., Ure, A.M., Garden, L.M., 1998. A critical evaluation of the three-stage BCR sequential extraction procedure to assess the potential mobility and toxicity of heavy metals in industrially-contaminated land. Analytica Chimica Acta 363, 45–55. doi:10.1016/S0003-2670(98)00057-9.
Davis, J.M., Svendsgaard, D.J., 1987. Low level lead exposure and child development. Nature 329, 297-300.
Day, J., Tylecote, R.F., 1991. The industrial evolution in metals. The Institute of Metals, London, 1991.
De Benedetto, F., Bernardini, G.P., Borrini, D., Emiliani, C., Cipriani, C., Danti, C., Caneschi, A., Gatteschi, D., Romanelli, M., 2002. Crystal chemistry of tetrahedrite solid-solution: EPR and magnetic investigations. Canadian Mineralogist 40, 837–847.
Dean, R.J., Shimmield, T.M., Black, K.D., 2007. Copper, zinc and cadmium in marine cage fish farm sediments: an extensive survey. Environmental Pollution. 145, 84–95.
Defra. 2002. Environment Agency, Soil Guideline Values for Lead Contamination. Report SGV10. Bristol:Department of the Environment, Food and Rural Affairs and the environment Agency.
Defra. 2007. The air quality strategy for England, Scotland, Wales and Northern Ireland. Volume 1, Cm7169 NIA 61/06-07.
Delves, H.T., Campbell, M.J., 1993. Identification and apportionment of sources of lead in human tissue. Environmental Geochemical Health 15, 75–84. doi:10.1007/BF02627825.
Denier van der Gon, H.A.C., Hulskotte, J.H.J., Visschedijk, A.J.H., Schaap, M., 2007. A revised estimate of copper emissions from road transport in UNECE-Europe and its impact on predicted copper concentrations. Atmospheric Environment 41, 8697–8710. doi:10.1016/j.atmosenv.2007.07.033.
Department for Transport. Birmingham City traffic profile for 2000 to 2014. Retrieved from http://www.dft.gov.uk/traffic-counts/area.php?region=West+Midlands&la=Birmingham . September 2015.
Department for Transport. City of Edinburgh traffic profile for 2000 to 2014. Retrieved from http://www.dft.gov.uk/traffic-counts/area.php?region=Scotland&la=City+of+Edinburgh . September 2015.
Department for Transport. Glasgow City Traffic counts points for 2014. Retrieved from http://www.dft.gov.uk/traffic-counts/cp.php?la=Glasgow+City . September 2015.
Department for Transport. Glasgow City traffic profile for 2000 to 2014. Retrieved from http://www.dft.gov.uk/traffic-counts/area.php?region=Scotland&la=Glasgow+City . September 2015.
Department for Transport. City of London traffic profile for 2000 to 2014. Retrieved from http://www.dft.gov.uk/traffic-counts/area.php?region=London&la=City+of+London . September 2015.
Díaz-Somoano M., Suárez-Ruiz I., Alonso J.I.G., Ruiz Encinar J, López-Antón M.A., Martínez-Tarazona M.R. 2007. Lead isotope ratios in Spanish coals of different characteristics and origin. International Journal of Coal Geology, 71:28–36.
Dobbs, R.A., Wise, R.H., Dean, R.B., 1972. The use of ultra-violet absorbance for monitoring the total organic carbon content of water and wastewater. Water Research. 6, 1173-1180.
Dobran, S., Zagury, G.J., 2006. Arsenic speciation and mobilization in CCA contamination soils; influence of organic matter content. Science of the Total Environment. 364, 239–250.
Dodd, M., Pergantis, S.A., Cullen, W.R., Li, H., Eigendorf, G.K., Reimer, K.J., 1996. Antimony speciation in freshwater plant extracts by using hydride generation–gas chromatography–mass spectrometry. Analyst 121, 223–228. doi:10.1039/AN9962100223.

Dold, B., Fontboté, L., 2001. Element cycling and secondary mineralogy in porphyry copper tailings as a function of climate, primary mineralogy, and mineral processing. Journal of Geochemical Exploration 74, 3–55. doi:10.1016/S0375-6742(01)00174-1.

Dong, T.T., Lee, B.K., 2009. Characteristics, toxicity, and source apportionment of polycylic aromatic hydrocarbons (PAHs) in road dust of Ulsan, Korea. Chemosphere 74, 1245–1253. doi:10.1016/j.chemosphere.2008.11.035.

Drever, J.I., 1997. The geochemistry of natural waters. Prentice-Hall, Incorporation.

Druller, P.R., Gallagher, M.J., Hall, A.J., Russell, M.J., 1997. Glendinning deposit-an example of turbidite-hosted arsenic-antimony-gold mineralization in the Sothern Uplands, Scotland. Transactions-Institution of Mining and Metallurgy. Institute of Mining & Metallurgy 106, B119-B134.

Douthwaite, R., Duckett, S., Yarwood, J., 2014. Spectroscopic Properties of Inorganic and Organometallic Compounds: Techniques, Materials and Applications. Royal Society of Chemistry.

Dore, C.J., Murrells, T.P., Passant, N.R., Hobson, M.M., Thistlethwaite, G. Wagner, A., Li, Y *et al.* 2008. UK emissions of air pollutants 1970 to 2006. UK emissions inventory team, AEA.

Dore, A.J., Hallsworth, S., McDonald, A.G., Werner, M., Kryza, M., Abbot, J., Nemitz, E., Dore, C.J., Malcolm, H., Vieno, M., Reis, S., Fowler, D., 2014. Quantifying missing annual emission sources of heavy metals in the United Kingdom with an atmospheric transport model. Science of the Total Environment 479–480, 171–180. doi:10.1016/j.scitotenv.2014.02.001.

Dudka, S., Adriano, D.C., 1997. Environmental Impacts of Metal Ore Mining and Processing: A Review. Journal of Environment Quality 26, 590. doi:10.2134/jeq1997.00472425002600030003x.

Eades, L.J., Farmer, J.G., MacKenzie, A.B., Kirika, A., Bailey-Watts, A.E. 1998. High-resolution record of radiocaesium deposition in Loch Lomond sediments. Journal Environmental Radioactivity, 39, pp. 107–115.

Eades, L.J., Farmer, J.G., MacKenzie, A.B., Kirika, A., Bailey-Watts, A.E., 2002. Stable lead isotopic characterisation of the historical record of environmental lead contamination in dated freshwater lake sediment cores from northern and central Scotland. Science of the Total Environment 292, 55–67. doi:10.1016/S0048-9697(02)00026-8.

Edinburgh City Council Freedom of Information. 2012. Edinburgh's 10 busiest roads and estimated total traffic. 407129/SD.32/CH-AM.

Edinburgh World Heritage, British Geological Survey, 2005. Setts in the city.

EFSA, 2009. EFSA panel on contaminants in the food chain, scientific opinion on arsenic in food. EFSAJ.7,1351.

EHS. Environment and Heritage Service. 2005. Natural heritage, formation of a peat bog. Fact sheet NH 008.

Elliott, W.Y., May, E.S., Rowe, J.W.F., Skelton, A., Wallace, D.H., 1937. International control of the non-ferrous metals, McMillan, New York.

Elliott, H. A., Liberati, M. R., Huang, C. P. 1986. Competitive adsorption of heavy metals by soils. Journal of Environment Quality 15:214-219.

Erel, Y., Veron, A., Halicz, L., 1997. Tracing the transport of anthropogenic lead in the atmosphere and in soils using isotopic ratios. Geochimica et Cosmochimica Acta 61, 4495–4505. doi:10.1016/S0016-7037(97)00353-0.

Espi, E., Boutron, C.F., Hong, S., Pourchet, M., Ferrari, C., Shotyk, W., Charlet, L., 1997. Changing concentrations of Cu, Zn, Cd and Pb in a high altitude peat bog from Bolivia during the past three centuries. Water, Air, & Soil Pollution 100, 289–296. doi:10.1023/A:1018364208168.

Essumang, D.K., Dodoo, D.K., Adjei, J.K., 2013. Effect of smoke generation sources and smoke curing duration on the levels of polycyclic aromatic hydrocarbon (PAH) in different suites of fish. Food and Chemical Toxicology 58, 86–94. doi:10.1016/j.fct.2013.04.014.

Ettler, V., Johan, Z., 2014. 12 years of leaching of contaminants from Pb smelter slags: Geochemical/mineralogical controls and slag recycling potential. Applied Geochemistry 40, 97–103. doi:10.1016/j.apgeochem.2013.11.001.

European Commission.1991. Council Directive 91/441/EEC of 26 June 1991 amending Directive 70/220/EEC on the approximation of the laws of the Member States relating to measures to be taken against air pollution by emissions from motor vehicles.

European Commission. 2000. Directive 2000/53/EC of the European Parliament and the council of 18 September 200 on end-of life vehicles.

European Commission. 2000. Directive 2000/60/EC of the European Parliament and of the Council of 23 October 2000 establishing a framework for Community action in the field of water policy (Water Framework Directive). European Commission.
European Commission. 2001. Directive 76/464/EEC Article 7 of the European Parliament and of the Council on pollution reduction programmes (Water Framework Directive). European Commission.
European Commission. 2008. Directive 2002/95/EC (RoHS Directive) of the European Parliament and of the Council on the restriction of the use of certain hazardous substances in electrical and electronic equipment(recast). 2008/0240 (COD). Brussels: European Commission.
European Commission 2008. Commission Regulation No692/2008 of 18 July 2008 Implementing and amending Regulation (FC) No 715/2007 on type-approval of vehicles with respect to emissions from light passenger and commercial vehicles (Euro 5 and Euro 6) and on access to vehicle repair and maintenance information.
European Commission. 2013. Directive 2013/39/EU of the European Parliament and of the Council of 12 August 2013 amending Directives 2000/60/EC and 2008/105/EC as regards priority substances in field of water policy. European Commission.
European Environment Agency Air quality in Europe — 2013 report ISBN 978-92-9213-406-8 doi:10.2800/92843.
European Environment Agency-Passenger car ownership in the EEA. URL http://www.eea.europa.eu/data-and-maps/figures/passenger-car-ownership-in-the-eea (accessed 06.28.14).
Fakour, H., Lin, T.F., 2014. Experimental determination and modeling of arsenic complexation with humic and fulvic acids. Journal of Hazardous Materials 279, 569–578. doi:10.1016/j.jhazmat.2014.07.039.
FAO/WHO food standards programme, Codex alimentarius commission, Twenty-fourth session, Geneva, Switzerland, 2–7 July 2001.
Fan, J.-X., Wang, Y.-J., Fan, T.-T., Cui, X.D., Zhou, D.M., 2014. Photo-induced oxidation of Sb(III) on goethite. Chemosphere 95, 295–300. doi:10.1016/j.chemosphere.2013.08.094.
Farmer, J. G., Lyon, T.D.B., 1977. Lead in Glasgow Street Dirt and Soil. Science of the Total Environment 8, 89–93. doi:10.1016/0048-9697(77)90064-X.
Farmer, J.G., Lovell, M.A., 1986. Natural enrichment of arsenic in Loch Lomond sediments. Geochimica et Cosmochimica Acta 50, 2059–2067. doi:10.1016/0016-7037(86)90259-0.
Farmer, J.G., MacKenzie, A.B., Sugden, C.L., Bryant, C.L., Eades, L.J., Bailey-Watts, A.E., Kirika, A., 1993. The history of environmental lead pollution in Scotland. In: R.J. Allan and J.O. Nriagu (Editors), Proceedings of the Ninth International Conference on Heavy Metals in the Environment. CEP, Edinburgh, Vol.2, pp. 211-214.
Farmer, J.G., Eades, L.J., MacKenzie, A.B., Kirika, A. and Bailey-Watts, A.E., 1996. Stable lead isotope record of lead pollution in Loch Lomond sediments since 1630 A.D, Environmental Science & Technology. 30 p.3080-3083.
Farmer, J.G., MacKenzie, A.B., Eades, L.J., Kirika, A., Bailey-Watts, A.E., 1997. Influences on the extent and record of heavy metal pollution in sediment cores from Loch Tay in a mineralised area of Scotland. Journal of Geochemical Exploration 58, 195–202. doi:10.1016/S0375-6742(96)00060-X.
Farmer, J.G., MacKenzie, A.B., Sugden, C.L., Edgar, P.J. and Eades, L.J. 1997. A comparison of the historical lead pollution records in freshwater lake sediments and peat cores from central Scotland.Water, Air, Soil Pollution 100 p.253-270.
Farmer, J.G., Eades, L.J., Graham, M.C., 1999. The lead content and isotopic composition of British coals and their implications for past and present releases of lead to the UK environment. Environmental Geochemistry and Health 21, 257–272. doi:10.1023/A:1006688515919.
Farmer, J.G., Eades, L.J., Graham, M.C., Bacon, J.R., 2000. The changing nature of the $^{206}Pb/^{207}Pb$ isotopic ratio of lead in rainwater, atmospheric particulates, pine needles and leaded petrol in Scotland, 1982–1998. Journal of Environmental Monitoring. 2, 49–57. doi:10.1039/A907558E
Farmer, J.G., Thomas, R.P., Graham, M.C., Geelhoed, J.S., Lumsdon, D.G., Paterson, E., 2002. Chromium speciation and fractionation in ground and surface waters in the vicinity of chromite ore processing residue disposal sites. Journal of Environmental Monitoring. 4, 235–243. doi:10.1039/B108681M.
Farmer, J.G., Graham, M.C., Bacon, J.R., Dunn, S.M., Vinogradoff, S.I., MacKenzie, A.B., 2005. Isotopic characterisation of the historical lead deposition record at Glensaugh, an organic-rich,

upland catchment in rural N.E. Scotland. Science of the Total Environment 346, 121–137. doi:10.1016/j.scitotenv.2004.11.020.

Farmer, J.G., MacKenzie, A.B., Moody, G.H., 2006. Human teeth as historical biomonitors of environmental and dietary lead: some lessons from isotopic studies of 19th and 20th century archival material. Environmental Geochemistry and Health 28, 421–430. doi:10.1007/s10653-006-9041-5.

Farmer, J.G., Graham, M.C., Yafa, C., Cloy, J.M., Freeman, A.J., MacKenzie, A.B., 2006. Use of $^{206}Pb/^{207}Pb$ ratios to investigate the surface integrity of peat cores used to study the recent depositional history and geochemical behaviour of inorganic elements in peat bogs. Global and Planetary Change 53, 240–248. doi:10.1016/j.gloplacha.2006.03.006.

Farmer, J.G., Eades, L.J., Graham, M.C., Cloy, J.M., Bacon, J.R., 2010. A comparison of the isotopic composition of lead in rainwater, surface vegetation and tree bark at the long-term monitoring site, Glensaugh, Scotland, in 2007. Science of the Total Environment 408, 3704–3710.

Farmer, J.G., Broadway, A., Cave, M.R., Wragg, J., Fordyce, F.M., Graham, M.C., Ngwenya, B.T., Bewley, R.J.F., 2011. A lead isotopic study of the human bioaccessibility of lead in urban soils from Glasgow, Scotland. Science of the Total Environment 409, 4958–4965. doi:10.1016/j.scitotenv.2011.08.061.

Farmer, J.G., MacKenzie, A.B., Graham, M.C., Macgregor, K., Kirika, A., 2015. Development of recent chronologies and evaluation of temporal variations in Pb fluxes and sources in lake sediment and peat cores in a remote, highly radiogenic environment, Cairngorm Mountains, Scottish Highlands. Geochimica et Cosmochimica Acta 156, 25–49. doi:10.1016/j.gca.2015.02.003.

Fawcett, S.E., Jamieson, H.E., Nordstrom, D.K., McCleskey, R.B., 2014. Arsenic and antimony geochemistry of mine wastes, associated waters and sediments at the Giant Mine, Yellowknife, Northwest Territories, Canada. Applied Geochemistry. doi:10.1016/j.apgeochem.2014.12.012.

Fergusson, J.E., Kim, N.D., 1991. Trace elements in street and house dusts: sources and speciation. Science of the Total Environment 100, 125–150.

Filella, M., Belzile, N., Chen, Y.W., 2002a. Antimony in the environment: a review focused on natural waters: I. Occurrence. Earth-Science Reviews 57, 125–176. doi:10.1016/S0012-8252(01)00070-8.

Filella, M., Belzile, N., Chen, Y.W., 2002b. Antimony in the environment: a review focused on natural waters: II. Relevant solution chemistry. Earth-Science Reviews 59, 265–285. doi:10.1016/S0012-8252(02)00089-2.

Filella, M., Belzile, N., Lett, M.C., 2007. Antimony in the environment: A review focused on natural waters. III. Microbiota relevant interactions. Earth-Science Reviews 80, 195–217. doi:10.1016/j.earscirev.2006.09.003.

Filella, M., Philippo, S., Belzile, N., Chen, Y., Quentel, F., 2009. Natural attenuation processes applying to antimony: A study in the abandoned antimony mine in Goesdorf, Luxembourg. Science of the Total Environment 407, 6205–6216.

Filella, M., 2011. Antimony interactions with heterogeneous complexants in waters, sediments and soils: A review of data obtained in bulk samples. Earth-Science Reviews 107, 325–341.

Filella, M., Williams, P.A., 2012. Antimony interactions with heterogeneous complexants in waters, sediments and soils: A review of binding data for homologous compounds. Chemie der Erde - Geochemistry, Antimony 72, Supplement 4, 49–65. doi:10.1016/j.chemer.2012.01.006

Fluxnet. A global network. Auchencorth Moss – Scotland. http://fluxnet.ornl.gov/site/771 (accessed 27th of March 2015).

Flynn, H.C., Meharg, A.A., Bowyer, P.K., Paton, G.I., 2003. Antimony bioavailability in mine soils. Environmental Pollution 124, 93–100.

Food standards agency, 2012. Polycyclic aromatic hydrocarbons in cereals, cereal products, vegetables, vegetable products and traditional smoked foods. April, number 01/12.

Forbes, E.A., Posner, A. M., Quick, J. P. 1976. The specific adsorption of divalent Cd, Co, Pb, and Zn on goethite. Journal of Soil Science. 27:154-166.

Fordyce, F. M., Lass-Evans, S., Ó Dochartaigh, B. É. 2013. A Case Study to Identify Urban Diffuse Pollution in the Light Burn Catchment, Glasgow, UK. Stage 3 contribution to: Wade, R et al. (2013) A Critical Review of Urban Diffuse Pollution Control: Methodologies To Identify Sources, Pathways And Mitigation Measures With Multiple Benefits., CREW, the James Hutton Institute, Aberdeen. Available online at: crew.ac.uk/publications.2013.

Foster, S., Maher, W., Krikowa, F., Telford, K., Ellwood, M., 2005. Observations on the measurement of total antimony and antimony species in algae, plant and animal tissues. Journal of Environmental Monitoring 7, 1214–1219. doi:10.1039/b509202g.

Fu, Z., Wu, F., Amarasiriwardena, D., Mo, C., Liu, B., Zhu, J., Deng, Q., Liao, H., 2010. Antimony, arsenic and mercury in the aquatic environment and fish in a large antimony mining area in Hunan, China. Science of the Total Environment 408, 3403–3410. doi:10.1016/j.scitotenv.2010.04.031.

Fu, Y.R., Chen,M.L., Bi,X.Y., He,Y.S., Ren,L.M., Xiang,W., Qiao,S.Y., Yan,S., Li,Z.G., Ma, Z.D., 2011. Occurrence of arsenic in brown rice and its relationship to soil properties from Hainan Island, China. Environmental.Pollution.159, 1757–1762.

Fuentes, A., Lloréns, M., Sáez, J., Soler, A., Aguilar, M.I., Ortuño, J.F., Meseguer, V.F., 2004. Simple and sequential extractions of heavy metals from different sewage sludges. Chemosphere 54, 1039–1047. doi:10.1016/j.chemosphere.2003.10.029.

Furuta, N., Iijima, A., Kambe, A., Sakai, K. and Sato, K., 2005. Concentrations, enrichment and predominant sources of Sb and other trace elements in size classified airborne particulate matter collected in Tokyo from 1995 to 2004. Journal of Environmental Monitoring 7:1155–1161.

Gabriels, R., 1970. General method for calculating the detection limit in chemical analysis. Analytical Chemistry 42, 1439–1440. doi:10.1021/ac60294a025.

Gaertner, R.R.W., Thériault, G.P., 2002. Risk of bladder cancer in foundry workers: a meta-analysis. Occupational Environmental Medicine 59, 655–663.

Gaetke, L.M., Chow, C.K., 2003. Copper toxicity, oxidative stress, and antioxidant nutrients. Toxicology 189, 147–163.

Gál, J., Hursthouse, A., Cuthbert, S., 2007. Bioavailability of arsenic and antimony in soils from an abandoned mining area, Glendinning (SW Scotland). Journal of Environmental Science and Health, Part A 42, 1263–1274.

Gallagher, M.J., Stone, P., Kemp, A.E.S., Hills, M.G., Jones, R.C., Smith, R.T., Peachey, D., Vickers, B.P., Parker, M.E., Rollin, K.E., Skilton, B.R.H. 1983. Strata bound arsenic and vein antimony mineralisation in Silurian greywackes at Glendinning, South Scotland. Institute of Geological Sciences Mineral Reconnaissance Programme. Report no. 59.

Garrido, F., Helmhart, M., 2012. Lead and soil properties distributions in a roadside soil: Effect of preferential flow paths. Geoderma 170, 305–313.

Geocaching. 2015. The Mer Bleue Bog. http://www.geocaching.com/geocache/GC10MZP_mer-bleue-bog?guid=deea9eaf-08be-42b1-825d-9f3a79577808 (accessed 3rd of September 2015).

Gezici, O., Kara, H., Yanık, S., Ayyildiz, H.F., Kucukkolbasi, S., 2007. Investigating sorption characteristics of copper ions onto insolubilized humic acid by using a continuously monitored solid phase extraction technique. Colloids and Surfaces A: Physicochemical and Engineering Aspects, XVIIth European Chemistry at Interfaces Conference 298, 129–138. doi:10.1016/j.colsurfa.2006.12.007.

Gibson, M.J., Farmer, J.G., 1986. Multi-step sequential chemical extraction of heavy metals from urban soils. Environmental Pollution Series B, Chemical and Physical;11:117–135. doi:10.1016/0143-148X(86)90039-X.

Gieré, R., Sidenko, N.V., Lazareva, E.V., 2003. The role of secondary minerals in controlling the migration of arsenic and metals from high-sulfide wastes (Berikul gold mine, Siberia). Applied Geochemistry, Arsenic Geochemistry-selected papers from the 10th Water-Rock Interaction Symposium, Villasimius, Italy, 10-15 June 2001 18, 1347–1359. doi:10.1016/S0883-2927(03)00055-6.

Goldschmidt, V.M., 1937. The principles of distribution of chemical elements in minerals and rocks. The seventh Hugo Müller Lecture, delivered before the Chemical Society on March 17th, 1937. Journal Chemical Society. 655–673. doi:10.1039/JR9370000655.

Gondar, D., López, R., Fiol, S., Antelo, J.M., Arce, F., 2006. Cadmium, lead, and copper binding to humic acid and fulvic acid extracted from an ombrotrophic peat bog. Geoderma 135, 196–203. doi:10.1016/j.geoderma.2005.12.003.

Gondar, D., Iglesias, A., López, R., Fiol, S., Antelo, J.M., Arce, F., 2006. Copper binding by peat fulvic and humic acids extracted from two horizons of an ombrotrophic peat bog. Chemosphere 63, 82–88. doi:10.1016/j.chemosphere.2005.07.003.

González-Castanedo, Y., Moreno, T., Fernández-Camacho, R., Sánchez de la Campa, A.M., Alastuey, A., Querol, X., de la Rosa, J., 2014. Size distribution and chemical composition of particulate

matter stack emissions in and around a copper smelter. Atmospheric Environment 98, 271–282. doi:10.1016/j.atmosenv.2014.08.057.
Graham, M.C., Vinogradoff, S.I., Chipchase, A.J., Dunn, S.M., Bacon, J.R. and Farmer, J.G., 2006 Using size fractionation and Pb isotopes to study Pb transport in the waters of an organic-rich upland catchment. Environmental Science & Technology 40(4) p.1250-1256.
Graham, M.C., Oliver, I.W., MacKenzie, A.B., Ellam, R.M., Farmer, J.G., 2008. An integrated colloid fractionation approach applied to the characterisation of porewater uranium–humic interactions at a depleted uranium contaminated site. Science of the Total Environment 404, 207–217. doi:10.1016/j.scitotenv.2008.05.042.
Graham, M.C., Oliver, I.W., MacKenzie, A.B., Ellam, R.M., Farmer, J.G., 2011. Mechanisms controlling lateral and vertical porewater migration of depleted uranium (DU) at two UK weapons testing sites. Science of the Total Environment 409, 1854–1866.
Gray, D., Pollard, S.J.T., Spence, L., Smith, R., Gronow, J.R., 2005. Spray irrigation of landfill leachate: estimating potential exposures to workers and bystanders using a modified air box model and generalised source term. Environmental Pollution 133, 587–599. doi:10.1016/ j.envpol.2004.06.010.
Gregory, J., Foster, K., Tyler, H., Wiseman, M., 1990. The diet and health of adults in the United Kingdom. London, HMSO.
Grigoratos, T., Martini, G., 2015. Brake wear particle emissions: a review. Environmental Science and Pollution and Research 22, 2491–2504. doi:10.1007/s11356-014-3696-8.
Gulson, B., 2008. Stable lead isotopes in environmental health with emphasis on human investigations. Science of the Total Environment 400, 75–92. doi:10.1016/j.scitotenv.2008.06.059.
Gunawardana, C., Goonetilleke, A., Egodawatta, P., Dawes, L., Kokot, S., 2012. Source characterisation of road dust based on chemical and mineralogical composition. Chemosphere 87, 163–170. doi:10.1016/j.chemosphere.2011.12.012.
Guo, H.R.,Yu, H.S., Hu, H., Monson, R.R., 2001.Arsenic in drinking water and skin cancers: cell type specificity (Taiwan, ROC).Cancer Causes Control 12,909–916.
Gupta, I., Salunkhe, A., Kumar, R., 2010. Modelling 10-year trends of PM10 and related toxic heavy metal concentrations in four cities in India. Journal of Hazardous Materials 179, 1084–1095. doi:10.1016/j.jhazmat.2010.03.117.
Hall, G.E.M., Gauthier, G, Pelchat, J.C., Pelchat, P., Vaive, J.E., 1996. Application of a sequential extraction scheme to ten geological certified reference materials for the determination of 20 elements. Journal of Analytical Atomic Spectrometry. 11(9):787–796.
Hansen, H.K., Yianatos, J.B., Ottosen, L.M., 2005. Speciation and leachability of copper in mine tailings from porphyry copper mining: Influence of particle size. Chemosphere 60, 1497–1503. doi:10.1016/j.chemosphere.2005.01.086.
Hansen, H.R., Pergantis, S.A., 2008. Analytical techniques and methods used for antimony speciation analysis in biological matrices. Journal of Analytical Atomic Spectrometry 23, 1328. doi:10.1039/b807599a.
Harris, D.C., 1991. Quantitative chemical analysis. W.H.Freeman and Company 3rd edition.
Hatzakis, A., Kokkevi, A., Maravelias, C., Katsouyanni, K., Salaminios, F., Kalandidi, A., Koutselinis, A., Stefanis, C., Trichopoulos, D., 1989. Psychometric Intelligence Deficits in Lead-exposed Children, in: Smith, M.A., Grant, L.D., Sors, A.I. (Eds.), Lead Exposure and Child Development. Springer Netherlands, pp. 211–223.
He, M., Wang, X., Wu, F., Fu, Z., 2012. Antimony pollution in China. Science of the Total Environment 421–422, 41–50. doi:10.1016/j.scitotenv.2011.06.009.
Hickey, M. G. and J. A. Kittrick. 1984. Chemical partitioning of cadmium, copper, nickel, and zinc in soils and sediments containing high levels of heavy metals. Journal of Environmental Quality. 13:372-376.
Hiller, E., Lalinská, B., Chovan, M., Jurkovič, Ľ., Klimko, T., Jankulár, M., Hovorič, R., Šottník, P., Fľaková, R., Ženišová, Z., Ondrejková, I., 2012. Arsenic and antimony contamination of waters, stream sediments and soils in the vicinity of abandoned antimony mines in the Western Carpathians, Slovakia. Applied Geochemistry 27, 598–614.
Hitzel, A., Pöhlmann, M., Schwägele, F., Speer, K., Jira, W., 2013. Polycyclic aromatic hydrocarbons (PAH) and phenolic substances in meat products smoked with different types of wood and smoking spices. Food Chemistry 139, 955–962. doi:10.1016/j.foodchem.2013.02.011.

Hockmann, K., Lenz, M., Tandy, S., Nachtegall, M., Janousch, M., Schulin, R., 2014. Release of antimony from contaminated soil induced by redox changes. Journal of Hazardous Materials 30, 275, 215-21.

Hong, S., Candelone, J.P., Patterson, C.C., Boutron, C.F., 1994. Greenland ice evidence of hemispheric lead pollution two millennia ago by greek and roman civilizations. Science 265, 1841–1843. doi:10.1126/science.265.5180.1841.

Hudson-Edwards, K.A., Houghton, S.L., Osborn, A., 2004. Extraction and analysis of arsenic in soils and sediments. TrAC Trends in Analytical Chemistry 23, 745–752. doi:10.1016/j.trac.2004.07.010.

Hughes, M.F., Beck, B.D., Chen, C. Lewis, A.S., Thomas, D.J., 2011. Arsenic exposure and toxicology: A historical perspective. Toxicological Sciences 123 (2), 305-332.

Hulskotte, J.H.J., Roskam, G.D., Denier van der Gon, H.A.C., 2014. Elemental composition of current automotive braking materials and derived air emission factors. Atmospheric Environment 99, 436–445. doi:10.1016/j.atmosenv.2014.10.007.

Hur, J., Yim, S., Schlautman, M.A., 2003. Copper leaching from brake wear debris in standard extraction solutions. Journal of Environmental Monitoring. 5, 837–843. doi:10.1039/B303820C.

IARC. 1987. Monographs on the evaluation of the carcinogenic risk of chemicals to humans. Overall evaluation of carcinogenity: An updating of IARC monographs (Vols. 1–42). Lyon, France: International Agency for Research on Cancer Supplement 7.

IARC (International Agency for Research on Cancer). 1989. Antimony Trioxide and Antimony Trisulfide. In Monographs on the Evaluation of the Carcinogenic Risk of Chemicals to Humans. Volume 47. Some Organic Solvents, Resin Monomers and Related Compounds, Pigments and Occupational Exposures in Paint Manufacture and Painting (Vol. 47, pp. 291-305). International Agency for Research on Cancer, Lyon, France.

IARC. 2010. Monographs on the evaluation of carcinogenic risks to humans (Vol.92). Lyon, France: International Agency for Research on Cancer.

Iijima, A., Sato, K., Yano, K., Kato, M., Kozawa, K., Furuta, N., 2008. Emission Factor for Antimony in Brake Abrasion Dusts as One of the Major Atmospheric Antimony Sources. Environmental Science & Technology. 42, 2937–2942. doi:10.1021/es702137g.

International Agency for Research on Cancer (IARC), 1989. IARC Monograph, vol. 47, Lyon, France pp. 291.

Ip, C.C.M., Li, X.D., Zhang, G., Wong, C.S.C., Zhang, W.L., 2005. Heavy metal and Pb isotopic compositions of aquatic organisms in the Pearl River Estuary, South China. Environmental Pollution. 138, 494–504.

Jarvie, H.P., Neal, C., Burton, J.D., Tappin, A.D., 2000. Patterns in trace element chemistry in the freshwater tidal reaches of the River Trent. Science of the Total Environment. 251/252, 317–333.

JECFA, 1982. Evaluation of certain food additives and contaminants. Twenty-sixth report of the Joint FAO/WHO Expert Committee on Food Additives. WHO Technical Report Series No. 683.

Johnson, D.B., Hallberg, K.B., 2005. Acid mine drainage remediation options: a review. Science of the Total Environment 338, 3–14. doi:10.1016/j.scitotenv.2004.09.002.

Johnson, C.A., Moench, H., Wersin, P., Kugler, P., Wenger, C., 2005. Solubility of antimony and other elements in samples taken from shooting ranges. Journal of Environmental Quality 34, 248–254.

Johnson, B. Historic UK Newcastle-upon-tyne. http://www.historic-uk.com/HistoryMagazine/DestinationsUK/NewcastleuponTyne/ (accessed February 2016).

Kabata-Pendias, A., Szteke, B., 2015. Trace Elements in Abiotic and Biotic Environments. CRC Press.

Kadi, M.W., 2009. Soil Pollution Hazardous to Environment: A case study on the chemical composition and correlation to automobile traffic of the roadside soil of Jeddah city, Saudi Arabia. Journal of Hazardous Materials 168, 1280–1283.

Kalogeropoulos, N., Karavoltsos, S., Sakellari, A., Avramidou, S., Dassenakis, M., Scoullos, M., 2012. Heavy metals in raw, fried and grilled Mediterranean finfish and shellfish. Food and Chemical Toxicology 50, 3702–3708. doi:10.1016/j.fct.2012.07.012.

Kamal, A., Qamar, K., Gulfraz, M., Anwar, M.A., Malik, R.N., 2015. PAH exposure and oxidative stress indicators of human cohorts exposed to traffic pollution in Lahore city (Pakistan). Chemosphere 120, 59–67. doi:10.1016/j.chemosphere.2014.05.021.

Karsten Kalbitz, K.K., 2008. Contribution of dissolved organic matter to carbon storage in forest mineral soils. Journal of Plant Nutrition and Soil Science 171, 52–60. doi:10.1002/jpln.200700043.

Kalbitz, K., Solinger, S., Park, J-H., Michalzik, B., Matzner, E., 2000. Controls on the dynamics of dissolved organic matter in soils: a review. Soil Science 165, 277-304.

Keinonen, M., 1992. The isotopic composition of lead in man and the environment in Finland 1966–1987: isotope ratios of lead as indicators of pollutant source. Science of the Total Environment 113, 251–268. doi:10.1016/0048-9697(92)90004-C.

Keon, N.E., Swartz, C.H., Brabander, D.J., Harvey, C., Hemond, H.F., 2001. Validation of an Arsenic Sequential Extraction Method for Evaluating Mobility in Sediments. Environmental Science & Technology. 35, 2778–2784. doi:10.1021/es001511o.

Kim, J. Y., Myung, J. H., Ahn, J. S., & Chon, H. T. 1998. Heavy metal speciation in dusts and stream sediments in the Taejon area, Korea. Journal of Geochemical Exploration, 64, 409–419.

Kim, K.H., Jahan, S.A., Kabir, E., Brown, R.J.C., 2013. A review of airborne polycyclic aromatic hydrocarbons (PAHs) and their human health effects. Environment International 60, 71–80. doi:10.1016/j.envint.2013.07.019.

Kögel-Knabner, I., Totsche, K.U., 1998. Influence of dissolved and colloidal phase humic substances on the transport of hydrophobic organic contaminants in soils. Physics and Chemistry of the Earth 23, 179–185. doi:10.1016/S0079-1946(98)00010-X.

Komárek, M., Ettler, V., Chrastný, V., Mihaljevič, M., 2008. Lead isotopes in environmental sciences: A review. Environment International 34, 562–577. doi:10.1016/j.envint.2007.10.005.

Krachler, M., Emons, H., Zheng, J., 2001. Speciation of antimony for the 21st century: promises and pitfalls. Trends in Analytical Chemistry 20, 79–90. doi:10.1016/S0165-9936(00)00065-0.

Krachler, M., Zheng, J., Koerner, R., Zdanowicz, C., Fisher, D., Shotyk, W., 2005. Increasing atmospheric antimony contamination in the northern hemisphere: snow and ice evidence from Devon Island, Arctic Canada. Journal of Environmental. Monitoring. 7, 1169–1176. doi:10.1039/B509373B.

Krachler, M., Zheng, J., Fisher, D., Shotyk, W., 2008. Atmospheric Sb in the Arctic during the past 16,000 years: Responses to climate change and human impacts. Global Biogeochemistry Cycles 22, GB1015. doi:10.1029/2007GB002998.

Krachler, M., Shotyk, W., 2009. Trace and ultra-trace metals in bottled waters: Survey of sources worldwide and comparison with refillable metal bottles. Science of the Total Environment 407, 1089–1096. doi:10.1016/j.scitotenv.2008.10.014.

Kropschot, S.J., Doebirch, J.L., 2011. USGS Mineral Resource Program, Lead-soft and easy to cast. Factsheet 2011-3045.

Kukutschová, J., Roubíček, V., Malachová, K., Pavlíčková, Z., Holuša, R., Kubačková, J., Mička, V., MacCrimmon, D., Filip, P., 2009. Wear mechanism in automotive brake materials, wear debris and its potential environmental impact. Wear 267, 807–817.

Kumar, A.R., Riyazuddin, P., 2010. Preservation of inorganic arsenic species in environmental water samples for reliable speciation analysis. Trends in Analytical Chemistry 29, 1212–1223. doi:10.1016/j.trac.2010.07.009.

Kuo, S., P. E. Heilman and A. S. Baker. 1983. Distribution and forms of copper, zinc, cadmium, iron, and manganese in soils near a copper smelter. Soil Science.135:101-109.

Küttner, A., Mighall, T.M., De Vleeschouwer, F., Mauquoy, D., Martínez Cortizas, A., Foster, I.D.L., Krupp, E., 2014. A 3300-year atmospheric metal contamination record from Raeburn Flow raised bog, south west Scotland. Journal of Archaeological Science 44, 1–11. doi:10.1016/j.jas.2014.01.011.

Kuwae, M., Tsugeki, N.K., Agusa, T., Toyoda, K., Tani, Y., Ueda, S., Tanabe, S., Urabe, J., 2013. Sedimentary records of metal deposition in Japanese alpine lakes for the last 250 years: Recent enrichment of airborne Sb and In in East Asia. Science of the Total Environment 442, 189–197. doi:10.1016/j.scitotenv.2012.10.037.

Land Quality Management Ltd, Chartered Institute of Environmental Health, 2012. Generic assessment criteria for human health risk assessment. 2nd edition. May 2012.

Laskin, D., 2006. The Great London Smog. Weatherwise 59, 42–45. doi:10.3200/WEWI.59.6.42-45.

Le Vine, S., Jones, P., 2012. On the move. Making sense of car and train travel trends in Britain. RAC Foundation.

Lee, S.V., Cundy, A.B., 2001. Heavy Metal Contamination and Mixing Processes in Sediments from the Humber Estuary, Eastern England. Estuarine, Coastal and Shelf Science 53, 619–636. doi:10.1006/ecss.2000.0713.

Lee, K., Hur, S.D., Hou, S., Burn-Nunes, L.J., Hong, S., Barbante, C., Boutron, C.F., Rosman, K.J.R., 2011. Isotopic signatures for natural versus anthropogenic Pb in high-altitude Mt. Everest ice cores during the past 800 years. Science of the Total Environment 412–413, 194–202. doi:10.1016/j.scitotenv.2011.10.002.

Lee, P.W., Filip, P., 2013. Friction and wear of Cu-free and Sb-free environmental friendly automotive brake materials. Wear, Wear of Materials 2013 302, 1404–1413. doi:10.1016/j.wear.2012.12.046.

Leuz, A.K., Mönch, H., Johnson, C.A., 2006. Sorption of Sb(III) and Sb(V) to Goethite: Influence on Sb(III) Oxidation and Mobilization. Environmental Science & Technology. 40, 7277–7282. doi:10.1021/es061284b.

Li, N., Xia, Y., Mao, Z., Wang, L., Guan, Y., Zheng, A., 2012. Influence of antimony oxide on flammability of polypropylene/intumescent flame retardant system. Polymer Degradation and Stability 97, 1737–1744.

Li, P., Lin, C., Cheng, H., Duan, X., Lei, K., 2015. Contamination and health risks of soil heavy metals around a lead/zinc smelter in southwestern China. Ecotoxicology and Environmental Safety 113, 391–399. doi:10.1016/j.ecoenv.2014.12.025.

Li, M., Peng, B., Chai, L., Peng, N., Xie, X., Yan, H., 2013. Technological mineralogy and environmental activity of zinc leaching residue from zinc hydrometallurgical process. Transactions of Nonferrous Metals Society of China 23, 1480–1488. doi:10.1016/S1003-6326(13)62620-5.

Livett, E.A., Lee, J.A., Tallis, J.H., 1979. Lead, Zinc and Copper Analyses of British Blanket Peats. Journal of Ecology 67, 865–891. doi:10.2307/2259219.

Lim, L.H., Harrison, R.M., Harrad, S., 1999. The Contribution of Traffic to Atmospheric Concentrations of Polycyclic Aromatic Hydrocarbons. Environmental Science and Technology 33, 3538–3542. doi:10.1021/es990392d.

Lindemann, T., Prange, A., Dannecker, W., Neidhart, B., 2000. Stability studies of arsenic, selenium, antimony and tellurium species in water, urine, fish and soil extracts using HPLC/ICP-MS. Fresenius Journal of Analytical Chemistry 368, 214–220. doi:10.1007/s002160000475.

Lintschinger, J., Koch, I., Serves, S., Feldmann, J., Cullen, W.R., 1997. Determination of antimony species with high-performance liquid chromatography using element specific detection. Fresenius Journal of Analytical Chemistry 359, 484–491. doi:10.1007/s002160050618.

Lintschinger, J., Schramel, O., Kettrup, A., 1998. The analysis of antimony species by using ESI-MS and HPLC-ICP-MS. Fresenius Journal of Analytical Chemistry 361, 96–102. doi:10.1007/s002160050841.

Liu, J., Li, K., Xu, J., Zhang, Z., Ma, T., Lu, X., Yang, J., Zhu, Q., 2003. Lead toxicity, uptake, and translocation in different rice cultivars. Plant Science 165, 793–802. doi:10.1016/S0168-9452(03)00273-5.

Liu, M., Cheng, S.B., Ou, D.N., Hou, L.J., Gao, L., Wang, L.L., Xie, Y.S., Yang, Y., Xu, S.Y., 2007. Characterization, identification of road dust PAHs in central Shanghai areas, China. Atmospheric Environment 41, 8785–8795. doi:10.1016/j.atmosenv.2007.07.059.

Liu, W.X., Dou, H., Wei, Z.C., Chang, B., Qiu, W.X., Liu, Y., Tao, S., 2009. Emission characteristics of polycyclic aromatic hydrocarbons from combustion of different residential coals in North China. Science of the Total Environment 407, 1436–1446.

Lohmann, R., Northcott, G.L., Jones, K.C., 2000. Assessing the Contribution of Diffuse Domestic Burning as a Source of PCDD/Fs, PCBs, and PAHs to the U.K. Atmosphere. Environmental Science & Technology 34, 2892–2899. doi:10.1021/es991183w.

Lorenzi, D., Entwistle, J.A., Cave, M., Dean, J.R., 2011. Determination of polycyclic aromatic hydrocarbons in urban street dust: Implications for human health. Chemosphere 83, 970–977. doi:10.1016/j.chemosphere.2011.02.020.

Macgregor, K., Oliver, I., Duguid, A., Ridgway, I., 2011. Persistent organic pollutants in Scottish freshwater biota; Monitoring options, current levels and the way forward. Scottish Environment Protection Agency, chemistry and ecology departments.

Macgregor, K., MacKinnon, G., Farmer, J.G., Graham, M.C., 2015. Mobility of antimony, arsenic and lead at a former antimony mine, Glendinning, Scotland. Science of the Total Environment 529, 213–222. doi:10.1016/j.scitotenv.2015.04.039.

MacKenzie, A. B.; Logan, E. M.; Cook, G. T.; Pulford, I. D. 1998a. A historical record of atmospheric depositional fluxes of contaminants in west-central Scotland derived from an ombrotrophic peat core. Science of the Total Environment. 222, 157–166.

MacKenzie, A.B., Logan, E.M., Cook, G.T., Pulford, I.D., 1998b. Distributions, inventories and isotopic composition of lead in ^{210}Pb-dated peat cores from contrasting biogeochemical

environments: Implications for lead mobility. Science of the Total Environment 223, 25–35. doi:10.1016/S0048-9697(98)00302-7.
MacKenzie A.B., Pulford I.D. 2002. Investigation of metal dispersal from a disused mine site at Tyndrum, Scotland, using concentration gradients and stable Pb isotope ratios. Applied Geochemistry 17:1093 –103.
MacKenzie, A.B., Hardie, S.M.L., Farmer, J.G., Eades, L.J., Pulford, I.D., 2011. Analytical and sampling constraints in ^{210}Pb dating. Science of the Total Environment 409, 1298–1304. doi:10.1016/j.scitotenv.2010.11.040.
MacKinnon, G., MacKenzie, A.B., Cook, G.T., Pulford, I.D., Duncan, H.J., Scott, E.M., 2011. Spatial and temporal variations in Pb concentrations and isotopic composition in road dust, farmland soil and vegetation in proximity to roads since cessation of use of leaded petrol in the UK. Science of the Total Environment 409, 5010–5019.
Maiz I, Arambarri I, Garcia R, Millán E., 2000. Evaluation of heavy metal availability in polluted soils by two sequential extraction procedures using factor analysis. Environmental Pollution.110 (1): 3–9.
Maliszewska-Kordybach B. 1999. Sources, concentrations, fate and effects of polycyclic aromatic hydrocarbons (PAHs) in the environment. Part A: PAHs in air. Polish Journal of Environmental Studies 8: 13–136.
Maresky, L.S., Grobler, S.R., 1993. Effect of the reduction of petrol lead on the blood lead levels of South Africans. Science of the Total Environment 136, 43–48.
Martínez-Cortizas, A., Pontevedra-Pombal, X., Muñoz, J.C.N., García-Rodeja, E., 1997. Four Thousand Years of Atmospheric Pb, Cd and Zn Deposition Recorded by the Ombrotrophic Peat Bog of Penido Vello (Northwestern Spain). Water, Air, & Soil Pollution 100, 387–403. doi:10.1023/A:1018312223189.
Matschullat, J., 2000. Arsenic in the geosphere — a review. Science of the Total Environment 249, 297–312. doi:10.1016/S0048-9697(99)00524-0.
McArthur, J.M., Banerjee, D.M., Hudson-Edwards, K.A., Mishra, R., Purohit, R., Ravenscroft, P., Cronin, A., Howarth, R.J., Chatterjee, A., Talukder, T., Lowry, D., Houghton, S., Chadha, D.K., 2004. Natural organic matter in sedimentary basins and its relation to arsenic in anoxic ground water: the example of West Bengal and itsworldwide implications, Applied Geochemistry. 19 1255–1293.
McComb, K.A., Craw, D., McQuillan, A.J., 2007. ATR-IR Spectroscopic Study of Antimonate Adsorption to Iron Oxide. Langmuir 23, 12125–12130. doi:10.1021/la7012667.
McLean, J.E., Bledsoe, B.E., 1992. USEPA Ground water issue-Behaviour of metals in soils. EPA/540/S-92/018.
Merrington, G., Alloway, B.J., 1994. The flux of Cd, Cu, Pb and Zn in mining polluted soils. Water Air and Soil Pollution 73, 333–344. doi:10.1007/BF00477997.
Met Office. UK Climate. http://www.metoffice.gov.uk/public/weather/climate (accessed August 2015).
Met office. Eastern Scotland: climate. http://www.metoffice.gov.uk/climate/uk/regional-climates/es (accessed February, 2016).
Michazik, B., Matzner, E., 1999. Dynamics of dissolved organic nitrogen and carbon in a Central European Norway spruce ecosystem. European Journal of Soil Science. 50, 579–590.
Michalzik, E.M., 2001. Dynamics of dissolved organic nitrogen and carbon in a Central European Norway spruce ecosystem. European Journal of Soil Science 50, 579 – 590.
Michalski, R., Szopa, S., Jab&#x142, o&#x144, Ska, M., &#x0141, Yko, A., 2012. Application of Hyphenated Techniques in Speciation Analysis of Arsenic, Antimony, and Thallium. The Scientific World Journal, e902464. doi:10.1100/2012/902464.
Miguel, E. de, Llamas, J.F., Chacón, E., Berg, T., Larssen, S., Røyset, O., Vadset, M., 1997. Origin and patterns of distribution of trace elements in street dust: Unleaded petrol and urban lead. Atmospheric Environment 31, 2733–2740.
Mills, C., Simpson, I., Adderley, W.P., 2014. The lead legacy: the relationship between historical mining, pollution and the post-mining landscape. Landscape History 35, 47–72. doi:10.1080/01433768.2014.916912.
Miravet, R., Hernández-Nataren, E., Sahuquillo, A., Rubio, R., López-Sánchez, J.F., 2010. Speciation of antimony in environmental matrices by coupled techniques. TrAC Trends in Analytical Chemistry 29, 28–39. doi:10.1016/j.trac.2009.10.006.

Mitchell, R.G., Spliethoff, H.M., Ribaudo, L.N., Lopp, D.M., Shayler, H.A., Marquez-Bravo, L.G., Lambert, V.T., Ferenz, G.S., Russell-Anelli, J.M., Stone, E.B., McBride, M.B., 2014. Lead (Pb) and other metals in New York City community garden soils: Factors influencing contaminant distributions. Environmental Pollution 187, 162–169. doi:10.1016/j.envpol.2014.01.007.

Mitsunobu, S., Harada, T., Takahashi, Y., 2006. Comparison of antimony behaviour with that of arsenic under various soil redox conditions. Environmental Science & Technology. 40, 7270–7276.

Mitsunobu, S., Takahashi, Y., Terada, Y., Sakata, M., 2010. Antimony(V) incorporation into synthetic ferrihydrite, goethite, and natural iron oxyhydroxides. Environmental Science & Technology 44, 3712–3718.

Mohammad, B., Ure, A.M., Reglinski, J., Littlejohn, D., 1990. Speciation of antimony in natural waters: the determination of Sb (III) and Sb (V) by continuous flow hydride generation– atomic absorption spectrometry. Chemical Speciation and Bioavailability 3, 117–122.

Mondal, D., Banerjee,M., Kundu, M., Banerjee, N.,Bhattacharya, U., Giri,A.K., Ganguli, B., SenRoy,S., Polya,D.A., 2010.Comparison of drinking water, raw rice and cooking of rice as arsenic exposure routes in three contrasting areas of West Bengal, India. Environmental Geochemistry Health 32,463–477.

Monna F, Lancelot J, Croudace IW., 1997. Pb isotopic composition of airborne particulate material from France and the Southern United Kingdom: implications for Pb pollution sources in urban areas. Environmental Science & Technology 31:2277–86.

Moorbath S. 1962. Lead isotope abundance studies on mineral occurrences in the British Isles and their geological significance. Philosophical Transactions of the Royal Society A: Mathematical, Physical Engineering Science 254:295–360.

Mossop, K.F., Davidson, C.M., 2003. Comparison of original and modified BCR sequential extraction procedures for the fractionation of copper, iron, lead, manganese and zinc in soils and sediments. Analytica Chimica Acta 478, 111–118. doi:10.1016/S0003-2670(02)01485-X.

Morillo, J., Usero, J., Gracia, I., 2002. Partitioning of metals in sediments from the Odiel River (Spain). Environment International 28, 263–271. doi:10.1016/S0160-4120(02)00033-8.

Moses, C.A., 2008. Comparative evaluation of semi-synthetic jet fuels. CRC Project No. AV-2-04a. U.S.Air Force research laboratories contract F33415-02-D-2299.

Muller, J., Ruppert, H., Muramatsu, Y. & Schneider, J., 2000. Reservoir sediments - a witness of mining and industrial development (Malter reservoir, Eastern Erzgebirge, Germany). Environmental Geology, 39 (12), 1341-1351.

Mummullage, S., Egodawatta, P., Ayoko, G.A., Goonetilleke, A., 2016. Use of physicochemical signatures to assess the sources of metals in urban road dust. Science of the Total Environment 541, 1303–1309. doi:10.1016/j.scitotenv.2015.10.032.

Munksgaard, N.C., Lottermoser, B.G., Blake, K., 2011. Prolonged Testing of Metal Mobility in Mining-Impacted Soils Amended with Phosphate Fertilisers. Water Air and Soil Pollution 223, 2237–2255. doi:10.1007/s11270-011-1019-y.

Murozumi, M. T., Chow, T.J., Patterson, C.C. 1969. Chemical concentrations of pollutant aerosols, terrestrial dusts and sea salts in Greenland and Antarctic snow strata. Geochimica et Cosmochimica Acta 33, 1247–1294. doi:10.1016/0016-7037(69)90045-3.

Murray, K., Linder, P.W., 1984. Fulvic acids: structure and metal binding. II. Predominant metal binding sites. Journal of Soil Science. 35, 217–222.

Myers, H.P., 2003. Introductory Solid State Physics, 2nd Edition. Taylor & Francis.

Nair, C.K., Balchand, A.N., Nambisan, P.N.K., 1991. Heavy metal speciation in sediments of Cochin estuary determined using chemical extraction techniques. Science of the Total Environment 102, 113–128. doi:10.1016/0048-9697(91)90310-B.

Napier, F., D'Arcy, B., Jefferies, C., 2008. A review of vehicle related metals and polycyclic aromatic hydrocarbons in the UK environment. Desalination, 10th IWA International Specialized Conference on Diffuse Pollution and Sustainable Basin Management 18–22 September 2006, Istanbul, Turkey 10th IWA International Specialized Conference on Diffuse Pollution and Sustainable Basin Management 226, 143–150. doi:10.1016/j.desal.2007.02.104.

Napier, F., Jefferies, C., Heal, K.V., Fogg, P., Arcy, B.J.D., Clarke, R., 2009. Evidence of traffic-related pollutant control in soil-based sustainable urban drainage systems (SUDS). Water Science and Technology. 60, 221–230. doi:10.2166/wst.2009.326.

Nenadic, S. 2011. The rise of Edinburgh. BBC. http://www.bbc.co.uk/history/british/civil_war_revolution/scotland_edinburgh_01.shtml (accessed 18th of August 2015).
Needleman, H.L., Gunnoe, C., Leviton, A., Reed, R., Peresie, H., Maher, C., *et al*., 1979. Deficits in psychologic and classroom performance of children with elevated dentine lead levels. New England Journal of Medicine. 300, 689-695.
Netregs. Environmental huidence for your business in Northern Ireland and Scotland. 2015. http://www.netregs.org.uk/library_of_topics/materials__equipment/more_hazardous_materials_topic/wood_preservatives.aspx (accessed 18th of August 2015).
Neubauer, E., Kohler, S.J., Laudon, H., von der Kammer, F. Hofmann, T., 2013. Effect of pH and stream order on iron and arsenic speciation in boreal catchments. Environmental Science and Technology 47, 7120-7128.
Nguyen, V.K., Tran, T., Han, H.J., Lee, S.H., Lee, J.U., 2015. Possibility of bacterial leaching of antimony, chromium, copper, manganese, nickel, and zinc from contaminated sediment. Journal of Geochemical Exploration 156, 153–161. doi:10.1016/j.gexplo.2015.05.012.
Nichani, V., Li, W. I., Smith, M.A., Noonan, G., Kulkarni, M., Kodavor, M., Naeher, L.P., 2006. Blood lead levels in children after phase-out of leaded gasoline in Bombay, India. Science of the Total Environment 363, 95–106.
Nieminen, T.M., Ukonmaanaho, L., Shotyk, W., 2002. Enrichment of Cu, Ni, Zn, Pb and As in an ombrotrophic peat bog near a Cu-Ni smelter in Southwest Finland. Science of the Total Environment, Peat Bog Archives of Atmospheric Metal Deposition 292, 81–89. doi:10.1016/S0048-9697(02)00028-1.
Ning, L., Liyuan, Y., Jirui, D., Xugui, P., 2011. Heavy metal pollution in surface water of Linglong gold mining area, China. Procedia Environmental Sciences 10, Part A, 914–917.
Nirel, R.M.V., Morel, F.M.M. 1990. Pitfalls of sequential extractions. Water Research Volume 24, Issue 8, pp. 1055-1056.
Nishioka, K., Hirahara, A., Iwamoto, E. 2002. Determination of antimony in polyethylene terephthalate bottles by graphite furnace atomic absorption spectrometry using microwave sample preparation, Bull. Inst. Life Sci. Hiroshima Prefectural Women's University., 8, 35-42.Nordberg, G.F., Flower, B.A., Nordberg, M., and Friberg, L. 2007. Handbook on the Toxicology of Metals. 3rd edition, Academic Press lncorporation. New York.
Nordstrom, D.K., Alpers, C.N., 1999. Geochemistry of acid mine waters. In: Plumlee, G.S., Logsdon, M.J., (Eds.), The Environmental Geochemistry of Mineral Deposits. Part A: Processes, Techniques and Health Issues. Reviews in Economic Geology 6A, pp. 133–160.
Nriagu, J.O., 1978. Lead in soils, sediment and major rock types, the biogeochemistry of lead. Elsevier Biomedical Press, Amsterdam, pp 18-88.
Nriagu, J.O., 1989. Natural Versus Anthropogenic Emissions of Trace Metals to the Atmosphere, in: Pacyna, D.J.M., Ottar, D.B. (Eds.), Control and Fate of Atmospheric Trace Metals, NATO ASI Series. Springer Netherlands, pp. 3–13.
Nriagu, J.O., Pacyna, J.M., 1988. Quantitative assessment of worldwide contamination of air, water and soils by trace metals. Nature 333, 134–139. doi:10.1038/333134a0.
Nriagu, J.O., Bhattacharya, P., Mukherjee, A.B., Bundschuh, J., Zevenhoven, R., Loeppert, R.H., 2007. Arsenic in soil and groundwater: an overview, in: Prosun Bhattacharya, A.B.M., Jochen Bundschuh, Ron Zevenhoven and Richard H. Loeppert (Ed.), Trace Metals and Other Contaminants in the Environment, Arsenic in Soil and Groundwater Environment Biogeochemical Interactions, Health Effects and Remediation. Elsevier, pp. 3–60.
Mansor, N. 2008. Investigation of lead and zinc dispersion from an abandoned mine site at Tyndrum, Scotland. PhD thesis. University of Glasgow.
Olid, C., Garcia-Orellana, J., Martínez-Cortizas, A., Masqué, P., Peiteado-Varela, E., Sanchez-Cabeza, J.-A., 2010. Multiple site study of recent atmospheric metal (Pb, Zn and Cu) deposition in the NW Iberian Peninsula using peat cores. Science of the Total Environment 408, 5540–5549. doi:10.1016/j.scitotenv.2010.07.058.
Olmedo, P., Hernández, A.F., Pla, A., Femia, P., Navas-Acien, A., Gil, F., 2013. Determination of essential elements (copper, manganese, selenium and zinc) in fish and shellfish samples. Risk and nutritional assessment and mercury–selenium balance. Food and Chemical Toxicology 62, 299–307. doi:10.1016/j.fct.2013.08.076.

Ok, Y.S., Usman, A.R.A., Lee, S.S., Abd El-Azeem, S.A.M., Choi, B., Hashimoto, Y., Yang, J.E., 2011. Effects of rapeseed residue on lead and cadmium availability and uptake by rice plants in heavy metal contaminated paddy soil. Chemosphere 85, 677–682. doi:10.1016/j.chemosphere.2011.06.073.

Okkenhaug, G., Zhu, Y.G., Luo, L., Lei, M., Li, X., Mulder, J., 2011. Distribution, speciation and availability of antimony (Sb) in soils and terrestrial plants from an active Sb mining area. Environmental Pollution 159, 2427–2434.

Omstedt, G., Bringfelt, B., Johansson, C., 2005. A model for vehicle-induced non-tailpipe emissions of particles along Swedish roads. Atmospheric Environment 39, 6088–6097. doi:10.1016/j.atmosenv.2005.06.037.

Ordóñez, A., Loredo, J., Miguel, E.D., Charlesworth, S., 2003. Distribution of heavy metals in the street dusts and soils of an industrial city in northern Spain. Archives of Environmental Contamination Toxicology 44, 0160–0170.

Orsetti, S., de las Mercedes Quiroga, M., Andrade, E.M., 2006. Binding of Pb(II) in the system humic acid/goethite at acidic pH. Chemosphere, Environmental Chemistry 65, 2313–2321. doi:10.1016/j.chemosphere.2006.05.009.

Orsetti, S., Marco-Brown, J.L., Andrade, E.M., Molina, F.V., 2013. Pb(II) Binding to Humic Substances: An Equilibrium and Spectroscopic Study. Environmental Science & Technology. 47, 8325–8333. doi:10.1021/es400999q.

OS MasterMap Integrated Transport Network Layer [GML2 geospatial data], Coverage: Edinburgh, Updated Jan 2009, Ordnance Survey, GB. Using: EDINA Digimap Ordnance Survey Service, <http://edina.ac.uk/digimap>, Downloaded: June 2009.

OS MasterMap Integrated Transport Network Layer [GML2 geospatial data], Coverage: Glasgow, Updated Jan 2009, Ordnance Survey, GB. Using: EDINA Digimap Ordnance Survey Service, <http://edina.ac.uk/digimap>, Downloaded: June 2009.

Osterberg, E., Mayewski, P., Kreutz, K., Fisher, D., Handley, M., Sneed, S., Zdanowicz, C., Zheng, J., Demuth, M., Waskiewicz, M., Bourgeois, J., 2008. Ice core record of rising lead pollution in the North Pacific atmosphere. Geophysical Research Letters. 35, L05810. doi:10.1029/2007GL032680.

Pacyna, J.M., 1984. Estimation of the atmospheric emissions of trace elements from anthropogenic sources in Europe. Atmospheric Environment 18, 41–50. doi:10.1016/0004-6981(84)90227-0.

Pacyna, J.M., Pacyna, E.G., 2001. An assessment of global and regional emissions of trace metals to the atmosphere from anthropogenic sources worldwide. Environmental Review 9, 269–298. doi:10.1139/a01-012.

Pacyna, E.G., Pacyna, J.M., Fudala, J., Strzelecka-Jastrzab, E., Hlawiczka, S., Panasiuk, D., Nitter, S., Pregger, T., Pfeiffer, H., Friedrich, R., 2007. Current and future emissions of selected heavy metals to the atmosphere from anthropogenic sources in Europe. Atmospheric Environment 41, 8557–8566. doi:10.1016/j.atmosenv.2007.07.040.

Pacyna, J.M., Pacyna, E.G., Aas, W., 2009. Changes of emissions and atmospheric deposition of mercury, lead, and cadmium. Atmospheric Environment - Fifty Years of Endeavour. Atmospheric Environment. 43, 117–127. doi:10.1016/j.atmosenv.2008.09.066.

Pant, P., Harrison, R.M., 2013. Estimation of the contribution of road traffic emissions to particulate matter concentrations from field measurements: A review. Atmospheric Environment 77, 78–97. doi:10.1016/j.atmosenv.2013.04.028.

Pattrick, R.A.D., 1985. Pb-Zn and minor U mineralisation at Tyndrum, Scotland. Mineral Magazine. 49, 671–681.

Pauwels, H., Pettenati, M., Greffié, C., 2010. The combined effect of abandoned mines and agriculture on groundwater chemistry. Journal of Contaminant Hydrology 115, 64–78. doi:10.1016/j.jconhyd.2010.04.003.

Perera, F., Hemminki, K., Jedrychowski, W., Whyatt, R., Campbell, U., Hsu, Y., Santella, R., Albertini, R., O'Neill, J.P., 2002. In utero DNA damage from environmental pollution is associated with somatic gene mutation in newborns. Cancer Epidemiology Biomarkers Prevention. 11, 1134–1137.

Pirajno, F., Burlow, R., Huston, D., 2010. The Magellan Pb deposit, Western Australia; a new category within the class of supergene non-sulphide mineral systems. Ore Geology Reviews 37, 101–113. doi:10.1016/j.oregeorev.2010.01.001.

Pitman, A.L., Pourbaix, M., de Zoubov, N., 1957. Potential-pH diagram of the antimony-water system. Its applications to properties of the metal, its compounds, its corrosion, and antimony electrodes. Journal of Electrochemical Society. 104, 594– 600.

Plumlee, G.S., Smith, K.S., Montour, M.R., Fichlin, W.H., Mosier, E.L., 1999. Geologic control on the composition of natural waters and mine waters drainage diverse minerals-deposit types. In: Filipek, L.H., Plumlee, G.S. (Eds.), Environmental Geochemistry of Mineral Deposits. Part B: Case Studies and Research Topics. Reviews in Economic Geology 6B, pp. 373–432.

Potin-Gautier, M., Pannier, F., Quiroz, W., Pinochet, H., de Gregori, I., 2005. Antimony speciation analysis in sediment reference materials using high-performance liquid chromatography coupled to hydride generation atomic fluorescence spectrometry. Analytica Chimica Acta 553, 214–222. doi:10.1016/j.aca.2005.07.055.

Pulford, I.D., MacKenzie, A.B., Donatello, S., Hastings, L., 2009. Source term characterisation using concentration trends and geochemical associations of Pb and Zn in river sediments in the vicinity of a disused mine site: Implications for contaminant metal dispersion processes. Environmental Pollution, Special Issue Section: Ozone and Mediterranean Ecology: Plants, People, Problems 157, 1649–1656. doi:10.1016/j.envpol.2008.12.018.

Qi, C., Wu, F., Deng, Q., Liu, G., Mo, C., Liu, B., Zhu, J., 2011. Distribution and accumulation of antimony in plants in the super-large Sb deposit areas, China. Microchemical Journal 97, 44–51. doi:10.1016/j.microc.2010.05.016.

Quentel, F., Filella, M., 2002. Determination of inorganic antimony species in seawater by differential pulse anodic stripping voltammetry: stability of the trivalent state. Analytica Chimica Acta 452, 237–244. doi:10.1016/S0003-2670(01)01474-X.

Quinty. F., Rochefort, L., 2003. Peatland restoration guide, Canadian Sphagnum Peat Moss Association and New Brunswick Department of Natural Resources and Energy. Second edition, 106.

Quiroz, W., Cortés, M., Astudillo, F., Bravo, M., Cereceda, F., Vidal, V., Lobos, M.G., 2013. Antimony speciation in road dust and urban particulate matter in Valparaiso, Chile: Analytical and environmental considerations. Microchemical Journal 110, 266–272. doi:10.1016/j.microc.2013.04.006.

Rabinowitz, M.B., 1991. Toxicokinetics of bone lead. Environmental Health Perspective 91, 33–37.

Rabinowitz MB., 2002 Isotopic characterisation of various brands of corroding grade refined lead metal. Bull Environmental Contamination and Toxicology 69:501–8.

Rabinowitz MB. 2005. Lead isotopes in soils near five historic American lead smelters and refineries. Science of the Total Environment. 346:138–48.

Ragaini, R.C., Ralston, H.R., Roberts, N., 1977. Environmental trace metal contamination in Kellogg, Idaho, near a lead smelting complex. Environmental Science & Technology. 11, 773–781. doi:10.1021/es60131a004.

Rahman, M.A., Hasegawa, H., 2011. Aquatic arsenic: phytoremediation using floating macrophytes. Chemosphere. 83,633–646.

Ravenscroft,P., Brammer,H., Richards,K., 2009. Arsenic Pollution: a Global Synthesis. Wiley-Blackwell, UK, pp.318–485.

Ravindra, K., Sokhi, R., Van Grieken, R., 2008. Atmospheric polycyclic aromatic hydrocarbons: Source attribution, emission factors and regulation. Atmospheric Environment 42, 2895–2921. doi:10.1016/j.atmosenv.2007.12.010.

Redman, A. D.; Macalady, D. L.; Ahmann, D., 2002. Natural organic matter affects arsenic speciation and sorption onto hematite. Environmental Science and Technology 36, 2889-2896.

Reimann C, de Caritat P., 1998. Chemical elements in the environment. Berlin: Springer, 398.

Royal Society of Chemistry. Arsenic element information http://www.rsc.org/periodic-table/element/33/arsenic (accessed 18 March 2015).

Reimann, C., Arnoldussen, A., Englmaier, P., Filzmoser, P., Finne, T.E., Garrett, R.G., Koller, F., Nordgulen, Ø., 2007. Element concentrations and variations along a 120-km transect in southern Norway – Anthropogenic vs. geogenic vs. biogenic element sources and cycles. Applied Geochemistry 22, 851–871. doi:10.1016/j.apgeochem.2006.12.019.

Reimann, C., Matschullat, J., Birke, M., Salminen, R., 2010. Antimony in the environment: Lessons from geochemical mapping. Applied Geochemistry 25, 175–198. doi:10.1016/j.apgeochem.2009.11.011.

Renberg, I., Persson, M.W., Emteryd, O., 1994. Pre-industrial atmospheric lead contamination detected in Swedish lake sediments. Nature 368, 323–326. doi:10.1038/368323a0.
Ricca, B., D'Amore, G., 1965. Ricerche sugli antimoniati. Annali di Chimica. (Rome) 46, 483– 490.
Robbins, J.A. 1978. In:The biogeochemistry of lead. Edited by Nriago, J.P. Elsevier, Amsterdam.
Appleby, P.G., Oldfield, F., 1978. The calculation of lead-210 dates assuming a constant rate of supply of unsupported ^{210}Pb to the sediment. CATENA 5, 1–8. doi:10.1016/S0341-8162(78)80002-2.
Robbins, N., Zhang, Z.F., Sun, J., Ketterer, M.E., Lalumandier, J.A., Shulze, R.A., 2010. Childhood lead exposure and uptake in teeth in the Cleveland area during the era of leaded gasoline. Science of the Total Environment 408, 4118–4127.
Rogge, W.F., Mazurek, M.A., Hildemann, L.M., Cass, G.R., Simoneit, B.R.T., 1993. Quantification of urban organic aerosols at a molecular level: Identification, abundance and seasonal variation. Atmospheric Environment. Part A. General Topics 27, 1309–1330. doi:10.1016/0960-1686(93)90257-Y.
Rognerud, S., Hongve, D., Fjeld, E., Ottesen, R.T., 1999. Trace metal concentrations in lake and overbank sediments in southern Norway. Environmental Geology 7, 723–732.
Roper, A.J., Williams, P.A., Filella, M., 2012. Secondary antimony minerals: Phases that control the dispersion of antimony in the supergene zone. Chemie der Erde - Geochemistry. doi:10.1016/j.chemer.2012.01.005.
Rosman, K.J.R., Chisholm, W., Hong, S., Candelone, J.-P., Boutron, C.F., 1997. Lead from carthaginian and roman Spanish mines isotopically identified in Greenland ice dated from 600 B.C. to 300 A.D. Environ. Sci. Technol. 31, 3413–3416. doi:10.1021/es970038k.
Rothwell, J.J., Evans, M.G., Lindsay, J.B., Allott, T.E.H. 2007. Scale-dependent spatial variability in peatland lead pollution in the southern Pennines, UK. Environmental Pollution 145: 111-120. eScholarID:1b6283 | DOI:10.1016/j.envpol.2006.03.037.
Rouxel, O., Ludden, J., Fouquet, Y., 2003. Antimony isotope variations in natural systems and implications for their use as geochemical tracers. Chemical Geology 200, 25–40. doi:10.1016/S0009-2541(03)00121-9.
Rowell, C., Kuiper, N., Al-Saad, K., Nriagu, J., Shomar, B., 2014. A market basket survey of As, Zn and Se in rice imports in Qatar: Health implications. Food and Chemical Toxicology 70, 33–39. doi:10.1016/j.fct.2014.04.041.
Salminen, R. (chief ed.), Batista M.J., Bidovec M., Demetriades A., De Vivo B., De Vos W *et al*. 2005. Geochemical Atlas of Europe. Part 1 - Background Information, Methodology and Maps. Geological Survey of Finland, Otamedia Oy, Espoo, 525 pp.
Sander L.C., Wise S.A., 1997. Polycyclic aromatic hydrocarbon structure index. NIST Special Publication 922, NSPUE2. United States Department of Commerce Technology Administration, National Institute of Standards and Technology, Gaithersburg, MD, pp 1–105.
Sanders, P.G., Xu, N., Dalka, T.M., Maricq, M.M., 2003. Airborne brake wear debris: size distributions, composition, and a comparison of dynamometer and vehicle tests. Environmental Science & Technology 37 (18), 4060-4069.
Sankar, T.V., Zynudheen, A.A., Anandan, P.G., Viswanathan, N.P.G., 2006. Distribution of organochlorine pesticides and heavy metal residues in fish and shellfish from Calicut region, Kerala, India. Chemosphere 65, 583–590.
Sartorious, US. http://www.sartorius.us/us/services/laboratory/download-center/?tx_solr[q]=&tx_solr[page]=182 (accessed 27th of March 2015).
Scheetz, C.D., Donald Rimstidt, J., 2008. Dissolution, transport, and fate of lead on a shooting range in the Jefferson National Forest near Blacksburg, VA, USA. Environmental Geology 58, 655–665. doi:10.1007/s00254-008-1540-5.
SCHER (Scientific Committee on Health and Environmental Risks), 2011. Opinion on Lead Standard in Drinking Water, 11 January 2011.
Schroeder, W.H., Dobson, M., Kane, D.M., Johnson, N.D., 1987. Toxic Trace Elements Associated with Airborne Particulate Matter: A Review. Journal of the Air Pollution Control Association 37, 1267–1285. doi:10.1080/08940630.1987.10466321.
Schroth, A.W., Bostick, B.C., 2008. Lead sequestration and species redistribution during soil organic matter decomposition. Environmental Science & Technology 42, 3627–33.
Schwikowski, M., 2004. Reconstruction of European Air Pollution from Alpine Ice Cores, in: Cecil, L.D., Green, J.R., Thompson, L.G. (Eds.), Earth Paleoenvironments: Records Preserved in Mid-

and Low-Latitude Glaciers, Developments in Paleoenvironmental Research. Springer Netherlands, pp. 95–119.
SEPA, Scottish Government, 2013 Implementing the water environment and water services (Scotland) Act 2003: Environmental standards for water environment, a consultation.
SEPA , Scottish Environment Protection Agency, 2008. Control of priority and dangerous substances and specific pollutants in the water environment. EP061 v1.
SEPA, Scottish Environment Protection Agency, 2013. Supporting Guidance (WAT-SG-53)-Environmental standards for discharges to surface waters. Ver:4.0.
SEPA, Scottish Environment Protection Agency, 2014. Supporting guidance-Environment quality standards and standards for discharges to surface water, (WAT-SG-53). July, version 5.1.
SEPA, Scottish Environment Protection Agency. Scottish Pollutant Release Inventory (SPRI) http://www.sepa.org.uk/air/process_industry_regulation/pollutant_release_inventory.aspx (accessed 18 March 2015).
Scottish Natural Heritage, 2001, Boglands-Scotland's living landscapes. ISBN:1853971020.
Settle, D.M., Patterson, C.C., 1980. Lead in albacore: guide to lead pollution in Americans. Science 207, 1167–1176. doi:10.1126/science.6986654.
Sh, T., Liu, C.Q., Feng, C., 2012. Solubility, toxicity and sorption of antimony from smelter release. Journal of Geochemical Exploration 118, 14–18. doi:10.1016/j.gexplo.2012.03.007.
Shepherd, T.J., Chenery, S.R.N., Pashley, V., Lord, R.A., Ander, L.E., Breward, N., Hobbs, S.F., Horstwood, M., Klinck, B.A., Worrall, F., 2009. Regional lead isotope study of a polluted river catchment: River Wear, Northern England, UK. Science of the Total Environment 407, 4882–4893. doi:10.1016/j.scitotenv.2009.05.041.
Shen, H., Tao, S., Wang, R., Wang, B., Shen, G., Li, W., Su, S., Huang, Y., Wang, X., Liu, W., Li, B., Sun, K., 2011. Global time trends in PAH emissions from motor vehicles. Atmospheric Environment 45, 2067–2073. doi:10.1016/j.atmosenv.2011.01.054.
Shi, Z., Allen, H.E., Di Toro, D.M., Lee, S.Z., Harsh, J.B., 2013. Predicting Pb^{II} adsorption on soils: the roles of soil organic matter, cation competition and iron (hydr)oxides. Environmental Chemistry 10, 465-474.
Shikazono, N., Zakir, H.M., Sudo, Y., 2008. Zinc contamination in river water and sediments at Taisyu Zn–Pb mine area, Tsushima Island, Japan. Journal of Geochemical Exploration 98, 80–88. doi:10.1016/j.gexplo.2007.12.002.
Shirahata, H., Elias, R.W., Patterson, C.C., Koide, M., 1980. Chronological variations in concentrations and isotopic compositions of anthropogenic atmospheric lead in sediments of a remote subalpine pond. Geochimica et Cosmochimica Acta 44, 149–162. doi:10.1016/0016-7037(80)90127-1.
Shotyk, W., Cheburkin, A.K., Appleby, P.G., Fankhauser, A., Kramers, J.D., 1996. Two thousand years of atmospheric arsenic, antimony, and lead deposition recorded in an ombrotrophic peat bog profile, Jura Mountains, Switzerland. Earth and Planetary Science Letters 145, E1–E7. doi:10.1016/S0012-821X(96)00197-5.
Shotyk, W., Blaser, P., Grunig, A., Cheburkin, A.K., 2000. A new approach for quantifying cumulative, anthropogenic, atmospheric lead deposition using peat cores from bogs: Pb in eight Swiss peat bog profiles. The Science of the Total Environment 249, 281e295.
Shotyk, W., Krachler, M., Martinez-Cortizas, A., Cheburkin, A.K., Emons, H., 2001. A peat bog record of natural, pre-anthropogenic enrichments of trace elements in atmospheric aerosols since 12 370 14C yr BP, and their variation with Holocene climate change. Earth and Planetary Science Letters 199, 21–37. doi:10.1016/S0012-821X(02)00553-8.
Shotyk, W., Weiss, D., Heisterkamp, M., Cheburkin, A.K., Appleby, P.G., Adams, F.C., 2002. New peat bog record of atmospheric lead pollution in Switzerland: Pb concentrations, enrichment factors, isotopic composition, and organolead species. Environmental Science & Technology. 36, 3893–3900.
Shotyk, W., Krachler, M., Chen, B., 2004. Antimony in recent, ombrotrophic peat from Switzerland and Scotland: Comparison with natural background values (5,320 to 8,020 14C yr BP) and implications for the global atmospheric Sb cycle. Global Biogeochemical Cycles 18, GB1016. doi:10.1029/2003GB002113.
Shumway. L.A., 2000. Trace element and polyaromatic hydrocarbon analysis of jet fuels:jetA, JP5, and JP8. Technical report 1845. SPAWAR Systems centre San Diego.

Skupinska K, Misiewicz I, Kasprzycka-Guttman T. 2004. Polycyclic aromatic hydrocarbons: physiochemical properties, environmental appearance and impact on living organisms. Acta Poloniae Pharmaceutica. 61(3):233–40.

Smichowski, P., 2008. Antimony in the environment as a global pollutant: A review on analytical methodologies for its determination in atmospheric aerosols. Talanta 75, 2–14. doi:10.1016/j.talanta.2007.11.005.

Smith, M.A., Grant, L.D., Sors, A.I., 1989. Lead Exposure and Child Development: An International Assessment. Kluwer Academic, Dordrecht, The Netherlands, pp. 211-223.

Smith, D.J.T., Edelhauser, E.C., Harrison, R.M., 1995. Polycyclic aromatic hydrocarbon concentrations in road dust and soil samples collected in the United Kingdom and Pakistan. Environmental Technology 16, 45–53.

Smith J. T., Appleby P. G., Hilton J. and Richardson N. (1997) Inventories and fluxes of ^{210}Pb, ^{137}Cs and ^{241}Am determined from the soils of three small catchments in Cumbria, UK. Journal of Environmental Radioactivity. 37, 127–142.

Smith, E., Naidu, R., and Alston, A.M., 1999, Chemistry of As in soil: I. Sorption of arsenate and arsenite by four Australian soils. Journal of Environmental Quality, 28, 1719–1726.

Smith, A.M.L., Hudson-Edwards, K.A., Dubbin, W.E., Wright, K., 2006. Dissolution of jarosite [KFe3(SO4)2(OH)6] at pH 2 and 8: Insights from batch experiments and computational modelling. Geochimica et Cosmochimica Acta 70, 608–621. doi:10.1016/j.gca.2005.09.024.

Souchay, P., Peschanski, D., 1948. Contribution a` l'e´tude des phe´nome`nes de condensation en chimie mine´rale. III. Emploi des mesures d'absorption lumineuse. Bulletin de la Societe Chimique. 439– 446.

Spencer, K.L., Cundy, A.B., Croudace, I.W., 2003. Heavy metal distribution and early-diagenesis in salt marsh sediments from the Medway Estuary, Kent, UK. Estuarine, Coastal and Shelf Science 57, 43–54. doi:10.1016/S0272-7714(02)00324-4.

Sproal, R., Turoczy, N.J., Stagnitti, F., 2002. Chemical and physical speciation of arsenic in a small pond receiving gold mine waste effluent. Ecotoxicolgy and Environmental Safety. 53, 370–375.

Steely, S., Amarasiriwardena, D., Xing, B., 2007. An investigation of inorganic antimony species and antimony associated with soil humic acid molar mass fractions in contaminated soils. Environmental Pollution 148, 590–598. doi:10.1016/j.envpol.2006.11.031

Steinnes, E., Berg, T., Uggerud, H.T., 2011. Three decades of atmospheric metal deposition in Norway as evident from analysis of moss samples. Science of the Total Environment 412–413, 351–358. doi:10.1016/j.scitotenv.2011.09.086

Stephan, C.H., Courchesne, F., Hendershot, W.H., McGrath, S.P., Chaudri, A.M., Sappin-Didier, V., Sauvé, S., 2008. Speciation of zinc in contaminated soils. Environmental Pollution 155, 208–216.Boni, M., Mondillo, N., 2015. The "Calamines" and the "Others": The great family of supergene nonsulfide zinc ores. Ore Geology Reviews 67, 208–233. doi:10.1016/j.oregeorev.2014.10.025

Sugden, C.L., Farmer, J.G., MacKenzie,A.B. 1991a. Lead and 206Pb/207Pb profiles in ^{210}Pb dated ombrotrophic peat cores from Scotland. In: J.G. Farmer (Editor), Proceedings of the Eight International Conference on Heavy Metals in the Environment. CEP, Edinburgh, Vol 1, pp, 90-93.

Sugden, C.L., Farmer, J.G., MacKenzie,A.B. 1991b. Isotopic characterisation of lead inputs and behaviour in recent Scottish freshwater loch sediments. In: J.G. Farmer (Editor), Proceedings of the Eight International Conference on Heavy Metals in the Environment. CEP, Edinburgh, Vol 1, pp, 511-514.

Sugden, C.L., Farmer, J.G., Mackenzie, A.B., 1993. Isotopic ratios of lead in contemporary environmental material from Scotland. Environmental Geochemical Health 15, 59–65. doi:10.1007/BF02627823.

Sturges, W.T., Barrie, L.A., 1987. Lead 206/207 isotope ratios in the atmosphere of North America as tracers of US and Canadian emissions. Nature 329: 144–6.

Su, Y.-H., Zhu, Y.-G., 2008. Uptake of selected PAHs from contaminated soils by rice seedlings (Oryza sativa) and influence of rhizosphere on PAH distribution. Environmental Pollution 155, 359–365. doi:10.1016/j.envpol.2007.11.008.

Sutherland, R.A., 2010. BCR®-701: A review of 10-years of sequential extraction analyses. Analytica Chimica Acta 680, 10–20. doi:10.1016/j.aca.2010.09.016.

Sutherland R.C. and Jelen S.L., 1996. Studies Show Sweeping has Beneficial Impact on Stormwater Quality, Published APWA Reporter, Volume 63, No.10, pp.8.Taiwan National Science Council (2002).

Świetlik, R., Trojanowska, M., Strzelecka, M., Bocho-Janiszewska, A., 2015. Fractionation and mobility of Cu, Fe, Mn, Pb and Zn in the road dust retained on noise barriers along expressway – A potential tool for determining the effects of driving conditions on speciation of emitted particulate metals. Environmental Pollution 196, 404–413. doi:10.1016/j.envpol.2014.10.018

Taylor, S.R., 1964. Abundance of chemical elements in the continental crust: a new table. Geochimica et Cosmochimica Acta 28, 1273–1285

Taylor, H.T. 2001. Inductively Coupled Plasma-Mass Spectrometry. Academic press.

Tchounwou, P.B., Udensi, U.K., Isokpehi, R.D., Yedjou, C.G., Kumar, S., 2015. Arsenic and Cancer, in: Flora, S.J.S. (Ed.), Handbook of Arsenic Toxicology. Academic Press, Oxford, 23, pp. 533–555.

Telford, K., Maher, W., Krikowa, F., Foster, S., 2008. Measurement of total antimony and antimony species in mine contaminated soils by ICPMS and HPLC-ICPMS. Journal of Environmental Monitoring 10, 136. doi:10.1039/b715465h.

Tella, M., Pokrovski, G.S., 2012. Stability and structure of pentavalent antimony complexes with aqueous organic ligands. Chemical Geology 292–293, 57–68. doi:10.1016/j.chemgeo.2011.11.004.

Tella, M., Pokrovski, G.S., 2009. Antimony (III) complexing with O-bearing organic ligands in aqueous solution: an X-ray absorption fine structure spectroscopy and solubility study, Geochimica Cosmochimica Acta 73, 268–290.

Tera, O., Schwartzman, D.W., Watkins, T.R., 1985. Identification of gasoline lead in children's blood using isotopic analysis. Archives of Environmental Health 40:120–.3

Tessier, A., Campbell, P.G.C., Bisson, M., 1979. Sequential extraction procedure for the speciation of particulate trace metals. Analytical Chemistry. 51, 844–851. doi:10.1021/ac50043a017.

Tessier, A., P. G. C. Campbell, and M Bisson. 1980. Trace metal speciation in the Yamaoka and St. Francois Rivers (Quebec). Canadian Journal of Earth Sciences. 17:90-105.

Thanabalasingam, P., Pickering, W.F., 1990. Specific sorption of antimony (III) by the hydrous oxides of Mn, Fe, and Al. Water Air Soil Pollution 49, 175–185. doi:10.1007/BF00279519.

Tian, H., Zhou, J., Zhu, C., Zhao, D., Gao, J., Hao, J., He, M., Liu, K., Wang, K., Hua, S., 2014. A comprehensive global inventory of atmospheric Antimony emissions from anthropogenic activities, 1995-2010. Environmental Science & Technology. 48, 10235–10241. doi:10.1021/es405817u.

Tighe, M., Lockwood, P., Wilson, S., 2005. Adsorption of antimony(V) by floodplain soils, amorphous iron(III) hydroxide and humic acid. Journal Environmental Monitoring. 7, 1177–1185. doi:10.1039/B508302H.

Tipping, E., 2002. Cation Binding by Humic Substances. Cambridge University Press.

Tobiszewski, M., Namieśnik, J., 2012. PAH diagnostic ratios for the identification of pollution emission sources. Environmental Pollution 162, 110–119.

Tongesayi, T., Smart, R.B., 2007. Abiotic reduction mechanism of As(V) by fulvic acid in the absence of light and the effect of Fe(III), Water South Africa 33 615–618.

Topsoil. The contaminated land exposure assessment (CLEA) Department for environment food and rural affairs, 2007. The air quality strategy for England, Scotland, Wales and Northern Ireland. Cm 7169 NIA 61/06-07. July 2007.

Tsaihwa J, John L. Lead isotopes in North American coals. Science 1972;176:510–1 Tchounwou, P.B., Udensi, U.K., Isokpehi, R.D., Yedjou, C.G., Kumar, S., 2015. 23 - Arsenic and Cancer, in: Flora, S.J.S. (Ed.), Handbook of Arsenic Toxicology. Academic Press, Oxford, pp. 533–555.

Tylenda, C.A., Sullivan Jr., D.W., Fowler, B.A., 2015. Chapter 27 - Antimony, in: Nordberg, G.F.N.A.F. (Ed.), Handbook on the Toxicology of Metals (Fourth Edition). Academic Press, San Diego, pp. 565–579.

UKpia. 2015. Statistical Review.

UKTAG. 2008. Proposals for Environmental Quality Standards for Annex VIII Substances. UK Technical Advisory Group on the Water Framework Directive.

UKTAG. 2010. Water Framework Directive: An approach to the revoked directives:-the freshwater fish directive, the shellfish directive and the dangerous substances directive. UK Technical Advisory Group on the Water Framework Directive.

Ulrich, N., 1998. Speciation of antimony(III), antimony(V) and trimethylstiboxide by ion chromatography with inductively coupled plasma atomic emission spectrometric and mass spectrometric detection. Analytica Chimica Acta 359, 245–253. doi:10.1016/S0003-2670(97)00656-9.

United Nations, 2001. Synthesis Report on Arsenic in Drinking Water.
University of Cambridge, physics. http://www-outreach.phy.cam.ac.uk/camphy/xraydiffraction/xraydiffraction7_1.htm (accessed 27th of March 2015).
Ure, A.M., Quevauviller, P.H., Muntau, H., Griepink, B., 1993. Speciation of heavy metals in soils and sediments. An account of the improvement and harmonization of extraction techniques undertaken under the auspices of the BCR of the commission of the European communities. International Journal of Environmental Analytical Chemistry.51:135–151.
U.S. Department of Agriculture, Agricultural Research Service. 2011. USDA National Nutrient Database for Standard Reference, Release 24. Nutrient Data Laboratory Home Page, http://www.ars.usda.gov/ba/bhnrc/ndl
U.S. Geological Survey, 2013, Mineral commodity summaries 2013: U.S. Geological Survey, p.198.
USDA. 1999. Soil Taxonomy. A basic system of soil classification for making and interpreting soil surveys. Second edition.
Vallius, H., 2014. Heavy metal concentrations in sediment cores from the northern Baltic Sea: Declines over the last two decades. Marine Pollution Bulletin 79, 359–364. doi:10.1016/j.marpolbul.2013.11.017.
Valotto, G., Rampazzo, G., Visin, F., Gonella, F., Cattaruzza, E., Glisenti, A., Formenton, G., Tieppo, P., 2015 Environmental and traffic-related parameters affecting road dust composition: A multi-technique approach applied to Venice area (Italy). Atmospheric Environment. 122, 596-608. Doi:10.1016/j.atmosenv.2015.10.006.
Van de Velde, K., Ferrari, C., Barbante, C., Moret, I., Bellomi, T., Hong, S., Boutron, C., 1999. A 200 Year Record of Atmospheric Cobalt, Chromium, Molybdenum, and Antimony in High Altitude Alpine Firn and Ice. Environmental Science and Technology. 33, 3495–3501. doi:10.1021/es990066y.
Van den Berg, G.A., Loch, J.P.G., van der Heijdt, L.M., Zwolsman, J.J.G., 1998. Vertical distribution of acid-volatile sulfide and simultaneously extracted metals in a recent sedimentation area of the river Meuse in the Netherlands. Environmental Toxicology and Chemistry 17, 758–763. doi:10.1002/etc.5620170433.
Vane, C.H., Harrison, I., Kim, A.W., 2007. Assessment of polyaromatic hydrocarbons (PAHs) and polychlorinated biphenyls (PCBs) in surface sediments of the Inner Clyde Estuary, UK. Marine Pollution Bulletin 54, 1301–1306. doi:10.1016/j.marpolbul.2007.04.005.
Vane, C.H., Chenery, S.R., Harrison, I., Kim, A.W., Moss-Hayes, V., Jones, D.G., 2011. Chemical signatures of the Anthropocene in the Clyde estuary, UK: sediment-hosted Pb, 207/206Pb, total petroleum hydrocarbon, polyaromatic hydrocarbon and polychlorinated biphenyl pollution records. Philosophical Transactions of the Royal Society of London A: Mathematical, Physical and Engineering Sciences 369, 1085–1111. doi:10.1098/rsta.2010.0298.
Vane, C.H., Kim, A.W., Beriro, D.J., Cave, M.R., Knights, K., Moss-Hayes, V., Nathanail, P.C., 2014. Polycyclic aromatic hydrocarbons (PAH) and polychlorinated biphenyls (PCB) in urban soils of Greater London, UK. Applied geochemistry 51, 303–314.
Vanhaecke, F., Balcaen, L., Malinovsky, D., 2009. Use of single-collector and multi-collector ICP-mass spectrometry for isotopic analysis. Journal of Analytical Atomic Spectrometry. 24, 863–886. doi:10.1039/B903887F.
Varrica, D., Bardelli, F., Dongarrà, G., Tamburo, E., 2013. Speciation of Sb in airborne particulate matter, vehicle brake linings, and brake pad wear residues. Atmospheric Environment 64, 18–24. doi:10.1016/j.atmosenv.2012.08.067.
Véron, A., Flament, P., Bertho, M.L., Alleman, L., Flegal, R., Hamelin, B., 1999. Isotopic evidence of pollutant lead sources in Northwestern France. Atmospheric Environment 33:3377–3388. doi:10.1016/S1352-2310(98)00376-8.
Vile, M.A., Wieder, R.K., Novák, M., 1999. Mobility of Pb in Sphagnum-derived peat. Biogeochemistry 45, 35–52. doi:10.1023/A:1006085410886.
Von Gunten, H.R., Sturm, M., Moser, R.N., 1997. 200-Year Record of Metals in Lake Sediments and Natural Background Concentrations. Environmental Science & Technology. 31, 2193–2197. doi:10.1021/es960616h.
VROM, 2000. Dutch target and intervention values. Annex I.
Wang, W.H., Wong, M.H., Leharne, S., Fisher, B., 1998. Fractionation and Biotoxicity of Heavy Metals in Urban Dusts Collected from Hong Kong and London. Environmental Geochemistry and Health 20, 185–198. doi:10.1023/A:1006530300522.

Wang, Z., Chen, J., Qiao, X., Yang, P., Tian, F., Huang, L., 2007. Distribution and sources of polycyclic aromatic hydrocarbons from urban to rural soils: A case study in Dalian, China. Chemosphere 68, 965–971. doi:10.1016/j.chemosphere.2007.01.017.

Wang, S., Mulligan, C.N., 2008. Speciation and surface structure of inorganic arsenic in solid phases: A review. Environment International 34, 867–879. doi:10.1016/j.envint.2007.11.005.

Walker, F.P., Schreiber, M.E., Rimsdidt, J.D., 2006. Kinetics of arseonopyrite oxidative dissolution by oxygen. Geochimica Cosmochimica Acta 70, 1668–1676.

Washington University in St Louis. School of engineering & applied science. http://eecelabs.seas.wustl.edu/ICP-MS.aspx (accessed 20th of March 2015).

Weatheronline. Edinburgh Airport. http://www.weatheronline.co.uk/weather/maps/city?WMO=03160&CONT=ukuk&LAND=UK&ART=WDR&LEVEL=162&MOD=tab (accessed February 2016)

Webster, L., Russell, M., Walsham, P., Phillips, L.A., Packer, G., Scurfield, J.A., Dalgarno, E.J.,Moffat, C.F., 2008. Long term monitoring of persistent organic pollutants (POPS) in wild and rope grown blue mussels (*mytilius edulis*) from Scottish coastal waters, Fisheries Research Services Internal Report No 28/08. December.

Wedepohl, K.H., 1995. The composition of the continental crust. Geochimica et Cosmochimica Acta 59, 1217–1232.

Weiss, D., Shotyk, W., Boyle, E.A., Kramers, J.D., Appleby, P.G., Cheburkin, A.K., 2002. Comparative study of the temporal evolution of atmospheric lead deposition in Scotland and eastern Canada using blanket peat bogs. Science of the Total Environment, Peat Bog Archives of Atmospheric Metal Deposition 292, 7–18. doi:10.1016/S0048-9697(02)00025-6.

WHO, 1978. Evaluation of certain food additives and contaminants. WHO technical report Series, No. 631.

WHO, 1996. Trace elements in human nutrition and health. ISBN 9241581734.

WHO, 2003. Copper in drinking-water. Background document for preparation of WHO Guidelines for drinking-water quality. Geneva, World Health Organization (WHO/SDE/WSH/03.04/88).

WHO, 2008. Guidelines for drinking-water quality, third edition, incorporating first and second agenda. Geneva: World Health Organization.

WHO, 2011. Guidelines for Drinking Water Quality. vol.4. World Health Organisation, Geneva, pp.315–318.

Wick, A.F., Haus, N.W., Sukkariyah,B.F., Haering, K.C., Lee Daniels, W., 2011. Remediation of PAH-contaminated soils and sediments:A literature review. Virgina Polytechnic Institute and State University.

Wilson, G.V., 1921. In: The lead, Zinc, Copper and Nickel Ores of Scotland. Member of the Geological Survey. Great Britain Mineral Resource 17:93-106.

Wilson, P., Mairs, A., Bailey, S., 2005. Building with Scottish Stone. Arcamedia. ISBN 1-904320-02-3.

Windfinder.com - Wind and weather statistic Edinburgh Airport. Windfinder.com. URL http://www.windfinder.com/windstats/windstatistic_edinburgh.htm (accessed 30th of March 2015).

Wilson, G.V., 1921. In: The lead, zinc, copper and nickel ores of Scotland. Memoirs of the Geological Survey. G.B. Mineral Resource. 17:93-106.

Wilson, G.V., 1921. Special Reports on the Mineral Resources of Great Britain, Memoirs of the Geological Survey, Scotland, Volume XVII.

Wilson, S.C., Lockwood, P.V., Ashley, P.M., Tighe, M., 2010. The chemistry and behaviour of antimony in the soil environment with comparisons to arsenic: A critical review. Environmental Pollution 158, 1169–1181.

Winneke, G., Kramer, U., Brockhaus, A., Ewers, U., Kujanek, G., Lechner, H., *et al.*, 1983. Neuropsychological studies in children with elevated tooth-lead concentrations: II. Extended studies. International Archives of. Occupational Environmental Health 51, 231-252.

Winneke, G., Collet, W., Lilienthal, H., 1988. The effects of lead in laboratory animals and environmentally-exposed children. Toxicology 49, 291-298.

World Business Council for Sustainable Development. 2013. Mobility: Meeting the challenges to sustainability.

Wu, F., Fu, Z., Liu, B., Mo, C., Chen, B., Corns, W., Liao, H., 2011. Health risk associated with dietary co-exposure to high levels of antimony and arsenic in the world's largest antimony mine area. Science of the Total Environment 409, 3344–3351. doi:10.1016/j.scitotenv.2011.05.033.

Wu, D., Wang, Z., Chen, J., Kong, S., Fu, X., Deng, H., Shao, G., Wu, G., 2014. Polycyclic aromatic hydrocarbons (PAHs) in atmospheric PM2.5 and PM10 at a coal-based industrial city: Implication for PAH control at industrial agglomeration regions, China. Atmospheric Research 149, 217–229. doi:10.1016/j.atmosres.2014.06.012.

Xia, K., Bleam, W., Helmke, P.A., 1997. Studies of the nature of Cu^{2+} and Pb^{2+} binding sites in soil humic substances using X-ray absorption spectroscopy. Geochimica et Cosmochimica Acta 61, 2211–2221. doi:10.1016/S0016-7037(97)00079-3.

Xu, L., Wu, F., Zheng, J., Xie, Q., Li, H., Liao, H., Zhao, X., Guo, F., 2011. Sediment records of Sb and Pb stable isotopic ratios in Lake Qinghai. Microchemical Journal, Antimony: Emerging Global Contaminant in the Environment 97, 25–29. doi:10.1016/j.microc.2010.05.012.

Yafa, C., Farmer, J.G., 2006. A comparative study of acid-extractable and total digestion methods for the determination of inorganic elements in peat material by inductively coupled plasma-optical emission spectrometry. Analytica Chimica Acta 557, 296–303.

Yafa, C., Farmer, J.G., Graham, M.C., Bacon, J.R., Barbante, C., Cairns, W.R.L., Bindler, R., Renberg, I., Cheburkin, A., Emons, H., Handley, M.J., Norton, S.A., Krachler, M., Shotyk, W., Li, X.D., Martinez-Cortizas, A., Pulford, I.D., MacIver, V., Schweyer, J., Steinnes, E., Sjøbakk, T.E., Weiss, D., Dolgopolova, A., Kylander, M., 2004. Development of an ombrotrophic peat bog (low ash) reference material for the determination of elemental concentrations. Journal of Environmental. Monitoring. 6, 493–501. doi:10.1039/B315647H.

Yang, Y., Ratté, D., Smets, B.F., Pignatello, J.J., Grasso, D., 2001. Mobilization of soil organic matter by complexing agents and implications for polycyclic aromatic hydrocarbon desorption. Chemosphere. 43, 1013–1021. doi:10.1016/S0045-6535(00)00498-7.

Yang,Q., Shu, W., Qiu, J.W., Wang, H.B., Lan, Y. 2004. Lead in paddy soils and rice plants Lechang and its potential health risk around lead/zinc Mine, Guangdong, China. Environment international 30, 883–9. doi:10.1016/j.envint.2004.02.002.

Yang, H., Rose, N., 2005. Trace element pollution records in some UK lake sediments, their history, influence factors and regional differences. Environment International 31, 63–75. doi:10.1016/j.envint.2004.06.010.

Yunker, M.B., Macdonald, R.W., Vingarzan, R., Mitchell, R.H., Goyette, D., Sylvestre, S., 2002. PAHs in the Fraser River basin: a critical appraisal of PAH ratios as indicators of PAH source and composition. Organic Geochemistry 33, 489–515. doi:10.1016/S0146-6380(02)00002-5.

Zaharescu, D.G., Hooda, P.S., Soler, A.P., Fernandez, J., Burghelea, C.I., 2009. Trace metals and their source in the catchment of the high altitude Lake Respomuso, Central Pyrenees. Science of the Total Environment 407, 3546–3553. doi:10.1016/j.scitotenv.2009.02.026.

Zhang, Y., Tao, S., 2009. Global atmospheric emission inventory of polycyclic aromatic hydrocarbons (PAHs) for 2004. Atmospheric Environment 43, 812–819.

Zhao, J., Tang, X., W. Huang, W., 2002. Abundance of trace elements in coals of China. Coal Geology China, 14, 5–14.

Zhao, P., Feng, Y., Zhu, T., Wu, J., 2006. Characterizations of resuspended dust in six cities of North China. Atmospheric Environment 40, 5807–5814. doi:10.1016/j.atmosenv.2006.05.026.

Zhao, F.J., McGrath, S.P., Meharg, A.A., 2010. Arsenic as a food chain contaminant: mechanism of plant uptake and metabolism and mitigation strategies. Annual Review of Plant Biology. 61,535–559.

Zhao, H., Li, X., Wang, X., 2011. Heavy Metal Contents of Road-Deposited Sediment along the Urban–Rural Gradient around Beijing and its Potential Contribution to Runoff Pollution. Environ. Sci. Technol. 45, 7120–7127. doi:10.1021/es2003233.

Zhang, D., Lee, D.-J., Pan, X., 2014. Potentially harmful metals and metalloids in urban street dusts of Urumqi City: Comparison with Taipei City. Journal of the Taiwan Institute of Chemical Engineers 45, 2447–2450. doi:10.1016/j.jtice.2014.04.018.

Zheng, J., Ohata, M., Furuta, N., 2000. Antimony Speciation in Environmental Samples by Using High-Performance Liquid Chromatography Coupled to Inductively Coupled Plasma Mass Spectrometry. Analytical Sciences 16, 75–80.

Zheng, J., Iijima, A., Furuta, N., 2001. Complexation effect of antimony compounds with citric acid and its application to the speciation of antimony(III) and antimony(V) using HPLC-ICP-MS. Journal of Analytical Atomic Spectrometry 16, 812–818. doi:10.1039/b101943k.

Zhou, J., Tian, H., Zhu, C., Hao, J., Gao, J., Wang, Y., Xue, Y., Hua, S., Wang, K., 2015. Future trends of global atmospheric antimony emissions from anthropogenic activities until 2050. Atmospheric Environment 120, 385–392. doi:10.1016/j.atmosenv.2015.09.018.

Zhu, C., Zhu, Y., Lu, R., He, R., Xia, Z., 2012. Perceptions and aspirations for car ownership among Chinese students attending two universities in the Yangtze Delta, China. Journal of Transport Geography 24, 315–323.

Zuna, M., Mihaljevič, M., Šebek, O., Ettler, V., Handley, M., Navrátil, T., Goliáš, V., 2011. Recent lead deposition trends in the Czech Republic as recorded by peat bogs and tree rings. Atmospheric Environment 45, 4950–4958. doi:10.1016/j.atmosenv.2011.06.007.

Appendix 1 Calculation of solid phase sample concentrations from acid digest ICP-OES/MS concentration measurements

Equation A1 shown below, was used to calculate solid phase concentrations from acid digest samples analysed by ICP-OES/MS as described in sections 3.3.11 and 3.3.12.

$$\text{Mass of Sb in 25 ml volumetric} = \left(\text{Instrument readout } (\text{mg L}^{-1}) - \text{Sample blank } (\text{mg L}^{-1})\right) \times \left(\text{Volume correction } (\text{L}^{-1}) \; \frac{25}{1000}\right) \times \left(\frac{\text{Sample weight used (mg)}}{1000}\right)$$

Equation A1

Example: Calculation taken for Sb from Auchencorth Moss 0-1 cm profile, sample 1

$$\text{Mass of Sb in 25 ml volumetric} = \left(1.5 - 0.0\right) \times \left(\frac{25}{1000}\right) \times \left(\frac{1000}{0.2528}\right)$$

$$= 0.15 \text{ mg kg}^{-1}$$

Appendix 2 Rainwater pH from five locations in, or near, Edinburgh

Table A1: Mean rainwater pH and S.D. from five locations in, or near, Edinburgh

Edinburgh location	pH value ± 1SD
Bonnyrigg	6.6 ± 0.9
Red moss of Balerno	5.1 ± 0.4
Flotterstone	6.4*
Blackford	6.2 ± 0.6
George square	6.0 ± 0.2

* Only one sample successfully collected rainwater for this location

Appendix 3 Edinburgh Road dust sequential extraction results used in Figures 5.soil core profiles

Table A2: Antimony BCR sequential extraction results for Edinburgh road dust sites

Road dust Site	BCR concentrations (mg kg^{-1})			Aqua regia (mg kg^{-1})	BCR Total (mg kg^{-1})	Aqua regia digest total (mg kg^{-1})	% Recovery
	Step 1	Step 2	Step 3				
A90	0.08	0.13	0.48	10.7	11.4	8.74	130
A70	0.1 ± 0.010	0.02 ± 0.002	0.22 ± 0.039	3.26 ± 0.085	3.59 ± 0.1	2.51	143
A8	0.29 ± 0.052	0.42 ± 0.063	0.66 ± 0.074	2.05 ± 0.037	43.42 ± 0.2	2.68	128
A1	0.12 ± 0.010	0.02 ± 0.006	0.29 ± 0.099	10.7 ± 1.52	11.1 ± 1.6	15.4	72.1
Hillpark Drive	0.04 ± 0.010	0.04 ± 0.010	0.05 ± 0.008	1.13 ± 0.170	1.25 ± 0.2	1.65	75.8
Thistle Street	0.09 ± 0.003	0.07 ± 0.004	0.42 ± 0.018	2.46 ± 0.306	3.04 ± 0.3	8.17	37.2
Redhall Drive	0.09 ± 0.010	0.04 ± 0.005	0.56 ± 0.018	3.39 ± 0.633	4.08 ± 0.7	4.14	98.5
Belmont Crescent	0.05 ± 0.001	0.01 ± 0.001	0.15 ± 0.004	4.68 ± 0.322	4.89 ± 0.3	4.20	116
Cambusnethan Street	0.18 ± 0.001	0.15 ± 0.006	1.08 ± 0.471	4.64 ± 0.181	6.04 ± 0.3	7.96	75.8

Table A3: Lead BCR sequential extraction results for Edinburgh road dust sites

Road dust Site	BCR concentrations (mg kg^{-1})			Aqua regia (mg kg^{-1})	BCR Total (mg kg^{-1})	Aqua regia digest total (mg kg^{-1})	% Recovery
	Step 1	Step 2	Step 3				
A90	1.66 ± 0.49	1.09 ± 0.20	2.96 ± 0.43	15.5 ± 3.14	21.2 ± 4.3	19.0	112
A70	5.18 ± 0.09	2.58 ± 0.36	2.66 ± 0.54	13.9 ± 4.65	24.3 ± 4.6	22.8	105
A8	3.77 ± 1.46	1.44 ± 0.48	9.50 ± 1.16	33.5 ± 1.50	48.2 ± 4.6	30.5	158
A1	7.70 ± 0.09	5.60 ± 0.08	8.34 ± 2.45	18.6 ± 3.22	40.2 ± 5.65	59.3	67.8
Hillpark Drive	0.76 ± 0.08	8.51 ± 0.80	1.72 ± 0.19	34.2 ± 14.5	45.2 ± 14	37.8	120
Thistle Street	54.0 ± 2.74	7.53 ± 0.93	86.0 ± 8.03	172 ± 0.12	319 ± 6.1	297	107
Redhall Drive	1.52 ± 0.07	1.12 ± 0.08	15.0 ± 0.27	39.5 ± 3.21	57.1 ± 3.6	59.0	96.7
Belmont Crescent	5.64	2.60	6.64	17.0	31.9	37.3	85.5
Cambusnethan Street	32.0 ± 11.27	10.6 ± 2.72	75.8 ± 33.6	172 ± 26.2	290 ± 74	337	86.0

Table A4: Copper BCR sequential extraction results for Edinburgh road dust sites

Road dust Site	BCR concentrations (mg kg^{-1})			Aqua regia (mg kg^{-1})	BCR Total (mg kg^{-1})	Aqua regia digest total (mg kg^{-1})	% Recovery
	Step 1	Step 2	Step 3				
A90	76.6 ± 13.3	3.98 ± 0.10	57.1 ± 13.0	89.0 ± 18.1	227 ± 8.17	233	97.4
A70	48.6	6.59	12.7	11.6	79.5	72.0	110
A8	100 ± 6.96	5.00 ± 0.72	11.5 ± 1.00	69.1 ± 6.41	186 ± 15.1	183	102
A1	48.6 ± 3.93	7.55 ± 0.15	17.6 ± 0.10	52.9 ± 3.37	127 ± 0.80	97.4	130
Hillpark Drive	4.87 ± 0.86	4.86 ± 0.85	8.86 ± 3.06	39.8 ± 1.55	58.4 ± 3.22	40.0	146
Thistle Street	14.4 ± 1.32	0.65 ± 0.07	22.3 ± 3.08	45.5 ± 1.48	82.8 ± 5.96	95.8	86.4
Redhall Drive	5.41 ± 0.54	0.14 ± 0.02	35.3 ± 6.15	34.6 ± 2.47	75.5 ± 9.18	71.6	105
Belmont Crescent	19.3 ± 3.21	3.80 ± 1.25	19.3 ± 9.21	46.6 ± 2.83	89.0 ± 14.0	80.1	111
Cambusnethan Street	17.7 ± 0.10	0.39 ± 0.03	34.8 ± 3.29	59.0 ± 0.46	112 ± 2.96	105	107

Table A5: Zinc BCR sequential extraction results for Edinburgh road dust sites

Road dust site	BCR concentrations (mg kg^{-1})			Aqua regia (mg kg^{-1})	BCR Total (mg kg^{-1})	Aqua regia digest total (mg kg^{-1})	% Recovery
	Step 1	Step 2	Step 3				
A90	126 ± 40.7	22.9 ± 3.89	53.3 ± 7.67	94.0 ± 16.9	296 ± 54	355	83.3
A70	48.6 ± 8.76	6.59 ± 0.75	27.4 ± 1.77	55.8 ± 1.80	138 ± 12	141	98.5
A8	172 ± 2.20	27.6 ± 0.34	45.7 ± 1.81	81.0 ± 0.32	326 ± 4.7	235	139
A1	172 ± 9.42	9.54 ± 0.04	49.5 ± 0.26	40.4 ± 1.02	272 ± 11	228	120
Hillpark Drive	47.9 ± 0.96	25.6 ± 0.61	33.6 ± 0.70	26.6 ± 0.42	134 ± 0.8	140	95.7
Thistle Street	223 ± 58.0	31.9 ± 5.89	39.3 ± 2.98	148 ± 8.55	443 ± 75	398	111
Redhall Drive	88.7 ± 4.72	23.0 ± 2.15	28.3 ± 2.1	101 ± 0.01	241 ± 9.0	238	101
Belmont Crescent	93.0 ± 11.9	6.68 ± 0.93	46.3 ± 1.08	37.1 ± 0.86	183 ± 15	162	113
Cambusnethan Street	223 ± 3.96	41.4 ± 2.23	48.2 ± 11.4	152 ± 4.29	465 ± 17	495	93.9

Appendix 4 Glendinning Sb mine analysis results where for solid phase, sequential extraction, porewater and colloidal fractions obtained from C1, SpH1-surface, SpH1-deep and S1-S6 sample locations

Tables A6-A15 show data used in Figures 1-7 and Tables 1-3 presented in Chapter 6.

Table A6: Profile section results for pH, %OM and elemental concentrations for Glendinning C1 location

Depth (cm)	pH	%OM	Fe (%)	Sb (mg kg^{-1})	As (mg kg^{-1})	Pb (mg kg^{-1})
0-2	-	95.3	0.11 ± 0.1	0.80 ± 0.5	0.52 ± 0.02	3.07 ± 1.4
2-4	-	85.8	0.43 ± 0.2	0.70 ± 0.5	0.43 ± 0.08	6.45 ± 0.1
4-6	4.1	35.5	1.52 ± 0.1	0.41 ± 0.3	0.63 ± 0.03	34.4 ± 1.0
6-8	4.0	28.5	1.86 ± 0.1	0.43 ± 0.1	0.72 ± 0.03	40.2 ± 0.4
8-10	3.9	18.8	2.21 ± 0.2	1.18 ± 0.4	0.70 ± 0.05	43.2 ± 0.5
10-12	4.0	18.2	1.94 ± 0.1	0.41 ± 0.2	0.91 ± 0.34	57.1 ± 21
12-14	4.0	19.0	2.30 ± 0.1	0.63 ± 0.5	0.85 ± 0.3	38.7 ± 1.5
14-16	4.0	17.3	3.35 ± 0.4	0.84 ± 0.4	0.65 ± 0.02	40.7 ± 0.2
16-18	4.1	15.0	2.49 ± 0.1	0.92 ± 0.3	0.67 ± 0.01	39.0 ± 0.4
18-20	4.1	14.8	2.74 ± 0.1	0.78 ± 0.5	0.68 ± 0.02	33.9 ± 0.3

-indicates insufficient sample material

Table A7: Replicate results for pH, %OM and elemental concentrations for Glendinning SpH1-surface samples

Replicate Number	%OM	Fe (%)	Sb (mg kg^{-1})	As (mg kg^{-1})	Pb (mg kg^{-1})
1	9.7	5.10	174	81.5	9222
2	9.5	5.37	302	85.0	1020
3	7.4	3.99	210	77.5	873
4	7.3	5.05	256	74.0	949
5	10.9	5.11	203	83.5	934
6	8.1	5.26	180	79.7	917
Mean result		4.98	221	80.2	937
SD		0.5	50	4.0	50

Table A8: Replicate results for pH, %OM and elemental concentrations for Glendinning SpH1-deep samples

Replicate Number	%OM	Fe (%)	Sb (mg kg^{-1})	As (mg kg^{-1})	Pb (mg kg^{-1})
1	2.8	4.46	402	125	478
2	3.2	420	342	104	476
3	3.2	4.31	300	110	421
4	-	-	-	-	-
5	3.6	411	329	119	527
6	3.8	410	541	115	621
Mean result		3.53	382	115	405
SD		1.7	96	8.0	15

-indicates spilled sample

Table A9: Profile section results for pH, %OM and elemental concentrations for Glendinning S1, S2 and S3 locations

Depth (cm)	%OM	Fe (%)	Sb (mg kg^{-1})	As (mg kg^{-1})	Pb (mg kg^{-1})
Sample site **(S1)**					
0-2	38.6	3.83 ± 0.1	132 ± 40	34.9 ± 2.2	398 ± 8.7
2-4	25.4	4.77 ± 0.1	102 ± 2.6	45.0 ± 0.1	462 ± 18
4-6	12.3	5.65 ± 0.2	106 ± 0.3	57.2 ± 1.4	487 ± 50
6-8	6.6	5.80	55.4	46.6	390
Sample site **(S2)**					
0-2	77.2	1.02 ± 0.1	149 ± 1.3	5.68 ± 0.4	91.6 ± 2.7
2-4	68.3	1.93 ± 0.3	222 ± 42	16.3 ± 2.0	211 ± 30
4-6	36.4	4.22 ± 0.5	117 ± 47	45.2 ± 5.5	475 ± 40
6-8	26.4	4.81 ± 0.4	129 ± 3.0	47.7 ± 8.9	710 ± 33
8-11	21.0	4.86 ± 0.3	95.5 ± 26	55.6 ± 1.7	498 ± 9.8
Sample site **(S3)**					
0-2	44.9	2.44 ± 0.3	261 ± 7.1	11.7 ± 2.0	85.0 ± 11
2-4	41.3	2.84 ± 0.1	183 ± 10	13.9 ± 1.3	97.1 ± 2.1
4-6	31.5	3.55 ± 0.1	183 ± 10	17.4 ± 0.2	114 ± 1.8
6-8	36.8	6.63 ± 0.1	224 ± 8.5	15.8 ± 1.0	104 ± 4.8
8-10	18.0	4.02 ± 0.8	82.7	18.2 ± 0.2	104 ± 0.5
10-12	14.3	5.48 ± 0.2	50.8 ± 16	19.1 ± 0.5	90.9 ± 2.1

Table A10: Profile section results for pH, %OM and elemental concentrations for Glendinning S4, S5 and S6 locations

Depth (cm)	%OM	Fe (%)	Sb (mg kg^{-1})	As (mg kg^{-1})	Pb (mg kg^{-1})
Sample site **(S4)**					
0-2	53.6	2.51 ± 0.1	121 ± 12	18.4 ± 0.5	52.2 ± 24
2-4	43.7	4.04 ± 0.1	157 ± 6.3	28.4 ± 1.6	419 ± 0.1
4-6	36.1	4.60 ± 0.1	170 ± 50	38.0 ± 2.7	468 ± 7.9
6-8	28.8	5.61 ± 0.1	171 ± 22	53.8 ± 2.2	521 ± 0.3
8-10	25.0	6.28 ± 0.6	188	75.3 ± 9.0	546 ± 34
10-12	23.2	5.87 ± 0.1	146	34.2 ± 0.2	632 ± 6.7
Sample site **(S5)**					
0-2	48.4	2.08 ± 0.1	65.9 ± 10	3.09 ± 0.1	31.0 ± 0.5
2-4	45.2	2.60 ± 0.1	76.1 ± 8.7	3.87 ± 0.1	40.2 ± 0.2
4-6	38.2	2.90 ± 0.1	91.2 ± 26	4.34 ± 0.2	46.3 ± 0.8
6-8	30.7	3.17 ± 0.1	71.0 ± 1.0	5.16 ± 0.1	50.6 ± 0.8
8-10	27.7	3.27 ± 0.2	71.7 ± 8.8	5.28 ± 0.3	52.1 ± 5.0
10-12	22.8	3.46 ± 0.2	67.7 ± 7.9	5.92 ± 0.5	48.9 ± 3.8
Sample site **(S6)**					
0-2	44.6	1.94 ± 0.6	6.78 ± 5.7	0.36 ± 0.2	27.9 ± 13
2-4	32.1	2.91 ± 0.1	16.8 ± 3.5	1.10 ± 0.1	70.2 ± 0.2
4-6	18.3	4.29 ± 0.1	16.7 ± 0.1	1.28 ± 0.1	83.7 ± 0.1
6-9	13.0	4.50 ± 0.2	21.7 ± 2.9	1.40 ± 0.4	88.6 ± 1.6

Table A11: Glendinning sequential extraction results for soil core profiles S2 (2-4cm), S2 (6-8 cm), S3 (2-4 cm), S4 (4-6 cm), S4 (8-10 cm) and S5 (4-6 cm)

Element	BCR concentrations (mg kg^{-1})			Aqua regia (mg kg^{-1})	BCR Total (mg kg^{-1})	HF digest total (mg kg^{-1})	% Recovery
	Step 1	Step 2	Step 3				
S2: 2-4 cm							
Sb	2.51 ± 0.1	1.29 ± 0.1	90.2 ± 4.5	42.6 ± 0.8	137	221	61.8
As	2.91 ± 0.1	1.33 ± 0.1	10.8 ± 1.0	1.77 ± 0.3	16.8	16.3	103
Pb	0.48 ± 0.2	0.28 ± 0.1	103 ± 2.3	46.9 ± 4.9	151	211	71.6
Fe	8.36 ± 0.1	377 ± 6.8	6670 ± 424	3860 ± 180	10900	19300	56.5
S2: 6-8 cm							
Sb	3.45 ± 0.1	3.00 ± 0.1	9.21 ± 0.4	170 ± 1.1	186	129	144
As	1.52 ± 0.1	3.75 ± 0.1	4.83 ± 0.2	15.2 ± 2.3	25.3	47.7	53.0
Pb	2.31 ± 0.2	9.31 ± 0.2	139 ± 2.0	439 ± 10	590	710	63.0
Fe	8.77 ± 0.2	2430 ± 87	4380 ± 410	23500 ± 1700	30300	48100	73.9
S3: 2-4 cm							
Sb	4.15 ± 0.1	2.39 ± 0.1	29.6 ± 2.2	124 ± 2.7	160	183	87.4
As	1.71 ± 0.1	1.84 ± 0.1	5.55 ± 0.1	8.29 ± 0.1	17.4	13.9	125
Pb	0.39 ± 0.1	0.33 ± 0.1	17.8 ± 1.5	62.7 ± 1.2	81.2	97.1	83.6
Fe	7.06 ± 0.1	740 ± 61	3920 ± 0.8	12500 ± 203	17200	28400	60.6
S4: 4-6 cm							
Sb	3.01 ± 0.1	2.67 ± 0.1	18.2 ± 1.0	126 ± 48	150	170	88.2
As	1.00 ± 0.1	1.24 ± 0.1	7.87 ± 0.7	28.4 ± 19	38.5	38.0	101
Pb	1.65 ± 0.1	7.15 ± 0.1	83.9 ± 0.7	229 ± 144	322	468	68.8
Fe	16.1 ± 0.6	2870 ± 153	4740 ± 745	15900 ± 1420	23500	45900	51.2

Table A11 ***continued.***

Element	BCR concentrations (mg kg^{-1})			Aqua regia (mg kg^{-1})	BCR Total (mg kg^{-1})	HF total	% Recovery
	Step 1	Step 2	Step 3				
S4: 8-10 cm							
Sb	4.50 ± 0.5	3.81 ± 0.1	7.87 ± 1.0	201 ± 25	217	188	116
As	0.82 ± 0.1	2.89 ± 0.2	4.50 ± 0.4	29.2 ± 1.8	37.4	75.3	50.0
Pb	1.49 ± 0.2	5.94 ± 0.5	56.2 ± 4.5	331 ± 20	395	546	72.2
Fe	15.3 ± 1.6	4020 ± 112	4040 ± 218	27800 ±2520	35900	48200	57.1
S5: 4-6 cm							
Sb	0.56 ± 0.1	0.72 ± 0.1	10.9*	50.3*	62.5*	91.2	68.5
As	0.10 ± 0.1	0.78 ± 0.1	1.41*	1.00*	3.29*	4.4	74.8
Pb	0.30 ± 0.1	0.26 ± 0.1	14.7*	24.1*	39.4*	46.3	85.1
Fe	7.30 ± 0.1	667 ± 13	3980*	14080*	18700*	29000	64.5

***** Sample loss

Table A12: Porewater and ultrafiltration concentrations and mass balance for S2

Depth (cm)	Total porewater concentration (µg/l)				Retentate concentration (µg/l)				Filtrate concentration (µg/l)				Total retentate and filtrate concentration (µg/l)				Ultrafiltration / porewater % recovery			
	Sb	As	Pb	Fe	Sb	As	Pb	Fe	Sb	As	Pb	Fe	Sb	As	Pb	Fe	Sb	As	Pb	Fe
2-4	13.9	1250	48.9	2050	8.80	697	36.0	1560	4.90	711	4.0	61.7	13.7	1410	40.0	1620	98.6	113	81.8	79.1
4-6	23.9	1570	80.6	3580	18.3	1020	80.0	3090	7.80	642	1.0	85.4	26.1	1660	81.0	3180	109	106	100	88.7
6-8	34.2	1700	87.1	3620	18.4	1020	73.0	3240	15.8	664	0.7	96.7	34.2	1680	73.7	3340	100	99.1	54.6	92.2
8-10	29.9	1260	58.2	2310	13.2	718	47.0	2190	17.0	565	0.6	77.9	30.2	1280	47.6	2270	101	102	81.8	98.2
10-13					23.0	838	51.0	2300	51.3	763	2.0	94.6	74.3	1600	53.0	2390				

Table A13: Porewater and ultrafiltration concentrations and mass balance for S3

Depth (cm)	Total porewater concentration (µg/l)				Retentate concentration (µg/l)				Filtrate concentration (µg/l)				Total retentate and filtrate concentration (µg/l)				Ultrafiltration / porewater % recovery			
	Sb	As	Pb	Fe	Sb	As	Pb	Fe	Sb	As	Pb	Fe	Sb	As	Pb	Fe	Sb	As	Pb	Fe
0-2	98	327	0.7	2141	36.0	133	1.0	2240	165	508	0.2	16.1	201	641	1.2	2260	206	196	171	106
2-4	206	651	3.6	6522	35.6	160	2.5	4650	160	424	0.2	12.5	196	584	2.7	4660	95.1	89.7	75.0	71.5
4-6	268	682	20.6	29510	6.2	289	11.9	22600	209	271	5.9	19.0	215	560	17.8	22600	80.2	82.1	86.4	76.6
6-8	402	842	40.1	57770	44.7	475	23.4	44000	316	190	11.0	18.0	361	665	34.4	44000	89.8	79.0	85.8	76.1
8-10	524	837	51.4	75930	90.4	601	35.7	64700	386	123	10.0	11.8	476	724	45.7	64700	90.8	86.5	88.9	85.2

Table A14: Porewater and ultrafiltration concentrations and mass balance for S4

Depth (cm)	Total porewater concentration (µg/l)				Retentate concentration (µg/l)				Filtrate concentration (µg/l)				Total retentate and filtrate concentration (µg/l)				Ultrafiltration / porewater % recovery			
	Sb	As	Pb	Fe	Sb	As	Pb	Fe	Sb	As	Pb	Fe	Sb	As	Pb	Fe	Sb	As	Pb	Fe
0-2	1060	3900	3.7	575	216	977	2.4	384	973	3345	<0.1	8.4	1190	4320	2.4	392	112	111	64.9	68.2
2-4	1150	3250	9.5	1240	116	547	5.7	750	1090	2717	<0.1	7.0	1210	3260	5.7	757	105	100	60.0	61.0
4-6	2100	3260	13.1	1550	581	1190	6.6	801	1850	2370	<0.1	6.3	2430	3560	6.6	807	116	109	50.4	52.1
6-8	1680	3080	9.1	1120	78.1	309	5.0	603	1600	2582	<0.1	9.8	1680	2890	5.0	613	100	93.8	54.9	54.7
8-10	1550	3380	11.9	1510	191	652	7.9	961	1400	2693	<0.1	3.5	1590	3340	7.9	965	103	98.8	66.4	63.9
10-13	1290	4370	12.8	1520	128	590	7.1	849	1160	3505	<0.1	4.9	1290	4100	7.1	853	100	93.8	55.5	56.1

Table A15: Porewater and ultrafiltration concentrations and mass balance for S5

Depth (cm)	Total porewater concentration (µg/l)				Retentate concentration (µg/l)				Filtrate concentration (µg/l)				Total retentate and filtrate concentration (µg/l)				Ultrafiltration / porewater % recovery			
	Sb	As	Pb	Fe	Sb	As	Pb	Fe	Sb	As	Pb	Fe	Sb	As	Pb	Fe	Sb	As	Pb	Fe
0-2					7.6	51.9	1.2	5320	12.5	93.8	<0.1	13.5	20.1	145	1.2	5330				
2-4	32.2	184	5.4	20300	12.4	80.0	4.4	16100	17.8	82.5	<0.1	11.3	30.2	162	4.4	16100	93.8	87.9	81.5	79.3
4-6	62.3	324	14.2	54500	33.8	223	12.3	44500	26.6	49.2	<0.1	11.4	60.4	272	12.3	44500	97.0	84.1	86.6	81.7
6-8	128	434	16.5	74800	56.3	353	14.0	63900	73.0	30.2	0.5	11.2	129	383	14.5	63900	101	88.3	87.9	85.4
8-10	309	320	17.5	48500	103	301	15.1	56000	218	43.3	0.5	17.5	321	344	15.6	56000	104	108	89.1	116
10-13	786	377	19.3	56600	39.6	179	9.1	32800	641	128	7.2	767	681	307	16.3	33600	86.7	81.5	84.5	59.4

Table A16: Distribution of Sb, As, Pb and Fe across gel electrophoresis fractions obtained for the colloid fraction (3kDa-0.2µm) isolated from S2-S5

Sample Site	Fraction number	Sb (µg/fraction)	As (µg/fraction)	Pb (µg/fraction)	Fe (µg/fraction)
S2	1	32.2	1340	206	6780
	2	16.0	349	90.4	2420
	3	4.41	52.3	30.5	2600
	4	4.55	51.4	75.9	1870
	5	2.42	16.3	45.6	3780
	6	1.35	1.0	40.6	1230
	7	11.9	< 0.1	22.1	584
	8	2.64	< 0.1	57.4	1740
S3	1	24.0	494	43.7	4530
	2	13.3	102	17.3	2660
	3	17.7	371	17.1	1370
	4	17.6	10.3	28.2	3000
	5	16.9	< 0.1	16.6	968
	6	3.37	< 0.1	10.7	1360
	7	0.33	< 0.1	17.5	898
	8	< 0.1	< 0.1	108	608
S4	1	22.7	84.4	40.4	1120
	2	35.2	26.5	50.3	1210
	3	109	20.2	63.7	814
	4	88.6	19.6	90.9	2750
	5	49.3	40.9	140	902
	6	40.0	166.0	146	5480
	7	4.65	20.8	140	849
	8	4.73	10.8	108	553
S5	1	26.1	97.8	93.8	1850
	2	14.6	60.2	120	1390
	3	13.8	36.5	83.6	1270
	4	5.28	13.8	273	664
	5	4.71	22.7	218	576
	6	< 0.1	11.5	253	380
	7	2.17	4.52	94.6	496
	8	1.39	6.44	77.5	347

Appendix 5 Calculation of element inventories for Loch Tay, Great Moss and Auchencorth Moss

Using the formula shown below, Sb and Pb inventories were calculated and presented in chapter 6 and 7 for Loch Tay, Great Moss and Auchencorth Moss.

$$\text{Sb INV}\,(\text{mg m}^{-2}) = \left(\frac{\text{sample dry mass}\ (\text{g}) \times \text{Sb}\ (\text{mg kg}^{-1})^{*}}{\text{core area}\ (\text{cm}^{2})} \right) \times 10$$

*This value can be changed to calculate an Anthropogenic Sb INV (mg m^{-2}). For this instance, the following formula should be used to correct Sb (mg kg^{-1}):

Anthropogenic Sb (mg kg^{-1}) = Sb (mg kg^{-1}) – Sb upper continental crust value

Example: Calculation taken for Sb from Auchencorth Moss 0-1 cm profile

$$\text{Sb INV}\,(\text{mg m}^{-2}) = \left(\frac{10.4\ (\text{g}) \times 0.1\ (\text{mg kg}^{-1})^{*}}{225\ (\text{cm}^{2})} \right) \times 10$$

$$\text{Sb INV}\,(\text{mg m}^{-2}) = 0.05$$

Appendix 6 Loch Tay Mini-Mackereth and Jenkin sediment core data tables, and Great Moss and Auchencorth Moss peat core data tables

Table A17: Mini-Mackereth sediment core data used in chapter 6 for Figures 6.8 – 6.12, 6.18 and 6.19

Depth (cm)	Dry wt (g)	Sb (mg kg^{-1})	Anthropogenic Sb (mg kg^{-1})	Anthropogenic Sb/Pb ratio	Sb inventory (mg g^{-2})	Section year	Sb flux (mg cm^{-2} y^{-1})
0-1	1.88	0.66	0.24	0.0020	0.133	1990.9	0.067
1-2	3.59	0.75	0.33	0.0025	0.353	1988.0	0.092
2-3	4.11	0.82	0.40	0.0028	0.495	1983.9	0.113
3-4	4.90	0.95	0.53	0.0035	0.778	1979.1	0.149
4-5	5.02	1.38	0.96	0.0059	1.451	1973.8	0.271
5-6	4.67	1.39	0.97	0.0058	1.364	1968.6	0.274
6-7	5.42	1.50	1.08	0.0064	1.771	1963.3	0.307
7-8	6.01	1.37	0.95	0.0059	1.726	1957.2	0.270
8-9	6.73	1.28	0.86	0.0058	1.753	1950.4	0.245
9-10	5.51	1.42	1.00	0.0055	1.664	1943.9	0.284
10-11	6.73	1.59	1.17	0.0067	2.376	1937.4	0.332
11-12	6.32	1.61	1.19	0.0064	2.269	1930.4	0.337
12-13	6.24	1.65	1.23	0.0049	2.314	1923.8	0.348
13-14	6.56	1.68	1.26	0.0026	2.495	1916.9	0.357
14-15	7.39	1.80	1.38	0.0029	3.066	1909.5	0.390
15-16	8.12	1.65	1.23	0.0070	3.009	1901.3	0.348
16-17	7.38	1.55	1.13	0.0064	2.520	1893.0	0.320
17-18	8.58	1.37	0.95	0.0056	2.443	1884.5	0.267
18-19	8.38	1.32	0.90	0.0054	2.268	1875.5	0.254
19-20	9.04	1.38	0.96	0.0057	2.627	1866.2	0.273

Table A17 ***continued***

Depth (cm)	Dry wt (g)	Sb (mg kg^{-1})	Anthropogenic Sb (mg kg^{-1})	Anthropogenic Sb/Pb ratio	Sb inventory (mg g^{-2})	Section year	Sb flux (mg cm^{-2} y^{-1})
20-22	16.003	1.29	0.87	0.0048	4.204	1852.9	0.247
22-24	17.65	0.93	0.51	0.0026	2.698	1834.9	0.144
24-26	23.07	0.86	0.44	0.0029	3.090	1813.3	0.126
26-28	20.91	0.64	0.22	0.0014	1.413	1789.8	0.063
28-30	18.80	0.62	0.20	0.0012	1.138	1768.7	0.057
30-32	18.45	0.54	0.12	0.0008	0.652	1748.9	0.033
32-34	18.89	0.58	0.16	0.0008	0.890	1729.0	0.044
34-36	19.08	0.61	0.19	0.0010	1.103	1708.8	0.054
36-38	19.91	0.58	0.16	0.0012	0.976	1688.0	0.046
38-40	16.98	0.60	0.18	0.0007	0.905	1668.4	0.050
40-45	39.90	0.45	0.03	0.0001	0.388	1638.1	0.009
45-50	40.41	0.47	0.05	0.0003	0.650	1595.3	0.015
50-55	43.13	0.51	0.09	0.0012	1.139	1550.8	0.025
55-60	41.92	0.46	0.04	0.0053	0.468	1505.5	0.010
60-65	40.83	0.44					
65-70	42.30	0.45					
70-75	45.82	0.41					
75-80	46.72	0.42					
80-85	49.31	0.40					
85-90	46.55	0.39					

Table A18: Jenkin sediment core data used in chapter 6 for Figures 6.13 – 6.19.

Depth (cm)	Dry wt (g)	Mn (%)	Fe (%)	As (mg kg^{-1})	Sb (mg kg^{-1})	Pb (mg kg^{-1})	$^{206}Pb/^{207}Pb$ Ratio	$^{208}Pb/^{207}Pb$ Ratio	$^{208}Pb/^{206}Pb$ Ratio
0-1	2.391	1.83 ± 0.01	8.84 ± 0.1	32.9 ± 2.2	1.06 ± 0.02	209 ± 1.0	1.154 ± 0.001	2.433 ± 0.001	2.109 ± 0.006
1-2	3.617	0.41 ± 0.01	8.33 ± 0.6	42.2 ± 1.2	0.94 ± 0.05	195 ± 2.5	1.153 ± 0.003	2.427 ± 0.004	2.104 ± 0.006
2-3	4.514	0.37 ± 0.02	7.12 ± 0.4	47.4 ± 3.4	1.07 ± 0.07	197 ± 0.6	1.156 ± 0.005	2.428 ± 0.006	2.099 ± 0.000
3-4	5.433	0.32 ± 0.01	6.57 ± 0.8	57.3 ± 1.4	1.02 ± 0.02	187 ± 19	1.148 ± 0.001	2.427 ± 0.001	2.115 ± 0.005
4-5	5.412	0.33 ± 0.01	7.02 ± 0.2	61.5 ± 4.7	1.28 ± 0.01	218 ± 2.9	1.153 ± 0.003	2.424 ± 0.007	2.100 ± 0.006
5-6	5.845	0.31 ± 0.01	6.30 ± 0.2	52.4 ± 0.2	1.42 ± 0.01	220 ± 2.6	1.147 ± 0.004	2.419 ± 0.004	2.112 ± 0.001
6-7	5.634	0.32 ± 0.01	6.46 ± 0.2	59.0 ± 0.8	1.44 ± 0.03	231 ± 1.7	1.145 ± 0.001	2.415 ± 0.004	2.106 ± 0.001
7-8	5.727	0.31 ± 0.01	6.00 ± 0.1	59.9 ± 0.8	1.48 ± 0.02	217 ± 0.8	1.148 ± 0.002	2.425 ± 0.006	2.113 ± 0.006
8-9	6.772	0.28 ± 0.01	6.05 ± 0.2	47.9 ± 0.3	1.44 ± 0.07	212 ± 4.7	1.154 ± 0.002	2.439 ± 0.004	2.116 ± 0.002
9-10	7.543	0.31 ± 0.01	5.95 ± 0.4	35.8 ± 0.8	1.27 ± 0.02	192 ± 7.2	1.155 ± 0.003	2.456 ± 0.003	2.119 ± 0.002
10-11	8.149	0.27 ± 0.01	6.48 ± 0.2	45.4 ± 1.6	1.30 ± 0.06	231 ± 13	1.158 ± 0.003	2.448 ± 0.006	2.116 ± 0.008
11-12	7.519	0.27 ± 0.01	5.82 ± 0.1	53.8 ± 3.3	1.47 ± 0.01	212 ± 3.1	1.156 ± 0.004	2.449 ± 0.003	2.120 ± 0.006
12-13	7.135								
13-14	7.808	0.22 ± 0.01	5.30 ± 0.4	48.6 ± 4.0	1.38 ± 0.10	258 ± 10	1.155 ± 0.001	2.431 ± 0.002	2.111 ± 0.001
14-15	8.66	0.24 ± 0.01	5.39 ± 0.1	49.5 ± 0.8	1.68 ± 0.01	630 ± 8.1	1.147 ± 0.002	2.425 ± 0.004	2.111 ± 0.001
15-16	9.01	0.23 ±0.01	5.11 ± 0.1	41.7 ± 0.5	1.78 ± 0.01	292 ± 0.7	1.157 ± 0.006	2.439 ± 0.006	2.108 ± 0.002
16-17		0.25 ± 0.01	5.46 ± 0.1	39.6 ± 1.1	1.57 ± 0.03	244 ± 18	1.158 ± 0.005	2.460 ± 0.001	2.123 ± 0.006
17-18		0.25 ± 0.02	5.55 ± 0.1	42.3 ± 1.3	1.45 ± 0.06	230 ± 6.2	1.161 ± 0.001	2.462 ± 0.001	2.122 ± 0.001
18-19		0.25 ± 0.01	5.17 ± 0.1	40.4 ± 1.1	1.31 ± 0.11	229 ± 19	1.162 ± 0.002	2.462 ± 0.004	2.114 ± 0.001

Table A18 *continued*

Depth (cm)	Dry wt (g)	Anthropogenic Sb (mg kg^{-1})	Anthropogenic Pb (mg kg^{-1})	Anthropogenic Sb/Pb ratio	Sb inventory (mg g^{-2})	Pb inventory (mg g^{-2})	Section year	Anthropogenic flux (mg cm^{-2} y^{-1})	
								Sb	Pb
0-1	2.391	0.64	192	0.0033	0.41	123	1990.9	0.181	54.3
1-2	3.617	0.52	178	0.0029	0.50	172	1987.9	0.146	50.3
2-3	4.514	0.65	180	0.0036	0.79	217	1984.1	0.184	50.8
3-4	5.433	0.60	169	0.0036	0.88	246	1979.4	0.171	47.9
4-5	5.412	0.86	201	0.0043	1.25	290	1974.3	0.244	56.7
5-6	5.845	1.00	203	0.0050	1.57	317	1968.9	0.284	57.3
6-7	5.634	1.02	214	0.0048	1.53	322	1963.5	0.288	60.5
7-8	5.727	1.06	200	0.0053	1.63	307	1958.2	0.301	56.6
8-9	6.772	1.02	194	0.0053	1.85	352	1952.2	0.289	55.0
9-10	7.543	0.85	175	0.0049	1.72	353	1945.5	0.242	49.6
10-11	8.149	0.88	213	0.0041	1.92	465	1938.1	0.249	60.4
11-12	7.519	1.05	195	0.0054	2.10	391	1930.7	0.296	55.1
12-13	7.135						1923.7		
13-14	7.808	0.96	241	0.0040	2.00	504	1916.7	0.271	68.3
14-15	8.66	1.26	613	0.0021	2.93	1420	1908.9	0.358	173.5
15-16	9.01	1.36	275	0.0049	3.28	663	1900.5	0.385	77.8
16-17		1.15	227	0.0051					
17-18		1.03	213	0.0049					
18-19		0.89	212	0.0042					

Table A19: Great Moss peat core data used in chapter 7 for Figures 7.2-7.5, 7.15, 7.16 and 7.18

Depth (cm)	Dry wt (g)	Sb (mg kg^{-1})	Anthropogenic Sb/Ti (mg kg^{-1})	Lithogenic Sb (mg kg^{-1})	Anthropogenic Sb (mg kg^{-1})	Sb inventory (mg g^{-2})	Section year	Total Sb flux (mg cm^{-2} y^{-1})	Anthropogenic Sb flux (mg cm^{-2} y^{-1})
0-2	17.4	0.49 ± 0.11	0.010	0.0051	0.49	0.53	2010.6	0.138	0.137
2-4	17.2	0.54 ± 0.03	0.009	0.0057	0.53	0.56	2006.5	0.133	0.131
4-6	41.4	0.77 ± 0.05	0.010	0.0074	0.76	1.95	1999.4	0.199	0.197
6-8	109	1.30 ± 0.02	0.012	0.0107	1.29	7.12	1982.1	0.291	0.288
8-10	65.6	2.41 ± 0.05	0.016	0.0145	2.39	7.93	1961.8	0.502	0.499
10-12	51.3	2.62 ± 0.02	0.020	0.0129	2.61	6.75	1949.1	0.714	0.711
12-14	53.3	2.21 ± 0.16	0.018	0.0121	2.20	5.91	1938.2	0.487	0.485
14-16	99.2	2.11 ± 0.25	0.016	0.0134	2.10	10.50	1924.3	0.673	0.669
16-18	108	1.11 ± 0.07	0.007	0.0163	1.09	5.97	1908.4	0.381	0.375
18-20	113	0.53 ± 0.09	0.003	0.0147	0.52	2.70	1888.6	0.117	0.114
20-22	77.2	0.33 ± 0.01	0.002	0.0150	0.31	1.11	1868.4	0.071	0.068
22-24	82.0	0.54 ± 0.01	0.001	0.0174	0.22	0.85	1854.0	0.073	0.068
24-26	86.7	0.21 ± 0.05	0.001	0.0178	0.19	0.70	1840.6	0.054	0.050
26-28	132	0.15 ± 0.01	0.001	0.0134	0.14	0.73	1823.0	0.038	0.035
28-30	130	0.13 ± 0.03	0.001	0.0119	0.12	0.60	1802.4	0.033	0.029
30-32	131	0.12 ± 0.02	0.001	0.0093	0.11	0.58	1782.0	0.031	0.028

Table A19 continued

Depth (cm)	Dry wt (g)	Sb (mg kg^{-1})	Anthropogenic Sb/Ti (mg kg^{-1})	Lithogenic Sb (mg kg^{-1})	Anthropogenic Sb (mg kg^{-1})	Sb inventory (mg g^{-2})	Section year	Total Sb flux (mg cm^{-2} y^{-1})	Anthropogenic Sb flux (mg cm^{-2} y^{-1})
32-34	146.0	0.17 ± 0.13	0.001	0.0074	0.07	0.42	1760.5	0.020	0.018
34-36	168.0	0.10 ± 0.02	0.001	0.0063	0.09	0.62	1736.1	0.025	0.024
36-38	118.0	0.29 ± 0.33	0.001	0.0051	0.05	0.22	1713.9	0.013	0.012
38-40	62.7	0.03 ± 0.01	0.001	0.0022	0.03	0.12	1696.0	0.007	0.007
40-42	59.0	0.07 ± 0.03	0.002	0.0030	0.07	0.29	1678.4	0.017	0.016
42-44	50.3	0.05 ± 0.01	0.002	0.0023	0.05	0.20	1661.4	0.013	0.012
44-46	54.4	0.08 ± 0.05	0.003	0.0024	0.08	0.35		0.020	0.020
46-48	63.8	0.07 ± 0.01	0.003	0.0021	0.07	0.36	1624.1	0.016	0.016
48-50	56.6	0.07 ± 0.01	0.003	0.0024	0.06	0.30			

Table A20: Auchencorth Moss peat core data used in chapter 7 for Figures 7.6, 7.9, 7.10, 7.12, 7.15, 7.16 and 7.18

Depth (cm)	Dry wt (g)	Mn (%)	Fe (%)	Ti (mg kg^{-1})	Sb (mg kg^{-1})	Pb (mg kg^{-1})	$^{206}Pb/^{207}Pb$ Ratio	$^{208}Pb/^{207}Pb$ Ratio	$^{208}Pb/^{206}Pb$ Ratio
0-2	10.4	377 ± 1.1	0.19 ± 0.05	141 ± 27	0.10 ± 0.06	19.0 ± 6.5	1.152 ± 0.004	2.412 ± 0.006	2.094 ± 0.003
2-4	14.6	248 ± 27	0.12 ± 0.07	78 ± 9.1	0.18 ± 0.03	57.5 ± 11	1.140 ± 0.002	2.398 ± 0.005	2.106 ± 0.001
4-6	8.25	129 ± 0.3	0.30 ± 0.01	119 ± 3 .1	0.29 ± 0.01	104 ± 0.5	1.136 ± 0.001	2.394 ± 0.001	2.108 ± 0.001
6-8	14.4	112 ± 2.5	0.39 ± 0.06	776 ± 210	0.49 ± 0.15	104 ± 7.1	1.133 ± 0.001	2.391 ± 0.001	2.108 ± 0.001
8-10	26.4	105 ± 1.5	0.93 ± 0.11	158 ± 4.6	0.43 ± 0.01	109 ± 3.1	1.134 ± 0.004	2.391 ± 0.006	2.111 ± 0.002
10-12	22.8	99.5 ± 6.0	0.93 ± 0.11	90 ± 16	0.51 ± 0.08	117 ± 2.7	1.131 ± 0.001	2.390 ± 0.001	2.110 ± 0.003
12-14	20.4	80.0 ± 3.3	0.99 ± 0.11	103 ± 9.8	0.82 ± 0.03	129 ± 2.8	1.138 ± 0.004	2.398 ± 0.007	2.107 ± 0.001
14-16	24.1	62.0 ± 1.5	1.08 ± 0.08	117 ± 3.8	1.41 ± 0.06	171 ± 2.0	1.143 ± 0.002	2.406 ± 0.002	2.104 ± 0.001
16-18	25.4	52.4 ± 2.2	1.27 ± 0.01	184 ± 17	1.43 ± 0.06	182 ± 8.2	1.149 ± 0.002	2.410 ± 0.001	2.101 ± 0.003
18-20	31.8	39.9 ± 1.6	1.43 ± 0.17	225 ± 6.5	1.79 ± 0.06	188 ± 3.6	1.159 ± 0.001	2.447 ± 0.005	2.109 ± 0.003
20-22	34.0	43.3 ± 0.1	1.64 ± 0.05	251 ± 16	1.85 ± 0.03	194 ± 6.9	1.158 ± 0.002	2.441 ± 0.003	2.106 ± 0.003
22-24	43.7	43.9 ± 0.1	1.48 ± 0.05	420 ±8.7	1.77 ± 0.01	137 ± 2.9	1.173 ± 0.002	2.460 ± 0.004	2.095 ± 0.003
24-26	48.7	42.8 ± 0.2	1.17 ± 0.03	338 ± 4.5	1.33 ± 0.04	91.9 ± 3.6	1.177 ± 0.002	2.476 ± 0.001	2.104 ± 0.005
26-28	66.4	42.2 ± 1.5	1.32 ± 0.07	208 ± 2.9	0.36 ±0.02	48.0 ± 0.8	1.174 ± 0.001	2.437 ± 0.001	2.076 ± 0.004
28-30	48.6	40.7 ± 1.4	0.94 ± 0.02	452 ± 54	0.54 ± 0.01	41.8 ± 0.3	1.176 ± 0.004	2.443 ± 0.002	2.073 ± 0.001
30-32	42.9	37.9 ± 4.4	1.05 ± 0.02	569 ± 28	0.57 ± 0.04	31.9 ± 0.7	1.179 ± 0.001	2.442 ± 0.003	2.073 ± 0.003
32-34	46.6	41.8 ± 0.2	0.99 ± 0.07	713 ± 30	0.54 ± 0.03	28.1 ± 0.5	1.176 ± 0.001	2.461 ± 0.005	2.096 ± 0.002
34-36	53.0	48.4 ± 4.8	1.00 ± 0.03	1621 ± 5.4	0.46 ± 0.01	25.6 ± 0.1	1.178 ± 0.004	2.453 ± 0.003	2.085 ± 0.009
36-38	105	50.9 ± 0.2	0.78 ± 0.13	3940 ±456	0.33 ± 0.03	21.7 ± 1.6	1.180 ± 0.004	2.449 ± 0.003	2.074 ± 0.003

Table A20 continued

Depth (cm)	Dry wt (g)	Anthropogenic Sb/Pb ratio	Lithogenic Sb (mg kg^{-1})	Lithogenic Pb (mg kg^{-1})	Anthropogenic Sb inventory (mg kg^{-1})	Anthropogenic Pb inventory (mg kg^{-1})	Section year	Total flux (mg cm^{-2} y^{-1})		Anthropogenic flux (mg cm^{-2} y^{-1})	
								Sb	Sb	Sb	Pb
0-2	10.4	0.0050	0.0141	0.7714	0.04	8.38	2008.5	0.01	0.01	0.01	2.62
2-4	14.6	0.0030	0.0077	0.4247	0.11	37.1	2006.0	0.09	0.08	0.08	27.9
4-6	8.25	0.0027	0.0118	0.6496	0.10	37.8	2004.2	0.04	0.04	0.04	14.7
6-8	14.4	0.0041	0.0772	4.234	0.26	63.6	2001.5	0.10	0.08	0.08	20.4
8-10	26.4	0.0038	0.0157	0.8632	0.49	128	1997.8	0.12	0.12	0.12	30.4
10-12	22.8	0.0042	0.0090	0.4922	0.50	119	1992.8	0.10	0.10	0.10	23.9
12-14	20.4	0.0063	0.0102	0.5616	0.73	116	1987.5	0.13	0.13	0.13	20.3
14-16	24.1	0.0082	0.0116	0.6384	1.49	182	1981.5	0.22	0.21	0.21	26.1
16-18	25.4	0.0078	0.0183	1.006	1.59	204	1972.0	0.12	0.12	0.12	15.2
18-20	31.8	0.0094	0.0224	1.227	2.50	265	1954.2	0.12	0.12	0.12	12.5
20-22	34.0	0.0095	0.0249	1.367	2.75	290	1933.5	0.17	0.17	0.17	18.0
22-24	43.7	0.0129	0.0418	2.290	3.37	262	1919.8	0.21	0.21	0.21	16.4
24-26	48.7	0.0144	0.0336	1.842	2.80	195	1905.5	0.23	0.22	0.22	15.7
26-28	66.4	0.0072	0.0207	1.133	1.00	139	1901.9	0.12	0.12	0.12	16.6
28-30	48.6	0.0126	0.0450	2.466	1.07	85.0	1893.4	0.04	0.03	0.03	2.95
30-32	42.9	0.0179	0.0566	3.105	0.98	54.9					
32-34	46.6	0.0195	0.0709	3.886	0.98	50.1					
34-36	53.0	0.0178	0.1612	8.839	0.70	39.6					
36-38	105										

Appendix 7 Statistical output from Microsoft Excel

Output 1, page 161

Sb t-Test: Two-Sample Assuming Equal Variances

	Variable 1	*Variable 2*
Mean	5.096710517	5.56706213
Variance	6.437819093	9.91594528
Observations	10	10
Pooled Variance	8.176882188	
Hypothesized Mean Difference	0	
Df	18	
t Stat	-0.36780174	
P(T<=t) one-tail	0.358655192	
t Critical one-tail	1.734063592	
P(T<=t) two-tail	0.717310385	
t Critical two-tail	2.100922037	

Pb t-Test: Two-Sample Assuming Equal Variances

	Variable 1	*Variable 2*
Mean	108.6486	161.5802
Variance	14998.33	18777.19
Observations	10	10
Pooled Variance	16887.76	
Hypothesized Mean Difference	0	
Df	18	
t Stat	-0.91078	
P(T<=t) one-tail	0.187224	
t Critical one-tail	1.734064	
P(T<=t) two-tail	0.374447	
t Critical two-tail	2.100922	

Cu t-Test: Two-Sample Assuming Equal Variances

	Variable 1	*Variable 2*
Mean	87.36625	95.39102
Variance	1607.378	3316.878
Observations	10	10
Pooled Variance	2462.128	
Hypothesized Mean Difference	0	
Df	18	
t Stat	-0.36163	
P(T<=t) one-tail	0.36092	
t Critical one-tail	1.734064	
P(T<=t) two-tail	0.72184	
t Critical two-tail	2.100922	

Zn t-Test: Two-Sample Assuming Equal Variances

	Variable 1	*Variable 2*
Mean	223.9473	272.1869
Variance	16422.21	26198.82
Observations	10	10
Pooled Variance	21310.52	
Hypothesized Mean Difference	0	
Df	18	
t Stat	-0.73891	
P(T<=t) one-tail	0.234744	
t Critical one-tail	1.734064	
P(T<=t) two-tail	0.469488	
t Critical two-tail	2.100922	

Output 2, page 161

Traffic No. and Sb road dust conc. Regression Statistics	
Multiple R	0.394869
R Square	0.155921
Adjusted R Square	-0.12544
Standard Error	13889.17
Observations	5

				Significance
df	*SS*	*MS*	*F*	*F*
1	1.07E+08	1.07E+08	0.554172	0.510627
3	5.79E+08	1.93E+08		
4	6.86E+08			

	Standard				*Upper*	*Lower*	*Upper*
Coefficients	*Error*	*t Stat*	*P-value*	*Lower 95%*	*95%*	*95.0%*	*95.0%*
12519.05	18081.17	0.69238	0.538479	-45023.3	70061.4	-45023.3	70061.4
1867.202	2508.24	0.744427	0.510627	-6115.14	9849.539	-6115.14	9849.539

Traffic No. and Pb road dust conc. Regression Statistics	
Multiple R	0.182096
R Square	0.033159
Adjusted R Square	-0.28912
Standard Error	14864.91
Observations	5

df	*SS*	*MS*	*F*	*Significance F*
1	22734921	22734921	0.102889	0.769436
3	6.63E+08	2.21E+08		
4	6.86E+08			

Coefficients	*Standard Error*	*t Stat*	*P-value*	*Lower 95%*	*Upper 95%*	*Lower 95.0%*	*Upper 95.0%*
27965.94	10987.06	2.545352	0.084284	-6999.8	62931.68	-6999.8	62931.68
-32.8142	102.3004	-0.32076	0.769436	-358.38	292.7514	-358.38	292.7514

Traffic No. and Cu road dust conc. Regression Statistics	
Multiple R	0.399654
R Square	0.159724
Adjusted R Square	-0.26041
Standard Error	5661.119
Observations	4

ANOVA

	df	*SS*	*MS*	*F*	*Significance F*
Regression	1	12183761	12183761	0.380169	0.600346
Residual	2	64096539	32048269		
Total	3	76280300			

	Coefficients	*Standard Error*	*t Stat*	*P-value*	*Lower 95%*	*Upper 95%*	*Lower 95.0%*	*Upper 95.0%*
Intercept	20431.78	7431.607	2.749309	0.110749	-11543.8	52407.41	-11543.8	52407.41
X Variable 1	-40.311	65.37854	-0.61658	0.600346	-321.612	240.9902	-321.612	240.9902

Traffic No. and Zn road dust conc. Regression Statistics	
Multiple R	0.481026
R Square	0.231386
Adjusted R Square	-0.15292
Standard Error	5414.339
Observations	4

ANOVA

	df	*SS*	*MS*	*F*	*Significance F*
Regression	1	17650166	17650166	0.602085	0.518974
Residual	2	58630134	29315067		
Total	3	76280300			

	Coefficients	*Standard Error*	*t Stat*	*P-value*	*Lower 95%*	*Upper 95%*	*Lower 95.0%*	*Upper 95.0%*
Intercept	12674.74	5283.083	2.399118	0.138532	-10056.5	35406.01	-10056.5	35406.01
X Variable 1	13.90515	17.92036	0.775941	0.518974	-63.1999	91.01026	-63.1999	91.01026

Output 3, page 168

SUMMARY OUTPUT

Traffic No. and Sb road dust conc. Regression Statistics	
Multiple R	0.814438
R Square	0.66331
Adjusted R Square	0.494965
Standard Error	3583.491
Observations	4

ANOVA

	df	*SS*	*MS*	*F*	*Significance F*
Regression	1	50597478	50597478	3.940181	0.185562
Residual	2	25682822	12841411		
Total	3	76280300			

	Coefficients	*Standard Error*	*t Stat*	*P-value*	*Lower 95%*	*Upper 95%*	*Lower 95.0%*	*Upper 95.0%*
Intercept	7253.46	4847.844	1.496224	0.273257	-13605.1	28112.05	-13605.1	28112.05
X Variable 1	2272.353	1144.769	1.984989	0.185562	-2653.19	7197.894	-2653.19	7197.894

SUMMARY OUTPUT

Traffic No. and Pb road dust conc. Regression Statistics	
Multiple R	0.597387
R Square	0.356872
Adjusted R Square	0.035308
Standard Error	4952.677
Observations	4

ANOVA

	df	*SS*	*MS*	*F*	*Significance F*
Regression	1	27222285	27222285	1.1098	0.402613
Residual	2	49058015	24529007		
Total	3	76280300			

	Coefficients	*Standard Error*	*t Stat*	*P-value*	*Lower 95%*	*Upper 95%*	*Lower 95.0%*	*Upper 95.0%*
Intercept	13232.59	3746.98	3.531535	0.071668	-2889.36	29354.55	-2889.36	29354.55
X Variable 1	23.50273	22.30981	1.05347	0.402613	-72.4886	119.4941	-72.4886	119.4941

Traffic No. and Cu road dust conc. Regression Statistics	
Multiple R	0.399654
R Square	0.159724
Adjusted R Square	-0.26041
Standard Error	5661.119
Observations	4

ANOVA

	df	*SS*	*MS*	*F*	*Significance F*
Regression	1	12183761	12183761	0.380169	0.600346
Residual	2	64096539	32048269		
Total	3	76280300			

	Coefficients	*Standard Error*	*t Stat*	*P-value*	*Lower 95%*	*Upper 95%*	*Lower 95.0%*	*Upper 95.0%*
Intercept	20431.78	7431.607	2.749309	0.110749	-11543.8	52407.41	-11543.8	52407.41
X Variable 1	-40.311	65.37854	-0.61658	0.600346	-321.612	240.9902	-321.612	240.9902

Traffic No. and Zn road dust conc. Regression Statistics	
Multiple R	0.481026
R Square	0.231386
Adjusted R Square	-0.15292
Standard Error	5414.339
Observations	4

ANOVA

	df	*SS*	*MS*	*F*	*Significance F*
Regression	1	17650166	17650166	0.602085	0.518974
Residual	2	58630134	29315067		
Total	3	76280300			

	Coefficients	*Standard Error*	*t Stat*	*P-value*	*Lower 95%*	*Upper 95%*	*Lower 95.0%*	*Upper 95.0%*
Intercept	12674.74	5283.083	2.399118	0.138532	-10056.5	35406.01	-10056.5	35406.01
X Variable 1	13.90515	17.92036	0.775941	0.518974	-63.1999	91.01026	-63.1999	91.01026

Output 4, page 172

Sb: t-Test: Two-Sample Assuming Unequal Variances

	Variable 1	*Variable 2*
Mean	5.331886326	4.51
Variance	7.804738558	4.372111111
Observations	20	10
Hypothesized Mean Difference	0	
Df	23	
t Stat	0.903527529	
P(T<=t) one-tail	0.1878062	
t Critical one-tail	1.713871528	
P(T<=t) two-tail	0.3756124	
t Critical two-tail	2.06865761	

Pb: t-Test: Two-Sample Assuming Unequal Variances

	Variable 1	*Variable 2*
Mean	135.114374	250.94
Variance	16736.234	79991.5982
Observations	20	10
Hypothesized Mean Difference	0	
Df	11	
t Stat	-1.2321895	
P(T<=t) one-tail	0.12178362	
t Critical one-tail	1.79588482	
P(T<=t) two-tail	0.24356723	
t Critical two-tail	2.20098516	

Cu: t-Test: Two-Sample Assuming Unequal Variances

	Variable 1	*Variable 2*
Mean	91.37863488	114.68
Variance	2349.488893	5156.164
Observations	20	10
Hypothesized Mean Difference	0	
Df	13	
t Stat	-0.92607967	
P(T<=t) one-tail	0.185638933	
t Critical one-tail	1.770933396	
P(T<=t) two-tail	0.371277867	
t Critical two-tail	2.160368656	

Zn: t-Test: Two-Sample Assuming Unequal Variances

	Variable 1	*Variable 2*
Mean	248.067071	509.81
Variance	20801.29246	532761.961
Observations	20	10
Hypothesized Mean Difference	0	
Df	9	
t Stat	-1.123078274	
P(T<=t) one-tail	0.14523441	
t Critical one-tail	1.833112933	
P(T<=t) two-tail	0.290468821	
t Critical two-tail	2.262157163	

Output 5, page 174

PAH: t-Test: Two-Sample Assuming Equal Variances

	Variable 1	*Variable 2*
Mean	4598.086851	25675.30467
Variance	7068719.438	3134740140
Observations	10	10
Pooled Variance	1570904430	
Hypothesized Mean Difference	0	
Df	18	
t Stat	-1.18911376	
P(T<=t) one-tail	0.12492282	
t Critical one-tail	1.734063592	
P(T<=t) two-tail	0.249845641	
t Critical two-tail	2.100922037	

Output 6, page 179

Pb isotope ratios: t-Test: Two-Sample Assuming Unequal Variances

	Variable 1	*Variable 2*
Mean	1.143957	1.113825
Variance	3.06E-05	6.74E-05
Observations	13	4
Hypothesized Mean Difference	0	
Df	4	
t Stat	6.876011	
P(T<=t) one-tail	0.001172	
t Critical one-tail	2.131847	
P(T<=t) two-tail	0.002344	
t Critical two-tail	2.776445	

Output 7a and 7b, page 189

PAH / Cu association SUMMARY OUTPUT

Regression Statistics	
Multiple R	0.845509004
R Square	0.714885476
Adjusted R Square	0.67924616
Standard Error	31709.30363
Observations	10

ANOVA

	df	*SS*	*MS*	*F*	*Significance F*
Regression	1	20168821769	20168821769	20.05890027	0.002059295
Residual	8	8043839492	1005479937		
Total	9	28212661261			

	Coefficients	*Standard Error*	*t Stat*	*P-value*	*Lower 95%*	*Upper 95%*
Intercept	-49928.44448	19634.28469	-2.54292149	0.034553275	-95205.18613	-4651.702831
X Variable 1	659.2583637	147.1980608	4.478716364	0.002059295	319.8190271	998.6977004

PAH / Zn association SUMMARY OUTPUT

Regression Statistics	
Multiple R	0.977346497
R Square	0.955206175
Adjusted R Square	0.949606947
Standard Error	12568.57694
Observations	10

ANOVA

	df	*SS*	*MS*	*F*	*Significance F*
Regression	1	26948908251	2.69E+10	170.596	1.12115E-06
Residual	8	1263753011	1.58E+08		
Total	9	28212661261			

	Coefficients	*Standard Error*	*t Stat*	*P-value*	*Lower 95%*	*Upper 95%*	*Lower 95.0%*
Intercept	-12544.73019	4935.550762	-2.54171	0.034619	-23926.13064	-1163.329729	-23926.1306
X Variable 1	74.9691745	5.73981968	13.06124	1.12E-06	61.7331266	88.20522241	61.733126

Output 8, page 193

Cu BCR distribution t-Test: Two-Sample Assuming Unequal Variances

	Variable 1	*Variable 2*
Mean	40.2863774	18.60058
Variance	85.5821365	159.5514
Observations	4	5
Hypothesized Mean Difference	0	
Df	7	
t Stat	2.97021606	
P(T<=t) one-tail	0.01040069	
t Critical one-tail	1.8945786	
P(T<=t) two-tail	0.02080137	
t Critical two-tail	2.36462425	

Output 9a, 9b and 9c, page 218

Regression Statistics for Sb and OM	
Multiple R	0.952650952
R Square	0.907543837
Adjusted R Square	0.884429796
Standard Error	4.246752893
Observations	6

ANOVA

	df	*SS*	*MS*	*F*	*Significance F*
Regression	1	708.1181413	708.1181	39.26375	0.003309822
Residual	4	72.13964053	18.03491		
Total	5	780.2577819			

	Coefficients	*Standard Error*	*t Stat*	*P-value*	*Lower 95%*	*Upper 95%*	*Lower 95.0%*	*Upper 95.0%*
Intercept	7.215098932	4.195654554	1.71966	0.160614	-4.433905619	18.86410348	-4.433905619	18.86410348
X Variable 1	0.94045738	0.15008706	6.266079	0.00331	0.523748898	1.357165863	0.523748898	1.357165863

Regression Statistics for Sb and DOM	
Multiple R	0.997946
R Square	0.995896
Adjusted R Square	0.994528
Standard Error	8.946987
Observations	5

ANOVA

	df	*SS*	*MS*	*F*	*Significance F*
Regression	1	58270.71558	58270.71558	727.94198	0.000111733
Residual	3	240.1457144	80.04857146		
Total	4	58510.86129			

	Coefficients	*Standard Error*	*t Stat*	*P-value*	*Lower 95%*	*Upper 95%*	*Lower 95.0%*	*Upper 95.0%*
Intercept	112.2483	7.895020418	14.21760131	0.00075389	87.12277406	137.3737	87.12277406	137.3737312
X Variable 1	0.379879	0.0140798	26.98039992	0.00011173	0.335070435	0.424687	0.335070435	0.424686852

SUMMARY OUTPUT

Regression Statistics for Sb and Fe	
Multiple R	0.987839
R Square	0.975826
Adjusted R Square	0.967769
Standard Error	21.71342
Observations	5

ANOVA

	df	*SS*	*MS*	*F*	*Significance F*
Regression	1	57096.4429	57096.4429	121.102306	0.001606868
Residual	3	1414.418395	471.4727983		
Total	4	58510.86129			

	Coefficients	*Standard Error*	*t Stat*	*P-value*	*Lower 95%*	*Upper 95%*	*Lower 95.0%*	*Upper 95.0%*
Intercept	171.9293	14.87125723	11.56117821	0.0013896	124.6022773	219.2562	124.6022773	219.2562325
X Variable 1	0.004484	0.000407498	11.00464927	0.00160687	0.003187534	0.005781	0.003187534	0.005781216

SUMMARY OUTPUT

Regression Statistics for Sb and Fe association	
Multiple R	0.981053767
R Square	0.962466494
Adjusted R Square	0.949955326
Standard Error	37.35102588
Observations	5

ANOVA

	df	*SS*	*MS*	*F*	*Significance F*
Regression	1	107323.0027	107323.0027	76.92858525	0.00312162
Residual	3	4185.297403	1395.099134		
Total	4	111508.3001			

	Coefficients	*Standard Error*	*t Stat*	*P-value*	*Lower 95%*	*Upper 95%*	*Lower 95.0%*	*Upper 95.0%*
Intercept	123.9021657	26.07393425	4.751955134	0.017685301	40.92327001	206.8810615	40.92327001	206.8810615
X Variable 1	0.005108418	0.000582428	8.77089421	0.00312162	0.003254871	0.006961966	0.003254871	0.006961966

Output 10, page 219

S2, Fe and Pb porewater t-Test: Two-Sample Assuming Equal Variances

	Variable 1	*Variable 2*
Mean	58.97669	2561.622
Variance	299.9628	490949.1
Observations	5	5
Pooled Variance	245624.5	
Hypothesized Mean Difference	0	
Df	8	
t Stat	-7.98424	
P(T<=t) one-tail	2.21E-05	
t Critical one-tail	1.859548	
P(T<=t) two-tail	4.43E-05	
t Critical two-tail	2.306004	

S3, Fe and Pb porewater t-Test: Two-Sample Assuming Equal Variances

	Variable 1	*Variable 2*
Mean	20.35713549	27639.88224
Variance	381.1881506	709815106.1
Observations	5	5
Pooled Variance	354907743.7	
Hypothesized Mean Difference	0	
Df	8	
t Stat	-2.318080287	
P(T<=t) one-tail	0.024533126	
t Critical one-tail	1.859548038	
P(T<=t) two-tail	0.049066251	
t Critical two-tail	2.306004135	

S4, Fe and Pb porewater t-Test: Two-Sample Assuming Equal Variances

	Variable 1	*Variable 2*
Mean	5.80822799	731.224191
Variance	3.67735077	41001.0745
Observations	6	6
Pooled Variance	20502.3759	
Hypothesized Mean Difference	0	
Df	10	
t Stat	-8.77497	
P(T<=t) one-tail	2.5965E-06	
t Critical one-tail	1.81246112	
P(T<=t) two-tail	5.193E-06	
t Critical two-tail	2.22813885	

S5, Fe and Pb porewater t-Test: Two-Sample Assuming Equal Variances

	Variable 1	*Variable 2*
Mean	10.77692	36563.44
Variance	41.01111	5.19E+08
Observations	6	6
Pooled Variance	2.59E+08	
Hypothesized Mean Difference	0	
Df	10	
t Stat	-3.93146	
P(T<=t) one-tail	0.001407	
t Critical one-tail	1.812461	
P(T<=t) two-tail	0.002814	
t Critical two-tail	2.228139	

Output 11, page 269

Mn: t-Test: Two-Sample Assuming Equal Variances

	Variable 1	*Variable 2*
Mean	0.522778	0.376884
Variance	0.230915	0.134203
Observations	18	18
Pooled Variance	0.182559	
Hypothesized Mean Difference	0	
Df	34	
t Stat	1.02437	
P(T<=t) one-tail	0.156447	
t Critical one-tail	1.690924	
P(T<=t) two-tail	0.312894	
t Critical two-tail	2.032245	

Fe: t-Test: Two-Sample Assuming Equal Variances

	Variable 1	*Variable 2*
Mean	6.215	6.27239
Variance	0.548509	1.06823
Observations	18	18
Pooled Variance	0.808369	
Hypothesized Mean Difference	0	
Df	34	
t Stat	-0.19149	
P(T<=t) one-tail	0.424639	
t Critical one-tail	1.690924	
P(T<=t) two-tail	0.849279	
t Critical two-tail	2.032245	

As: t-Test: Two-Sample Assuming Equal Variances

	Variable 1	*Variable 2*
Mean	45.38889	47.64054
Variance	168.6046	70.77959
Observations	18	18
Pooled Variance	119.6921	
Hypothesized Mean Difference	0	
Df	34	
t Stat	-0.61743	
P(T<=t) one-tail	0.270531	
t Critical one-tail	1.690924	
P(T<=t) two-tail	0.541062	
t Critical two-tail	2.032245	

Sb: t-Test: Two-Sample Assuming Equal Variances

	Variable 1	*Variable 2*
Mean	1.338143	1.353538
Variance	0.111404	0.05064
Observations	18	18
Pooled Variance	0.081022	
Hypothesized Mean Difference	0	
Df	34	
t Stat	-0.16226	
P(T<=t) one-tail	0.436032	
t Critical one-tail	1.690924	
P(T<=t) two-tail	0.872065	
t Critical two-tail	2.032245	

Pb: t-Test: Two-Sample Assuming Equal Variances

	Variable 1	*Variable 2*
Mean	213.6111	244.7035
Variance	11089.78	9912.583
Observations	18	18
Pooled Variance	10501.18	
Hypothesized Mean Difference	0	
Df	34	
t Stat	-0.91024	
P(T<=t) one-tail	0.184552	
t Critical one-tail	1.690924	
P(T<=t) two-tail	0.369103	
t Critical two-tail	2.032245	

Appendix 8 Published research paper 1

Mobility of antimony, arsenic and lead at a former antimony mine, Glendinning, Scotland

Kenneth Macgregor [a], Gillian MacKinnon [b], John G. Farmer [a], Margaret C. Graham [a]

[a] School of GeoSciences, University of Edinburgh, Crew Building, Alexander Crum Brown Road, Edinburgh EH9 3FF, United Kingdom

[b] Scottish Universities Environmental Research Centre, Scottish Enterprise Park, East Kilbride, Glasgow G75 0QF, United Kingdom

HIGHLIGHTS

• Solid phase speciation of antimony, arsenic, lead and iron differed between sites.

• Elevated soil porewater antimony concentrations were linked to DOM and spoil leaching.

• Leaching from spoil resulted in elevated antimony concentrations in stream water.

Abstract

Elevated concentrations of antimony (Sb), arsenic (As) and lead (Pb) in upland organic-rich soils have resulted from past Sb mining activities at Glendinning, southern Scotland. Transfer of these elements into soil porewaters was linked to the production and leaching of dissolved organic matter and to leaching of spoil material. Sb was predominantly present in truly dissolved (<3 kDa) forms whilst As and Pb were more commonly associated with large Fe-rich/organic colloids. The distinctive porewater behaviour of Sb accounts for its loss from deeper sections of certain cores and its transport over greater distances down steeper sections of the catchment. Although Sb and As concentrations decreased with increasing distance down a steep gully from the main spoil heap, elevated concentrations (~6-8 and 13-20 μg L^{-1}, respectively) were detected in receiving stream waters. Thus, only partial attenuation occurs in steeply sloping sections of mining-impacted upland organic-rich soils and so spoil-derived contamination of surface waters may continue over time periods of decades to centuries.

Capsule abstract: Production and leaching of dissolved organic matter led to the concomitant transfer of truly dissolved Sb to soil porewaters. Leaching of spoil-derived Sb impacted on the quality of receiving stream waters.

Keywords: Antimony, Humic substances, Colloids, Iron (oxy)hydroxides

1. Introduction

The marked rise in global antimony (Sb) production, e.g. from 55 kt in 1990 to 180 kt in 2012 (Butterman and Carlin, 2004; USGS, 2013), is largely attributable to its use in flame retardants, car brake liner lubricants, catalysts for the production of polyethylene terephthalate (PET) and alloy additives (Filella *et al.,* 2002a; Ceriotti and Amarasiriwardena, 2009; Bach *et al*., 2012; USGS, 2013). Currently, ~84% of global Sb production takes place in China (He *et al*., 2012) and, although some large-scale mines have recently closed (USGS, 2013), many are operational, e.g. at the Dachang and Zhazaixi deposits in Guangxi and Hunan provinces, respectively. Significant environmental and human health impacts are associated with on-going ore extraction and smelting processes but there are also environmental concerns relating to historical sites. In the UK, Sb mining and smelting activities ceased in the mid-20th century (Flynn *et al*., 2003) but impacts upon soils and waters are still observed in the 21st century (Flynn *et al*., 2003; Gál *et al.,* 2007). In addition,

Sb mining and smelting processes usually release arsenic (As) and lead (Pb) to the environment since all three elements commonly co-occur in the sulfidic ore deposits. In Europe, Sb is a list II pollution reduction substance (EC, 2001), with some chemical forms considered to be carcinogenic (IARC, 1989). Arsenic is similarly classified whilst Pb is a list I priority hazardous substance by the EU Water Framework Directive (EC, 2000).

This study focuses on the Glendinning mine located in Dumfries and Galloway, SW Scotland (Fig. 1(a)–(b)), from which ~200 t of Sb ores were extracted during three main production periods, 1793–1798, 1888–1891 and 1919–1922 (Gallagher *et al*., 1983). Ore smelting took place at Jamestown, ~1 km downhill of the mine (Gallagher *et al.,* 1983). Several spoil heaps in the vicinity of the mine are still evident, and previous studies have reported Sb concentrations of 14.0–673 mg kg^{-1} (Flynn *et al.,* 2003) and 10.3–1200 mg kg^{-1} (Gál *et al*., 2007) in the surrounding soils. Whilst these studies demonstrated that the soil Sb concentrations were significantly elevated above background levels, the geochemical associations, lateral and vertical elemental mobility and transport mechanisms for Sb, As and Pb at the site remain poorly defined. The mobility of contaminants in soil is often influenced by key variables such as drainage, pH, redox status, organic matter content and the abundance of major elements such as iron (Fe) in the soil. Many of these factors are interlinked and, for example, drainage and pH are particularly important with respect to redox cycling of Fe. Iron oxides are major natural sorbents for Sb (Johnson *et al*., 2005; Mitsunobu *et al*., 2006, 2010; Wilson *et al.,* 2010; Okkenhaug *et al*., 2011), and Filella *et al.* (2002b) noted the importance of Fe (oxy)hydroxides in limiting Sb mobility, particularly in acidic soils typical of those found at the Glendinning site. As in many upland areas of the UK, the soils are also organic-rich and previous work has shown that Sb, As and Pb bind to organic matter to varying extents (e.g. Buschmann and Sigg, 2004; Buschmann *et al*., 2006). For example, several studies have shown significant binding of Sb to soil humic acids (Buschmann and Sigg, 2004), whilst others found only limited organic complexation within soils (Filella, 2011). Lead has been shown to be largely immobile in upland organic-rich soils in NE Scotland but during storm events it can be released in association with organic-rich colloids (Graham *et al*., 2006). A recent study also showed that phase associations of Pb were influenced by soil pH with significant adsorption to organic matter at pH <5 but preferential adsorption to Fe (oxy)hydroxides at higher pH (Shi *et al*., 2013). Iron (oxy)hydroxides also act as a control on As mobility due to the high affinity of As for these phases under oxic conditions. Some studies, however, have shown that these interactions can be modified and sometimes enhanced by the presence of natural organic matter (NOM) (e.g. Redman *et al*., 2002). Subtle differences in associations, e.g. direct binding to Fe oxides vs bridging between NOM and Fe oxides vs direct binding to NOM, are important because they may influence the form in which such elements are released into soil porewaters and their subsequent fate (e.g. Neubauer *et al*., 2013).

This study determines the concentrations and associations of Sb, As and Pb in soil, porewater, surface flow and stream waters in order to assess elemental mobility and transport processes operating in the vicinity of a large spoil heap at the abandoned Glendinning Sb mine in Scotland.

2. Materials and methods

2.1. Sample collection

To demonstrate connectivity between spoil heap 1 (SpH1) and the receiving water, the Glenshanna Burn, 250 mL water samples were collected in pre-cleaned polyethylene bottles from surface flows in the small gully leading steeply down from SpH1 towards the Burn and directly from the Burn itself. In February 2013, stream waters W1 and W2 were collected upstream whilst W3 was collected downstream of SpH1. The two surface flows collected at the same time were designated W4 and W5 (Fig. 1(c)). Sampling was repeated in October

2014 at W1, W3, W4 and W5. Composite surface (0–5 cm; SpH1-surface) and subsurface (30–35 cm; SpH1-deep) spoil samples collected in February 2013 were stored in labelled polyethylene bags. Depending upon soil depth, ≤12 cm-deep cores also collected in February 2013 were taken using a spade and also placed in labelled polyethylene bags. These were collected at: (i) three locations (S1–3) along a 30-m transect from spoil heap 2 (SpH2) which was near the mine entrance towards a path; (ii) three locations (S4–6) along a 50-m transect down-gully from SpH1 towards the Glenshanna Burn; and (iii) a control site (C1) approximately 500 m further up the Glenshanna valley (Fig. 1). Soil core dimensions were ~20 cm × 20 cm × ~12 cm depth and each core was sliced into 2-cm depth sections. Each section was weighed, air dried (25 °C; ~20 days), reweighed, sieved to <2 mm and ground using a mortar and pestle until a fine homogenised powder was achieved.

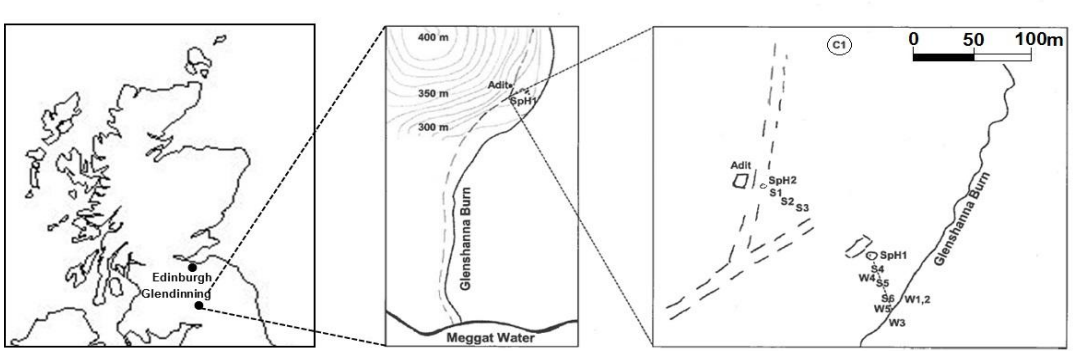

Fig. 1. (a) Map of Scotland showing the location of Glendinning; (b) schematic of the Glendinning mining site showing the location of the adit and main spoil heap (SpH1); and (c) enlarged schematic showing the location of soil and water sampling sites in relation to the adit and SpH1.

2.2. Sample preparation

2.2.1. Stream and surface flow water

Sub-samples (200 mL) of the stream water samples were acidified with 100 μL c.HNO_3 (Aristar, VWR International Ltd., Leics., UK), filtered through 1 μm membranes (Whatman cellulose nitrate membrane filter paper; VWR International Ltd., Leics., UK) and slowly concentrated tenfold on a hotplate. Reagent blanks were similarly prepared. The surface flow waters did not require pre concentration.

2.2.2. Soil samples

Soil pH was determined in soil suspensions (2.5 g soil in 12.5 mL 0.01 M $CaCl_2$) using a calibrated pH meter (Jenway model 3505). Approximately 0.25 g of each soil section was oven-dried (105 °C; 12 h). The organic matter (OM) content was determined relative to the oven-dried mass after ashing (450 °C; 4 h). The ash residue was digested using a MARS 6 microwave digestion system (CEM) and the modified US EPA Method 3052 (HF–HNO_3 Aristar, VWR International Ltd., Leics., UK) published by Yafa and Farmer (2006). With every batch of ten samples, duplicate reagent blanks and duplicate samples of a peat certified reference material (NIMT/UOE/FM001 (Yafa *et al.*, 2004)) were taken through the same procedure (see SI file).

2.2.3. Porewater extraction and ultrafiltration

In accordance with the method in Graham *et al.* (2008), porewaters were isolated by centrifuging fresh soil at 8873 ×g for 10 min. The supernatant was filtered through 0.2 μm (Whatman, hydrophilic) membranes. For S2–5 porewaters, the UV absorbance at 252 nm was used as a proxy for dissolved organic matter (DOM) concentration (Graham *et al.*, 2008). A 20 mL subsample of the 0.2 μm-filtrate was then ultracentrifuged (3 kDa Vivaspin 20; polyethersulfone membranes; VWR International Ltd., Leics., UK) at 6655 ×g (60 min). The ultra-filtrate (truly dissolved fraction) and ultrafilter retentate (colloidal fraction) were quantitatively removed and stored in separate sterilin tubes ready for measurement of UV absorbance at 252 nm (Unicam UV2 spectrometer) and elemental analysis (see Analysis section below).

2.2.4. Sequential extraction

The three-stage BCR sequential extraction detailed by Davidson *et al*.(1998) was followed (see SI file). In brief, BCR1, 2 and 3 remove the exchangeable/acid-soluble, reducible (e.g. Fe/Mn (oxy)hydroxide) and oxidisable (e.g. organic matter, sulfide) phases, respectively, from the soil whilst the residual fraction comprises non-extractable phases.

2.2.5. Gel electrophoresis

The ultrafiltration retentate (3 kDa–0.2 μm) from selected soil porewaters underwent gel electrophoretic fractionation (Fisherbrand horizontal miniplus unit) as described in Graham *et al*. (2008).

2.3. Analysis

Concentrations of Sb (206.836 nm), As (228.812 nm), Pb (220.353 nm) and Fe (239.562 nm) in soil digests were determined by Inductively Coupled Plasma-Optical Emission Spectroscopy (ICP-OES) using a Perkin–Elmer Optima 5300DV instrument (Perkin–Elmer, Beaconsfield, UK). Calibration standards (0.01–300 mg L−1) were prepared using a 1000 mg L^{-1} ICP standard solution (in 1 M HNO_3; Fisher Scientific) for Sb, and an ICP Multielement Standard Solution IV CentiPUR (Merck) for As, Pb and Fe. Calibration curves for both low and high-concentration samples were obtained. Analytical precision (±RSD) for the independent reference solution, ICP Multielement Standard Solution VI (Pb: 10 mg L^{-1}; As and Fe: 100 mg L^{-1}), was <3.3% (n = 10). Analysis of ombrotrophic peat reference material NIMT/UOE/FM001 (Yafa *et al.*, 2004) gave concentrations (Sb 2.00 ± 0.43, As 3.00 ± 0.56, Pb 159 ± 6 and Fe 803 ± 46, all in mg kg^{-1}; n = 12) which were in good agreement with the certified (Pb 174 ±8 mg kg^{-1}), and information only values (As 2.44 ± 0.55; Sb 2.37 ± 0.34; Fe 921 ± 84 mg kg^{-1}) (Yafa *et al*., 2004; Cloy *et al.*, 2009).

Elemental (Sb, As, Pb and Fe) concentrations in stream water, surface flow, porewater and gel electrophoresis samples were determined by Inductively Coupled Plasma-Mass Spectrometry (ICP-MS) using an Agilent 7500ce instrument (Agilent Technologies, Stockport, UK) with nickel cones. Calibration standards (0.01–1000 μg L^{-1}) and curves for both low- and high-elemental concentrations were prepared. Analysis of the National Institute of Standards and Technology (NIST) Standard Reference Material (SRM) 1640 Trace Elements in Water gave values of Sb 58.2 ± 2.9 μg L^{-1}, As 58.3 ± 1.6 μg L^{-1}, Pb 21.9 ± 2.6 μg L^{-1} and Fe 100.1 ± 5.0 μg L^{-1} (n = 5) which compared well with the certified values (Sb 58.3, As 64.3, Pb 19.6 and Fe 98.1 μg L^{-1}).

3. Results

3.1. Soil pH, OM content and elemental (Fe, Sb, As and Pb) concentrations in soil and soil porewaters

3.1.1. Soil pH

There was typically little variation in soil pH with increasing depth. The lowest pH values (3.9–4.1) were obtained for the control soil (C1) but low pH values were also obtained for S4 (4.7–4.9) and S1 (4.4–5.2), i.e. those closest to the spoil heaps, SpH1 and SpH2, respectively. The pH values for the soils at S2, S3, S5 and S6 were slightly less acidic and ranged from 5.4–6.3 (Table 1).

3.1.2. OM content

The OM content for C1 soils was in the range of ~15–95% w/w and highest in the top 0–5 cm sections. The exceptionally high OM content, especially in the top sections (SI file), may account for the low pH of the control soil. With the exception of S2 which had a maximum value of ~77%, peak OM content for S1–6 soils was typically ~39–54% w/w (Table 1). The vertical OM profiles for S1–6 all showed similar trends, decreasing from the surface towards the bottom of the cores (Fig. 2), and were consistent with the soil type for the area which comprises a peaty layer overlying silty-clay mineral soils (Gallagher *et al.*, 1983). The porewaters extracted from the soils were pale brown-coloured, indicating the presence of dissolved humic substances. With the exception of S5, where absorbance values at 252 nm (a measure of colour) remained approximately constant, the maximum absorbance occurred at depths of 5–8 cm in each core. This was ~5 cm below the maximum solid phase OM content (Fig. 2), similar to results observed in many other studies (e.g. Michalzik and Matzner, 1999). The DOM profile shape is the result of production and leaching in the upper layers and removal via adsorption in the deeper layers (Kalbitz *et al.*, 2000; Kalbitz and Kaiser, 2008).

3.2. Iron

The Fe concentrations in the control soil core C1 were ~0.1–3.4% w/w (Table 1) whilst those for S1–6 were in the range of ~0.2–6.3% w/w (Fig. 2), with highest values occurring in the soils closest to SpH1 and SpH2. In contrast with OM content, the vertical profiles for Fe showed very low concentrations in the top sections and then a general trend of increasing concentration with increasing depth, reflecting the transition from the peaty surface layer to mineral-rich material. Porewater Fe concentrations were also typically greater at depth than at the surface but there was no strong relationship with solid phase Fe concentration. Consistent with a transition to reducing conditions, for S2, S4 and S5 there was a clear subsurface maximum at ~5–10 cm and, for S3, the Fe concentration continued to increase to the bottom of the core. Highest porewater concentrations of ~80 mg L^{-1} were obtained for the deeper sections of S3 and S5.

3.3. Antimony

The mean and range of Sb concentrations in soils from C1 were 0.7 ± 0.3 mg kg^{-1} and 0.4–1.2 mg kg^{-1} (Table 1), respectively, consistent with the values of 0.6–1.05 mg kg^{-1} for local soils obtained as part of the FOREGS study (Salminen *et al.*, 2005) and indicative of no

influence from the nearby mining activities. In contrast, concentrations in S1–6 soils were several orders of magnitude higher. Maximum values of ~260 mg kg^{-1} were found in S3 soils and, for S4–6, there was a clear trend of decreasing concentration with increasing distance downslope from SpH1 (Fig. 2). The porewater Sb concentrations for S4 and S5 also reflected this trend with distance from SpH1 (Fig. 2).

Regression analysis showed that there was a strong relationship between solid phase OM content and Sb concentrations at S3 ($P < 0.01$, $R^2 = 0.95$). Although the porewater Sb and solid phase Sb profiles for S2–5 appeared to be unrelated, there were strong correlations between the porewater concentration profiles of Sb and DOM (e.g. S3: $P < 0.01$, $R^2 = 0.95$) and of Sb and Fe (e.g. S3: $P < 0.01$, $R^2 = 0.98$). An exception was S5, however, where the Sb porewater profile was distinctly different from those of both Fe and DOM (Fig. 2).

3.4. Arsenic

Arsenic concentrations of <1 mg kg^{-1} at C1 (Table 1) were again in good agreement with those reported in the FOREGS study for the locality (Salminen *et al*., 2005), similar to those in soils from S6 (<1.4 mg kg^{-1}) but at least an order of magnitude lower than those for S1–5. The highest As concentration of ~75 mg kg^{-1} was obtained at S4, the site closest to SpH1, and, as for Sb, As concentrations decreased with increasing distance downslope from SpH1. In agreement with the vertical Fe concentration profiles, however, As concentrations showed a general increase with increasing soil depth. For S2 and S5, there was also a strong relationship between porewater As and Fe concentrations, suggesting concomitant release from the soil solid phase.

3.5. Lead

In contrast with Sb and As, the C1 soil Pb concentrations were higher than expected based on its crustal abundance (~12–15 mg kg^{-1}) (Taylor, 1964; Wedepohl, 1995). Concentrations of up to 57 mg kg^{-1} were attributable to atmospheric deposition of Pb emissions from coal combustion, smelting and leaded gasoline in the industrial and post-industrial periods (Salminen *et al*., 2005; Cloy *et al.*, 2009; Farmer *et al*., 2010). However, considerably higher values (up to 710 mg kg^{-1}) were observed for S1–4, consistent with the additional contribution of mining-derived Pb to these soils, whilst those for S5–6 were similar to C1. The vertical concentration profiles for S1 and S3 had slight sub-surface maxima at ~5 cm depth whilst there was a general increase towards the bottom of each of the other cores. Highest concentrations of ~600–700 mg kg^{-1} were observed towards the bottom of S2 and S4. Akin to Sb and As, porewater Pb profiles bore little resemblance to the respective solid phase profiles; in the main, there was a strong similarity between the vertical porewater profiles of Pb and Fe.

Table 1: Elemental concentration range found in control soil (C1), spoil (SpH1), soil profile (S1-6) and water (W1-5) samples taken in the vicinity of Glendinning antimony mine

Samples collected	pH	%OM	Fe %	Sb mg kg^{-1}	As mg kg^{-1}	Pb mg kg^{-1}
C1	3.9 – 4.1	14.8 – 95.3	0.11 – 3.35	0.41 – 1.18	0.43 – 0.91	3.07 – 57.1
SpH1-surface†	5.0	7.31 – 10.9	3.98 – 5.26	174 – 302	74.0 – 85.0	873 – 1020
SpH1-deep†	6.6	2.82 – 3.77	4.02 – 4.46	300 – 541	104 – 170	421 – 621
S1	4.4 – 5.2	6.60 – 38.6	3.83 – 5.80	55.4 – 132	34.9 – 57.2	390 – 486
S2	6.0 – 6.3	21.0 – 77.2	0.21 – 4.86	95.5 – 222	5.68 – 55.6	91.6 – 710
S3	5.4 – 5.6	14.3 – 44.9	2.45 – 5.48	50.7 – 261	13.9 – 19.1	90.9 – 114
S4	4.7 – 4.9	23.2 – 53.6	2.51 – 6.28	120 – 188	18.4 – 75.3	52.2 – 632
S5	5.6 – 6.0	22.8 – 48.4	2.08 – 3.46	65.9 – 91.2	3.87 – 5.92	40.2 – 52.1
S6	5.7 – 6.0	13.0 – 44.6	1.94 – 4.50	6.77 – 21.7	0.36 – 1.40	27.9 – 88.6
Water sites			Fe µg L^{-1}	Sb µg L^{-1}	As µg L^{-1}	Pb µg L^{-1}
W1* 02/13			32.8 ± 0.04	0.10	1.13 ± 0.09	0.08 ± 0.03
10/14				0.26	0.89	0.38
W2*			32.0 ± 0.09	0.11	1.00 ± 0.01	0.08 ± 0.00
W3* 02/13			22.2 ± 3.79	5.88 ± 0.29	13.2 ± 1.14	0.07 ± 0.03
10/14				7.53	20.2	0.68
W4*			4.95 ± 2.69	83.8 ± 0.90	181 ± 26.4	0.55 ± 0.68
W5 02/13			5.31	783	1770	0.06
10/14				674	1480	0.21

† 6 sub-samples of spoil; ***** mean from duplicate analysis

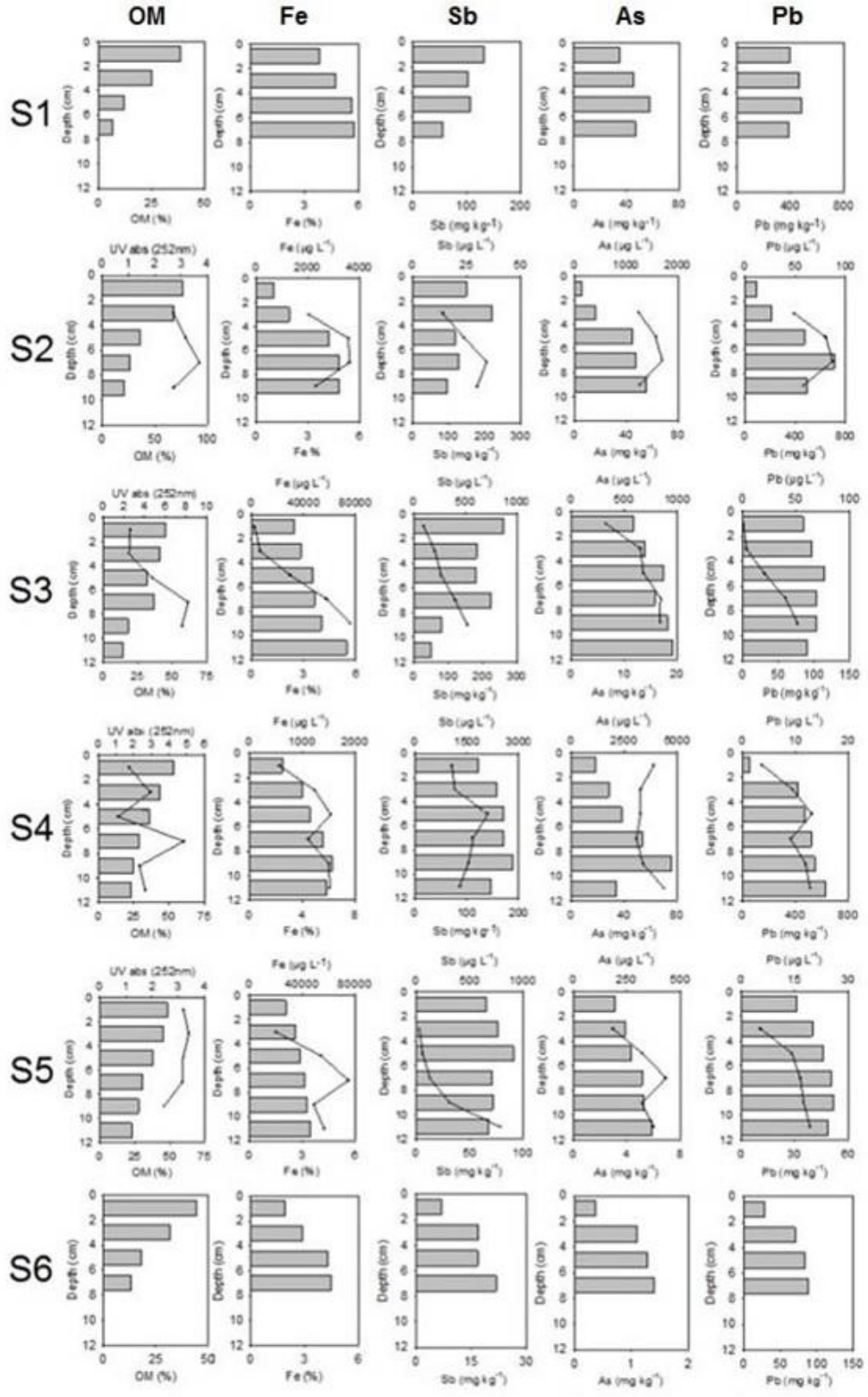

Figure 2: Vertical variations in the concentrations of OM, Fe, Sb, As and Pb in solid phase soils (S1-6) and their respective porewaters (S2-5)

3.6. OM content and elemental (Sb, As, Pb and Fe) concentrations in SpH1

As expected, the spoil samples had lower OM content than the surrounding soils (Table 1). There was, however, a thin coverage of soil like material supporting heathers and mosses and this was reflected in an OM content of ~7–11% w/w for SpH1-surface. With less soil present at depth, the OM content for SpH1-deep dropped to ~3–4% w/w. The ore material at Glendinning comprised stibnite (Sb2S3) and semseyite ($Pb_9Sb_8S_{21}$) in association with a stratiform arsenopyrite (FeAsS)–pyrite (FeS_2) mineralisation (Gallagher *et al*., 1983) and SpH1 samples contained elevated concentrations of Sb, As, Pb and Fe. The composition of the spoil was not uniform and the range of values reflects the analysis of six aliquots of these samples. Higher Sb and As concentrations of ~300–540 mg kg^{-1} and ~100–170 mg kg^{-1}, respectively, were obtained for SpH1-deep. In contrast, SpH1-surface had higher Pb concentrations of ~870–1020 mg kg^{-1}. The median Fe concentrations were 5.1% w/w and 4.2% w/w for SpH1-surface and SpH1-deep, respectively, and the range of Fe concentrations was also greater for the surface sample. The variation in composition may be attributable to changes in the nature of weathering processes operating at the surface and at greater depth within the spoil.

3.7. Stream water and surface flow elemental (Sb, As, Pb and Fe) concentrations

For samples collected in February 2013, aqueous phase Sb concentrations were ~0.1 μg L^{-1} at W1–2 (upstream of the gully) but ~5.9 ± 0.3 μg L^{-1} at W3 (downstream of the gully). Similar results of ~0.3 μg L^{-1} at W1 and 7.5 μg L^{-1} at W3 were obtained in October 2014, demonstrating that the waters flowing down the gully from SpH1 were transferring measurable Sb concentrations to the Glenshanna Burn. The W3 values were, however, ~ 100-fold lower than the values of ~780 μg L^{-1} (02/2013) and ~670 μg L^{-1} (10/2014) obtained at W5 (surface flow furthest down-gully from SpH1) (Table 1) and so considerable dilution had taken place upon entering the Burn. As for Sb, As concentrations were also lower at the upstream sites (~ 0.9–1.0 μg L^{-1}) than the values of ~13.2 ± 1.1 μg L^{-1} (02/2013) and 20.2 μg L^{-1} (10/2014) at the downstream site. Again, since the As concentrations at W5 were ~1770 μg L^{-1} (02/2013) and ~1480 μg L^{-1} (10/2014) the dilution upon entering the Burn was, to a first approximation, ~100-fold. Pb concentrations were generally low (0.06–0.08 μg L^{-1}) and there was no difference between upstream and downstream waters nor was there any elevation in the surface flow, W5. Iron concentrations in stream waters W1–3 were higher than in W4–5 and, in contrast with the other elements, Fe concentration in the downstream sample, W3, was slightly lower than in the upstream samples (W1–2).

3.8. BCR sequential extraction of selected soil samples

Samples from 2–4 cm or 4–6 cm for each of S2–5 and from 6–8 cm and 8–10 cm for S2 and S4, respectively, were selected as exemplar near-surface and deeper sections (Fig. 3). Typical recoveries for Sb, As and Pb were ~80–100% whilst those for Fe were ~60%, the latter being attributable to the use of aqua regia rather than HNO3/HF for the digestion of the residual phase. The results for Sb showed that very little was extracted in BCR1 and 2 (<5% in total) from any of the samples. Approximately 66% was extracted in BCR3 from S2 2–4 cm which had ~70% w/w OM whilst ~15–20% was extracted from the other near surface samples which had ~45–55% OM. The two samples from the deeper sections of S2 and S4 had lower OM contents and <10% Sb was extracted in BCR3. For As, ~5–18% was extracted in BCR1 from the samples taken from S2 and S3 whilst <3% was found in the same fraction for samples from S4 and S5. About 3–24% was extracted in BCR2 with the greater proportions being extracted from the samples from the deeper sections of S2 and S4, and especially the S5 4–6 cm section. As for Sb, the greatest proportion of As (~65%)

extracted in BCR3 was for the sample which had the highest OM content, S2 2–4 cm. The lowest proportions extracted in this fraction were again for the deeper sections of S2 and S4. In these samples and in S4 4–6 cm, the greatest proportion (60–~ 80%) of As was in the residual phase. For Pb, <1% was extracted in BCR1 and 2 from each of the samples. Approximately 65% Pb was in BCR3 for S2 2–4 cm whilst in all other samples, ~18–39% was extracted in this fraction. Thus the majority of Pb was present in the residual fraction in all samples except the highly organic S2 2–4 cm sample. For Fe the pattern was quite similar to that for Pb but with up to 12% in BCR2, 10–55% in BCR3 and the remainder in the residual phase. Although the overall extractability (sum of BCR 1–3) increased in the order Sb < Fe < Pb < As, the between-site and "with-depth" trends were quite similar for all four elements.

3.9. Elemental (Sb, As, Pb and Fe) concentrations in colloidal and dissolved fractions of the soil porewaters from S2–5

In general, the proportion in the colloidal fraction increased in the order Sb ≤ As b Pb ≤ Fe (Fig. 4) but there were considerable variations with depth for both Sb and As. At S2, there was ~ 65–70% colloidal Sb in the near-surface porewaters which decreased to ~30% towards the bottom of the core. At S5, values ranged from 6–55% but at S3 and S4 there was <25% Sb in the colloidal fraction of the porewaters. The distribution of As between colloidal and truly dissolved forms was similar to Sb in the S4 porewaters but, for S2, S3 and S5 there were distinct differences, e.g. there was an increase from ~20% to ~80% As in the colloidal fraction of S3 porewaters with increasing depth whilst the amount of colloidal Sb remained <20%. Similar trends were evident for the S5 porewaters and it was clear that there were site-specific differences between the porewater distributions of Sb and As. With the exception of Pb in the porewaters of S3 and the bottom section of S5, both Pb and Fe were almost exclusively present in the colloidal fraction, These results are consistent with previously published work (e.g. Graham *et al*., 2006; Schroth *et al*., 2008) showing that Pb solubility is enhanced by association with both organic and Fe-rich colloids.

3.10. Gel electrophoretic patterns

For the 4–6 cm ultrafilter retentate from S2 and S5, the highest concentrations of Sb, As and Fe were found in the fractions closest to the gel well (Fig. 5 and SI file). Thus Sb and As were associated with large Fe rich humic colloids. In comparison, for the 4–6 cm samples from S3 and S4, Sb and As were associated with smaller organic colloids (SI file). The distribution of Pb was similar to that of Fe at S2 and S3 but, at both S4 and S5, Pb was predominantly associated with small organic colloids and there was little correlation between the distribution of Pb and those of Sb or Fe (Fig. 5 and SI file).

4. Discussion

4.1. Antimony and other elemental concentrations in the spoil heap (SpH1)

Antimony, As and Pb concentrations in the spoil material from SpH1 were typically higher than those in all six soil cores (S1–6) and the control soil (C1) (Table 1). Excavation of the lower mining area (Gallagher *et al*., 1983), which ran underground from the adit to a shaft near SpH1 (Fig. 1(b)–(c)), resulted in spoil with high mineral content (stibnite (Sb_2S_3), arsenopyrite (FeAsS) and galena (PbS)) being deposited on the surrounding land and this has subsequently been exposed to the atmosphere and subject to infiltration of rainwater. Biver and Shotyk (2012) studied the kinetics of Sb release from stibnite and showed that higher rates of dissolution occurred as pH decreased from 5.1 to 1.1 and also with increasing

dissolved oxygen concentrations from 0.05 to 0.8 atm. The lower concentrations of antimony in the surface spoil are most likely a consequence of greater stibnite weathering rates in the surface spoil. Oxidative dissolution of arsenopyrite also releases As and Fe into solution but the latter tends to hydrolyse and precipitate in the form of Fe (oxy)hydroxides (e.g. Walker *et al*., 2006). Moreover, coatings on the surface of Sb-containing munitions have been shown to be enriched in both Fe and Pb (Ackerman *et al*., 2009). Thus at Glendinning, we propose that oxidative dissolution processes lead to the loss of Sb (Biver and Shotyk, 2012) and As (Walker *et al*., 2006) whilst precipitation favours the enrichment of Fe and Pb in surface spoil. At depth, reductive dissolution of Fe (oxy)hydroxides favours the loss of both Fe and Pb from surface coatings, accounting for the lower concentrations of these elements in SpH1-deep.

4.2. Processes controlling the spatial distribution and associations of Sb, As, Pb and Fe in soils at the Glendinning site

4.2.1. Down-slope from the adit

Core S1 was situated below SpH2 on a shallow slope leading down from the adit whilst S2–3 were in a water-logged area at the base of this slope (Fig. 1(b)–(c)). Antimony concentrations consistently decreased with increasing soil depth whilst the profiles for As, Pb and Fe showed either increased or near-constant concentrations with increasing depth. Based on the similarity of their vertical profiles, Sb may be strongly retained by OM in the near-surface sections of S1–3. This would be consistent with results for shooting range soils which attributed strong retention in surface organic layers to Sb(V) binding by humic acids (Steely *et al*., 2007).

The soil concentrations of Sb increased along the transect from S1 to S3 but this trend was not observed for As and Pb (Table 1 and Fig. 2). Thus, although originating from the same source material, the processes controlling not only vertical but also lateral mobility have affected Sb differently from As and Pb. There was little variation in pH with increasing soil depth (Table 1) nor was there an obvious relationship between pH and elemental concentration with distance downslope from SpH2. The profiles of As and Pb generally followed the trend for Fe at each of S1–3 and so sequential extraction was expected to reveal a major difference between the solid phase associations of Sb and those of As and Pb. In contrast with the anticipated results, all four elements behaved similarly. For example, the majority of each was associated with OM at S2 (2–4 cm) whilst at S3 (2–4 cm) the majority of Sb, Pb, Fe and ~50% As was in the residual phase. Comparison of the data for the 2–4 cm and 6–8 cm sections for the S2 core also revealed a consistent change for all four elements with increasing depth: the proportion associated with OM decreased markedly, resulting in a concomitant increase in the percentage present in the residual fraction (Fig. 3). Thus, solid phase associations per se do not explain the observed differences in vertical and lateral distribution of Sb in comparison with As and Pb (Fig. 2).

A further confounding feature of the data was that at S2 and at S3 the porewater profiles for Sb, As and Pb were very similar to each other and, in each case, were similar to those of both DOM and Fe (Fig. 2). However, when the distribution between colloidal and truly dissolved forms was considered (Fig. 4), there was a significant difference between the distributions of Sb and As and those of Pb, Fe and DOM (colour strongly retained in the colloidal fraction; data not shown). For the latter group, the vast majority (70–100%) was present in the colloidal fraction whilst up to ~90% Sb and up to ~80% As were present in the truly dissolved fraction. Moreover, for S2, there was a major change from colloidal Sb in the near-surface sections to truly dissolved forms at depth whilst, at S3, the proportion in the truly dissolved phase remained almost constant with depth. At both locations, this strongly

contrasted with the distribution of As: at S2, there was little change with depth whilst at S3, the proportion of colloidal As increased with increasing depth and thus the behaviour of As became more similar to that of Pb, Fe and OM. We propose that lateral transport promotes the removal of truly dissolved Sb species from these deeper sections of the soil whilst association of As and Pb with large Fe-rich/organic colloids favours their retention.

Fig. 3. Distribution of Sb, As, Pb and Fe amongst BCR fractions (exchangeable, reducible and oxidisable) and the residual phase of selected soil samples from S2–5.

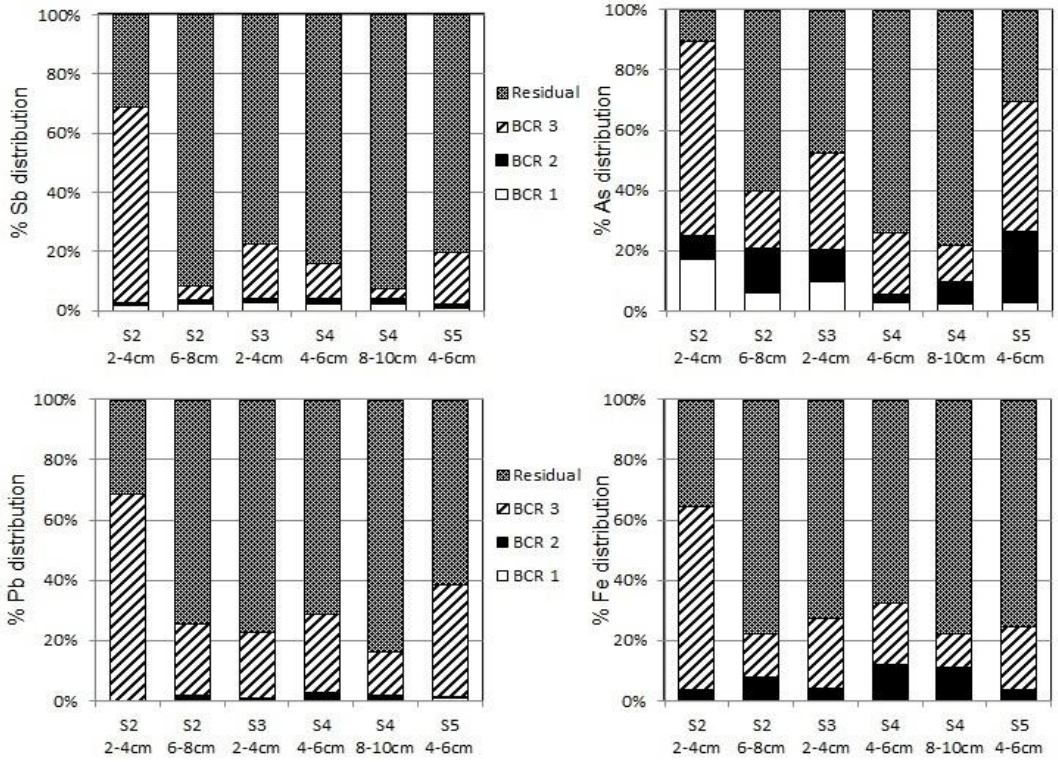

For S2 4–6 cm, where the solid phase associations indicated that large proportions of Sb, As, Pb and Fe were associated with organic matter, more than 50% of each element was in colloidal forms within the porewater. Gel electrophoresis confirmed a strong association of Sb, As and Pb with very large Fe-rich organic colloids which have low mobility. For S3 4–6 cm, where the solid phase association with organic matter was lower, Sb was mainly in the truly dissolved fraction and gel electrophoresis showed that, within the colloidal fraction, the greater proportion of As was again associated with very large Fe-rich colloids. Overall, the results of both ultrafiltration and gel electrophoresis point to differences in associations, which may start to explain the differences in the vertical distribution of Sb compared with As, Pb and Fe.

4.2.2. Down-gully from SpH1

There were ~2-fold and ~9-fold decreases in the maximum Sb concentration in the solid phase soils between S4 and S5 and S4 and S6, respectively (Table 1). Arsenic and Pb concentrations decreased much more rapidly between S4 and S5 (Table 1), suggesting that mobilised Sb may be transported over longer distances than both As and Pb before being attenuated by the gully soils. Mitsunobu *et al.* (2006) found that, where Sb and As behaved

differently in soil, Sb was almost exclusively present in its oxidised form (Sb^{V}) whilst As was present as a mixture of As^{III} and As^{V}, indicative of the greater stability of Sb^{V} in soil–water systems. In addition to its stability in the soil porewaters (Mitsunobu *et al.,* 2006), Sb^{V} sorbs less strongly to Fe oxides than As^{V} over a wide pH range (Leuz *et al.,* 2006). In this study, there was a distinct change in solid phase associations of As with distance down-gully. The sequential extraction data for S5 soils showed that, in contrast with Sb, the majority of solid phase As was associated with Fe oxides and with organic matter, which may also be intimately associated with Fe oxides. Moreover, the porewater profile of As was very similar to that of Fe, the majority of this As was in the colloidal fraction and, from the gel electrophoresis, As was mainly associated with large Fe-rich organic colloids. Although Sb was also associated with the same type of colloids, a greater proportion was present in truly dissolved forms. Thus the extent of sorption to Fe oxides may at least in part explain the observed trends with distance down-gully from SpH1.

As for the results for S3 soils, sequential extraction data for 4–6 cm samples from both S4 and S5 revealed that ~80% Sb was present in the residual phase. At 8–10 cm in S4, there was a decrease in association with organic matter and the percentage in the residual phase had increased to >90%. The distributions of As and Pb were similar to that of Sb at both 4–6 cm and 8–10 cm in S4, which suggests a very low potential for remobilisation of all three elements at this location. At S5, however, because As was almost evenly distributed amongst the iron oxide, organic matter and residual phases and could thus be more susceptible to redox-related remobilisation and loss from the soils should prevailing conditions change in the future.

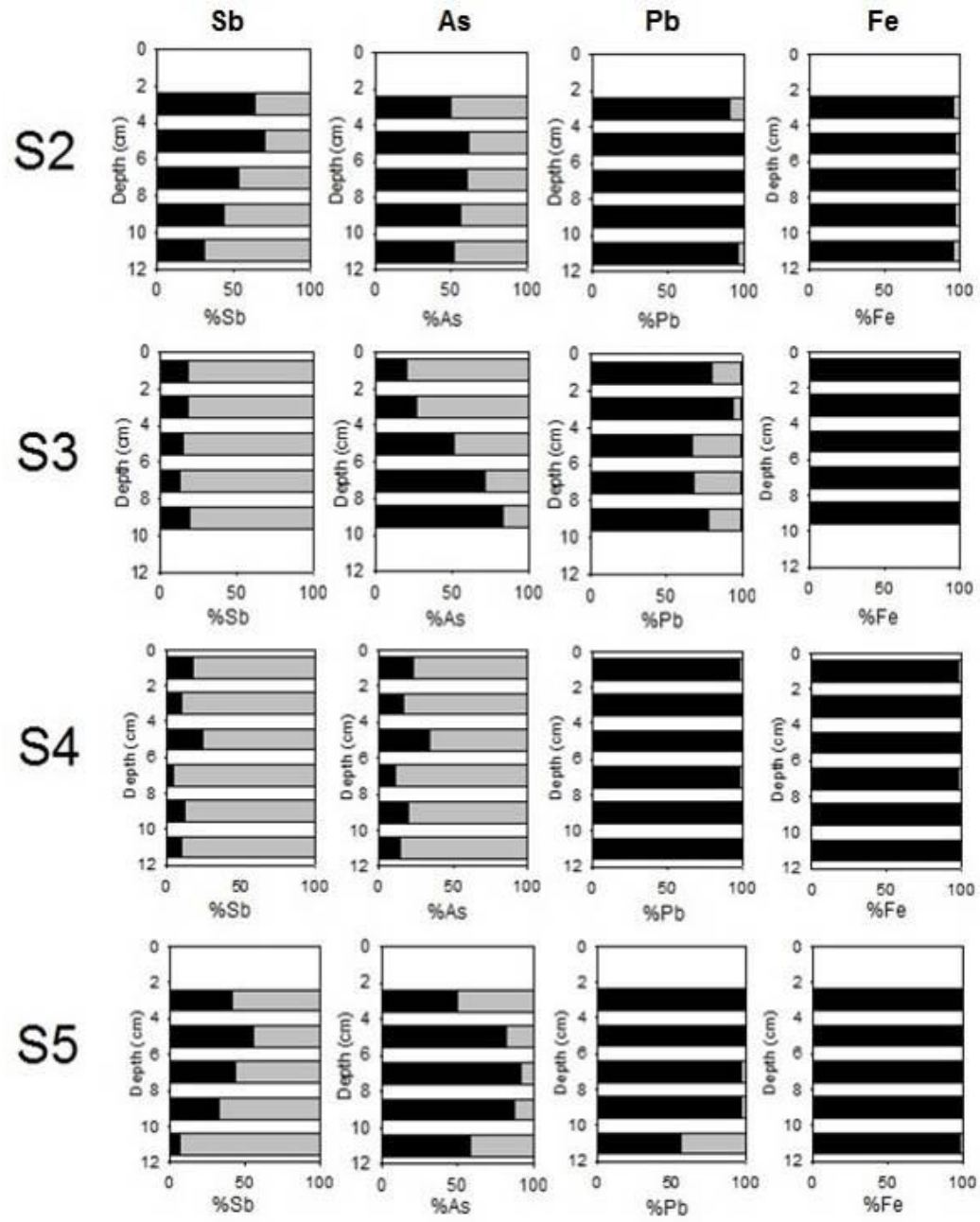

Fig. 4. Vertical variations in the distribution of Sb, As, Pb and Fe amongst colloidal (3 kDa–0.2 µm) and dissolved fractions (<3 kDa) of the porewaters from S2–5. Colloidal fraction in the black: dissolved fraction in light grey.

The Sb concentrations in the porewaters at S4 were ~2–4 times greater than at S3, whilst the S4 solid phase concentrations were only slightly higher than those at S3. Since the sequential extraction data showed very little difference in the solid phase associations of Sb, and the pH of the S4 soils (~4.7–4.9) was similar to that of the surface spoil (~4.8), the higher S4

porewater Sb concentrations are attributed to rainwater-induced leaching from the spoil, which was ~5 m upslope (cf Filella *et al*., 2009; Biver and Shotyk, 2013). Moreover, the much higher solid phase Pb concentrations at S4 in comparison with S3 were not reflected in higher porewater concentrations, suggesting a lower leachability of Pb from the spoil in comparison with Sb. This is consistent with the data for the spoil which, as discussed above, indicated preferential loss of Sb (and As) from SpH1-surface samples (Table 1). In the S4 porewaters, both Sb and As were predominantly present in truly dissolved form. The small amount of Sb present in colloidal forms was associated with smaller organic colloids which had a low Fe content. In contrast, the small amount of colloidal As at S4 was mainly associated with larger Fe-rich colloids, providing an additional explanation for its more rapid removal to the solid phase during its down-gully transport.

Comparing S4 and S5 porewaters, the maximum Sb concentration decreased by a factor of ~2 whilst that of As decreased by ~10. Thus for Sb and As, this trend mirrored that described above for the solid phase, providing further support for the poorer attenuation of Sb by the gully soils. One potential anomaly, however, was that the distributions of Pb and As at S5 were similar and, although the solid phase Pb concentration had decreased by a factor of ~15, porewater Pb concentrations were similar to those at S4. In the porewaters of both S4 and S5, Pb, Fe and DOM (colour retention) were almost exclusively found in the colloidal fraction whilst >~50% Sb and ≤70% As was present in the truly dissolved fraction. Gel electrophoretic fractionation of the colloid fraction of porewaters from the 4–6 cm section of S5 then revealed further important differences in elemental speciation. Antimony and As present within the colloidal fraction were both associated with large Fe rich organic colloids whilst Pb was associated with smaller organic colloids which contained low concentrations of iron (Fig. 5). In agreement with Graham *et al.* (2011) and Crançon et al. (2010), who showed that association with small Fe-poor organic colloids inhibited the removal of depleted uranium (DU) from firing range soils, small organic-colloidal association of Pb inhibits its removal from the porewaters to the solid phase of the S5 gully soils. Fig. 5. Distribution of Sb, As, Pb and Fe across gel electrophoretic fractions obtained for the colloid fraction (3 kDa–0.2 μm) isolated from S5 porewaters.

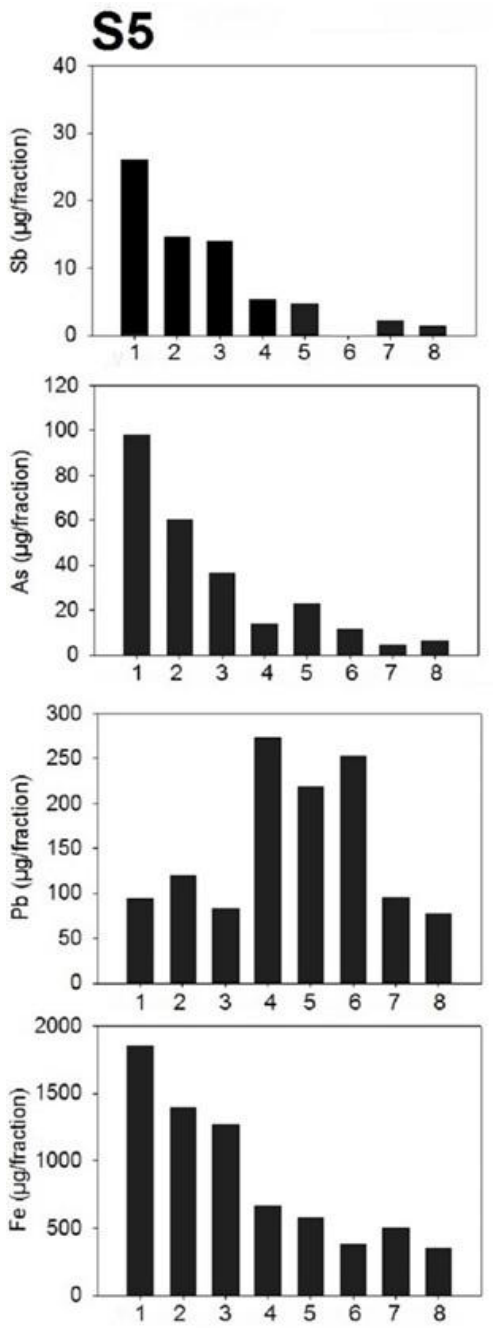

Fig. 5. Distribution of Sb, As, Pb and Fe across gel electrophoretic fractions obtained for the colloid fraction (3 kDa–0.2 µm) isolated from S5 porewaters.

4.3. Impact upon receiving waters

The Sb concentrations of ~6–8 µg L^{-1} and ~84 µg L^{-1} for W3 (downstream of gully) and W4 (surface flow closest to SpH1), respectively, were in reasonable agreement with those previously reported for downstream (14.3 µg L^{-1}) and spoil heap drainage (60.4 µg L^{-1}) samples (Mohammad *et al.*, 1990). The Sb concentrations at W3 were more than an order of magnitude higher than the value of 0.11 µg L^{-1} in the upstream waters (W1–2). The latter was in line with those published in an extensive review by Filella *et al.* (2002b) where concentrations ranged from 0.17 µg L−1 in pristine water at Loch Ewe, Scotland, to 1.9 µg

L^{-1} in the urbanised River Trent (Apte and Howard, 1986; Filella *et al*., 2002b; Jarvie et al., 2000). For As, water concentrations can be more variable due to local mineralogy, with natural concentrations ranging between 1 and 10 μg L−1 (Jarvie *et al.,* 2000). The values of ~1–1.1 μg L^{-1} for W1–2 fell within this range whilst that for W3 (~13–20 μg L^{-1}) only slightly exceeded the natural concentration range and was much lower than concentrations of ≤283 μg L^{-1} found downstream of an abandoned Slovakian Sb mine (Hiller *et al.*, 2012). Nevertheless, the water from W4 and W5 exceeded the 50.0 μg L^{-1} As freshwater Environmental Quality Standard (EQS) (SEPA, 2013).

5. Conclusions

In the vicinity of the small spoil heap, SpH2, at Glendinning, Scotland, Sb, As, Pb and Fe are released into soil porewaters as a consequence of DOM production and leaching. The extent of colloid association and indeed the speciation within the colloid fraction varied for each element. Importantly, Sb was mainly present in truly dissolved forms towards the bottom of the soil profiles whilst greater proportions of As, Pb and Fe were present in the colloidal fraction. The decreasing solid phase Sb concentrations with depth were therefore a consequence of the loss of truly dissolved Sb from the deepest sections of the soil profiles. The movement of rainwater through the main spoil heap, SpH1, mobilised Sb and As, which were then transported down a steep gully via soil porewaters and surface flows to the Glenshanna Burn. Arsenic was more rapidly removed from the porewaters to the solid phase as a consequence of its stronger associations with Fe oxides. There were clear trends of decreasing solid phase concentrations of Sb, As and Pb with distance down-gully, demonstrating a degree of natural attenuation for all three elements even in steeply sloping organic-rich parts of the catchment. The transport of Sb and As from mineral-rich spoil to the Glenshanna Burn demonstrates mobility in the surrounding area. Although the Glendinning Sb mine has been closed for approximately a century, its environmental impact has left a legacy in the surrounding area, and whilst the Glenshanna Burn complies with the current EQS values, this may not be the case in the future, especially if environmental change leads to increasingly stormy conditions.

References

Ackerman, S., Giere, R., Newville, M., Majzlan, J., 2009. Antimony sinks in the weathering crust of bullets from Swiss shooting ranges. Sci. Total Environ. 407, 1669–1682.

Apte, S.C., Howard, A.G., 1986. Determination of dissolved inorganic antimony (V) and antimony (III) species in natural waters by hydride generation atomic absorption spectrometry. J. Anal. At. Spectrom. 1, 221–225.

Bach, C., Dauchy, X., Chagnon, M.-C., Etienne, S., 2012. Chemical compounds and toxicological assessments of drinking water stored in polyethylene terephthalate (PET) bottles: a source of controversy reviewed. Water Res. 46, 571–583.

Biver, M., Shotyk, W., 2012. Stibnite (Sb_2S_3) oxidative dissolution kinetics from pH 1 to 11. Geochim. Cosmochim. Acta 79, 127–139.

Biver, M., Shotyk, W., 2013. Stibiconite (Sb_3O_6OH), senarmontite (Sb_2O_3) and valentinite (Sb_2O_3): dissolution rates at pH 2–11 and isoelectric points. Geochim. Cosmochim. Acta 109, 268–279.

Buschmann, J., Sigg, L., 2004. Antimony(III) binding to humic substances: influence of pH and type of humic acid. Environ. Sci. Technol. 38, 4535–4541.

Buschmann, J., Kappeler, A., Lindauer, U., Kistler, D., Berg, M., Sigg, L., 2006. Arsenite and arsenate binding to dissolved humic acids: influence of pH, type of humic acid and aluminum. Environ. Sci. Technol. 40, 6015–6020.

Butterman, W.C., Carlin, J.F., 2004. Mineral Commodity Profiles—Antimony. U.S. Department of the Interior, U.S. Geological Survey (Open-file report 03-019).

Ceriotti, G., Amarasiriwardena, D., 2009. A study of antimony complexed to soil-derived humic acids and inorganic antimony species along a Massachusetts highway. Microchem. J. 91, 85–93.

Cloy, J.M., Farmer, J.G., Graham, M.C., MacKenzie, A.B., 2009. Retention of As and Sb in ombrotrophic peat bogs: records of As, Sb, and Pb deposition at four Scottish sites. Environ. Sci. Technol. 43, 1756–1762.

Crançon, P., Pili, E., Charlet, L., 2010. Uranium facilitated transport by water-dispersible colloids in field and soil columns. Sci. Total Environ. 408, 2118–2128.

Davidson, C.M., Duncan, A.L., Littlejohn, D., Ure, A.M., Garden, L.M., 1998. A critical evaluation of the three-stage BCR sequential extraction procedure to assess the potential mobility and toxicity of heavy metals in industrially-contaminated land. Anal. Chim. Acta 363, 45–55.

European Commission, 2000. Directive 2000/60/EC of the European Parliament and of the Council of 23 October 2000 Establishing a Framework for Community Action in the Field of Water Policy (Water Framework Directive). European Commission. European Commission, 2001. Directive 76/464/EEC Article 7 of the European Parliament and of the Council on Pollution Reduction Programmes (Water Framework Directive). European Commission.

Farmer, J.G., Eades, L.J., Graham, M.C., Cloy, J.M., Bacon, J.R., 2010. A comparison of the isotopic composition of lead in rainwater, surface vegetation and tree bark at the long term monitoring site, Glensaugh, Scotland, in 2007. Sci. Total Environ. 408, 3704–3710.

Filella, M., 2011. Antimony interactions with heterogeneous complexants in waters, sediments and soils: a review of data obtained in bulk samples. Earth Sci. Rev. 107, 325–341.

Filella, M., Belzile, N., Chen, Y.-W., 2002a. Antimony in the environment: a review focused on natural waters: I. Occurrence. Earth Sci. Rev. 57, 125–176.

Filella, M., Belzile, N., Chen, Y.-W., 2002b. Antimony in the environment: a review focused on natural waters: II. Relevant solution chemistry. Earth Sci. Rev. 59, 265–285.

Filella, M., Philippo, S., Belzile, N., Chen, Y., Quentel, F., 2009. Natural attenuation processes applying to antimony: a study in the abandoned antimony mine in Goesdorf, Luxembourg. Sci. Total Environ. 407, 6205–6216.

Flynn, H.C., Meharg, A.A., Bowyer, P.K., Paton, G.I., 2003. Antimony bioavailability in mine soils. Environ. Pollut. 124, 93–100.

Gál, J., Hursthouse, A., Cuthbert, S., 2007. Bioavailability of arsenic and antimony in soils from an abandoned mining area, Glendinning (SW Scotland). J. Environ. Sci. Health A 42, 1263–1274.

Gallagher, M.J., Stone, P., Kemp, A.E.S., Hills, M.G., Jones, R.C., Smith, R.T., Peachey, D., Vickers, B.P., Parker, M.E., Rollin, K.E., Skilton, B.R.H., 1983. Strata bound arsenic and vein antimony mineralisation in Silurian greywackes at Glendinning, South Scotland. Institute of Geological Sciences Mineral Reconnaissance Programme (Report no. 59).

Graham, M.C., Vinogradoff, S.I., Chipchase, A.J., Dunn, S.M., Bacon, J.R., Farmer, J.G., 2006. Using size fractionation and Pb isotopes to study Pb transport in organic-rich upland catchments, NE Scotland. Environ. Sci. Technol. 40, 1250–1256.

Graham, M.C., Oliver, I.W., MacKenzie, A.B., Ellam, R.M., Farmer, J.G., 2008. An integrated colloid fractionation approach applied to the characterisation of porewater uranium–humic interactions at a depleted uranium contaminated site. Sci. Total Environ. 404, 207–217.

Graham, M.C., Oliver, I.W., MacKenzie, A.B., Ellam, R.M., Farmer, J.G., 2011. Mechanisms controlling lateral and vertical porewater migration of depleted uranium (DU) at two UK weapons testing sites. Sci. Total Environ. 409, 1854–1866.

He, M., Wang, X., Wu, F., Fu, Z., 2012. Antimony pollution in China. Sci. Total Environ. 421–422, 41–50.

Hiller, E., Lalinská, B., Chovan, M., Jurkovič, Ľ., Klimko, T., Jankulár, M., Hovorič, R., Šottník, P., Fľaková, R., Ženišová, Z., Ondrejková, I., 2012. Arsenic and antimony contamination of waters, stream sediments and soils in the vicinity of abandoned antimony mines in the Western Carpathians, Slovakia. Appl. Geochem. 27, 598–614.

International Agency for Research on Cancer (IARC), 1989. IARC Monograph vol. 47. World Health Organisation, Lyon, France, p. 291 ISBN 92 83212479; ISSN 02509555.

Jarvie, H.P., Neal, C., Burton, J.D., Tappin, A.D., 2000. Patterns in trace element chemistry in the freshwater tidal reaches of the River Trent. Sci. Total Environ. 251/252, 317–333.

Johnson, C.A., Moench, H., Wersin, P., Kugler, P., Wenger, C., 2005. Solubility of antimony and other elements in samples taken from shooting ranges. J. Environ. Qual. 34, 248–254.

Kalbitz, K., Solinger, S., Park, J.-H., Michalzik, B., Matzner, E., 2000. Controls on the dynamics of dissolved organic matter in soils: a review. Soil Sci. 165, 277–304.

Kalbitz, K., Kaiser, K., 2008. Contribution of dissolved organic matter to carbon storage in forest mineral soils. J. Plant Nutr. Soil Sci. 171, 52–60.

Leuz, A.-K., Mönch, H., Johnson, C.A., 2006. Sorption of Sb(III) and Sb(V) to goethite: influence on Sb(III) oxidation and mobilization. Environ. Sci. Technol. 40, 7277–7282.

Michazik, B., Matzner, E., 1999. Dynamics of dissolved organic nitrogen and carbon in a Central European Norway spruce ecosystem. Eur. J. Soil Sci. 50, 579–590.

Mitsunobu, S., Harada, T., Takahashi, Y., 2006. Comparison of antimony behaviour with that of arsenic under various soil redox conditions. Environ. Sci. Technol. 40, 7270–7276.

Mitsunobu, S., Takahashi, Y., Terada, Y., Sakata, M., 2010. Antimony(V) incorporation into synthetic ferrihydrite, goethite, and natural iron oxyhydroxides. Environ. Sci. Technol. 44, 3712–3718.

Mohammad, B., Ure, A.M., Reglinski, J., Littlejohn, D., 1990. Speciation of antimony in natural waters: the determination of Sb (III) and Sb (V) by continuous flow hydride generation–atomic absorption spectrometry. Chem. Speciat. Bioavailab. 3, 117–122.

Neubauer, E., Kohler, S.J., Laudon, H., von der Kammer, F., Hofmann, T., 2013. Effect of pH and stream order on iron and arsenic speciation in boreal catchments. Environ. Sci. Technol. 47, 7120–7128.

Okkenhaug, G., Zhu, Y.-G., Luo, L., Lei, M., Li, X., Mulder, J., 2011. Distribution, speciation and availability of antimony (Sb) in soils and terrestrial plants from an active Sb mining area. Environ. Pollut. 159, 2427–2434.

Redman, A.D., Macalady, D.L., Ahmann, D., 2002. Natural organic matter affects arsenic speciation and sorption onto hematite. Environ. Sci. Technol. 36, 2889–2896.

Salminen, R. (chief Ed.), Batista, M.J., Bidovec, M., Demetriades, A., De Vivo, B., De Vos, W. *et al.*, 2005. Geochemical Atlas of Europe. Part 1 — Background Information, Methodology and Maps. Geological Survey of Finland, Otamedia Oy, Espoo, 525 pp.

Schroth, A.W., Bostick, B.C., Kaste, J.M., Friedland, A.J., 2008. Lead sequestration and species redistribution during soil organic matter decomposition. Environ. Sci. Technol. 42, 3627–3633.

SEPA, Scottish Environment Protection Agency, 2013. Supporting Guidance (WAT-SG-53)—Environmental Standards for Discharges to Surface Waters. Ver: 4.0.

Shi, Z., Allen, H.E., Di Toro, D.M., Lee, S.-Z., Harsh, J.B., 2013. Predicting Pb^{II} adsorption on soils: the roles of soil organic matter, cation competition and iron (hydr)oxides. Environ. Chem. 10, 465–474.

Steely, S., Amarasiriwardena, D., Xing, B., 2007. An investigation of inorganic antimony species and antimony associated with soil humic acid molar mass fractions in contaminated soils. Environ. Pollut. 148, 590–598.

Taylor, S.R., 1964. Abundance of chemical elements in the continental crust: a new table. Geochim. Cosmochim. Acta 28, 1273–1285.

U.S. Geological Survey, 2013. Mineral Commodity Summaries 2013. U.S. Geological Survey, p. 198.

Walker, F.P., Schreiber, M.E., Rimstidt, J.D., 2006. Kinetics of arsenopyrite oxidative dissolution by oxygen. Geochim. Cosmochim. Acta 70, 1668–1676.

Wedepohl, K.H., 1995. The composition of the continental crust. Geochim. Cosmochim. Acta 59, 1217–1232.

Wilson, S.C., Lockwood, P.V., Ashley, P.M., Tighe, M., 2010. The chemistry and behaviour of antimony in the soil environment with comparisons to arsenic: a critical review. Environ. Pollut. 158, 1169–1181.

Yafa, C., Farmer, J.G., 2006. A comparative study of acid-extractable and total digestion methods for the determination of inorganic elements in peat material by inductively coupled plasma-optical emission spectrometry. Anal. Chim. Acta 557, 296–303.

Yafa, C., Farmer, J.G., Graham, M.C., Bacon, J.R., Barbante, C., Cairns, W.R.L., Bindler, R., Renberg, I., Cheburkin, A., Emons, H., Handley, M.J., Norton, S.A., Krachler, M., Shotyk, W., Li, X.D., Martinez-Cortizas, A., Pulford, I.D., MacIver, V., Schweyer, J., Steinnes, E., SjØbakk, T.E., Weiss, D., Dolgopolova, A., Kylander, M., 2004. Development of an ombrotrophic peat bog (low ash) reference material for the determination of elemental concentrations. J. Environ. Monit. 6, 493–501.

Appendix 9 Published research paper 2

Development of recent chronologies and evaluation of temporal variations in Pb fluxes and sources in lake sediment and peat cores in a remote, highly radiogenic environment, Cairngorm Mountains, Scottish Highlands

John G. Farmer[a], Angus B. MacKenzie[b], Margaret C. Graham[a], Kenneth Macgregor[a], Alexander Kirika[c]

[a] School of GeoSciences, University of Edinburgh, Edinburgh EH9 3FF, Scotland, UK
[b] Scottish Universities Environmental Research Centre, East Kilbride G75 0QF, Scotland, UK
[c]NERC Centre for Ecology and Hydrology, Bush Estate, Penicuik EH26 0QB, Scotland, UK

Abstract

The use of stable Pb isotope analyses in conjunction with recent (^{210}Pb and anthropogenic radionuclide) chronologies has become a well-established method for evaluating historical trends in depositional fluxes and sources of atmospherically deposited Pb using archival records in lake sediment or peat cores. Such studies rely upon (i) simple radioactive disequilibrium between unsupported ^{210}Pb and longer-lived members of the ^{238}U decay series and (ii) well-defined values for the isotopic composition of contaminant Pb and indigenous Pb in the study area. However, areas of high natural radioactivity can present challenging environments for such studies, with potential complications arising from more complex disequilibria in the ^{238}U decay series and the occurrence, at local or regional level, of anomalous, ill-defined stable isotope ratios due to the presence of elevated levels of radiogenic Pb. Results are presented here for a study of a sediment core from a freshwater lake, Loch Einich, in the high natural radioactivity area of the Cairngorm Mountains of Scotland. ^{238}U decay series disequilibria revealed recent diagenetic re-deposition of both U and ^{226}Ra, the latter resulting in a requirement to use a modified calculation to derive a ^{210}Pb chronology for the core. Confidence in the chronology was provided by good agreement with the independent ^{241}Am chronology, but the ^{137}Cs distribution was affected by significant post-depositional mobility in the organic-rich sediment. The systematics of variations in ^{230}Th, ^{232}Th and stable Pb isotope ratio distributions were used to establish the indigenous Pb characteristics of the sediment. The relatively high radiogenic content of the indigenous Pb resulted in complications in source apportionment, in particular during the 20th century, with multiple natural and anthropogenic sources precluding the use of a simple binary mixing model. Consequently, ^{206}Pb/^{207}Pb ratios in Scottish moss samples from an archive collection were used to provide the input term for atmospheric deposition in order to establish historical trends in indigenous and anthropogenic Pb fluxes. A test of the accuracy of the derived Pb fluxes was provided by analysis of a core from a nearby blanket peat deposit, Great Moss. Independent atmospheric and basal inputs gave a complex distribution of ^{210}Pb in the peat, but this did not affect calculation of a ^{210}Pb chronology. Once again, the ^{210}Pb chronology was supported by the ^{241}Am distribution. Temporal trends in anthropogenic Pb deposition derived for the Loch Einich sediment core were in generally good agreement with those for the Great Moss peat core, other peat cores and some other lake sediment cores from northern Scotland, providing confidence in the use of the archive moss data to characterise atmospheric deposition. However, sustained input of Pb to Loch Einich sediment at relatively high levels in the late 20th century, after the regional decline in atmospheric Pb

deposition suggested that catchment-derived Pb is now a significant component of the depositional flux for Loch Einich.

1. Introduction

Extensive use has been made of Pb concentration and stable Pb isotope profiles in ^{210}Pb-dated lake sediment and ombrotrophic peat cores to reconstruct historical trends in atmospheric deposition and to apportion sources of anthropogenic Pb (e.g. Farmer et al., 1996, 2005; Shotyk et al., 1996, 2002, 2005; MacKenzie et al., 1997, 1998; Schell et al., 1997; Brannvall et al., 2001a; Novak et al., 2003; Cloy et al., 2008; Martınez Cortizas et al., 2012; Allan et al., 2013; Miller et al., 2014). Such studies, supported by independent records derived from analyses of archived grass (Bacon et al., 1996) and moss (Farmer et al., 2002) samples, have established the general historical trends in atmospheric depositional fluxes of Pb in Europe (Renberg et al., 2001; Bindler, 2011), which exhibited a marked increase following the start of the Industrial Revolution in the mid-19th century, maximum values in the mid-20th century and a subsequent decrease in the late 20th century in response to reduced emissions. Anthropogenic Pb deposited in the UK in the 19th century was characterised by an average ^{206}Pb/^{207}Pb ratio of about 1.175 (Bacon et al., 1996; Farmer et al., 1996, 2005; Cloy et al., 2008), reflecting the dominant use of locally derived Pb ores and coal. The use of imported Australian Pb ore (^{206}Pb/^{207}Pb ~1.04), starting at the end of the 19th century, resulted in a decrease in the ^{206}Pb/^{207}Pb ratio of atmospherically deposited Pb, in particular from the 1930s to the 1990s when leaded petrol, which had an average ratio of ~1.08 (Sugden et al., 1993; Farmer et al., 2000), was used. Minimum ^{206}Pb/^{207}Pb ratios of about 1.12 were observed in the late 1980s–early 1990s (Cloy et al., 2008), after which the use of unleaded petrol reversed the trend, with values tending back towards those of indigenous Pb (e.g. Farmer et al., 2002, 2010). The characteristic difference in ^{206}Pb/^{207}Pb ratio between industrial and petrol Pb allowed the use of a simple binary mixing model to apportion the relative contribution of each to total contaminant Pb deposition (e.g. Farmer et al., 1996).

The concentration profile of anthropogenic Pb in sediment cores, and to a lesser extent in peat cores, is superimposed upon the natural Pb concentration profile and, in order to derive the isotope ratio of contaminant Pb, correction for the natural component can be made using the intrinsic geological ^{206}Pb/^{207}Pb ratio for the sediment (Farmer et al., 1996). Correction for the natural Pb component has a relatively small effect for ombrotrophic peat and for sediment with high concentrations of contaminant Pb, but is progressively more important in deeper sections of cores with lower levels of contamination or in cores from areas remote from pollution sources.

Background geological ^{206}Pb/^{207}Pb ratios in much of the UK and western/central Europe lie in the approximate range 1.17–1.20 (Sugden et al., 1993; Farmer et al., 1996,2005; Shotyk et al., 1996, 2002, 2005; MacKenzie et al.,1997, 1998; Novak et al., 2003; Bacon and Hewitt, 2005;Merilainen et al., 2011), meaning that anthropogenic Pb deposited in the 19th and early 20th centuries, with a ^{206}Pb/^{207}Pb ratio of about 1.175, was isotopically very similar to indigenous Pb.

Significant variations in the natural geological Pb isotopic composition in rocks and derived soils occur, at both regional and local scales, in response to differences in bedrock U and Th concentrations and age of emplacement. For example, on a regional basis, isotopic differences between the rocks of the Baltic Shield and those of western/central Europe result in ^{206}Pb/^{207}Pb ratios of around 1.3–2.0 in soils in Sweden (Brannvall et al., 2001b; Klaminder et al., 2008, 2011), contrasting with lower values of 1.17–1.20 in Europe and the UK. At the local level, Pb in the Pb–Zn mineralisation at Tyndrum in Scotland is characterised by a ratio of 1.146 (MacKenzie and Pulford, 2002), which contrasts with typical intrinsic geological ^{206}Pb/^{207}Pb ratios of 1.17–1.20 for much of Scotland (Sugden et al., 1993; Farmer et al., 1996, 2000, 2005; MacKenzie et al., 1997, 1998; Bacon and Hewitt, 2005). The Tyndrum ^{206}Pb/^{207}Pb ratio is intermediate between those for industrial Pb and petrol Pb, thereby

complicating source apportionment (Farmer et al., 1997a). Thus, accurate characterisation of the natural background Pb isotopic composition is important when correcting observed sediment concentrations for natural Pb content.

In areas of high natural radioactivity, the use of archival peat and sediment records for reconstruction of historical trends in Pb fluxes can potentially be complicated both by variations in stable Pb isotope ratios and by disequilibria within the natural decay series affecting distributions of ^{210}Pb and ^{226}Ra. ^{210}Pb dating is based on the assumption of simple radioactive disequilibrium produced by deposition of unsupported ^{210}Pb as a result of atmospheric decay of ^{222}Rn (Goldberg, 1963; Robbins and Edgington, 1975; Appleby and Oldfield, 1978). Age-depth modelling by ^{210}Pb dating, supported by nuclear fallout studies (e.g.^{137}Cs, ^{241}Am), is by now generally well established (e.g. Appleby, 2001, 2008), although refinements continue to be suggested (e.g. MacKenzie et al., 2011; Hansson et al., 2014). However, geochemical processes operating in areas with elevated concentrations of U and Th can result in additional decay series disequilibria by, for example, diagenetic redistribution of U (e.g. Scott et al., 1991; Read et al., 1993) or ^{226}Ra (e.g. Fanning et al., 1981) or by additional generation of unsupported ^{210}Pb as a consequence of elevated fluxes of ^{222}Rn (Card and Bell, 1985). Such processes can present complications in ^{210}Pb dating, in particular if they result in disequilibrium between ^{226}Ra and supported ^{210}Pb (Brenner et al., 1994, 2004). Additionally, if these and other processes, such as mineral weathering (e.g. Shirahata et al., 1980; Erel et al., 1994), operate over geological timescales, they could influence stable Pb isotopic composition, potentially giving variations at the local level. Thus, understanding the geochemical processes operating and resultant decay series disequilibrium is critical in both ^{210}Pb dating and stable Pb isotope studies in areas of high natural radioactivity.

The present work focussed on evaluating the significance of such effects in sediment and peat deposits in the high natural radioactivity environment of the Cairngorm Mountains in Scotland. The study entailed analysis of an archived (2001) freshwater lake sediment core from Loch Einich and of a recent (2012) peat core from the nearby Moine Mhor (Great Moss) blanket peat deposit, which lies on metamorphic Moine rocks to the south of Loch Einich, close to the junction with the Cairngorm pluton (Thomas et al., 2004) (Fig. 1). Loch Einich is located in the Caledonian granites of the Cairngorm intrusion, which have high levels of natural radioactivity, with average U and Th specific activities of 157 Bq kg^{-1} (12.6 mg kg^{-1}) and 108 Bq kg^{-1} (26.8 mg kg^{-1}), respectively, (Brown et al., 1979) and estimates of emplacement age ranging from 390 to 425 Ma (Plant et al., 1990; Thomas et al., 2004)). Consistent with this, Jones et al. (1993) have reported 226Ra activities in sediments of Cairngorm plateau lochs (e.g. Loch Coire an Lochain and Lochan Uaine) an order of magnitude greater than those typical of other UK sites, while Yang et al. (2007) have observed high radiogenic ^{206}Pb/^{207}Pb ratios of up to 1.35 for sediments from Lochnagar, a freshwater lake lying on (Lochnagar) granite just to the southeast of the Cairngorm Mountains. Yang et al. (2002, 2007) also found that catchment, rather than the declining direct atmospheric, input to Lochnagar had come to dominate the flux of anthropogenic Pb to the lake sediments in recent decades, indicative not only of a lag but also of a potentially significant future environmental pollution problem for freshwater lakes.

The work described here involved analysis of long-lived members of the ^{238}U and ^{232}Th natural decay series in order to provide an understanding of the system sufficient to enable development of ^{210}Pb chronologies and to rationalise variations in stable Pb isotope ratios in order to define indigenous regional values. The aims of the work were to establish reliable recent chronologies and to derive an estimate of the indigenous stable Pb isotope variations in this complex, highly radiogenic system in order to deconvolute the elemental, isotopic and radionuclide profiles in the Loch Einich sediment core. Specific objectives included (i) the development of a ^{210}Pb chronology for Loch Einich and the derivation of both natural and anthropogenic Pb fluxes to its sediments and (ii) through comparison of these findings with

those from the Great Moss peat core and various other Scottish records, the assessment of influences upon, and the implications of, the derived historical Pb deposition flux information.

2. MATERIALS AND METHODS

2.1. Site description

2.1.1. The Cairngorm Mountains

The Cairngorms, the north-eastern spur of the Grampian Mountains in the Scottish Highlands (Fig. 1a), lie between the rivers Spey to the north-west and Dee to the south, occupying an area of 32 km x 19 km (Watt and Jones, 1948). A detailed description of the area by Thomas et al. (2004) indicates that the central and larger part consists of a mass of granite (Fig. 1b), the Cairngorm Granite pluton, intruded at ~425 Ma in late Silurian-early Devonian times into metamorphosed Dalradian metasedimentary rocks during the later stages of the Caledonian mountain building period. The Cairngorm Granite became exposed at the surface ~390 Ma ago, with subsequent erosion, including the influence of Quaternary glaciation from ~2 Ma ago, resulting in landscape features of plateaus and classic glacial troughs and corries (Gordon, 1993; Thomas et al., 2004). Braeriach (1296 m), one of the characteristic complex plateaus of the western sector of the Cairngorms massif, is terminated abruptly to the west by the deep, glacial chasm of Glen Einich, containing Loch Einich at its head (Fig. 1c). To the west of Glen Einich is a high ridge comprising the principal summit of Sgor Gaoith (1118 m) and its outliers of Sgoran Dubh Mor and Carn Ban Mor, while to the south of Glen Einich is a remote sprawling plateau known as the Moine Mhor or Great Moss (Gordon, 1993). The steep headwall above Loch Einich at the southern tip of Glen Einich coincides with the contact between the Cairngorm Granite and metasedimentary country rocks (Thomas et al., 2004) (Fig. 1b and c). The Cairngorm Granite underlies all of the high land (including Loch Einich) of the Cairngorm Mountains except for the Moine Mhor area in the southwest (Gordon et al., 2006), where the blanket peat of Great Moss lies on metamorphosed Dalradian sandstones and siltstones (Barron et al., 2011).

2.1.2. Loch Einich

Lying at the head of the U-shaped glaciated valley of Glen Einich (Fig. 1c), 503 m above sea level, Loch Einich is an oligotrophic loch, ~1.9 km long and up to 500 m wide, with a mean depth of ~19 m and a maximum depth of ~40 m. The loch has an area of 0.796 x 106 m^2 and volume of 15.107 x 10^6 m^3, with a catchment (mean altitude 869 m) area of 11.067 x 10^6 m^2, annual rainfall of 1800 mm (potential evaporation 229 mm) and total run-off of 18.600 x 10^6 m^3 (Lyle, 1987). The loch has an average water retention time of 296.4 days, with the north-flowing Allt na Beinne Moire the main outflow. Loch Einich, which enjoys more sheltered conditions than the higher altitude Cairngorm lochs, has a catchment consisting of bare rock, thin soils (sub-alpine/rankers/lithosols) and an area of blanket peat (Helliwell et al., 2002; Barron et al., 2011).

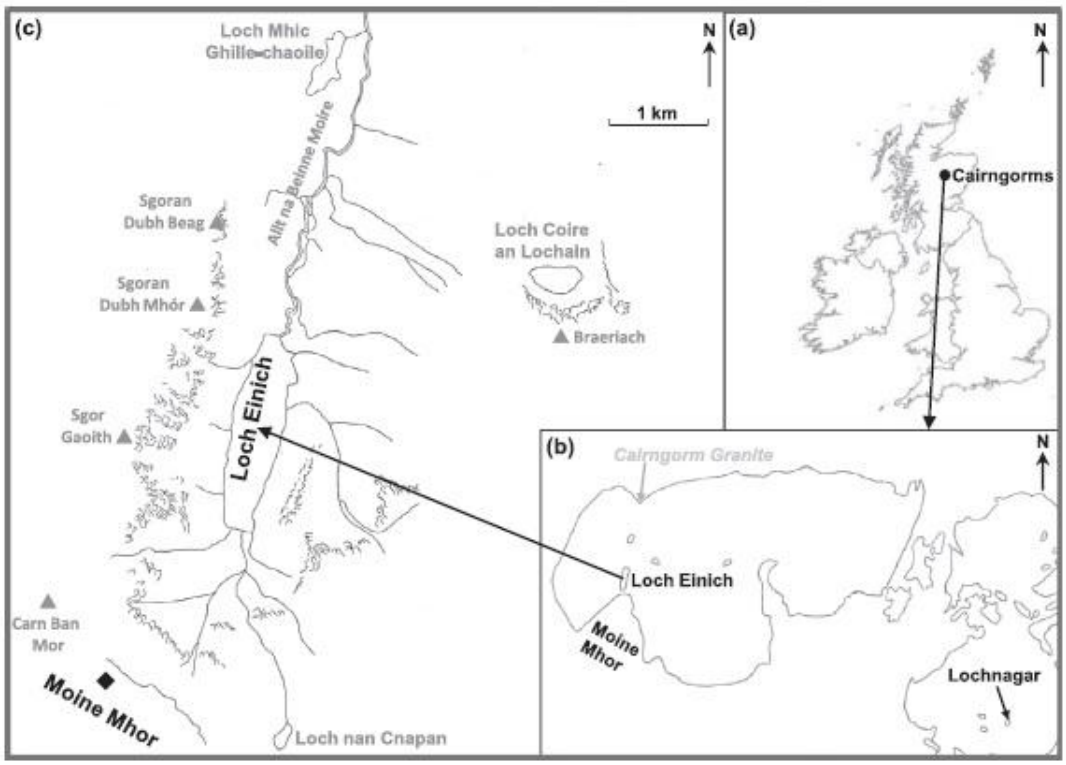

Fig. 1. Maps showing location of (a) Cairngorm Mountains in the UK, (b) Loch Einich on the Cairngorm Granite (and Lochnagar (altitude 785 m) on the Lochnagar Granite) and Moine Mhor (Great Moss) adjacent to the Cairngorm Granite and (c) the sampling sites on Loch Einich and Great Moss, as well as the locations of other lochs, Loch Mhic Ghille-chaoile (altitude 500 m), Loch Coire an Lochain (920 m) and Loch nan Cnapan (870 m) (Rose et al., 2012) nearby.

2.1.3. Moine Mhor (Great Moss)

At 900–945 m, Moine Mhor (Great Moss) (Fig. 1c) has the largest extent of high-altitude blanket peat in the Cairngorms (Watt and Jones, 1948). The predominant vegetation on the plateau is dissected Empetrum–Eriphorum bog on deep peat with Racomitrium heath on the higher ground and Nordus grassland where snow lies late (McVean, 1962). Barber et al. (2000) have reported that there is a remarkable preservation in the underlying peat of abundant macrofossils, presumably due to the sub-arctic climate, which mirror the humification and bulk density with alterations of Sphagnum-rich and Racomitrium-dominated peat, representing relatively wet and dry periods, respectively. The peat contains a proportion of sand and silt derived from the glacial debris of Moine rocks and not from the Cairngorm Granite (McVean, 1962).

2.2. Sample collection

2.2.1. Loch Einich sediment

The Jenkin coring technique was used to collect a sediment core, 21 cm in length, from a water depth of ~40 m, in the centre of Loch Einich (57°4'7"N, 3°47'31"W) (Fig. 1c) on 2 August 2001. The core was cut into 1-cm depth increments (cross-sectional area 37.39 cm^2), which were returned to the laboratory for subsequent weighing before and after oven-drying at 80°C.

2.2.2. Great Moss peat

A monolith core, 50 cm in length (nominally 15 cm x 9 cm cross section), was collected at an altitude of 949 m from Great Moss (57°2'47.0"N, 3°48'53.5"W), about 1.75 km south of Loch Einich (Fig. 1c), on 20 June 2012. The core was cut into 2-cm depth increments (with individually measured cross-sectional area varying from 117 cm^2 (13 cm x 9 cm) to 252 cm^2 (18 cm x 14 cm) over the length of the core), which were returned to the laboratory for subsequent weighing before and after air-drying at room temperature. The material in the core changed from predominantly living surface vegetation (0–2 cm) to decaying surface vegetation (2–4 cm) and decaying surface vegetation and peat (4–6 cm), underlain by peat (6–50 cm), below which there was a layer of mineral material.

2.3. Sample preparation (for elemental and Pb isotopic analysis)

2.3.1. Sediment

Duplicate to quintuplicate sub-samples (~0.2 g) of dried sediment sections were oven-dried at 105°C overnight and dry-ashed at 450°C for 4 h before digestion in 30 mL 8M HNO_3 (Aristar, Merck, Poole, UK) on a hot-plate at 90°C for 2–3 h. The solutions were then cooled, filtered (Whatman 540, ashless), evaporated to ~1 mL and diluted to 25 mL with 2% (v/v) HNO3 (Farmer et al., 1999, 2002) for analysis by inductively coupled plasma-optical emission spectrometry (ICP-OES) and inductively coupled plasma mass spectrometry (ICP-MS) after appropriate subsequent dilution.

2.3.2. Peat

Duplicate to quadruplicate sub-samples (~0.25 g) of air-dried, manually ground peat were oven-dried at 105°C overnight and weighed before ashing in a furnace at 450°C for 4 h. Using a modified US EPA Method 3052 Protocol, ashed samples were digested in 9 mL conc. HNO_3 and 1 mL conc. HF (Aristar, Merck, Poole, UK) in Teflon microwave digestion vessels in a MARS 6 (CEM, Buckingham, UK) microwave digestion system (Yafa et al., 2004; Yafa and Farmer, 2006). Digests were evaporated to 1 mL on a hot-plate and then made up to 25 mL with 2% (v/v) HNO_3.

2.4. Sample analysis (elements and Pb isotopes)

2.4.1. ICP-OES

Lead, Mn and Fe concentrations in the sediment digests, as well as Mn, Fe and Ti concentrations in the peat digests, were determined by ICP-OES using a Perkin- Elmer Optima 5300 DV instrument (Perkin-Elmer, Beaconsfield, UK) in axial mode, employing an RF forward power of 1400 W, with argon gas flows of 15, 0.2 and 0.75 L min^{-1} for plasma, auxiliary and nebuliser flows, respectively. A peristaltic pump was used to take sample solutions into a Gem Tip cross-flow nebuliser and Scott spray chamber at a rate of 1.5 mL min_1. The use of Pb (220.353 nm), Mn (259.372 nm), Fe (239.562 nm) and Ti (336.121 nm) emission lines and calibration standards in the appropriate concentration range enabled calculation of sample Pb, Mn, Fe and Ti concentrations. Overall mean analytical precision for replicate sample analyses (n = 2–5) for Pb, Mn and Fe in all sediment sections was ±7%, ±7% and ±5%, respectively; for Mn, Fe and Ti in all peat sections, the corresponding figures were ±10%, ±8% and ±7%, respectively.

2.4.2. ICP-MS

Lead concentrations and isotope ratios ($^{206}Pb/^{207}Pb$, $^{208}Pb/^{206}Pb$ and $^{208}Pb/^{207}Pb$) in the peat sample solutions were determined by quadrupole ICP-MS using an Agilent 7500ce (with octopole reaction system) instrument (Agilent Technologies, Stockport, UK), with nickel cones, employing an RF forward power of 1540 W and reflected power of 1 W, with argon gas flows of 0.82 and 0.20 L min^{-1} for carrier and makeup flows, respectively, and peristaltic

pumping or free aspiration rates into the Mira mist nebuliser of 0.2 or 1.2 mL min^{-1}, respectively. A common Pb isotopic reference material from the National Institute of Standards and Technology (NIST), SRM 981, was used for mass bias correction. Employing appropriate calibration standards and sample dilution to <25 μg L^{-1}, sample concentrations were calculated using isotope analysis acquisition and the fully quantitative mode (three points per unit mass, with integration times of 0.3 s per point and five replicate runs per sample). Overall mean analytical precision for Pb determination in replicate (n = 2–4) peat samples of >8 mg kg^{-1} (n = 18) and <8 mg kg^{-1} (n = 7) averaged ±4.6% and ±12.5%, respectively. Overall mean analytical precision for Pb isotope ratio determination in duplicate peat samples (n = 25) was ±0.27%, ±0.23% and ±0.24% for $^{206}Pb/^{207}Pb$, $^{208}Pb/^{206}Pb$ and $^{208}Pb/^{207}Pb$, respectively. Overall mean analytical precision for the similarly determined Pb isotope ratios in replicate (n = 2–4) sediment samples was ±0.30%, ±0.22% and ±0.26% for $^{206}Pb/^{207}Pb$, $^{208}Pb/^{206}Pb$ and $^{208}Pb/^{207}Pb$, respectively.

2.4.3. Quality assurance

2.4.3.1. Sediment.

The mean Pb concentration (n = 9) of 114 ± 3 mg kg^{-1} obtained by dry ash/8M HNO_3 digestion for a secondary Loch Lomond reference material, previously calibrated against IAEA Lake Sediment SL reference material, was in good agreement with the 120 ± 11 mg kg^{-1} of Eades et al. (2002). For the Czech Metrological Institute CMI7003 soil reference material, a mean concentration (n = 9) of 25.4 ± 1.7 mg kg^{-1} was obtained (certified, 22.7 ± 1.3 mg kg^{-1}, extractable by boiling 2 M HNO3). The corresponding CMI7003 data for Mn and Fe were 493 ± 24 mg kg^{-1} (certified, 476 ± 28 mg kg^{-1}, extractable by boiling 2M HNO3) and 2.85 ± 0.05% (non-certified matrix element, 2.90%), respectively. The mean $^{206}Pb/^{207}Pb$ ratio of 1.142 ± 0.002 for the secondary Loch Lomond sediment reference material, previously calibrated against the IAEA SL-I material (Viczian et al., 1990; Eades et al., 2002), agreed with the previously obtained value of 1.140 ± 0.002 (Eades, 1999).

2.4.3.2. Peat.

The mean values of 173 ± 10 mg kg^{-1} obtained for the total Pb concentration of the Ombrotrophic Peat reference material NIMT/UOE/FM/ 001 agreed with the certified Pb value of 174 ± 8 mg kg^{-1}. The corresponding NIMT/UOE/FM/001 data for Mn, Fe and Ti were 6.4 ± 0.6 mg kg^{-1} (certified, 7.52 ± 0.41 mg kg_1), 879 ± 87 mg kg^{-1} (information only, 921 ± 84 mg kg^{-1}) and 339 ± 26 mg kg^{-1} (information only, 357 ± 18 mg kg^{-1}), respectively. The mean isotope ratios of $^{206}Pb/^{207}Pb$, $^{208}Pb/^{206}Pb$ and $^{208}Pb/^{207}Pb$ determined in NIMT/UOE/ FM/001 (n = 12, ±1 SD) as 1.177 ± 0.002, 2.094 ± 0.004 and 2.463 ± 0.003, respectively, were in good agreement with corresponding reported information only values of 1.176 ± 0.001, 2.092 ± 0.002 and 2.461 ± 0.003 (Yafa et al., 2004).

2.5. Radionuclide analyses

2.5.1. Gamma spectroscopy

^{210}Pb (half-life 22.3 years), ^{226}Ra (half-life 1600 years), ^{241}Am (half-life 432.7 years) and ^{137}Cs (half-life 30 years) were measured by gamma spectroscopy using a low background EG&G Ortec planar HPGe detector (diameter 51.4 mm, depth 19.4 mm) housed in a graded Pb–Cd–Cu shield. Prior to analysis, samples were sealed in polycarbonate containers and stored for a period of at least 30 days to ensure radioactive equilibrium between ^{226}Ra and ^{222}Rn (half-life 3.825 days). ^{210}Pb, ^{241}Am and ^{137}Cs were measured using their gamma emissions at 46.5 keV, 59.5 keV and 661.7 keV, respectively, while ^{226}Ra was determined indirectly using the 351.9 keV and 609.3 keV gamma emissions of its decay chain

descendants ^{214}Pb (half-life 26.8 minutes) and ^{214}Bi (half-life 19.9 minutes), respectively. Detection efficiencies were established using standards which were prepared by addition of known activities of the radionuclides of interest, in solutions derived from Amersham certified standards, to peat or sediment in which activities of unsupported ^{210}Pb and anthropogenic radionuclides were below limits of detection.

2.5.2. Alpha spectroscopy

Loch Einich sediment samples were analysed for ^{238}U (half-life 4.47 x 10^9 years), ^{234}U (half-life 4.25 x 10^5 years), ^{232}Th (half-life 1.41 x 10^{10} years) and ^{230}Th (half-life 7.54 x 10^4 years) by addition of a known activity of a ^{232}U/^{228}Th standard solution (Harwell) to the sample before total digestion by sequential HCl/HNO_3 and HF digestions. U and Th were separated by anion exchange and electroplated onto stainless steel planchettes (MacKenzie et al., 1994) prior to alpha spectroscopy analysis using an EG&G Octet spectrometer. Alpha particle energies used in the analyses were: ^{238}U 4.147 MeV (23%) and 4.196 MeV (77%); ^{234}U 4.724 MeV (27.5%) and 4.776 MeV (72.5%); ^{232}U 5.264 MeV (31.2%) and 5.320 MeV (68.6%); ^{232}Th 3.952 MeV (23%) and 4.010 MeV (77%); ^{230}Th 4.621 MeV (23.4%) and 4.688 MeV (76.3%); ^{228}Th 5.340 MeV (26.7%) and 5.423 MeV (72.7%).

2.5.3. Quality assurance

Accuracy for gamma spectroscopy was evaluated by analysis of the IAEA reference soil IAEA-447 giving mean values of 408 ± 28 Bq kg^{-1} (n = 9) for ^{210}Pb, 23.8 ± 7.5 Bq kg^{-1} (n = 9) for ^{226}Ra and 432 ± 16 (n = 12) Bq kg^{-1} for ^{137}Cs, relative to certified values of 420 ± 20, 25.1 ± 2.0 and 425 ± 10 Bq kg^{-1}, respectively. Accuracy for U/Th analysis was assessed using the CANMET reference material DL1a, giving average values (n = 3) for ^{238}U, ^{234}U, ^{230}Th and ^{232}Th specific activities of 1400 ± 33, 1427 ± 33, 1423 ± 40 and 300 ± 12 Bq kg^{-1}, respectively, relative to a certified value of 1429 Bq kg^{-1} for each of ^{238}U, ^{234}U, ^{230}Th and 309 Bq kg^{-1} for ^{232}Th.

3. RESULTS AND DISCUSSION

3.1. Loch Einich

3.1.1. Sediment core geochemistry

The depth profiles of wet weight/dry weight ratio, Loss On Ignition (LOI) and Mn and Fe concentrations are displayed in Fig. 2a–d. The wet weight/dry weight ratio (Fig. 2a) decreased steadily from the highly porous surface layers to relatively constant values (3.5 ± 0.3) in the more compacted layers below 12 cm, although there was a noticeable slight dip for sections between 5 and 7 cm, possibly indicative of a coarser grain size. The LOI (Fig. 2b), indicative of the trend in organic carbon content, decreased from a mean of 25 ± 6% (range 19–34%) for 0–5 cm to 17 ± 1% (15.5–18%) for 5–10 cm and 14 ± 2.5% (range 11.5–18%) for 10–21 cm. The Mn and Fe profiles (Fig. 2c and d) reflected the influence of classic natural, redox-related, diagenetic enrichment (e.g. Farmer and Lovell, 1986), with near-surface peaks of 2.77% at 1–2 cm and 6.35%, 1 cm below, at 2–3 cm, respectively. As with the wet weight/dry weight ratio profile, there was a dip at 5–7 cm in the Fe concentration, consistent with a coarser sediment grain size.

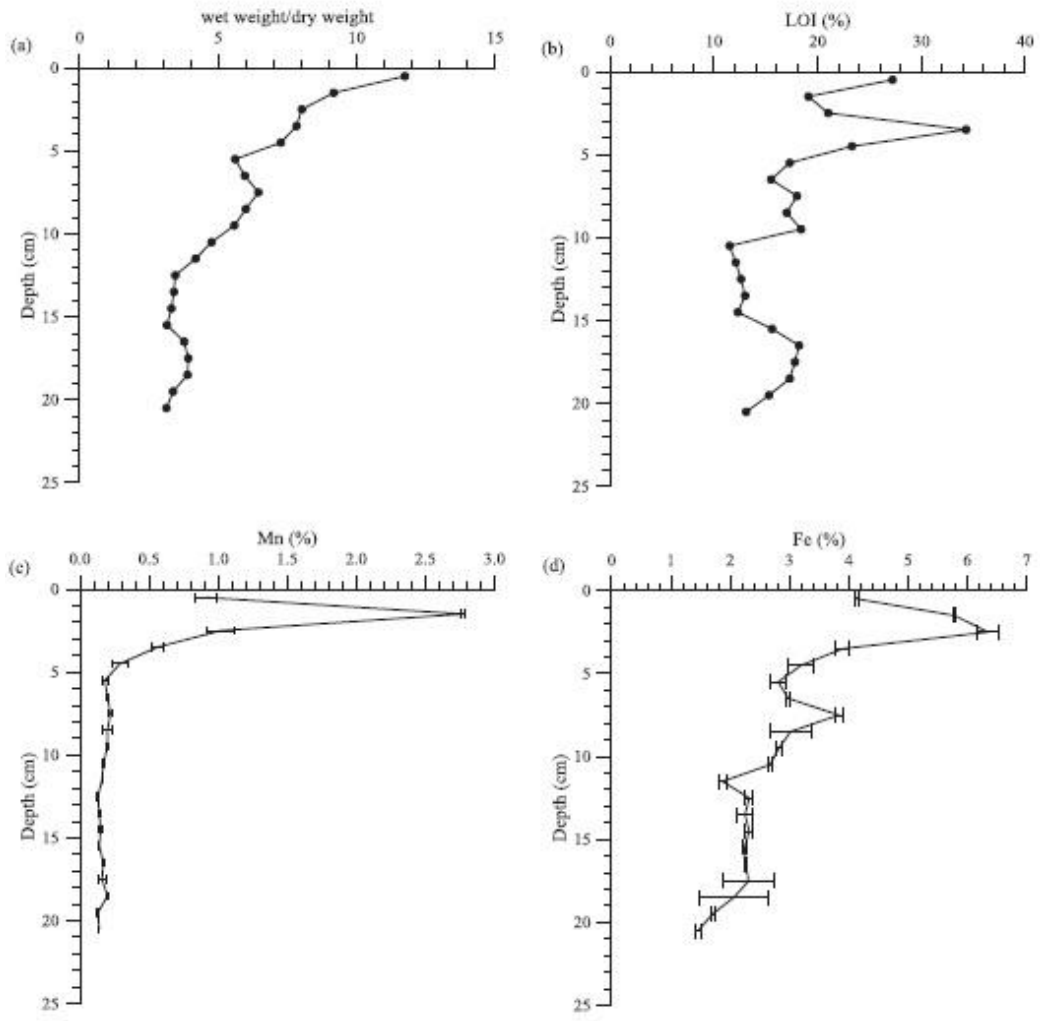

Fig. 2. Depth profiles of (a) wet weight/dry weight ratio (b) LOI, (c) Mn concentration and (d) Fe concentration for the Loch Einich sediment core.

3.1.2. Radionuclides

3.1.2.1. Decay series disequilibrium.

Natural decay series radionuclide specific activity and activity ratio profiles are shown in Fig. 3a–f. ^{238}U specific activities, ranging from 1327 to 2794 Bq kg^{-1} (Fig. 3a), are an order of magnitude higher than the regional average value of 157 Bq kg^{-1} for the Cairngorm intrusion (Brown et al., 1979), indicating localised enrichment of U. The profile exhibits an irregular form, with the lowest specific activities in the section from 10 to 15 cm. There is no systematic trend in the ^{238}U profile as a function of depth and the distribution bears no quantitative relationship to the concentration of organic matter, inferred from the LOI data (Fig. 2b), or to variations in redox conditions inferred from the Mn and Fe distributions (Fig. 2c and d). This suggests that the variations in specific activity of ^{238}U probably result from variable input of detrital minerals, which would be consistent with the steep gradients and lack of vegetation cover in the catchment. There is, however, apparent limited dilution of ^{238}U by Mn and Fe enrichment at 1–3 cm. ^{232}Th specific activities (Fig. 3b), in the range 134–398 Bq kg^{-1}, are slightly higher than the regional average of 108 Bq kg^{-1} (Brown et al., 1979). Values for samples from below 11 cm (range 312– 398 Bq kg^{-1}) are higher than those

above 11 cm (range 134–295 Bq kg^{-1}), which decrease irregularly towards the surface. This decrease can be partially attributed to higher concentrations of organic matter, Mn and Fe with decreasing depth in the core (Fig. 2b–d).

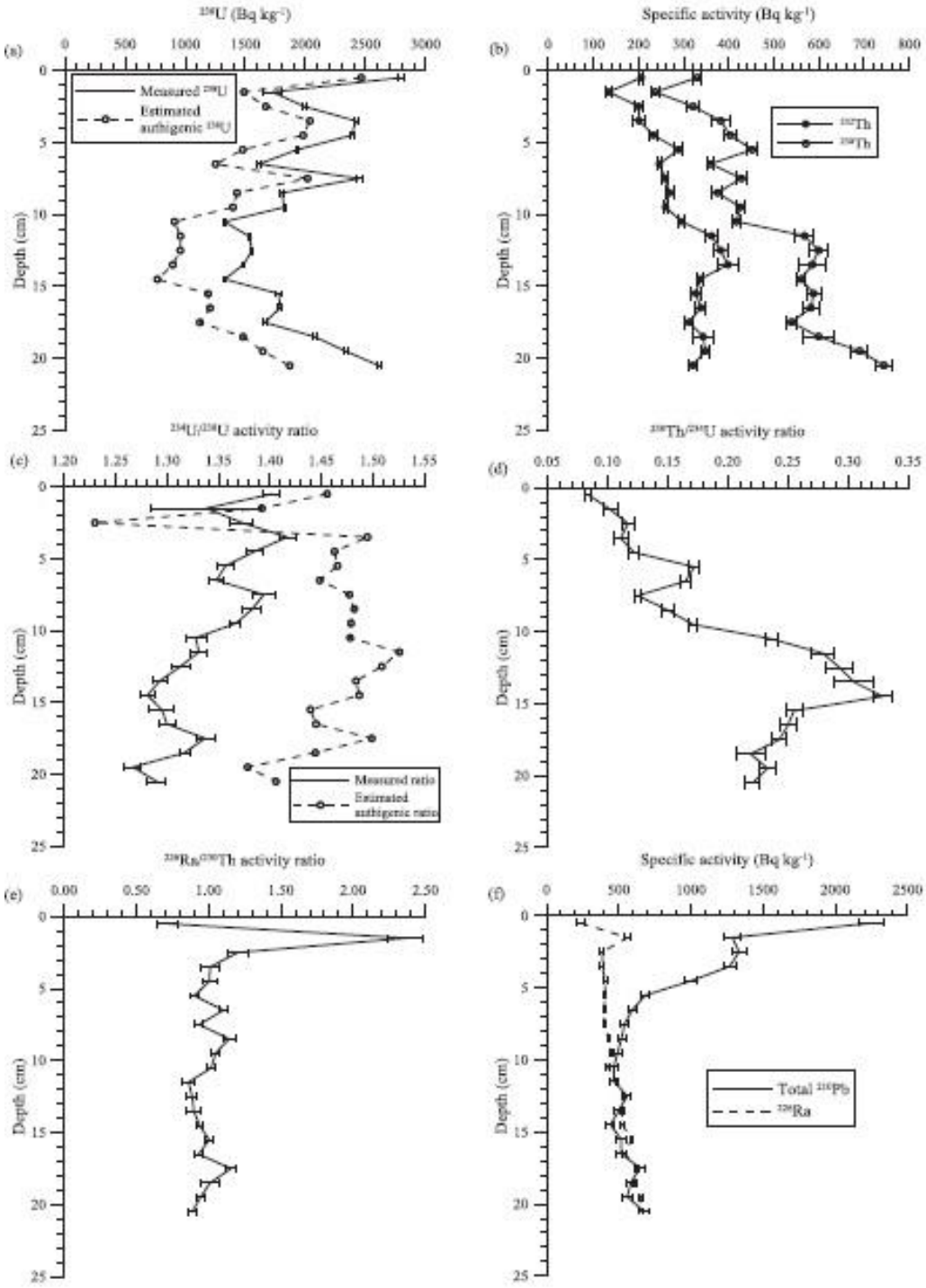

Fig. 3. Natural decay series radionuclide specific activity and activity ratio profiles for the Loch Einich sediment core: (a) ^{238}U, (b) ^{230}Th, ^{232}Th, (c) ^{234}U/^{238}U, (d) ^{230}Th/^{234}U, (e) ^{226}Ra/^{230}Th and (f) ^{226}Ra, total ^{210}Pb.

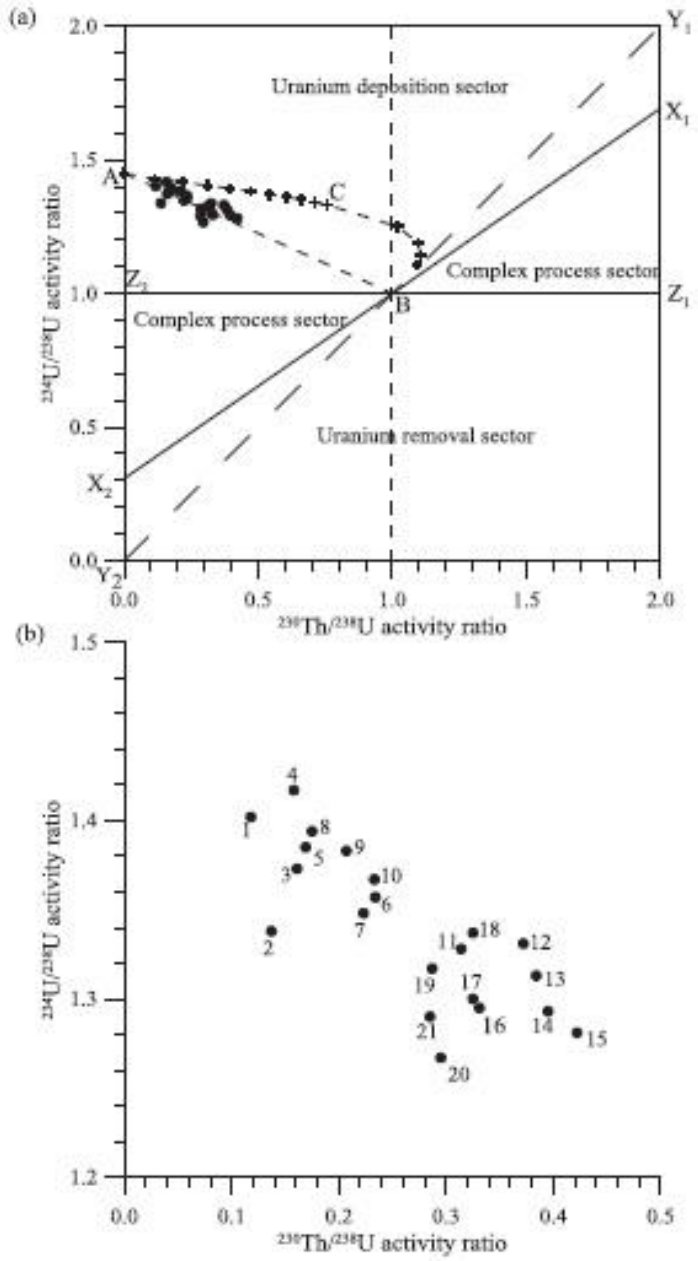

Fig. 4. Plot of 234U/^{238}U activity ratio versus ^{230}Th/^{238}U activity ratio (Scott et al., 1992) for the Loch Einich sediment core. Labels in (b) are sample numbers, representing increasing depth from 1 to 21 cm in 1-cm depth increments. Explanatory note: The underlying assumption is that the system initially starts at equilibrium (point B). Uranium is then either removed to solution in groundwater or deposited from solution in groundwater moving the system away from equilibrium. Uranium removed to, or deposited from, groundwater will have ^{234}U/^{238}U activity ratio greater than or equal to unity. Removal or deposition processes can be either continuous or sudden (i.e. occurring over a short time relative to the ^{234}U and ^{230}Th half-lives of 2.45 x 10^5 years and 7.54 x 10^4 years, respectively). The graph is divided into a number of sectors corresponding to different processes as indicated below by the bounding lines: Z_2-B-X_1: U deposition; Y_1-B-X_1: U deposition but cannot be attained by a continuous process; X_2-B-Z_1: U removal; Y_2-B-X_2: U removal but cannot be attained by a continuous

process; X_1-B-Z_1 and X_2-B-Z_2: complex process sectors that cannot be attained by any single process.

Mn and Fe with decreasing depth in the core (Fig. 2b–d). However, the magnitude of the decrease in ^{232}Th specific activity is greater than can be accounted for by these effects, again suggesting variable detrital mineral input from the catchment. ^{234}U/^{238}U activity ratios (Fig. 3c) are all greater than unity (range 1.27–1.42) indicative of authigenic re-deposition of U from groundwater, which typically has ^{234}U/^{238}U activity ratios of greater than unity as a result of preferential dissolution of ^{234}U from minerals as a consequence of radiation-influenced lattice damage and recoil effects (Thiel et al., 1983; Scott et al., 1992). Ratios for samples above 11 cm are generally higher than those in deeper sections, suggesting a higher concentration of authigenic U in the upper section of the core. ^{230}Th/^{234}U activity ratios (Fig. 3d) are all less than unity (range 0.084–0.33), again consistent with re-deposition of U. The ^{230}Th/^{234}U activity ratio increases from the base of the core to 14.5 cm, corresponding to a decreasing trend in ^{238}U specific activity. Above this depth, the ^{230}Th/^{234}U activity ratio decreases while ^{238}U specific activities increase. The results are therefore consistent with re-deposition of U, with higher ^{230}Th/^{234}U activity ratios corresponding to lower ^{238}U specific activities. Values for samples from below 11 cm (range 0.22–0.33) are higher than those above 11 cm (range 0.084–0.24), again suggesting higher concentrations of authigenic U closer to the surface. The trends in the ^{230}Th specific activity profile (Fig. 3b) are very similar to those of the ^{232}Th profile (linear correlation $r^2 = 0.76$), suggesting that both are contained in the same detrital minerals. With the exception of the top two samples, ^{226}Ra/^{230}Th activity ratios (Fig. 3e) are at or close to equilibrium, consistent with input of a detrital mineral phase in which the ^{238}U series is in secular equilibrium. There is clear enrichment of ^{226}Ra in the 1–2 cm sample (Fig. 3f), coincident with the peak in Mn concentration (Fig. 2c), implying diagenetic re-deposition of ^{226}Ra at this depth.

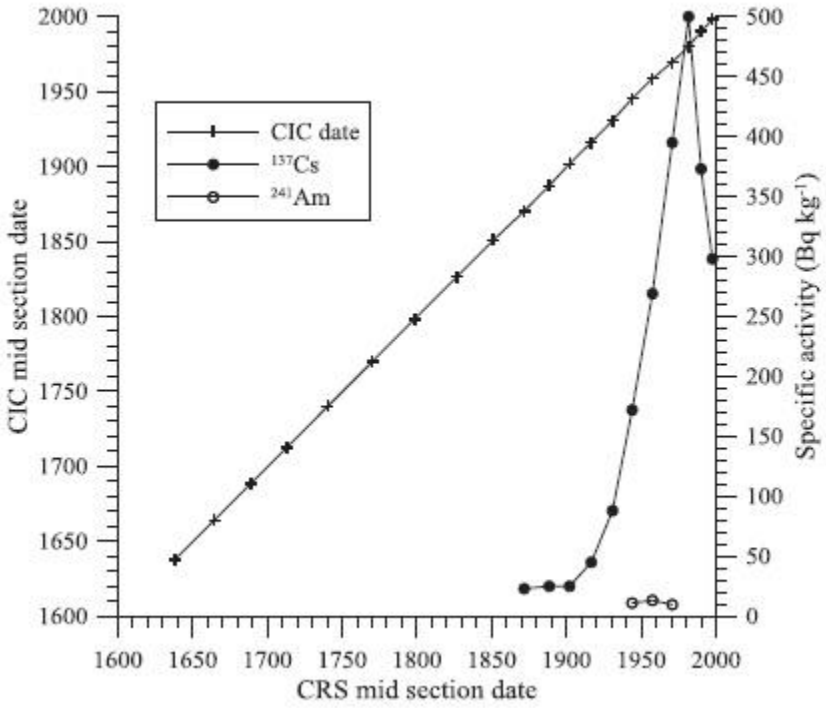

Fig. 5. Plot of ^{210}Pb CIC mid-section date and ^{137}Cs and ^{241}Am specific activities versus ^{210}Pb CRS mid-section date for the Loch Einich sediment core.

The results therefore indicate that U is present both in a detrital mineral phase, in which the ^{238}U series is in equilibrium, and in an authigenic phase and that the distribution of the mineral phase is probably best indicated by the ^{230}Th and ^{232}Th distributions. If the assumption is made that the ^{230}Th specific activity represents the secular equilibrium value for the ^{238}U decay series in the detrital mineral phase, then subtraction of the ^{230}Th specific activity from the measured values for ^{238}U and ^{234}U provides an estimate of the authigenic component of each isotope. As shown in Fig. 3a, the estimated authigenic phase is the dominant component and determines the overall trends in the total ^{238}U specific activity profile. $^{234}U/^{238}U$ activity ratios for the authigenic U (Fig. 3c) have a relatively small variation, with an average value of 1.45 ± 0.06. The one exception to this is the 2–3 cm sample which has an estimated ratio of 1.23. This is co-incident with the Fe peak and could indicate limited involvement of U in diagenetic recycling at this depth.

In the plot of $^{234}U/^{238}U$ activity ratio against $^{230}Th/^{238}U$ activity ratio (Thiel et al., 1983; Scott et al., 1992), all of the samples lie in the U deposition sector (Fig. 4a). With the assumption, as above, that the sediment contains detrital minerals with the ^{238}U series in equilibrium plus an additional authigenic component, the specific locations of individual samples in this plot will be determined by the relative contributions of the detrital and authigenic components. Consistent with this, the samples are distributed along a tie line between point A, representing the estimated authigenic component with $^{234}U/^{238}U = 1.45$ and $^{230}Th/^{234}U = 0$, and the detrital minerals with the ^{238}U series in secular equilibrium (point B).

Fig. 4b shows an expanded version of the plot with sample numbers added. The samples fall into two clear groups in the plot with samples 1–10 lying further from equilibrium than samples 11–21, consistent with the above conclusion that there is a higher concentration of authigenic U in the upper section of the core. An indication of the timescale for the deposition of the authigenic U is given by the curve A–C–B in Fig. 4a, which represents the return towards equilibrium of the authigenic component. The first 10 increments on the curve, in the section A–C, represent progressive 10,000-year periods while those in section C–B represent further incremental 100,000-year periods up to 500,000 years. The results therefore indicate that the re-deposition of the authigenic U probably occurred on a timescale substantially shorter than the ^{230}Th half-life (7.54×10^4 years) and would be consistent with rapid, post-glacial weathering. The absence of any relationship between the ^{238}U and $^{234}U/^{238}U$ profiles and either depth or core chemistry suggests that the variations in these parameters are the result of rock–water interactions in the catchment prior to in wash of detrital minerals to the loch.

3.1.2.2. Core chronology. Developing a ^{210}Pb chronology

for the core is complicated by the diagenetic enrichment of ^{226}Ra in the 1–2 cm section (Fig. 3f), since the excess ^{226}Ra will initially be deposited in the absence of descendant radionuclides in the decay series, but there will be post-depositional in growth of ^{210}Pb over the timespan represented by the section depth. The total supported ^{210}Pb in the section will therefore comprise a component in detrital minerals plus a component that has grown in from ^{226}Ra decay. To deal with this, it was assumed that the ^{230}Th specific activity of 237 Bq kg^{-1} represents the secular equilibrium value for the complete ^{238}U decay series, including supported ^{210}Pb, in the detrital minerals. The ^{230}Th specific activity was then subtracted from that of ^{226}Ra to give the excess ^{226}Ra specific activity. An approximate accumulation rate of 0.013 g cm^{-2} y^{-2} was derived using a Constant- Initial-Concentration (CIC) calculation (Appleby and Oldfield, 1978), assuming that measured ^{226}Ra specific activities represent supported ^{210}Pb, to give an estimated value of 9 years for the timespan for the 1–2 cm section. The assumption was made that the true timespan for the section was in the range 5–15 years and ingrowth of ^{210}Pb was calculated, on a summed annual incremental basis, for timespans in this range. The ingrown component was then added to the assumed equilibrium value for the detrital minerals to obtain the total supported specific activity. A series of

Constant-Rate-of-Supply (CRS) calculations (Appleby and Oldfield, 1978) was performed using each of the calculated total supported ^{210}Pb values to estimate the unsupported specific activity. In each case, the CRS calculation yielded a value of close to 7 years for the timespan covered by the 1–2 cm section, indicating that the ingrown component has only a minor effect on chronology calculations. Consequently, a 7-year ingrowth period for the 1–2 cm section was assumed for developing chronologies. This gave a total unsupported ^{210}Pb inventory of 10.37 kBq m^{-2}, corresponding to an average annual depositional flux of 322 Bq m^{-2} y^{-1}.

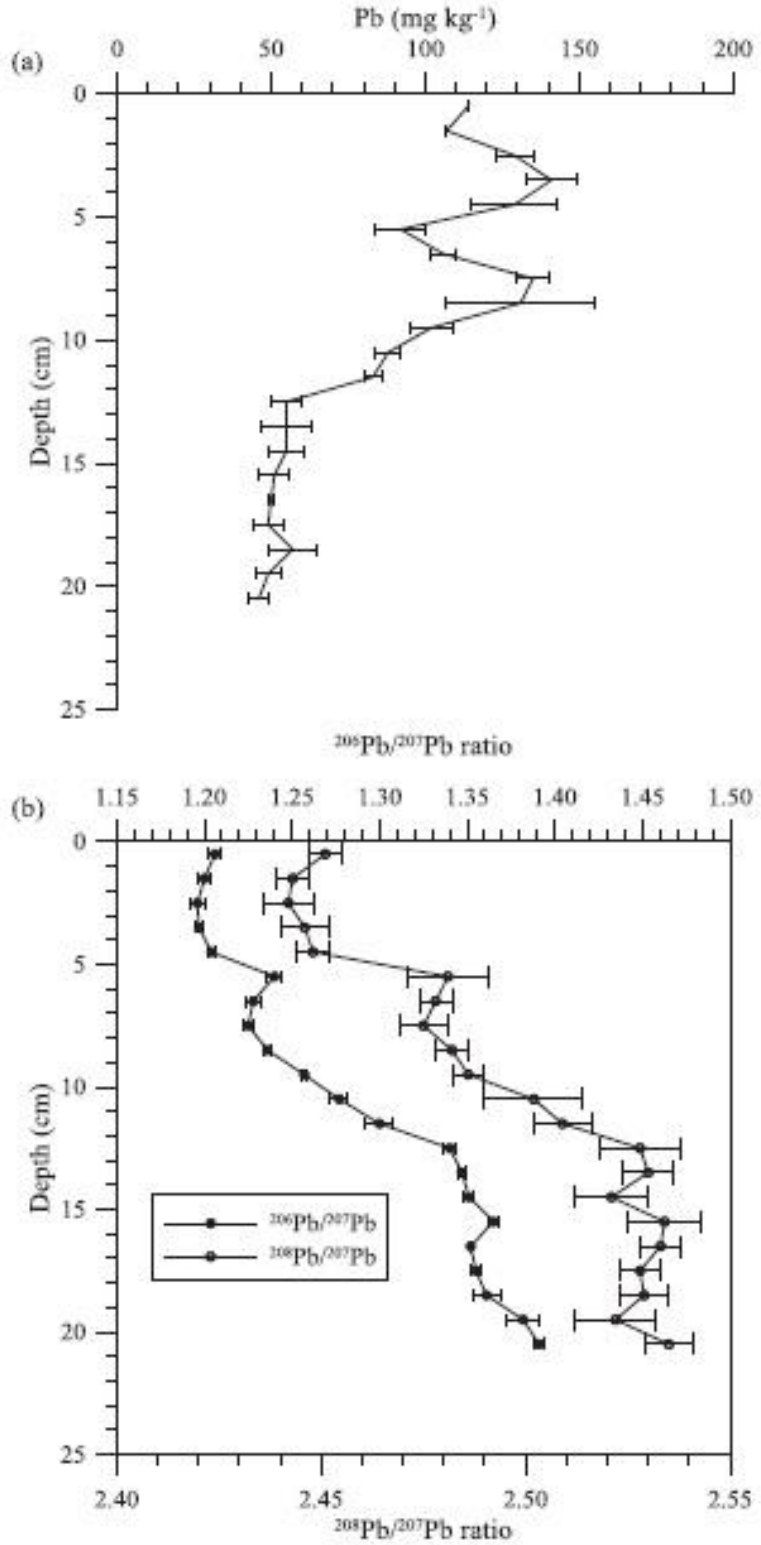

Fig. 6. Depth profiles of (a) Pb concentration and (b) $^{206}Pb/^{207}Pb$ ratio and $^{208}Pb/^{207}Pb$ ratio for the Loch Einich sediment core.

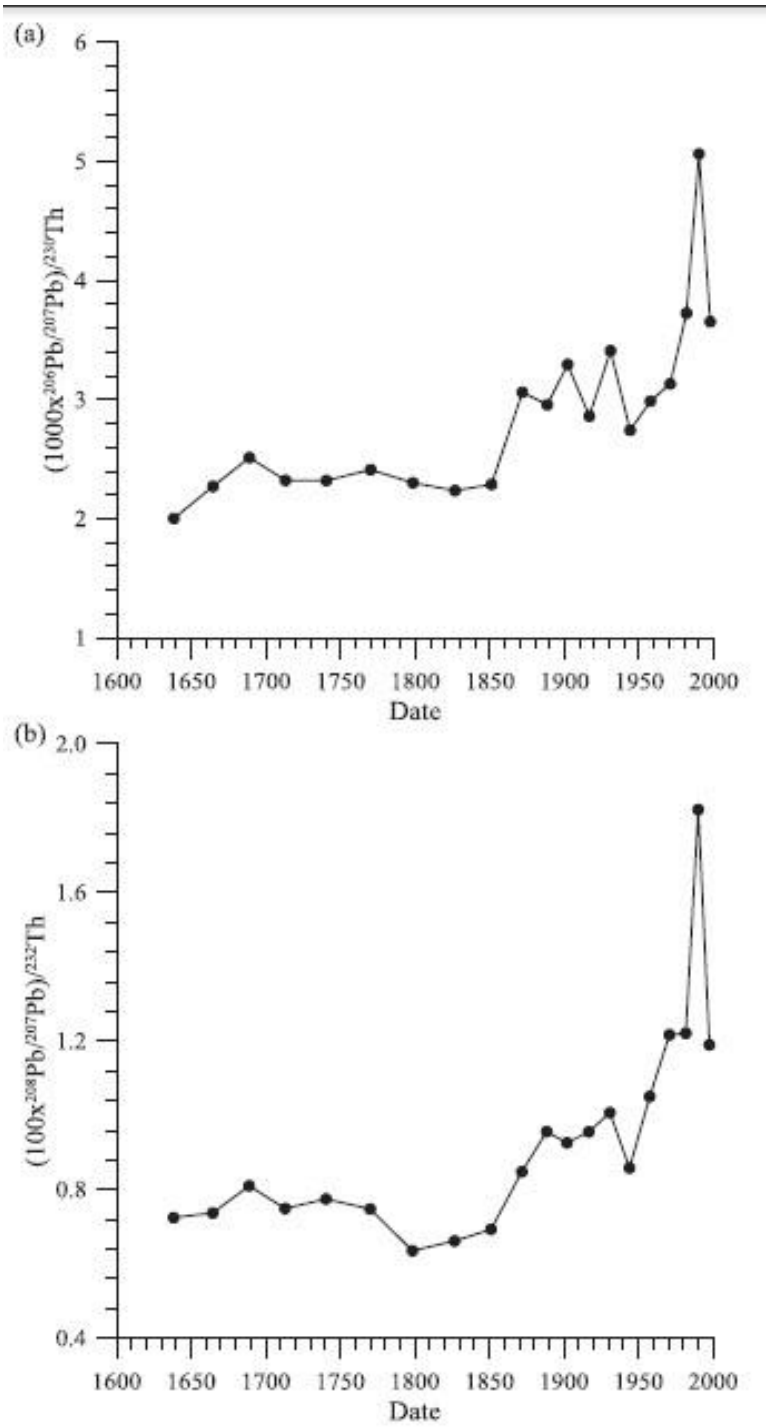

Fig. 7. Plots of (a) (1000 _ $^{206}Pb/^{207}Pb$ ratio)/^{230}Th specific activity and (b) (100_ $^{208}Pb/^{206}Pb$ ratio)/^{232}Th specific activity versus ^{210}Pb CRS mid-section dates for the Loch Einich sediment core.

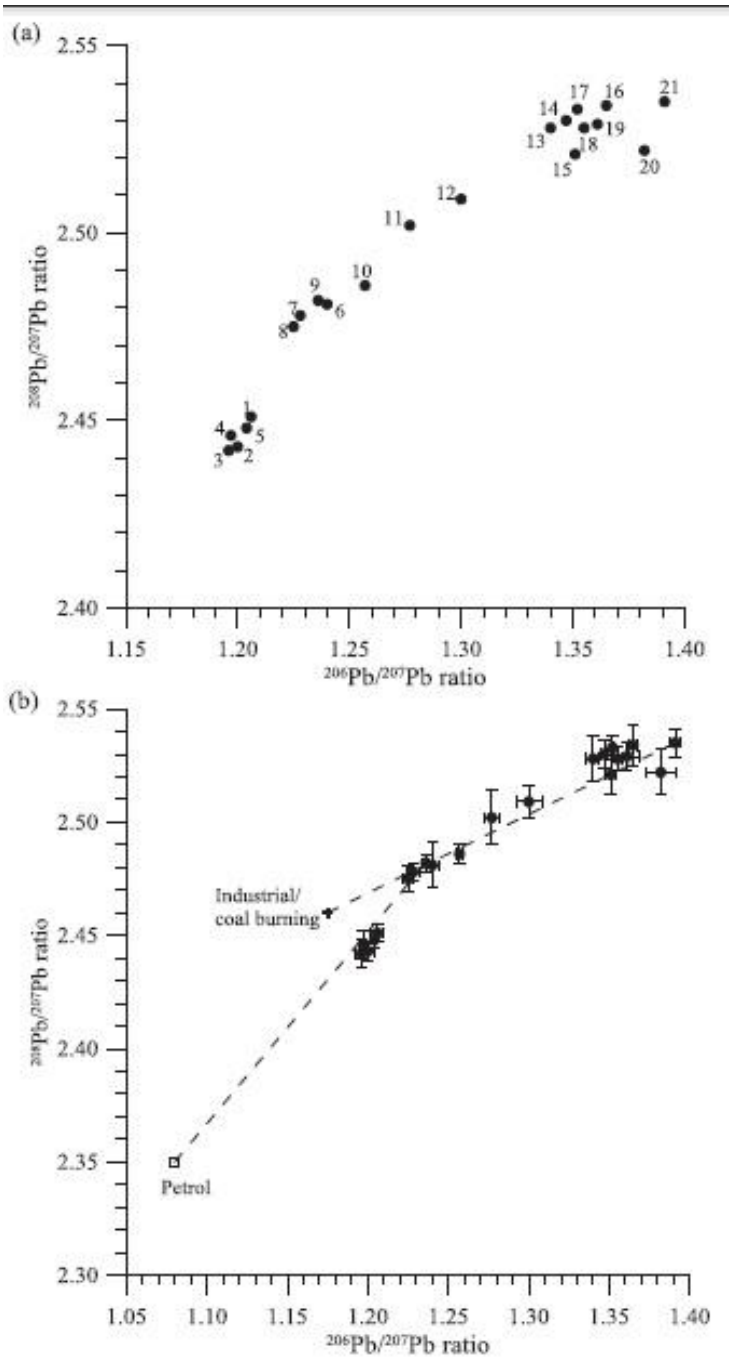

Fig. 8. Plots of $^{208}Pb/^{207}Pb$ ratio versus $^{206}Pb/^{207}Pb$ ratio for the Loch Einich sediment core (a) showing sample numbers and (b) with data points representing the stable Pb isotopic composition of combined industrial emissions and coal burning and of petrol Pb.

Following the recommendation of Appleby (2001), both CRS and CIC calculations were performed. The CRS calculation used summation of measured ^{210}Pb activities in individual sections to derive inventories and, with a limit of detection of ~3 Bq kg^{-1}, ages calculated in this way should not be biased by inaccuracies in estimation of inventories until greater than 100 years (MacKenzie et al., 2011). ^{210}Pb reached limit of detection at a depth corresponding to 1872 in the CRS chronology and 1871 in the CIC chronology, so estimation of ages

beyond these dates relied upon extrapolation. In the case of the CIC chronology, this was achieved simply by assuming that the average accumulation rate (0.0127 g cm^{-2} y^{-1}) applied to the entire core. For extrapolation of the CRS chronology, the equation for the best-fitting straight line for the linear relationship between cumulative weight and CRS age was derived and applied to the sections of the core below the depth corresponding to 1872. Clearly there is a risk that a change in accumulation rate could have affected deeper sections of the core, which would result in inaccuracies in extrapolated ages beyond 1872.

Fig. 5 shows a plot of the extrapolated CIC chronology against the extrapolated CRS chronology along with measured specific activities for ^{137}Cs and ^{241}Am. There was excellent agreement between the CRS and CIC chronologies, with linear regression r^2 values of 0.998 for the chronologies back to 1872 and 0.999 for the extrapolated chronologies. ^{241}Am was detected in three sections of the core with CRS mid-section ages of 1943 (section timespan 1937–1950), 1957 (timespan 1950–1965) and 1971 (timespan 1965–1976) and maximum activity in the section incorporating 1963. The ^{241}Am distribution thus provides strong independent support for the ^{210}Pb chronologies. In contrast, the ^{137}Cs profile does not show the two peaks that would be expected on the basis of maximum weapons testing fallout deposition in 1963 and Chernobyl fallout in 1986, but exhibits a single peak at a position corresponding to 1982 (timespan 1977– 1987) in the CRS chronology and 1980 in the CIC chronology (timespan 1975–1985). Moreover, ^{137}Cs was detected to depths corresponding to sediment deposited in the mid-19th century, suggesting significant post-depositional mobility by diffusion in this organic-rich (LOI values of up to 34.3%) sediment (Torgersen and Longmore, 1984; Klaminder et al., 2012).

Although the effect on ^{210}Pb-derived age of correcting for the diagenetic enrichment of ^{226}Ra results in an addition of only 1.4 years (by CRS) and of only 2.2 years (by CIC) by a depth of 11 cm and an addition of only ~6 years (by extrapolated CIC) by the bottom of the core, it is of greater significance for the uppermost two sections of the core (by CRS). With correction, 0–1 and 1–2 cm correspond to sectional timespans of 7.04 and 7.99 years, respectively, compared with uncorrected values of 8.41 and 5.19 years, an overall increase of 1.4 years. [Note: this redistribution of the enhanced number of years between these two sections has the important subsequent effect of increasing the ratio of the calculated Pb fluxes (CRS) for the sections (i.e. 0–1 cm: 1–2 cm) by a factor of 1.43 (cf. 3.3.1)].

3.1.3. Pb and Pb isotopes

Lead concentrations (Fig. 6a) range from 46 to 141 mg kg^{-1} with higher values in the upper half of the core, where there is a distinct bimodal distribution with peaks at 3–4 cm and 7–8 cm. Despite the remote location of Loch Einich, the maximum concentrations are similar to those of ~150 mg kg^{-1} observed in sediments from the southern basin of Loch Lomond, which is close to the central Scotland industrial belt (Farmer et al., 1996). Below 12 cm, however, Pb concentrations show only small variations in the range 46–57 mg kg^{-1}, ~3–4 times those found at depth in Loch Lomond sediment.

^{206}Pb/^{207}Pb and ^{208}Pb/^{207}Pb ratios respectively lie in the ranges 1.196–1.391 and 2.442–2.535 (Fig. 6b), corresponding to a higher radiogenic Pb content than observed, for example, in Loch Lomond sediments (e.g. Farmer et al., 1996, 1997b; Eades et al., 2002). Both the ^{206}Pb/^{207}Pb ratio and the ^{208}Pb/^{207}Pb ratio show relatively small variations below 12 cm, with a slightly increasing trend with increasing depth (Fig. 6b). There is a more pronounced decrease in both ratios with decreasing depth above 12 cm, with a small reversal of the trend at 5–6 cm. The trends in the ratio profiles are therefore very similar to each other and to those in the ^{232}Th and ^{230}Th profiles (Fig. 3b), suggesting that both Th isotopes and the radiogenic Pb are contained in the same minerals and implying geologically long-term closed conditions for the minerals. On this basis, the mineral phase would be characterised by constant values for the ratio of the ^{206}Pb/^{207}Pb atom ratio to the ^{230}Th specific activity and of the ^{208}Pb/^{207}Pb atom ratio to ^{232}Th specific activity and deviations from these values would indicate input of Pb from an external source. Fig. 7a and b shows these ratios plotted against

CRS mid-section dates. For ease of visual presentation, the (^{206}Pb/^{207}Pb)/^{230}Th ratio has been multiplied by 1000 and the (^{208}Pb/^{207}Pb)/^{232}Th ratio by 100. Assuming the deepest sample represents the indigenous mineral component, both graphs suggest a relatively small, fairly constant input of Pb from an external source with a relatively constant Pb isotopic composition up to ca. 1850, but a much larger and more variable input thereafter. Assuming an emplacement age of U of ~400 Ma (Plant et al., 1990; Thomas et al., 2004) and a closed system, ingrown radiogenic Pb would have a ^{206}Pb/^{207}Pb ratio of about 18.2. If the indigenous Pb in Loch Einich is a binary mix of radiogenic Pb with this ratio and primordial Pb with a ^{206}Pb/^{207}Pb ratio of 0.914 (Patterson, 1956), then the radiogenic component constitutes about 2.7% of the indigenous Pb in the deepest sample.

The plot of ^{208}Pb/^{207}Pb ratio against ^{206}Pb/^{207}Pb ratio (Fig. 8a) shows a general trend towards more radiogenic character of the Pb with increasing depth, with samples 13–21, corresponding to CRS mid-section dates of 1616–1826, forming a cluster in the most radiogenic position. There is no trend as a function of depth within the cluster, but the deepest sample, 21, has the most radiogenic composition. Samples 6–13 (CRS dates 1826–1943) lie on a linear trend with samples 8–13 (dates 1826–1916) in sequence according to depth, but with samples 6 and 7 slightly out of sequence. Samples 1–5 (dates 1957–1997) are located in the least radiogenic area of the graph, with sample 3 (1982) having the lowest radiogenic content. Fig. 8b shows the ^{208}Pb/^{207}Pb versus ^{206}Pb/^{207}Pb plot with the addition of data points representing the isotopic composition of atmospheric deposition in Scotland from combined industrial emissions and coal burning and of petrol Pb (Farmer et al., 1999, 2000, 2002). Samples 9–21 (dates 1616–1902) lie approximately along a tie line between the industrial/ coal data point and sample 21, while samples 1- 8 (dates 1916–1997) lie on the tie line between the petrol Pb data point and sample 9 (date 1902). The data can therefore be treated as representing binary mixing of indigenous Pb, represented by sample 21, with industrial/coal Pb until the end of the 19th century, followed by three-component (indigenous – industrial/coal - imported Australian Pb) mixing from the start of the 20th century. Source apportionment up to the end of the 19th century is therefore straightforward using ^{206}Pb/^{207}Pb values of 1.391, the ratio for sample 21, and 1.175, the average for industrial/coal burning. The three-component system in the 20th century is more complex and in order to distinguish between indigenous mineral and combined external inputs, the ^{206}Pb/^{207}Pb data for archived moss samples (Farmer et al., 2002) (cf. Fig. 16) were used to represent those of atmospherically deposited Pb during this period. Values for the ^{206}Pb/^{207}Pb ratio were calculated as the average of the moss values over timespans corresponding to CRS age spans for each depth increment of the core. Resultant average fluxes for total Pb, indigenous Pb and external (anthropogenic) Pb deposition are shown in Fig. 9 (see Section 3.3.1 for discussion).

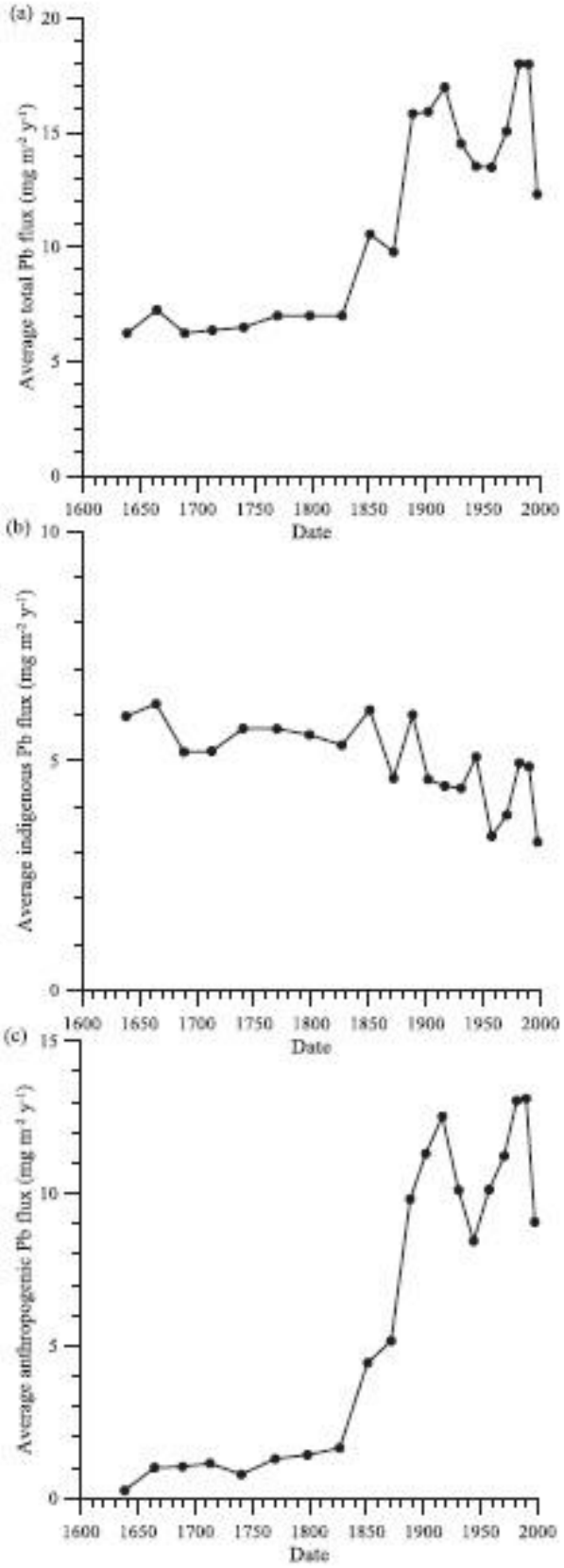

Fig.9. Estimated average annual fluxes for (a) total Pb, (b) indigenous Pb and (c) anthropogenic Pb for the ^{210}Pb-dated (CRS) Loch Einich sediment core.

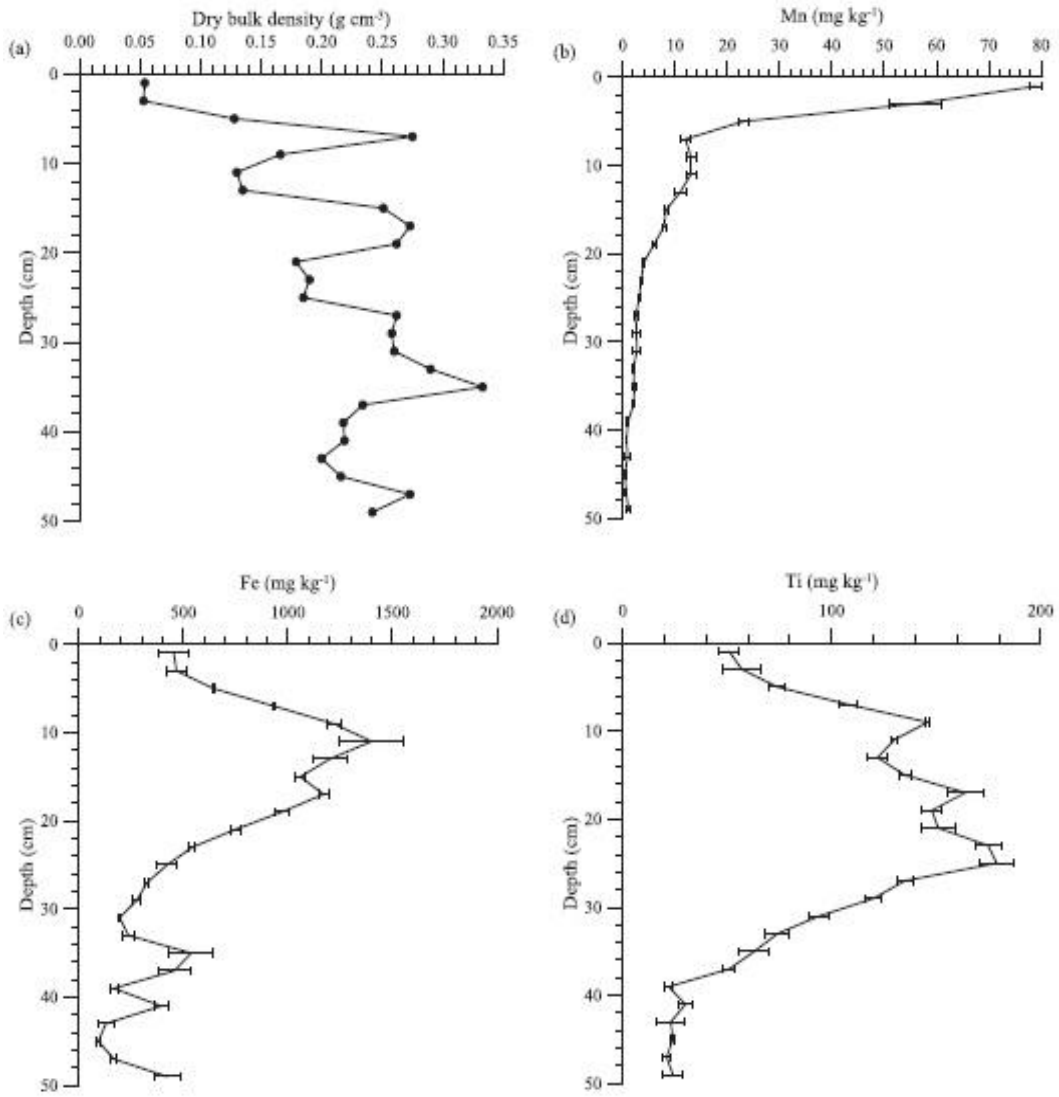

Fig.10. Depth profiles of (a) Dry bulk density and (b) Mn, (c) Fe and (d) Ti concentration for the Great Moss peat core

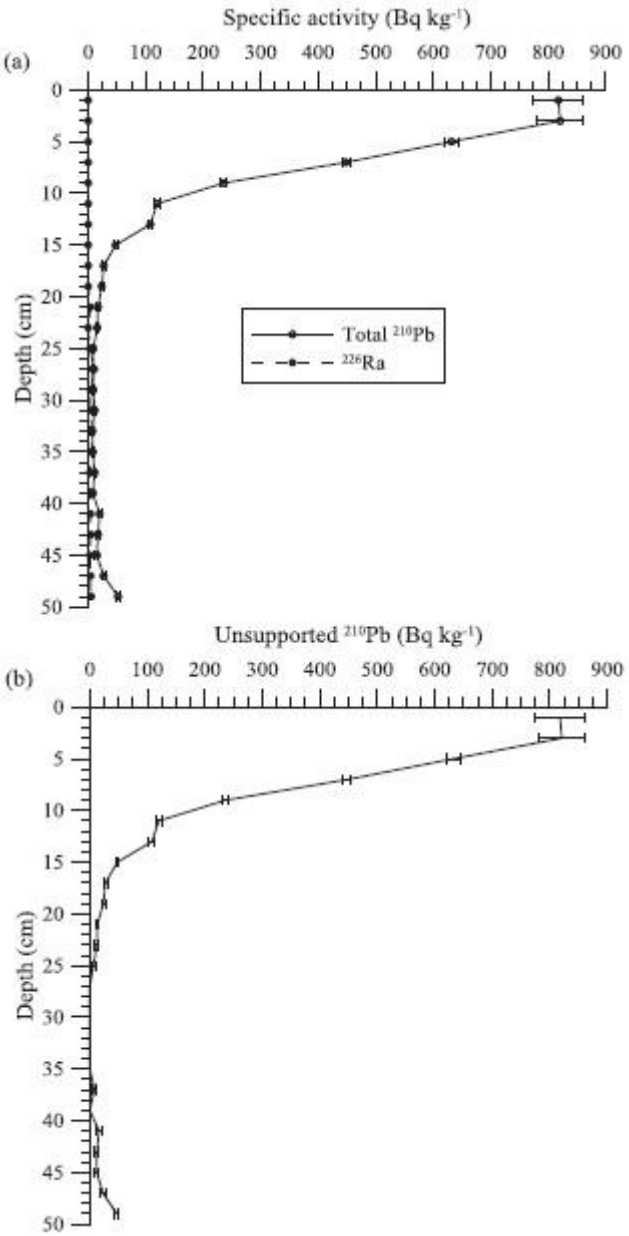

Fig.11. Depth profiles of (a) total ^{210}Pb and ^{226}Ra specific activity and (b) unsupported ^{210}Pb specific activity for the Great Moss peat core.

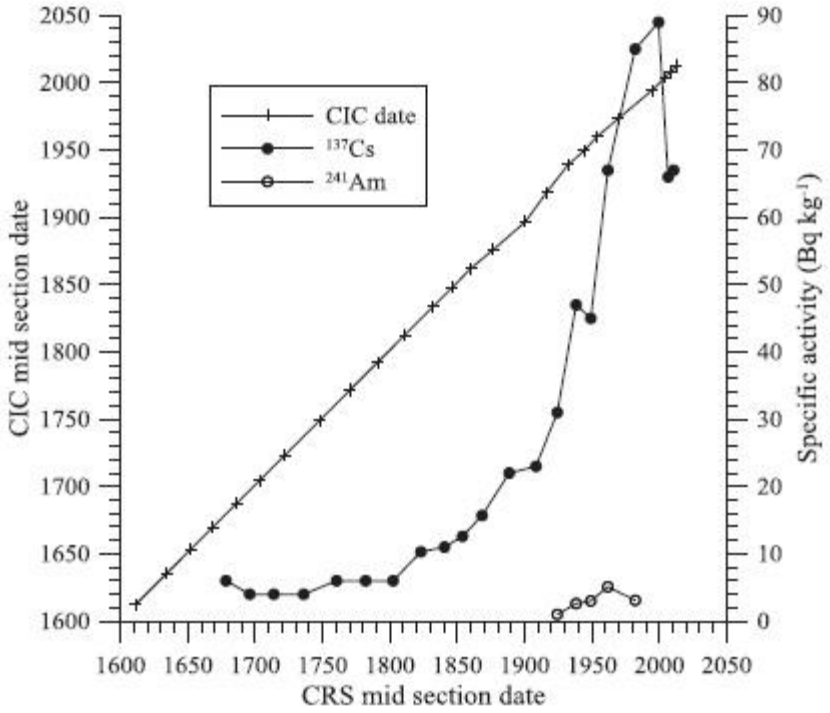

Fig. 12. Plot of CIC mid-section date and ^{137}Cs and ^{241}Am specific activities versus CRS mid-section date for the ^{210}Pb-dated Great Moss peat core.

3.2. Great Moss

3.2.1. Peat core geochemistry

Dry bulk density, Mn, Fe and Ti profiles are shown in Fig. 10. The dry bulk density (Fig. 10a) increased somewhat irregularly with increasing depth, broadly in line with ash content, and the mean value of 0.21 ± 0.07 g cm^{-3} suggests a highly compacted peat. Both this mean dry bulk density value, much higher than for ombrotrophic peat, and the mean dry ash value of 2.1 ± 0.8% for the core are comparable with those reported for shallow blanket peat elsewhere in the uplands of the British Isles (Cannell et al., 1993; Holden et al., 2001; Lindsay, 2010). Variations in the dry bulk density of peat with depth are usually related to variations in the degree of compaction of the peat itself related to variations in the degree of decomposition of the peat and to variations in the water content of the core. From 8 to 50 cm, i.e. below the surface region of living and decaying vegetation in the Great Moss core, the water content varied from 67.6% to 77.9%, with mean values of 72.5% for 8–22 cm, 69.3% for 22–36 cm and 74.9% for 36–50 cm. Variations in wetness of the Great Moss peat with depth have been reported by Barber et al. (2000) as indicators of climate change. The near-surface concentration profile of Mn (Fig. 10b), rising to a peak of 79 mg kg^{-1} in the top section (0–2 cm), is characteristic of plant recycling of nutrients (Cloy et al., 2009), although redox-related diagenesis could also be a factor. The latter may also have affected the profile of Fe (Fig. 10c), which peaked at 1400 mg kg^{-1} (10–12 cm), although industrial emissions and atmospheric deposition of Fe-containing particles will have been a major source. The concentration profile of Ti (Fig. 10d), which rose steadily from 21–30 mg kg^{-1} (38–50 cm) to a maximum of 179 mg kg^{-1} at 25 cm and a broad peak (122– 164 mg kg^{-1}) extending to 8 cm before a rapid fall to 51 mg kg^{-1} at the surface, reflects the influence of soil dust input, arising primarily from the clearance of land for agricultural purposes (Cloy et al., 2008).

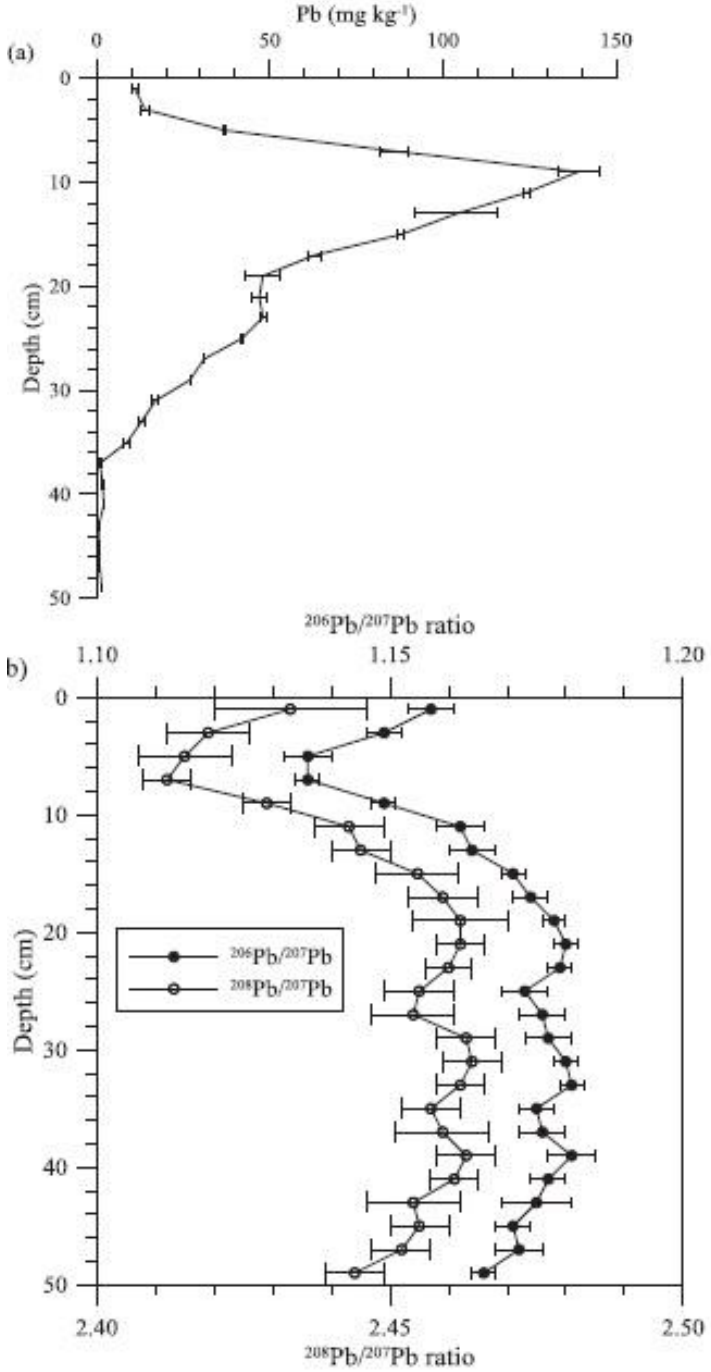

Fig.13. Depth profiles of (a) Pb concentration and (b) $^{206}Pb/^{207}Pb$ ratio and $^{208}Pb/^{207}Pb$ ratio profiles for the Great Moss peat core.

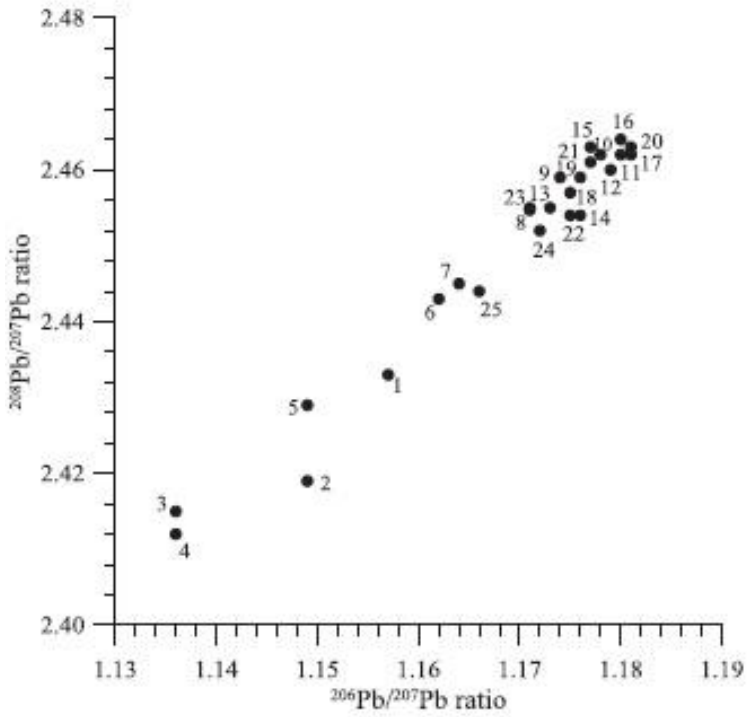

Fig.14. Plot of $^{208}Pb/^{207}Pb$ ratio versus $^{206}Pb/^{207}Pb$ ratio for the Great Moss peat core. Labels are sample section numbers, representing increasing depth from 0 to 50 cm in 2-cm depth increments.

3.2.2. Radionuclides

Total ^{210}Pb specific activity (Fig. 11a) decreased from a maximum of 818 Bq kg^{-1} at the surface to a minimum of 7 Bq kg^{-1} at 32–34 cm, below which values increased again to reach 52 Bq kg^{-1} at 48–50 cm. ^{226}Ra was below the limit of detection from the surface to 20 cm, below which it was present at specific activities varying irregularly in the range 3.0 10.5 Bq kg_1. Unsupported ^{210}Pb specific activity (Fig. 11b) decreased from 818 Bq kg^{-1} at the surface to reach the limit of detection at 24–26 cm and remained below the detection limit until 36–38 cm. In deeper sections of the core, unsupported ^{210}Pb increased irregularly from 8 Bq kg^{-1} at 36–38 cm to 47 Bq kg^{-1} at 48–50 cm. Similar to the glacial sand and silt noted by McVean (1962), the peat was underlain by a thin layer of coarse mineral matter, with total ^{210}Pb and ^{226}Ra specific activities of 47 ± 3 and 50 ± 3 Bq kg^{-1}, respectively.

The distribution of unsupported ^{210}Pb indicates separate inputs from (i) atmospheric deposition at the surface and (ii) a basal input, almost certainly due to production in deeper sections of the core from in situ decay of bedrock derived ^{222}Rn (half-life = 3.825 days) (Card and Bell, 1985). The inventory of unsupported ^{210}Pb below 36 cm was 678 Bq m^{-2} y^{-1}, corresponding to an average input of 21 Bq m^{-2} y^{-1}. The irregular distribution was not amenable to quantitative interpretation in terms of advection and/or diffusion, but the fact that unsupported ^{210}Pb was below detection limit from 26 to 36 cm indicates that there is insignificant migration of bedrock-derived ^{222}Rn above 36 cm. It was therefore concluded that the upper section of the core was unaffected by the basal input and was therefore suitable for conventional ^{210}Pb dating and both CRS and CIC chronologies were derived.

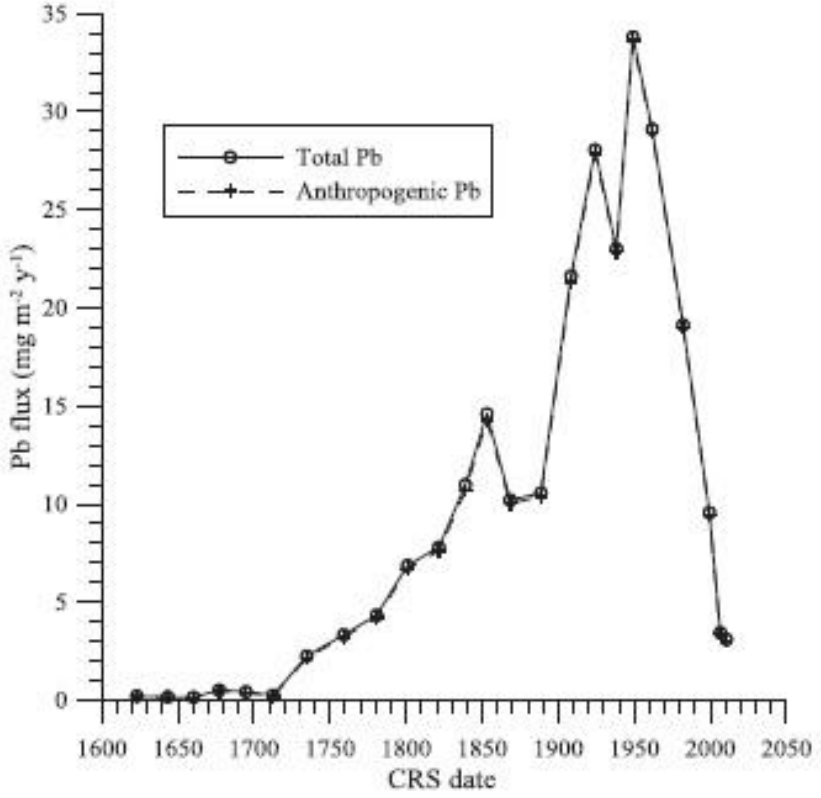

Fig. 15. Plot of average annual depositional fluxes of total and anthropogenic Pb versus CRS date for the ^{210}Pb-dated Great Moss peat core.

The CRS chronology was calculated using summation of measured sectional ^{210}Pb activities to derive inventories, giving directly calculated ages to 1823 and extrapolated ages, as described above for Loch Einich, for older sections. There was good agreement between the two chronologies as shown in Fig. 12, with linear regression r2 values of 0.994 and 0.999 for calculated chronologies to 1823 and for the extrapolated chronologies, respectively. The total inventory of unsupported ^{210}Pb was 8.80 kBq m^{-2}, corresponding to an average annual depositional flux of 273 Bq m^{-2} y^{-1}. ^{241}Am was detected in five sections of the core (Fig. 12), with maximum activity in the section spanning the period 1953–1969, consistent with maximum weapons testing fallout in 1963 and providing support for the ^{210}Pb chronology. ^{241}Am was also detected in the sections corresponding to 1916–1932 and 1969–1994. The latter could represent the effects of Chinese nuclear weapons tests in the 1970s (UNSCEAR, 1993; MacKenzie, 2000), but the former is indicative of a limited degree of post-depositional spreading of ^{241}Am (e.g. Hansson et al., 2014). The ^{137}Cs distribution, with peak activity over two sections spanning 1969–2004 with corresponding mid-section dates of 1982– 1999 and extending to a depth corresponding to the early 18th century, did not reflect the historical deposition pattern, confirming a high degree of post-depositional mobility by diffusion.

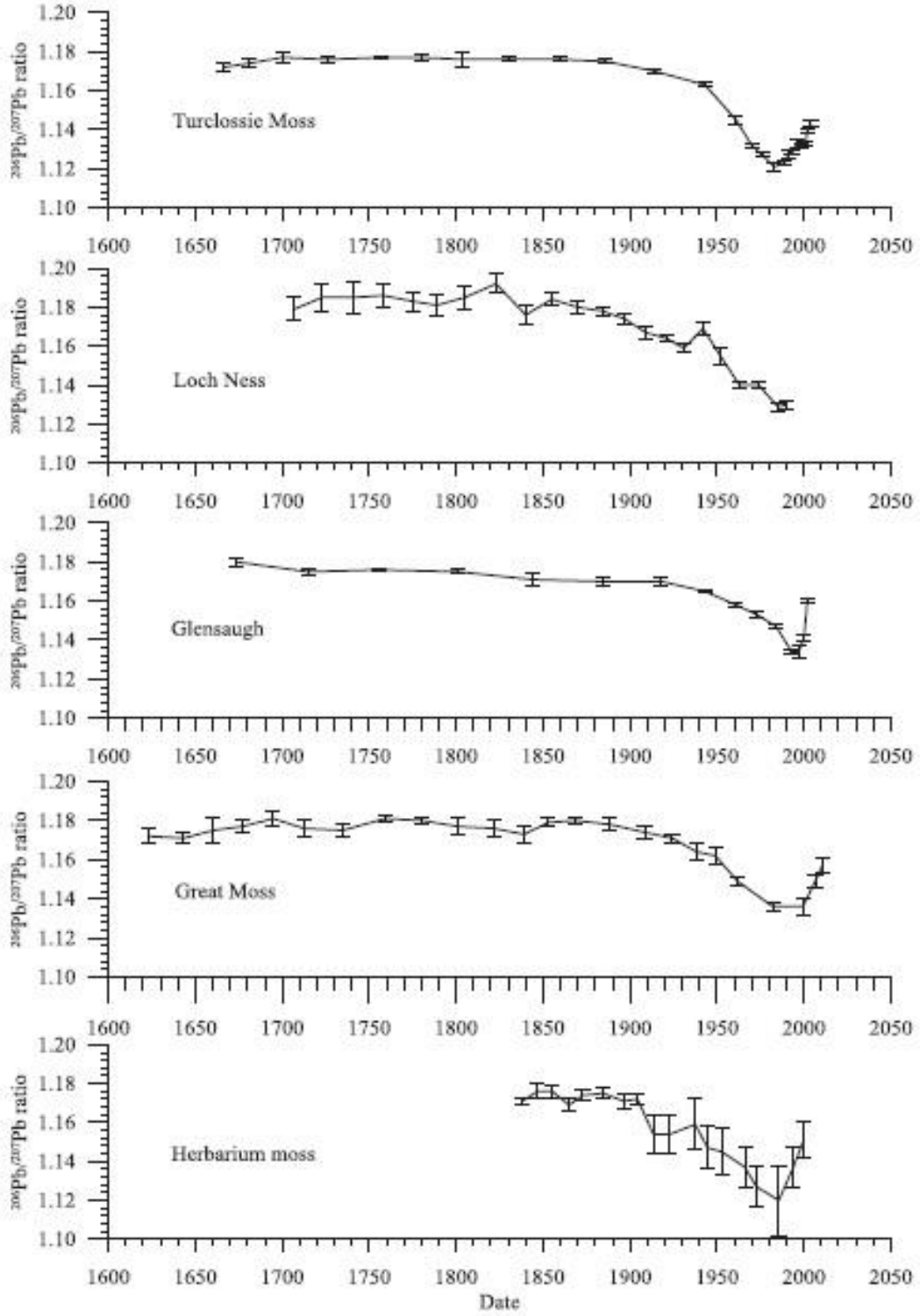

Fig. 16. Comparison of $^{206}Pb/^{207}Pb$ ratio versus date for Scottish herbarium moss (Farmer et al., 2002), Great Moss peat, Glensaugh peat (Farmer et al., 2005), Loch Ness sediment (anthropogenic Pb) (Eades et al., 2002) and Turclossie Moss peat (Cloy et al., 2008).

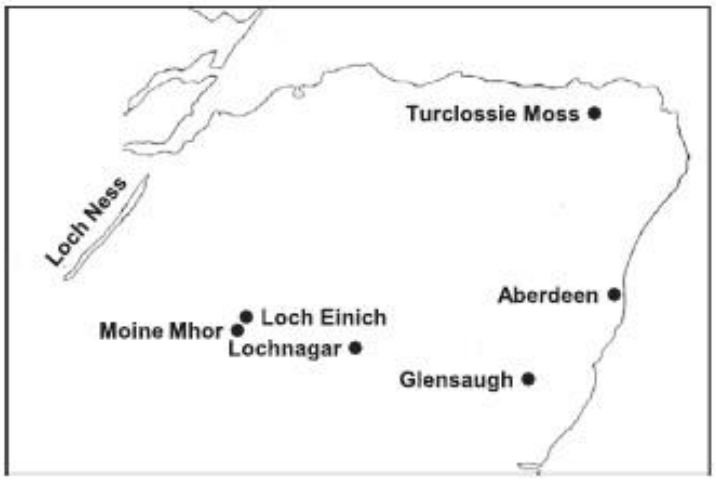

Fig. 17. Map showing the locations of Loch Einich and Great Moss (Moine Mhor) relative to Glensaugh, Loch Ness and Turclossie Moss (cf. Figs. 16 and 18) and Lochnagar (cf. Fig. 19)

3.2.3. Pb and Pb isotopes

Pb concentrations increased rapidly from 11 mg kg^{-1} at the surface to a maximum of 139 mg kg^{-1} at 8–10 cm, below which they gradually decreased with increasing depth, to reach values of around 1 mg kg^{-1} in the sections below 36 cm (Fig. 13a). The peak value of 139 mg kg^{-1} is at the lower end of the range previously reported for Scottish peats, with most peak values lying in the range 200– 1000 mg kg^{-1} (MacKenzie et al., 1997, 1998; Farmer et al., 2005; Cloy et al., 2008). The $^{206}Pb/^{207}Pb$ profile (Fig. 13b) and the plot of $^{208}Pb/^{207}Pb$ ratio against $^{206}Pb/^{207}Pb$ ratio (Fig. 14) both conform with the well established pattern for Scottish peat (MacKenzie et al., 1997, 1998; Farmer et al., 2005; Cloy et al., 2008) reflecting variations in input of contaminant Pb from industrial/coal burning and petrol Pb sources.

The CRS chronology and Pb concentrations were used to calculate average annual total deposition fluxes for Pb as shown in Fig. 15. A small correction was made for the natural Pb content of the peat, estimated on the basis of the Pb/Ti ratio (cf. Cloy et al., 2008), to derive anthropogenic Pb fluxes, which were almost indistinguishable from the total Pb fluxes (Fig. 15). Fig. 16 demonstrates the excellent agreement in temporal trends of the $^{206}Pb/^{207}Pb$ ratio between Great Moss peat, Scottish herbarium moss (1838–2000) and archives at other locations (Glensaugh peat, Loch Ness sediment and Turclossie Moss peat) in the north-east of Scotland (Fig. 17) since the mid-17th century, with respect to (i) the late 19th/early 20th century onset of decline from values of typically 1.17–1.18, (ii) the dates (1982–1993) of minimum values (1.120–1.136) and (iii) the subsequent increase (to 1.143–1.160) by the early 2000s after measures in the mid-1980s to reduce and, in 2000, ban the use of Pb in petrol.

Similarly, for deposition fluxes of anthropogenic Pb (Fig. 18), there is excellent agreement between Great Moss peat, Glensaugh peat, Loch Ness sediment and Turclossie Moss peat with respect to (i) the major trends of increase since the onset of the Industrial Revolution, (ii) the dates (1949–1961) of mid-20th century maxima and (iii) the subsequent steep decline (for the three peat locations) to only 6–9% of the maxima and comparable to pre-1750 values by the first decade of the 21st century.

3.3. Comparison of Loch Einich and Great Moss

3.3.1. Temporal trends in average annual total and contaminant Pb fluxes

Fig. 19 compares temporal trends in total Pb flux for Great Moss peat and Loch Einich sediment (both CIC and CRS-based chronologies) with those derived from dated sediment cores from three lochs at the western end of the Cairngorm Mountains (Fig. 1c), Loch Coire an Lochain, Loch Mhic Ghille-chaoile and Loch nan Cnapan (Rose et al., 2012), and also Lochnagar (Fig. 17), which lies on Lochnagar granite (Fig. 1b) to the south-east (Yang et al., 2002).

After the increase in total Pb fluxes from the mid-19th century to ca. 1910–1920 for all, the decline in Pb fluxes from 1924 to 1938 for Great Moss peat is also evident over a similar time period in sediment cores from Loch Einich and, most notably, Loch Coire an Lochain, with smaller but still discernible decreases for Loch nan Cnapan and Loch Mhic Ghille-chaoile. Such a dip has also been reported for a sediment core (LL-10L) from the northern basin of Loch Lomond (Farmer, 1994) and attributed to reduced industrial activity during the economic slump of the interwar period.

While the steep decline in total Pb fluxes from the subsequent maximum in mid-20th century to the beginning of the 21st century for Great Moss peat is mirrored in the Pb flux trend for Loch Coire an Lochain, there is no such decline observed for Loch Einich. Instead the Pb flux trend stays relatively constant in the second half of the 20th century, similar to those of Loch Mhic Ghille-chaoile and Lochnagar sediment and quite unlike either the steep declines in Great Moss peat and Loch Coire an Lochain sediment or the steep increase in Loch nan Cnapan sediment. Rose et al. (2012) have rationalised the differences in these recent total Pb flux trends between Loch Coire an Lochain, Loch Mhic Ghille-chaoile and Loch nan Cnapan in terms of the differing nature of the loch catchments and the role that catchment soil erosion plays in the transfer of metals to the lochs. For Loch Coire an Lochain, thin catchment soils (with limited catchment input) are considered to give rise to temporal trends in Pb deposition to lake sediments similar to those of atmospheric emissions and deposition. This is supported here by the agreement observed between total Pb flux trends in Loch Coire an Lochain sediment and Great Moss peat in our work, with Great Moss peat directly recording the decline in atmospheric Pb emissions and deposition. In contrast, for Loch nan Cnapan, the significantly eroded catchment soils (with continuing Great Moss catchment input) are held to be responsible for the maintenance of increasing trends in Pb fluxes through the most recent decades. Rose et al. (2012) consider Loch Mhic Ghille-chaoile to be intermediate, the comparatively non-eroded soils of its catchment (Glen Einich) yielding a pattern with some similarity to atmospheric Pb deposition patterns, but with a reduced recent decline when compared with Loch Coire an Lochain and Great Moss peat. Yang et al. (2002) have interpreted the continuing deposition of Pb to Lochnagar sediments at rates comparable to those of the mid-20th century, despite the considerable decline in Pb emissions to the atmosphere (e.g. from 9.9 kt in 1973 to 3.8 kt in 1986, 0.14 kt in 2001 and 0.061 kt in 2012, according to the UK National Atmospheric Emissions Inventory (2014)), as indicative of continuing and proportionately greater input of Pb from the catchment relative to the atmosphere, amounting to ~90% of the Pb input to the lake by the end of the 20th century. On the basis of the total Pb flux trends in Fig. 19, Loch Einich resembles Loch Mhic Ghille-chaoile and Lochnagar rather than Loch Coire an Lochain or Loch nan Cnapan.

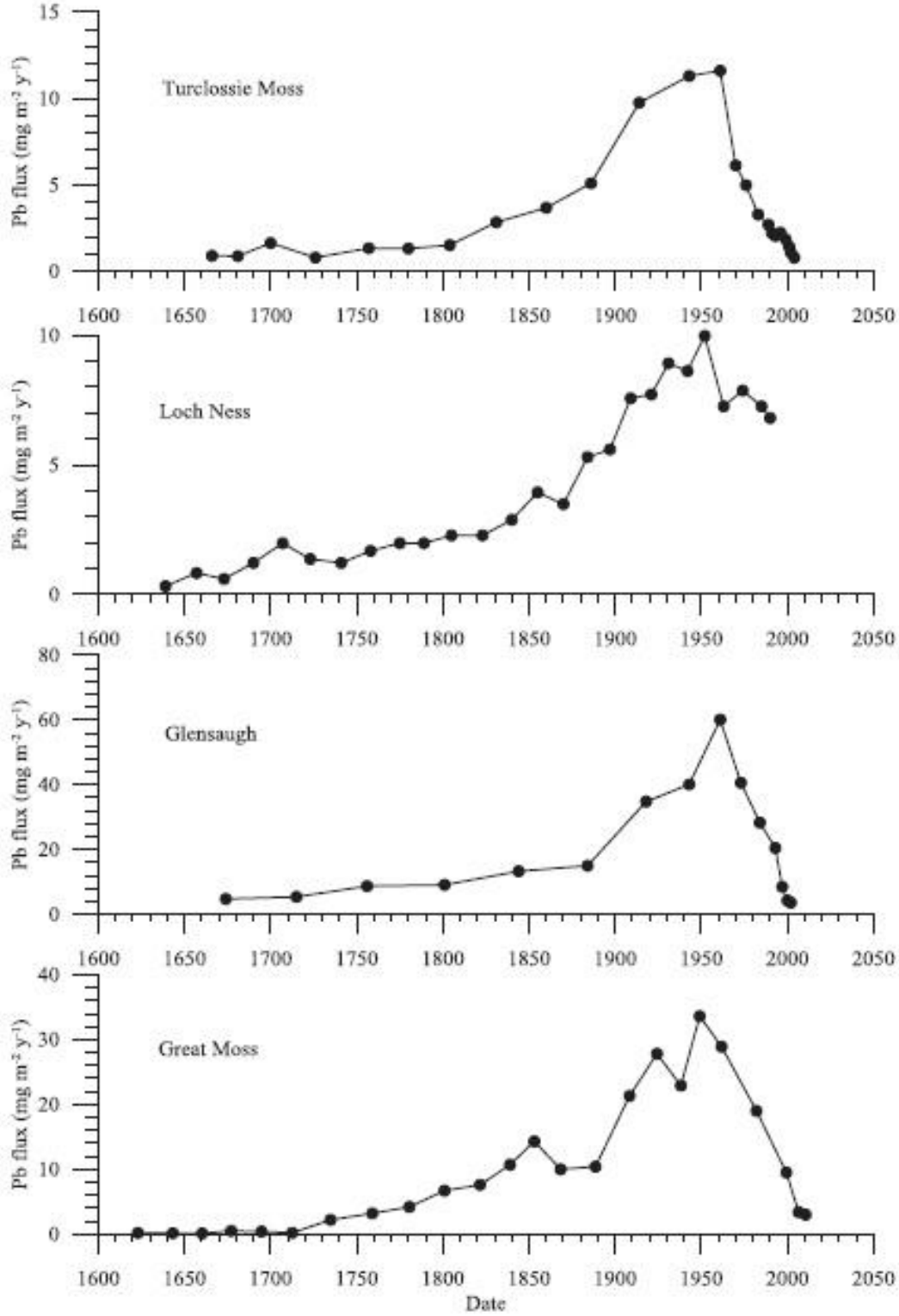

Fig.18. Comparison of anthropogenic Pb flux versus ^{210}Pb date for Great Moss peat, Glensaugh peat (total Pb) (Farmer et al., 2005), Loch Ness sediment (Eades et al., 2002) and Turclossie Moss peat (Cloy et al., 2008).

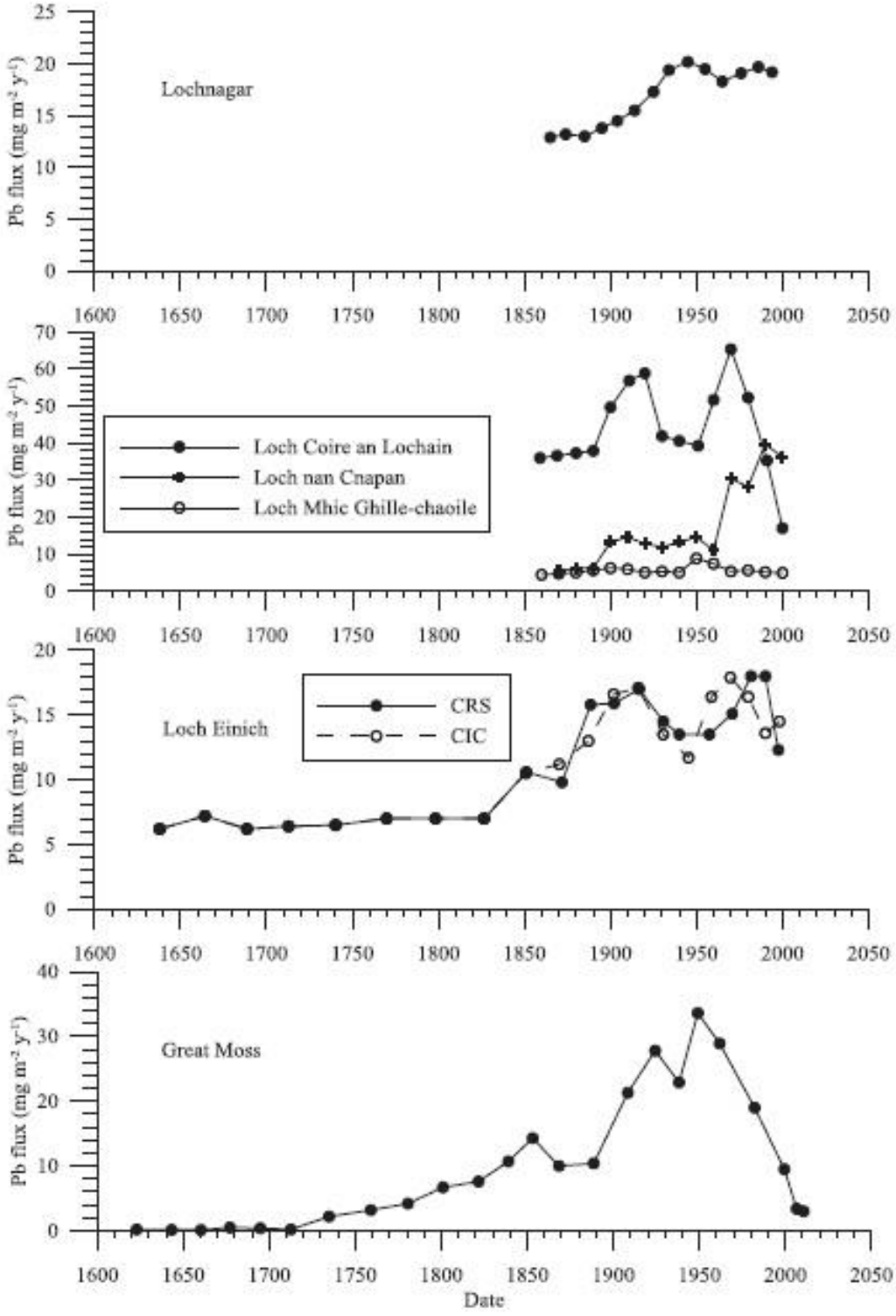

Fig.19. Comparison of total Pb flux versus ^{210}Pb date for Great Moss peat and Loch Einich sediment (both CRS and CIC chronology), Loch Coire an Lochain, Loch nan Cnapan and Loch Mhic Ghille-chaoile sediment (Rose et al., 2012) [for locations see Fig. 1] and Lochnagar sediment (Yang et al., 2002)].

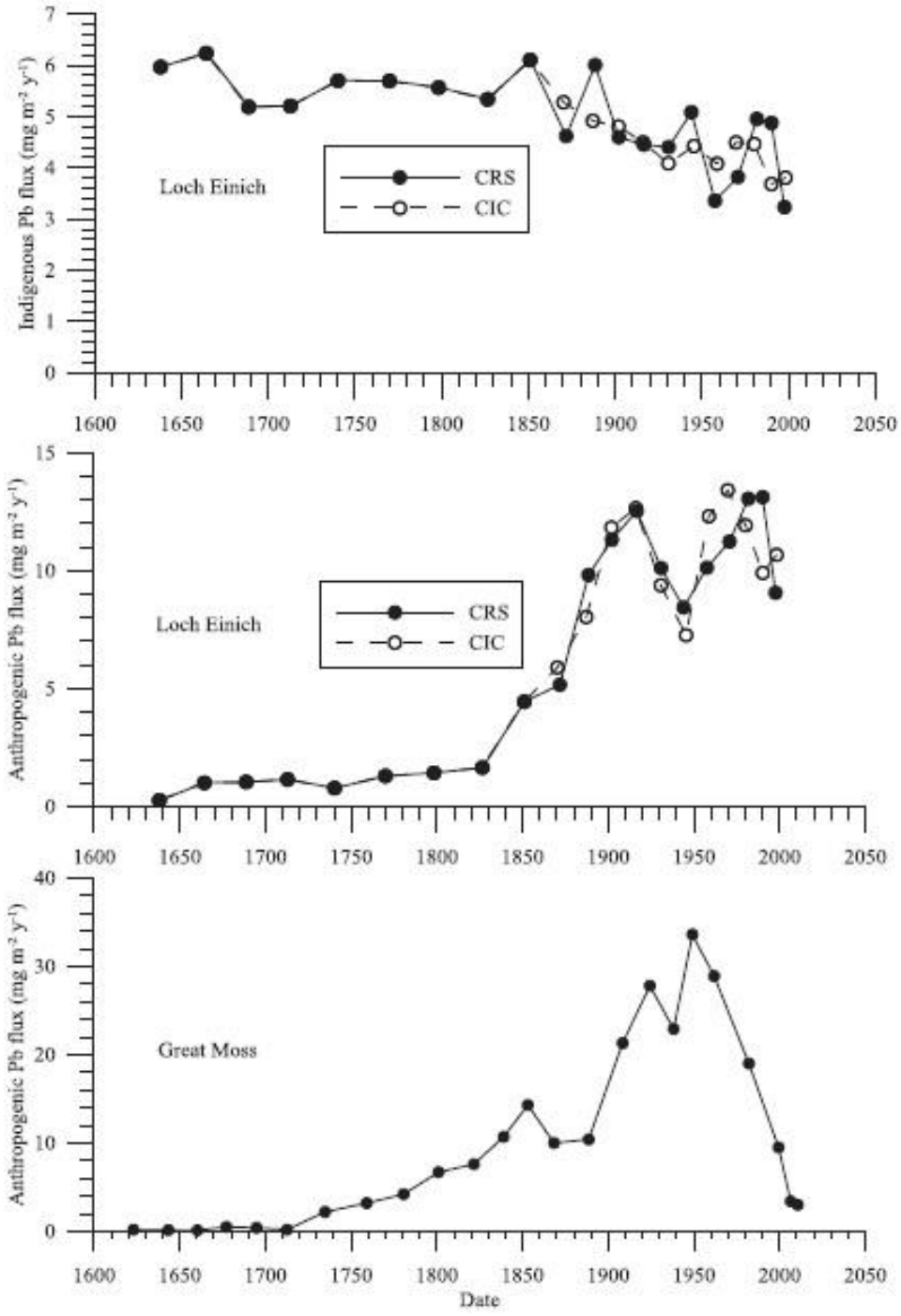

Fig.20. Comparison of Pb flux versus ^{210}Pb date for Great Moss peat anthropogenic Pb, Loch Einich sediment anthropogenic Pb (both CRS and CIC chronology) and Loch Einich sediment indigenous Pb (both CRS and CIC chronology).

This latter phenomenon is seen even more clearly if the total Pb flux for Loch Einich is separated into indigenous and contaminant Pb components (cf. 3.1.3 and Fig. 9) and compared directly with the atmospheric contaminant Pb flux deposition trend as represented by the Great Moss peat (Fig. 20). Thus, continuing input of previously deposited contaminant Pb from the catchment was contributing significantly (9–13 mg m^{-2} y^{-1}) to the deposition of Pb to Loch Einich sediment during the late 20th century and at about three times the rate of deposition of indigenous Pb (3–4 mg m^{-2} y^{-1}).

3.3.2. Anthropogenic Pb inventories

The comparison of inventories of anthropogenic Pb for different time periods (cf. the approach of Eades et al., 2002; Farmer et al., 2005) since the 17th century for cores from Turclossie Moss, Loch Ness, Glensaugh, Great Moss and Loch Einich (Table 1) reveals broad agreement in the relative distributions (% of total anthropogenic Pb inventory) with time, although it is noteworthy that Loch Einich is the highest (at 17% of total) for the post-1975 period, perhaps reflective of the continuing input from the catchment at a time of declining atmospheric emissions and deposition. The absolute magnitude of the inventories at the different locations can of course be influenced by a variety of factors other than geographical variation, such as sediment focusing in lochs (e.g. Rose, 2007) and variable deposition over and retention by peat bogs (e.g. Bindler et al., 2004). The 3.70 g m^{-2} for Great Moss peat, however, is close to the estimated soil storage of 4.40 g m^{-2} for anthropogenically derived Pb in the Glen Einich catchment of Loch Mhic Ghille-chaoile (Rose et al., 2012). It is especially noteworthy that when the post-1860 inventories of anthropogenic Pb for Loch Einich and Great Moss are compared with those for Lochnagar and its catchment (Yang et al., 2002), not only are the magnitudes similar for (i) Loch Einich and Lochnagar sediments and (ii) Great Moss peat and the Lochnagar catchment (Table 2) but also the inventory ratios of 0.49 for Einich/Great Moss and 0.64 for Lochnagar/Lochnagar catchment.

It is also instructive to compare the inventories of anthropogenic Pb with those of unsupported ^{210}Pb for Loch Einich, Great Moss and a variety of other locations in the area for which such data are available (Table 3). The average annual ^{210}Pb flux, derived from the unsupported ^{210}Pb inventory, can vary with factors such as altitude and the extent of rainfall. Thus, on the basis of 77 ± 14 Bq m^{-2} y^{-1} per 1000 mm rainfall (Smith et al., 1997), Farmer et al. (2005) deduced that the 198 Bq m^{-2} y^{-1} for Glensaugh peat was approximately double the value anticipated and attributed this to enhanced deposition of ^{210}Pb under the conditions (e.g. occult deposition from clouds) pertaining at the altitude (426 m) of the collected peat core near the top of the Glensaugh catchment. Rose (2007) considered sediment focusing (by a factor of _2.0) and catchment input to be responsible for the 7.80 kBq m^{-2} inventory and derived average annual flux of 242 Bq m^{-2} y^{-1} for Lochnagar sediments. Both Great Moss peat (273 Bq m^{-2} y^{-1}) and Loch Einich sediment (322 Bq m^{-2} y^{-1}) are also elevated, a figure of ~140 Bq m^{-2} y^{-1} being anticipated on the basis of the average annual rainfall of 1800 mm at Loch Einich. Similar enhancement factors could be operating at Great Moss (altitude 949 m) and Loch Einich as proposed for Glensaugh and Lochnagar, respectively, and there is also the possibility, in the case of Loch Einich, of additional ^{210}Pb from decay of ^{222}Rn introduced by groundwater flow (Norton et al., 1985) as previously suggested for another Cairngorm loch, Lochan Uaine (Jones et al., 1993). It is worth noting, however, that the unsupported ^{210}Pb average annual ^{210}Pb flux (and inventory) for Great Moss peat is only ~15% less than that for Loch Einich sediment, while the anthropogenic Pb inventory for Great Moss is 2.15 times (or 2.0 times, post-1860) that for Loch Einich. This suggests that significant loss of anthropogenic Pb introduced to Loch Einich (water retention time 296 days) is occurring by outflow via the Allt na Beinne Moire before it can be deposited in the bottom sediments.

Table 1
Comparison of inventories of anthropogenic Pb for different time periods for cores from Turclossie Moss, Loch Ness, Glensaugh, Great Moss and Loch Einich.

Loch/Peat Bog	Anthropogenic Pb inventory					
	Pre-1820 g m^{-2} (% of total)	1820–1900 g m^{-2} (% of total)	1901–1930 g m^{-2} (% of total)	1931–1975 g m^{-2} (% of total)	1976-top g m^{-2} (% of total)	Total g m^{-2}
Turclossie Moss[a]	0.18	0.30	0.345	0.46	0.075	1.36
ca. 1660–2004	*(13)*	*(22)*	*(25)*	*(34)*	*(6)*	
Loch Ness[a]	0.27	0.31	0.23	0.38	0.11	1.30
ca. 1630–1990	*(21)*	*(24)*	*(18)*	*(29)*	*(8)*	
Glensaugh[a]	1.20	1.15	1.08	2.06	0.52	6.01
ca. 1650–2002	*(20)*	*(19)*	*(18)*	*(34)*	*(9)*	
Great Moss	0.45	0.83	0.78	1.17	0.47	3.70
ca. 1610–2012	*(12)*	*(22)*	*(21)*	*(32)*	*(13)*	
Loch Einich	0.20	0.41	0.36	0.46	0.29	1.72
ca. 1625–2001	*(12)*	*(24)*	*(21)*	*(27)*	*(17)*	

[a] Values for Turclossie Moss, Loch Ness and Glensaugh based on data in Cloy et al. (2008), Eades et al. (2002) and Farmer et al. (2005), respectively, and extrapolated ^{210}Pb dates.

Table 2
Comparison of inventories of anthropogenic Pb since 1860 for cores from Loch Einich, Great Moss, Lochnagar and Lochnagar catchment.

Loch sediment/Peat	Post-1860 Anthrop. Pb inventory g m^{-2}	Loch sediment/Peat	Post-1860 Anthrop. Pb inventory g m^{-2}
Loch Einich ca. 1860–2001	1.40	Lochnagar[a] ca. 1860–1997	1.55
Great Moss ca. 1860–2012	2.83	Lochnagar Catchment[a] ca. 1860–1997	2.41

[a] Lochnagar and Lochnagar catchment data from Yang et al. (2002).

Table 3
Comparison of inventories of anthropogenic Pb and unsupported ^{210}Pb for cores from Turclossie Moss, Loch Ness, Glensaugh, Lochnagar, Great Moss and Loch Einich.

Loch / Peat Bog	Anthrop. Pb inventory g m^{-2}	Unsupported ^{210}Pb inventory kBq m^{-2}	Average annual ^{210}Pb flux Bq m^{-2} y^{-1}
Turclossie Moss[a] ca. 1660–2004	1.36	2.62	81
Loch Ness[a] ca. 1630–1990	1.30	3.22	100
Glensaugh[a] ca. 1650–2002	6.01	6.40	198
Lochnagar[b] ca. 1625–1997	1.90	7.80	242
Great Moss ca. 1610–2012	3.70	8.80	273
Loch Einich ca. 1625–2001	1.72	10.37	322

[a] Values for Turclossie Moss, Loch Ness and Glensaugh based on data in Cloy et al. (2008), Eades et al. (2002) and Farmer et al. (2005), respectively, and extrapolated ^{210}Pb dates.
[b] Values for Lochnagar are based on (i) pro-rata extrapolation from Lochnagar and Loch Einich Pb data in Table 2 and (ii) ^{210}Pb data in Rose (2007).

4. CONCLUSIONS

Radionuclide, elemental and isotopic analysis of a sediment core from Loch Einich, which lies on Cairngorm Granite in the Cairngorm Highlands, Scotland, led to the following conclusions:

(i) The sediment is enriched in U by an order of magnitude relative to the surrounding catchment bedrock. Decay series radionuclide profiles, activity ratios and stable Pb isotope systematics show that U in the sediment is present in both a dominant authigenic phase and as a minor component in detrital minerals in which the ^{238}U decay series is in secular equilibrium. Decay series disequilibria, in conjunction with core geochemistry, suggest that re-deposition of the authigenic component is probably a consequence of a post-glacial weathering process in the catchment.
(ii) The sediment core exhibited classical redox-driven, near-surface enrichment in Mn and Fe, with clear evidence of diagenetic enrichment of ^{226}Ra in association with Mn, for which suitable correction was necessary in order to derive a ^{210}Pb chronology. This correction significantly affected the relative magnitude of the Pb fluxes subsequently calculated for the uppermost two sections of the core using the sectional timespans derived from the CRS method of ^{210}Pb dating. There was excellent agreement between derived ^{210}Pb (CRS, CIC) and ^{241}Am chronologies, but ^{137}Cs exhibited a high degree of mobility in the organic-rich sediment. The study reveals the value of developing a full understanding of decay series disequilibria in complex, high natural radioactivity systems in order to derive ^{210}Pb chronologies.
(iii) Consistent with the location, Pb isotope ratios were more radiogenic than observed in lake sediments from other parts of Scotland outwith the Cairngorm area. The Pb in the detrital minerals was estimated to have 2.7% radiogenic content. It is important to define accurately the indigenous stable Pb isotopic composition in this type of environment. Systematics of variations in ^{232}Th and ^{230}Th specific activities and ^{208}Pb/^{207}Pb and ^{206}Pb/^{207}Pb ratios indicated that the Pb deposited in the core up to the end of the 19th century can be treated as a binary mixture of indigenous Pb and atmospherically deposited Pb, with a ^{206}Pb/^{207}Pb ratio of about 1.175 as a consequence of dominant input from industrial emissions and coal burning. This allowed the use of a simple binary mixing model for this period. A more complex situation applied to Pb deposited in the 20th century, with three significant components: indigenous Pb, industrial/ coal-derived Pb and petrol Pb. This system is not amenable to source apportionment by a simple binary mixing calculation, so ^{206}Pb/^{207}Pb ratios for samples of archived herbarium moss were used to estimate the ratio for atmospheric deposition from combined industrial/coal and petrol Pb sources in order to estimate temporal variations in anthropogenic and indigenous Pb fluxes.

Similar analysis of a monolith core from the nearby Great Moss blanket peat deposit, which lies on metamorphosed Dalradian sandstones and siltstones, showed that:

(i) The shallow (0.5 m) Great Moss peat deposit has separate basal and atmospheric inputs of unsupported ^{210}Pb. There was very good agreement between ^{210}Pb (CRS, CIC) and ^{241}Am chronologies for the peat core. The value in calculating both CRS and CIC ^{210}Pb chronologies and of corroborating them with the independent ^{241}Am chronology is emphasised for both lake sediment and peat by this study.
(ii) There was an excellent level of agreement (at least until recent decades) between Loch Einich and Great Moss cores with respect to the temporal trends in calculated total and anthropogenic Pb fluxes, providing strong support for the use of the archived moss data to estimate the isotopic composition of atmospheric deposition. This demonstrates the value of independent data sets from archived moss or grass samples. Both the Loch Einich and Great

Moss cores indicated a dip in anthropogenic Pb deposition in the early mid- 20th century, consistent with decreased emissions during the economic depression of the 1930s. Further strong support for the estimated temporal variations in Pb fluxes was provided by a very high degree of consistency with corresponding trends derived for numerous other Scottish lake sediment or peat cores.
(iii) Pb fluxes in Loch Einich towards the end of the 20th century were higher than would be anticipated on the basis of the Great Moss and other peat core data, indicating that catchment-derived material constitutes a significant component of contemporary Pb input to the loch. This has also been observed for Lochnagar, to the southeast of the Cairngorm Mountains, with susceptibility to input from catchment erosion the key factor in this type of upland environment. This represents a general change from direct atmospheric inputs dominating to catchment inputs now being more important. The characterisation of such fluxes is fundamental to understanding the long-term fate of contaminant Pb in the environment.

Overall, this study highlights the requirement to develop an adequate understanding of the geochemical processes operating and of the resultant decay series disequilibria in order to establish chronologies and Pb fluxes for lake sediments and peat in areas with high natural radioactivity levels.

ACKNOWLEDGEMENTS
We thank Lorna Eades for her technical expertise in ICP-OES and ICP-MS analysis and David Blair and Lauri Koresaar for laboratory assistance at UoE, Ian Oliver for support in the field, and Caroline Donnelly for radionuclide analyses at SUERC.

REFERENCES
Allan M., Le Roux G., De Vleeschouwer F., Bindler R., Blaauw M., Piotrowska N., Sittorski J. and Fagel N. (2013) Highresolution reconstruction of atmospheric deposition of trace metals and metalloids since AD 1400 recorded by ombrotrophic peat cores in Hautes-Fagnes, Belgium. Environ. Pollut. 178,
381–394.

Appleby P. G. (2001) Chronostratigraphic techniques in recent sediments. In Tracking Environmental Change using Lake Sediments, vol. 1 (eds. W. M. Last and J. P. Smol), pp. 171– 203. Basin Analysis Coring and Chronological Techniques. Kluwer Academic Publishers, Dordrecht.

Appleby P. G. (2008) Three decades of dating recent sediments by fallout radionuclides: a review. The Holocene 18, 83–93.

Appleby P. G. and Oldfield F. (1978) The calculation of lead-210 dates assuming a constant rate of supply of unsupported ^{210}Pb to the sediment. Catena 5, 1–8.

Bacon J. R. and Hewitt I. E. (2005) Heavy metals deposited from the atmosphere on upland Scottish soils: chemical and lead isotope studies of the association of metals with soil components. Geochim. Cosmochim. Acta 69, 19–33.

Bacon J. R., Jones K. C., McGrath S. P. and Johnston A. E. (1996) Isotopic character of lead deposited from the atmosphere at a grassland site in the United Kingdom since 1860. Environ. Sci. Technol. 30, 2511–2518.

Barber K. E., Maddy D., Rose N., Stevenson A. C., Stoneman R. and Thompson R. (2000) Replicated proxy-climate signals over the last 2000 yr from two distant UK peat bogs: new evidence for regional palaeoclimate teleconnections. Quatern. Sci. Rev. 19, 481–487.
Barron H. F., Gillespie M. R. and Merritt J.W. (2011) Geodiversity of the Cairngorms National Park. British Geological Survey Open Report, OR/10/19, NERC, Edinburgh, 43 p.

Bindler R. (2011) Contaminated land environments of man: reviewing the lead isotopic evidence in sediments, peat and soils for the temporal and spatial patterns of atmospheric lead pollution in Sweden. Environ. Geochem. Health 33, 311–329.

Bindler R., Klarqvist M., Klaminder J. and Fo¨ rster J. (2004) Does within-bog variability of mercury and lead constrain reconstruction of absolute deposition rates from single peat records? The example of Store Mosse, Sweden. Global Biogeochem. Cycles 18, GB3020. http://dx.doi.org/10.1029/2004GB002270.

Bra¨nnvall M.-L., Bindler R., Emteryd O. and Renberg I. (2001a) Four thousand years of atmospheric lead pollution in northern Europe: a summary from Swedish lake sediments. J. Paleolimnol. 25, 421–435.

Bra¨nnvall M.-L., Kurkkio H., Bindler R., Emtryd O. and Renberg I. (2001b) The role of pollution versus natural geological sources for lead enrichment in recent lake sediments and surface forest soils. Environ. Geol. 40, 1057–1065.

Brenner M., Peplow A. J. and Schelske C. L. (1994) Disequilibrium between ^{226}Ra and supported ^{210}Pb in a sediment core from a shallow Florida lake. Limnol. Oceanogr. 39, 1222–1227.

Brenner M., Schelske C. L. and Kenney W. F. (2004) Inputs of dissolved and particulate ^{226}Ra to lakes and implications for ^{210}Pb dating recent sediments. J. Paleolimnol. 32, 53–66.

Brown G. C., Plant J. and Lee M. K. (1979) Geochemical and geophysical evidence of the geothermal potential of Caledonian granites in Britain. Nature 280, 129–131.

Cannell M. G. R., Dewar R. C. and Pyatt D. G. (1993) Conifer plantations on drained peatlands in Britain: a net gain or loss of carbon?. Forestry 66 353–369.

Card J. W. and Bell K. (1985) The relationship of soil ^{210}Po and ^{210}Pb geochemical dispersion patterns to uranium mineralisation. J. Geochem. Explor. 23, 101–115.

Cloy J. M., Farmer J. G., Graham M. C., MacKenzie A. B. and Cook G. T. (2008) Historical records of atmospheric Pb deposition in four Scottish ombrotrophic peat bogs: an isotopic comparison with other records from western Europe and Greenland. Global Biogeochem. Cycles 22, GB2016. http://dx.doi.org/10.1029/2007GB003059.

Cloy J. M., Farmer J. G., Graham M. C. and MacKenzie A. B. (2009) Retention of As and Sb in ombrotrophic peat bogs: records of As, Sb and Pb deposition at four Scottish sites. Environ. Sci. Technol. 43, 1756–1762.

Eades L. J. (1999) Radiochronological investigations of the pollution history of lead and other heavy metals in Scottish freshwater loch sediments. Ph. D. thesis, University of Edinburgh.

Eades L. J., Farmer J. G., MacKenzie A. B., Kirika A. and Bailey- Watts A. E. (2002) Stable lead isotopic characterisation of the historical record of environmental lead contamination in dated freshwater lake sediment cores from northern and central Scotland. Sci. Total Environ. 292, 55–67.

Erel Y., Harlavan Y. and Blum J. D. (1994) Lead isotope systematics of granitoid weathering. Geochim. Cosmochim. Acta 58, 5299–5306.

Fanning K. A., Byrne R. H., Breland, II, J. A., Betzer P. R., Moore W. S., Elsinger R. J. and Pyle T. E. (1981) Geothermal springs of the West Florida continental shelf: evidence for dolomitization and radionuclide enrichment. Earth Planet. Sci. Lett. 52, 345–354.

Farmer J. G. (1994) Environmental change and the chemical record in Loch Lomond sediments. Hydrobiology 290, 39–49.

Farmer J. G. and Lovell M. A. (1986) Natural enrichment of arsenic in Loch Lomond sediments. Geochim. Cosmochim. Acta 50, 2059–2067.

Farmer J. G., Eades L. J., MacKenzie A. B., Kirika A. and Bailey-Watts A. E. (1996) Stable lead isotopic record of lead pollution in Loch Lomond sediments since 1630 A.D. Environ. Sci. Technol. 30, 3080–3083.

Farmer J. G., MacKenzie A. B., Eades L. J., Kirika A. and Bailey-Watts A. E. (1997a) Influences on the extent and record of heavy metal pollution in sediment cores from Loch Tay in a mineralised area of Scotland. J. Geochem. Explor. 58, 195–202.

Farmer J. G., MacKenzie A. B., Sugden C. L., Edgar P. J. and Eades L. J. (1997b) A comparison of the historical lead pollution records in peat and freshwater lake sediments from central Scotland. Water Air Soil Pollut. 100, 253–270.

Farmer J. G., Eades L. J. and Graham M. C. (1999) The lead content and isotopic composition of British coals and their implications for past and present releases of lead to the U.K. environment. Environ. Geochem. Health 21, 257–272.

Farmer J. G., Eades L. J., Graham M. C. and Bacon J. R. (2000) The changing nature of the $^{206}Pb/^{207}Pb$ isotopic ratio of lead in rainwater, atmospheric particulates, pine needles and leaded petrol in Scotland, 1982–1998. J. Environ. Monit. 2, 49–57.

Farmer J. G., Eades L. J., Atkins H. and Chamberlain D. F. (2002) Historical trends in the lead isotopic composition of Sphagnum mosses from Scotland (1838–2000). Environ. Sci. Technol. 36, 152–157.

Farmer J. G., Graham M. C., Bacon J. R., Dunn S. M., Vinogradoff S. I. and MacKenzie A. B. (2005) Isotopic characterisation of the historical lead deposition record at Glensaugh, an organic-rich, upland catchment in rural N. E. Scotland. Sci. Total Environ. 346, 121–137.

Farmer J. G., Eades L. J., Graham M. C., Cloy J. M. and Bacon J. R. (2010) A comparison of the isotopic composition of lead in rainwater, surface vegetation and tree bark at the long-term monitoring site, Glensaugh, Scotland, in 2007. Sci. Total Environ. 408, 3704–3710.
Goldberg E. D. (1963) Geochronology with Lead-210. In Radioactive Dating. International Atomic Energy Agency, Vienna, pp. 121–131.

Gordon J. E. (1993) The Cairngorms, eastern Grampian Mountains. In Quaternary of Scotland, vol. 6 (eds. J. E. Gordon and D. G. Sutherland), pp. 259–276. Geological Conservation Review Series. Chapman and Hall, London (Chapter 9).

Gordon J., Wignall R., Brazier N. and Bruneau P. (2006) Cairngorms: A Landscape Fashioned by Geology, second ed. Scottish Natural Heritage, Perth.

Hansson S. V., Kaste J. M., Olid C. and Bindler R. (2014) Incorporation of radiometric tracers in peat and implications for estimating accumulation rates. Sci. Total Environ. 493, 170–177.

Helliwell R. C., Wright R. F., Evans C. D., Jenkins A. and Ferrier R. C. (2002) A comparison of loch chemistry from 1955 and 1999 in the Cairngorms, N. E. Scotland. Water Air Soil Pollut.: Focus 2, 47–59.

Holden J., Burt T. P. and Cox N. J. (2001) Macroporosity and infiltration in blanket peat: the implications of tension disc infiltrometer measurements. Hydrol. Proc. 15, 289–303.

Jones V. J., Flower R. J., Appleby P. G., Natkanski J., Richardson N., Rippey B., Stevenson A. C. and Battarbee R. W. (1993) Palaeolimnological evidence for the acidification and atmospheric contamination of lochs in the Cairngorm and Lochnagar areas of Scotland. J. Ecol. 81, 3–24.

Klaminder J., Bindler R. and Renberg I. (2008) The biogeochemistry of atmospherically derived Pb in the boreal forest of Sweden. Appl. Geochem. 23, 2922–2931.

Klaminder J., Farmer J. G. and MacKenzie A. B. (2011) The origin of lead in the organic horizon of tundra soils: atmospheric deposition, plant translocation from the mineral soil or soil mineral mixing? Sci. Total Environ. 409, 4344–4350.

Klaminder J., Appleby P., Crook P. and Renberg I. (2012) Post-deposition diffusion of 137Cs in lake sediment: implications for radiocaesium dating. Sedimentol 59, 2259–2267. http://dx.doi.org/10.1111/j.1365-3091.2012.01343.x.

Lindsay R. (2010) Peatbogs and Carbon: A Critical Synthesis. RSPB Scotland, 344 p.

Lyle A. A. (1987) The bathymetry and hydrology of some lochs vulnerable to acid deposition in Scotland. In Acidification and Fish in Scottish Lochs (eds. P. S. Maitland, A. A. Lyle and R. N. B. Campbell). Institute of Terrestrial Ecology, Grange-over-Sands, pp. 22–34.

MacKenzie A. B. (2000) Environmental radioactivity: experience from the 20th century – trends and issue for the 21st century. Sci. Total Environ. 249, 313–329.

MacKenzie A. B. and Pulford I. D. (2002) Investigation of contaminant metal dispersal from a disused mine site at Tyndrum, Scotland, using concentration gradients and stable Pb isotope ratios. Appl. Geochem. 17, 1093–1103.

MacKenzie A. B., Scott R. D., Linsalata P., Miekeley N. and Coutinho de Jesus H. (1994) Interlaboratory comparison of analytical methods for the determination of natural series uranium and thorium isotopes in rock samples. J. Radioanal. Nucl. Chem. 182, 21–34.

McVean D. N. (1962) Cladonia Elongata (Jacq.) Hoffm in the Cairngorms. The Lichenologist 1, 94–96.

Merila¨inen J. J., Kustula V. and Witick A. (2011) Lead pollution history from 256 BC to AD 2005 inferred from the Pb isotope ratio ($^{206}Pb/^{207}Pb$) in a varve record of Lake Korttaja¨rvi in Finland. J. Paleolimnol. 45, 1–8.

Martınez Cortizas A., Peiteado Valera E., Bindler R., Biester H. and Cheburkin A. (2012) Reconstructing historical Pb and Hg pollution in NW Spain using multiple cores from Chao de Lamoso bog (Xistral Mountains). Geochim. Cosmochim. Acta 82, 68–78.

Miller H., Croudace I. W., Bull J. M., Cotterill C. J., Dix J. K. and Taylor R. N. (2014) A 500 year sediment lake record of anthropogenic and natural inputs to Windermere (English Lake District) using double-spike lead isotopes, radiochronology and sediment microanalysis. Environ. Sci. Technol. 48, 7254–7263.

Norton S. A., Hess C. T., Blake G. M., Morrison M. L. and Baron J. (1985) Excess unsupported ^{210}Pb in lake sediments from Rocky Mountain Lakes: a groundwater effect. Can. J. Fish. Aquat. Sci. 42, 1249–1254.

Novak M., Emmanuel S., Vile M. A., Erel Y., Veron A., Paces T., Wider R. K., Vanecek M., Stepanova M., Brizova M. and Hovorka J. (2003) Origin of lead in eight central European peat bogs determined from isotope ratios, strengths and operational times of regional pollution sources. Environ. Sci. Technol. 37, 437–445.

Patterson C. (1956) Age of meteorites and the earth. Geochim. Cosmochim. Acta 10, 230–237.

Plant J., Henney P. J. and Simpson P. R. (1990) The genesis of tin–uranium granites in the Scottish Caledonides: implications for metallogenesis. Geol. J. 25, 431–442.

Read D., Bennett D. G., Hooker P. J., Ivanovich M., Longworth G., Milodowski A. E. and Noy D. J. (1993) The migration of uranium into peat-rich soils at Broubster, Caithness, Scotland, UK. J. Contaminant Hydrol. 13, 291–308.

Renberg I., Bindler R. and Brannvall M.-L. (2001) Using the historical atmospheric lead-deposition record as a chronological marker in sediment deposits in Europe. Holocene 11, 511–516.

Robbins J. A. and Edgington D. N. (1975) Determination of recent sedimentation rates in Lake Michigan using Pb-210 and Cs-137. Geochim. Cosmochim. Acta 39, 285–304.

Rose N. L. (2007) The sediments of Lochnagar: Distribution, accumulation and composition. In Lochnagar: The Natural History of a Mountain Lake (ed. N. L. Rose). Springer, Dordrecht, pp. 155–175 (Chapter 8).

Rose N. L., Yang H., Turner S. D. and Simpson G. L. (2012) An assessment of the mechanisms for the transfer of lead and mercury from atmospherically contaminated organic soils to lake sediments with particular reference to Scotland, UK.
Geochim. Cosmochim. Acta 82, 113–135.

Schell W. R., Tobin M. J., Wieder R. K. and Mitchell P. I. (1997) Deposition history of trace metals and fallout radionuclides in wetland ecosystems using ^{210}Pb chronology. Water Air Soil Pollut. 100, 233–239.

Scott R. D., MacKenzie A. B., Ben Shaban Y. A., Hooker P. J. and Houston C. M. (1991) Uranium transport and retardation at the Needle's Eye natural analogue site, South West Scotland. Radiochim. Acta 52/53, 357–365.

Scott R. D., MacKenzie A. B. and Alexander W. R. (1992) The interpretation of ^{238}U–^{234}U–^{230}Th–^{226}Ra disequilibria produced by rock–water interactions. J. Geochem. Explor. 45, 323–343.

Shirahata H., Elias R. W. and Patterson C. C. (1980) Chronological variations in concentrations and isotopic compositions of anthropogenic atmospheric lead in sediments of a remote sub-alpine pond. Geochim. Cosmochim. Acta 44, 149–162.

Shotyk W., Cheburkin A. K., Appleby P. G., Fankhauser A. and Kramers J. D. (1996) Two thousand years of atmospheric arsenic, antimony and lead deposition recorded in an ombrotrophic peat bog profile, Jura Mountains, Switzerland. Earth Planet. Sci. Lett. 145, E1 E7.

Shotyk W., Weiss D., Heisterkamp M., Cheburkin A. K., Appleby P. G. and Adams F. C. (2002) New peat bog record of atmospheric lead pollution in Switzerland: Pb concentrations, enrichment factors, isotopic composition and organolead species. Environ. Sci. Technol. 36, 3893–3900.

Shotyk W., Goodsite M. E., Roos-Barraclough F., Givelet N., Le Roux G., Weiss D., Cheburkin A. K., Knudsen K., Heinemeier J., van Der Knaap W. O., Norton S. A. and Lohse C. (2005) Accumulation rates and predominant atmospheric sources of natural and anthropogenic Hg and Pb on the Faroe Islands. Geochim. Cosmochim. Acta 69, 1–17.

Smith J. T., Appleby P. G., Hilton J. and Richardson N. (1997) Inventories and fluxes of ^{210}Pb, ^{137}Cs and ^{241}Am determined from the soils of three small catchments in Cumbria, UK. J. Environ. Radioact. 37, 127–142.

Sugden C. L., Farmer J. G. and MacKenzie A. B. (1993) Isotopic ratios of lead in contemporary environmental material from Scotland. Environ. Geochem. Health 15, 59–65.

Thiel K., Vorwerk R., Saager R. and Stupp H. D. (1983) ^{235}U fission tracks and ^{238}U-series disequilibria as a means to study recent mobilization of uranium in Archaean pyritic conglomerates. Earth Planet. Sci. Lett. 65, 249–262.

Thomas C. W., Gillespie M. R., Jordan C. and Hall A. M. (2004) Geological structure and landscape of the Cairngorm Mountains. Scottish Natural Heritage Commissioned Report No. 064 (ROAME No. F00AC103).

Torgersen T. and Longmore M. E. (1984) 137Cs diffusion in the highly organic sediment of Hidden Lake, Fraser Island, Queensland. Aust. J. Mar. Freshw. Res. 35, 537–548.

UK National Atmospheric Emissions Inventory (2014), Lead, http://naei.defra.gov.uk (accessed July 2014).

UNSCEAR (1993) Sources and effects of ionising radiation. Report to the General Assembly by the United Nations Scientific Committee on the Effects of Ionizing Radiation, United Nations, New York.

Viczia´n M., Lasztity A. and Barnes R. M. (1990) Identification of potential environmental sources of childhood lead poisoning by inductively coupled plasma mass spectrometry. Verification and case studies. J. Anal. Atom. Spectrom. 5, 293–300.

Watt A. A. and Jones E. W. (1948) The Ecology of the Cairngorms: Part 1. The Environment and the Altitudinal Zonation of the Vegetation. J. Ecol. 36, 283–304.

Yafa C. and Farmer J. G. (2006) A comparative study of total and acid-extractable digestion methods for the determination of inorganic elements in peat material by inductively coupled plasma-optical emission spectrometry. Anal. Chim. Acta 557, 296–303.